

European Wind Turbine Standards II

The book is based on work done in an R&D project in the framework of an ongoing programme of the European Commission. This programme, called JOULE, supports research and development into renewable energy technologies. It is managed by the Directorate General XII for Science, Research and Development. The work done, as published in this book, has been supported by the Commission under EC contract No JOR3-CT95-0064.

Published by

ECN Solar & Wind Energy
PO Box 1
1755 ZG Petten
The Netherlands

Reproduction is authorised, except for commercial purposes, provided the source is acknowledged.

Realisation: BetaText, Bergen, The Netherlands

EUROPEAN WIND TURBINE STANDARDS II

J.W.M. Dekker
J.T.G. Pierik
(Editors)



This book contains results of the "European Wind Turbine Standards - II" project carried out within the JOULE-III RD programme of the European Commission, contract nr. JOR3-CT95-0064.

PARTICIPANTS OF THE EWTS-II PROJECT

CRES, Centre for Renewable Energy Sources (Greece)
CIEMAT, Centro de Investigaciones Energeticas, Medioambientales y Tecnologicas (Spain)
DEWI, Deutsches Windenergie-Institut (Germany)
ECN, Energieonderzoek Centrum Nederland (Netherlands)
Germanische Lloyd (Germany)
NEL, National Engineering Laboratory (United Kingdom)
RNL, Risø National Laboratories (Denmark)
Teknikgruppen AB (Sweden)
Windtest (Germany)

Project administration:
EUREC-Agency, European Renewable Energy Centres Agency
Kapeldreef 75
B3001 Leuven
Belgium

PREFACE

The number of installed wind turbines, world wide as well as in Europe, is increasing rapidly. At the end of 1997, the total amount of wind power had reached 7600 MW, almost 4800 MW was found in Europe¹. Wind energy has realized a substantial improvement in system reliability as well as a considerable reduction in costs over the recent years. The electricity production in regions with high average wind speeds is now competitive with conventional production methods².

The increase in industrial activity in wind energy in turn generates a demand for standardized methods of design, testing and certification of wind turbines. This demand is partly covered by the activities of standardization bodies (CEN/CEGELEC, IEC), however a number of bottle-necks in knowledge and technical harmonization still exists. It was the objective of the European Wind Turbine Standards project (EWTS), the predecessor of the current project, to remove some of the constraints and bottle-necks and contribute to the harmonization. EWTS was completed in the beginning of 1996, but during its execution a number of technical items evolved that still required further investigation. Therefore, a continuation of the project was defined: EWTS-II, to address items that could not be completed. These items were:

- 1. load spectra and extreme wind conditions;*
- 2. quantification of failure probabilities;*
- 3. integration of blade tests in design;*
- 4. power performance in complex terrain;*
- 5. site evaluation..*

This report presents the results of these investigations.

Furthermore, the previous EWTS project started to establish an organisation of qualified measurement institutes in the field of wind energy, the MEASNET organisation. MEASNET unifies measurement procedures of the participating institutes and guarantees qualified measurements and mutual acceptance among its members. MEASNET was formally established during EWTS-II. A summary on its results is included in the executive summary. More details on the structure of MEASNET, its in house measurement procedures and the rules for acceptance are presented in a separate report³.

We want to express our gratitude to the European Commission and to the national governments for sponsoring this project and we hope that it has brought the work on wind turbine standardisation a step further.

*Jos Dekker and Jan Pierik,
June 1998,
Petten, The Netherlands*

¹ International Wind Energy Development: World Market Update 1997. BTM Consult

² Inaugural speech of Prof. dr. ir. G.A.M. van Kuik, June 1998, Delft

³ Implementation of the Network of European Measurement Institutes, MEASNET

LIST OF CONTENTS

PREFACE	V
EXECUTIVE SUMMARY	IX
1. WIND FARMS-WIND FIELD AND TURBINE LOADING	Part 1 Sub A.1
2. COMPLEX TERRAIN AND FATIGUE LOADING	Part 1 Sub B.1
3. EXTREME WIND CLIMATE EVENTS	Part 1 Sub C.1
4. QUANTIFICATION OF FAILURE PROBABILITIES	Part 2.1
5. INTEGRATION OF BLADE TEST IN DESIGN	Part 3.1
6. POWER PERFORMANCE IN COMPLEX TERRAIN	Part 4.1
7. SITE EVALUATION	Part 5.1

EXECUTIVE SUMMARY

1. LOAD SPECTRA AND EXTREME WIND CONDITIONS

1.1 Introduction

The subproject Load Spectra and Extreme Wind Conditions will generate technical background information to facilitate the development and improvement of the European Wind Turbine Standards in the framework of CENELEC.

The objective of this subproject is to provide guidelines for:

- description of the wind condition in wind farms,
- description of the wind condition in complex terrain
- investigation and evaluation of extreme wind conditions.

All the investigations were performed with reference to the IEC-1400-1 standard.

The turbine classifications in IEC-1400-1 are defined in terms of mean wind speeds, turbulence intensities, and a procedure to determine the extremes. The IEC-1400-1 defines four standard classes I, II, III, IV and an S class. In the S-class, all the wind field parameters have to be specified by the manufacturer. The mean wind speeds in class I to IV are 10m/s, 8.5m/s, 7.5m/s and 6m/s, respectively. The wind speed is assumed to be Raleigh distributed. In addition the standard classes are divided into a high and low turbulence class A and B.

The turbulence classes are defined to cover an extended range of wind turbine operation, including operation in wind farms and complex terrain. Even so, the standard states, that the modified turbulence structure in complex terrain and wake effects must be taken into account in the fatigue analysis of the wind turbines. However no commonly accepted procedures or guidelines exist for the estimation of the relevant turbulence parameter for the two above mentioned types of wind turbine operation. Based on the knowledge of the ambient wind and turbulence distribution, and assumptions of the wind farm configuration, the presented subproject “Load Spectra and Extreme Wind Conditions” provides guidelines for estimation of the wake turbulence for wind farm operation. In the same way, the fatigue relevant turbulence characteristics for complex terrain are investigated. The extreme wind conditions given in the IEC 1400-1 are evaluated from a theoretical and practical point of view. Guidelines are given how to estimate the extreme wind conditions from the actual wind distribution and the turbulence intensity level.

1.2 Wind farms-Wind field and turbine loading

When operating under wake conditions, an increase in fatigue consumption of wind turbines has been observed. The changes in the load patterns originate both from modifications in the mean wind field and from modifications in the turbulence field. By means of a parameter study, the significant wind field parameters, in relation to the increased wind turbine fatigue consumption in wakes, are identified. The analysis is based on a large number of aeroelastic simulations for five significantly different wind turbine concepts. The effect on selected equivalent loads, originating from realistic perturbations in the selected parameters, is determined by means of a two level factorial method.

It has been demonstrated that the deterministic wake deficit as well as the modified turbulence characteristics (turbulence length scale, turbulence intensity, and coherence decay) all are of primary importance in relation to fatigue loading in wake conditions. Furthermore the effects of each of the above parameters appeared to be approximately additive in a fatigue life consumption sense.

Finally a set of simple models has been investigated and subsequently proposed for the quantification of the identified key parameters. The result is that the wind farm effects are easily included in the IEC 1400-1 by including wake load cases simply defined by suitable modifications in the parameters presently used in definition of the conventional load cases.

1.2.1 Conclusions

A procedure for wake load predictions, and its possible inclusion in the IEC-code framework is established. The overall philosophy is to preserve the existing division in four wind turbine classes, and simply supplement the existing load specifications with quantitative wake load specifications.

This procedure is limited to single wake situations, but it is supposed to apply also for multiple wake situations. A detailed investigation has been performed to quantify the wake load situation. The investigation falls into three phases: a crude identification of key wake wind field parameters, a quantification of the identified key parameters and finally a detailed key parameter identification based on predicted wake characteristics.

Applying a two level-factorial method it has been demonstrated that, in the present analysis, 10-minutes simulation time series are a sufficient representation of the individual load situations to yield significant results.

The main findings from the investigation are:

- All four investigated parameters representing the wake wind field, wake deficit, wake turbulence, length scale, and wake coherence—were demonstrated to be significant in relation to increased fatigue life consumption in wakes compared to ambient conditions.
- It is possible to quantify the relevant wake parameters by use of simple models.
- The fatigue contributions, caused by the investigated four parameters, are shown to behave additively. This implies, that a simple approximate method, involving only a very limited number of aeroelastic calculations, can be applied for fatigue estimates taking into account the detailed wind farm topology and the particular wind turbine concept.
- The effect due to increased turbulence intensity is crucial and usually dominates the fatigue effects caused by the other investigated parameters with a factor of 2 to 3.
- The different turbine concepts and different load types act differently with respect to parameter sensitivity. This fact demonstrates the appropriateness of a detailed wake load estimation based on the philosophy applied here, compared to the “all factors in one parameter” approach previously used.

1.3 Complex terrain and fatigue loading

The aims of this subtask are:

- to investigate the effect of the terrain complexity on the wind field properties that drive the fatigue loading of wind turbines (like wind shear, Reynolds stresses, etc.).
- to investigate and quantify the impact of the above properties on fatigue loading for machines of different size and design philosophy.

The first goal is met by analysing the available experimental complex terrain wind databases, as well as by performing systematic parametric runs for simple, 2-D, configurations including single and tandem hill

layouts. In the latter case, results are presented in terms of speed-up and turbulent kinetic energy distributions. The second goal is met through parameter identification (PI) procedures applied on both measurements and computational -aeroelastic- results. “Fatigue influence” matrices are, thus, established for different machine sizes and concepts. Recommendations are made on how to include the present findings into the IEC Standards.

When a turbine is erected at a site which differs significantly from the design conditions of the IEC standard, the fatigue and the extreme loads have to be recalculated. The estimation of the turbulence parameters at a specific site must be part of the site assessment procedure. If a turbine, designed according to the standard classes, is intended to operate at a site with a Weibull shape factor k lower than 1.8, the fatigue load has to be recalculated using the actual Weibull parameters. The actual extreme wind speed events at the site need to be re-evaluated also.

It is felt that the 16% to 18% turbulence intensity values used in the IEC 1400-1 standard can cover complex terrain operation with turbulent intensities from 13% up to 15% respectively, without additional design calculations. It was estimated that this 3% extra turbulent intensity value can compensate a 20 % increase in fatigue loading due to overall complex terrain effects. When a machine is intended to operate at a complex terrain site with a turbulent intensity larger than 15%, the fatigue loads have to be re-evaluated based on the actual values of the Weibull parameters and turbulence conditions at the site.

The wind shear law used in the standards can be maintained, having in mind that a conservative estimation of complex terrain loading is thus achieved.

Sites with wind inclination more than 20 degrees should be considered within the (S)pecial class context.

A site assessment of a complex terrain site must, as a minimum include the following parameters:

- Weibull scale and shape factors C and k ;
- turbulence intensity;
- flow tilt (inclination) angle;

Characteristic values of the remaining wind field parameters can be selected on basis of these values.

1.4 Extreme wind climate events

Critical loads result in responses that exceed the limits beyond which structural damage or irreversible change may be expected. Thus the designer is interested in the number of times, or the probability, that large loads and resulting large responses may occur during the life of the system.

In the IEC 1400-1 standard divides the wind regime for load and safety considerations into normal wind conditions which will occur frequently during normal operation of the wind turbine, and extreme wind conditions which are defined as having a 1 year or 50 year recurrence period. The extreme wind conditions are used to determine critical design loads which the turbine must withstand during its lifetime. These extreme conditions include peak wind speeds due to storms and rapid changes in wind speed and direction.

The objective of this part of the project is to review the models for extremes of the IEC 1400-1 standard, in particular to investigate whether the specified values for the extremes correspond to the assigned probability .

To this end a theoretical approach is adopted by using Extreme Value Theory rather than to perform yet another analysis of wind speed time series. Although measurements should ultimately be decisive, it is obviously dangerous to infer statistics of extremes from a necessarily limited set of data.

Using Extreme Value Theory it is shown that, given a certain knowledge of the climatology, it is possible

to derive statistical characteristics of extreme wind conditions which are believed to be important for wind turbine design, e.g. the survival wind speed, extreme gusts and extreme wind direction changes. In the present report the limit distributions of these three extreme wind conditions have been investigated, assuming that the climatology (the Weibull distribution, the annual average turbulence intensity, the turbulence model etc.) is defined by the IEC wind turbine classes I through IV. In addition the sensitivity of the extremes for the shape parameter k investigated.

With the assumptions given above the derivation of the probability density functions (pdf) and the limit distributions (cdf) for the 10-minute average and 3-second average extreme wind speed is straightforward. It is shown that, given a certain confidence level, the magnitude of the extreme wind speed strongly depends on the shape, k , and scale parameter, C , of the parent Weibull distribution. Smaller shape parameters lead to higher extreme values and vice versa. The influence of the shape parameter becomes pronounced when $k \leq 1.8$.

Comparison with the IEC values shows that the reference wind speed V_{ref} is acceptable for sites with $k \geq 1.77$, i.e. for most flat terrain sites in Europe. This is also the case for the extreme 3-second average wind speeds V_{e1} and V_{e50} (the so-called ‘survival wind speeds’) given in the IEC extreme wind speed model (EWM). But it should be noted that the annual extreme 3-second average wind speed with a recurrence period of one year, V_{e1} , has been redefined to the “*annual characteristic largest 3-second average wind speed.*”

If a wind turbine has to be designed for complex terrain ($1.4 \leq k \leq 1.5$, say), then it is recommended to increase the ratio of the reference wind speed to the annual wind speed to $V_{\text{ref}}/V_{\text{ave}} = 6.6$. In that case, the expressions for V_{e50} and V_{e1} , given by the IEC, still hold.

Assuming longitudinal wind speed fluctuations u_{T1} and u_{T2} at the same location but at different instants t_1 and t_2 to be jointly normal, the conditional pdf $f(u_{T2} - u_{T1} | u_{T1})$ is derived and the limit distribution function is computed through numerical integration. For extreme gusts not only a strong dependence on the parameters of the parent Weibull distribution is found, but also on the assumed turbulence model, viz. Von Kármán or Kaimal, which determines the temporal correlation as function of the time lag $\tau = t_2 - t_1$ and the integral time scale (L/U).

The magnitude of the extreme gust is inversely proportional to the shape parameter k of the parent Weibull distribution. The gust speed increases for increasing time lag τ until the time lag is greater than the integral time scale (L/U), then the gust speed hardly changes anymore. Given the same confidence level, gust values are greater for a starting wind speed at V_{rated} than for a starting wind speed at V_{out} .

The values found for the extreme 3-sec average gusts with a confidence level of 98% are much larger than the values specified by the IEC 1400-1 standard. This was to be expected because experience using the IEC standard has shown that the Normal Turbulence Model (NTM) leads in most cases to higher loads than the extreme operating gust, indicating that the extreme operational gust model is too benign with respect to actual external conditions.

New analysis of the extreme operating gust, performed by a working group of the IEC (TC88/WG7), based on measurements from the German lowland and from Californian sites, shows a ratio of gust magnitude, V_{gust1} , to standard deviation, σ_1 , of about 4.8, indicating that ‘real’ extremes will yield much higher ratio’s, close to values found in the present project, which are estimated to vary between 4.4 for wind turbine class IV and 7 for wind turbine class I. Therefore it must be concluded that acceptance of the new model of the extreme operating gust for the second edition of the IEC standard, proposed by the above mentioned working group, would definitely be an improvement.

The derivation of a probability density function $f_{\theta}(\theta)$ for the wind direction can be found in the literature. It can be shown that this angular pdf only depends on the reciprocal value of the turbulence intensities and

the non-dimensional ratio of the standard deviation of the u and v component of the wind (a measure of the anisotropy of the fluctuations). Because of the non-Gaussian tail of $f_{\theta}(\theta)$ it cannot be assumed that the density function $f_{\theta_1, \theta_2}(\theta_1, \theta_2)$ is jointly normal and it turns out to be impossible to derive, from first principles, this density function in closed form. Numerical integration proved to be too costly.

To circumvent this problem an exponential type density function is fitted to $f_{\theta}(\theta)$ and the extreme value analysis is performed in much the same way as for the extreme gusts. Given the uncertainties in the present analysis the comparison with the IEC values is very limited. It is clear, however, that the IEC values are too benign. Again the newly proposed formulation for the next edition of the IEC standard will be an improvement.

Finally some attention is given to some rare meteorological phenomena— tornadoes and downbursts— which quite likely will induce extreme wind loads, but which are not included in the extreme climate events of the IEC standard.

To conclude:

- Probability density functions and distribution functions have been derived for extreme wind speeds, extreme gusts and extreme wind direction changes. With these density functions it is not only possible to assign a probability to certain extreme wind conditions, but it is also possible to construct a standard where the model for extreme winds and the model for ‘normal’ turbulence and the site classification are logically related, both mathematically and physically.
- The derived distribution functions have been used to compute the magnitude of extreme wind speeds, extreme gusts and extreme wind direction changes with a confidence level of 98%. Comparison with the values given by the IEC 1400-1 standard confirms the observation that the IEC values for extreme gusts are generally too benign. It is recommended however to re-evaluate the distribution function for the extreme wind direction change.
- Finally a rare meteorological phenomenon, called a downburst, is described, which should be included in the extreme climate events of the IEC standard.

2. QUANTIFICATION OF FAILURE PROBABILITIES

Presently, wind turbines are being designed in accordance with deterministic design rules embedded in standards like the IEC 1400-1 and various national standards and certification criteria. These rules concern the design of the load carrying components and the design of safety and control systems.

2.1 Target values for structural reliability

For a safe design of load carrying components a margin is introduced between the design value of the strength and the characteristic value of the load. Over the years various methods to define safety margins have been used, but nowadays the concept of the partial safety factors is commonly embodied in the structural design codes. The determination of the magnitude of the partial safety factors can be done empirically. However, a probabilistic approach is preferred, because in this way uncertainties in the load and the strength can be considered in a more rational manner. This probabilistic method has been applied already in other branches of industry like offshore and civil engineering, but is not introduced in the wind energy branch yet. As the concept of probabilistic calibration of partial safety factors is fairly new in the

wind turbine community the principles behind the method were examined as part of the EWTS-I subproject “Calibration of Safety Factors”. To calibrate partial safety factors based on a probabilistic method target values for the structural reliability of load carrying components have to be drawn up. This aspect has been considered in the current subproject by means of a literature study. From this literature study it is concluded that:

- The Scandinavian countries and The Netherlands seem to be leading in the application of structural reliability methods.
- The code which is not local to a country, but shall be applied Europe-wide, is the Eurocode 1.

Therefore, it is recommended to apply the safety level of the Eurocode to wind turbines, which would mean a yearly safety index of 4.7, corresponding to a failure probability of 10^{-6} /year.

2.2 Guidelines for data collection and parameter estimation

Generally, the control systems have to keep the wind turbine within its design limits during normal operation and have to ensure that electrical energy is generated and supplied to the grid in an efficient manner. In case of a failure or in case of abnormal external conditions, the control systems in combination with the safety systems also have to keep the turbine within its design envelope to prevent damage or unsafe operation. As a consequence of a failure of a safety system, the wind turbine can run into overspeed and is operating beyond design conditions. This can lead to catastrophic failures like blade rupture. Scenarios, how a wind turbine can run into overspeed or failed operation, are derived by means of a qualitative Probabilistic Safety Assessment (PSA). With a quantitative PSA it is also possible to calculate the frequency of occurrence of for example overspeed. PSA’s for wind turbines have been carried out successfully in various countries. Because it is expected that PSA’s will be used more and more, guidelines or recommended practices were formulated as part of the EWTS-I subproject “Assessment of Wind Turbine Safety; Recommended Practices”.

Because the treatment of data for the quantification was beyond the scope of the EWTS-I project, this aspect has been considered in the current subproject. Guidelines to collect data for quantitative safety and reliability analyses have been formulated, based on a limited benchmark study.

As guidelines for data collection and parameter estimation, it is recommended to use as starting basis:

- the guidelines as outlined in the LW 15/75 and NEWECs-45 studies reports; and
- the recommended practices from the EWTS-I project.

In addition to these reports, the following is recommended:

1. The recommendations set out in the LW15/75 and NEWECs-45 studies can be used for design of specific data collection and parameter estimation. Also, the recommendations of the LW 15/75 study on the use of generic data are still valid.
2. Preferably, use should be made of standard, proven methods as laid down in reliability handbooks. Preferably, computerised versions of (generic) databases and existing software for reliability data analysis should be used.
3. Generic wind turbine data sources can be used if no specific data are available or if there are no time or resources available to collect design specific data.
4. Generic wind turbine data sources can be used to provide data on a high level, e.g., an estimate of blade failure frequency to be used in risk studies, or for frequencies of certain initiating events, e.g., grid loss.
5. If generic data are used to estimate a particular parameter (e.g., a failure rate), the following should be documented clearly for each parameter estimated:
 - *the reference(s) to the source(s) used,*
 - *a discussion why the source is considered valid or why the source is used,*

- *the calculation procedure to arrive at the final estimate if multiple sources are used.*
6. If engineering judgement is used to provide an estimate, the reason for this should be indicated. Engineering judgement should be used to provide an estimate if design specific or generic sources do not provide an adequate answer.

2.3 Risks to the public

As mentioned above failure of the safety system might lead to catastrophic failures like blade rupture, which can cause risks to the public. In that way it is of great interest for e.g. authorities, especially in densely populated areas. To judge whether a risk is unacceptable, limits have to be indicated above which the risks become unacceptable (maximum permissible levels).

From a literature study it is concluded that risk criteria related to the risk to the public, applicable for wind turbines are:

- the individual risk and
- the group risk (as defined in the official Dutch premises for risk management).

For these two criteria, the following target values are recommended:

Individual risk

For the use of the individual risk a risk target level of 10^{-5} /year is recommended. The individual risk is independent of the site of the wind turbine (park) and can be calculated without knowing the exact location of the installation. Note that the term ‘risk limit’ is not used but instead the term ‘risk target’, because risk limits are not commonly used in all EU countries.

Group risk

The target value for the group risk is that the likelihood of an accident with 10 deaths occurring should not exceed one in every hundred thousand years (10^{-5} /year). The aim of setting target values for group risk is to prevent social disruption (the death of a group of people all at once). Accidents with even more serious consequences lead to correspondingly greater degrees of disruption. It is therefore assumed that an n -times larger impact than 10 deaths should correspond with an n -squared smaller probability of such an accident occurring. The actual group risk is expressed as a so-called Complementary Cumulative Distribution Function (CCDF).

2.4 Final recommendations

The main recommendations resulting from this EWTS-II subproject are summarised as follows:

- The guidelines formulated as part of this EWTS-II subproject can be an aid to collect data and to use it wisely for the purpose of safety and reliability studies of wind turbine designs.
- Qualitative safety and reliability studies are recommended very strongly as a minimum, as these studies result often in the identification of design errors (e.g., no or too less redundancy, no defence for certain events). Quantification, even with only the use of generic data sources, often results in a good ranking of the important event sequences, component failure modes, and systems. A combination of generic data and engineering judgement can always be used, although the reliability analyst should be aware of the limitations. In this way, a design can be made (more) balanced.
- Quantitative safety and reliability studies should be used primarily for the ‘relative’ (qualitative) purposes outlined above. The use of absolute figures and absolute criteria should be avoided.

3. INTEGRATION OF BLADE TEST IN DESIGN

3.1 Introduction

The objective of this part of the project is to develop a recommended methodology to include full-scale blade tests in the wind turbine design process. Actual test and measurement procedures do not need to be addressed here, especially because they are in development under the co-ordination of a working group of IEC TC-88WG8.

During the performance of the work a continuing discussion has been held whether the general objective, the deliverables and the activities to be performed are in compliance with each other. Full scale blade tests, as performed nowadays, are executed to demonstrate adequate safety margins and to verify design calculations. This means that the performance of mechanical tests on rotor blades is already a fact today, although the tests are usually performed at the end of the design process. Consequently the test results are not used to upgrade the design, unless the experiments showed that the design criteria are not met. So the tests are performed to demonstrate, to a reasonable level of certainty, that specified limit states of the rotor blades are not reached, provided that they are produced according to the specifications. In other words that the rotor blade will survive the design load spectrum. The usefulness of these tests for the designer to improve the design formed the main discussion point within this EWTS II subproject.

Use has been made of the reports and guidelines of the SFAT and IEC-TC88 WG8 documents.

The deliverables of the work as reported, contain information concerning recommended methodologies to include blade tests in the wind turbine design process in order to, demonstrate adequate safety margins and to verify design calculations.

3.2 Technical description

General

The full scale tests as discussed here, are split up in (blade) property tests, i.e. the eigenfrequencies, mass etc. , strength tests, and fatigue tests.

Property tests

These tests are intended to check whether properties, like mass, centre of gravity, eigenfrequencies and static strength are (almost) equal to the values assumed in the load spectrum calculations. When they differ to much, the loads used to verify the structural design are not valid any more. The actual allowable margin, between measured values and the values assumed in the aeroelastic calculations can easily be determined using calculations in which the most critical parameters are varied some percents up or down. When the most important statistics, such as maximum, minimum and standard deviation, or for example a fatigue equivalent load range, differ a lot, the sensitivity of that parameter is large and consequently the allowable margin is small.

Mass and centre of gravity are the most easiest measurements to perform. The values give a very good indication whether the blade has been produced according to the specifications.

Stiffness is very important, it indicates whether tower clearance is sufficient and together with the mass distribution it provides the input for the calculation of the natural frequencies. The stiffness distribution is not that easy to determine, especially when the lay-up of the laminates across the cross-section is not symmetric and coupling between deformation modes has to be taken into account.

Natural vibration tests. Results are very important to verify whether the aeroelastic calculations have been

performed on an accurate model of the wind turbine (rotor blades). The eigenfrequencies are not that difficult to determine, however the actual mode shape is more difficult to measure. Differences compared with the assumed values should be consistent with the differences between assumed mass and stiffness distribution.

Static tests

The static test results are used to verify whether the structural design is sufficient. This test can be performed in a number of selected directions.

When it is the intention to go to ultimate load or failure load one has to be very careful which direction is tested first. The most likely direction to fail first should be tested last.

The results, usually strain gauge readings on a number of selected spots give a fair indication whether the structural design is accurate enough to predict the strains/stresses. Strain/stress concentrations are difficult to determine due to the fact that only a limited number of strain gauges will or can be monitored.

When failure occurs at an early stage in the test, a careful examination of the failure and the (test) loading compared to the design loading, has to be made in order to make sure that differences between design and test loading are not the cause of the early failure.

Fatigue tests

The fatigue test has limited value for the designer, especially when the designer wants to improve the design from the test results.

The main reason is that the test loading differs much from the design loading, due to the fact that a test is made up of only $3 \cdot 10^6$ to 10^7 cycles and the design loading comprises up to $5 \cdot 10^8$ cycles. For coupon fatigue tests the scatter in allowable number of cycles is almost a factor of 10. When only 1/3 of that scatter is present at a full scale test, the results of two or even more tests are needed to obtain clear conclusions, except when a failure occurs early in the fatigue test.

3.3 Conclusions

For designers the blade property and static test are the most important tests. The design load spectrum and structural integrity can be checked to a large extent. The fatigue test which is of less use for the designer, is however a very valuable test to check all details of design and manufacturing. Errors or design flaws which remain unnoticed easily during the other tests, will show up clearly in a fatigue test. Spots with high strains e.g. in corners where strain gauges can not be applied, will crack and this will indicate that the design requirements are not met.

4. POWER PERFORMANCE IN COMPLEX TERRAIN

4.1 Introduction

It is widely accepted that in spite of the fact that during the last years the wind energy technology and industry attained an outstanding progress, further research is needed on specific technical and non-technical issues. The prominent issues are related to system integration, cost-effectiveness improvement as well as standardisation and certification. All these issues are strongly dependent on the power performance verification and assessment practices. Recently, several EU funded research projects as well as standardisation bodies were concentrated on the different aspects of this issue.

The research, presented within this EWTS II subproject, is intended to clarify the status of power performance verification and assessment in complex terrain, putting emphasis on the following items:

- power performance verification for wind turbines operating in complex terrain,
- assessment of developed, applied and verified tools for WECS power performance in complex terrain.,
- assessment of the available international and national standards.

The major achievements of the project are:

- presentation and assessment of various power performance measurements regarding wind turbines of different size and control strategy,
- presentation and assessment of alternative power performance verification practices
- identification and quantification of the terrain induced effects on the power performance of wind turbines,
- assessment of the existing recommendation and standardisation documents and identification of all inefficiencies that influence the power performance assessment and verification in complex terrain,
- construction of the technical basis for the development of a reliable procedure for power performance measurements in complex terrain.

4.2 Technical description

The project scientific and technical description and progress is presented for each task separately, as follows:

Inventory of existing information on the issue of power performance measurements in complex terrain.

The literature research resulted in many topic-related articles and documents, yet it provided a limited readily exploitable information for complex terrain measurements. The survey and the resulting conclusions regarded topography effects, effect of obstacles, site calibration practices, alternative power curve measurement procedures and site dependent wind characteristics effect on power curve.

Assessment of power performance measurement campaigns and site calibration techniques. Focus on comparison of different power curve measurements at different sites through annual energy production estimation and uncertainty estimation for power curve and annual energy production.

Several power performance campaigns have been analysed in order to assess the recommended procedures regarding site calibration, power curve determination and annual energy production uncertainty estimation. The analysed data regarded wind turbines of different size and control strategy operating at different sites, as shown in table 1.1 where an overview of the experimental and analysis work performed within the project is presented.

In the field of site calibration different techniques were assessed, namely a nacelle cup anemometer at a downwind parked turbine and the use of a meteorological mast prior wind turbine erection. Moreover the application of numerical site calibration was judged also.

Table 1.1. Overview of experimental and analytical research within EWTS-II.IV.

Wind turbine	Terrain	Institute	Site calibration technique	AEP estimation	Uncertainty estimation	Parameter identification
WINCON 110XT (110kW, stall)	complex	CRES	nacelle cup on running WT nacelle cup on parked WT rotor disk measurements	Yes	Yes	Yes
VESTAS V27 (225kW, pitch)	complex	CRES	nacelle cup on parked WT	Yes	Yes	Yes
	flat	RISO	reference mast	Yes	Yes	No
	flat	DEWI	reference mast	Yes	Yes	No
	flat	WINDTEST	reference mast	Yes	Yes	No
MADE AE-30	flat	CIEMAT	reference mast	Yes	Yes	Yes
	complex	CIEMAT	reference mast	Yes	Yes	Yes
NORDTANK 500/37 (500kW, stall)	complex	CRES	calibration prior WT erection nacelle cup on parked WT	Yes	Yes	Yes
	flat	RISO	reference mast	Yes	Yes	Yes
	complex	NEL	numerical simulation	Yes	Yes	Yes
	complex	NEL	numerical simulation	Yes	Yes	Yes
	flat	DEWI	reference mast	Yes	Yes	Yes
	flat	WINDTEST	reference mast	Yes	Yes	Yes
NEDWIND 500kW	complex	DEWI	nacelle cup on running WT	Yes	Yes	No
ELKRAFT 1MW	flat	RISO	nacelle cup on running WT	Yes	Yes	No

Assessment of power curve evaluation using nacelle anemometers.

The assessment of the nacelle anemometer on running machines was performed on a wide range of wind turbine sizes ranging from 110kW up to 1MW machines (see table 1.1).

The following conclusions were drawn from this research:

- the correct application of the methodology and the transfer of the calibration formula to other wind turbines of the same make and type, presupposes that the wind turbine rotor settings, yaw behaviour, the position on the nacelle anemometer are unchanged as well as that the terrain remains flat.
- the dependency of the calibration formula to wind and wind turbine parameters was found to be limited. On the other hand these effects are expected to be magnified in cases where wind structure and wind turbine response at the calibration site compared with the testing site are quite different.
- lower scatter in the measured power curve as a function of the nacelle wind speed may be obtained.
- the introduction of the nacelle cup calibration formula introduces a statistical error that should be taken into account in the uncertainty estimation.
- The use of nacelle wind speed measurements may decrease the error induced by site calibration significantly in cases where large discrepancies are encountered between the measured and reference wind speed.

Parametric analysis of the available power curve measurements for the identification of the site related effects influencing the power performance behaviour.

The parameter identification of wind turbine power performance regarded the quantification of the dependency of power characteristics on wind deterministic and stochastic characteristics, especially mean value and standard deviation.

The following issues were clarified by means of this parameter identification procedure:

- identification and quantification of the wind parameters that affect power performance,
- assessment of the sensitivity of power characteristics for wind turbines of different size and control system,
- assessment of the sensitivity of power characteristics for the same wind turbine type when operated in different sites,
- assessment of causal parameters in relation to complex terrain characteristics
- assessment of a power curve normalising procedure based on parameter identification results .

An analytic method is introduced covering parameter identification tasks in power performance measurements. The developed tool is based on multivariate regression analysis with a backward parameter elimination technique in order to account for the statistically insignificant parameters. The method was applied for the parameter identification of the power performance of wind turbines operating at different sites, both flat and complex. The parameters chosen to comprise the model set describe the deterministic part of the wind, the main turbulent characteristics, the turbulence length scale as well as the wind speed distribution. The examined dependent variables were the mean power output, the standard deviation of the power output and in the case of pitch controlled machine the response of the control system. The effect of the above parameters was identified and quantified. It appeared that except from the mean wind speed other parameters, related to the deterministic as well to the stochastic wind characteristics are affecting the power performance of the turbine and should be considered within power performance assessment procedures. The parameter identification procedure was applied to the following cases: 225kW pitch regulated, 110kW stall regulated, 300kW stall regulated and 500kW stall regulated. Moreover, a separate investigation on the sensitivity of power performance on turbulence, wind shear and atmospheric stability has been performed on a 3MW wind turbine.

Assessment of existing guidelines and their validity for complex sites. Identification of drawbacks connected to the application of existing guidelines and recommendations for power performance measurements in complex sites. The assessment was focused on the recommendations of IEC 1400-1 ed.2. Certain inefficiencies, related to site calibration and uncertainty estimation procedures, were identified.

The assessment of the existing standards and recommendations regarded the following issues:

- status of wind turbine power performance assessment and verification (existing standards, EU project results, contractual matters, market needs etc.),
- review of characteristics of complex terrain and their effect to power performance ,
- points that are not adequately described by the present IEC 1400-1 ed.2 document, particularly in relation to complex terrain (site calibration, uncertainty estimation etc.),
- recommendations for performing power performance assessment and verification in complex terrain.

The discussed critical points regarded the following issues:

- test site requirements,
- characterisation of wind speed sensors,
- influence of wind mean and turbulent structure,
- site calibration,
- response system ,
- measurement analysis,
- contractual aspects.

The derived practical recommendations for power performance assessment in complex terrain followed from the identified inefficiencies of the IEC 1400-1 ed.2. and regarded the following issues:

- definition of site complexity,
- selection and characterisation of instrument configuration,
- wind turbine control system response,
- site calibration,
- normalisation procedure,
- uncertainty estimation procedure,
- power curve measurements of wind farms.

Drafting of a status report providing a comprehensive overview of the up to date available information on power performance in complex terrain and of the proposed solutions and results of the parameter identification.

The final technical report includes the following items:

- introductory review on project background, objective, working methodology and project scientific and technical performance,
- review on power performance measurements focusing on the effects of terrain orography on wind field, site calibration, alternative methodologies for power measurements and effects of turbulence and shear on power curves,
- presentation of the experimental research and analysis performed by the participants within the project,
- review of the experimental research on alternative power performance methodologies, namely using a nacelle cup anemometer on a running wind turbine or by using the upwind rotor averaged wind speed as reference,
- presentation of the parameter identification procedure background and results. Analysis was performed on all available data bases regarding wind turbines of different size and control strategy,
- review of the assessment of existing guidelines for power performance,
- presentation of practical recommendations and conclusions.

5. SITE EVALUATION

Over the ten to fifteen years that commercial wind farm development has been a reality throughout Europe, the term “site assessment” or “site evaluation” has generally tended to be associated with the prediction of the energy yield potential of a site prior to the installation of wind turbines. Hence, historically, the evaluation has usually been restricted to the assessment of the site annual average wind speed and wind speed distribution. However, as the economic and design margins on wind turbines and wind farms become tighter, the need to quantify and minimise all aspects of risk has become more important. The site evaluation is at the core of this risk evaluation process and consequently needs to consider more than just energy yield potential if other aspects such as turbine integrity and safety are to be assessed.

This is addressed in the latest draft edition of the IEC wind turbine safety standard (IEC-1400-1 “Safety of Wind Turbine Systems”, Edition 2) which necessitates a site evaluation. Although IEC 1400-1 (ed2) explicitly states what the scope of the site evaluation must be, it does not give guidance on how to do it. Therefore, the intention of this sub-project has been to provide information and methods which will be of practical use to those involved in the application of the IEC standard.

The approach taken may be summarised as follows:

- a survey of consultants and test organisations offering site assessment/evaluation services in each of the EC countries taking part in the ongoing project was made in order to determine the various methodologies used .
- the survey results were collated in a database and interpreted to identify national or other trends.
- with regard to mean wind speed prediction, which is but one aspect of site evaluation, a detailed review of the results of numerous well documented modelling and measurement based evaluation techniques was carried out and hence guidelines for the application of the techniques were proposed.
- the more promising new or revised modelling based evaluation techniques for mean wind speed determination were implemented using various test cases to assess their repeatability and usefulness.
- a detailed investigation of the background principles and theory relating to “other” site wind parameters was carried out and summarised. Hence a list of instructions for the practical determination of these other parameters was written, including a summary of instrumentation requirements.

5.1 Survey of European Consultants

Consultants and test organisations in Denmark, Germany, Greece, Netherlands, Spain and United Kingdom were individually contacted to determine the scope and methods used for site evaluation, with the emphasis on mean wind speed prediction techniques as it was anticipated that this was the most commonly assessed parameter. Consequently 71 responses to the survey were received out of a total of about 100 consultants approached.

5.2 Database

The survey results reveal strong national and topographical trends governing the extent and method of site assessment. Countries with generally flat or simple terrain rely mainly on modelling or calculation based techniques whereas the countries with complex terrain primarily use measurement based techniques, sometimes in combination with modelling for short distance spatial extrapolation of wind speed. In certain countries the mean wind speed evaluation is carried out as a legal requirement but primarily with regard to the aspect of energy yield rather than structural integrity. Of the measurement based techniques used, variations on the Measure-Correlate-Predict (MCP) technique are most common whereas the most popular model in use is WASP. Of the other parameters assessed by measurement, turbulence intensity and the mean shear layer characteristic were typically determined.

As a separate exercise a review of the sources and types of input data available commercially within each country for use with modelling or MCP type techniques was carried out. The main specifications of terrain contour maps and long term wind speed data available in each country are summarised.

5.3 Mean Wind Speed Prediction

A comprehensive review of the technical status of modelling and measurement based techniques was carried out. As dictated by the results of the survey, specific emphasis was placed on WASP and MCP with a view to proposing guidelines for use.

In the case of WASP the main recommendations for successful implementation are:

- both the reference and predicted sites are subject to the same weather regime
- neutral atmospheric conditions prevail
- the surrounding terrain is sufficiently gentle and smooth to ensure mostly attached flows
- the reference data are reliable
- the description of the background roughness length must be as accurate as possible The MCP technique can be successfully applied where the following conditions can be satisfied:

- validated, long-term and short-term concurrent measured reference wind speed data are available at a reference site within the same climatological zone as the prediction site.
- validated prediction site wind speed measurements are available for a period of at least 8 months and more typically 12 months or more.

5.4 Mean Wind Speed Modelling Technique Enhancements

Perhaps the major shortcoming in the commercial use of wind flow models (and MCP) is the difficulty in the quantification of uncertainties. In this report a philosophy for the assessment of uncertainty is proposed which, although not necessarily easy to apply to wind models, does highlight the components of uncertainty of relevance. Derivation of a specific parameter (Ruggedness Index) for categorising terrain has been summarised from recent literature and is proposed as a useful technique for identifying when the limits of applicability of a model may have been exceeded.

5.5 Other Parameters

Methods for assessing parameters other than mean wind speed are proposed. In each case, the theoretical background is also presented.

The following parameters have been considered:

- reference wind speed
- characteristic turbulence intensity at 15 m/s
- annual average wind speed distribution
- normal wind profile
- turbulence length scales
- coherence
- standard deviation ratios
- negative gust

Recommendations for instrumentation and measurement requirements are given in each case. As certain parameters require the use of an ultra-sonic anemometer and as this is still a rather specialised instrument a review of important points on the use and interpretation of data arising from this device is presented.

It is believed that the information presented in this report will provide useful guidance to those involved in site evaluations and, especially with regard to the other parameters, collates relevant practical information and knowledge in one convenient document for the first time. However, more practical experience of applying the recommended techniques should be gained to determine if all of the proposals are indeed sufficient.

6. IMPLEMENTATION OF EUREC-AGENCY MEASNET

6.1 Introduction

More than three years ago the six the European institutes CIEMAT, CRES, DEWI, ECN, NEL, RISØ later joined by WINDTEST, decided to improve their measurement quality jointly in order to avoid any problems of future mutual recognition. Measurements performed by the institutes, even applying the existing IEA, IEC and other standards and recommendations, showed remarkable differences in their results, a situation which is unacceptable in an open international market. To improve this unsatisfactory situation the above mentioned test centres worked together in the projects “European Wind Turbine Standards I and II” co-financed by the European Commission and agreed to form a grouping called: MEASNET, Network of European Measuring Institutes.

During the two projects special attention was given to the anemometer calibration procedure. Due to the third power dependence of power from wind speed, the main emphasis had to be concentrated on a accurate anemometer calibration. Specially the problem of the use of different wind tunnels for anemometer calibration had to be solved. Basis for all performed harmonisation and quality evaluation work were round robin tests and agreed quality evaluation procedures.

Within the two above mentioned projects, the main task of the project team consisted of creating an organisational structure and of establishing rules and requirements which will guarantee that high quality measurements are carried out by the participants. In effect, the objective of this project was to arrive at the situation where the measuring institutes are able to perform measurements of equal quality which are sufficient for the mutual comparison and acceptance.

MEASNET is not restricted to the actual founding members but also open for other institutions as long as they are independent of industry and fulfil the membership requirements set up by MEASNET. All member institutes ensure compliance with the agreed measurement procedures by obtaining and maintaining EN 45001 accreditation. Measurements will not be done by MEASNET but by each participating institute. Customers therefore have the advantage to contract that MEASNET member for a measurement, which offers the best commercial conditions.

6.2 Internal Structure and Requirements of MEASNET

6.2.1 Structure of MEASNET

To ensure high quality measurements, uniform interpretation of standards and recommendations as well as interchangeability of results, the members established an organisational structure for MEASNET (Fig. 6.1). Within this structure mutual periodical quality procedures for measurements and evaluations will be performed. The highest tier is the Council of Members. An Executive Board, composed of three representatives from different member institutes executes the tasks delegated by the Council of Members. One or more Expert Groups, specialising in certain measurement tasks, advise and support the Executive Board and the Council of Members on the definition of the measurement procedures. Assessment Teams are established to perform assessments for the admission of new members and for quality confirmation of MEASNET members. MEASNET members must be accredited to EN 45001 for the MEASNET approved measurements.

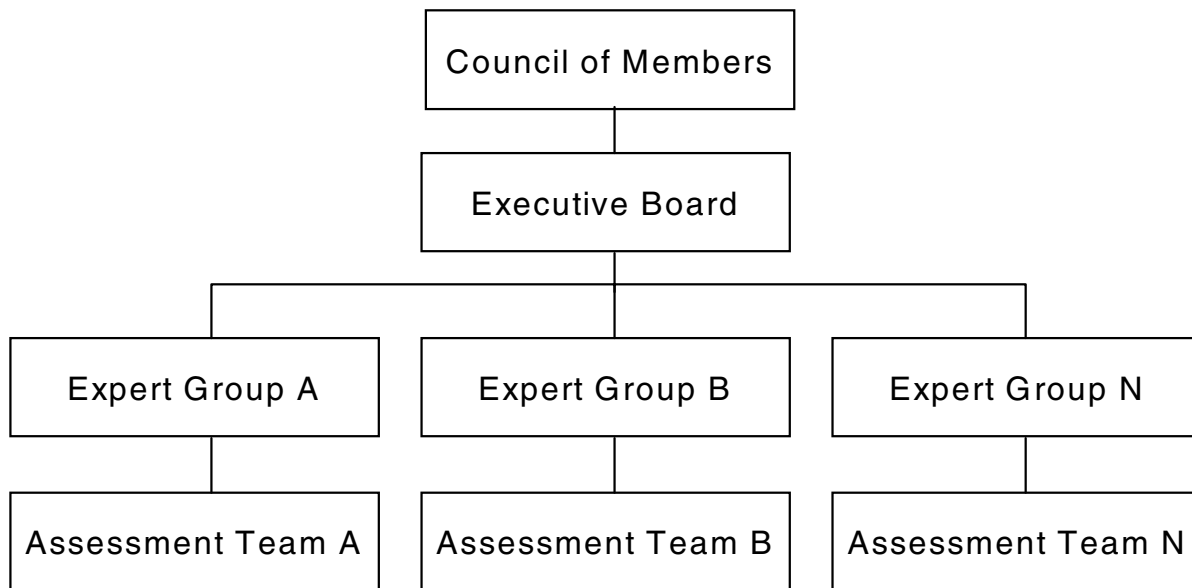


Figure 6.1 Organisational structure of MEASNET

6.2.2 Requirements of MEASNET

In order to ensure generally acceptable, high quality measurements the member institutes shall fulfil the following requirements:

- legally independent from industry.
- adequate experience in the field of wind energy and wind energy related measurements.
- qualified and experienced measurement staff.
- carry out measurements according to the MEASNET rules and procedures, at least power performance measurements.
- EN 45001 accreditation of the agreed measurement procedures. If the EN 45000 accreditation system is not implemented in the home country of the organisation, the agreed alternative acceptance requirements will be applied*).
- presentation of measurement results according to the MEASNET format.
- accept the policy of co-operation and exchange of information on measurement and evaluation procedures and on problems arising in measurement campaigns.
- MEASNET members will accept each other results as far as they are carried out according to the MEASNET procedures.
- MEASNET members will subject themselves to an internal MEASNET quality evaluation programme.

*) If the EN 45000 accreditation system is not implemented in a country, the MEASNET Council of Members will decide on alternative acceptance procedures for the candidate organisation.

MEASNET membership is not restricted to the member institutes but is open for other organisations as long as they are independent of industry and fulfil the membership requirements set up by MEASNET. The seat of MEASNET is the address of the institute of the current Executive-Chairman of MEASNET. Actual address for 1997 and 1998 is DEWI in Germany. As this seat will change with the Executive-Chairman the formal contact address of MEASNET for initial contacts is the seat of the EUREC-Agency in Leuven.

MEASNET c/o EUREC-Agency
Kapeldreef 75
3001 Leuven - Heverlee, Belgium
Tel.: ++32-16-281-522
Fax.: ++32-16-281-510

All commercial contacts can be made of course directly with the desired member institutes.

6.3 MEASNET Recognised Measurements

During the course of the two projects, the members of MEASNET agreed on the following measurement and quality evaluation procedures to be performed under the MEASNET quality criteria:

- anemometer calibration
- power performance
- noise
- power quality.

Special attention was given to the calibration of anemometers as the most crucial part of a power curve measurement. As an intermediate result of the round robin tests was agreed that not all MEASNET members are approved for absolute anemometer calibrations. Absolute anemometer calibration is considered to be a general commercial service offered to customers. The not approved institutes may perform relative calibrations which allow for own power curve measurements only. In the beginning of the project it was not foreseen to distinguish between the two calibration methods, but it turned out to be necessary. Until the end of the project the participants did not obtain an agreement about relative calibration method due to missing experience.

All agreed measurement procedures except power quality, take into account the final and draft documents of international organisations, e.g. IEC, IEA and in addition requirements derived from results of related projects and measurement experiences. The agreed noise measurement procedure is an example for the necessity of additional MEASNET measurement requirements. The performed round robin evaluation of a measured data set led, after some necessary correction measures of the different institutes, to comparable results because the IEC recommendation concerning the evaluation of tonality was improved.

For the power quality measurement procedure a IEC standard is not yet existing. Therefore the members of MEASNET decided to use the respective German guidelines until IEC recommendations will be worked out. At the moment Germany is the only country, where such measurements are required by the utilities. In Germany this guidelines for power quality measurements had been worked out during the last two years by a group of experts coming from the involved measurement institutes, industry, utilities and state governments. They include two years of experience gained by the three German measurement institutes and therefore are already a good starting point for a future international harmonisation within MEASNET.

A MEASNET member must at least be approved for power performance measurements. This requirement was established to guarantee that MEASNET members have enough experience and understanding in wind energy related questions. In the actual status of the project not all founding members have finished yet the quality evaluation procedure for the different agreed measurements. A member must not be approved for all measurement types and can be approved for additional measurements at any time he performed successfully the quality evaluation procedure. The MEASNET measurement approval is valid for five years as far as the institute passes successfully all internal quality evaluation programmes during this time and maintains the accreditation to EN 45001. An official MEASNET acceptance document indicates the measurement types for which the MEASNET member is approved for. Customers should ask the institute of their choice to present this document.

Measurement reports performed under the quality criteria of MEASNET will be stamped by the measuring institute with a stamp which consists of the MEASNET logo and, written around the logo, the name of the institute. As an example the general logo of MEASNET is shown in Fig. 6.2.

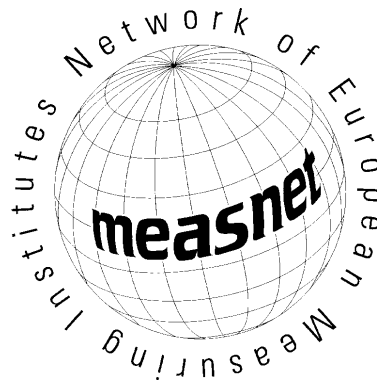


Figure 6.2 Logo of MEASNET

MEASNET is now operative and the institutes are allowed to offer their MEASNET approved, high quality measurements from October 1997 on.

6.4 Performed Quality Evaluations

Several quality evaluations have been made during the two projects. The most intensive one was for anemometer calibration, because a procedure had to be found, how to judge the quality of the wind tunnel which should be used for the anemometer calibration. The standard anemometers in use by each institute were sent around for calibration to each of the MEASNET founding members. One of the evaluation difficulties was how to define the correct wind speed reference to which the calibration results of each institute had to be compared. After an additional evaluation of the influence of anemometers under skew wind flow conditions and after several correction measures a mutually agreed comparison base was found. As a result of this round robin the institutes decided to have the above mentioned two types of approved anemometer calibrations, the absolute and the relative anemometer calibration.

Other round robin evaluations were performed for power performance and noise measurements. In both cases a set of measured data were sent around for evaluation by the individual institutes. Differences in the evaluation results were discussed and led to correction measures concerning the established measurement and quality evaluation procedures. All round robin tests showed, that the idea of MEASNET to harmonise the interpretation of standards and the applied measurement methods is of very high importance. Guidelines for evaluation, for example stated in the existing IEC standards, even when correctly applied led to different interpretations of requirements and consequently to differences in the results.

6.5 Conclusion

MEASNET members are interested commercially in performing measurements in the field of wind energy. In spite of all difficulties encountered during the project the institutes always found a solution which could be accepted finally by all members. It was of great advantage for the progress of the work that the experts of the founding members are used to work together in many other joint European research projects since more than a decade. As a result of their intensive and detailed work, MEASNET members now mutually accept their measurement results and guarantee high quality by regularly performed quality evaluation programmes.

The advantages for the industry to contract a MEASNET institute are:

- the measurements are accepted in other countries,
- are of high and comparable quality,
- and can be ordered on the basis of competitive offers from the member institutes.

For the first time measurement institutes work together and were able to find agreed procedures with the goal to harmonise the interpretation of measurement procedures established in international standards and recommendations. The different performed quality evaluation tests during the course of the two projects showed the necessity of such a grouping, if measurements performed by different institutes shall be comparable to each other. The fact that all MEASNET members are also engaged in the different existing IEC, IEA and CENELEC working groups will help to integrate the gained MEASNET experience in the respective international measurement standards and recommendations.

At the moment MEASNET is only a wind energy activity. But the participants are convinced that measuring institutes engaged in other renewable energies will encounter the same harmonisation problems when they have to enter a real commercial market situation. Perhaps MEASNET serves as an example for them of how to work together and solve the harmonisation and quality evaluation problems.

EUROPEAN WIND TURBINE STANDARDS II
PART 1
LOAD SPECTRA AND EXTREME WIND CONDITIONS
SUB A
WIND FARMS – WIND FIELD AND TURBINE LOADING

G.C. Larsen (ed.) Risø National Laboratory
I. Carlén Teknikgruppen AB
G.J. Schepers Netherlands Energy Research Foundation ECN

Abstract

When operating under wake conditions, an increase in fatigue life consumption on wind turbines has been observed. The changes in the load patterns originate both from modifications in the mean wind field, and from modifications in the turbulence field. By performing a parameter study, the significant wind field parameters, in relation to the increased wind turbine fatigue consumption in wakes, are identified. The analysis is based on a large number of aeroelastic simulations and it has been performed for five significantly different wind turbine concepts. For each of these the effect on selected equivalent loads, originating from realistic perturbations in the selected parameters, is determined by means of a two level factorial method.

It has been demonstrated that the deterministic wake deficit as well as the modified turbulence characteristics – turbulence length scale, turbulence intensity, and coherence decay – all are of primary importance in relation to fatigue loading under wake conditions. The effects of each of the above parameters was furthermore shown to be approximately additive in a fatigue life consumption sense.

Finally a set of simple models has been investigated which subsequently resulted in a recommendation for the quantification of the identified key parameters. The recommendation can serve as a resource for certifying bodies and is further, if it is found appropriate, easily included in the IEC-code framework. The wake load cases is thus simply defined by suitable modifications in the parameters presently used in definition of the conventional load cases.

CONTENTS OF PART 1Sub A

1	INTRODUCTION	7
2	WAKE WIND FIELD STRUCTURE	9
2.1	Delimitations	9
2.2	Preliminary parameter study	10
2.2.1	Reference sets	11
	Wake deficit	12
	Turbulence intensity	12
	Turbulence length scale	12
	Coherence decay factor	12
2.2.2	Results	13
2.3	Wake measurements	13
2.4	Wake models	14
2.4.1	GCL–model	14
	Deficit	14
	Turbulence Intensity	15
	Turbulence Length Scale	17
	Coherence decay	19
	Transversal turbulence	21
	Turbulence intensity	22
	Turbulence length scales	23
2.4.2	SF–model	24
2.4.3	DR–model	24
2.4.4	TNO–model	28
	Turbulence Intensity	28
	Deficit	29
2.4.5	MM–model	29
	Velocity deficit	32
	Turbulence intensity	32
	Length scale	34

2.4.6	UPMWAKE-model	34
	Velocity deficit	34
	Turbulence intensity	37
2.4.7	Concluding remarks	38
3	WAKE LOADING	41
3.1	Method	41
3.1.1	Reference sets	42
	Flat terrain	42
	Wake	42
3.1.2	Factorial method and calculation scheme	43
3.1.3	Fatigue determination	44
	Replicated simulations	44
3.2	Results and Analysis	44
3.2.1	Benchmark	45
3.2.2	Results	46
3.2.3	Discussion	54
4	CONCLUSIONS	55
5	RECOMMENDATIONS	57
5.1	Mean Wind Deficit	57
5.2	Turbulence Intensity	57
5.3	Turbulence Length Scales	58
5.4	Coherence Decay Factors	59
	ACKNOWLEDGEMENTS	60
	REFERENCES	61
A	VESTAS V27 TURBINE	63
B	VARIABLE SPEED 500 KW TURBINE	65
B.1	Background	65

B.2	Rated Conditions and Losses	67
B.3	Generator curve	67
B.4	Pitch control	67
C	DANWIN 180 KW TURBINE	69
D	NÄSUDDEN 3 MW TURBINE	73
E	NORDTANK NTK500 TURBINE	77
F	EXPERIMENTAL WAKE CHARACTERIZATION	81
G	GRAPHIC COLLOCATION OF RESULTS	83

1 INTRODUCTION

An increasing part of the future wind turbines will be erected in wind farms due to the diverted reduction in grid costs, the limited number of sites with optimal wind potential, and environmental requirements. Therefore, prediction of the wind induced loads in wind farms is of vital importance.

Measurements have revealed an increased loading of wind turbines sited in wind farm configurations compared to stand alone turbines, other things being equal. The fatigue loads on a turbine is a combination of periodic deterministic loads, associated with gravity and mean wind field, and turbulence induced loads. The increase in fatigue consumption in wind farms originates both from modified mean wind field and from modified turbulence field. One possible strategy to account for increased wake loads is to collect the total impact from wake operation in only one parameter – often chosen as the turbulence intensity which is a parameter experienced to be of significant importance [1]. However, this method has the drawback that its generality is affected by the fact that it is based on the choice of a specific fatigue evaluation model and a limited number of predefined Wöhler exponents and wind turbine concepts. Moreover, it excludes the detailed wind farm topology from being taken into account and fails to reflect, that the induced loads on different component categories respond individually on the different elements in the total wind load modification.

Therefore a more detailed description is required, not only for design approval of a specific site, but especially in relation to optimization of wind turbines suited for wake operation. Consequently it is of importance to investigate in details the impact arising from wake modifications of the individual parameters constituting the conventional wind field description.

One of the important conclusions from the "Dynamic Loads in Wind Farms II" project [1]¹ is that the stochastic component of the fatigue loading, caused by wake turbulence, is dominant compared to the periodic deterministic contribution, and that partial wake operation does not represent a significantly more severe fatigue loading regime than a full wake operation. Based on this knowledge it has been decided to (conservatively) limit the present investigation to an *artificial situation* defined by a partial wake deficit combined with a full wake turbulence formulation. For decreasing spacing, the degree of conservatism associated with the partial wake formulation of the deficit is believed to increase.

In order to simplify the task further, only *single wake* situations are considered and in turn assumed representative for wake loading in general. Bearing in mind that the turbulence part of the fatigue loading in a wind farm is dominant compared to the periodic deterministic contribution, the single wake approach is justified by measurements from the Sexbierum wind farm. Here it has been observed that double wake situations mainly differ from single wake situations by reducing further the mean wake wind speed, whereas the turbulence field is only marginally modified².

Based on the above described simplifications, a detailed analyses has been performed in order to quantify the wake load situation. The analysis falls into three phases.

The first phase embraces a parameter study aiming at identifying the key wake wind field parameters responsible for increased wind turbine fatigue life consumption in wakes compared to ambient conditions. In this part of the analysis, crude estimated wake characteristics are obtained from relevant measurements and these are only meant to be of the correct order of magnitude.

¹Final report p. 105–106.

²Dynamic Loads in Wind Farms II – Final report p. 104.

The second phase deals with a possible quantification of the identified key parameters from the first phase. This phase embraces collection of significant wake measuring data and a subsequent verification of simple models predicting the key parameters.

The third and final step is to repeat the parameter study performed in the first phase, with the simple experimentally based wake characteristics replaced by more detailed predictions from selected models, and to draw the final conclusions.

2 WAKE WIND FIELD STRUCTURE

When operating in a wake situation, the mean wind profile as well as the turbulence characteristics experienced by a turbine, are modified compared to the ambient situation.

For relevant turbine spacings, the modified *mean wind profile* is characterized by adding a bell-shaped velocity deficit to the a priori wind shear profile associated with the undisturbed flow. The modified *turbulence field* is primarily the consequence of creation of turbulence in the free shear layer between the retarded wake flow and the undisturbed free stream. Hence the modified wake turbulence field is in general characterized by an increased turbulence intensity, a decreased turbulence length scale and an increase in the coherence decay. As no significant qualitative modifications in the spectral shape has been observed, the turbulence description in the present study follows the traditional description of turbulence in flat and homogeneous terrain³. Thus, the wind farm effects are condensed only in the modification of the mean wind shear profile and three parameters defining the turbulence field.

2.1 Delimitations

Basically, the present investigation is associated with wake conditions in flat and homogeneous terrain, as only turbulence structures typical for those terrain conditions have been considered.

In order to simplify the situation only *single wake* situations are considered, and these are in addition assumed to be representative for wake loading in general. This delimitation is closely linked to an important conclusion from the "Dynamic Loads in Wind Farms II" project [1]⁴ where it is stated that the stochastic component of the fatigue failure loading, caused by wake turbulence, is dominant compared to the periodic deterministic contribution. Bearing that in mind, the approach is justified by measurements from the Sexbierum wind farm, where it has been observed that double wake situations mainly differ from single wake situations by reducing further the mean wake wind speed, whereas the turbulence field is only marginally modified⁵.

An other important result, originating from the same report, is that partial wake operation does not represent a significantly more severe fatigue loading regime than a full wake operation. Based on this knowledge it has been decided to (conservatively) limit the present investigation to an artificial situation defined by a *partial wake deficit* combined with a *full wake turbulence* formulation. It is assumed that this artificial wake situation, to a reasonable degree, is representative for fatigue wake loading in general. For decreasing spacing, the degree of conservatism associated with the partial wake formulation of the deficit is believed to increase.

The situation is further simplified by assuming the mean velocity field modifications in the *mean wind direction* to be of "first order importance", whereas mean wind field modifications related to the two remaining directions are considered to be of "second order importance". Only modifications of "first order importance" are considered.

At down stream distances, corresponding to traditional spacings in wind farms, it is *assumed* that only the surface- and wake shear mechanisms contribute significantly to the turbulence production. When the two shear turbulence contributions have scales of comparable orders of magnitude, it is reasonable to

³The Kaimal turbulence spectrum and the Davenport coherence model are applied in the analysis.

⁴Final report p. 105–106.

⁵Dynamic Loads in Wind Farms II – Final report p. 104.

expect the resulting spectral shape to be qualitatively invariant, which is also confirmed by measurements. However, the parameters characterizing the particular spectra will be modified. Modifications related to turbulence intensity and turbulence length scale for all three turbulence components are considered, whereas only possible changes in the uu -autocorrelation is investigated. In other words wake aspects related to auto- and cross correlations, involving any of the v - and w - turbulence components, are neglected.

2.2 Preliminary parameter study

The present section deals with a preliminary parameter study aiming at identifying the key wake wind field parameters, responsible for increased wind turbine fatigue consumption in wakes compared to ambient conditions. In the previous section, the array of parameters, with potential significant impact on wake fatigue life consumption, has been limited to mean wake velocity deficit, turbulence intensity, turbulence length, and coherence decay.

In this initial parameter study the situation is further simplified, as the turbulence intensity- and turbulence length scale wake modifications, associated with turbulence components perpendicular to the mean wind direction, have been neglected due to an assumed dominating influence from the u -component. To summarize, the parameters included in the present parameter investigation are :

- Longitudinal mean wind field wake deficit (the only parameter with a deterministic character).
- Standard deviation of the u -turbulence component expressed in terms of turbulence intensity.
- Turbulence length scale related to the u -turbulence component.
- Spatial uu -coherence expressed in terms of coherence decay.

Crude estimates of the above wake characteristics are obtained from relevant measurements⁶, supplemented with a numerical determination of the wake deficit form, and at this stage the wake parameters are only meant to be of the correct order of magnitude.

Basically, the analysis is defined by selecting a number of turbine concepts and turbine spacings. In order to represent a broad spectrum of different wind turbine concepts and sizes, four fundamentally different horizontal axis wind turbine types have been considered – a stall regulated three-bladed turbine, a pitch regulated three-bladed turbine, a three bladed variable speed turbine, and a large two-bladed pitch regulated turbine. The main data, describing the investigated turbines, are summarized in the Appendices A–D. For each turbine type, two turbine spacing situations (5 rotor diameter spacing (5D) and 8 rotor diameter spacing (8D)) have been investigated based on criteria as relevance, representative situations, and finally that the scenarios are covered by the available measurements.

The basic philosophy in the parameter investigation is then, for each wind turbine concept, to choose two sets of reference situations – one related to a wind farm configuration with 5D spacing, and an other related to a wind farm configuration with 8D spacing.

Each set of reference situations contains a (common) reference situation, related to ambient conditions in flat and homogeneous terrain, and a reference situation related to the wake situation (5D or 8D spacing).

⁶The order of magnitude of the selected parameter variations are based on analysis of measurements performed at the Danish Noerrekaer Enge and Vindeby wind farms.

For each reference set, the effect on selected fatigue loads, originating from first order variations in each of the investigated parameters (for a number of different mean wind speeds), is subsequently determined from aeroelastic simulations. For each mean wind speed regime and for each turbine concept, a two level factorial design method [16] is subsequently used to identify the effect of each parameter. The procedure is described in more detail in chapter 3.

2.2.1 Reference sets

The defining parameters are given in Table 2.1 and Table 2.2, where I^u denotes the turbulence intensity associated with the turbulence u -component, L^u is the length scale related to the turbulence u -component, and a^u is the coherence decay constant in a Davenport formulation of the spatial uu -coherence. The maximum value of the deterministic wake deficit is denoted V_d . The reference situation corresponding to ambient conditions has been selected with *no* mean wind shear. Usually the shear is relatively small across the rotor plane, and as the present investigation moreover focus only on relative differences, the simplification is justified for the present purpose.

The wake deficit, the wake turbulence intensity, the wake length scale, and the wake coherence decay factor depend on the ambient mean wind velocity and on the turbine concept. However, as the quantities in the tables below are only meant to be of the correct order of magnitude, constant values have been specified for reasons of simplicity.

The interpretation of the above described parameters, in terms of load case definitions, is specified below.

Table 2.1 Reference set no. 1 (5D spacing).

	Ambient conditions	Wake conditions (5D spacing)
yaw-error	0 deg.	0 deg.
slope of terrain	0 deg.	0 deg.
$\Delta \bar{V}$	0 m/s	1.5 m/s
I^u	15 %	18 %
L^u	600 m	300 m
a^u	8.8	25

Table 2.2 Reference set no. 2 (8D spacing).

	Ambient conditions	Wake conditions (8D spacing)
yaw-error	0 deg.	0 deg.
slope of terrain	0 deg.	0 deg.
$\Delta \bar{V}$	0 m/s	1 m/s
I^u	15 %	17 %
L^u	600 m	360 m
a^u	8.8	25

Wake deficit

The focus is on a (partial) single wake situation, which is assumed to be the most severe case of operation, although no dramatic deviation compared to the full wake situation is expected. The partial wake situation to be considered is (rather arbitrarily) defined as the situation where the blade tip passes through the center of the wake (and thus including the wake deficit part characterized by a large horizontal gradient). It is presumed, that the deficit is positioned at the side of the rotor giving rise to maximum impact on the fatigue loads.

The explicit shape of the wake deficit has been based on UPMWAKE⁷ calculations through an iterative procedure, where the particular wind turbine thrust coefficient was adjusted until the specified deficit magnitude was obtained.

Turbulence intensity

The turbulence intensity is always defined with the ambient mean wind speed at hub height, \bar{V}_a , as the normalizing factor.

Turbulence length scale

The longitudinal turbulence length scale is given with reference to a standard Kaimal formulation of the turbulence spectrum, $S(f)$, as formulated in the Danish Code of Practice [18] :

$$\frac{f S(f)}{\sigma_u^2} = \frac{f L_u / \bar{V}_a}{\left(1 + 1.5 \frac{f L_u}{\bar{V}_a}\right)^{5/3}}, \quad (2.2.1.1)$$

where σ_u^2 denotes the variance of the longitudinal turbulence component, and f is the frequency measured in hertz.

If the Kaimal formulation given in the IEA 1400–1 document is adopted, the length scales specified in Table 2.1 and Table 2.2 should be divided by a factor of 4.

Coherence decay factor

The coherence function is, in the present context, defined as the *magnitude* of the complex cross-spectral density of the longitudinal wind velocity components, corresponding to two spatial separated points, divided by the squareroot of the product of the respective autospectrum functions. The standard Davenport formulation is adopted :

$$\text{Coh}(s, f) = \exp \left[-a^u \left(\frac{f s}{\bar{V}_a} \right) \right], \quad (2.2.1.2)$$

where s denotes the magnitude of the projection of the separation vector between the two spatial points on a plane perpendicular to the average wind direction.

⁷A brief description of this code is presented in section 2.4.6.

2.2.2 Results

The main conclusions from the investigation are :

- The mean wind deficit, increased turbulence intensity, decreased turbulence length scale as well as increased coherence decay should all be considered as significant in relation to increased wind turbine fatigue life consumption in wakes compared to ambient conditions.
- The effects on fatigue loading, originating from the investigated parameters, act approximately additively.

2.3 Wake measurements

In order to form a general view of the available experimentally based wake characteristics, and furthermore to establish a basis for verifying available wake models against experimental data, it was decided to establish a database of wake measurements. Each of the project participants have selected at most 15 of their most suitable measured campaigns and these are collected in the table presented in Appendix F. The table contains parameters describing the wake situation (turbine separation measured in rotor diameters, turbine type, atmospheric stability expressed in terms of the Richardson number, ambient mean wind speed at hub height etc.) as well as parameters describing the wake wind field. The wake wind field parameters are defined as follows :

- The *wake deficit* is described in terms of the maximum wake deficit $\Delta \bar{V}$ within the wake.
- The *ambient turbulence intensity*, I_a^u , is defined as the standard deviation of the horizontal turbulence component (as it is usually obtained from cup anemometer measurements) divided by the undisturbed mean wind speed \bar{V}_a . Both values refer to turbine hub height.
- The *wake turbulence intensity*, I_{wt}^u , is defined as the maximum standard deviation of the horizontal turbulence component within the wake divided by the undisturbed mean wind speed at turbine hub height.
- The *ambient turbulence length scale*, L_a^u , is defined as the (Kaimal) length scale of the u -turbulence component, corresponding that particular frequency, f_L , where half of the turbulence energy relates to frequencies higher than f_L . L_a^u refers to the turbine hub height.
- The *wake turbulence length scale*, L_w^u , is defined in analogy with the ambient turbulence length. L_w^u refers to the position within the wake where the reduction in the length scale takes its maximum.
- The *ambient transversal turbulence component*, σ_a^v , refers to the turbine hub height.
- The *wake transversal turbulence component*, σ_w^v , refers to the position within the wake where the maximum value is obtained.
- The *ambient coherence decay factor*, a_a , relates to a Davenport coherence description. Both horizontal and vertical separation are accepted, and to facilitate the use of cup anemometers, the decay factor relates to the horizontal turbulence component. Vertical and horizontal separation are indicated by adding a "V" or a "H" to the table value.

- The *wake coherence decay factor*, a_w , relates to a Davenport coherence description. Both horizontal and vertical separation is accepted, and the decay factor relates to the horizontal turbulence component. Vertical and horizontal separation are again indicated by adding a "V" or a "H" to the table value.

2.4 Wake models

The overall conclusion from the initial parameter study is that the induced mean wind deficit, the increased turbulence intensity, the decreased turbulence length scale, as well as the increased coherence decay should all be considered as significant modifications in relation to increased wind turbine fatigue life consumption in wakes compared to ambient conditions.

The present section is concerned with a possible quantification of these parameters, in a wake situation, as function of the involved turbine characteristics and the ambient meteorological conditions. The performance of a number of available models is investigated. The study is based on the wake measurements supplied by Teknikgruppen, ECN and Risoe, and described in the previous section 2.3. The measurements include a wide range of different wind turbines and ambient meteorological conditions.

2.4.1 GCL-model

The model [2] encompass a *semi-analytical* description of the wake deficit and a set of simple *empirical relations* providing the relevant characteristics (turbulence intensity as well as the turbulence length scale) for the turbulence field in a wake. The empirical expressions are based on full scale measurements and are applicable for both stall-, pitch- and variable speed regulated turbines.

In order to enable the treatment of data from model experiments performed in wind tunnels, the expression for the turbulence intensity has been made non-dimensional and is thus slightly modified compared to the expression given in the above reference. Moreover, one of the boundary conditions for the deficit model was modified in order to reflect the blocking effect from the ground (in a simple manner).

Deficit

Neglecting the blocking effect originating from the ground, the wake behind a wind turbine is considered a free turbulence region. Problems involving free turbulence are often of the same nature as boundary layer problems in the sense that the size of the free turbulence region in the direction perpendicular to the mean flow is considerably smaller than the size in the mean flow direction. The model is thus based on the *presumption* that the wake region can be adequately described by Prandtl's (rotational symmetric) turbulent boundary layer equations (*large Reynolds numbers* assumed).

Assuming similarity between deficits at different distances from the upstream turbine and moderate amplitudes of the deficit, the following asymptotic expressions are obtained for the mean wind speed deficit, $\Delta\bar{V}$, and for the wake radius, R_w :

$$R_w = \left(\frac{35}{2\pi}\right)^{\frac{1}{5}} (3c_1^2)^{\frac{1}{5}} (C_T Ax)^{\frac{1}{5}}, \quad (2.4.1.1)$$

$$\Delta \bar{V} = -\frac{\bar{V}_a}{9} (C_T A x^{-2})^{\frac{1}{3}} \left\{ r^{\frac{3}{2}} (3c_1^2 C_T A x)^{-\frac{1}{2}} - \left(\frac{35}{2\pi} \right)^{\frac{3}{10}} (3c_1^2)^{-\frac{1}{5}} \right\}^2, \quad (2.4.1.2)$$

where x and r denote axial and radial directions, A is the rotor area, C_T denotes the rotor drag coefficient, \bar{V}_a the ambient mean wind velocity at hub height, and c_1 is the non-dimensional mixing length defined by

$$c_1 = l(C_T A x)^{-\frac{1}{3}}, \quad (2.4.1.3)$$

with l being Prandtl's mixing length.

This expression separates to some degree the rotor specific drag dependence, and l is consequently expected to be relatively insensitive to both the size and the design of the rotor.

With C_T determined either from measurements or from a simple aerodynamic calculations, two parameters have to be evaluated from boundary conditions – one is the position of the rotor relative to the applied coordinate system, and the second is the non-dimensional mixing length c_1 .

The first boundary condition to be satisfied is that the wake radius at the rotor position equals the rotor radius.

The second boundary condition is an empirical relationship stating that the wake radius at 9.5 rotor diameters distance from the turbine can be determined by $R_{w,9.5D} = \max(1.08D, 1.08D + 21.7D(I_a^h - 0.05))$, where D and I_a^h denotes the rotor diameter and the (horizontal) ambient turbulence intensity, respectively. This boundary condition essentially states that the expansion of the wake is dominated by ambient cross flow turbulence – however for sufficiently small ambient turbulence intensity the turbulence contributions from wake shear, blade tip vortices, and hub vortices ensures a turbulence intensity level corresponding to minimum 5%. If the wake radius, determined according to the above prescription, exceeds the hub height, the blocking effect is taken into account by applying a wake radius equal to the mean of $R_{w,9.5D}$ and the hub height as a "design wake radius" at 9.5 rotor diameters distance from the turbine.

The performance of the model appears from the Table 2.3, where S denotes the turbine spacing expressed in rotor diameters, and $\Delta \bar{V}$ is the mean wind deficit.

Some deviation between measurements and model predictions are encountered, especially for the results associated with the Sexbierum wind farm. However, no systematic trend was observed in the deviations. As the model is based on an asymptotic theory, it might be somewhat conservative for very close spacings [19].

Turbulence Intensity

At down stream distances corresponding to traditional spacings in wind farms, it is *assumed* that only the surface- and wake shear mechanisms contribute significantly to the turbulence production. It is moreover *assumed* that the turbulence fluctuations, originating from these two sources, are *statistically independent* such that the turbulent energies are additive in the energy sense. Normalizing with respect to the *undisturbed mean wind velocity*, the total turbulence intensity of the along wind turbulence component in the wake, I_{wt}^u , is expressed as

Table 2.3 Measured wake deficit values compared to GCL–model predictions.

S [D]	D [m]	Hub Height [m]	C_T	Stability Ri	Amount of Data [hours]	\bar{V}_a [m/s]	I_a [%]	Mea. $\Delta\bar{V}$	Est. $\Delta\bar{V}$	Rel. dev. [%]
2.0	28	31	0.67	neutral	0.5	9.9	14.0	4.4	2.1	-52
5.3	28	31	0.76	neutral	9.0	7.3	11.9	1.2	1.2	0
5.3	28	31	0.70	neutral	4.5	9.1	12.9	1.4	1.2	-14
5.3	28	31	0.59	neutral	7.5	11.5	13.7	1.6	1.2	-25
7.5	28	31	0.76	neutral	4.5	7.5	10.9	0.6	1.1	83
7.5	28	31	0.70	neutral	1.5	9.1	14.2	0.7	0.8	14
14.5	28	31	0.75	neutral	16.0	7.9	11.7	0.5	0.6	20
14.5	28	31	0.69	neutral	11.0	9.3	12.7	0.5	0.6	20
14.5	28	31	0.59	neutral	4.0	11.7	13.8	0.3	0.6	100
4.2	23	30	0.44	0.04	0.33	14.2	5.6	4.5	3.4	-24
6.1	23	30	0.67	-0.3	0.33	9.7	6.4	2.4	2.3	-4
6.1	23	30	0.87	-0.15	0.33	6.3	6.9	1.6	1.8	13
6.1	23	30	0.87	-1.25	0.33	6.7	5.4	1.8	2.7	50
6.1	23	30	0.81	-0.5	0.5	7.8	6.3	1.9	2.3	21
4.2	23	30	0.86	-1.0	0.33	6.9	4.8	3.0	3.9	30
6.1	23	30	0.79	-2.0	0.5	8.0	6.3	1.8	2.3	28
4.2	23	30	0.83	-6.5	0.33	7.5	6.0	3.0	2.9	-3
4.2	23	30	0.71	-1.7	0.33	9.6	7.7	3.4	2.5	-27
4.2	23	30	0.83	0.07	0.5	7.9	3.8	4.3	5.2	21
4.2	23	30	0.3	0.01	0.166	17.4	7.0	4.6	2.2	-52
4.2	23	30	0.52	0.03	0.166	13.4	4.3	5.3	4.6	-13
4.2	23	30	0.5	0.03	0.166	13.7	5.9	5.3	3.4	-36
4	30	35	0.75		0.285	7.3	10.5	3.6	1.6	-56
4	30	35	0.75		0.356	7.7	8.9	3.6	2.0	-44
4	30	35	0.75		0.356	8.1	10.9	3.5	1.7	-51
7	30	35	0.57		0.711	13.6	7.2	2.8	1.9	-32
7	30	35	0.75		0.569	10.1	9.5	2.7	1.8	-33
7	30	35	0.74		0.996	10.0	9.1	2.3	1.8	-22
7	30	35	0.74		0.356	8.9	9.6	2.3	1.5	-35
5	0.27	0.31	0.91		0.006	4.13	9.0	1.05	1.2	14
7.5	0.27	0.3	0.87		0.008	4.1	9.0	1.03	0.9	-13

$$I_{wt}^u = \sqrt{I_a^2 + I_w^2}, \quad (2.4.1.4)$$

where subscripts a and w refer to ambient and wake, respectively. The specific wake contribution, I_w , depends on both the down wind distance and the undisturbed mean wind velocity, and is (for spacings larger than two rotor diameters) determined as :

$$I_w = 0.29 S^{-1/3} \sqrt{1 - \sqrt{1 - C_T}}, \quad (2.4.1.5)$$

where S denotes the spacing expressed in rotor diameters and C_T is the rotor thrust coefficient.

The proposed model has the correct qualitative– and asymptotic features as I_w increases for increasing C_T , decreases for increasing S , and tends to zero for S approaching infinity.

The performance of the model appears from the Table 2.4.

The model is based on the maximal change in a standard deviation profile (which is usually associated to the upper part of the rotorplane) normalized with the *undisturbed mean wind velocity* at hub height. The reason is, that the wind field modelling in most aeroelastic models operate with only one value for the turbulence intensity – we have then selected a slightly conservative value for that parameter.

In some of the experiments the spatial resolution was limited, and as a consequence the estimated values were expected to be moderately conservative. This is also reflected in the table above, except for a few very large deviations related to measurements with practically no increase in the turbulence intensity, originating from the wake situation. In general, a satisfactory agreement is encountered.

Turbulence Length Scale

When the two shear turbulence contributions have scales of comparable orders of magnitude, it is reasonable to expect the resulting spectral shape to be qualitatively invariant compared to the ambient situation. However, the resulting length scale is modified. The modified length scale depends on the rotor thrust coefficient, the spacing distance, the rotor diameter, and the undisturbed turbulence length scale. *Assuming* an approximate linear relationship between thrust coefficient and mean wind speed (for a stall controlled turbine), and referring to a Kaimal formulation of the turbulence spectrum, the length scale for the u turbulence component inside a wake, L_w^u , is determined from :

$$L_w^u = L_a^u \left(1 - \min \left(\frac{12.2 \left(1 - \frac{D}{L_a} \right)}{\bar{V}_a S_r^{0.6}}, 0.9 \right) \right), \quad (2.4.1.6)$$

where L_a^u denotes the u -turbulence length scale in the undisturbed flow, \bar{V}_a is the undisturbed mean wind velocity at hub height, and the reduced spacing, S_r , between the turbines is defines as :

$$S_r = 2^{0.8} + (S - 2)^{0.8} \quad \text{for } S \geq 2. \quad (2.4.1.7)$$

The undisturbed length scale and the resulting wake length scale refer to conditions at hub height. L_w^u is seen to be monotonous in \bar{V}_a , L_a^u , S_r , and D . However, the dependence on D is not pronounced for

Table 2.4 Wake turbulence intensities compared to GCL-model predictions.

S [D]	D [m]	Hub Height [m]	C_T	Stability Ri	Amount of Data [hours]	\bar{V}_a [m/s]	I_a [%]	Mea. I_{wt} [%]	Est. I_{wt} [%]	Rel. dev. [%]
2.0	28	31	0.67	neutral	0.5	9.9	14.0	16.5	20.5	24
5.3	28	31	0.76	neutral	9.0	7.3	11.9	16.2	16.8	4
5.3	28	31	0.70	neutral	4.5	9.1	12.9	16.2	17.1	6
5.3	28	31	0.59	neutral	7.5	11.5	13.7	17.5	16.9	-3
8.5	35	37	0.52	neutral	4.0	11.1	6.8	11.0	10.4	-5
9.5	35	37	0.57	neutral		10.0	7.2	11.3	10.8	-4
7.5	28	31	0.76	neutral	4.5	7.5	10.9	14.0	15.2	9
7.5	28	31	0.70	neutral	1.5	9.1	14.2	14.3	17.3	21
14.5	28	31	0.75	neutral	16.0	7.9	11.7	12.3	14.4	17
14.5	28	31	0.69	neutral	11.0	9.3	12.7	12.6	15.0	19
14.5	28	31	0.59	neutral	4.0	11.7	13.8	14.7	15.5	5
4.2	23	30	0.44	0.04	0.33	14.2	5.6	6.6	10.6	61
6.1	23	30	0.67	-0.3	0.33	9.7	6.4	11.4	12.2	7
6.1	23	30	0.87	-0.15	0.33	6.3	6.9	11.3	14.4	27
6.1	23	30	0.87	-1.25	0.33	6.7	5.4	12.5	13.8	10
6.1	23	30	0.81	-0.5	0.5	7.8	6.3	12.9	13.5	5
4.2	23	30	0.86	-1.0	0.33	6.9	4.8	15.6	15.0	-4
6.1	23	30	0.79	-2.0	0.5	8.0	6.3	13.5	13.3	-1
4.2	23	30	0.83	-6.5	0.33	7.5	6.0	16.0	15.0	-6
4.2	23	30	0.71	-1.7	0.33	9.6	7.7	13.0	14.4	11
4.2	23	30	0.83	0.07	0.5	7.9	3.8	10.7	14.3	34
4.2	23	30	0.3	0.01	0.166	17.4	7.0	9.3	10.1	9
4.2	23	30	0.52	0.03	0.166	13.4	4.3	6.6	10.9	65
4.2	23	30	0.5	0.03	0.166	13.7	5.9	6.6	11.4	73
4	30	35	0.75		0.285	7.3	10.5	15.1	16.6	10
4	30	35	0.75		0.356	7.7	8.9	13.7	15.7	15
4	30	35	0.75		0.356	8.1	10.9	15.4	16.9	10
7	30	35	0.57		0.711	13.6	7.2	9.3	11.4	23
7	30	35	0.75		0.569	10.1	9.5	12.2	14.3	17
7	30	35	0.74		0.996	10.0	9.1	11.9	14.0	18
7	30	35	0.74		0.356	8.9	9.6	11.1	14.3	29
5	0.27	0.31	0.91		0.006	4.13	9.0	14.1	16.8	19
7.5	0.27	0.3	0.87		0.008	4.1	9.0	12.3	14.9	21

Table 2.5 Wake length scales for u -turbulence components compared to GCL-model predictions.

S [D]	D [m]	Hub Height [m]	C_T	Stability Ri	Amount of Data [hours]	V_a [m/s]	L_a^u [%]	Mea. L_w^u [m]	Est. L_w^u [m]	Rel. dev. [%]
2.0	28	31	0.67	neutral	0.5	9.9	1070	140	149	7
5.3	28	31	0.76	neutral	9.0	7.3	1052	359	343	-5
5.3	28	31	0.70	neutral	4.5	9.1	1035	421	475	13
5.3	28	31	0.59	neutral	7.5	11.5	1363	788	776	-2
8.5	35	37	0.66	neutral	14.0	9.0	940	505	530	5
4.2	23	30	0.44	0.04	0.33	14.2	1306	598	797	33
6.1	23	30	0.67	-0.3	0.33	9.7	1380	846	717	-15
6.1	23	30	0.87	-0.15	0.33	6.3	1776	672	448	-33
6.1	23	30	0.87	-1.25	0.33	6.7	1849	975	559	-43
6.1	23	30	0.81	-0.5	0.5	7.8	1730	837	687	-18
4.2	23	30	0.86	-1.0	0.33	6.9	1592	635	317	-50
6.1	23	30	0.79	-2.0	0.5	8.0	1711	828	705	-15
4.2	23	30	0.83	-6.5	0.33	7.5	1868	616	479	-22
4.2	23	30	0.71	-1.7	0.33	9.6	1196	690	504	-27
4.2	23	30	0.83	0.07	0.5	7.9	672	598	210	-65
4.2	23	30	0.3	0.01	0.166	17.4	1840	1270	1251	-1
4.2	23	30	0.52	0.03	0.166	13.4	902	543	531	-2
4.2	23	30	0.5	0.03	0.166	13.7	1693	708	1008	42
4	30	35	0.67		0.285	7.3	644	138	159	15
4	30	35	0.67		0.356	7.7	920	184	253	37
4	30	35	0.67		0.356	8.1	736	230	233	1

the usual size of wind turbines. For large turbine spacings or for large mean wind speeds, L_w^u tends to approach L_a^u , and the expression thus exhibit the correct asymptotic behaviour.

In the Table 2.5, the performance of the model has been compared to measured values. The model is calibrated to a Kaimal formulation of the length scale, and where data were given with reference to a Von Karman formulation, they have been converted into a Kaimal formulation.

Considering the large uncertainties related to the determination of the length scale in general, the agreement between measurements and predictions is considered satisfactory – especially when bearing in mind that fatigue estimates, based on aeroelastic calculations, is rather unsensible to relatively moderate variations in the length scale.

In analogy with the turbulence intensity parameter, and for the same reasons, the present model is based on the maximal changes in a length scale profile. This is also reflected in the estimates, as most of these underpredict the measured values.

Coherence decay

Initiated by the indications from the initial parameter study, a simple attempt has been performed to extend the original model–complex also to take into account modification of the cross–correlation between turbulence components in a wake situation. In accordance with the assumptions introduced in beginning

of this chapter, the considerations to follow are limited to only uu -coherences. The investigation is based on a relatively slender data material⁸.

The tendencies displayed, in the Swedish and the Danish measured uu -coherence decay factors, seems at first to be somewhat contradicting, as the Danish results indicate no wake effect on vertical coherence for a 7.5 diameter spacing, whereas the Swedish results show a marked effect for a 6.1 diameter spacing. However, forcing the wake effect to be neglectable for spacings larger than 7.5 diameters and maximal for a 2 diameter spacing, introduces some harmony in the interpretation.

The two sets of experiments operate with different values of the vertical spacing, as the Danish results relates to a 13 m spacing, whereas the Swedish measurements operate with 6.4 m and 4.7 m spacing. Thus the coherences evaluated based on the Danish measurements will decay somewhat faster with the frequency than the Swedish coherences. However, the Danish results are based on very long runs which (more than) compensate for the loss in statistical significance due to the faster decay⁹.

The coherence is given a Davenport-formulation and is thus expressed as

$$\text{Coh}(s, f) = \sqrt{\exp\left(-\frac{asf}{\bar{V}_a}\right)}, \quad (2.4.1.8)$$

where f is the frequency in [Hz], s is the separation in [m], \bar{V}_a is the (ambient) mean wind speed in [m/s]. The ambient (undisturbed) coherence decay factor, a_a , is determined by [8]

$$a_a = \begin{cases} 12 + \frac{11|z_2 - z_1|}{z_{average}} & \text{for vertical separation} \\ 12 + \frac{11\Delta y}{z_{average}} & \text{for lateral separation} \end{cases}, \quad (2.4.1.9)$$

with the measuring heights denoted by z_1, z_2 , the average of these equal to $z_{average}$, and Δy being the lateral separation.

Intuitively, it is felt that the relative change of the coherence decay factors for lateral and vertical separations should be of the same order of magnitude. Both the lateral and the vertical coherences is, as expected, strongly effected by the wake for small wind turbine separations, whereas for moderate separations they are unaffected. As stated above, the wake influence is assumed to be negligible for spacings larger than 7.5 rotor diameters, and maximal for a spacing equal to 2 rotor diameters.

Basing the lateral wake coherence decay modification on the Danish measurements and the vertical wake coherence decay modification on both Swedish and Danish data, the following expression for the wake coherence decay factor, a_w , is proposed

$$a_w = \begin{cases} (1 + K_w)a_a & \text{for } 2 \leq S < 7.5 \\ a_a & \text{for } 7.5 \leq S \end{cases}, \quad (2.4.1.10)$$

where S denote the spacing expressed in rotor diameters and the wake correction factor, K_w , is given by

⁸The data material reproduced in the Appendix F.

⁹The coherence decay is mainly determined based on values in the frequency band corresponding to coherence values between 0.3 and 1.0

Table 2.6 Measured wake coherence decay compared to model predictions.

S [D]	Stability Ri	Amount of Data [hours]	\bar{V}_a [m/s]	Mea. $1 + K_w^H$	Est. $1 + K_w^H$	Mea. $1 + K_w^V$	Est. $1 + K_w^V$
2	neutral	3.0	~ 11.3	2.6	2.8		
2	neutral	1.5	~ 11.7	3.2	1.9		
2	neutral	1.5	~ 14.7	3.8	2.9		
4.2	-1.0	0.33	6.9			1.8	1.8
4.2	-6.5	0.33	7.5			1.9	1.9
4.2	-1.7	0.33	9.6			2.4	2.3
4.2	0.03	0.166	13.4			3.0	3.1
4.2	0.03	0.166	13.7			3.4	3.1
4.2	0.04	0.33	14.2			3.3	3.2
4.2	0.01	0.166	17.4			2.1	3.4
6.1	-0.15	0.33	6.3			1.2	1.3
6.1	-1.25	0.33	6.7			1.5	1.3
6.1	-0.5	0.5	7.8			1.7	1.4
6.1	-2.0	0.5	8.0			1.9	1.4
6.1	-0.3	0.33	9.7			1.9	1.6

$$K_w = \begin{cases} \frac{7.5-S}{5.5} & \text{for } \bar{V}_a < 6 \\ \frac{7.5-S}{5.5} \left(\frac{1}{3} \bar{V}_a - C_s \right) & \text{for } 6 \leq \bar{V}_a \leq 15 \\ \frac{4(7.5-S)}{5.5} & \text{for } 15 < \bar{V}_a \end{cases} \quad (2.4.1.11)$$

For vertical separation $C_s \equiv 1$ and for horizontal separation $C_s \equiv 2$. For spacings less than 2 rotor diameters the value of the wake coherence decay factor is assumed to equal the value related to a 2 diameter spacing.

The model performance is illustrated below, where K_w^V refers to vertical separation, and K_w^H refers to horizontal separation.

The agreement is satisfactory. However, the data material is somewhat limited which might affect the generality of the proposed estimation procedure.

Most turbulence generators do not have the ability to take into account coherence decay factors depending on spacing direction, nor on the magnitude of the spacing. In general, the turbulence generators presume constant coherence decay factors, and the derived coherences (referring to a particular site) thus depend only on frequency and on the absolute value of the spacing. In this situation the mean of coherence decay factors estimated for horizontal- and vertical separation, respectively, is recommended, and in case the ambient coherence factor is determined from the above expression (2.4.1.9), a vertical separation of 2/3 of the rotor diameter should be specified in order to assure satisfactory agreement for eddies with the maximal potential for aerodynamic impact.

Transversal turbulence

So far the investigations have concentrated on the along wind turbulence component u only, as this

component is the main responsible for the fatigue load generation, and as most available measured data are based on cup anemometer recordings (giving the horizontal velocity component and in a first order approximation the along wind turbulence intensity). However, the fatigue effect originating from the transversal components is not negligible. Therefore, a relation between the v - and w -turbulence components and the u -component is of interest. The derivation to follow is also an extension compared to the original model concept.

In analogy with the considerations related to the u -component, it is assumed that the transversal turbulence can be properly described by adjusting the spectral parameters related to a traditional description of the ambient turbulence in flat homogeneous terrain. Thus, the qualitative characteristics of the turbulence are *presumed* to be preserved, and here the wind farm effects are condensed in a suitable modification of only a few parameters.

At this stage, there is limited information available on the wake behaviour of the transversal components, and the available material is dealing with only two of the above mentioned parameters – the turbulence intensity and the turbulence length scales.

Turbulence intensity

For flat and homogeneous terrain, the following relations express the standard deviations of the turbulence components, σ^u , σ^v , and σ^w as

$$\sigma_a^v \approx \frac{3}{4}\sigma_a^u, \quad (2.4.1.12)$$

$$\sigma_a^w \approx \frac{1}{2}\sigma_a^u, \quad (2.4.1.13)$$

where subscript "a" indicate ambient values.

In a wake, the turbulence tends to be more isotropic, and the above relations are modified to [9]¹⁰

$$\sigma_w^v \approx 0.8\sigma_w^u, \quad (2.4.1.14)$$

$$\sigma_w^w \approx 0.6\sigma_w^u, \quad (2.4.1.15)$$

where subscript "w" indicate wake-values.

¹⁰In the analysis, the relation between turbulence components turn out to depend on the measuring height, and the presented values is the most conservative ones in the sence that they produce the largest standard deviations.

Turbulence length scales

Let the u -, v -, and w - turbulence components inside as well as outside the wake be described by power density spectra of the Kaimal form,

$$S_k(L^k, f) = (\sigma^k)^2 \frac{L^k / \bar{V}}{(1 + \frac{3}{2} f L^k / \bar{V})^{5/3}}, \quad (2.4.1.16)$$

in the neutral regime, where k substitutes either u , v or w . Assuming local isotropy in the inertial subrange for sufficiently small eddies, the following relations hold for the spectral components:

$$\lim_{f \rightarrow \infty} \frac{S_u(L^u, f)}{S_v(L^v, f)} = \lim_{f \rightarrow \infty} \frac{S_u(L^u, f)}{S_w(L^w, f)} = \frac{3}{4}. \quad (2.4.1.17)$$

The proportion 3:4 in relation (2.4.1.17) does not express lack of isotropy, but is a consequence of the turbulence component u being directed along the mean wind direction.

For *flat and homogeneous terrain*, combining expressions (2.4.1.12), (2.4.1.16), and (2.4.1.17) leads to the following relation

$$\lim_{f \rightarrow \infty} \frac{S_u(L_a^u, f)}{S_v(L_a^v, f)} = \lim_{f \rightarrow \infty} \frac{L_a^u}{(\frac{3}{4})^2 L_a^v} \left(\frac{\frac{1}{f} + \frac{3}{2} L_a^v / \bar{V}_a}{\frac{1}{f} + \frac{3}{2} L_a^u / \bar{V}_a} \right)^{5/3} = \frac{3}{4},$$

from where the proportion between the v - and u length scales can be derived as¹¹

$$\frac{L_a^v}{L_a^u} = \left(\frac{3 \times 9}{4 \times 16} \right)^{3/2} = 0.27. \quad (2.4.1.18)$$

In analogy, the value for the proportion between the w - and u length scales in homogeneous terrain can be determined to

$$\frac{L_a^w}{L_a^u} = 0.08. \quad (2.4.1.19)$$

Similar considerations related to the *wake situation*, and thus based on relations (2.4.1.14), (2.4.1.15), (2.4.1.16), and (2.4.1.17), lead to

$$\frac{L_w^v}{L_w^u} = 0.33 \quad (2.4.1.20)$$

$$\frac{L_w^w}{L_w^u} = 0.14. \quad (2.4.1.21)$$

¹¹Using the value 0.8 as the proportion between the v and u standard deviations, we arrive at the value 0.33 for proportion between the v and u length scales, which corresponds to the value given in the code IEC-1400-1.

2.4.2 SF-model

Also the present empirical method [3] is based on full scale measurements and works by specifying an effective turbulence intensity (or design turbulence intensity) in the mean wind direction, aiming at substituting a detailed wake calculation, when determining fatigue life consumption by means of aeroelastic models.

The wake effects, associated with the mean wind deficit, the decreased turbulence length scale, and the increased coherence decay, concerning the fatigue loading of a wind turbine is thus included in this effective turbulence intensity. As a consequence the effective turbulence intensity is usually conservative compared with measured physical values.

The effective turbulence intensity, I_{we}^u ¹², is determined from :

$$I_{we}^u = \sqrt{\frac{1.2C_T}{S^2} + I_a^2}. \quad (2.4.2.1)$$

The performance of the model appears from the Table 2.7. Apparently the model is not capable of handling near wake situations, as the 2D situation is leading to a 185% deviation. It is often found in wind tunnel measurements that up to 2D spacing, the shear stress profile develops very slowly in single wakes, by which transfer of momentum from the outer flow to the wake is limited [10],[11].

As expected, the model is somewhat conservative when compared to the measured (physical) wake values. However, as the model contain all wake effects in one number, a quantitative comparison is difficult.

2.4.3 DR-model

This model describes the increased fatigue loading in wakes by modifying the ambient turbulence intensity and is the procedure applied in the present "Danish Recommendation".

When wind turbines are erected in a wind farm cluster with a distance between the turbines of at least 5 rotor diameters, or in a wind farm array with a mutual distance of at least 3 rotor diameters, the increase in fatigue loading, originating from the change in mean wind field and turbulence structure, can be taken into account by specifying a design turbulence intensity¹³, I_d , as :

$$I_d = \sqrt{I_a^2 + I_w^2}, \quad (2.4.3.1)$$

where I_w is an additional wake contribution expressed by

$$I_w = \beta_v \beta_l 0.15. \quad (2.4.3.2)$$

In the above expression, β_v denotes a correction factor related to the mean wind hub velocity, whereas β_l is a correction factor related to the distance between the wind turbines. These correction factors are obtained from Figures 2.1, 2.2 and 2.3, respectively.

¹²Normalized with respect to the ambient mean wind speed at hub height.

¹³Normalized with respect to the ambient mean wind speed at huh height.

Table 2.7 Wake turbulence intensities compared to SF-model predictions.

S [D]	D [m]	Hub Height [m]	C_T	Stability Ri	Amount of Data [hours]	\bar{V}_a [m/s]	I_a [%]	Mea. I_{we} [%]	Est. I_{we}^u [%]	Rel. dev. [%]
2.0	28	31	0.67	neutral	0.5	9.9	14.0	16.5	47.0	185
5.3	28	31	0.76	neutral	9.0	7.3	11.9	16.2	21.6	33
5.3	28	31	0.70	neutral	4.5	9.1	12.9	16.2	21.6	33
5.3	28	31	0.59	neutral	7.5	11.5	13.7	17.5	21.0	20
8.5	35	37	0.52	neutral	4.0	11.1	6.8	11.0	11.5	5
9.5	35	37	0.57	neutral		10.0	7.2	11.3	11.3	0
7.5	28	31	0.76	neutral	4.5	7.5	10.9	14.0	16.8	20
7.5	28	31	0.70	neutral	1.5	9.1	14.2	14.3	18.7	31
14.5	28	31	0.75	neutral	16.0	7.9	11.7	12.3	13.4	9
14.5	28	31	0.69	neutral	11.0	9.3	12.7	12.6	14.2	12
14.5	28	31	0.59	neutral	4.0	11.7	13.8	14.7	15.0	2
4.2	23	30	0.44	0.04	0.33	14.2	5.6	6.6	18.2	176
6.1	23	30	0.67	-0.3	0.33	9.7	6.4	11.4	16.0	41
6.1	23	30	0.87	-0.15	0.33	6.3	6.9	11.3	18.1	60
6.1	23	30	0.87	-1.25	0.33	6.7	5.4	12.5	17.6	41
6.1	23	30	0.81	-0.5	0.5	7.8	6.3	12.9	17.3	34
4.2	23	30	0.86	-1.0	0.33	6.9	4.8	15.6	24.7	58
6.1	23	30	0.79	-2.0	0.5	8.0	6.3	13.5	17.2	27
4.2	23	30	0.83	-6.5	0.33	7.5	6.0	16.0	24.5	53
4.2	23	30	0.71	-1.7	0.33	9.6	7.7	13.0	23.3	79
4.2	23	30	0.83	0.07	0.5	7.9	3.8	10.7	24.1	125
4.2	23	30	0.3	0.01	0.166	17.4	7.0	9.3	15.9	71
4.2	23	30	0.52	0.03	0.166	13.4	4.3	6.6	19.3	192
4.2	23	30	0.5	0.03	0.166	13.7	5.9	6.6	19.4	193
4	30	35	0.75		0.285	7.3	10.5	15.1	25.9	72
4	30	35	0.75		0.356	7.7	8.9	13.7	25.3	85
4	30	35	0.75		0.356	8.1	10.9	15.4	26.1	69
7	30	35	0.57		0.711	13.6	7.2	9.3	13.8	49
7	30	35	0.75		0.569	10.1	9.5	12.2	16.6	36
7	30	35	0.74		0.996	10.0	9.1	11.9	16.2	37
7	30	35	0.74		0.356	8.9	9.6	11.1	16.5	48
5	0.27	0.31	0.91		0.006	4.13	9.0	14.1	22.8	61
7.5	0.27	0.3	0.87		0.008	4.1	9.0	12.3	16.3	33

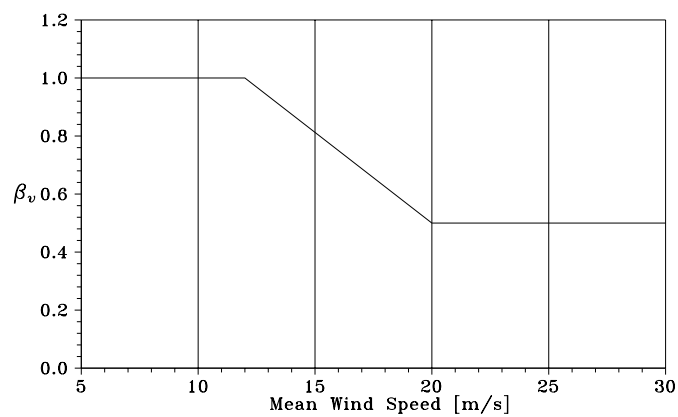


Figure 2.1 Wind speed correction factor.

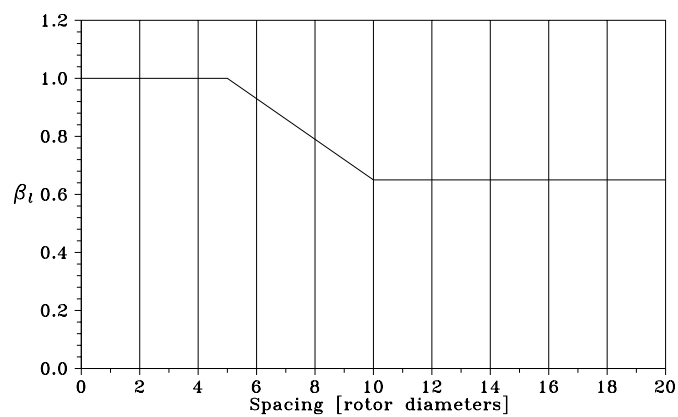


Figure 2.2 Distance correction factor for wind turbines in a wind farm array.

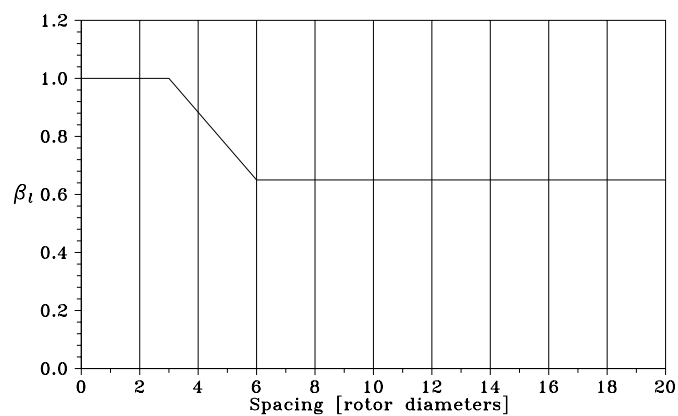


Figure 2.3 Distance correction factor for wind turbines in a wind farm cluster.

The performance of the model appears from the Table 2.8.

Table 2.8 Wake turbulence intensities compared to DR-model predictions.

S [D]	D [m]	Hub Height [m]	C_T	Stability Ri	Amount of Data [hours]	\bar{V}_a [m/s]	I_a [%]	Mea. I_{wt} [%]	Est. I_{wt} [%]	Rel. dev. [%]
5.3	28	31	0.76	neutral	9.0	7.3	11.9	16.2	16.2	0
5.3	28	31	0.70	neutral	4.5	9.1	12.9	16.2	16.9	5
5.3	28	31	0.59	neutral	7.5	11.5	13.7	17.5	17.6	0
8.5	35	37	0.52	neutral	4.0	11.1	6.8	11.0	10.1	-8
9.5	35	37	0.57	neutral		10.0	7.2	11.3	10.4	-8
7.5	28	31	0.76	neutral	4.5	7.5	10.9	14.0	13.2	-6
7.5	28	31	0.70	neutral	1.5	9.1	14.2	14.3	16.1	12
14.5	28	31	0.75	neutral	16.0	7.9	11.7	12.3	13.9	13
14.5	28	31	0.69	neutral	11.0	9.3	12.7	12.6	14.7	17
14.5	28	31	0.59	neutral	4.0	11.7	13.8	14.7	15.7	7
4.2	23	30	0.44	0.04	0.33	14.2	5.6	6.6	12.5	89
6.1	23	30	0.67	-0.3	0.33	9.7	6.4	11.4	9.9	-14
6.1	23	30	0.87	-0.15	0.33	6.3	6.9	11.3	10.2	-10
6.1	23	30	0.87	-1.25	0.33	6.7	5.4	12.5	9.2	-26
6.1	23	30	0.81	-0.5	0.5	7.8	6.3	12.9	9.8	-24
4.2	23	30	0.86	-1.0	0.33	6.9	4.8	15.6	13.8	-12
6.1	23	30	0.79	-2.0	0.5	8.0	6.3	13.5	9.8	-27
4.2	23	30	0.83	-6.5	0.33	7.5	6.0	16.0	14.2	-11
4.2	23	30	0.71	-1.7	0.33	9.6	7.7	13.0	15.0	16
4.2	23	30	0.83	0.07	0.5	7.9	3.8	10.7	13.4	26
4.2	23	30	0.3	0.01	0.166	17.4	7.0	9.3	11.1	19
4.2	23	30	0.52	0.03	0.166	13.4	4.3	6.6	12.5	90
4.2	23	30	0.5	0.03	0.166	13.7	5.9	6.6	13.0	96
4	30	35	0.67		0.285	7.3	10.5	15.1	16.9	12
4	30	35	0.67		0.356	7.7	8.9	13.7	16.0	17
4	30	35	0.67		0.356	8.1	10.9	15.4	17.2	11
7	30	35	0.42		0.711	13.6	7.2	9.3	9.9	6
7	30	35	0.66		0.569	10.1	9.5	12.2	12.1	-1
7	30	35	0.66		0.996	10.0	9.1	11.9	11.8	-1
7	30	35	0.66		0.356	8.9	9.6	11.1	12.2	10
5	0.27	0.31	0.91		0.006	4.13	9.0	14.1	14.6	4
7.5	0.27	0.3	0.87		0.008	4.1	9.0	12.3	11.7	-5

Despite the simplicity of the model, the agreement between model predictions and measurements is satisfactory except for a few very large deviations. This is somewhat surprising, as the philosophy behind the model is the same as for the the SF-model – namely to concentrate all wake effects in only one parameter (turbulence intensity). Therefore more conservative results were expected.

2.4.4 TNO-model

This empirical model [4] originates from work carried out in the "Dynamic Loads in Wind Farms (I)" Joule project and has been further assessed by the Dutch TNO laboratory. It is based on extensive measurements of wind turbine arrays in an atmospheric boundary layer wind tunnel. The model specifies the increased turbulence intensity in the wake, I_{wt}^u ¹⁴, compared to the ambient conditions as well as the maximal wake deficit, $\Delta\bar{V}$.

Turbulence Intensity

The wake turbulence intensity is determined from the expression

$$I_{wt}^u = \sqrt{I_a^2 + I_w^2}, \quad (2.4.4.1)$$

with the additional wake contribution determined from

$$I_w = 1.31 C_T^{0.7} I_a^{0.68} \left(\frac{X}{X_F} \right)^{-0.96}, \quad (2.4.4.2)$$

where C_T denotes the rotor thrust coefficient, X is the downwind distance, and X_F denotes the beginning of the far wake section given by

$$X_F = \frac{d(1-e)X_N}{e(1-d)}, \quad (2.4.4.3)$$

with d and e conveniently introduced as

$$d = \sqrt{0.214 + 0.144m}, \quad (2.4.4.4)$$

$$e = \sqrt{0.134 + 0.124m}, \quad (2.4.4.5)$$

and m determined by

$$m = \frac{1}{\sqrt{1 - C_T}}. \quad (2.4.4.6)$$

The extension of the wake near field, X_N , is expressed by

$$X_N = \frac{R_0}{\sqrt{\left(\frac{dR}{dx}\right)_m^2 + \left(\frac{dR}{dx}\right)_\lambda^2}}, \quad (2.4.4.7)$$

where the involved quantities are determined by

¹⁴Normalized with respect to the undisturbed ambient mean wind speed.

$$\left(\frac{dR}{dx}\right)_m = \frac{(1-m)\sqrt{1.49+m}}{9.76(1+m)}, \quad (2.4.4.8)$$

$$\left(\frac{dR}{dx}\right)_\lambda = \sqrt{0.075I_a^{0.21} + 0.457 \times 10^{-3}\lambda^{(0.71I_a+2.62)}}, \quad (2.4.4.9)$$

and

$$R_0 = \frac{D}{2} \sqrt{\frac{m+1}{2}}, \quad (2.4.4.10)$$

where λ denotes the tip speed ratio, and D is the rotor diameter.

The performance of the TNO–model, regarding turbulence intensities, appears from the Table 2.9.

Some deviations are encountered between measurements and model predictions. However, there is no systematic trend, except that the model tend to yield conservative results in situations with low ambient turbulence intensities.

Deficit

With the nomenclature introduced above, the maximal wake deficit is expressed as

$$\Delta\bar{V} = \Delta\bar{V}_N \left(\frac{X}{X_N}\right)^{-1.25}, \quad (2.4.4.11)$$

where X denotes the down wind distance from the turbine, and

$$\Delta\bar{V}_N = 0.56C_T + 0.255. \quad (2.4.4.12)$$

The performance of the deficit prediction is illustrated in the Table 2.10.

Some deviations between measurements and model predictions are encountered, and there is a clear tendency for the model to underpredict the deficit.

2.4.5 MM–model

The MM–model predicts velocity deficit as well as turbulence intensity and turbulence length scale in wake situations. Contrary to most other models, the present approach operate with the concept "transport time" instead of downstream distance. The transport time is calculated using Taylors hypothesis. The model is described in detail in model [5].

Table 2.9 Wake turbulence intensities compared to TNO-model predictions.

S [D]	D [m]	Hub Height [m]	C_T	Stability Ri	Amount of Data [hours]	\bar{V}_a [m/s]	I_a [%]	Mea. I_{wt} [%]	Est. I_{wt} [%]	Rel. dev. [%]
2.0	28	31	0.67	neutral	0.5	9.9	14.0	16.5	36.7	122
5.3	28	31	0.76	neutral	9.0	7.3	11.9	16.2	16.2	0
5.3	28	31	0.70	neutral	4.5	9.1	12.9	16.2	18.0	11
5.3	28	31	0.59	neutral	7.5	11.5	13.7	17.5	18.7	7
8.5	35	37	0.52	neutral	4.0	11.1	6.8	11.0	8.1	-27
9.5	35	37	0.57	neutral		10.0	7.2	11.3	8.3	-27
7.5	28	31	0.76	neutral	4.5	7.5	10.9	14.0	13.3	-5
7.5	28	31	0.70	neutral	1.5	9.1	14.2	14.3	17.1	19
14.5	28	31	0.75	neutral	16.0	7.9	11.7	12.3	12.5	2
14.5	28	31	0.69	neutral	11.0	9.3	12.7	12.6	13.5	8
14.5	28	31	0.59	neutral	4.0	11.7	13.8	14.7	14.6	0
4.2	23	30	0.44	0.04	0.33	14.2	5.6	6.6	9.8	48
6.1	23	30	0.67	-0.3	0.33	9.7	6.4	11.4	9.7	-15
6.1	23	30	0.87	-0.15	0.33	6.3	6.9	11.3	10.4	-7
6.1	23	30	0.87	-1.25	0.33	6.7	5.4	12.5	9.0	-28
6.1	23	30	0.81	-0.5	0.5	7.8	6.3	12.9	10.0	-23
4.2	23	30	0.86	-1.0	0.33	6.9	4.8	15.6	10.7	-32
6.1	23	30	0.79	-2.0	0.5	8.0	6.3	13.5	9.9	-27
4.2	23	30	0.83	-6.5	0.33	7.5	6.0	16.0	12.4	-22
4.2	23	30	0.71	-1.7	0.33	9.6	7.7	13.0	14.5	11
4.2	23	30	0.83	0.07	0.5	7.9	3.8	10.7	9.4	-12
4.2	23	30	0.3	0.01	0.166	17.4	7.0	9.3	10.1	9
4.2	23	30	0.52	0.03	0.166	13.4	4.3	6.6	8.8	33
4.2	23	30	0.5	0.03	0.166	13.7	5.9	6.6	10.8	64
4	30	35	0.75		0.285	7.3	10.5	15.1	18.0	19
4	30	35	0.75		0.356	7.7	8.9	13.7	15.9	16
4	30	35	0.75		0.356	8.1	10.9	15.4	18.5	20
7	30	35	0.57		0.711	13.6	7.2	9.3	8.8	-5
7	30	35	0.75		0.569	10.1	9.5	12.2	12.5	2
7	30	35	0.74		0.996	10.0	9.1	11.9	11.9	0
7	30	35	0.74		0.356	8.9	9.6	11.1	12.5	12
5	0.27	0.31	0.91		0.006	4.13	9.0	14.1	21.9	56
7.5	0.27	0.3	0.87		0.008	4.1	9.0	12.3	15.7	28

Table 2.10 Measured wake deficit values compared to TNO-model predictions.

S [D]	D [m]	Hub Height [m]	C_T	Stability Ri	Amount of Data [hours]	\bar{V}_a [m/s]	I_a [%]	Mea. $\Delta\bar{V}$	Est. $\Delta\bar{V}$	Rel. dev. [%]
2.0	28	31	0.67	neutral	0.5	9.9	14.0	4.4	5.4	23
5.3	28	31	0.76	neutral	9.0	7.3	11.9	1.2	1.0	-17
5.3	28	31	0.70	neutral	4.5	9.1	12.9	1.4	1.4	0
5.3	28	31	0.59	neutral	7.5	11.5	13.7	1.6	1.9	19
7.5	28	31	0.76	neutral	4.5	7.5	10.9	0.6	0.7	17
7.5	28	31	0.70	neutral	1.5	9.1	14.2	0.7	0.9	29
14.5	28	31	0.75	neutral	16.0	7.9	11.7	0.5	0.3	-40
14.5	28	31	0.69	neutral	11.0	9.3	12.7	0.5	0.4	-20
14.5	28	31	0.59	neutral	4.0	11.7	13.8	0.3	0.5	67
4.2	23	30	0.44	0.04	0.33	14.2	5.6	4.5	3.2	-29
6.1	23	30	0.67	-0.3	0.33	9.7	6.4	2.4	1.4	-42
6.1	23	30	0.87	-0.15	0.33	6.3	6.9	1.6	0.8	-50
6.1	23	30	0.87	-1.25	0.33	6.7	5.4	1.8	0.9	-50
6.1	23	30	0.81	-0.5	0.5	7.8	6.3	1.9	1.1	-42
4.2	23	30	0.86	-1.0	0.33	6.9	4.8	3.0	1.6	-47
6.1	23	30	0.79	-2.0	0.5	8.0	6.3	1.8	1.1	-39
4.2	23	30	0.83	-6.5	0.33	7.5	6.0	3.0	1.7	-43
4.2	23	30	0.71	-1.7	0.33	9.6	7.7	3.4	2.3	-32
4.2	23	30	0.83	0.07	0.5	7.9	3.8	4.3	2.0	-54
4.2	23	30	0.3	0.01	0.166	17.4	7.0	4.6	3.4	-26
4.2	23	30	0.52	0.03	0.166	13.4	4.3	5.3	3.3	-38
4.2	23	30	0.5	0.03	0.166	13.7	5.9	5.3	3.3	-38
4	30	35	0.75		0.285	7.3	10.5	3.6	1.6	-56
4	30	35	0.75		0.356	7.7	8.9	3.6	1.7	-53
4	30	35	0.75		0.356	8.1	10.9	3.5	1.8	-49
7	30	35	0.57		0.711	13.6	7.2	2.8	1.2	-57
7	30	35	0.75		0.569	10.1	9.5	2.7	1.1	-59
7	30	35	0.74		0.996	10.0	9.1	2.3	1.1	-52
7	30	35	0.74		0.356	8.9	9.6	2.3	1.0	-57
5	0.27	0.31	0.91		0.006	4.13	9.0	1.05	1.24	18
7.5	0.27	0.3	0.87		0.008	4.1	9.0	1.03	0.78	-24

Velocity deficit

The decay of the relative maximal velocity deficit downstream a wind turbine is expressed as the sum of the thrust coefficient, C_T , and a function of the transport time downstream the wind turbine, together with a time scale, t_0 :

$$\frac{\Delta \bar{V}}{\bar{V}_a} = 0.4 \ln \left(\frac{t_0}{t} \right) + C_T. \quad (2.4.5.1)$$

The transport time $t = \frac{x}{\bar{V}_a}$ is used since it was found that the development of the flow is depending on how long time the processes have been active.

Immediately downstream the turbine, the relative velocity deficit has two peaks, situated at the middle section of the blades, but with increasing transport time behind the turbine, momentum transport towards the centre gradually wipes out the two peaks and one maximum will occur at the centre line. The time needed to obtain only one maximum is defined as t_0 , and depends on atmospheric stability, turbine characteristic, and the roughness length at the site. For *neutral* stratification t_0 can be written :

$$t_0 = \frac{1}{\omega} \ln \left(\frac{H}{z_0} \right) \frac{R}{H}, \quad (2.4.5.2)$$

where ω is the rotational frequency in [Hz], R rotor radius, H hub height, and z_0 the roughness length.

For sufficiently long transport time the calculated relative velocity deficit becomes smaller than zero; hence the model is not valid for very large transport times. When this situation occurred in the calculations, the deficit was set equal to zero. Also, the model is not valid for transport times shorter than the time t_0 , although a value can be calculated.

For transport times where the model is applicable, the spatial distribution $\Delta v(y, z)$ in the vertical (z) and lateral (y) directions is approximated by a Gaussian distribution as

$$\frac{\Delta v(y, z)}{\bar{V}_a} = \frac{\Delta V}{\bar{V}_a} \exp \left(-\frac{\left(\frac{y}{R}\right)^2}{2\sigma_y^2} \right) \left(\exp \left(-\frac{\left(\frac{z+H}{R}\right)^2}{2\sigma_z^2} \right) + \exp \left(-\frac{\left(\frac{z-H}{R}\right)^2}{2\sigma_z^2} \right) \right), \quad (2.4.5.3)$$

where σ_y and σ_z are the normalized lateral and vertical standard deviations.

The performance of the model is illustrated in the Table 2.11.

The results reveal some deviations, especially for large turbine spacings. The agreement with the Swedish measurements, which has been used for the calibration of the model, is excellent.

It is a prerequisite for application of the model that a representative surface roughness can be defined, and consequently situations with roughness changes might cause problems.

Turbulence intensity

The centreline turbulence intensity found in the wake, \tilde{I}_{wt}^u , can be expressed as

Table 2.11 Measured wake deficit values compared with the MM-model predictions.

S [D]	D [m]	Hub Height [m]	C_T	Stability Ri	Amount of Data [hours]	V_a [m/s]	I_a [%]	Mea. $\Delta\bar{V}$	Est. $\Delta\bar{V}$	Rel. dev. [%]
2.0	28	31	0.67	neutral	0.5	9.9	14.0	4.4	6.86	56
5.3	28	31	0.76	neutral	9.0	7.3	11.9	1.2	1.3	9
5.3	28	31	0.7	neutral	4.5	9.1	12.9	1.4	1.89	35
5.3	28	31	0.59	neutral	7.5	11.5	13.7	1.6	2.2	37
7.5	28	31	0.76	neutral	4.5	7.5	10.9	0.6	0.39	-35
7.5	28	31	0.7	neutral	1.5	9.1	14.2	0.7	0.63	-10
14.5	28	31	0.75	neutral	16.0	7.9	11.7	0.5	0	-100
14.5	28	31	0.69	neutral	11.0	9.3	12.7	0.5	0	-100
14.5	28	31	0.59	neutral	4.0	11.7	13.8	0.3	0	-100
4.2	23	30	0.44	0.04	0.33	14.2	5.6	4.5	4.7	6
6.1	23	30	0.67	-0.3	0.33	9.7	6.4	2.4	2.6	10
6.1	23	30	0.87	-0.15	0.33	6.3	6.9	1.6	1.8	15
6.1	23	30	0.87	-1.25	0.33	6.7	5.4	1.8	1.7	-4
6.1	23	30	0.81	-0.5	0.5	7.8	6.3	1.9	2.0	6
4.2	23	30	0.86	-1.0	0.33	6.9	4.8	3.0	2.8	-6
6.1	23	30	0.79	-2.0	0.5	8.0	6.3	1.8	1.9	5
4.2	23	30	0.83	-6.5	0.33	7.5	6.0	3.0	3.1	1
4.2	23	30	0.71	-1.7	0.33	9.6	7.7	3.4	3.7	7
4.2	23	30	0.83	0.07	0.5	7.9	3.8	4.3	4.3	0
4.2	23	30	0.3	0.01	0.166	17.4	7.0	4.6	4.9	5
4.2	23	30	0.52	0.03	0.166	13.4	4.3	5.3	5.2	-1
4.2	23	30	0.5	0.03	0.166	13.7	5.9	5.3	5.2	-2
4	30	35	0.75		0.285	7.3	10.5	3.6	2.1	-42
4	30	35	0.75		0.356	7.7	8.9	3.6	2.2	-38
4	30	35	0.75		0.356	8.1	10.9	3.5	2.4	-33
7	30	35	0.57		0.711	13.6	7.2	2.8	0.04	-98
7	30	35	0.75		0.569	10.1	9.5	2.7	0.65	-76
7	30	35	0.74		0.996	10.0	9.1	2.3	0.54	-77
7	30	35	0.74		0.356	8.9	9.6	2.3	0.48	-79
5	0.27	0.31	0.91		0.006	4.13	9.0	1.05	1.09	-4
7.5	0.27	0.3	0.87		0.008	4.1	9.0	1.03	0.9	8

$$\tilde{I}_{wt}^u = I_a + 0.6 \left(1 - \frac{t_0}{t} \right) \frac{\Delta \bar{V}}{\bar{V}_a}. \quad (2.4.5.4)$$

The turbulence intensity determined according to the above procedure, corresponds to the measured value normalised with the local *mean wake velocity*, which is indicated by equipping the turbulence intensity parameter with a "tilde".

The performance of the model is illustrated in the Table 2.12, where the results presented have been recalculated and normalised with the ambient wind speed, using the ratio between measured wake velocity and ambient velocity.

Some deviations are encountered but there is no systematic trend.

Length scale

In the MM-model, the characteristic length scale calculated is L_{max} – the wavelength with most energy.

$$L_{max} = \left(\frac{D}{\frac{\Delta \bar{V}}{\bar{V}_a}} \right) \quad (2.4.5.5)$$

This model can only be compared with data from Alsvik, since there has not been any calculations of this variable for the other sites.

The agreement between predictions and measurements is satisfactory.

2.4.6 UPMWAKE-model

In contradiction to the other presented models, the UPMWAKE model requires more comprehensive calculations. The model [6] takes into account the atmospheric stability, described by the Monin–Obukhov length, and the surface roughness in the description of the undisturbed flow. The perturbations, introduced in the basic flow by a wind turbine, are described in terms of fluid dynamic equations for conservation of mass, momentum, energy, turbulent kinetic energy, and dissipation rate of the turbulent kinetic energy. The modeling of the turbulent transport terms is based on the k-ε model for closure of the turbulent flow equations.

The set of equations is discretized by means of the finite difference method and solved numerically using the SIMPLE algorithm [7]. The parabolic approximation has been made, and the numerical solution of the parabolic equations has been carried out using an alternating direction implicit (ADI) method. The resulting wake model is three dimensional, and the output is velocity deficit and turbulence intensities.

Velocity deficit

The performance of the model is illustrated by the example calculations given in the Table 2.14.

Table 2.12 Measured turbulence intensity values compared with the MM-model predictions.

S [D]	D [m]	Hub Height [m]	C_T	Stability Ri	Amount of Data [hours]	\bar{V}_a [m/s]	I_a [%]	Mea. I_{wt} [%]	Est. I_{wt} [%]	Rel. dev. [%]
2.0	28	31	0.67	neutral	0.5	9.9	14.0	16.5	6.4	-61
5.3	28	31	0.76	neutral	9.0	7.3	11.9	16.2	16.8	4
5.3	28	31	0.7	neutral	4.5	9.1	12.9	16.2	18.4	14
5.3	28	31	0.59	neutral	7.5	11.5	13.7	17.5	18	3
7.5	28	31	0.76	neutral	4.5	7.5	10.9	14.0	12.4	-11
7.5	28	31	0.7	neutral	1.5	9.1	14.2	14.3	16.1	-13
8.5	35	37	0.52	neutral	4	11.1	6.8	11	17.3	-58
9.5	35	37	0.57	neutral		10	7.2	11.3	10.6	-6
14.5	28	31	0.75	neutral	16.0	7.9	11.7	12.3	11.7	-5
14.5	28	31	0.69	neutral	11.0	9.3	12.7	12.6	12.7	1
14.5	28	31	0.59	neutral	4.0	11.7	13.8	14.7	13.8	-6
4.2	23	30	0.44	0.04	0.33	14.2	5.6	6.6	7	6
6.1	23	30	0.67	-0.3	0.33	9.7	6.4	2.4	2.6	8
6.1	23	30	0.87	-0.15	0.33	6.3	6.9	11.3	15.1	34
6.1	23	30	0.87	-1.25	0.33	6.7	5.4	12.5	12.8	2
6.1	23	30	0.81	-0.5	0.5	7.8	6.3	12.9	13.5	5
4.2	23	30	0.86	-1.0	0.33	6.9	4.8	15.6	12.1	-22
6.1	23	30	0.79	-2.0	0.5	8.0	6.3	13.5	13.2	-2
4.2	23	30	0.83	-6.5	0.33	7.5	6.0	16.0	13.7	-14
4.2	23	30	0.71	-1.7	0.33	9.6	7.7	13.0	13.2	2
4.2	23	30	0.83	0.07	0.5	7.9	3.8	10.8	9.3	-14
4.2	23	30	0.3	0.01	0.166	17.4	7.0	9.3	5.8	-38
4.2	23	30	0.52	0.03	0.166	13.4	4.3	6.6	6.5	-2
4.2	23	30	0.5	0.03	0.166	13.7	5.9	6.6	7.2	9
4	30	35	0.75		0.285	7.3	10.5	15.1	22	46
4	30	35	0.75		0.356	7.7	8.9	13.7	20	46
4	30	35	0.75		0.356	8.1	10.9	15.4	22	43
7	30	35	0.57		0.711	13.6	7.2	9.3	7.2	-23
7	30	35	0.75		0.569	10.1	9.5	12.2	12.4	2
7	30	35	0.74		0.996	10.0	9.1	11.9	11.5	-3
7	30	35	0.74		0.356	8.9	9.6	11.1	12.0	8
5	0.27	0.31	0.91		0.006	4.13	9.0	14.1	16.2	15
7.5	0.27	0.3	0.87		0.008	4.1	9.0	12.3	15	22

Table 2.13 Measured L_{max_w} values compared with the MM-model predictions.

S [D]	D [m]	Hub Height [m]	C_T	Stability Ri	Amount of Data [hours]	\bar{V}_a [m/s]	L_a [%]	Mea. L_w [m]	Est. L_w [m]	Rel. dev. [%]
4.2	23	30	0.44	0.04	0.33	14.2	234	59	73	24
6.1	23	30	0.67	-0.3	0.33	9.7	168	82	93	13
6.1	23	30	0.87	-0.15	0.33	6.3	114	69	92	33
6.1	23	30	0.87	-1.25	0.33	6.7	290	66	87	32
6.1	23	30	0.81	-0.5	0.5	7.8	605	70	96	37
4.2	23	30	0.86	-1.0	0.33	6.9	852	44	53	21
6.1	23	30	0.79	-2.0	0.5	8.0	490	75	99	32
4.2	23	30	0.83	-6.5	0.33	7.5	440	57	57	0
4.2	23	30	0.71	-1.7	0.33	9.6	317	60	64	7
4.2	23	30	0.83	0.07	0.5	7.9	106	36	42	17
4.2	23	30	0.3	0.01	0.166	17.4	685	132	87	-34
4.2	23	30	0.52	0.03	0.166	13.4	166	71	58	-18
4.2	23	30	0.5	0.03	0.166	13.7	137	53	59	11

Table 2.14 Measured wake deficit values compared to UPMWAKE predictions.

S [D]	D [m]	Hub Height [m]	C_T	Stability Ri	Amount of Data [hours]	\bar{V}_a [m/s]	I_a [%]	Mea. $\Delta\bar{V}$	Est. $\Delta\bar{V}$	Rel. dev. [%]
5.3	28	31	0.76	neutral	9.0	7.3	11.9	1.2	1.67	39
5.3	28	31	0.70	neutral	4.5	9.1	12.9	1.4	1.69	21
5.3	28	31	0.59	neutral	7.5	11.5	13.7	1.6	1.79	12
7.5	28	31	0.76	neutral	4.5	7.5	10.9	0.6	1.26	110
7.5	28	31	0.70	neutral	1.5	9.1	14.2	0.7	1.12	60
14.5	28	31	0.75	neutral	16.0	7.9	11.7	0.5	0.75	50
14.5	28	31	0.69	neutral	11.0	9.3	12.7	0.5	0.66	32
4.2	23	30	0.44	0.04	0.33	14.2	5.6	4.5	3.15	-30
6.1	23	30	0.67	-0.3	0.33	9.7	6.4	2.4	2.11	-12
6.1	23	30	0.81	-0.5	0.5	7.8	6.3	1.9	2.20	16
4.2	23	30	0.3	0.01	0.166	17.4	7.0	4.6	2.46	-47
4	30	35	0.75		0.285	7.3	10.5	3.6	3.58	0
4	30	35	0.75		0.356	7.7	8.9	3.6	3.83	6
4	30	35	0.75		0.356	8.1	10.9	3.5	3.93	12
7	30	35	0.57		0.711	13.6	7.2	2.8	3.19	14
7	30	35	0.75		0.569	10.1	9.5	2.7	3.85	43
7	30	35	0.74		0.996	10.0	9.1	2.3	4.02	75
7	30	35	0.74		0.356	8.9	9.6	2.3	3.35	46
5	0.27	0.31	0.91		0.006	4.13	9.0	1.05	1.63	55
7.5	0.27	0.3	0.87		0.008	4.1	9.0	1.03	1.08	5

Table 2.15 Wake turbulence intensities compared to UPMWAKE predictions.

S [D]	D [m]	Hub Height [m]	C_T	Stability Ri	Amount of Data [hours]	V_a [m/s]	I_a [%]	Mea. I_{wt} [%]	Est. I_{wt} [%]	Rel. dev. [%]
5.3	28	31	0.76	neutral	9.0	7.3	11.9	16.2	21.7	34
5.3	28	31	0.70	neutral	4.5	9.1	12.9	16.2	20.7	28
5.3	28	31	0.59	neutral	7.5	11.5	13.7	17.5	19.1	9
8.5	35	37	0.52	neutral	4.0	11.1	6.8	11.0	12.1	10
9.5	35	37	0.57	neutral		10.0	7.2	11.3	12.8	13
7.5	28	31	0.76	neutral	4.5	7.5	10.9	14.0	19.3	38
7.5	28	31	0.70	neutral	1.5	9.1	14.2	14.3	19.8	38
14.5	28	31	0.75	neutral	16.0	7.9	11.7	12.3	16.4	33
14.5	28	31	0.69	neutral	11.0	9.3	12.7	12.6	16.2	29
6.1	23	30	0.67	-0.3	0.33	9.7	6.4	11.4	15.9	39
6.1	23	30	0.81	-0.5	0.5	7.8	6.3	12.9	19.4	50
4.2	23	30	0.3	0.01	0.166	17.4	7.0	9.3	9.3	0
4	30	35	0.75		0.285	7.3	10.5	15.1	18.7	24
4	30	35	0.75		0.356	7.7	8.9	13.7	16.8	23
7	30	35	0.57		0.711	13.6	7.2	9.3	10.9	17
7	30	35	0.75		0.569	10.1	9.5	12.2	18.7	53
7	30	35	0.74		0.996	10.0	9.1	11.9	18.3	54
5	0.27	0.31	0.91		0.006	4.13	9.0	14.1	19.2	36
7.5	0.27	0.3	0.87		0.008	4.1	9.0	12.3	18.1	47

Roughly speaking the deviations between measurements and model predictions are of the same order of magnitude as for the simple models.

Turbulence intensity

The performance of the model is illustrated by the example calculations given in table 2.15.

The deviations between measurements and model predictions reflect model estimates that are somewhat more conservative than observed for the semiempirical models.

Most likely, the explanation is that wake meandering (tending to reduce deficit as well as turbulence intensity in measurements) has not been taken into account in the calculations, whereas it to some extent is included in the calibration of the simple models. This is confirmed by the fact that, generally speaking, the degree of conservatism increases with down stream distance and decreases with increasing ambient wind speed ¹⁵. Furthermore, the UPMWAKE results have larger spatial resolution than the measurements. Since maximum values are compared, the UPMWAKE turbulence intensities are expected to exceed the measured values moderately.

¹⁵The latter tendency reflects that for low wind speeds, the wind direction fluctuations are stronger.

2.4.7 Concluding remarks

The performance of 7 models has been investigated with respect to prediction of one or more of the wake characteristics : mean wind deficit, turbulence intensity, turbulence length scale, and coherence decay. Each of the wake characteristics have been represented by only one value, and the spatial distribution across the rotor plane has thus not been investigated. However, most of the models offer a spatial description of the wake deficit, and the UPMWAKE-model furthermore predict a spatial distribution of the turbulence intensity. To facilitate a comparison, Appendix G contain a graphical representation of the results embracing wake deficits and wake turbulence intensities.

Some of the models fail to represent the turbulent wake situation with $C_T > 1$ creating backflow in the wake, when momentum theory does not give a solution anymore (GCL-model and TNO-model). However, these turbulent wake situations usually occur at very low wind speeds, which make them of less practical importance as they hardly contribute to the fatigue damage. Therefore, and because none of the available measurements reflects this situation, this complex of problems has not been investigated further.

The effect of wake meandering caused by wind direction changes is obviously integrated in the (full scale) measurements and has the effect of smoothing out the wake in the mean wind direction, leading to less pronounced time averaged values of the wake characteristics. The effect is increasing with increasing distance from the upstream turbine. Most of the semiempirical models are calibrated under such conditions which makes a direct comparison with measurements meaningful. However, for models which are not adjusted to these situations conservative results is expected, especially for large rotor spacings.

Some uncertainty is related to a comparison between model prediction and measurements. This is caused both by uncertainties in the measurements¹⁶ and by uncertainties in the model input (f. ex. the C_T values in the stall region of a stall controlled turbine).

Based on the performed investigation the following general conclusions has been drawn :

- Three of the models provide information on the wake deficit – the GCL-model, the TNO-model, and the MM-model. The three models display deviations of the same order of magnitude.
- The turbulence intensity inside a wake is predicted by all the investigated models. The SF-model gives somewhat conservative results which originate from the fact that the model aim at concentrating the wake fatigue effect, from changes in all atmospheric parameters, in the turbulence intensity. Also the UPMWAKE-model seems to be somewhat conservative, which might be related to the fact that wake meandering has not been modelled in the analysis. The remaining models display acceptable deviations of the same order of magnitude.

The maximal turbulence intensity is often seen in the upper part of the rotor plane (where maximal vertical shear appears). Due to limited spatial resolution of measurements not all of these refer to maximum turbulence intensity. Usually, only one representative value of turbulence intensity can be specified in turbulence models for aeroelastic calculations. Therefore it might be suggested to recommend a model which gives slightly conservative results in the comparison.

¹⁶The 5D wind tunnel experiment performed by TNO was repeated in the Marchwood wind tunnel under seemingly identical experimental conditions. However, the measured deficits were 1.44 m/s and 1.05 m/s, respectively. The discrepancy is to some extent caused by the fact that the flow in the wind tunnel has not fully developed at the measurement positions – however, it still illustrates the uncertainty related to the measurements. The observed deviation is of the same order of magnitude as has been identified between model predictions and measurements.

- Turbulence wake length scales are only provided by the GCL–, and the MM–models. These models operate with two different definitions of the length scale, but the deviations between measurements and predictions are of the same order of magnitude.
- A simple model for estimating the coherence decay factor inside a wake is proposed. However, the model is founded on a limited data material which might affect its generality.
- The GCL–model has been extended also to handle wake–modifications of the turbulence components perpendicular to the mean wind direction, reflecting the more isotropic character of wake turbulence compared to ambient turbulence. The model extension is based on analysis of measurements and simple assumptions concerning the spectral behaviour, and it links the wake v – and w –components to the previously predicted wake u –component. However, no systematic experimental verification was performed.

In conclusion, two models (GCL–model and MM–model) initially provided information on all the relevant wind wake parameters except the coherence. The GCL–model has subsequently been extended with a simple coherence prediction module which, however, is founded on a very limited data material possibly limiting its generality. Further, the GCL–model has been extended also to handle wake–modifications of the turbulence components perpendicular to the mean wind direction.

No significant differences between the performance of the MM– and the GCL–model have been revealed in the present verification, and both of these models rest on simple engineering formulas which can be programmed very easy. Neither of the models is designed for near wake situations, and the MM–model is furthermore not valid for very large spacings. Concerning the wake length scale modification, the GCL–model reflects the observed tendency towards decreasing wake modification with increasing ambient mean wind speed.

3 WAKE LOADING

In the initial phase of the parameter investigation, calculations were performed using the *same* basic wake parameters for all the four investigated wind turbines. Having identified the key wake parameters on this basis, these were quantified in the second phase. Based on the findings in the model verification part, it was decided to use the GCL–model for prediction of wake parameters. The MM–model for wake deficit and turbulence intensity was also considered, but the performance was not found to be robust enough for the quite large variations of fundamental data (C_T , D , rotational speed etc.) corresponding to the analysed turbines.

Basically, the purpose of the present section is to verify the result obtained in the initial parameter study, but under more realistic loading conditions. Thus, the rather restrictive assumptions, put forward in that analysis, are now modified to approach the load situation defined in section 2.1. More specific, the following adjustments have been performed :

- An ambient wind gradient, corresponding to the specified turbine hub height and the ambient turbulence intensity (at hub height), is now included. A conventional logarithmic shear is presumed.
- The wake load parameters is now adjusted to depend explicitly on the individual wind turbines and operational situations (turbine spacing, ambient mean wind speed). This is accomplished by use of the GCL–wake–model.
- The influence, caused by the transversal turbulence components, is included in the description of the ambient loading as well as in the wake loading.

3.1 Method

The method applied is basically analogues to the procedure briefly described and subsequently used in the initial parameter study. However, in the present investigation a few new aspects are included, and a more thorough description is therefore appropriate.

Like the previous investigation, the present investigation is also based on the four wind turbines described in Appendices A–D. In addition to these, the medium sized stall controlled turbine, described in Appendix E, has been included in order to serve as a common reference object for a small benchmark test performed with the involved program packages.

Three different load categories have been considered for each of the investigated turbines – corresponding to (undisturbed) mean wind speeds 10 m/s, 14 m/s, and 18 m/s, which in turn represent the regimes "below stall", "stall", and "deep stall" for the stall regulated turbines.

As in the previous investigation reference sets, corresponding to wind farms with 5D spacing and 8D spacing, respectively, have been selected. However, in the present investigation the reference sets depend on the ambient mean wind speed as well as the particular turbine. The choice of wind farm spacings is believed to be representative for most existing wind farms.

For each load situation the fatigue loads, expressed in terms of equivalent moments, have been determined based on 10 minutes time series obtained from aeroelastic calculations using "state of the art" wind field generators and the aeroelastic codes PHATAS, HAWC, and VIDYN. In the simulations, the focus was

put on flapwise-, edgewise-, yaw-, and tilt moments, as well as on the thrust force, and these were subsequently analysed by means of a two-level factorial method [16].

3.1.1 Reference sets

Each set of reference situations contains one reference situation related to flat and homogeneous terrain (defined by the particular mean wind speed), and one reference situation related to the wind farm situation (5D or 8D spacing) depending on the particular turbine as well as on the particular (undisturbed) mean wind speed.

Flat terrain

The ambient situation has been defined with a turbulence intensity of the longitudinal turbulence component equal to 12 % at hub height, and a logarithmic mean wind shear consistent with this choice. The mean wind speed at altitude z , $\bar{V}_a(z)$, is thus derived from

$$\bar{V}_a(z) = \frac{I_a^u \bar{V}_a(H)}{2.5\kappa} \ln \left(\frac{z \exp(1/0.12)}{H} \right), \quad (3.1.1.1)$$

where the previously introduced notation is applied, and κ denotes the von Karman constant.

The magnitude of the energy in the transversal turbulence components are determined from expressions (2.4.1.12) and (2.4.1.13).

The u -turbulence length scale, corresponding to the Kaimal formulation given in [18], is specified to 1000 m, and assuming local isotropy in the inertial subrange for sufficiently small eddies, the ambient turbulence length scales in the v - and w -directions are determined from expressions (2.4.1.18) and (2.4.1.19).

Finally, the cross correlations between different Cartesian turbulence components have been neglected, and the coherence decay constants, corresponding to the remaining three cross correlations, were specified in accordance with expression (2.4.1.9) as an averaged compromise between values corresponding to a vertical- and a horizontal separation equal to 2/3 of the particular rotor diameter (corresponding to eddies with a size giving rise to maximal aerodynamic rotor impact).

Wake

The relevant wake situations have been determined from the GCL-model expressions outlined in section 2, and a conservative choice of the wake position has been adopted for the wake deficit, as the wake center was situated at the tip of a horizontal positioned blade (corresponding to maximal induced horizontal shear) on the side of the rotor giving the most unfavourable blade flap loads. As the applied wind field generators are not able to distinguish between vertical- and horizontal separation, the average value $C_s = 1.5$ is used in the estimation of the modified coherence decay factor describing the u -cross correlation.

3.1.2 Factorial method and calculation scheme

The basic idea in the Mounturb project [20] was to perform first order variations in each of the selected parameters. Two different expansion points, defined by each of the *reference situations*, were used.

For each turbine and for each mean wind situation, this "one-factor-at-a-time" approach requires 5 aeroelastic calculations in order to determine the requested partial derivatives related to each reference situation. For each reference set this equals 10 aeroelastic calculations. As seen, it is assumed that, over the parameter range of interest, the variables act additively on the equivalent moment. If furthermore the requested partial derivatives differ for the two reference situations contained within the same reference set, an interpretation is difficult.

To circumvent these shortcomings, a more general approach – a two level factorial design procedure [16] – is applied here. The factorial design procedure is here based on aeroelastic simulations with all possible combinations of parameter variations contained within the same reference set. In the present case this requires a total of 16 aeroelastic simulations within each reference set (describing one particular turbine operating at one particular mean wind speed situation). In return for the 6 additional simulations, compared to the "one-factor-at-a-time" approach, the following is gained :

- Each main parameter effect – an effect caused by the isolated modification of only one parameter – is determined with superior significance, as it is based on 8 realisations of differens load series instead of 2. Effectively, it means that the a main parameter effect is computed as the average of 8 gradient estimates, corresponding to 8 different expansion points.
- In case the involved parameters do *not* act additively, the method can detect and estimate interactions that quantify the particular non-additivity.

For each turbine, each reference set, and each mean wind speed the simulation matrix to be performed appears from Table 3.1 below.

Table 3.1 Specification of aeroelastic calculations. Within a given reference set, "A" denotes ambient conditions and "W" denotes wake conditions of a particular parameter.

Simulation	$\Delta\bar{V}$	$I^{u,v,w}$	$L^{u,v,w}$	a	Simulation	$\Delta\bar{V}$	$I^{u,v,w}$	$L^{u,v,w}$	a
1	A	A	A	A	9	W	A	A	W
2	A	A	A	W	10	W	A	W	A
3	A	A	W	A	11	W	W	A	A
4	A	W	A	A	12	A	W	W	W
5	W	A	A	A	13	W	A	W	W
6	A	A	W	W	14	W	W	A	W
7	A	W	A	W	15	W	W	W	A
8	A	W	W	A	16	W	W	W	W

3.1.3 Fatigue determination

Based on the results produced by the performed aeroelastic time simulations, the Rainflow Counting Procedure is used to determine the involved load cycles for each of the selected load signals. The Rainflow Counting Procedure synthesizes local maximas and minimas to load range cycles, interpreted as closed hysteresis curves in the load history of the particular material. In the present situation 50 levels were used to resolve the load range interval.

Having evaluated the Rainflow Spectrum, the fatigue effects, of the associated spectral components, are subsequently decoupled applying the Palmgren–Miner approach to concentrate the spectral information in only one number, expressing the corresponding fatigue damage. In the present analysis, the fatigue damage estimation has been based on the Wöhler exponents 4, 8, and 12. The results are presented in terms of equivalent moments giving identical fatigue damage with reference to a 1 Hz cycle frequency.

Usually, more than one (typically between 3 and 6) 10 minutes load time series are required in order to make fatigue estimates converge to an acceptable level. This is primarily due to the demand for sufficient statistical significance of the low-frequency turbulence contribution to the fatigue life consumption. However, as the postprocessing involving the two-level-factorial method averages 8 simulations to predict main effects, it is a priori expected that only one simulation of each individual load situation is sufficient. Performing a number of replicated simulations, the robustness of the results from the factorial analysis are further investigated.

Replicated simulations

In order to investigate the statistical significance of the results, based on one single aeroelastic calculation for each combination of parameters, some replicated sets of calculations were performed. By extending the set of 16 combinations, specified in Table 3.1, to a new set of 32 combinations, a fifth factor was hereby introduced – the random seed used as input for the turbulence field generator. A significant effect of this fifth factor would then indicate a need for averaging equivalent loads from several 10 min load series, using different random seeds in the involved turbulence simulations. The conclusion from this exercise was that, for this specific study, the need for replicated runs was not found to be essential. The analysis was performed using the VIDYN code, with the Nordtank 500 kW turbine as the example turbine, and covered the three mean wind speed load cases involved in the parameter analysis.

3.2 Results and Analysis

The knowledge extracted from the analysis of the replicated runs legalizes the use of 10 minutes time series representations of the involved load cases as basis for the present parameter analysis. To avoid influence from irrelevant parameter changes, all the involved turbulence fields, associated with the investigation of a particular wind turbine concept, have been generated using the same random seed.

As previously mentioned, the aeroelastic simulations involve different program packages. In order to secure a common reference for the analysis, a small benchmark test has been performed based on one of the turbines exposed to identical load cases.

Table 3.2 Benchmark results for a 5 diameter spacing. The relative changes in equivalent moments/forces are presented for the HAWC simulations (Risoe), and for the VIDYN simulations (TG).

Load Type	Wake Par.	10 m/s		14 m/s		18 m/s	
		Risoe	TG	Risoe	TG	Risoe	TG
Flap	$\Delta \bar{V}$; m=12	0.06	0.08	0.02	0.10	0.01	0.04
	$I^{u,v,w}$; m=12	0.32	0.30	0.22	0.19	0.18	0.12
	$L^{u,v,w}$; m=12	0.09	0.07	0.03	0.05	0.03	0.04
	a ; m=12	0.02	-0.06	0.02	-0.03	-0.02	0.02
Edge	$\Delta \bar{V}$; m=12	0.04	0.00	0.02	0.03	-0.01	0.01
	$I^{u,v,w}$; m=12	0.11	0.06	0.10	0.04	0.09	0.04
	$L^{u,v,w}$; m=12	0.03	0.03	0.02	0.02	0.03	0.02
	a ; m=12	0.06	0.03	0.17	0.05	0.18	0.09
Tilt	$\Delta \bar{V}$; m=4	0.01	-0.03	0.01	0.01	0.00	0.01
	$I^{u,v,w}$; m=4	0.37	0.33	0.24	0.20	0.19	0.11
	$L^{u,v,w}$; m=4	0.14	0.13	0.08	0.08	0.05	0.05
	a ; m=4	0.12	0.04	0.15	0.02	0.07	0.02
Yaw	$\Delta \bar{V}$; m=4	-0.01	0.00	-0.02	0.00	-0.01	0.00
	$I^{u,v,w}$; m=4	0.36	0.32	0.23	0.19	0.19	0.10
	$L^{u,v,w}$; m=4	0.16	0.13	0.08	0.08	0.05	0.05
	a ; m=4	0.09	0.05	0.13	0.09	0.05	0.06
Thrust	$\Delta \bar{V}$; m=4	-0.02	-0.03	-0.01	0.02	-0.01	0.02
	$I^{u,v,w}$; m=4	0.35	0.33	0.24	0.17	0.18	0.11
	$L^{u,v,w}$; m=4	0.15	0.12	0.08	0.08	0.05	0.06
	a ; m=4	0.00	-0.01	0.06	0.08	0.03	0.08

3.2.1 Benchmark

The Nordtank 500 kW turbine was used as example turbine for the validation of the simulation packages, and the investigated load cases correspond to the load cases involved in the parameter analysis. Only two of the codes, HAWC (Risoe) and VIDYN (Teknik Gruppen), were involved in the benchmark test, as the time did not permit ECN to finetune FATAS to the Nordtank 500 kW turbine simulations.

The results obtained from the HAWC and VIDYN simulations are presented in Table 3.2 and in Table 3.3 below, where the relative changes in equivalent moments/forces, caused by the specified wake parameter variations, are presented. For the blade material, the Wöhler exponent $m = 12$ was considered representative, whereas for the tower loading, a Wöhler exponent equal to 4 was selected.

In general there is an acceptable degree of agreement between results produced by the two codes for the 5D spacing. However, there is a tendency of increasing discrepancies with increasing mean wind speed. The phenomenon is especially pronounced for the "deep stall" load situation, and it might thus be associated with different stall modeling. For the "below stall" and "stall" regimes the agreement is good, except for the relative increase in flap- and tilt moments caused by the coherence decay variation and for the relative increase in the edge moment originating from the turbulence intensity variation. The latter might be caused by different structural damping in the edge wise direction where the aerodynamic

Table 3.3 Benchmark results for a 8 diameter spacing. The relative changes in equivalent moments/forces are presented for the HAWC simulations (Risoe), and for the VIDYN simulations (TG).

Load Type	Wake Par.	10 m/s		14 m/s		18 m/s	
		Risoe	TG	Risoe	TG	Risoe	TG
Flap	$\Delta \bar{V}$; m=12	0.04	0.02	0.01	0.04	0.01	0.00
	$I^{u,v,w}$; m=12	0.26	0.24	0.16	0.14	0.15	0.08
	$L^{u,v,w}$; m=12	0.06	0.05	0.03	0.05	0.02	0.02
	a ; m=12	0.00	0.00	0.00	0.00	0.00	0.00
Edge	$\Delta \bar{V}$; m=12	0.03	0.00	0.01	0.01	0.00	0.01
	$I^{u,v,w}$; m=12	0.06	0.04	0.06	0.03	0.03	0.02
	$L^{u,v,w}$; m=12	0.02	0.02	0.02	0.02	0.01	0.01
	a ; m=12	0.00	0.00	0.00	0.00	0.00	0.00
Tilt	$\Delta \bar{V}$; m=4	0.00	-0.02	0.00	-0.01	0.00	0.01
	$I^{u,v,w}$; m=4	0.29	0.25	0.18	0.14	0.15	0.08
	$L^{u,v,w}$; m=4	0.12	0.10	0.06	0.06	0.03	0.04
	a ; m=4	0.00	0.00	0.00	0.00	0.00	0.00
Yaw	$\Delta \bar{V}$; m=4	-0.01	0.00	-0.01	-0.01	0.00	0.00
	$I^{u,v,w}$; m=4	0.28	0.25	0.18	0.14	0.15	0.07
	$L^{u,v,w}$; m=4	0.13	0.10	0.06	0.06	0.03	0.03
	a ; m=4	0.00	0.00	0.00	0.00	0.00	0.00
Thrust	$\Delta \bar{V}$; m=4	-0.01	0.00	0.00	0.01	-0.01	0.00
	$I^{u,v,w}$; m=4	0.28	0.26	0.19	0.13	0.15	0.08
	$L^{u,v,w}$; m=4	0.12	0.08	0.05	0.06	0.03	0.03
	a ; m=4	0.00	0.00	0.00	0.00	0.00	0.00

damping is modest.

In the 8D spacing situation the agreement is very convincing, resulting in an identical mutual ranking of the involved parameters regarding fatigue life consumption in wake situations. However, also in the 8D situation, the turbulence intensity variation in the "deep stall" situation display some differences.

3.2.2 Results

The described parameter analysis has been performed for the four different wind turbines introduced previously. From the analysis it appears, that the effects, originating from the investigated parameter variations, act approximately additively. In the tables 3.4 through 3.23 the relative changes in equivalent moments/forces, originating from the specified single parameter variations, are presented for the involved load cases and turbines, based on selected representative Wöhler exponents.

The notation in the tables is to be interpreted as follows : "Pitch; 5D" refers to results associated with the Vestas V27 turbine and a 5D turbine spacing, "Var.; 5D" refers to results associated with the artificial 500 kW variable speed turbine and a 5D turbine spacing, "Stall; 5D" refers to results associated with the Danwin 180 kW turbine and a 5D turbine spacing, and "2-BL; 5D" refers to results associated with the

Näsudden turbine and a 5D turbine spacing. The 8D spacing examples are indicated analogues with "5D" replaced by "8D".

Table 3.4 Relative increase in equivalent flapwise moment based on Wöhler exponent 12 and caused by the wake deficit.

Load Case	10 m/s	14 m/s	18 m/s
Pitch; 5D	2%	0%	1%
Var.; 5D	-8%	3%	0%
Stall; 5D	7%	9%	1%
2-Bl.; 5D	5%	0%	4%
Pitch; 8D	1%	-1%	1%
Var.; 8D	-9%	1%	0%
Stall; 8D	0%	8%	2%
2-Bl.; 8D	5%	-6%	2%

Table 3.5 Relative increase in equivalent edgewise moment based on Wöhler exponent 12 and caused by the wake deficit.

Load Case	10 m/s	14 m/s	18 m/s
Pitch; 5D	3%	1%	1%
Var.; 5D	-7%	-3%	-3%
Stall; 5D	2%	1%	-1%
2-Bl.; 5D	2%	3%	1%
Pitch; 8D	3%	0%	1%
Var.; 8D	-5%	-2%	-2%
Stall; 8D	1%	1%	-1%
2-Bl.; 8D	1%	2%	1%

Table 3.6 *Relative increase in equivalent tilt moment based on Wöhler exponent 4 and caused by the wake deficit.*

Load Case	10 m/s	14 m/s	18 m/s
Pitch; 5D	-2%	0%	0%
Var.; 5D	-11%	-1%	-1%
Stall; 5D	-2%	3%	2%
2-Bl.; 5D	12%	9%	3%
Pitch; 8D	-1%	0%	0%
Var.; 8D	-10%	1%	0%
Stall; 8D	4%	1%	0%
2-Bl.; 8D	7%	7%	2%

Table 3.7 *Relative increase in equivalent yaw moment based on Wöhler exponent 4 and caused by the wake deficit.*

Load Case	10 m/s	14 m/s	18 m/s
Pitch; 5D	-3%	-1%	0%
Var.; 5D	-12%	1%	0%
Stall; 5D	-5%	-3%	1%
2-Bl.; 5D	5%	7%	2%
Pitch; 8D	-2%	0%	0%
Var.; 8D	-9%	1%	0%
Stall; 8D	3%	-2%	1%
2-Bl.; 8D	4%	3%	2%

Table 3.8 *Relative increase in equivalent thrust force based on Wöhler exponent 4 and caused by the wake deficit.*

Load Case	10 m/s	14 m/s	18 m/s
Pitch; 5D	-1%	-1%	0%
Var.; 5D	-31%	2%	-2%
Stall; 5D	-1%	3%	-7%
2-Bl.; 5D	-25%	-14%	-5%
Pitch; 8D	1%	0%	0%
Var.; 8D	-24%	0%	-2%
Stall; 8D	-10%	-7%	3%
2-Bl.; 8D	-17%	-12%	-3%

Table 3.9 Relative increase in equivalent flapwise moment based on Wöhler exponent 12 and caused by modified turbulence intensity.

Load Case	10 m/s	14 m/s	18 m/s
Pitch; 5D	31%	17%	12%
Var.; 5D	33%	13%	7%
Stall; 5D	24%	22%	10%
2-Bl.; 5D	26%	16%	9%
Pitch; 8D	24%	11%	11%
Var.; 8D	26%	10%	5%
Stall; 8D	2%	9%	9%
2-Bl.; 8D	22%	12%	7%

Table 3.10 Relative increase in equivalent edgewise moment based on Wöhler exponent 12 and caused by modified turbulence intensity.

Load Case	10 m/s	14 m/s	18 m/s
Pitch; 5D	3%	2%	3%
Var.; 5D	2%	2%	1%
Stall; 5D	2%	2%	1%
2-Bl.; 5D	4%	5%	3%
Pitch; 8D	0%	1%	2%
Var.; 8D	1%	1%	1%
Stall; 8D	1%	2%	1%
2-Bl.; 8D	3%	3%	2%

Table 3.11 Relative increase in equivalent tilt moment based on Wöhler exponent 4 and caused by modified turbulence intensity.

Load Case	10 m/s	14 m/s	18 m/s
Pitch; 5D	31%	17%	12%
Var.; 5D	40%	17%	8%
Stall; 5D	24%	20%	13%
2-Bl.; 5D	20%	16%	8%
Pitch; 8D	22%	13%	10%
Var.; 8D	32%	14%	6%
Stall; 8D	4%	15%	10%
2-Bl.; 8D	17%	12%	6%

Table 3.12 *Relative increase in equivalent yaw moment based on Wöhler exponent 4 and caused by modified turbulence intensity.*

Load Case	10 m/s	14 m/s	18 m/s
Pitch; 5D	35%	21%	15%
Var.; 5D	41%	18%	8%
Stall; 5D	19%	14%	11%
2-Bl.; 5D	21%	13%	5%
Pitch; 8D	25%	16%	14%
Var.; 8D	33%	14%	7%
Stall; 8D	7%	10%	8%
2-Bl.; 8D	18%	10%	4%

Table 3.13 *Relative increase in equivalent thrust force based on Wöhler exponent 4 and caused by modified turbulence intensity.*

Load Case	10 m/s	14 m/s	18 m/s
Pitch; 5D	40%	22%	15%
Var.; 5D	37%	16%	8%
Stall; 5D	27%	16%	6%
2-Bl.; 5D	19%	19%	7%
Pitch; 8D	29%	17%	13%
Var.; 8D	28%	12%	6%
Stall; 8D	3%	12%	4%
2-Bl.; 8D	13%	13%	6%

Table 3.14 *Relative increase in equivalent flapwise moment based on Wöhler exponent 12 and caused by modified turbulence length scale.*

Load Case	10 m/s	14 m/s	18 m/s
Pitch; 5D	6%	0%	1%
Var.; 5D	0%	1%	0%
Stall; 5D	7%	4%	5%
2-Bl.; 5D	7%	4%	3%
Pitch; 8D	5%	-1%	0%
Var.; 8D	2%	1%	1%
Stall; 8D	3%	5%	3%
2-Bl.; 8D	5%	4%	1%

Table 3.15 Relative increase in equivalent edgewise moment based on Wöhler exponent 12 and caused by modified turbulence length scale.

Load Case	10 m/s	14 m/s	18 m/s
Pitch; 5D	1%	1%	0%
Var.; 5D	0%	0%	0%
Stall; 5D	1%	1%	1%
2-Bl.; 5D	2%	2%	2%
Pitch; 8D	-2%	0%	-1%
Var.; 8D	0%	0%	0%
Stall; 8D	1%	1%	0%
2-Bl.; 8D	1%	1%	1%

Table 3.16 Relative increase in equivalent tilt moment based on Wöhler exponent 4 and caused by modified turbulence length scale.

Load Case	10 m/s	14 m/s	18 m/s
Pitch; 5D	13%	5%	1%
Var.; 5D	2%	0%	1%
Stall; 5D	13%	8%	6%
2-Bl.; 5D	8%	5%	4%
Pitch; 8D	9%	3%	0%
Var.; 8D	3%	2%	2%
Stall; 8D	4%	6%	4%
2-Bl.; 8D	7%	5%	3%

Table 3.17 Relative increase in equivalent yaw moment based on Wöhler exponent 4 and caused by modified turbulence length scale.

Load Case	10 m/s	14 m/s	18 m/s
Pitch; 5D	16%	6%	2%
Var.; 5D	3%	1%	0%
Stall; 5D	10%	6%	5%
2-Bl.; 5D	8%	4%	3%
Pitch; 8D	10%	4%	0%
Var.; 8D	4%	2%	2%
Stall; 8D	5%	4%	4%
2-Bl.; 8D	7%	3%	2%

Table 3.18 Relative increase in equivalent thrust force based on Wöhler exponent 4 and caused by modified turbulence length scale.

Load Case	10 m/s	14 m/s	18 m/s
Pitch; 5D	15%	7%	3%
Var.; 5D	2%	1%	1%
Stall; 5D	11%	7%	3%
2-Bl.; 5D	6%	2%	2%
Pitch; 8D	11%	4%	1%
Var.; 8D	3%	3%	2%
Stall; 8D	2%	2%	2%
2-Bl.; 8D	4%	3%	1%

Table 3.19 Relative increase in equivalent flapwise moment based on Wöhler exponent 12 and caused by modified coherence decay.

Load Case	10 m/s	14 m/s	18 m/s
Pitch; 5D	-1%	-6%	-2%
Var.; 5D	-4%	-5%	3%
Stall; 5D	-2%	-1%	-2%
2-Bl.; 5D	-4%	-8%	-1%
Pitch; 8D	0%	0%	0%
Var.; 8D	0%	0%	0%
Stall; 8D	0%	0%	0%
2-Bl.; 8D	0%	0%	0%

Table 3.20 Relative increase in equivalent edgewise moment based on Wöhler exponent 12 and caused by modified coherence decay.

Load Case	10 m/s	14 m/s	18 m/s
Pitch; 5D	1%	4%	7%
Var.; 5D	0%	0%	0%
Stall; 5D	1%	1%	1%
2-Bl.; 5D	0%	0%	0%
Pitch; 8D	0%	0%	0%
Var.; 8D	0%	0%	0%
Stall; 8D	0%	0%	0%
2-Bl.; 8D	0%	0%	0%

Table 3.21 Relative increase in equivalent tilt moment based on Wöhler exponent 4 and caused by modified coherence decay.

Load Case	10 m/s	14 m/s	18 m/s
Pitch; 5D	8%	9%	7%
Var.; 5D	8%	8%	7%
Stall; 5D	3%	4%	0%
2-Bl.; 5D	-3%	-5%	-4%
Pitch; 8D	0%	0%	0%
Var.; 8D	0%	0%	0%
Stall; 8D	0%	0%	0%
2-Bl.; 8D	0%	0%	0%

Table 3.22 Relative increase in equivalent yaw moment based on Wöhler exponent 4 and caused by modified coherence decay.

Load Case	10 m/s	14 m/s	18 m/s
Pitch; 5D	8%	3%	-6%
Var.; 5D	9%	10%	11%
Stall; 5D	5%	3%	2%
2-Bl.; 5D	-12%	-14%	-10%
Pitch; 8D	0%	0%	0%
Var.; 8D	0%	0%	0%
Stall; 8D	0%	0%	0%
2-Bl.; 8D	0%	0%	0%

Table 3.23 Relative increase in equivalent thrust force based on Wöhler exponent 4 and caused by modified coherence decay.

Load Case	10 m/s	14 m/s	18 m/s
Pitch; 5D	7%	9%	6%
Var.; 5D	-1%	12%	17%
Stall; 5D	-2%	-4%	-2%
2-Bl.; 5D	0%	0%	5%
Pitch; 8D	0%	0%	0%
Var.; 8D	0%	0%	0%
Stall; 8D	0%	0%	0%
2-Bl.; 8D	0%	0%	0%

3.2.3 Discussion

A number of qualitative findings can be extracted from the analysis. The wind field modifications caused by the wake, and quantified in section 2, all tend to diminish with increasing wind turbine spacing. This behaviour is also reflected in the life time consumption, as a general tendency of decreasing wake effects, from the 5D situation to the 8D situation, is observed. The turbulence intensity– and the length scale modifications are seen to decrease for increasing wind speed, and this behaviour is also reflected in the investigated equivalent moments/forces.

The fatigue load dependance of the mean wind deficit with the mean wind speed is more complicated, as three factors contribute simultaneously – decrease in mean wind speed, introduction of horizontal shear, and modification of the vertical shear. In contradiction to the fatigue loading, caused by wake turbulence intensity, the fatigue loading associated with the wake deficit indicates no general tendency with the mean wind speed for the investigated turbine concepts and load types.

Tilt– and yaw moments exhibit the same behaviour except for the two–bladed turbine, where the increased wake coherence decay results in significant differences. The two–bladers are, however, born with distinct periodic properties of the rotor inertia often introducing phase–shifts in the turbine loads, even for very modest changes in the mechanical properties. These phase–shifts often affect the loading in an unexpected way, and the discrepancy between the tilt– and yaw loading, arising from an increased coherence in the turbulence field, is believed to originate from such a phenomenon.

All the four investigated parameters were demonstrated to be significant in relation to fatigue life consumption. However, in most of the investigated situations the effect originating from increase in the turbulence intensity dominates the other parameter effects with a factor of 2–3.

It is moreover evident that different turbine concepts act differently with respect to a particular parameter sensitivity, and that this also applies for different load types. More specific it is seen that the induced wake deficit generally is favourable for the thrust force, whereas it, for the majority of the investigated turbine concepts, introduces increased blade– and rotor fatigue loading.

Finally, it is observed that the increased wake coherence decay is favourable for the flap root moment, whereas increased wake turbulence intensity is in general introducing higher fatigue loading.

4 CONCLUSIONS

The present report deals with the establishment of a procedure for wake load predictions, and its possible inclusion in the IEC-code framework. The overall philosophy is to preserve the existing division in four wind turbine classes, and simply supplement the existing load specifications with quantitative wake load specifications.

The study is confined to single wake situations, but is anticipated to apply also for multiple wake situations. A detailed investigation has been performed to quantify the wake load situation. The investigation falls into three phases – a crude identification of key wake wind field parameters, a quantification of the identified key parameters, and finally a detailed key parameter identification based on predicted wake characteristics.

Applying a two-level-factorial method it has been demonstrated that, in the present analysis, 10-minutes simulation time series are a sufficient representation of the individual load situations to yield significant results.

The main findings from the investigation are :

- That all four investigated parameters – representing wake deficit, wake turbulence intensity, wake turbulence length scale, and wake coherence – were demonstrated to be significant in relation to increased fatigue life consumption in wakes compared to ambient conditions.
- That it is possible to quantify the relevant wake parameters by use of simple models.
- That the fatigue impact, caused by the investigated four parameters, are shown to act additively, which imply that a simple approximative method, involving only a very limited number of aeroelastic calculations, can be applied for fatigue estimates taking into account the detailed wind farm topology and the particular wind turbine concept [17].
- That the effect due to increased turbulence intensity is crucial and usually dominates the fatigue effects caused by the other investigated parameters with a factor of 2–3.
- That different turbine concepts and different load types act differently with respect to parameter sensitivity – this fact demonstrates the appropriateness in a detailed wake load estimation based on the philosophy applied here, compared to the "all factors in one parameter" approach previously used.

5 RECOMMENDATIONS

The present section deals with inclusion of wake load description in the IEC-code framework and contains, in a condensed version, the recommendations resulted from the present investigations.

When operating in a wake situation, the mean wind profile as well as the turbulence characteristics experienced by a turbine are modified compared to the ambient situation. The significant modifications are quantified in the following four subsections.

5.1 Mean Wind Deficit

The wake deficit in the mean wind direction, $\Delta\bar{V}$, and the wake extension, expressed in terms of the wake radius, R_w , are estimated according to the following expressions :

$$R_w = \left(\frac{35}{2\pi}\right)^{\frac{1}{5}} (3c_1^2)^{\frac{1}{5}} (C_T A(x + x_0))^{\frac{1}{5}},$$

$$\Delta\bar{V} = -\frac{\bar{V}_a}{9} (C_T A(x + x_0)^{-2})^{\frac{1}{3}} \left\{ r^{\frac{3}{2}} (3c_1^2 C_T A(x + x_0))^{-\frac{1}{2}} - \left(\frac{35}{2\pi}\right)^{\frac{3}{10}} (3c_1^2)^{-\frac{1}{5}} \right\}^2,$$

where x and r denote axial and radial directions, A is the rotor area, C_T denotes the rotor drag coefficient, \bar{V}_a the ambient mean wind velocity at hub height, and c_1 and x_0 are parameters approximated by :

$$x_0 = \frac{9.5D}{\left(\frac{2R_{9.5}}{D}\right)^3 - 1},$$

$$c_1 = \left(\frac{D}{2}\right)^{-\frac{1}{2}} (c_T A x_0)^{-\frac{5}{6}},$$

where D is the diameter of the upstream rotor. Denoting the ambient turbulence intensity by I_a and the hub height by H , $R_{9.5}$ is determined from :

$$R_{9.5} = \frac{1}{2} (R_{nb} + \min(H, R_{nb})),$$

$$R_{nb} = \max(1.08D, 1.08D + 21.7D(I_a - 0.05)).$$

The wake effect on the mean flow in directions perpendicular to the mean wind direction shall not be considered.

5.2 Turbulence Intensity

At down stream distances corresponding to traditional spacing in wind farms it is *assumed* that only the surface- and wake shear mechanisms contribute significantly to turbulence production. It is moreover

assumed that the turbulence fluctuations originating from these two sources are *statistically independent* such that the turbulent energies are additive in the energy sense. Normalizing with respect to the undisturbed mean wind velocity, \bar{V}_a , the *total* turbulence intensity of the along wind turbulence component in the wake, I_{wt}^u , is expressed as :

$$I_{wt}^u = \sqrt{I_a^2 + I_w^2},$$

where subscripts a and w refer to ambient and wake, respectively. The specific *wake contribution*, I_w , depends on both the down wind distance and the undisturbed mean wind velocity and is (for spacings larger than two rotor diameters) determined as :

$$I_w = 0.29 S^{-1/3} \sqrt{1 - \sqrt{1 - C_T}},$$

where S denotes the spacing expressed in rotor diameters.

Compared to ambient situations the wake turbulence tends to be more isotropic, and the energy content in the transversal turbulence components, v and w , are determined from :

$$\sigma_w^v \simeq 0.8 I_{wt}^u \bar{V}_a,$$

$$\sigma_w^w \simeq 0.6 I_{wt}^u \bar{V}_a,$$

where subscript "w" indicate wake-values.

5.3 Turbulence Length Scales

When the two shear turbulence contributions have scales of comparable orders of magnitude, it is reasonable to expect the resulting spectral shape to be qualitatively invariant. However, the resulting length scale is modified. The modified length scale depends on the rotor thrust coefficient, the spacing distance, the rotor diameter, and the undisturbed turbulence length scale.

Referring to the Kaimal formulation of the turbulence spectrum given in [18], the length scale for the u turbulence component inside the wake, L_w^u , is expressed as :

$$L_w^u = L_a^u \left(1 - \min \left(\frac{12.2 \left(1 - \frac{D}{L_a^u} \right)}{\bar{V}_a S_r^{0.6}}, 0.9 \right) \right),$$

where L_a^u denotes the u -turbulence length scale in the undisturbed flow, and S_r is defines as :

$$S_r = 2^{0.8} + (S - 2)^{0.8} \quad \text{for } S \geq 2.$$

Assuming local isotropy in the inertial subrange for sufficiently small eddies, the following relations can be derived for the wake turbulence length scales in the v - and w -directions :

$$\begin{aligned} L_w^v &= 0.33L_w^u \\ L_w^w &= 0.14L_w^u . \end{aligned}$$

5.4 Coherence Decay Factors

Assuming a Davenport-formulation of the coherence, the uu -coherence decay factor related to wake turbulence, a_w , shall determined according to :

$$a_w = \begin{cases} (1 + K_w)a_a & \text{for } 2 \leq S < 7.5 \\ a_a & \text{for } 7.5 \leq S \end{cases} ,$$

where a_a is the coherence decay factor related to ambient conditions, and the wake correction factor, K_w , is given by

$$K_w = \begin{cases} \frac{7.5-S}{5.5} & \text{for } \bar{V}_a < 6 \\ \frac{7.5-S}{5.5} \left(\frac{1}{3} \bar{V}_a - C_s \right) & \text{for } 6 \leq \bar{V}_a \leq 15 \\ \frac{4(7.5-S)}{5.5} & \text{for } 15 < \bar{V}_a \end{cases} .$$

For vertical separation $C_s \equiv 1$ and for horizontal separation $C_s \equiv 2$. For spacings less than 2 rotor diameters the value of the wake coherence decay factor is assumed to equal the value related to a 2 diameter spacing.

ACKNOWLEDGEMENTS

The work has been supported by the European Commission under contract JOR-CT95-00642. Stimulating discussions and assistance from our colleague Per Vølund, Wind Energy and Atmos. Phys. Dept., Risø National Laboratory, is furthermore acknowledged. Last but not least the contribution of Mikael Magnusson, Department of Meteorology, Uppsala University, is appreciated.

References

- [1] Adams, B.M. (1996). Dynamic loads in Wind Farms 2. Final report of Joule project JOU2-CT92-0094. GH-report 286/R/1, Garrad Hassan & Partners.
- [2] Larsen, G.C., Højstrup, J., and Madsen, H.Aa. (1996). Wind Fields in Wakes. EUWEC'96, Göteborg 1996.
- [3] Frandsen, S. et. al. (1996). Measurements on and Modelling of Offshore Wind Farms. Risoe-R-903(EN).
- [4] Verheij, F.J. (1993) Wind Data for Design of Wind Turbines Operating in Wind Farms (in Dutch). TNO – Environmental and Energy Research, 93-189.
- [5] Magnusson, M. (1996). Wind turbine "Wakes". Ph.d. dissertation, Acta Universitatis Upsaliensis, Uppsala.
- [6] Crespo, A. et al. (1985). Numerical Analysis of Wind Turbine Wakes. Proc. of the Delphi Workshop on Wind Energy Applications.
- [7] Patankar, S.V. and Spalding, D.B. (1972). A Calculation Procedure for Heat, Mass and Momentum Transfer in Three Dimensional Parabolic Flows. Int. Journal of Heat and Mass Transfer, Vol. 15.
- [8] Panofsky, H.A. and Dutton, J.A. (1983). Atmospheric Turbulence. John Wiley & Sons.
- [9] Højstrup, J. and Noergaard, P. (1990). Taendpibe Wind Farm Measurements 1988. Risoe-M-2894.
- [10] Papaconstantinou, A. and Bergeless, G. (1988). Hot-wire measurements of the flow field in the vicinity of a HAWG rotor. Journal of Wind Engineering and Industrial Aerodynamics, 31, p. 133-146.
- [11] Smith, D. (1990). Multiple wake measurements and analysis. Proceedings of 12'th BWEA Conference.
- [12] Tindal, A.J. (1993). Dynamic loads in wind farms I. GH-report 205/R/12, Garrad Hassan & Partners.
- [13] Seignette P.F.A.B (1996). On-line PVOPT user's manual, version 1.2. Netherlands Energy Research Foundation, ECN.
- [14] Schepers, J.G. (1996). PVOPT, Theory and test cases. ECN-C-96-057, Netherlands Energy Research Foundation, ECN.
- [15] Schepers, J.G. (1996). Design of variable speed turbine to be used in the WF-PNL program. Netherlands Energy Research Foundation, ECN.
- [16] Box, G.E.P. et al.(1978). Statistics for Experimenters – An Introduction to Design, Data Analysis, Data Analysis, and Model Building. John Wiley & Sons.
- [17] Petersen, S.M. et al. (1997). EWTS II – Load Spectra and Extreme Wind Conditions. EWEC'97, Dublin 1997.
- [18] Danish Code of Practice DS472 (1992). Loads and Safety of Wind Turbine Structures (in Danish). Teknisk Forlag.

- [19] Alberts, A. and Söker, H. (1997). Wind Speed and Turbulence Evaluations from Power data and the Nacelle Anemometer.
- [20] Fragoulis, A. et al. (1996). MOUNTURB FINAL REPORT – Load and Power Measurement Program on Wind Turbines Operating in Complex Mountaneous Regions. Final report of Joule project JOU2–CT93–0378. CRES.

A VESTAS V27 TURBINE

The present appendix contains a brief description of the V27 wind turbine, which is representing the pitch regulated turbine concept in the performed wake parameter analysis. Basically, the V27 turbine is a three bladed upwind horizontal axis wind turbine with active yaw and a high speed rotor. The main specifications of the turbine is given in Table A.1 below.

Table A.1 Main specifications for the Vestas V27 turbine.

ROTOR	
Power regulation	Pitch
Number of blades	3
Rotor diameter	27.00 m
Swept area	573 m ²
Hub height	28.65 m
Rotor speed	44 rpm/33 rpm
Blade tip angle	0° – 90° during operation
BLADES	
Manufacturer	Vestas
Spar and shell material	GRP
Total blade length	13.00 m
Profiled blade length	11.50 m
Root chord	1.30 m
Tip chord	0.50 m
Blade twist	13.0°
Blade profiles	NACA 63–600
First flapwise natural frequency	2.38 Hz
First edgewise natural frequency	3.41 Hz
GEAR BOX	
Gear ratio	1 : 27.6
GENERATOR	
Manufacturer	Siemens; double winding
Nominal power	225 kW
Voltage	480 V AC
Frequency	60 Hz
Rotational speed	1210 rpm (225 kW) / 910 rpm (50 kW)
TOWER	
Type	Lattice tower
Height	27.43 m
First bending natural frequency	1.31 Hz
CONTROL SYSTEM	
Manufacturer	Vestas
Cut-in wind speed	3.7 m/s
Cut-out wind speed	25.0 m/s

Table A.1 Main specifications for the Vestas V27 turbine (cont).

WEIGHTS	
Blade	≈ 600 kg
Rotor	≈ 2900 kg
Nacelle excl. rotor	≈ 7900 kg
Tower	≈ 600 kg
Total	≈ 19700 kg

A Theoretical thrust curve, which is vital for the quantification of wake effects, has been supplied from the manufacturer and is presented in Table A.2.

Table A.2 Calculated thrust curve for the Vestas V27 turbine.

Mean wind speed [<i>m/s</i>]	Thrust [<i>kN</i>]	Thrust coefficient C_T
3.5	3.8	0.88
4.0	4.9	0.88
5.0	7.7	0.88
6.0	10.0	0.79
7.0	12.5	0.73
8.0	18.0	0.80
9.0	21.0	0.74
10.0	24.6	0.70
11.0	26.7	0.63
12.0	27.8	0.55
13.0	26.7	0.45
14.0	22.7	0.33
15.0	20.5	0.26
16.0	18.9	0.21
17.0	17.2	0.17
18.0	17.0	0.15
19.0	15.2	0.12
20.0	15.4	0.11
21.0	13.9	0.09
22.0	13.6	0.08
23.0	13.0	0.07
24.0	12.1	0.06
25.0	13.2	0.06

Note, that the jump in C_T between the mean wind speeds 7 m/s and 8 m/s is caused by shift between generators.

B VARIABLE SPEED 500 KW TURBINE

The present appendix contains a brief description of an artificial wind turbine which represents the variable speed regulated turbine concept in the wake parameter analysis. The defined turbine is a three bladed, 500 kW, upwind horizontal axis wind turbine.

B.1 Background

The turbine has been designed in the ECN Basic Subsidy project "FyndFarm". The design is derived from the fixed speed, stall and pitch regulated, turbines which have been used in the development of wind farm design guidelines in the Dynamic Loads in Wind Farms II (DLWF-II) project [1]¹⁷.

Obviously, the design of these DLWF-II turbines needed some adjustment in order to account for variable speed operation :

- An optimal tip speed ratio ($\lambda_{design} = 7.5$) operation is assumed up to rated wind speed.
- Above V_{rated} the rotor speed and power are regulated by means of a pitch control algorithm. This algorithm is based on the one which is used for the constant speed, pitch regulated DLWF-II turbine.
- The aerodynamic design (chord and twist distribution) is found from an aerodynamic optimization, using the program PVOPT, [13] and [14].
- The mass and stiffness distributions are almost similar to the distributions of the DLWF-II turbines. However, some slight modifications were required in order to avoid operation a first flapwise natural frequency of 3P at rated conditions.

It should be noted that for the present study, only blade flexibility in the flapwise direction was taken into account. Hence the blade flexibility in the edgewise direction, the tower flexibility, and the drive train flexibility have been neglected.

The main specifications of the turbine are given in Table B.1. For a more detailed design report, reference is made to [15]. The calculated (stationary) thrust, power, pitch angle, and rotor speed are presented in Table B.2 as function of wind speed.

¹⁷See section 6.

Table B.1 Main specifications for the 500 kW variable speed turbine.

ROTOR	
Power regulation	Pitch / Variable speed
Number of blades	3
Rotor diameter	37.00 m
Swept area	1075 m ²
Hub height	34.95 m
Rotor speed range	20.2 rpm – 46.0 rpm; see also Table B.2
Tilt	2 deg
Coning	0 deg
Direction of rotation	Clockwise
BLADES	
Total blade length	18.5 m
Profiled blade length	15.0 m
Root chord	2.150 m
Tip chord	0.765 m
Blade twist	12.625 deg
Blade profiles	NACA 632xxx (inner) / NACA 634xxx (outer)
First flapwise natural frequency	2.239 Hz (standstill)
GEAR BOX	
Gear ratio	1 : 39.1
GENERATOR; see also section B.3	
Nominal power	500 kW
TOWER	
Type	Tapered tubular tower
Height	34.95 m
Top diameter	1.68 m
Base diameter	2.41 m
CONTROL SYSTEM, see also section B.4	
Cut-in wind speed	5 m/s
Rated wind speed	11.9 m/s
Cut-out wind speed	23 m/s
WEIGHTS	
Blade	1853 kg
Rotor incl. hub	8780 kg

Table B.2 Stationary rotor characteristics.

V [m/s]	$C_{P,aer}$	C_T	P_{aer} [kW]	Thrust [kN]	θ [deg]	Ω [rpm]
5.000	0.494	0.855	40.690	14.080	0.000	20.211
6.000	0.494	0.850	70.340	20.140	0.000	23.967
7.000	0.496	0.835	112.000	26.940	0.000	26.982
8.000	0.496	0.837	167.100	35.260	0.000	30.954
9.000	0.496	0.829	238.100	44.220	0.000	34.241
10.000	0.496	0.837	326.400	55.110	0.000	38.719
11.000	0.496	0.836	434.500	66.650	0.000	42.542
12.000	0.495	0.787	563.800	74.660	0.810	46.017
13.000	0.381	0.498	550.700	55.430	4.962	46.101
14.000	0.306	0.380	552.500	49.100	6.977	46.108
15.000	0.250	0.303	555.500	44.850	8.638	46.122
16.000	0.207	0.247	558.600	41.660	10.099	46.138
17.000	0.174	0.206	562.200	39.140	11.441	46.155
18.000	0.147	0.174	566.000	37.100	12.695	46.173
19.000	0.126	0.149	570.400	35.420	13.883	46.195
20.000	0.109	0.129	574.900	33.990	15.019	46.221
21.000	0.093	0.111	568.300	32.180	16.184	46.015
22.000	0.079	0.095	552.500	30.140	17.352	45.797
23.000	0.068	0.082	542.700	28.600	18.447	45.668

B.2 Rated Conditions and Losses

The losses at rated conditions remained unchanged from the losses of the DLWF-II turbines ($\approx 7\%$). As a consequence, the rated aerodynamic power was 537.5 kW, which resulted in a rated wind speed of 11.9 m/s. The rated rotorspeed was 46.03 rpm, see also Table B.2.

B.3 Generator curve

The generator curve (i.e. the generator power vs. the rotational speed) is basically a conventional third order curve. Above the rated power of 500 kW, the generator power is kept constant. Some modifications have been applied, in order to avoid operation at a rotational speed which is close to a multiple of the first flapwise natural frequency.

B.4 Pitch control

Above rated conditions it is attempted to keep the rotor speed (and consequently the power) at its rated values by means of a pitch control. The pitch control algorithm is almost similar to the one which was used to control the power of the fixed speed DLWF-II turbine; see [1] :

- PI proportional gain = $8.448 \cdot 10^{-7}$ rad/W.
- PI integral gain = $7.04 \cdot 10^{-6}$ rad/(Ws).
- Gain scheduling via pitch angle with scheduling factor equal to $\frac{1}{0.6375+20.77 \cdot \theta}$.
- Limits on schedule factor : $0.08677 < \text{fact} < 1$.
- The controller has been designed with a first order pitch actuator response with a time constant equal to 0.3 s.

However, for the present purpose, the controller should act on the rotor speed instead of the power. To this end, a dependency is introduced between the generator power set point and the rotor speed: if the rotor speed exceeds the rated value of 46.03 rpm, the set point is reduced with ΔP :

$$P_{\text{set}} = P_{\text{rated}} - \Delta P ,$$
$$\Delta P = k_n \int_0^T (\Omega - \Omega_{\text{rated}}) \cdot dt \quad (\Omega \text{ in rad/s}) ,$$
$$k_n = 1.0 \frac{\text{kW}}{\text{rad}} .$$

C DANWIN 180 KW TURBINE

The present appendix contains a brief description of the Danwin 180 kW wind turbine which, together with the Nordtank 500 kW turbine, is representing the stall regulated turbine concept in the performed wake parameter analysis.

The Danwin 180 kW turbine is a three bladed upwind horizontal axis wind turbine with active yaw. The main specifications of the turbine is given in Table C.1 below.

Table C.1 Main specifications for the Danwin 180 kW turbine.

ROTOR	
Power regulation	Stall
Number of blades	3
Rotor diameter	23.20 m
Swept area	422.7 m ²
Hub height	30.00 m
Rotor speed	42.8 rpm
Tilt	5°
Coning	0°
Blade tip angle	0.8°
BLADES	
Manufacturer	LM Glasfiber A/S
Type	LM 11H
Total blade length	10.80 m
Profiled blade length	8.80 m
Root chord	1.30 m
Tip chord	0.59 m
Blade twist	16.0°
Blade profiles	NACA 632xx
Air brakes	Pivotable blade tips
First flapwise natural frequency	2.40 Hz
First edgewise natural frequency	5.50 Hz
GEAR BOX	
Manufacturer	Jahnel/Kestermann
Gear ratio	1 : 41.7765
GENERATOR	
Manufacturer	Hawker Siddeley
Type	C315 M Sp
Nominal power	200 kW
Voltage	480 V
Frequency	60 Hz
Rotational speed	1000/750???? rpm

Table C.1 Main specifications for the Danwin 180 kW turbine (cont.).

MECHANICAL BRAKE	
Type	Disc
Function	Fail Safe
TOWER	
Type	Tapered tubular tower
Height	29.8 m
Number of sections	2
Top diameter	1.24 m
Base diameter	2.10 m
First bending natural frequency	1.10 Hz
CONTROL SYSTEM	
Manufacturer	Orbital
Cut-in system	Thyristors
Logic system	Microprocessor
Cut-in wind speed	4.0 m/s
Cut-out wind speed	25.0 m/s
WEIGHTS	
Blade	680 kg
Rotor incl. hub	3040 kg
Nacelle excl. rotor	6420 kg
Tower	10000 kg

A measured thrust curve was not available for the present turbine, and as a consequence the wake analysis is based on a calculated thrust curve which, for completeness, is presented in Table C.2. The thrust curve was determined with the aeroelastic code VIDYN.

Table C.2 Calculated thrust curve for the Danwin 180 kW turbine.

Mean wind speed [<i>m/s</i>]	Thrust [<i>kN</i>]	Thrust coefficient C_T
4.0	3.76	0.92
5.0	5.76	0.90
6.0	8.02	0.87
7.0	10.3	0.82
8.0	12.7	0.78
9.0	15.1	0.73
10.0	17.3	0.68
11.0	19.1	0.62
12.0	20.5	0.56
13.0	21.3	0.50
14.0	22.0	0.44
15.0	22.3	0.39
16.0	22.5	0.34
17.0	22.7	0.31
18.0	23.0	0.28
19.0	23.4	0.25
20.0	24.0	0.23
21.0	25.0	0.22
22.0	26.5	0.21
23.0	28.2	0.21
24.0	29.4	0.20
25.0	30.3	0.19

D NÄSUDDEN 3 MW TURBINE

The present appendix contains a brief description of the Näsudden 3 MW wind turbine which represents a large two bladed pitch regulated turbine concept in the performed wake parameter analysis.

The Näsudden II demonstration turbine is a two bladed upwind horizontal axis wind turbine with active yaw. The tower is very stiff on this prototype machine, and in order to approach a more realistic future design, the original tower has been replaced by the more flexible tower belonging to the sister turbine, Aeolus II, in the model calculations. The main specifications of the turbine, equipped with the soft tower, is given in Table D.1 below.

Table D.1 Main specifications for the Näsudden 3 MW turbine.

ROTOR	
Power regulation	Pitch
Number of blades	2
Rotor diameter	80.00 m
Swept area	5026.5 m ²
Hub height	92.00 m
Rotor speed	20.415 rpm
Tilt	8°
Coning	0°
BLADES	
Manufacturer	Messerschmitt–Bölkow–Blohm GmbH.
Total blade length	38.8 m
Profiled blade length	26.8 m
Root chord	4.40 m
Tip chord	0.65 m
Blade twist	7.2°
Blade profiles	FX–W–xxx
First flapwise natural frequency	1.66 Hz
First edgewise natural frequency	2.28 Hz
GEAR BOX	
Manufacturer	Lohmann&Stolterfoht
Type	Planetary/bevel
Gear ratio	1 : 73.475
GENERATOR	
Manufacturer	ABB
Type	Induction/2 speed
Nominal power	3MW
Voltage	6 kV
Frequency	50 Hz
Rotational speed	1000/1500 rpm

Table D.1 Main specifications for the Näsudden 3 MW turbine (cont.).

MECHANICAL BRAKE	
Manufacturer	Kvaener Turbin AB
Type	Disc
Function	Fail Safe
TOWER	
Type	Tapered tubular tower ¹⁸
Height	87.7 m
Top diameter	4.50 m
Base diameter	6.21 m
First bending natural frequency	0.42 Hz
CONTROL SYSTEM	
Manufacturer	Kvaener Turbin AB
Type	PLC
Cut-in wind speed	3.5 m/s
Cut-out wind speed	20.0 m/s
WEIGHTS	
Blade	9250 kg
Rotor incl. hub	38000 kg
Nacelle excl. rotor	138900 kg
Tower	1410000 kg

A measured thrust curve was not available for the present turbine, and as a consequence the wake analysis is based on a calculated thrust curve which, for completeness, is presented in Table D.2. The thrust curve was determined with the aeroelastic code VIDYN.

¹⁸Reinforced concrete.

Table D.2 Calculated thrust curve for the Näsudden 3 MW turbine.

Mean wind speed [m/s]	Thrust [kN]	Thrust coefficient C_T
3.5		
4.0	60	1.21
5.0	86	1.11
6.0	112	1.00
7.0	138	0.91
8.0	163	0.82
9.0	191	0.76
10.0	217	0.70
11.0	243	0.64
12.0	270	0.61
13.0	295	0.56
14.0	309	0.51
15.0	290	0.42
16.0	258	0.33
17.0	229	0.26
18.0	211	0.21
19.0	197	0.18
20.0	186	0.15

E NORDTANK NTK500 TURBINE

The present appendix contains a brief description of the Nordtank 500 kW wind turbine which, together with the Danwin 180 kW turbine, is representing the stall regulated turbine concept in the performed wake parameter analysis. The NTK500 turbine is moreover used as a "reference" turbine in the benchmark exercise performed with the three involved aeroelastic codes – HAWC, VIDYN, and PHATAS.

The Nordtank 500 kW turbine is a three bladed upwind horizontal axis medium sized wind turbine with active yaw. The main specifications of the turbine is given in Table E.1 below.

Table E.1 Main specifications for the Nordtank 500 kW turbine.

ROTOR	
Power regulation	Stall
Number of blades	3
Rotor diameter	37.00 m
Swept area	1075 m ²
Hub height	35.00 m
Rotor speed	30.2 rpm
Tilt	2°
Coning	0°
Blade tip angle	-2°
Direction of rotation	Clockwise
BLADES	
Manufacturer	LM Glasfiber A/S
Type	LM 17.0 m
Total blade length	17.00 m
Profiled blade length	14.50 m
Root chord	1.85 m
Tip chord	0.40 m
Blade twist	19.8°
Blade profiles	NACA 63; modified
Air brakes	Pivotable blade tips
First flapwise natural frequency	2.07 Hz
First edgewise natural frequency	3.43 Hz
GEAR BOX	
Manufacturer	FLENDER
Type	PEAK 4280
Gear ratio	1 : 50.142
MECHANICAL BRAKE	
Manufacturer	Svendborg Brakes
Type	BSFH 317
Function	Fail Safe

Table E.1 Main specifications for the Nordtank 500 kW turbine (cont.).

GENERATOR

Manufacturer	ABB
Type	HXR 355-LC 4B 3E
Nominal power	500 kW
Voltage	690 V
Nominal current	460 A
Cos phi	0.91
Frequency	50 Hz
Rotational speed	1500 rpm

TOWER

Type	Tapered tubular tower
Height	33.8 m
Number of sections	2
Top diameter	1.69 m
Base diameter	2.40 m
First bending natural frequency	0.81 Hz

CONTROL SYSTEM

Manufacturer	DANCONTROL
Type	NTK DC 04
Cut-in wind speed	4.0 m/s
Cut-out wind speed	25.0 m/s

WEIGHTS

Blade	1620 kg
Rotor incl. hub	8010 kg
Nacelle excl. rotor	15400 kg
Tower	22500 kg

A measured thrust curve was not available for the present turbine, and as a consequence the wake analysis is based on a calculated thrust curve which, for completeness, is presented in Table E.2. The thrust curve was determined with the aeroelastic code VIDYN.

Table E.2 Calculated thrust curve for the Nordtank 500 kW turbine.

Mean wind speed [<i>m/s</i>]	Thrust [<i>kN</i>]	Thrust coefficient C_T
4.0	17.1	1.61
5.0	22.3	1.34
6.0	27.5	1.16
7.0	33.0	1.02
8.0	38.1	0.90
9.0	44.0	0.82
10.0	49.3	0.75
11.0	53.3	0.67
12.0	56.1	0.59
13.0	58.1	0.52
14.0	59.0	0.46
15.0	59.6	0.40
16.0	60.2	0.36
17.0	60.8	0.32
18.0	61.8	0.29
19.0	62.5	0.26
20.0	63.4	0.24
21.0	64.4	0.22
22.0	65.4	0.20
23.0	66.5	0.19
24.0	67.5	0.18
25.0	68.6	0.17

F EXPERIMENTAL WAKE CHARACTERIZATION

For the Swedish results, the von Karman based length scales has been applied and then subsequently transformed to the required Kaimal formulation. The conversion is based on the specifications in the IEC-1400 document. The same transformation has been applied to the Dutch results.

Most of the Danish results are based on very long time series in order to improve the statistical significance. The specified parameter values are obtained as averages of a number of half hour statistics, for which the particular wake situation has occurred.

Table F.1 Wake characterization.

Spacing S [D]	Rotor Diam. D [m]	Hub Height H [m]	Thrust Coef. C_T	Stability R _i	Amount of Data [hours]	Wind Turbine Type	Ambient Mean Wind \bar{V}_a [m/s]	Max. Deficit ΔV [m/s]	Ambient Turb. int. I_a^u	Wake Turb. int. I_w^u	Ambient Leg. scale L_a^u [m]	Wake Leg. scale L_w^u [m]	Amb. transv. turb. comp. σ_a^v [m/s]	Wake transv. turb. comp. σ_w^v [m/s]	Amb. coh. Decay α_a	Wake coh. Decay α_w
2.0	28	31	0.67	neutral	0.5	NTK500	9.9	4.4	14.0	16.5	1070	140				
5.3	28	31	0.76	neutral	9.0	NTK500	7.3	1.2	11.9	16.2	1052	359				
5.3	28	31	0.70	neutral	4.5	NTK500	9.1	1.4	12.9	16.2	1035	421				
5.3	28	31	0.59	neutral	7.5	NTK500	11.5	1.6	13.7	17.5	1363	788				
8.5	35	37	0.66	neutral	14.0	Bonus450	9.0				940	505				
8.5	35	37	0.52	neutral	4.0	Bonus450	11.1		6.8	11.0						
9.5	35	37	0.57	neutral		Bonus450	10.0		7.2	11.3						
2.0	28	31		neutral	3.0	NTK500	6.9(wake)								12(H)	31(H)
2.0	28	31		neutral	1.5	NTK500	7.3(wake)								12(H)	38(H)
2.0	28	31		neutral	3.0	NTK500	10.3(wake)								12(H)	45(H)
7.5	28	31	0.76	neutral	4.5	NTK500	7.5	0.6	10.9	14.0					12(H)/16(V)	12(H)/16(V)
7.5	28	31	0.70	neutral	1.5	NTK500	9.1	0.7	14.2	14.3					12(H)/16(V)	12(H)/16(V)
14.5	28	31	0.75	neutral	16.0	NTK500	7.9	0.5	11.7	12.3					12(H)/16(V)	12(H)/16(V)
14.5	28	31	0.69	neutral	11.0	NTK500	9.3	0.5	12.7	12.6					12(H)/16(V)	12(H)/16(V)
14.5	28	31	0.59	neutral	4.0	NTK500	11.7	0.3	13.8	14.7					12(H)/16(V)	12(H)/16(V)
4.2	23	30	0.44	0.04	0.33	Danw180	14.2	4.5	5.6	6.6	1306	598	0.57	0.98	16(V)	53(V)
6.1	23	30	0.67	-0.15	0.33	Danw180	9.7	2.4	6.4	11.4	1380	846	0.50	1.03	14(V)	27(V)
6.1	23	30	0.87	-1.25	0.33	Danw180	6.26	1.57	6.9	11.3	1776	672	0.38	0.76	16(V)	19(V)
6.1	23	30	0.87	-1.25	0.33	Danw180	6.71	1.78	5.4	12.5	1849	975	0.30	0.84	17(V)	25(V)
6.1	23	30	0.81	-0.5	0.5	Danw180	7.76	1.85	6.3	12.9	1730	837	0.35	0.96	15(V)	22(V)
4.2	23	30	0.86	-1.0	0.33	Danw180	6.94	3.00	4.8	15.6	1592	635	0.30	0.90	11(V)	20(V)
6.1	23	30	0.79	-2.0	0.5	Danw180	7.95	1.84	6.3	13.5	1711	828	0.43	0.94	13(V)	25(V)
4.2	23	30	0.83	-6.5	0.33	Danw180	7.49	3.03	6.0	16.0	1868	616	0.48	1.13	13(V)	25(V)
4.2	23	30	0.71	-1.7	0.33	Danw180	9.55	3.43	7.7	13.0	1196	690	0.57	1.20	12(V)	29(V)
4.2	23	30	0.83	0.07	0.5	Danw180	7.93	4.33	3.8	10.7	672	598	0.31	0.56	33(V)	33(V)
4.2	23	30	0.30	0.01	0.166	Danw180	17.4	4.60	7.0	9.3	1840	1270	0.97	1.14	13(V)	27(V)
4.2	23	30	0.52	0.03	0.166	Danw180	13.37	5.28	4.3	6.6	902	543	0.46	0.88	18(V)	54(V)
4.2	23	30	0.50	0.03	0.166	Danw180	13.74	5.34	5.9	6.6	1693	708	0.61	1.04	17(V)	57(V)
4	30	35	0.75		0.285	WPS-30	7.3	3.6	10.5	15.1	644	138	0.80	1.08		
4	30	35	0.75		0.336	WPS-30	7.7	3.6	8.9	13.7	920	184	0.85	1.03		
4	30	35	0.75		0.336	WPS-30	8.1	3.5	10.9	15.4	736	230	0.89	1.16		
7	30	35	0.57		0.711	WPS-30	13.6	2.8	7.2	9.3						
7	30	35	0.75		0.569	WPS-30	10.1	2.7	9.5	12.2						
7	30	35	0.74		0.996	WPS-30	10.0	2.3	9.1	11.9						
7	30	35	0.74		0.336	WPS-30	8.9	2.3	9.6	11.1						
5	0.27	0.31	0.91		0.006	MODEL	4.13	1.05	9.0	14.1						
7.5	0.27	0.30	0.87		0.008	MODEL	4.1	1.03	9.0	12.3						

G GRAPHIC COLLOCATION OF RESULTS

The following contains a graphical representation of results associated with wake deficits and wake turbulence intensities.

The predictions by the investigated models are presented together with measurements (and relevant ambient characteristics).

Cases indicated by "R", "A", "S", and "T" refer to Risø measurements, Alsvik measurements, Sexbierum measurements, and wind tunnel measurements, respectively.

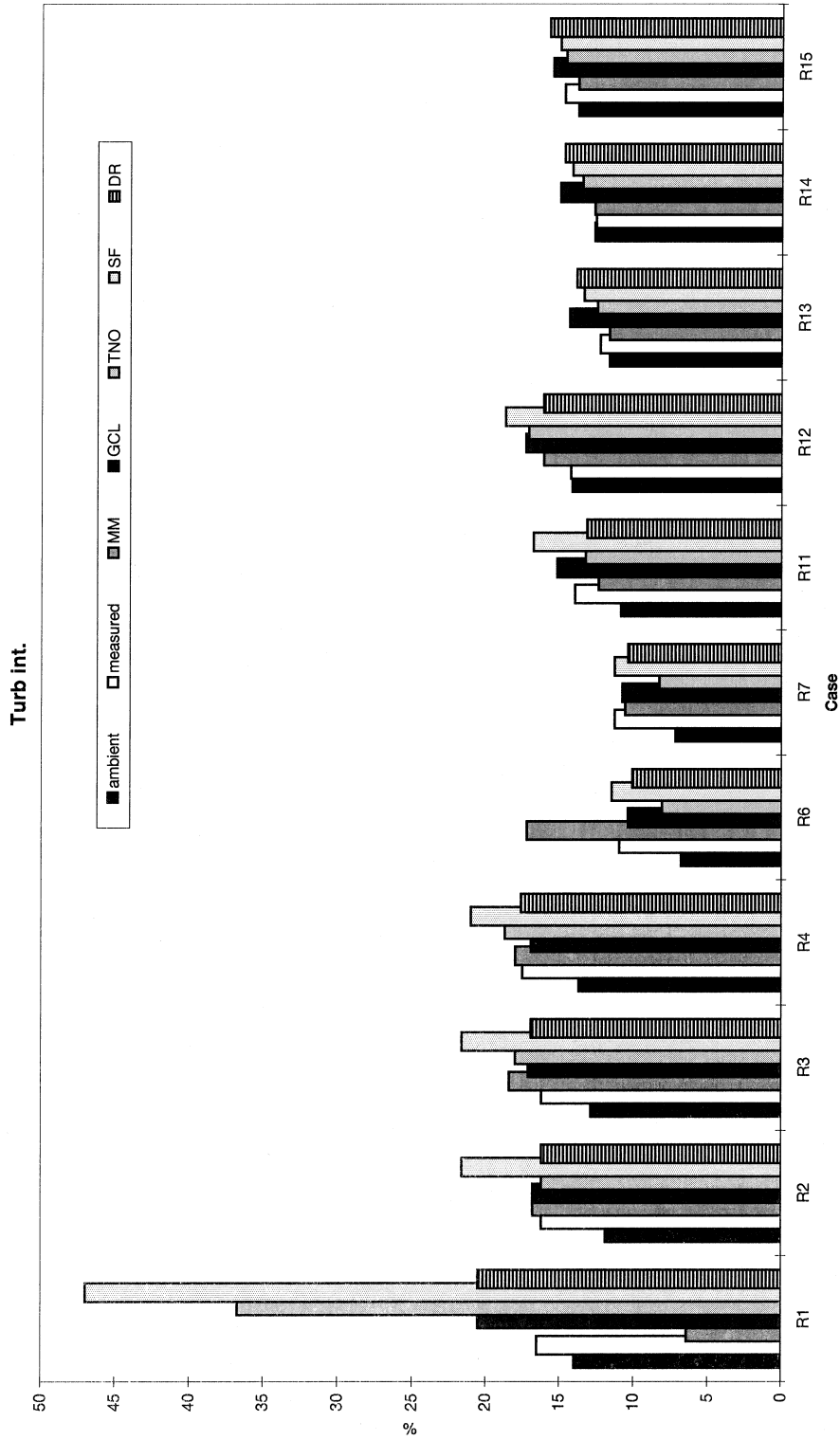


Figure G.1 Predictions of turbulence intensity compared to the Risø measurements.

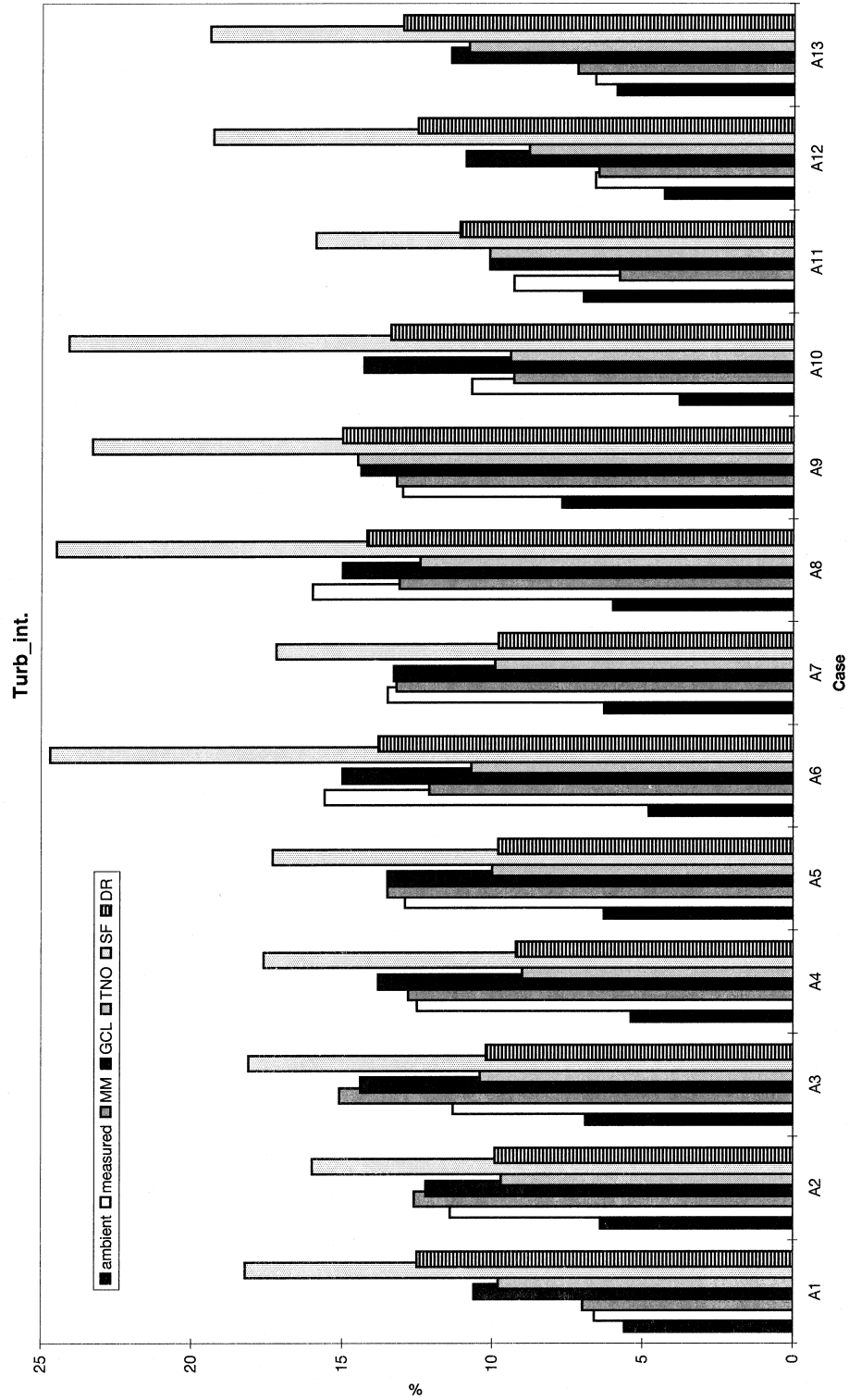


Figure G.2 Predictions of turbulence intensity compared to the Alsvik measurements.

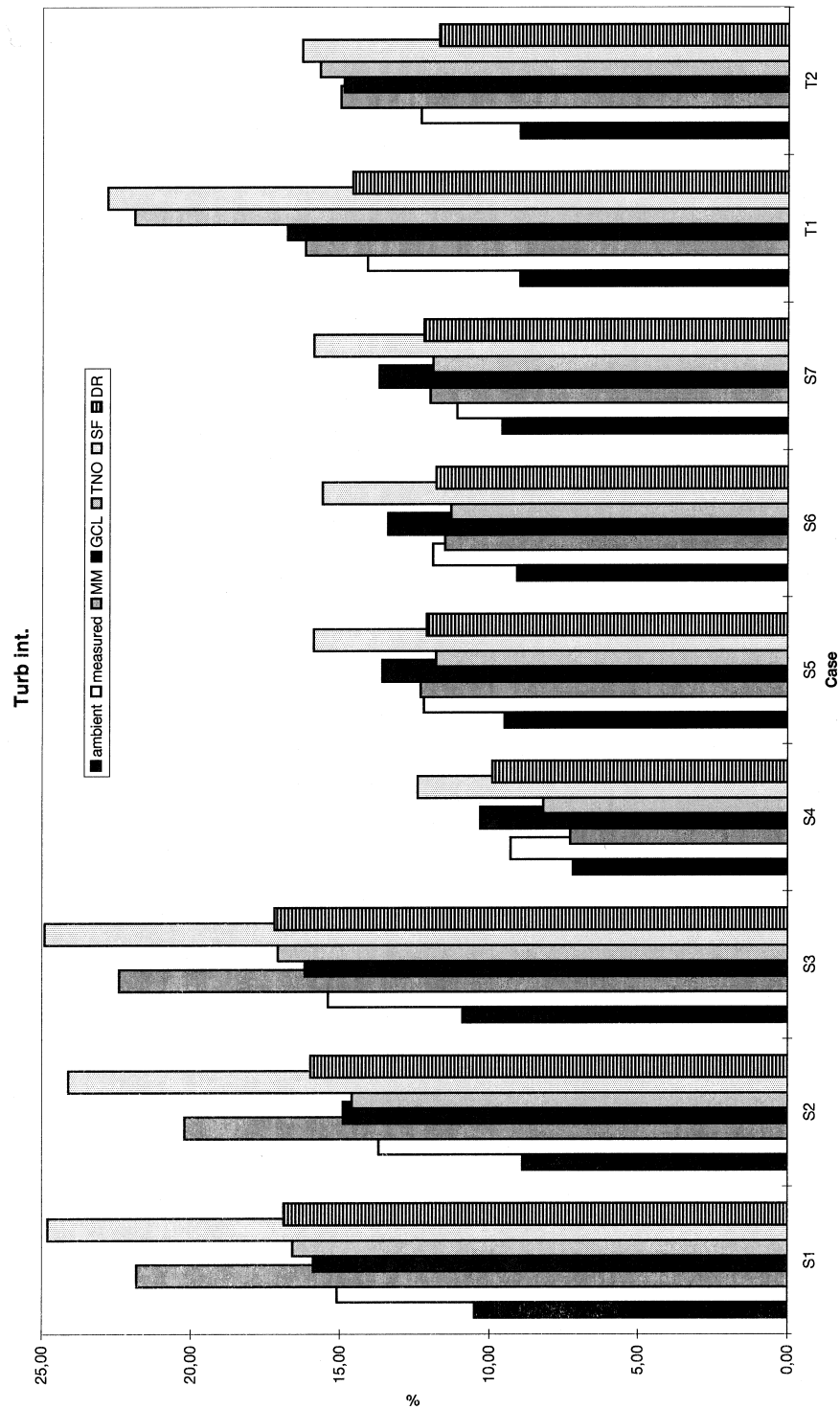


Figure G.3 Predictions of turbulence intensity compared to the TNO measurements.

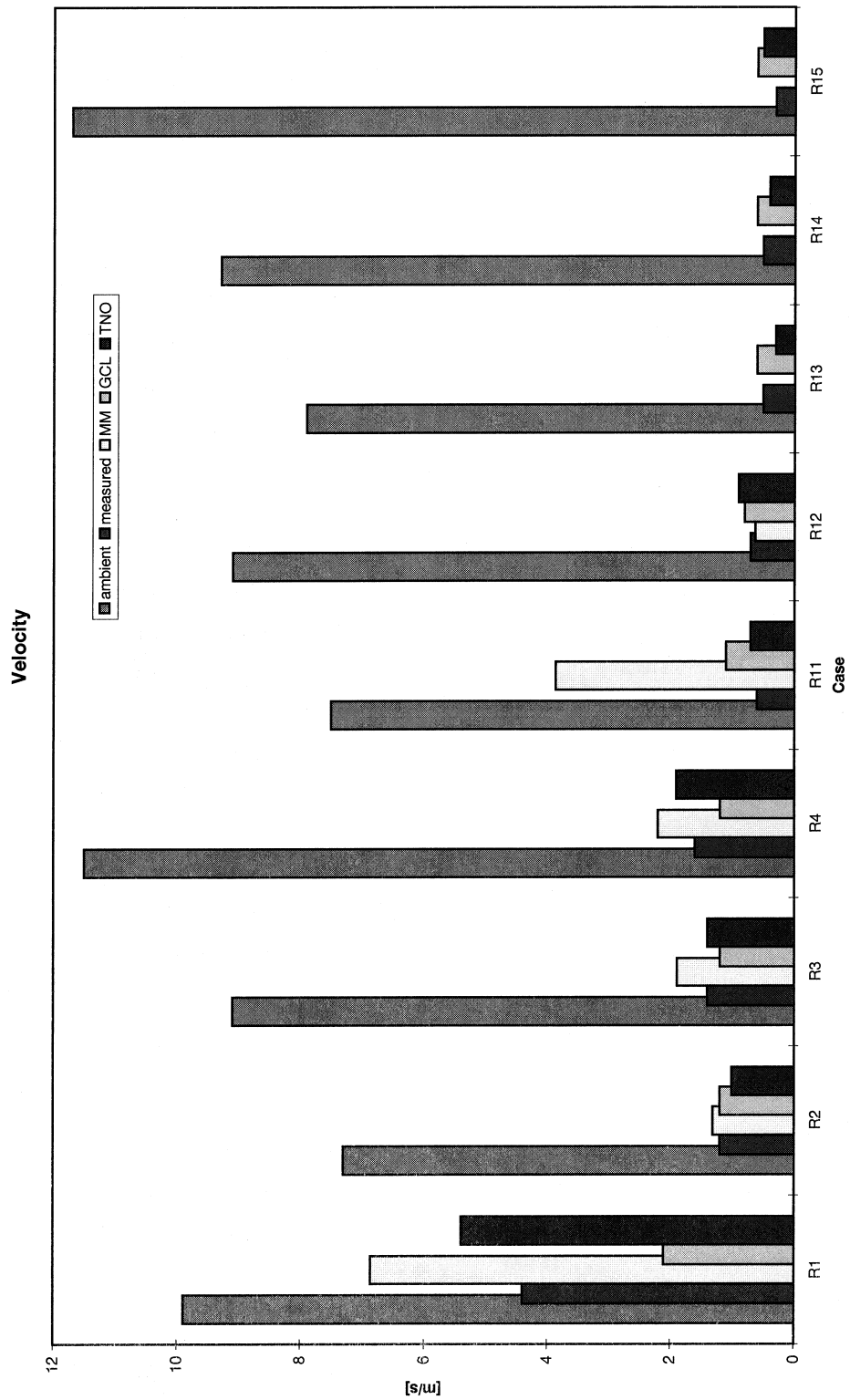


Figure G.4 Predictions of wake deficit compared to the Risø measurements.

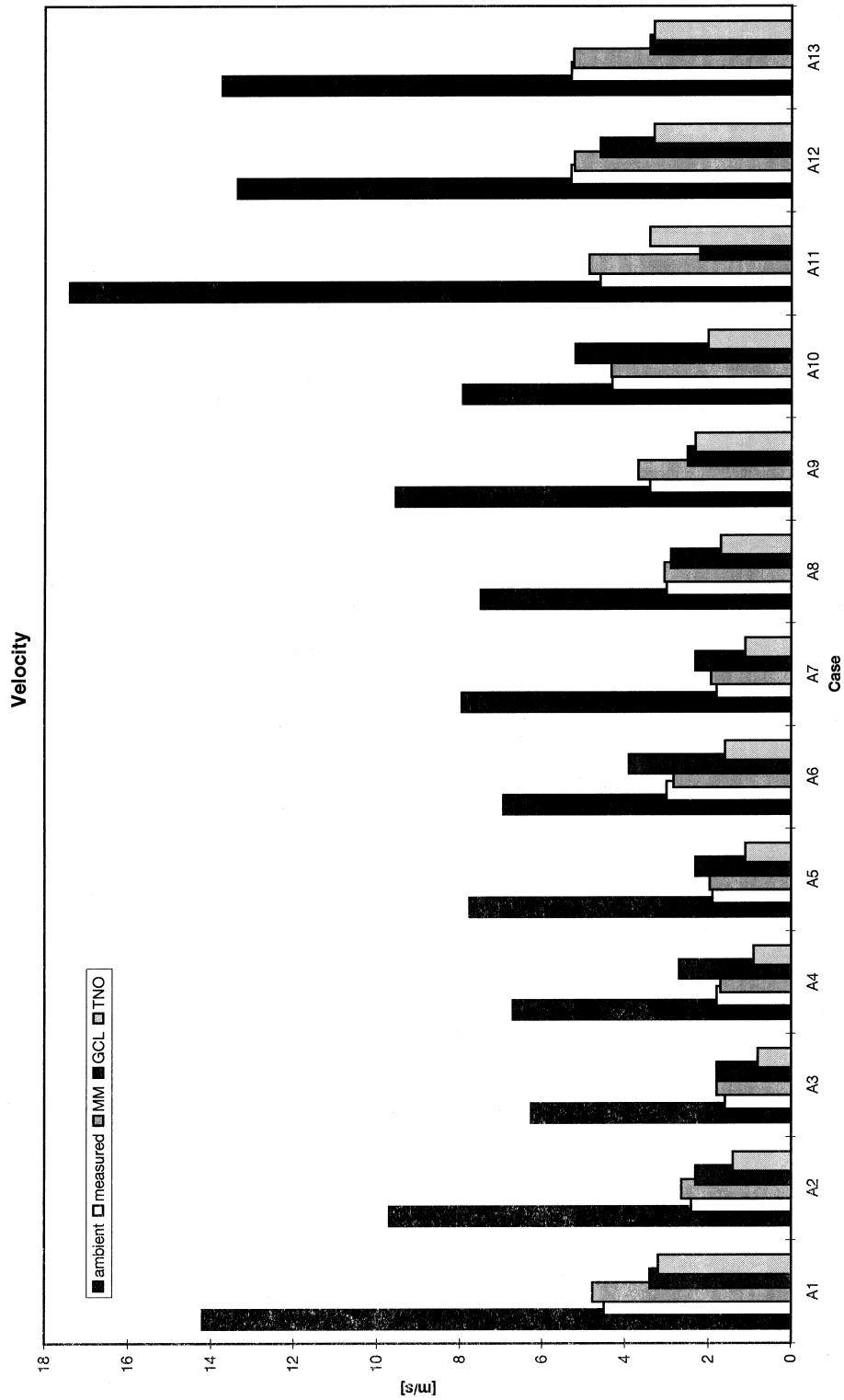


Figure G.5 Predictions of wake deficit compared to the Alsvik measurements.

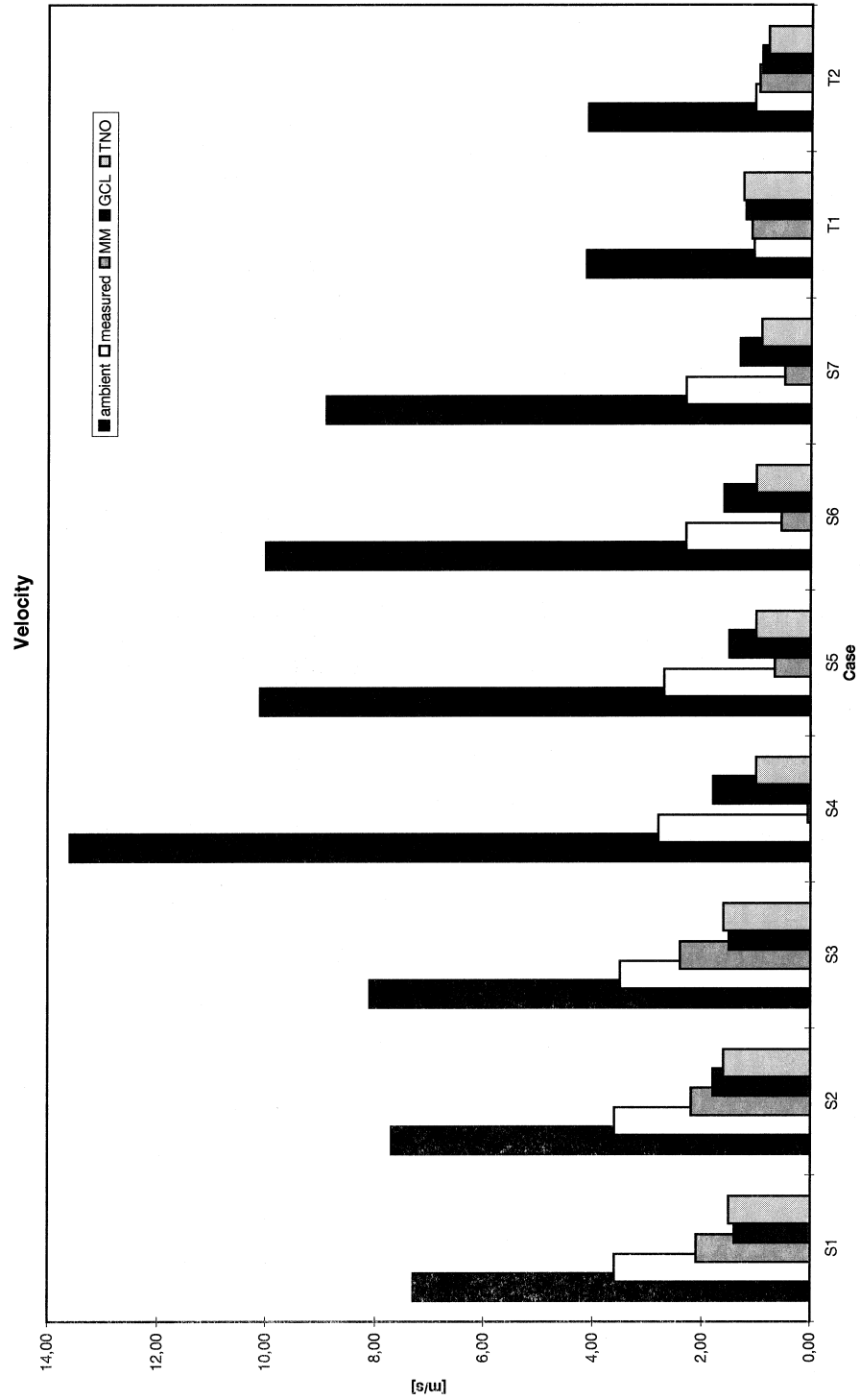


Figure G.6 Predictions of wake deficit compared to the TNO measurements.

EUROPEAN WIND TURBINE STANDARDS II
PART 1
LOAD SPECTRA AND EXTREME WIND CONDITIONS
SUB B
COMPLEX TERRAIN AND FATIGUE LOADING

P. Chaviaropoulos, (Editor)	CRES
G. Glinou, (Editor)	CRES
F.Mouzakis (Editor)	CRES
D. Winkelaar	Netherlands Energy Research Foundation ECN
B. Hendriks	Netherlands Energy Research Foundation ECN
B. Heijdra	Netherlands Energy Research Foundation ECN
S. Petersen	RISØ National Laboratory
P. Voelund	RISØ National Laboratory
G. Larsen	RISØ National Laboratory
I. Carlen	Technikgruppen AB
H. Ganander	Technikgruppen AB
E. Morfiadakis	CRES
K. Papadopoulos	CRES
D. Douvikas	CRES
P. Vionis	CRES
A. Fragoulis	CRES

CONTENTS OF PART 1 SUB B

1. SUMMARY.....	5
2. NOMENCLATURE.....	7
3. INTRODUCTION.....	9
4. MEAN WIND FIELD AND TURBULENCE STRUCTURE IN COMPLEX TERRAIN.....	11
4.1 Approach followed.....	11
4.2 Measured wind field characteristics.....	11
4.2.1 Mean wind field.....	11
4.2.2 Turbulence structure.....	12
4.3 Theoretical investigation.....	13
4.3.1 Parametric set-up.....	14
4.3.2 Flow model.....	14
4.3.3 Obtained results.....	15
4.3.4 Complex terrain and wind shear.....	17
4.3.5 Complex terrain and turbulent structure.....	17
4.4 Synthesis of the results.....	17
5. MACHINE LOADING IN COMPLEX TERRAIN.....	21
5.1 Approach followed.....	21
5.2 Modified wind field and machine loading; a measurement-based investigation.....	21
5.2.1 Machines and sites considered.....	22
5.2.2 Investigated parameters.....	22
5.3 Modified wind field and machine loading; a modelling-based investigation.....	24
5.3.1 Machines considered.....	25
5.3.2 Parametric set-up.....	26
5.3.3 Results and conclusions.....	28
5.4 Synthesis of the results.....	31
6. RECOMMENDATIONS.....	35
7. REFERENCES.....	37
Appendix A Speed-up and Turbulence Kinetic Energy computations for single and tandem hills.....	39
Appendix B A simplified wind shear law for hill-tops.....	63
Appendix C Theoretical investigation of the Reynolds Stress Tensor in complex terrain [C1].....	65
Appendix D Tables from measurement-based PI.....	71
Appendix E Tables from modelling-based PI.....	77

1. SUMMARY

The aim of this report is twofold. First to investigate the effect of the terrain complexity on the wind field properties that drive the fatigue loading of wind turbines (like wind shear, Reynolds stresses, etc.). Second, to investigate and quantify the impact of the above properties on fatigue loading for machines of different size and design philosophy. The first goal is met by analysing the available experimental complex terrain wind data bases, as well as by performing systematic parametric runs for simple, 2-D, configurations including single and tandem hill layouts. In the latter case, results are presented in terms of speed-up and turbulent kinetic energy distributions. The second goal is met through parameter identification (PI) procedures applied on both measurements and computational -aeroelastic- results. “Fatigue influence” matrices are, thus, established for different machine sizes and concepts. Recommendations are made in the last part of the report on how one could possibly include the present findings into the IEC Standards.

2. NOMENCLATURE

ϕ	Wind direction (degrees)
x,y,z	Cartesian, streamlined, coordinates (m)
z_0	Roughness length (m)
U,V,W	Cartesian, streamlined, mean wind speed vector components (m/s)
u	Normalized longitudinal wind component : $u(z) = U(z)/U_{ref}$
a_{ws}	Vertical wind shear exponent estimated from the power law model, $U(z)/U(H) = (z/H)^{a_{ws}}$
$\sigma_u, \sigma_v, \sigma_w$	Standard deviation of the u, v and w components of the wind speed (m/s)
σ_ϕ	Standard deviation of (horizontal) mean wind direction (degrees)
I or T.I	Turbulence intensity σ_u / U
$u'w', u'v', v'w'$	Reynolds stresses (non-diagonal entries to the Reynolds correlation tensor)
L_u, L_v, L_w	Length scales of the u,v and w wind velocity components estimated with the use of the Von Karman formulation (m)
A_{uu}, A_{vv}, A_{ww}	Coherence decay factors of the wind components at different heights estimated with the use of the Davenport model, $x(D,n) = e^{-AnD/U}$, where x expresses the square root of the coherence, D the separation distance between the points (m), n the frequency in Hz and U the mean wind speed in m/s.
K	Kinetic energy of turbulence defined as $\frac{1}{2}(\sigma_u^2 + \sigma_v^2 + \sigma_w^2)$ (m^2/sec^2)
k	Normalized kinetic energy of turbulence $k(z) = K(z)/U_{ref}^2$
Lsh	Linear shear coefficient $U(z_{tip})/U(z_{hub})$, z is the altitude
Yaw	Yaw error in degrees. Positive when the rotation vector turns clock-wise seen from the ground
S	Speed Up, $S = u(z) / u_{in}(z) = U(z) / U_{in}(z)$
T	Turbulence increase factor, $T = k(z) / k_{in}(z) = K(z) / K_{in}(z)$
Uskew	Skewness of the wind speed distribution estimated as $\frac{1}{N} \sum_{i=1}^N \left[\frac{u_i - U}{\sigma_u} \right]^3$
Ukurt	Kurtosis of the wind speed distribution estimated as $\frac{1}{N} \sum_{i=1}^N \left[\frac{u_i - U}{\sigma_u} \right]^4 - 3$
ref	subscript denoting far-field conditions (at the edge of the atmospheric layer)
in	subscript denoting properties at the inlet plane (resembling those of the flat-terrain)

This document is intended to produce the background information to help the introduction of complex terrain effects into the existing or future standards.

3. INTRODUCTION

Wind turbine (WT) classification is defined in the IEC context [1] in terms of wind speeds and turbulence intensities. The intention of these classifications is to cover most applications enabling the selection of representative values of the above two parameters so as to cover as many different sites as possible. The goal is to achieve WT classification with clearly varying robustness governed by wind speed and turbulence intensity. Four WT classes, I to IV, are thus introduced. To cover cases where special design conditions are needed, a further class “S” is foreseen where site-specific parameters are defined by the designer. Relying on the class-defining parameter values, a series of design load cases is, then, introduced for verifying the structural integrity of the load-carrying components of a machine within an appropriate safety level. Although not explicitly stated in the IEC standard, the semi-empirical frame suggested for the verification process is heavily relying on “flat terrain” experience / evidence. This is especially true for the turbulence models proposed and, consequently, for the evaluation of the fatigue loading of the WT’s. Any attempt, therefore, to include complex terrain operation within the current standardisation practice should first answer the following question: To what extent do the “complex terrain” wind conditions differ from the “flat terrain” ones and how these differences affect machine loading?

Recent work on complex terrain wind field [2],[3] has shown that both the deterministic and the stochastic wind properties do deviate significantly from the so called “flat terrain” conditions. More specifically:

- The vertical wind shear in complex terrain does not respect the log-law. In addition, the mean wind field strain tensor (including spatial derivatives of all three wind components) may be full and its entries may strongly vary with height.
- The wind vector can be strongly inclined, following the local terrain slope.
- The Reynolds stress tensor can be full and its entries may also vary with height. The kinetic energy of turbulence is split into its three components (longitudinal, transversal, vertical) at different portions than in flat terrain. More energy is now contained in the transversal and the lateral components.
- Turbulent length scales and spatial coherence are different in complex terrain. Smaller length scales and higher coherence decay factors are encountered at complex terrain turbulence measurements.
- Non-Gaussian behaviour of turbulence is often met in complex terrain.

These deviations become stronger as the terrain complexity (a non-quantifiable term, in general) increases. In the absence of a concise “complex terrain theory” and considering that the number of possible complex terrain layouts is infinite, the quantification of “complex terrain effects” can only be obtained indirectly. To do that the following two-step procedure is proposed and applied below:

1. Produce a complex terrain experimental database including as many sites as possible, to estimate the envelope of variation of the individual wind field parameters. Try to interpret these variations by introducing a suitable theory. Apply this theory in simple cases where the terrain complexity (single hill configurations, for instance) is well defined to identify trends and possible correlation between the parameters sought.
2. Interrelate wind-field properties and machine loading applying sensitivity analysis and parameter identification techniques for a variety of machine sizes and concepts. Define a procedure for translating specific site conditions to fatigue loading.

Most of the experimental work regarding step 1 has been accomplished in the framework of the concluded MOUNTURB [2] and the ongoing COMTERID [3] projects. Representative data are presented and discussed in chapter 2.

The theoretical work addressed in step 1 has been performed in the context of this project. This work includes Navier-Stokes computations of the mean flow field and turbulence around single- and double-hill configurations of different hill-slope(s) and separations (a measure of the terrain complexity for these model-problems). Results are presented in terms of velocity speed-up and turbulence increase factors. The set-up and the conclusions are discussed in chapter 2, while tabulated results are shown in Appendix A. The theoretical work is also supported by Appendix B, where a simplified wind shear law for hill-tops is presented, and Appendix C, where a discussion on the “complex terrain” Reynolds stress tensor is held.

Chapter 3 is devoted to the sensitivity analysis procedures mentioned above. Both load measurements and calculations are used for this purpose. Results obtained through a multi-regression analysis of the experimental data are presented in Appendix D. Fatigue influence matrices obtained for several machines through aeroelastic computations are tabulated in Appendix E.

Conclusions and recommendations are presented in chapters 4 and 5 respectively.

4. MEAN WIND FIELD AND TURBULENCE STRUCTURE IN COMPLEX TERRAIN

4.1 Approach followed

The investigation of mean wind field and turbulence structure is based on the analysis of the experimental “wind data bases” collated for a number of complex terrain sites (in terms of 10 minute blocks) and, also, on theoretical considerations. A hill catalogue, including two dimensional single and tandem hill configurations has been created through parametric mean flow field calculations. This catalogue can serve as a guide for providing a rough estimation of the wind shear and the turbulent intensity at a specific site, through an idealisation of its upwind surface section. The experimental approach is focusing on the identification of differences in the basic inflow parameters between flat and complex terrain.

4.2 Measured wind field characteristics

Experimental wind data bases have been analysed for the following complex terrain sites:

- Agia Marina , CRES test station at Lavrio (GR)
- Andros island, (GR)
- Marmari, (GR)
- Toplou, Crete island (GR)
- Sky River, RISØ measurements, (USA)

The findings regarding the mean wind field and turbulence properties are summarised in the next paragraphs.

4.2.1 Mean wind field

Typical wind profile shapes from Lavrio, Andros and Toplou, referring to a wide range of wind velocities, are shown in figure 4.1. The power law (1/7 exponent, recommended for flat terrain) is also plotted on the figure. It is seen that the actual wind shear is over-predicted by the fit in all cases. In reality, flat and even inverse profiles are observed.

Up to 20 degrees distortion of the horizontal mean wind component measured at 20 and 40 meters above ground level have been observed in Andros and Lavrio.

Up to 12 degrees flow tilt angle (wind vector inclination) have been observed at Marmari, at 40 meters a.g.l. In general, the flow tilt angle follows the local terrain slope, decreasing with increasing height.

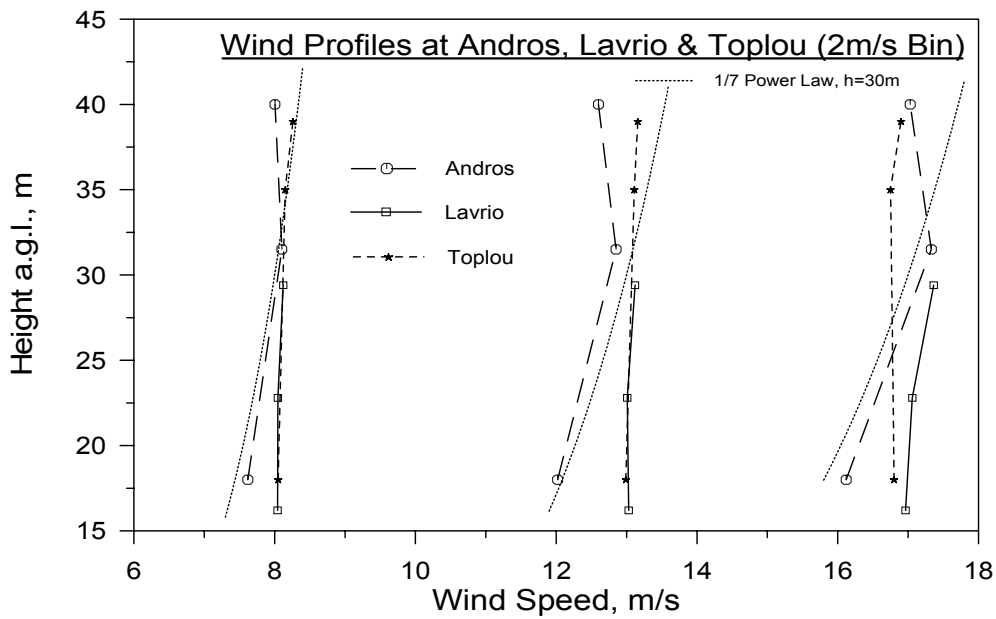


Figure 4.1 Vertical wind profiles of complex terrain sites

The horizontal spatial variation of mean wind field properties over distances of the order of a rotor diameter (20 m), measured at Lavrio were shown to be rather insignificant. This conclusion can be generalised provided that no significant terrain variations occur within the scale of interest.

4.2.2 Turbulence structure

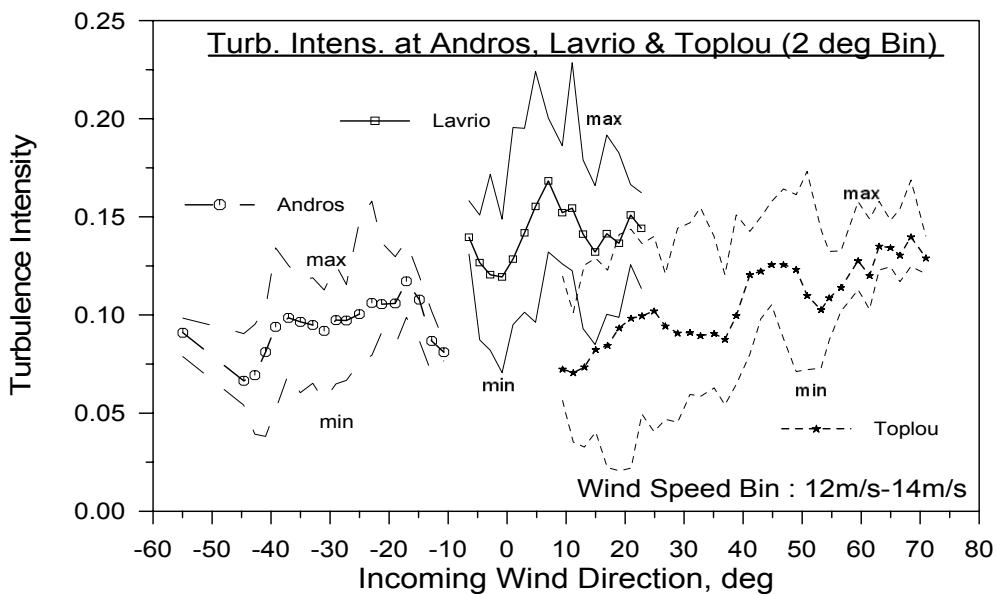


Figure 4.2 Turbulence intensity (TI) vs wind direction at the three sites

Turbulence intensity in complex terrain shows strong evidence of wind direction dependency. Representative plots are shown in figure 4.2, including mean and min_, max_ values. This is also true for all turbulence structure properties.

Mean, representative, values of the data bases over a wide sector centred at the prevailing wind direction for each site, are tabulated in table 1.

Table 1 Mean, representative, values of the data bases

SITE ID	Lavrio	Andros	Marmari	Toplou	Sky River
Height a.g.l (m)	22	31	40	40	43
Mean Wind Speed (m/s)	7.4	8.7	9.3	7.2	7.2
Weibull C(m/s),k	8.3 1.53	9.8 1.85	10.0 1.32	8.1 1.64	
TI= σ_u/U (%)	13	9.5	10	10	8
σ_v/σ_u	0.85	0.90	0.97		1.0
σ_w/σ_u	0.72	0.70	0.68		0.8
σ_ϕ/TI	47.3	56.0		38.5	
L_u (m)	20-120	20-120	20-200	20-120	10-250
L_v (m)	10-50	10-50	5-150		6-150
L_w (m)	5-20	5-20	4-40		6-54
	2-7	3-12	2-20	2-15	

Noticeable are the relatively low values of the Weibull shape parameter k which are definitely below the Rayleigh equivalent value 2.0 and most of the times even below 1.8. This finding is in accordance with the experience gained from the Wind Atlas [4] where the wind regime of a number of sites has been analysed. Low values of k are in favour of extreme wind events.

The turbulence intensities at all sites appear to be smaller compared to these used by the IEC1400-1 standard, namely 16 and 18%. The kinetic energy of turbulence is split to its three components at ratios different than the 1:0.8:0.5 characterising flat terrain. More turbulence energy is now distributed to the transversal and lateral wind components.

The rather crude procedure followed for estimating the length scales and coherence decay factors, as explained below, results in considerably scattered values. Nevertheless, a trend is evident for rather lower length scale values than the equivalent flat terrain values (71, 18, 4.5) presented in table 4 in the sequel.

Non Gaussian behaviour is indicated by the non-zero values of the higher order statistics (skewness and kurtosis coefficients). Slightly negative mean skewness values of the order (-0.3) have been observed at certain sites. However, the obtained values are neither that extreme, nor that persistent, to support a strong statement on non-Gaussian turbulence at complex terrain.

4.3 Theoretical investigation

The theoretical investigation is limited to flow calculations around two-dimensional hills of Gaussian shape. Single and double hill configurations are analysed using as free parameters the hill height over length (h/L), a maximum slope indicator, the separation (Dht) between the hills and the roughness length (z0). It is the intention of this work to interrelate wind shear and turbulence increase with terrain complexity, measured in this case by the two geometric parameters h/L and Dht. The obtained results,

which are presented in Appendix A along with the nomenclature adopted, include velocity and kinetic energy of turbulence distributions along the 10 m and 40 m heights above ground level, as well as the corresponding hill-top profiles.

4.3.1 Parametric set-up

All computations have been performed for the “hill half length” value $L = 250$ m. Disregarding Reynolds number effects the results can apply for different L values as soon as (h/L) and (z_0/L) are maintained.

Tables I-1 to I-7 present the single hill results. Parametric computations have been performed for four hill heights ($h = 50, 100, 150$ and 200 m) and three roughness length values, called (S)mall, (M)edium and (L)arge corresponding to $z_0 = 0.003$ m, 0.03 m and 0.3 m respectively. A case defined as $\{50 S\}$, for instance, corresponds to $h=50$ m and $z_0=(S)=0.003$ m. Table I-1 presents the considered single hill geometries. Table I-2 shows speed-up factors at the, so called, anemometer height, e.g. 10 meters above ground level. Speed-up factors at 40 m a.g.l. (so called hub-height) are shown in table I-3. Tables I-4 and I-5 present the evolution of the turbulence increase factor along the axial distance (x) at the two characteristic heights. Table I-6 presents normalised velocity profiles at the hill-top versus the height a.g.l. (linear scale). The inlet profile is also plotted. Table I-7 shows profiles of the kinetic energy of turbulence versus the height a.g.l. (logarithmic scale) at the inlet and the hill-top planes. Similar results are presented for the tandem-hill cases.

Tables I-8 to I-14 present results for tandem hills of equal height. The standard roughness ($z_0=0.03$ m) has been considered in all cases. Four different h/L ratios have been considered ($0.2, 0.4, 0.6$ and 0.8) along with five hill-tops separations ($D=4L, 6L, 8L, 10L$, and $12L$). Each case is marked with the corresponding $D(ht)$ and h/L values ($4L$ $h/L=0.2$ for the up-left case, for instance). The wind shear profiles at the two hill-tops (u_2 for the first hill and u_4 for the second) are compared against the corresponding single-hill result (u single) in table I-13. Turbulence profiles at the hill-top sections, called k_2 (first hill) and k_4 (second hill), are compared against the corresponding inlet-plane profile (k inlet).

Tables I-15 to I-21 present results of tandem-hills of different height. Four combinations of hill heights have been tested, (50 m - 100 m), (100 m - 50 m), (100 m - 200 m) and (200 m - 100 m), the first height corresponding to the first hill. Computations are performed for five separations per combination of heights. The standard roughness ($z_0=0.03$ m) has been considered in all cases.

4.3.2 Flow model

The flow model used for the parametric hill calculations is based on the Reynolds averaged incompressible Navier-Stokes equations. The k - ω model [5], supported with wall-function type boundary conditions (which take the roughness length into account), is used for turbulence closure. The constants of the model are suitably calibrated for atmospheric flows. The numerical integration of the governing equations is performed through a pressure-correction algorithm. Results are obtained on body-fitted structural grids.

It must be emphasised that the employed turbulence model is an isotropic one. In that respect the flow solver can only account for the global kinetic energy of turbulence but no information on how this energy is split into its three components σ_u , σ_v and σ_w is provided. The missing information is crucial since it is the longitudinal components of turbulence σ_u that mainly affects the fatigue loading of wind turbines while the two other have a rather secondary effect. To fill the gap some additional theoretical work on the Reynolds stresses is presented in Appendix C.

4.3.3 Obtained results

Analysing the obtained results the following qualitative conclusion can be drawn, regarding the influence of the hill height and the surface roughness on the flow properties over a hill (always referring to hill-top conditions):

- For a single hill, the speed up (S) and turbulence factor (T) increase as the h/L or the height h for a constant L, increases.
- For a single hill, the speed up increases with the surface roughness z0, while the (T) factor decreases as z0 increases.
- The wind shear profiles become fuller and more energetic as h/L increases and z0 decreases.
- The turbulence energy K increases with both h and z0.

The following conclusions can be made regarding the influence of a second hill on the turbulence and flow fields:

- The presence of an equal second hill reduces the speed up on both hills
- The presence of a second hill reduces the turbulence increase ratio on the first hill, but increases it for the second hill.
- The wind shear profiles become fuller and more energetic as the height h and distance between hills Dht increase.
- The turbulence energy profiles grow as the hill height h increases, but decreases as the separation between hills increases.
- When the height of the first hill is half the height of the second hill, the speed up at the top of the first hill depends on Dht, while on the contrary, the speed up at the top of the second hill has a small dependence on Dht.
- When the second hill is smaller, the dependence of the speed up results on Dht is reduced for the first hill, but is strongly increased for the second hill.
- When the first hill is smaller, the dependence of (T) in the distance between hills is small for the first hill. Nevertheless, it increases for the second hill.
- When the first hill is bigger than the second, (T) becomes independent of Dht for the first hill but not for the second.
- When the hills are different, turbulence is always bigger on the second hill, except for the instances where separation takes place.
- As the distance between hills Dht increases, the results converge to the single hill solution.

Regarding the turbulence variation with height it can always be seen from the corresponding hill-top profiles that there exist the, so called, inner layer where turbulence is getting very high, depending on the h/L ratio. Fortunately for the larger wind turbines, the depth of this inner layer is rather short (less than 10 meters in most of the cases examined here with L=250m). In the outer layer, turbulence is rather relaxed compared to its surface value.

Let us now quantify the results in terms of the turbulent intensity. By definition of the kinetic energy of turbulence (K) the following formula holds:

$$\sqrt{K} = \sigma_u \sqrt{\frac{1}{2} \left\{ 1 + \left(\frac{\sigma_v}{\sigma_u} \right)^2 + \left(\frac{\sigma_w}{\sigma_u} \right)^2 \right\}} \quad (1)$$

That is, to translate K into σ_u the ratios (σ_v / σ_u) and (σ_w / σ_u) must be known. Consider, now, two sets of such ratios, a flat terrain one with $\sigma_u: \sigma_v: \sigma_w=1:0.8:0.5$ and a complex terrain one with the, rather extreme, values $\sigma_u: \sigma_v: \sigma_w=1:1:0.8$. Then, by substitution

$$\begin{aligned}\sigma_u &= \sqrt{K} / 0.97 && \textit{flat} \\ \sigma_u &= \sqrt{K} / 1.15 && \textit{complex}\end{aligned}\tag{2}$$

indicating that less turbulent energy goes to the longitudinal direction in the complex terrain case. To avoid the dependence on the actual values of the turbulent ratios we now on adopt the unique, conservative, relation $\sigma_u=(K)^{1/2}$.

Let us now demonstrate the use of the results of Appendix A, which are presented in non-dimensional form.

For hill-tops where vertical profiles of k and u are given,

$$TI(z) = k(z)^{1/2} / u(z)\tag{3}$$

For **other than hill-top** locations (here $z = 10$ or 40 m)

$$\sigma_u(z) / \sigma_{u,in}(z) = (T)^{1/2}\tag{4}$$

In a similar way one may get the following formula for the turbulent intensity (TI):

$$TI(z) / TI_{in}(z) = (T)^{1/2} / S\tag{5}$$

where subscript (in) refers to the undisturbed far-stream conditions. Note that $TI_{in}(z)$ can be evaluated from the single-hill tables I-6 and I-7 applying equation (3).

Some examples of application follow below.

Example 1. Evaluate the turbulent intensity at 40 m above the top of a single hill with $h/L=0.4$ and $z_0=0.03m$.

From tables I-6 and I-7 we focus on the {100 M} plots since $100 = 0.4 \times L$ (250 m) and $z_0=0.03m$ (M case). Then, at 40 meters a.g.l $u=1.1$, $u_{in}=0.75$, $k=0.012$ and $k_{in}=0.0095$. Then, applying formula (3):

$$TI(40m) = k(40m)^{1/2} / u(40m) = (0.012)^{1/2} / (1.1) = 10 \%$$

Applying the formula for the “inflow” conditions (flat terrain equivalent)

$$TI(40m)_{in} = (0.0095)^{1/2} / (0.75) = 13 \%$$

In other words the turbulence intensity at the hill-top is decreased not because turbulence is less ($k=0.012$ in the first case while $k=0.0095$ in the second) but because of the speed-up effect. It is reminded that it is σ_u (or k in this case) that drives the fatigue loading and not the turbulence intensity itself.

Example 2. Using the setting of the previous case evaluate the turbulence intensity at $x = -100m$ (100 m up-stream the hill-top).

From tables I-3 and I-5 (40 m a.g.l) we get for $x=-100m$ the values: $S = 1.35$ and $T = 1.2$. Then, applying formula (5):

$$TI(40m) = / TI_{in}(40m) (T)^{1/2} / S = (13\%) (1.2)^{1/2} / (1.35) = 10.5 \%$$

Example 3. Consider two hills of equal height $h=100m$ (and $L=250m$). Let $z_0=0.03m$. Evaluate the turbulent intensity at 40m above the two hill tops for $Dht = 6L$ and $10L$.

From tables I-13 and I-14 and for the $\{6L \ h/L=0.4\}$ case we get:

1st hill : $u = 1.06$, $k = 0.012$ and, from relation (3) $TI = 10 \%$

2nd hill : $u = 1.04$, $k = 0.016$ and, from relation (3) $TI = 12 \%$

From the same tables and for the $\{10L \ h/L=0.4\}$ case we get:

1st hill : $u = 1.08$, $k = 0.011$ and, from relation (3) $TI = 10 \%$

2nd hill : $u = 1.08$, $k = 0.014$ and, from relation (3) $TI = 11 \%$

Comparing with the equivalent single hill case of example 1 ($TI=10\%$) it is seen that the TI at the first hill top is rather unaltered while TI at the second hill top increases as the distance between the hills decreases.

4.3.4 Complex terrain and wind shear

From the examined cases it appears that the complex terrain vertical shear, at least at hill-top conditions, acts favourable on machine loading compared to the flat terrain wind shear. In general, the velocity slopes (positive or negative when h/L is large) are smaller in absolute values than the log-law equivalent slope $du/dz = u_T/\kappa z$, κ being the Von Karman constant and u_T the friction velocity. In that respect, the use of the log-law for all, flat and complex terrain, cases within the standards is a conservative approach for the latter case.

If, however, a generalised wind shear law should be included in the standards, the analytical formulation presented in Appendix B is a possible candidate. The velocity variation with height is expressed in terms of the hill height h , its half-length L and the roughness length z_0 .

4.3.5 Complex terrain and turbulent structure

A theoretical investigation of the complex terrain turbulent structure, in terms of Reynolds stresses, is attempted in Appendix C. For the considered 2-D and quasi-3D cases it has been shown that

$$\left(\frac{\sigma_u}{\sigma_v}\right)^2 + \left(\frac{\sigma_w}{\sigma_v}\right)^2 \leq 2 \quad (6)$$

where the equality holds for all 2-D flows. Deviations from the equality denote three-dimensional effects. In the accelerating part of a 2-D flow the kinetic energy of turbulence increases (see Appendix A), while turbulent energy is transferred from the longitudinal u to the vertical w wind component. This implies that the turbulence in that area becomes more isotropic. In general, in the accelerating part of any complex terrain flow it is expected that σ_v and σ_w take higher values than the “flat terrain” equivalent while no such clear statement can be made for σ_u .

For the spectral properties of complex terrain turbulence (length scales, coherence) there is no concise theory available, to the authors knowledge. By intuition it is expected that the terrain effect should lead to some redistribution of the turbulent energy on the frequency domain, especially at its low frequency part. For a given topography the power spectra of turbulence should enjoy some self-preserving form which cannot be properly fitted either by the Kaimal or by the Von-Karman single-parametric representations. If one of the two representations is used for length-scale evaluation, the result will be heavily dependent on the selected area where the best-fit procedure applies. This is also true for the spatial coherence description in terms of the decay factor.

4.4 Synthesis of the results

Referring to complex terrain sites we hereafter imply locations, within a greater area with intense surface relief exhibiting a wind potential favourable for wind turbine installation e.g. to sites where the flow is

locally over-speeding, like hill-tops. Unattractive sites (where separated flow occurs, for instance) are excluded from this discussion.

Mean flow field properties

- Low values of the Weibull shape factor are often met at complex terrain sites.
- Mean wind field and turbulence structure are clearly affected by the upwind terrain features.
- The wind profile is clearly affected by the upwind fetch inducing local speed-up regions which vary with wind direction. Consequently, the logarithmic and power law are proved inadequate to describe the vertical wind shear. In most of the cases complex terrain wind shear seems to be less intense than its flat terrain equivalent.
- Depending on the actual site topography the mean flow field may be significantly distorted in the transversal direction, as well. The effect is stronger at the side-boarders (in respect to the wind direction) of local hills. Vertical deviations of wind direction of as much as 20 degrees have been recorded in some measurements.
- The flow inclination follows the local terrain slope and acts on the machine as a systematic vertical “yaw error”.

Turbulence structure

- Theoretical analysis and measurements indicate that the turbulence kinetic energy levels are higher in complex terrain and more importantly that the distribution mechanism of turbulent kinetic energy to its components is different from this observed in flat terrain cases. Numerical experimentation shows that the kinetic turbulence energy increase is more pronounced in the, so called, inner layer of the atmospheric boundary layer which, in most of the cases, is confined within the 10 meters above ground level. In the outer layer, where the large wind turbines operate, the turbulence increase is less significant. On the other hand, turbulence intensity seems to take lower values at complex than in flat terrain. This is due to the over-speeding of the mean wind vector.
- Differences from flat to complex terrain are also depicted in the stochastic wind characteristics as demonstrated by the values of the turbulence ratios σ_v / σ_u , σ_w / σ_u , σ_u^2 / K , σ_v^2 / K and σ_w^2 / K and Reynolds stresses ratios.
- The non-zero values of the non-diagonal entries of the Reynolds stress ($u'v'$ and $v'w'$ correlation's) tensor found in a number of cases gives evidence of the 3D character of the wind flow in complex terrain. Finally, a high correlation between the longitudinal and the vertical velocity component is noticed at complex terrain.
- The analysis of the data in the frequency domain revealed that in complex terrain a spectral gap is observed in the lower frequency part of the spectrum which can not be adequately modelled by the formulas existing in the literature. This is due to the fact that high frequencies corresponding to wavelengths smaller than the fetch over the terrain changes respond rapidly to changes imposed on the flow by streamline distortion and surface geometry whereas the low frequency of the spectra of the horizontal components are affected by the upstream terrain characteristics. Thus, the high frequency part is always in a state of quasi-equilibrium and the spectral shape conforms to this over uniform terrain while low frequency longitudinal spectral densities are reduced introducing the so called “spectral gap or lag” representing the different response times of inner and outer layer (small and large scales respectively).
- The significant scatter, associated with the uncertainty of the fitting process, observed in the length scale values in all the investigated sites did not allow for a well established comparison of the length scales between flat and complex terrain sites. Nevertheless, the results of this comparison indicate that the length scales characterising the turbulence kinetic energy distribution in its frequencies, is smaller in complex terrain (more energy in the high frequency part of the spectrum).

- The measured coherence exhibits the typical exponential decay with increasing turbulence frequency. The decay rates obtained through the application of the Davenport exponential decay model exhibit significant scatter, increasing with increasing longitudinal wind speed.
- Some deviations are observed in the distribution of wind speed with respect to the Gaussian in complex terrain sites. Noticeable is a trend for slightly negative values of skewness found in most of the analysed ten minutes time series, indicating an asymmetry in distribution, namely a shift (tail) towards the lower wind speeds. The minimum wind speed occurring in the time series is lower than the expected value from a Gaussian distribution ($U-3\sigma_w$). From the analysis performed at four complex terrain sites it is difficult to conclude whether the “tail” in the wind speed distribution is connected to the terrain, however this is the most probable assumption since this trend is observed in almost all the measurements obtained at these sites.

5. MACHINE LOADING IN COMPLEX TERRAIN

5.1 Approach followed

Fatigue loading of wind turbines is investigated through the analysis of existing “load” data bases and calculations. In both cases the emphasis is put in identifying the wind structure parameters that mainly affect fatigue loading and, then, in quantifying their influence by calculating the corresponding “partial derivatives” of the fatigue equivalent loads. In this way, systematic deviations of the wind structure parameters from one type of terrain to another can be directly translated to load deviations.

It must be emphasised that the approach followed is confined to the 10 minute time scale and does not “integrate” the findings to conclude on “machine life times”. The reason is that the integration procedure should rely on some mean-wind-speed probability distribution (of Weibull type, for instance) which, in principle, is terrain-type independent. Nevertheless, one should keep in mind that complex terrain measurements have shown that the shape factor of the Weibull distribution is taking significantly lower values (more energy at high wind speeds) than in flat terrain.

5.2 Modified wind field and machine loading; a measurement-based investigation

The procedure used in the measurement-based investigation comprises the following phases:

I. Identification of causative processes

The deterministic wind characteristics, wind turbulence characteristics as well as the wind speed distribution characteristics are regarded as the main causative processes when wind turbine fatigue loads are considered.

II. Determination of candidate independent variables for each process

Upon definition of the causative processes, a set of independent variables are selected in order to describe each process. The term independent is used according to the regression analysis nomenclature and does not imply that the predictive variables should be uncorrelated. The deterministic wind characteristics are described by the mean wind speed and wind shear. The wind turbulence is described by the standard deviation of the wind speed components and the turbulence length scale components. The wind speed distribution is described by the higher order descriptive statistics, namely skewness and kurtosis. In cases, where sonic measurements are available and the effect of the complex terrain characteristics is to be captured, the ratios of the standard deviations of the lateral and the vertical wind components against the longitudinal one are used. When cup and vane measurements are available the ratio of the standard deviation of wind direction against the turbulence intensity may be used instead.

III. Application of the full model

The regression analysis is performed for the selected full model.

IV. Iterative application of evaluation criteria and model reforming

The evaluation criterion is based on the p-values of the t-ratios of each independent variable. Large values for the p-value indicate that the rejection of the hypothesis " H_0 : the regression coefficient a_k is zero" is questionable, and consequently the parameter is rejected from the model and the regression analysis is performed again. According to statistics literature and numerical experimentation the rejection threshold values were set to be 5%.

V. Final selection and assessment

After the completion of the iterative process, the assessment of the regression findings is attained through the selected magnitudes, i.e. regression coefficients, dependence coefficients or t-statistics.

The above procedure has been applied for three machines operating at complex terrain sites. The theoretical background of the adopted methodology and the obtained results in tabulated form are presented in Appendix D.

5.2.1 Machines and sites considered

The above procedure has been applied to the experimental "load" data bases of three machines operating at complex terrain sites:

- The WXT110 (110 kW, three-bladed, stall) operating at the CRES test station at Lavrio (GR)
- The V27 (225 kW, three-bladed, pitch) operating at Andros island (GR)
- The NTK500 (500 kW, three-bladed, stall) operating at Toplou (GR)

5.2.2 Investigated parameters

The parameters considered for the fatigue analysis of the three machines are listed in the following table. In each case the analysis is performed for three individual velocity bins, representing linear, stall and post-stall operation. Mean values and standard deviations of the parameters at each velocity bin are, also, provided. As main fatigue driving parameters, the Reynolds stresses (normalised where appropriate) and the longitudinal length scale (Von Karman fit) have been selected. In one of the cases the wind shear exponent α_{ws} is included in the parameters list. When cup-anemometer wind measurements are only available, the normalised ratio of the wind direction standard deviation and the turbulence intensity (σ_φ/ TI) is used instead of σ_v/σ_u to account for the transversal variations of the wind vector. The influence of higher order statistics of turbulence, measured by the skewness (U_{skew}) and the kurtosis (U_{kurt}) coefficients of the recorded 10 min time series, is also taken into account.

Table 2.a Parameter set for WINCON W110XT data base

	U=5-8m/s		U=8-11m/s		U=13-17m/s	
	mean	sdv	mean	sdv	mean	sdv
U	7.2	0.63	9.4	0.84	14.8	1.15
α_{ws}	0.028	0.034	0.024	0.028	0.028	0.024
σ_u	0.98	0.29	1.36	0.33	2.14	0.45
σ_v/σ_u	0.94	0.20	0.87	0.16	0.81	0.13
σ_w/σ_u	0.77	0.15	0.72	0.12	0.67	0.09
Lu	67.0	29.4	85.5	34.7	106.1	39.4

Table 2.b Parameter set for VESTAS V27 data base

	U=5-7m/s		U=8-11m/s		U=13-16m/s	
	mean	sdv	mean	sdv	mean	sdv
U	6.52	0.33	9.7	0.83	14.1	0.76
α_{ws}	0.088	0.044	0.091	0.046	0.082	0.034
σ_u	0.60	0.18	0.95	0.18	1.35	0.27
σ_ϕ/TI	1.07	0.23	1.11	0.22	1.01	0.26
Lu	70,9	37,9	60.7	28,6	57.7	24.1
U_{skew}	-0.017	0.36	-0.048	0.27	-0.126	0.29
U_{kurt}	-0.16	0.71	-0.14	0.40	-0.20	0.37

Table 2.c Parameter set for NORDTANK NTK500/37 data base

	U=5-8m/s		U=8-11m/s		U=13-16m/s	
	mean	sdv	mean	sdv	mean	sdv
U	7.0	0.73	9.5	0.87	14.5	0.85
α_{ws}	-0.48e-3	0.055	0.091	0.51	0.11	0.42
σ_u	0.67	0.24	0.85	0.29	1.45	0.35
σ_ϕ/TI	0.94	0.25	1.03	0.22	0.91	0.12
Lu	28.3	13.8	32.5	15.6	46.3	17.2
U_{skew}	0.133	0.35	-0.18	0.35	-0.29	0.30
U_{kurt}	0.617	1.73	0.14	0.72	-0.014	0.61

3.2.3 Results and conclusions

Results are presented for the three machines in tables (D 1 to 3) of Appendix D. The column (Leq), where bold characters are used, provides the mean value of the corresponding equivalent load in kNm. The next columns provide the estimated values of the partial derivatives $\partial L_j / \partial x_i$. A measure of the significance of each parameter is the product of the corresponding partial derivative and the standard deviation of the parameter itself. This product indicates the increase of the equivalent load when the considered parameter increases one standard deviation with respect to its mean value. To demonstrate this, consider the following example:

Compare the significance of σ_u and Lu on the flap-wise bending load of a NTK500 blade in the wind-speed bin 8-11 m/s.

From table 2 we get the values $SDV_{\sigma_u} = 0.29$ m/s, $SDV_{Lu} = 15.6$ m. From table D.3 we get the values $\partial L / \partial \sigma_u = 45.3$ (kNm/m/s), $\partial L / \partial Lu = -0.1$ (kNm/m). The mean value of L is 46.88 kNm.

For 1-sdv increase of σ_u we get an increase in L

$$\Delta L = (45.3) * (0.29) = 13.14 \text{ kNm, or } (13.14)/(46.88) = 28\% \text{ increase of the load}$$

while for 1-sdv increase of Lu we get

$$\Delta L = (-0.1) * (15.6) = -1.56 \text{ kNm, or } (1.56)/(46.88) = 3.3\% \text{ decrease of the load}$$

In that respect Lu is almost 10 times less significant than σ_u .

Estimate the effect of a combined increase of σ_v/σ_u and σ_w/σ_u by 0.1 and 0.2 respectively on the tower bottom fatigue load in the wind speed bin of 8-11m/s for the WINCON 110XT turbine.

From table D.3 we get the values $\partial L / \partial \sigma_v/\sigma_u = 17,31$ (kNm/m/s), $\partial L / \partial \sigma_w/\sigma_u = 42,62$ (kNm/m). The mean value of L is 86,68 kNm.

For the selected parameter changes the resulting increase in L is:

$$\Delta L = (17,31) * (0.1) + (42,62) * (0.2) = 10,26 \text{ kNm, or } (10,26)/(86,68) = 12\% \text{ increase of the load}$$

From the tables of Appendix D it is seen that the partial derivatives related to the Reynolds stresses are always positive. When either σ_u , σ_v , σ_w or σ_ϕ/TI increases the fatigue load is also increasing. The longitudinal length scale has the opposite effect. The effect of σ_u is primary compared to the rest. The effect of σ_v , σ_w and σ_ϕ/TI becomes stronger at stalled operation. Skewness and kurtosis have also secondary effects.

5.3 Modified wind field and machine loading; a modelling-based investigation

In the framework of the MOUNTURB project, aeroelastic modellers were called upon to investigate the influence of some identified, terrain dependent, wind inflow parameters on the fatigue loading of the machines involved (WXT110, V27, MADE 300, NTK500). To do that, a sequence of representative test cases has been proposed, putting the emphasis on the wind inflow parameters that are hard to be investigated through the experiment. The expected result is a ‘fatigue influence matrix’ which is composed by the ‘partial derivatives’ of the fatigue loading in terms of the selected wind inflow parameters. For each machine the ‘fatigue influence matrix’ is formed for three different operating points (reference states), which are distinguished in terms of the mean wind speed at hub height. These reference states are selected in the linear, stall and post-stall zone, respectively. The input parameters which were identified as critical are: the mean wind speed at hub height, the longitudinal turbulence intensity, the yaw error, a wind shear parameter, the vertical mean wind component and the 3D turbulent characteristics of the incoming flow. To limit the requested computational effort in reasonable bounds the turbulent characteristics were grouped together to form three characteristic sets, one corresponding to flat terrain operation and two to complex terrain operation. The flat terrain set was identical to that proposed in the IEC International Standards draft report. The first complex terrain set relied on the mean values of turbulence measured from the experimental campaign at Andros island. The second complex terrain

turbulence set introduces some low probability ‘extremities’ on the length scales and coherence factor, in order to investigate their effect on fatigue. Fatigue damage was evaluated in terms of Rainflow Count (RFC) plots and 1 Hz equivalent loads of the blade root, tower bottom and low-speed shaft moments. Within the present project the MOUNTURB data sets were applied to three additional (DANWIN 180, NASSUDEN II and MAGLARP/WTS3) machines by T.G. Evidently, the MOUNTURB approach does not provide detailed information on the fatigue influence of the individual parameters (Reynolds stress tensor components, length scales, coherence decay factors) since all of them are blended within the three turbulent data sets. For this reason we shall call the MOUNTURB approach **Coarse Grain Parameter Identification (PI)**.

A detailed investigation of the influence of the individual turbulence structure parameters on fatigue is attempted within COMTERID project. Coupled-3D turbulence generators are used to investigate the possible influence of the wind components cross-correlation’s (off-diagonal components of the Reynolds stress tensor). Once again the analysis is performed for three wind speeds, representing linear, stall and post stall operation. The COMTERID approach will be called **Fine Grain PI**. Fatigue influence matrices are once again produced for selected machines following the MOUNTURB notation - guidelines.

5.3.1 Machines considered

The following machines have been modelled for the coarse grain PI analysis

- WXT110 : Three bladed, rotor diameter D=20m, stall controlled, fixed (rotational) speed and yaw , 110 kW.
- V27 : Three bladed, D=27m, pitch controlled, fixed speed and yaw, 225 kW.
- MADE AE/30 : Three bladed, D=30m, stall controlled, fixed speed and yaw, 300 kW.
- NTK500 : Three bladed, D=30m, stall controlled, fixed speed and yaw, 500 kW.
- V39 : Three bladed, D=29m, pitch controlled, fixed speed and yaw, 500 kW.
- DANWIN 180 : Three bladed, D=23m, stall controlled, fixed speed and yaw, 180 kW.
- NASUDDEN II : Two bladed, D=80m, pitch controlled, fixed speed yaw and teeter, 3MW.
- MAGLARP/WTS3 : Two bladed, downwind, D=84m, pitch,, teeter hinge, free yaw, 3MW.

The rotational speed and their first characteristic modes / eigen-frequencies are shown in the following table

Table 3 Rotational speed and first characteristic modes / eigen-frequencies

	WXT100	V-27	Made AE/30	NTK 500	V-39
Description of mode	meas.(Hz)	meas.(Hz)	simu.(Hz)	meas.(Hz)	meas.(Hz)
Rotational Speed	0.73	0.72	0.60	0.50	0.50
1 st Tower bending	1.47	1.05	1.06	0.94	0.89
1 st Shaft torsional	2.13	1.70	2.10	1.16	1.19
1 st asym. Rotor / yaw	2.41	2.15	2.29	1.70	1.26
1 st asym. Rotor / tilt	2.56	2.20	-	1.80	1.55
1 st sym. Rotor / flap	2.94	2.60	2.40	2.08	1.78
1 st asym. Rotor / edge	4.78	3.50	4.40	3.50	2.83
	DAN/180	NAS/ II	MAG/WTS3		
Description of mode	meas.(Hz)	meas.(Hz)	meas.(Hz)		
Rotational Speed	0.71	0.35	0.42		

1 st Tower bending	1.10	0.42	0.30
1 st blade flap	2.40	1.66	1.00
1 st blade edge	5.50	2.28	2.10

Presently, the fine grain PI has been only applied for the NTK500 and the V39 machines. Work is ongoing in the framework of the COMTERID project.

5.3.2 Parametric set-up

Data sets for **Coarse Grain PI**

To suppress the numerical effort the investigation is done for three turbulence data-sets, only, one typical for flat terrain and two for complex terrain operation. In all three cases the Von Karman non isotropic turbulence model is used for generating the turbulent time series. A common value of the coherence decay factor, called A, has been used for all three wind speed components in all rotor disk directions.

The FLAT terrain turbulence length scales have been derived from the Kaimal length scales suggested in the IEC International Standards Draft document. The equivalent Von Karman length scales are obtained from the Kaimal values after a suitable transformation which resulted in the following coefficients after a best fit procedure:

$$(L_u)_{Kaimal} = 2.3 (L_u)_{Von\ Karman}, (L_v)_{Kaimal} = 3.0 (L_v)_{Von\ Karman}, (L_w)_{Kaimal} = 3.0 (L_w)_{Von\ Karman}$$

For complex terrain turbulence simulations two data sets are proposed, a ‘normal’ set called CLX1 and an ‘extreme’ one called CLX2.

Table 4 Data sets for complex terrain turbulence simulations

CASE	σ_v / σ_u	σ_w / σ_u	L_u	L_v	L_w	A
FLAT	0.8	0.5	71	18	4.5	8.8
CLX1	0.95	0.70	50	30	10	6
CLX2	0.95	0.70	20	15	8	10

All turbulence properties are considered to be uniformly distributed on the rotor disk.

In order to form the ‘fatigue influence matrix’ it is proposed to perform the following 39 runs for each machine for the data sets presented below. To suppress the number of runs one, only, turbulent time series realisation per run is suggested with a common random seed initialisation for all turbulence simulations. Yaw effect is to be investigated for positive yaw error values, only, for the sake of economy. Since this work looking for trends and not for ‘exact’ solutions the wind shear and the vertical wind component effect, they are treated in an abstract way supposing linear shear for the longitudinal wind component, only, and a uniform vertical velocity component along the rotor disk.

The proposed 39 runs are divided into three similar groups representing deviations around three ‘reference states’ (rows in bold black). The reference states differ in terms of the hub wind velocity.

Table 5 Proposed runs for the formation of the ‘Fatigue influence matrix’

RUN No	U_{hub} (m/s)	σ_u / U_{hub}	Yaw (°)	Lsh (%)	W/U_{hub}	Turb. CASE
---------------	---------------------------------------	--	--------------------	--------------------	-------------------------------	-------------------

L1F-L1C	10	0.08	0	0	0.0	FLAT+CLX1
L2F-L2C-L2C+	>>	0.15	0	0	0.0	FLAT+CLX1+CLX2
L3F-L3C	>>	0.15	30	0	0.0	FLAT+CLX1
L4F-L4C	>>	0.15	0	15	0.0	FLAT+CLX1
L5F-L5C	>>	0.15	0	0	0.1	FLAT+CLX1
L6F-L6C	>>	0.25	0	0	0.0	FLAT+CLX1
S1F-S1C	14	0.08	0	0	0.0	FLAT+CLX1
S2F-S2C-S2C+	>>	0.15	0	0	0.0	FLAT+CLX1+CLX2
S3F-S3C	>>	0.15	30	0	0.0	FLAT+CLX1
S4F-S4C	>>	0.15	0	15	0.0	FLAT+CLX1
S5F-S5C	>>	0.15	0	0	0.1	FLAT+CLX1
S6F-S6C	>>	0.25	0	0	0.0	FLAT+CLX1
P1F-P1C	18	0.08	0	0	0.0	FLAT+CLX1
P2F-P2C-P2C+	>>	0.15	0	0	0.0	FLAT+CLX1+CLX2
P3F-P3C	>>	0.15	30	0	0.0	FLAT+CLX1
P4F-P4C	>>	0.15	0	15	0.0	FLAT+CLX1
P5F-P5C	>>	0.15	0	0	0.1	FLAT+CLX1
P6F-P6C	>>	0.25	0	0	0.0	FLAT+CLX1

Data sets for Fine Grain PI

The following specifications have been set for the fine grain PI which is restricted to the effect of the turbulence structure on fatigue loading:

1. The influence of the mean wind field is skipped (examined in MOUNTURB).
2. One, only, turbulent intensity value is considered T.I. ($\sigma_u/U=15\%$).
3. Three mean longitudinal wind speeds are considered ($U = 10, 14, 18$ m/s). No wind shear is assumed.
4. Emphasis is put on the 3-D turbulence structure. The “mean” values (reference state) and the 1 S.D.V. “worse” values are selected from the Ag. Marina experimental data base.
5. The following 3 (wind speeds) X 6 (states) are considered per machine. All dimensional quantities are given in S.I. units. Case No 1 is the reference state. The 6th case considers the u-v-w components in a de-coupled way (as done in MOUNTURB).

Table 6 Specifications for fine grain PI

No	σ_v/σ_u	σ_w/σ_u	L_u	L_v	L_w	A_u	A_{vv}	A_{ww}	u’w’ cor.	u’v’ cor.
1	0.85	0.66	60	30	15	5	5	5	active	active
2	1.00	0.66	60	30	15	5	5	5	active	active
3	0.85	0.76	60	30	15	5	5	5	active	active
4	0.85	0.66	30	30	15	5	5	5	active	active
5	0.85	0.66	60	30	15	7	5	5	active	active
6	0.85	0.66	60	30	15	5	5	5	non-active	non-active

Analysing wind data from the CRES test-station at Ag. Marina it appeared that the correlation between the v-w components is negligible compared to the u-w and u-v ones. In a first order approach one may also neglect the imaginary part of the u-w correlation and the real part of the u-v one. The procedure will be

therefore limited to the following (local) components of the spectral matrix: S_{uu} , S_{vv} , S_{ww} , $\text{Re}(S_{uw})$, $\text{Im}(S_{uv})$. To calculate the (complex) coherence between the components:

$$\begin{aligned}\text{Re}(\text{Coh}(uw)) &= \text{Re}(S_{uw}) / \sqrt{S_{uu} S_{ww}} \\ \text{Im}(\text{Coh}(uv)) &= \text{Im}(S_{uv}) / \sqrt{S_{uu} S_{vv}}\end{aligned}$$

the following expressions are considered, f denoting the frequency:

$$\begin{aligned}\text{Re}(\text{Coh}(uw)) &= B_{uw} \exp(-A_{uw} \cdot f) \\ \text{Im}(\text{Coh}(uv)) &= B_{uv} \exp(-A_{uv} \cdot f)\end{aligned}$$

A data fitting process provided the following representative values for the A and B coefficients $A_{uw} = 11.85$ and $B_{uw} = -0.55$, $A_{uv} = 16.6$ and $B_{uv} = 0.2$. These values are used in the present context when the u-w and u-v correlation's are active.

Output formats

Cumulative Rainflow Counting tables with Equivalent loads $m=4, 8, 12$ are presented in all cases for the following loads:

RFM : blade root flapping moment

REM : blade root edge moment

TBMx : tower bottom bending moment (normal to the mean flow)

TBMy : tower bottom bending moment (parallel to the mean flow)

TTM : tower torsion

DTM : drive train - low speed - torque

5.3.3 Results and conclusions

The full sets of obtained results are presented in table form in Appendix E. Dimensional moments (kNm) are only presented for the corresponding reference case. These are clearly designated using bold characters. All the other columns represent the ratio of the calculated moments versus the respective reference value. Tables D.1 to D.7 summarise the coarse grain PI results. Tables D.8 to D.9 summarise the fine grain PI ones.

To identify the influence of one single parameter (x_i) on a specific equivalent load L_j one has to calculate the corresponding partial derivative ($\partial L_j / \partial x_i$). Taking the linear part, only, of the Taylor expansion:

$$\begin{aligned}L_j(x_{1,ref}, x_{2,ref}, \dots, x_{i,ref} + \Delta x_i, \dots) &= L_j(x_{1,ref}, x_{2,ref}, \dots, x_{i,ref}, \dots) + \left[\frac{\partial L_j}{\partial x_j} \right]_{ref} \Delta x_i \quad \text{or} \\ L_j(x_i) &= L_{j,ref} + \left[\frac{\partial L_j}{\partial x_j} \right]_{ref} (x_i - x_{i,ref}) \quad \text{and} \\ \left[\frac{\partial L_j}{\partial x_j} \right]_{ref} &= \frac{L_{j,ref}}{(x_i - x_{i,ref})} \left[\frac{L_j(x_i)}{L_{j,ref}} - 1 \right]\end{aligned} \tag{7}$$

To estimate the partial derivatives one has to calculate $(x_i - x_{i,ref})$ from table 5 or table 6, depending on the sought parameter, and get the values $L_{j,ref}$ and $L_j(x_i)/L_{j,ref}$ from the corresponding table of Appendix E. To demonstrate the procedure consider the following example:

Evaluate the partial derivative of the flap equivalent load (m=12) in respect to the turbulence intensity for the NTK500 machine operating at flat terrain conditions at mean wind speed 10 m/s.

From table 5 we consider the reference T.I. value (0.15 case 2F) and the deviate T.I. (0.08 case 1F). Note that one could equally well use as the deviate the 6F case with T.I.=0.25. Then,

$$(x_i - x_{i,ref}) = (0.08) - (0.15) = -0.07$$

From Table D.4, (NTK500), m=12, V=10 m/s we get the following values:

$$\begin{aligned} L_{j,ref} &= 94.6 \text{ kNm (column F2)} \\ L_j(x_i)/L_{j,ref} &= 0.57 \quad (\text{column F1}) \end{aligned}$$

and the partial derivative is evaluated as:

$$(\partial L_j / \partial x_i) = (94.6 \text{ kNm}) / (-0.07) * (0.57 - 1) = (581 \text{ kNm})$$

This means, for instance, that if T.I. is increased by 3% from 0.15 to 0.18 under the assumed conditions, the equivalent load will increase

$$(581) * (0.18 - 0.15) \text{ kNm} = 17.43 \text{ kNm}$$

corresponding to a 18% increase of the equivalent load

Once the values of the partial derivatives have been evaluated, the effect of any combination of parameters deviation around the reference state can be estimated through a multi-variate Taylor expansion where the linear terms are only retained.

It must be emphasised that the selected range of variation of each individual parameter within the PI process represents some “realistic range of variation” (for instance T.I. from 0.08 to 0.25, L_u from 30 to 60 m, etc) which covers a variety of flat and complex terrain conditions. In that respect, the load ratios presented in Appendix E are also indicating the weight of each parameter on fatigue loading. Parameters leading to higher equivalent load ratios are more significant than the others (this is not true for the partial derivatives themselves).

Based on the last remark a review of the modelling PI results will be attempted herein.

Coarse Grain PI

Starting with the smaller machine, W110XT, it is seen from table D.1 that:

The main parameter influencing the equivalent loads is the turbulence intensity, or better, the standard deviation of the longitudinal velocity component σ_u . It is important to note that the increment of the equivalent loads with σ_u is of the same order of magnitude for all wind speeds and loads (with the exception of the blade-edge moment).

The second important parameter is the yaw misalignment, case 3 (30 degrees, a rather large value) which mainly affects the blade root flapping moment (RFM) equivalent load. The effect is stronger at higher wind speeds, most probably due to dynamic stall effects.

The third important parameter is related to the turbulence structure characteristics, cases 2C and 2C+. Concerning the turbulence structure properties it is important to note that:

- Both 2C and 2C+ cases correspond to increased turbulence kinetic energy in the rotor compared to the 2F case, since both the σ_v / σ_u and σ_w / σ_u ratios are increased. It is expected that part of this energy will be translated to fatigue load increase.
- The length scales of 2C are decreased compared to 2F but the coherence decay factor is also decreased leading to a contradictory effect on fatigue which can not be isolated through those limited runs.
- Case 2C+ has decreased length scales and increased decay factor in respect to 2C. Since both settings result in an increase of the equivalent loads it is expected that the 2C+ loads will be higher than those corresponding to 2C. The obtained results confirm the statement.
- Most of the employed turbulent wind generation models omit the cross-diagonal terms of the Reynolds stress tensor providing uncorrelated wind components. It was envisaged that the wind components coupling would further increase the fatigue loads.
- The additive effect of the turbulence structure properties is obvious in all C-(complex terrain) cases compared to the F-(flat terrain cases).
- For all investigated turbulence structure characteristics all load exhibit similar relative variations, except the blade load driven equivalent edge moment, which is less sensitive.

The linear shear, case 4 (15% corresponding to 8.5 degrees offset from vertical) has a quite dominant effect, especially on the blade-flap and the tower bending loads. The vertical wind component, case 5 (corresponding to 6 degrees slope) effect is not that pronounced. It is noted that the vertical wind component combined with the machine tilt angle introduces an effect similar to that of the yaw misalignment which sometimes is not included in the aerodynamic models and, thus, the obtained results for this case may be misleading.

The above stated general trends are confirmed for the MADE AE/30 and NTK500 machines, as well.

Similar conclusions can be drawn for the V27 machine. Some differences however exist. First, the yaw misalignment effect is milder, especially at the higher wind speeds, and this is probably due to the fact that the rotor is always running in its linear regime on account of the pitch control strategy. The effect of the turbulence structure properties (see cases 2C and, especially, 2C+) is extremely pronounced, at all wind speeds (as much as 70% increase of certain loads for 2C+).

Fine Grain PI

Although two, only, machines with similar dimensions have been considered, some preliminary conclusions can be drawn from tables D.8 and D.9.

- Surprisingly enough, it appears that a significant increase of the turbulent energy in the transversal (case 2) or the vertical (case 3) direction does not increase the loads more than 5%, in the worst case. The influence is negligible at low wind speeds.
- The only important effect is that of the longitudinal length scale (case 4). Tower loads seem to increase 20% and blade loads 10% when the length scale changes from 60 to 30 m.

- The effect of the coherence decay factor (case 5) and the cross-correlations (case 6) seem to be negligible.

In view of the above, it appears that the high loading encountered for the CLX1 and CLX2 turbulent sets considered for the coarse grain PI analysis are mainly attributed to the length scale decrement. Evidently, these conclusions may not be valid for machines of different size or control strategy.

5.4 Synthesis of the results

Both experimental and modelling-based parameter identification procedures have shown that the primary fatigue loading parameter is the turbulent intensity, or better the standard deviation of the longitudinal wind component. The analysis of the fatigue equivalent loads suggests that Leq is a quadratic function of σ_u . Considering that at higher wind speeds a constant value of turbulent intensity can be assumed for a given site, the above statement suggests that Leq is also a quadratic function of the mean wind speed. On that basis, the influence of the site Weibull parameters on fatigue loading will be investigated.. Let

$$Leq = aU^2 + bU = b(eU^2 + U) \quad , \quad e = a / b \quad (8)$$

where b is the linear part parameter and e stands for the quadratic parameter.

The damage caused by a load spectrum of n cycles with ranges L_i or by its equivalent load Leq is given by the formulae:

$$D = \sum_{i=1}^n \frac{1}{q(pL_i)^{-m}} = \frac{N_{eq}}{q(pLeq)^{-m}} \quad (9)$$

where q is a component constant and p is a constant for a particular location and load. The magnitude that decides the damage level is the m -moment of the equivalent load distribution over a large time period.

From the simplified expression for the short term equivalent load and after exponentiation we get:

$$Leq^m = b^m \left(e^m U^{2m} + \binom{m}{1} e^{m-1} U^{2m-1} + \dots + \binom{m}{i} e^{m-i} U^{2m-i} + \dots + U^m \right) \quad (10)$$

Given the fact that in general the quadratic parameter has small values ($e \ll 1$) the rejection of all terms that contain greater than second order factors of e is justified. Thus, the mean value of Leq^m , with the variable U following a Weibull distribution, is given by the following formula, $\langle \cdot \rangle$ denoting the expected value operator:

$$\langle L^m \rangle = b^m \langle U^m \rangle + meb^m \langle U^{m+1} \rangle \quad (11)$$

After introducing the analytic expressions for the higher moments for the U :

$$\langle U^m \rangle = c^m \Gamma\left(1 + \frac{m}{k}\right) = \langle U \rangle^m \frac{\Gamma\left(1 + \frac{m}{k}\right)}{\Gamma\left(1 + \frac{1}{k}\right)^m} \quad (12)$$

the mean value of Leq^m is finally given by the formula:

$$\langle Leq^m \rangle = b^m \langle U \rangle^m \left(\frac{\Gamma\left(1 + \frac{m}{k}\right)}{\Gamma\left(1 + \frac{1}{k}\right)^m} + me \langle U \rangle \frac{\Gamma\left(1 + \frac{m+1}{k}\right)}{\Gamma\left(1 + \frac{1}{k}\right)^{m+1}} \right) \quad (13)$$

In order to assess the effect of the Weibull shape parameter (k), in conjunction with the effect of the quadratic term, the equivalent load ratio defined below is introduced,

$$EquivalentLoadRatio = \left(\frac{\langle Leq(k, e, m, \langle U \rangle)^m \rangle}{\langle Leq(2, 0, m, \langle U \rangle)^m \rangle} \right)^{1/m} \quad (14)$$

indicating the load increase relative to a reference state corresponding to the Raleigh (k=2) shape factor and linear fatigue response to σ_u . Figures 5.1 and 5.2 show the equivalent load ratios for representative Weibull shape parameter values (k=1.4-2.2), quadratic term values (e=0,0.01,0.02) and S-N curve slopes (m=4,12). For all applications a mean wind speed of 7m/s was assumed.

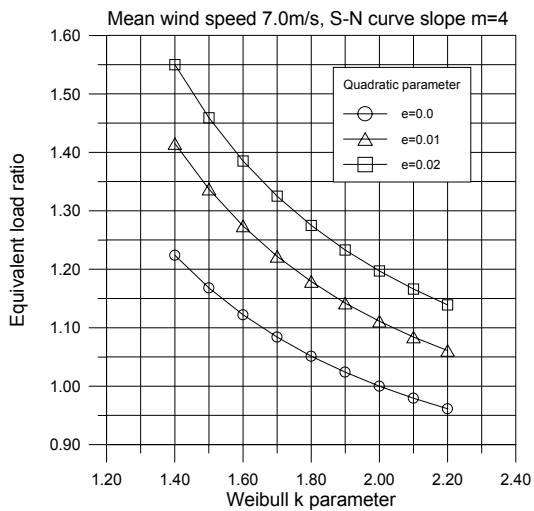


Figure 5.1 Equivalent load ratio vs k for m=4

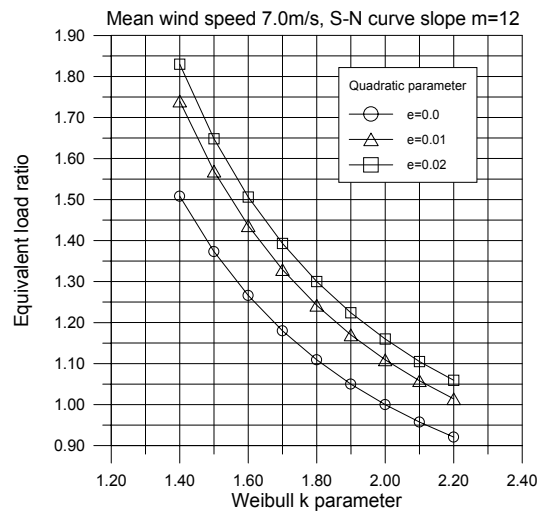


Figure 5.2 Equivalent load ratio vs k for m=12

It is seen that for two sites with the same mean wind speed $\langle U \rangle$ and turbulence intensity, the dependence of Leq on U suggests higher fatigue loading at the site with the smaller k . The effect is present for both m -values considered and becomes stronger as the machine response deviates from linearity. Evidently, k is not only important for extreme load considerations but also for fatigue loading. There is a strong evidence that complex terrain k values can be quite small.

A second important finding is that the increment of the equivalent loads with σ_u is of the same order of magnitude for all the wind speeds and loads (with the exception of the blade-edge moment). This implies that complex terrain standardisation could follow the current IEC approach if an “equivalent” -increased value- of turbulence intensity is used to account for the extra terrain-induced loading.

Yaw error was found to be the second parameter of significance. There is no reason to distinguish between flat and complex terrain operation regarding the yaw error (mostly depending on the control system of the

machine). Nevertheless flow inclination associated with complex terrain acts on the machine as a systematic “vertical yaw misalignment” which should be taken into account in fatigue analysis.

Wind shear has positive impact on fatigue loading, especially for two bladed teetered rotors. Complex terrain wind shear is, in general, milder than the flat terrain equivalent expressed through the log-law.

Both theoretical and experimental investigations have shown that the reinforcement of the turbulent kinetic energy in the lateral and vertical wind directions, due to the terrain, have a secondary effect (less than 5% increase) on fatigue loading. The effect is negligible at low wind speeds and related to the non-linear machine operation at post-stall conditions.

Low turbulence length scale values, often met at complex terrain, have a positive impact on fatigue. This is seen from both experimental and modelling PI's. The aeroelastic calculations overestimate this effect, showing that a longitudinal length scale drop from 60 to 30 meters would increase fatigue loading up to 20%. On the contrary the experimental investigation provides a 5% equivalent. This is rather due to the length scale estimation in-ambiguities discussed above. Similar conclusions can be drawn regarding coherence decay.

It is not so clear that complex terrain is responsible for non-Gaussian turbulence behaviour. Experimental investigations, at least for the data bases analysed, have not identified some strong effect on fatigue loading.

6. RECOMMENDATIONS

First, the Rayleigh distribution, wherever used within the present IEC standard should be replaced by the Weibull distribution with a k value less or equal than 1.8 when addressing at complex terrain sites. This is important for both the extreme and fatigue loading of a machine. When a machine is intended to operate at a site with k significantly lower than 1.8, it should be S(pecial) class certified.

It is felt that the 16% up to 18% turbulent intensity values used in the standards can cover complex terrain operation with TI's 13% up to 15% respectively, without additional care. It was estimated that this 3% extra TI value can afford a 20 % increase in fatigue loading due to overall complex terrain effects. When a machine is intended to operate at a complex terrain site with TI more than 15%, it should be S(pecial) class certified.

The wind shear law used in the standards can be maintained, having in mind that a conservative estimation of complex terrain loading is thus achieved.

Sites with wind inclination more than 20 degrees should be considered within the (S)pecial class context.

7. REFERENCES

- [1] Wind turbine generator systems Part 1: Safety requirements, IEC 88/1400-1/Ed.2, May 96.
- [2] A.N. Fragoulis et al., Load and Power Measurement Program on Wind Turbines operating in Complex Mountainous Regions, (MOUNTURB JOU2-CT93-0378), final report Vol: I to III, Nov. 1996.
- [3] A.N. Fragoulis, Investigation of Design Aspects and Design Options for Wind Turbines Operating in Complex Terrain Environments, (COMTERID JOR3-CT95-0033), Third Periodic report, July 1997.
- [4] E.L. Petersen et al., European Wind Atlas, Vol. II: Measurements and Modelling in Complex Terrain, Published for the European Commission.
- [5] D.C. Wilcox, Turbulence Modelling for CFD, @ 1993 by DCW Industries Inc., ISBN 0-9636051-0-0.

Appendix A Speed-up and Turbulence Kinetic Energy computations for single and tandem hills

Results of two-dimensional single and tandem Gaussian hill computations are presented in this Appendix. The flow model used is relying on the incompressible Reynolds averaged Navier-Stokes equations with k - ω turbulence closure. The constants of the model have been suitably calibrated for atmospheric flows. The work is fully reported in reference [A1].

A.1 Nomenclature

x	:	axial distance
z	:	height above ground level (a.g.l.)
z_0	:	roughness length
h	:	hill(s) height
L	:	hill half-length ; for the Gaussian hills considered here L is defined as the axial distance from the hill-top where $z = h/2$
D_{ht}	:	distance among hill-tops
U	:	longitudinal wind component
u	:	normalised longitudinal wind component : $u(z) = U(z)/U_{ref}$
K	:	kinetic energy of turbulence
k	:	normalised kinetic energy of turbulence $k(z) = K(z)/U_{ref}^2$
ref	:	subscript denoting far-field conditions (at the edge of the atmospheric boundary layer)
in	:	subscript denoting properties at the inlet plane (resembling those of the flat-terrain)
Speed Up	(S)	: $u(z) / u_{in}(z) = U(z) / U_{in}(z)$
Turbulence increase factor	(T)	: $k(z) / k_{in}(z) = K(z) / K_{in}(z)$
Anemometer height		: 10 m a.g.l.
Hub height		: 40 m a.g.l

A.2 References

[A1] J. Cardells, "Numerical Modelling of Wind Shear in Complex Terrain", CRES report, Sept. 1997.

A.3 Results of flow calculations

The results of the flow calculations are given as graphs, but denoted as table I-1 through I-21.

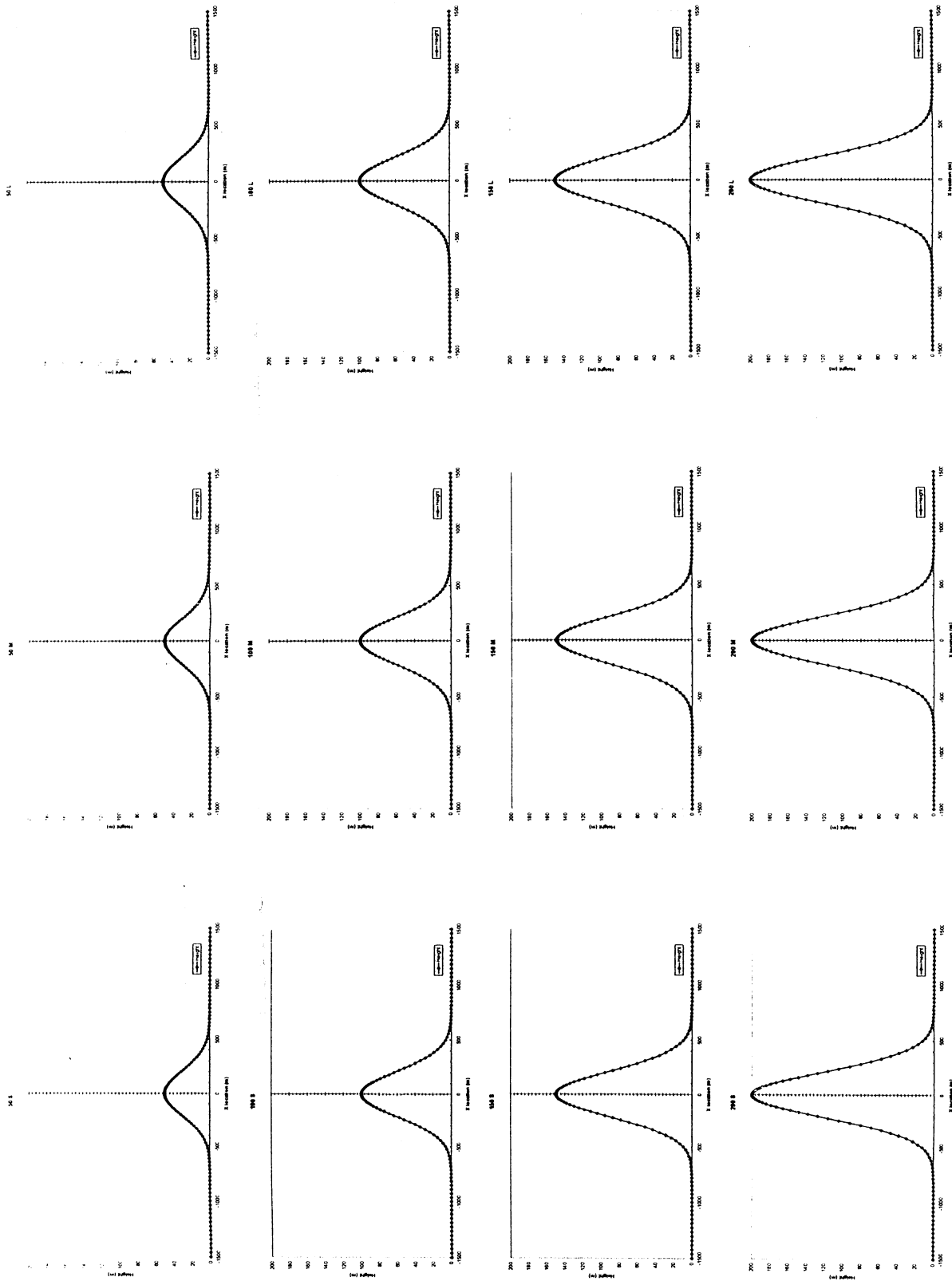


Table I-1: Hill geometry

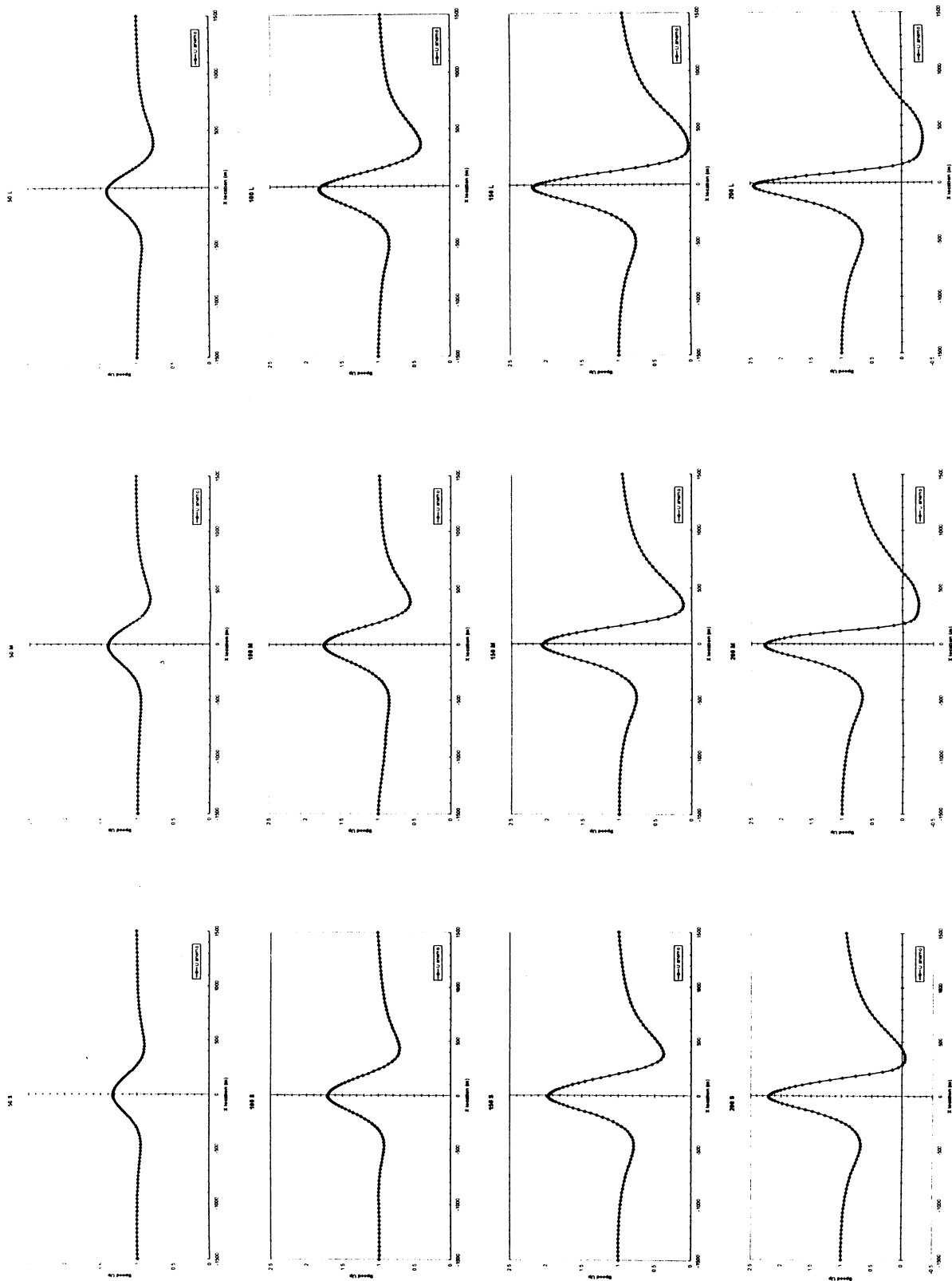


Table I-2: Speed up at anemometer height

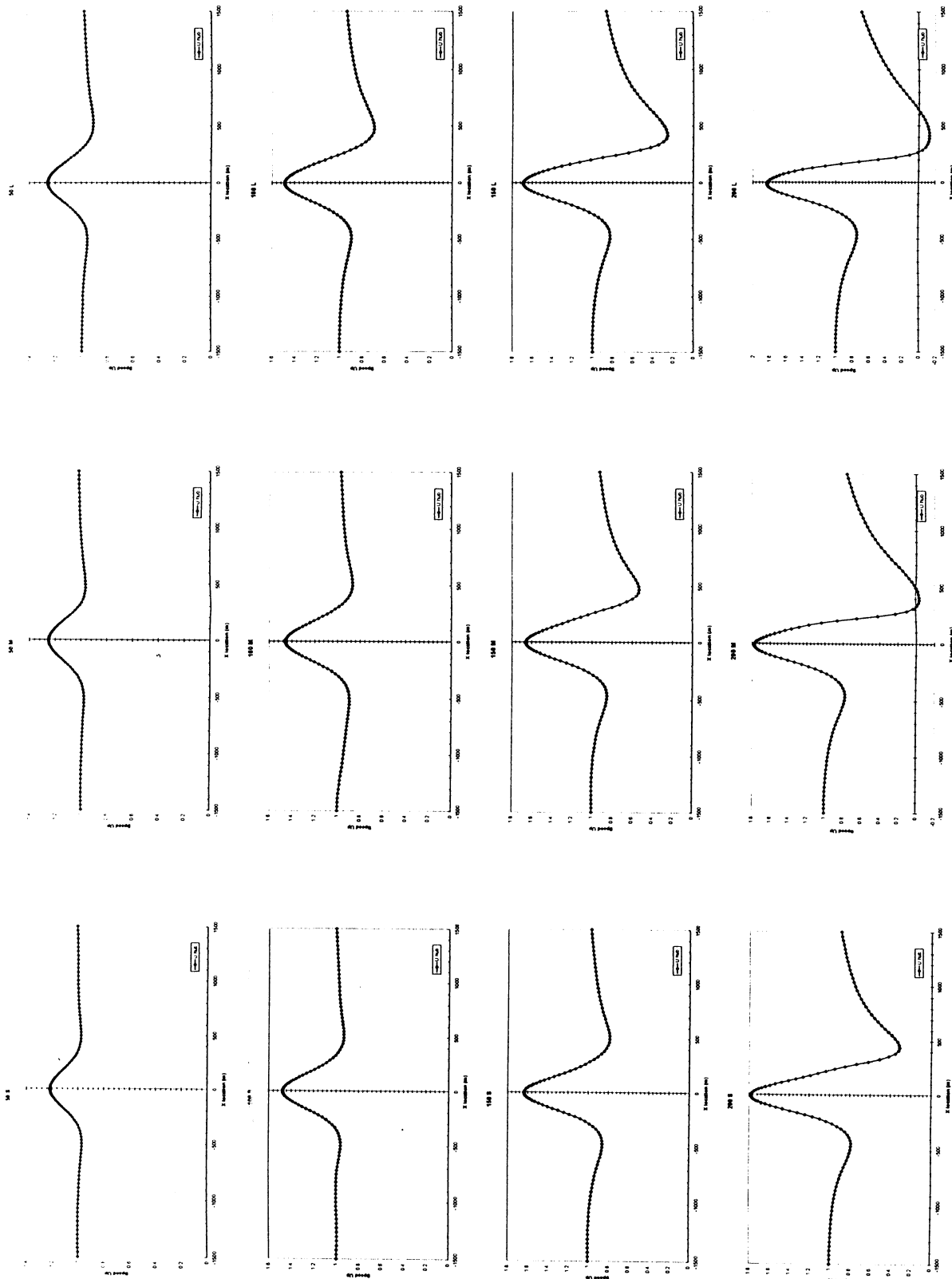


Table J-3: Speed up at hub height

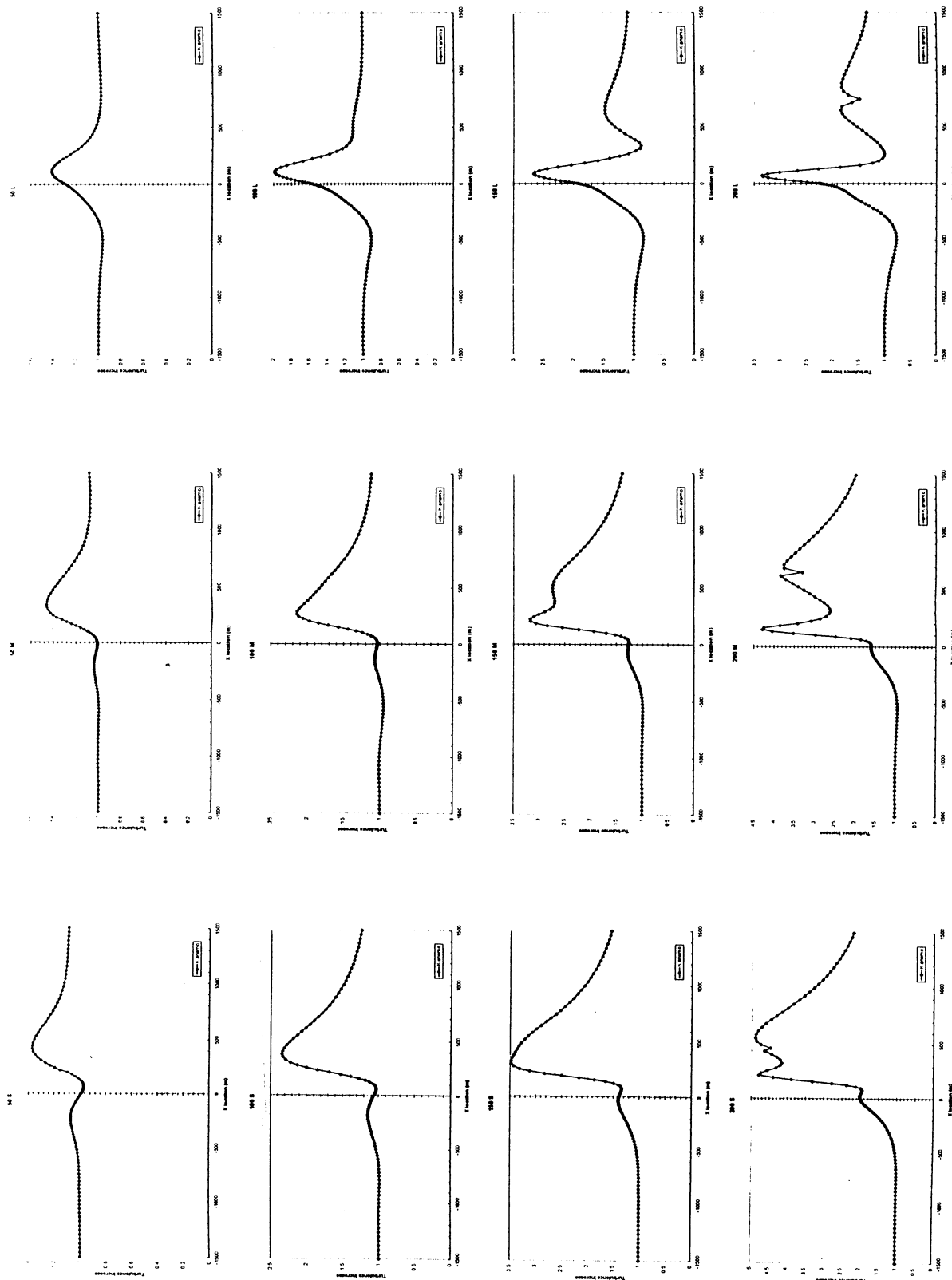


Table J-4: Turbulence increase at anemometer height

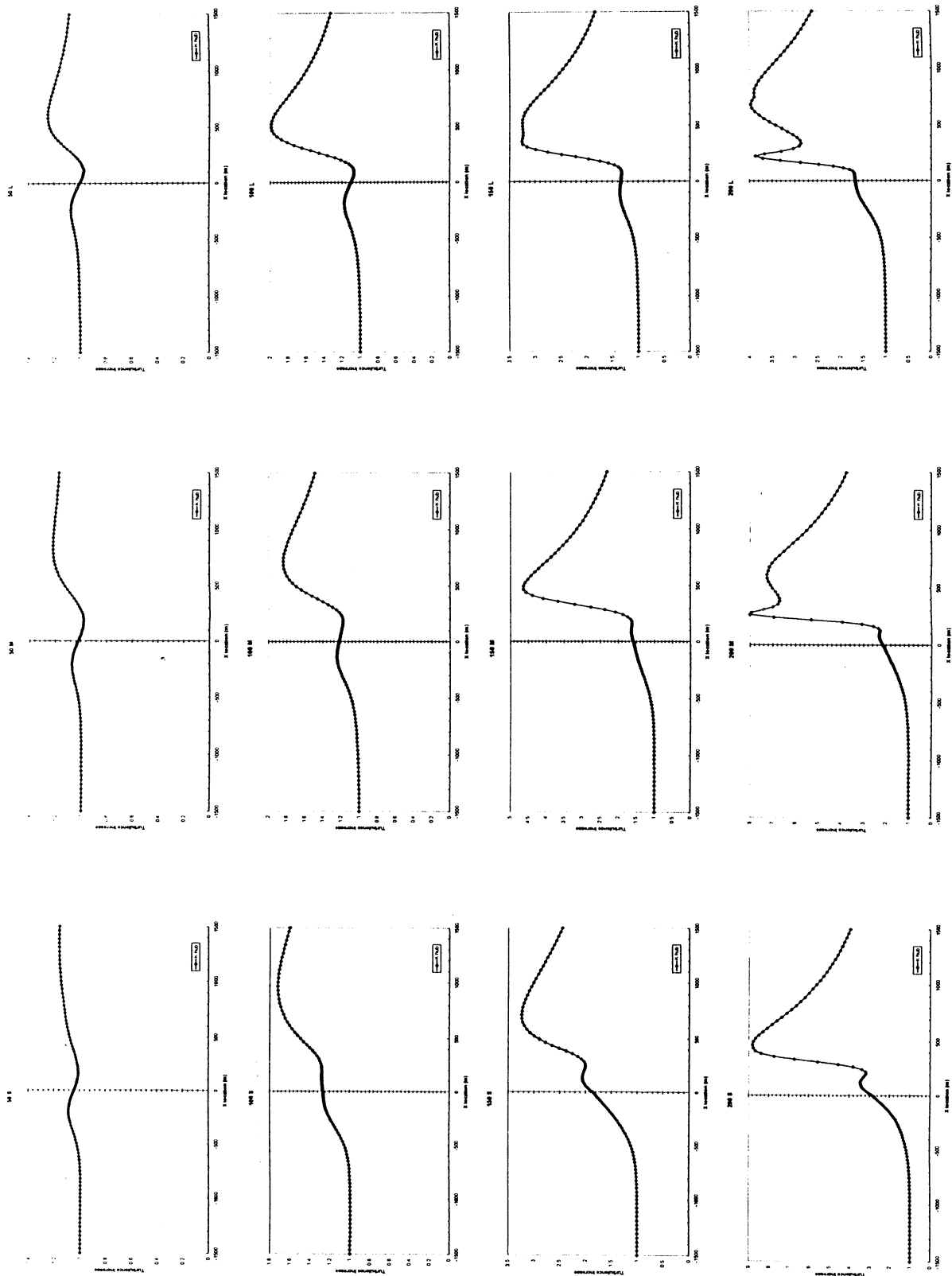


Table I-5: Turbulence increase at hub height

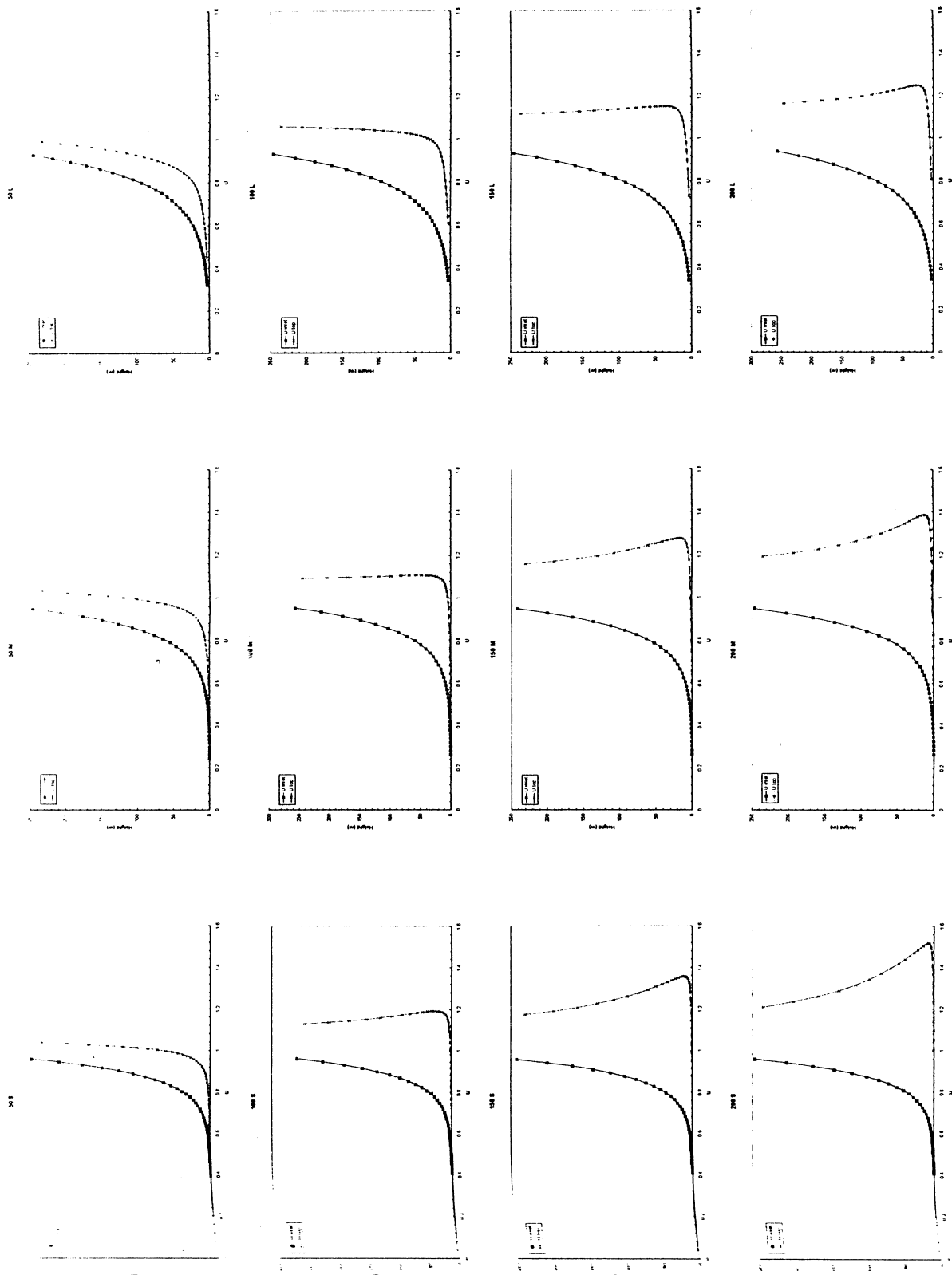


Table I-6: Wind shear profiles

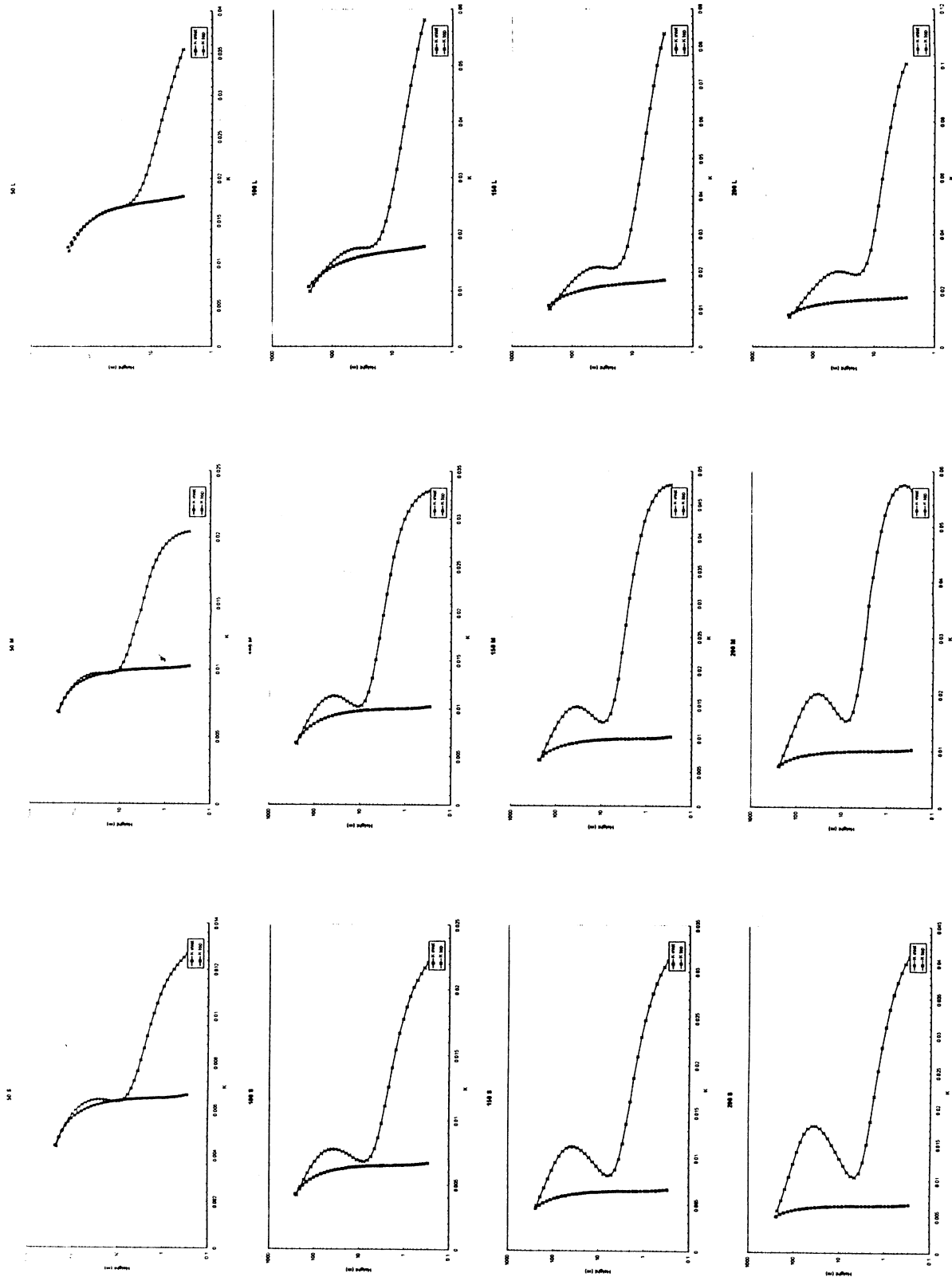


Table 1-7: Turbulence energy profiles

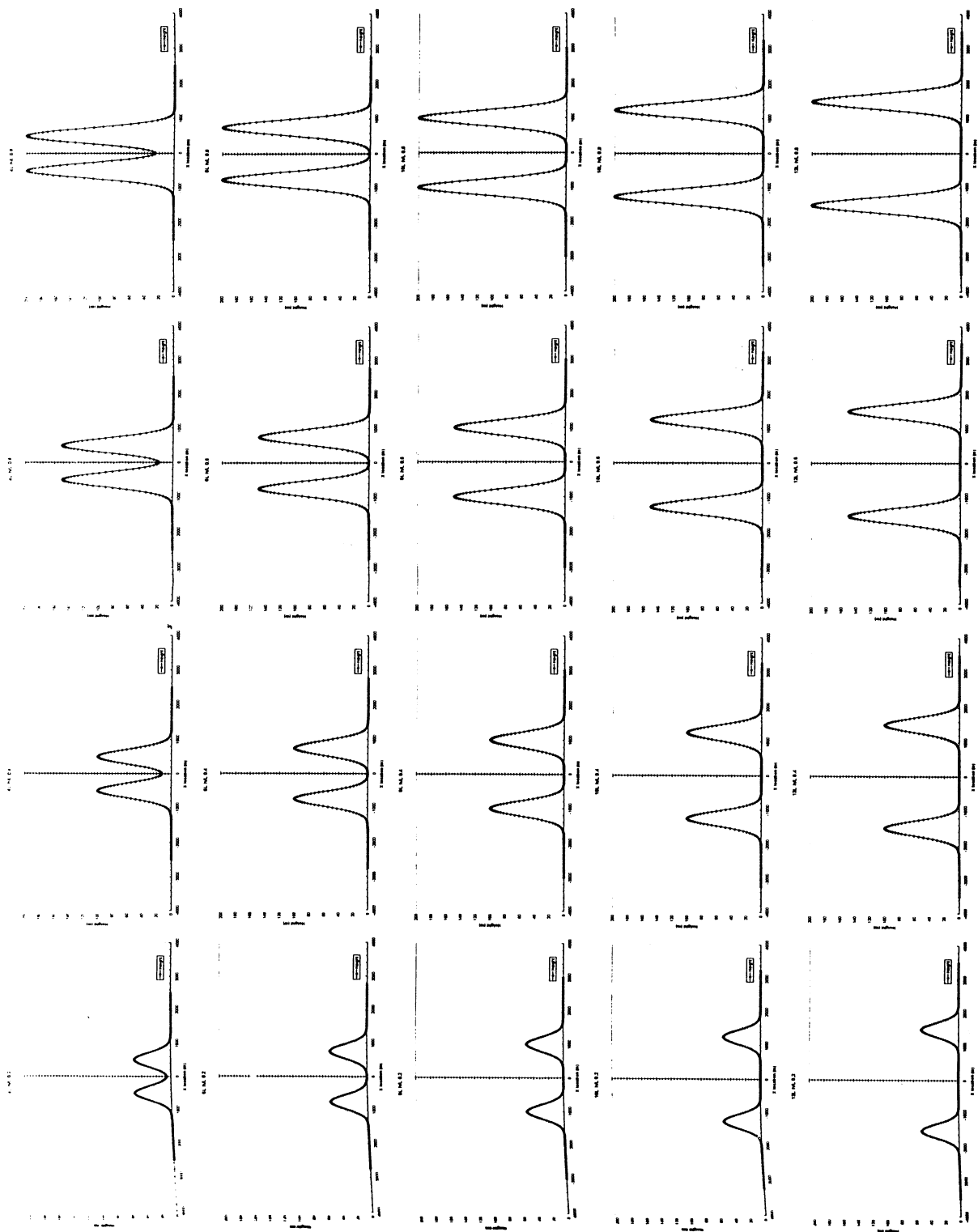


Table I-8: Hill geometry

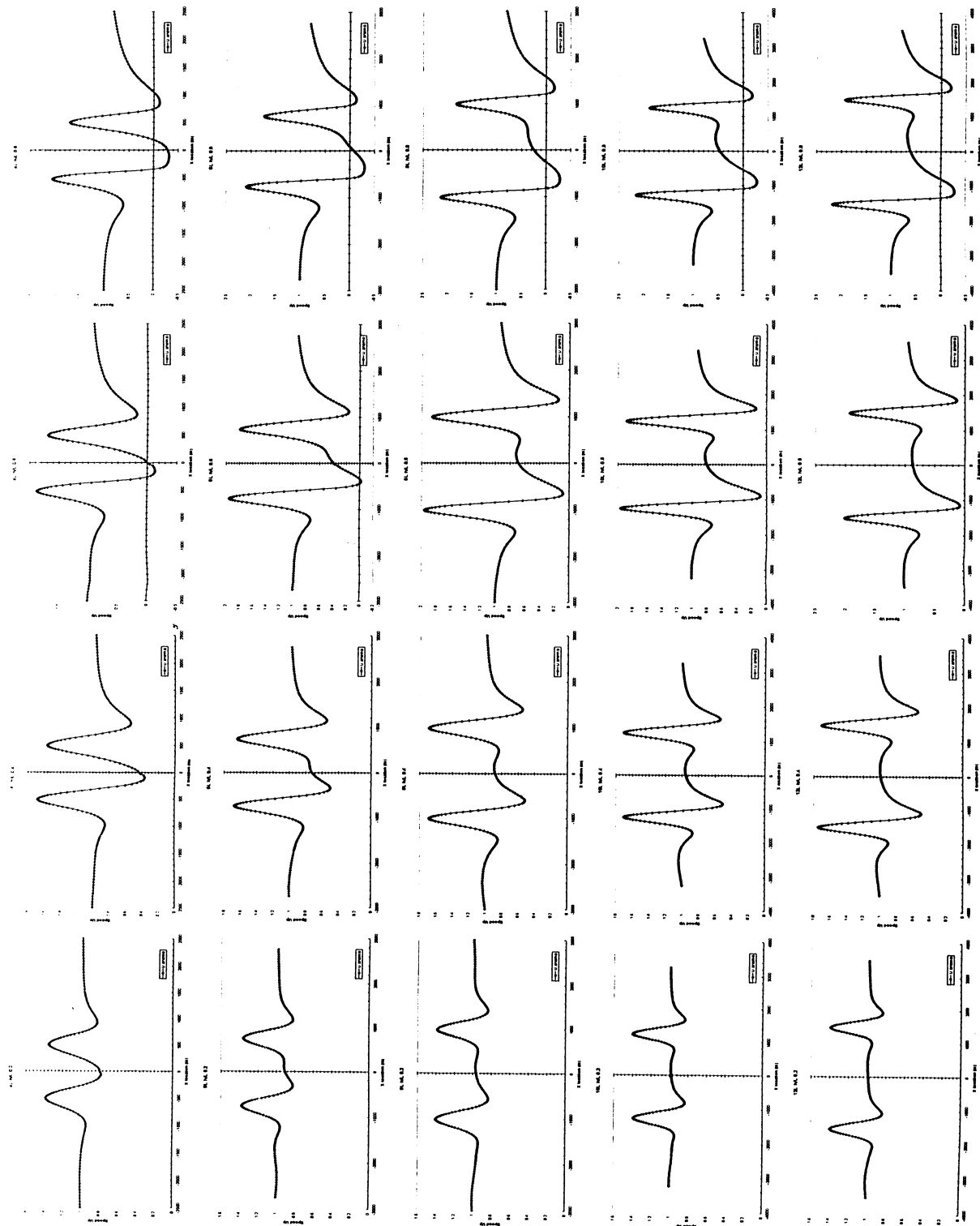


Table 1-9: Speed up at anemometer height

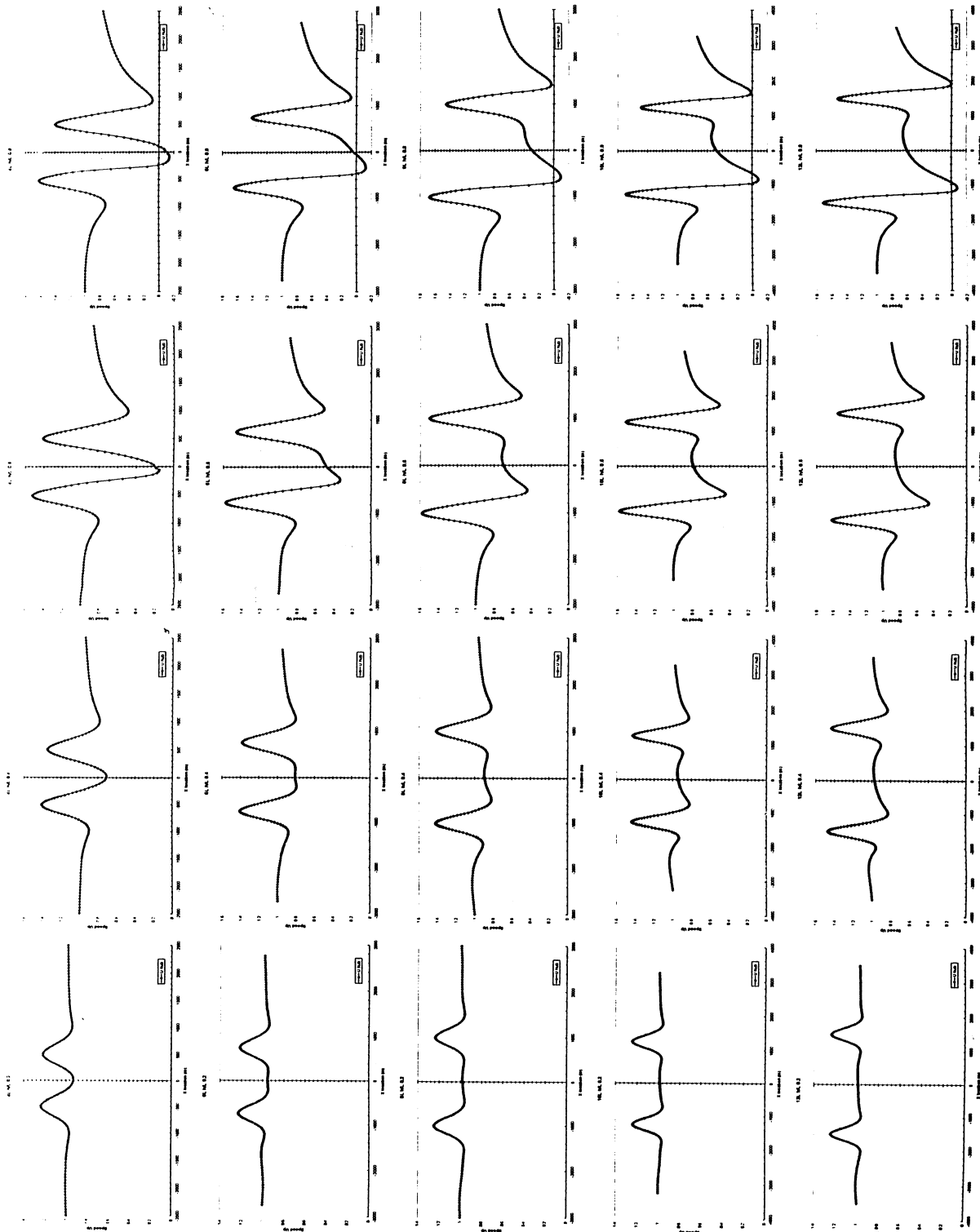


Table I-10: Speed up at hub height

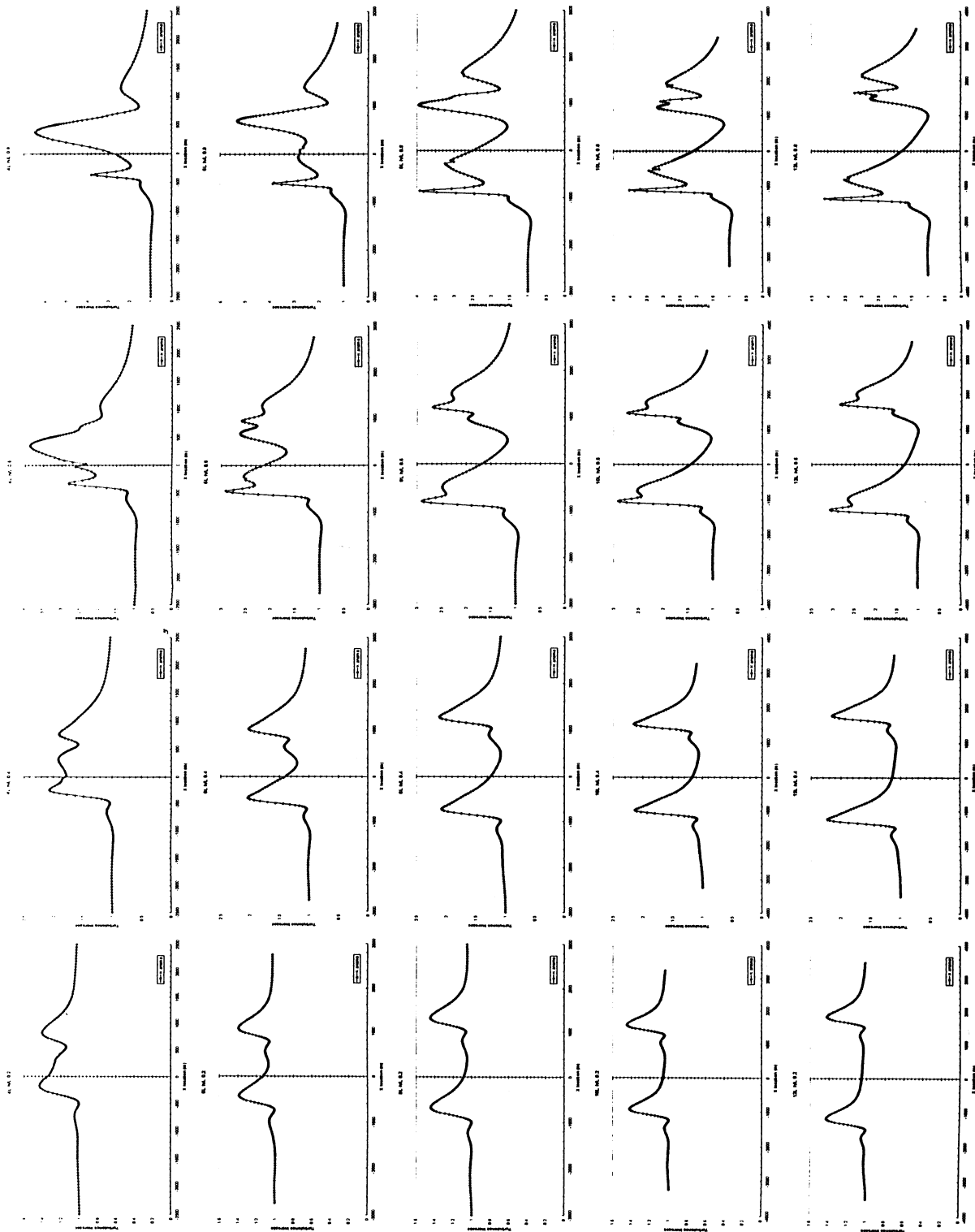


Table I-11: Turbulence increase at anemometer height

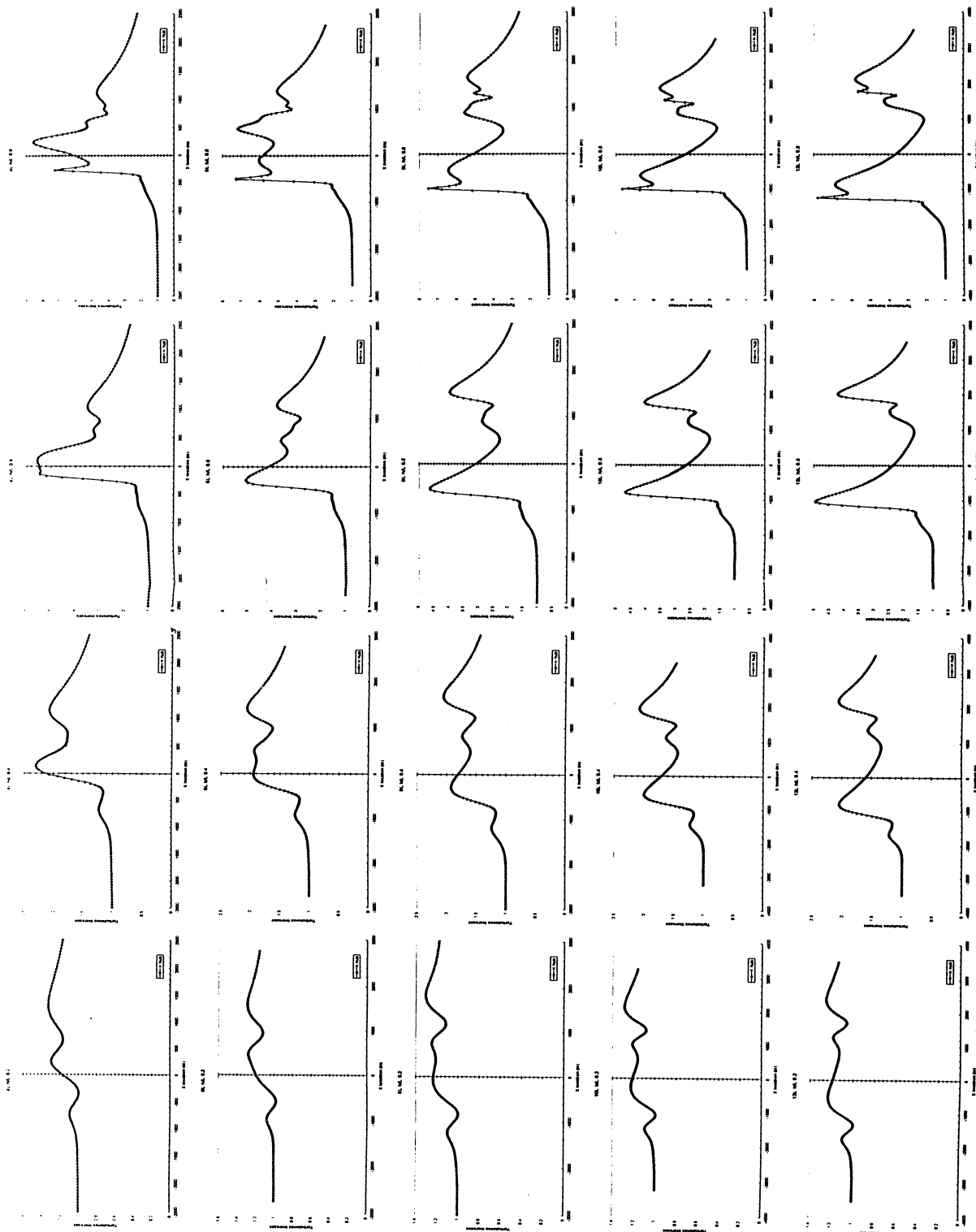


Table I-12: Turbulence increase at hub height

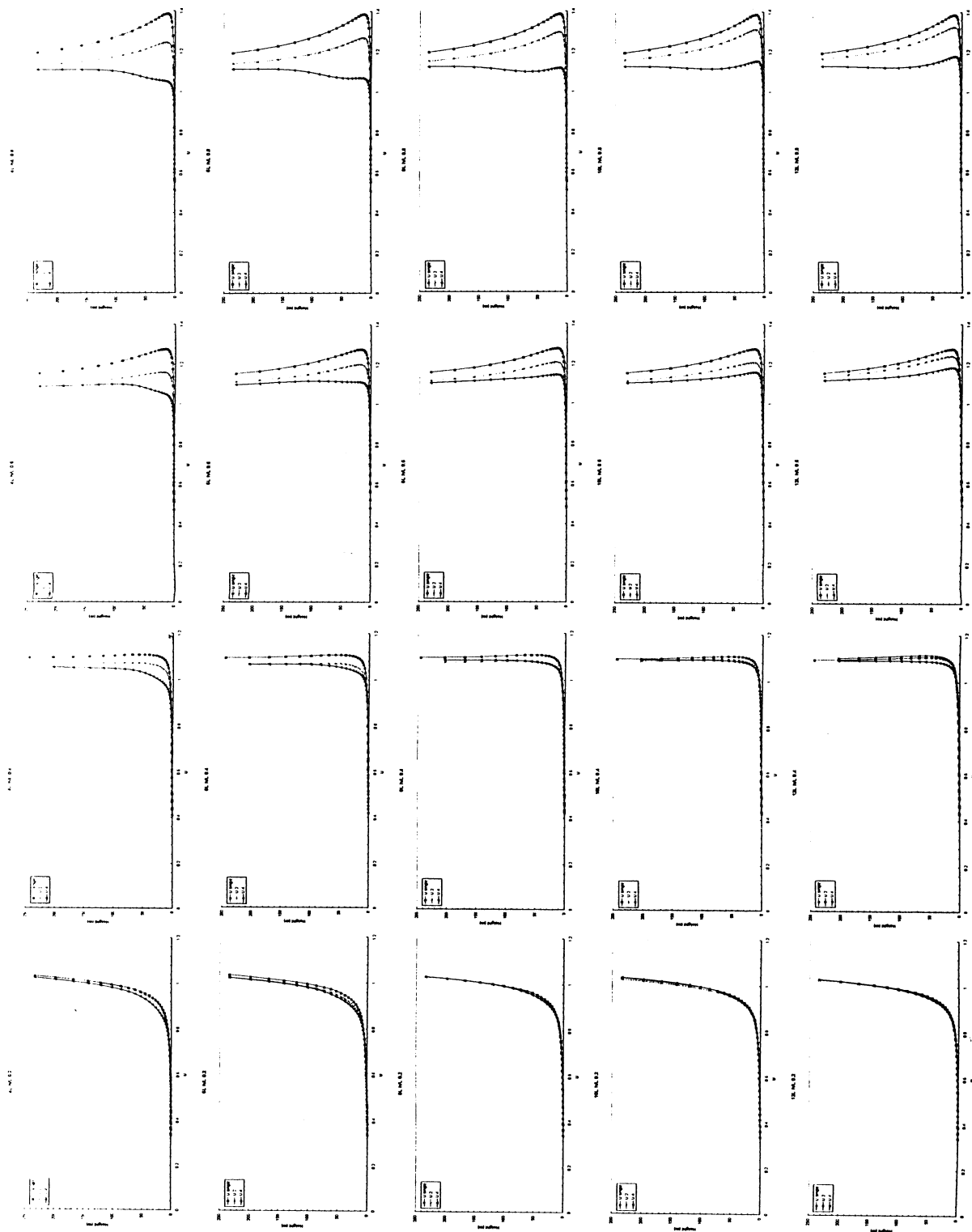


Table I-13: Single Hill - Double Hill Wind Shear Profiles Comparison

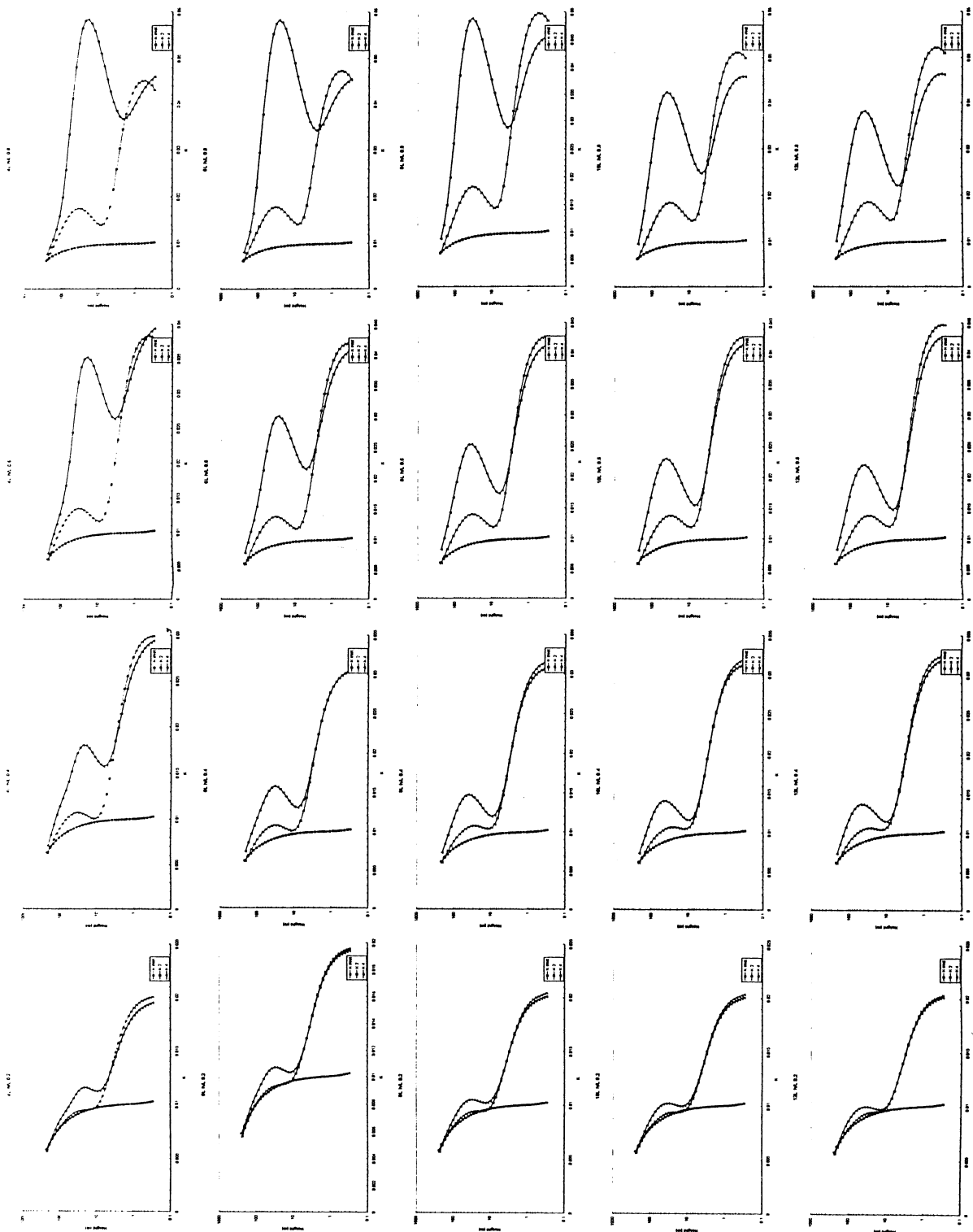


Table 1-14: Turbulence energy profiles

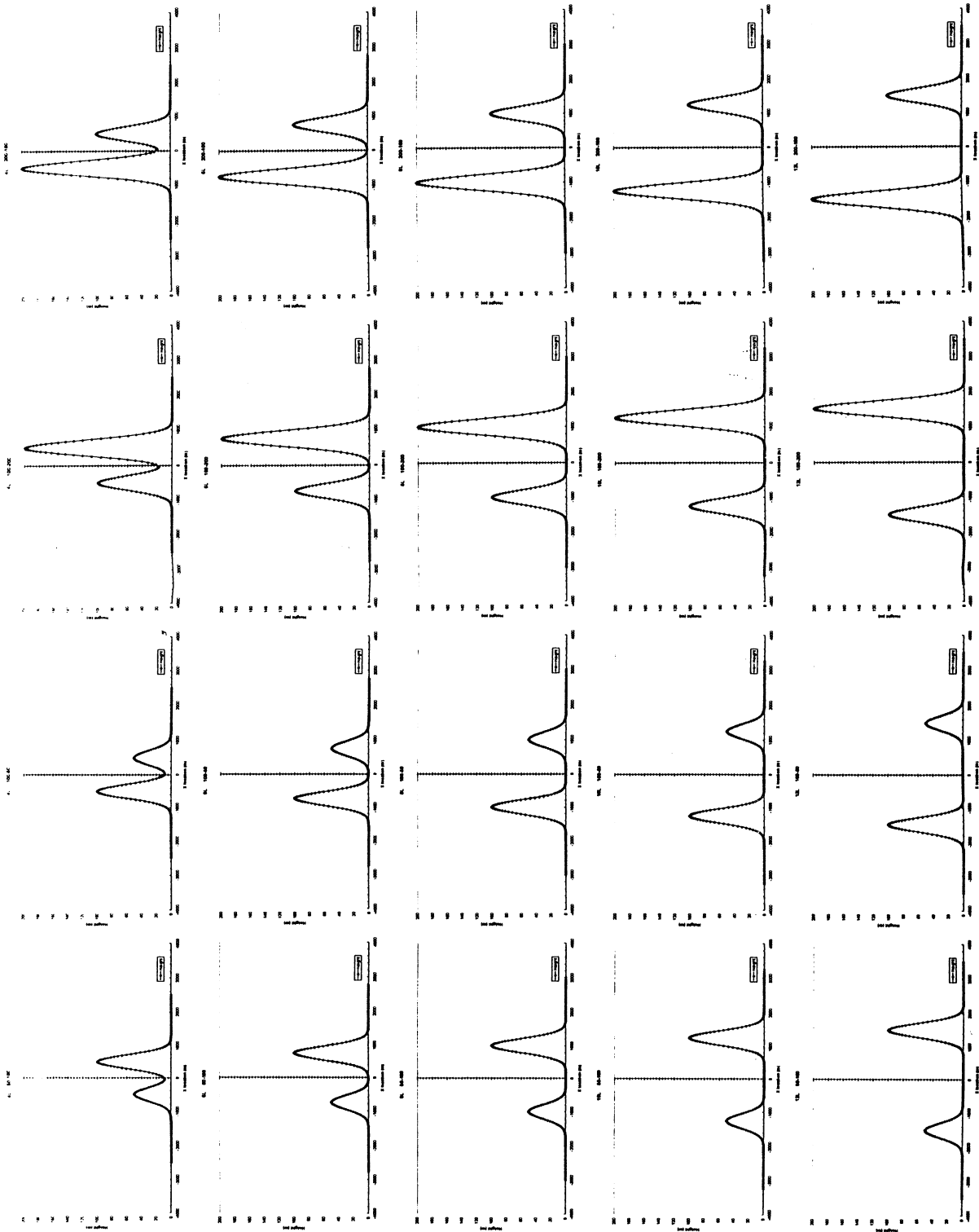


Table I-15: Hill geometry

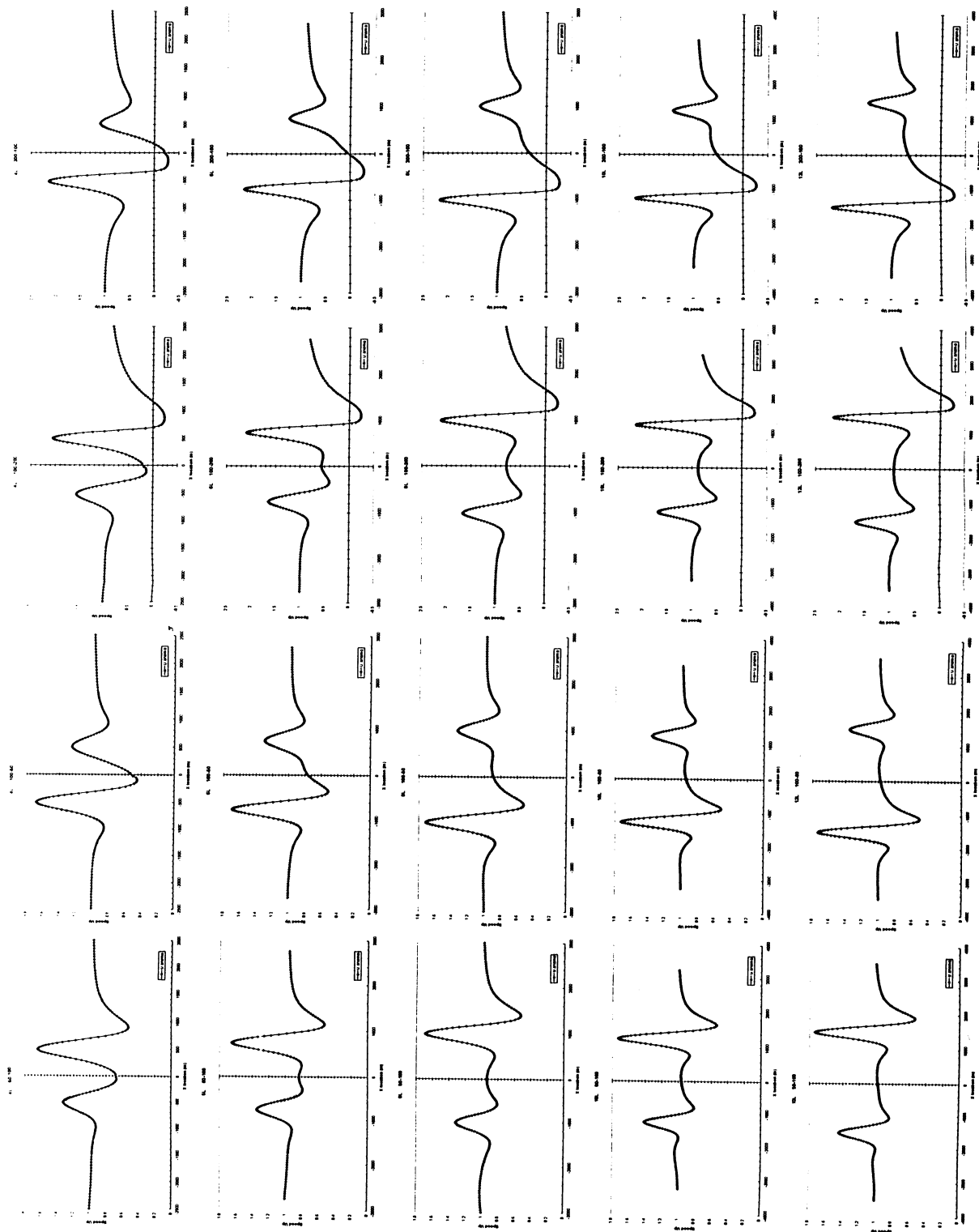


Table I-16: Speed up at anemometer height

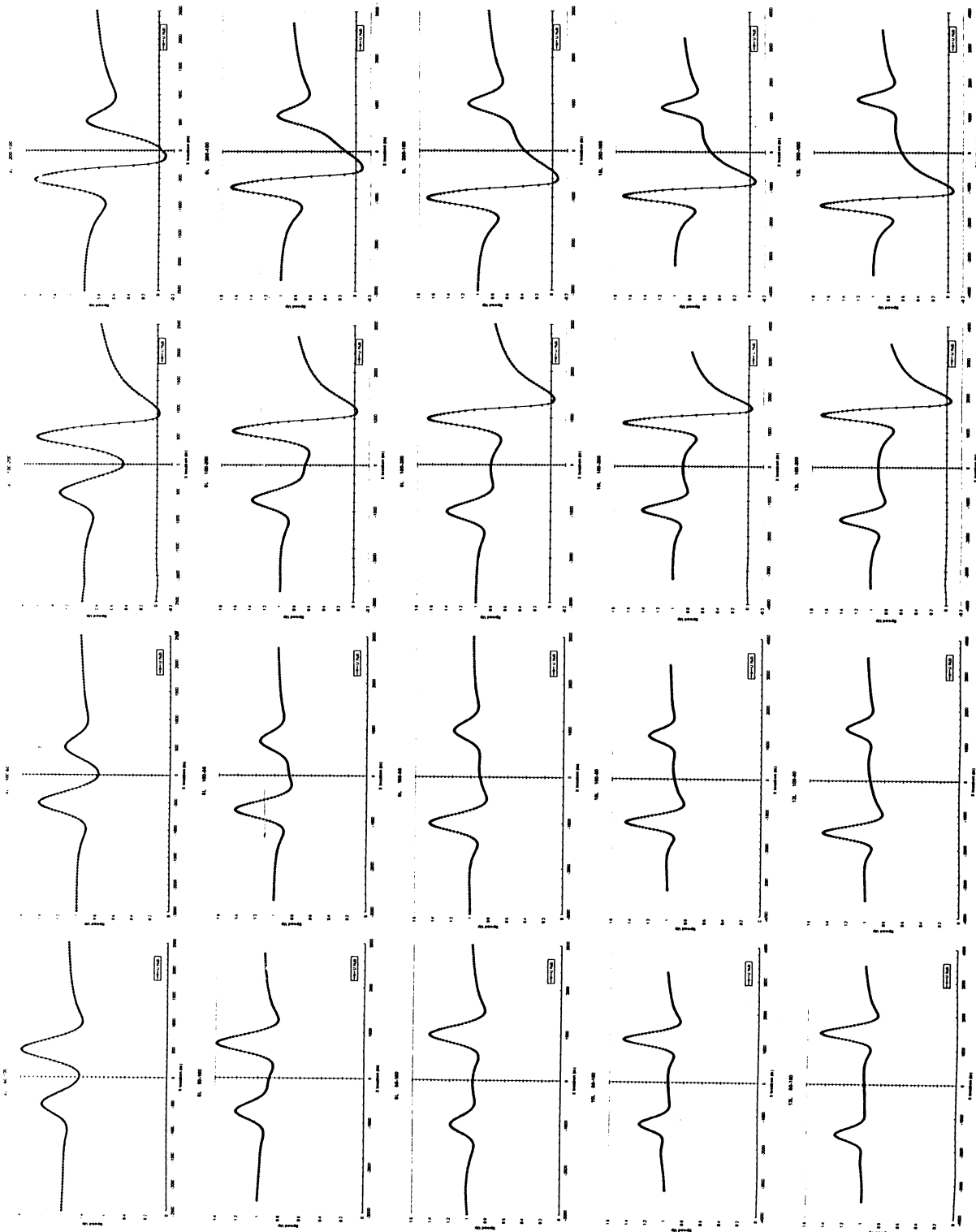


Table J-17: Speed up at hub height

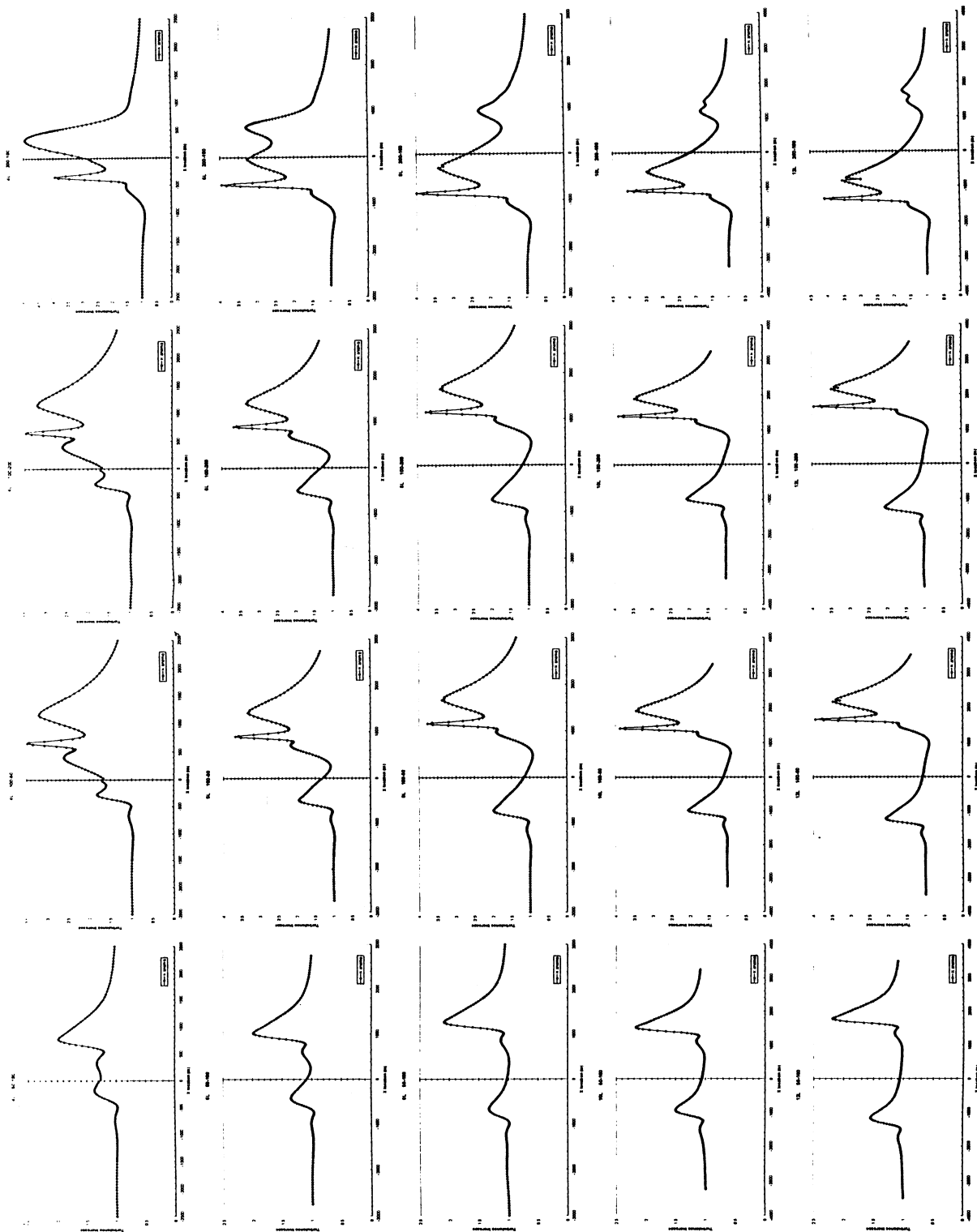


Table I-18: Turbulence energy at anemometer height

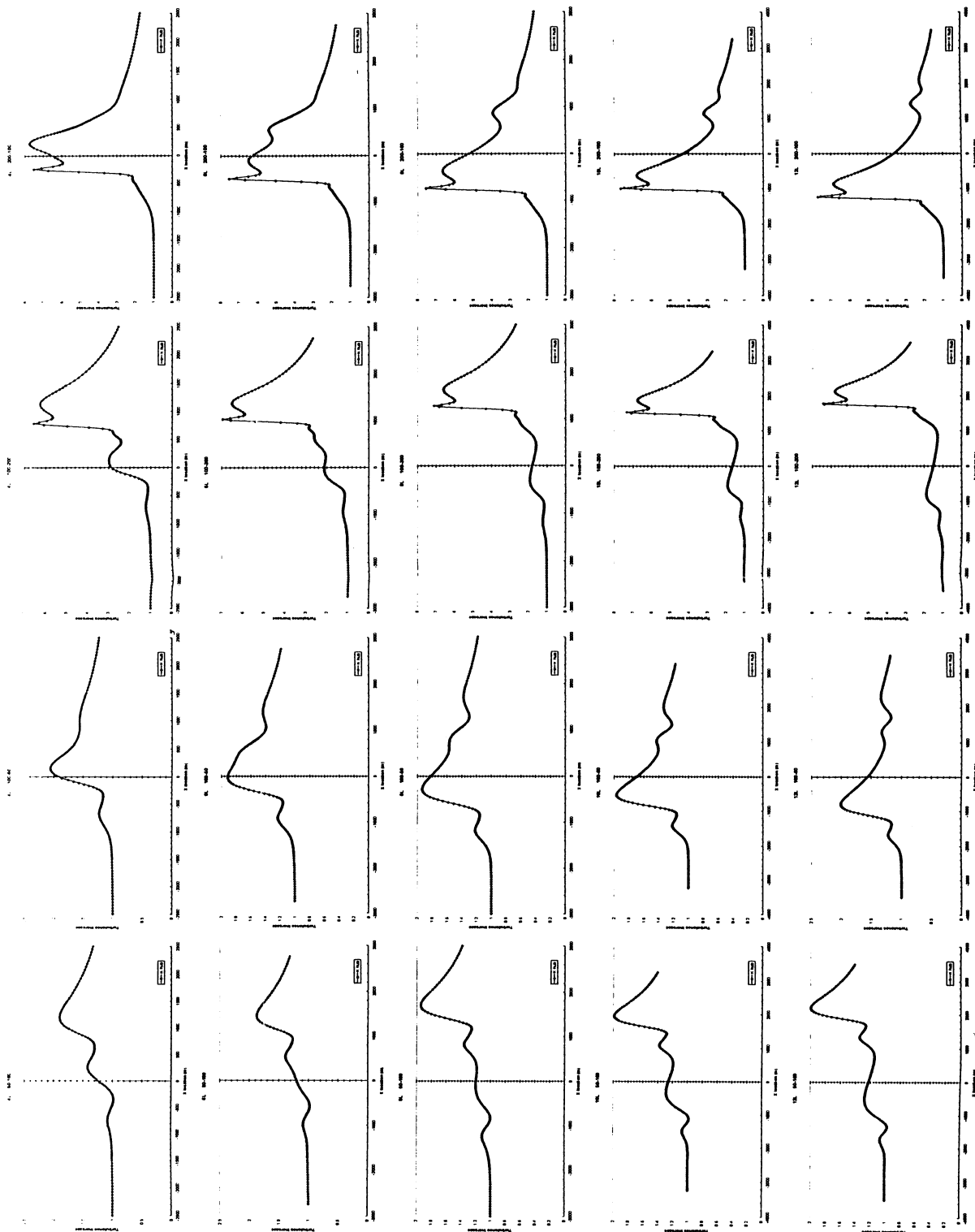


Table I-19: Turbulence energy at hub height

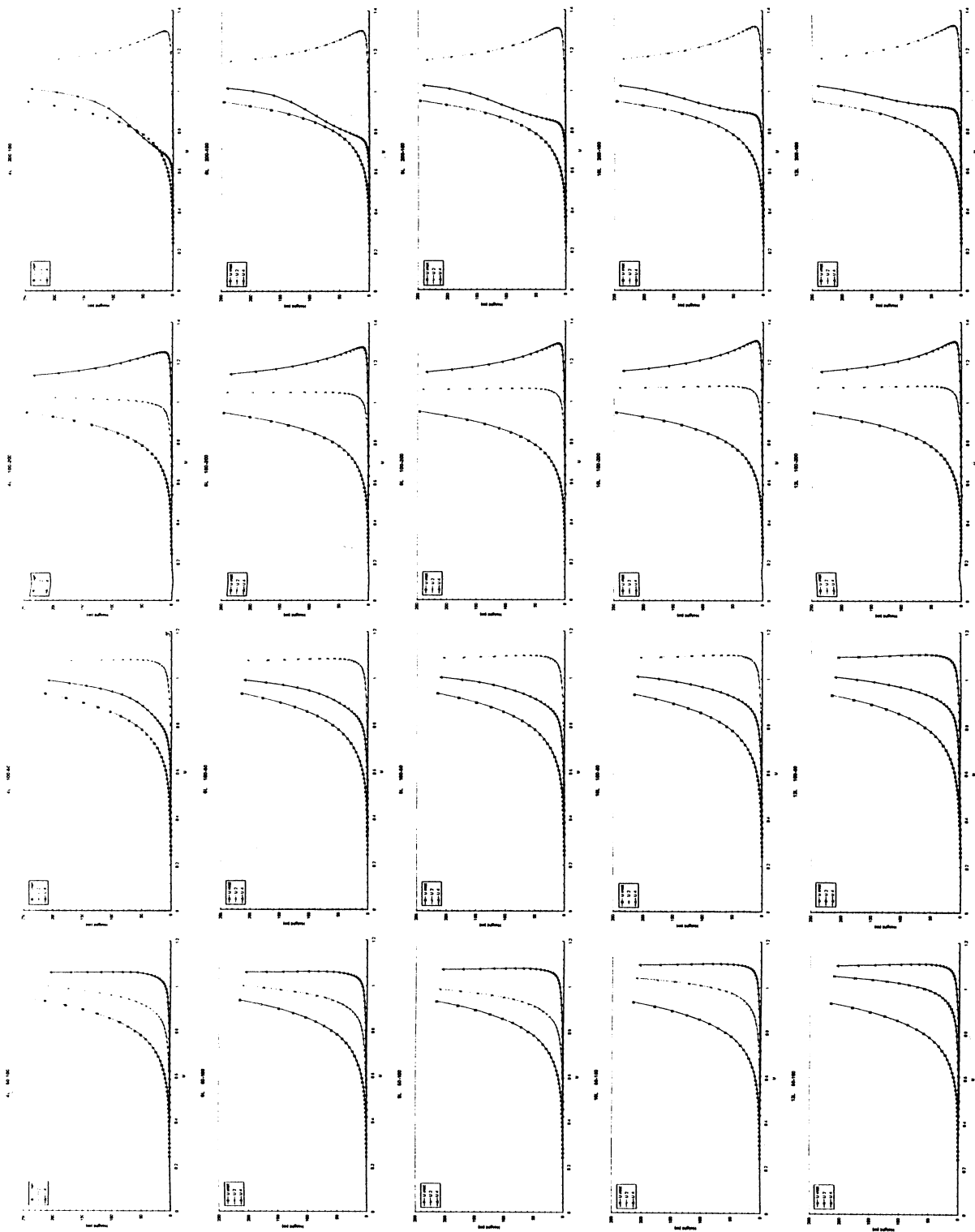


Table I-20: Wind shear profiles

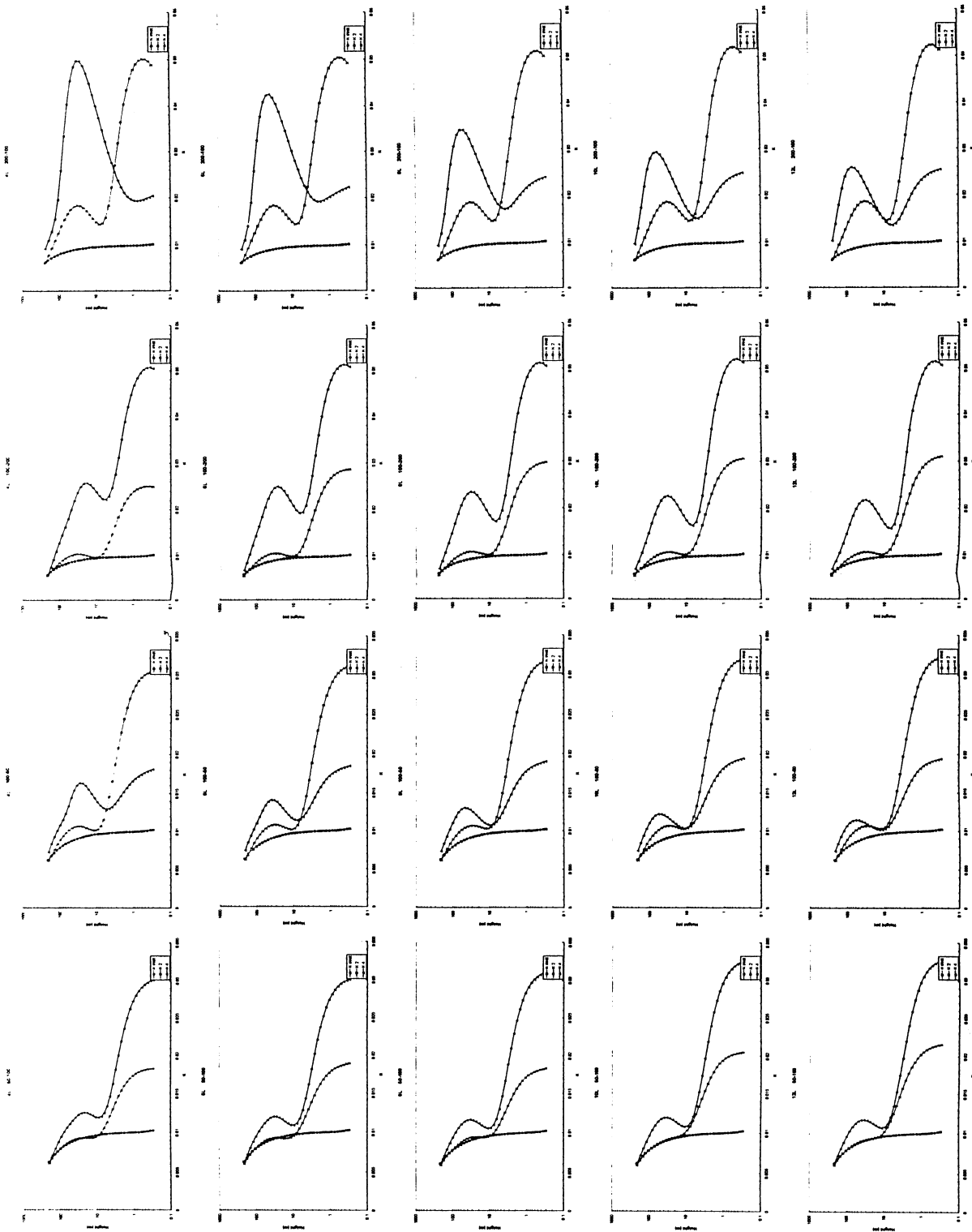


Table I-21: Turbulence profiles

Appendix B A simplified wind shear law for hill-tops

A semi-empirical wind shear law for hill-tops is presented here. The proposed formulas have been obtained by analysing parametric results obtained for Gaussian hills using the viscous-inviscid interaction method developed at CRES for mean wind field simulations in complex terrain. Further details on the method can be found in references [B1] and [B2].

B.1 Nomenclature

- z : height above ground level
 z_0 : roughness length
 H : hill height
 L : hill length at $\frac{H}{2}$ height
 u : normalised longitudinal wind component
 $u_{t,\beta}$: normalised “flat terrain equivalent” friction velocity (a function of the roughness length and the atmospheric boundary layer thickness)
 k : Von Karman Constant = 0.41

B.2 Single hill-top profile law

The resulted wind-shear law is the following

$$u(H, L, z_0, z) = 1 + f_1(H, L, z) + (1 + f_2(H, L, z_0))(1 + f_3(H, L, z_0)) + \frac{u_{t,\beta}}{k} (1 + f_2(H, L, z_0)) \ln \frac{z}{z_0}$$

where f_1 represents the potential flow part

$$f_1(H, L, z) = a_1 \left(\frac{H}{L} \right) \frac{1}{\left(1 + \frac{z}{L} \right)^2}$$

and the functions f_2, f_3 , corresponding to the viscous part, read

$$f_2(H, L, z_0) = \left(b_1 + b_2 \ln \left(\frac{z_0}{L} \right) + b_3 \ln^2 \left(\frac{z_0}{L} \right) \right) \left(\frac{H}{L} \right) - \left(b_4 + b_5 \ln \left(\frac{z_0}{L} \right) + b_6 \ln^2 \left(\frac{z_0}{L} \right) \right) \left(\frac{H}{L} \right)^2$$

$$f_3(H, L, z_0) = - \left(c_1 + c_2 \ln \left(\frac{z_0}{L} \right) + c_3 \ln^2 \left(\frac{z_0}{L} \right) \right) \left(\frac{H}{L} \right)$$

The best-fitted values of the model constants are:

$$a_1 = 1.05 \quad b_1 = 0.49 \quad b_2 = 0.167 \quad b_3 = 0.0066 \quad b_4 = 0.105$$

$$b_5 = 0.04 \quad b_6 = 0.0014 \quad c_1 = 0.165 \quad c_2 = 0.018 \quad c_3 = 0.00065$$

B.3 Example

The application of the above formulas for a Greek complex terrain site (Andros Island) with $H/L = 0.1$ and $z_0 = 0.15$ m is presented in figure B.1. Calculations (continuous curves) are compared against experimental data obtained at two neighbour masts, called M1 and M2. The dashed lines represent the corresponding estimation of the single-slope (flat terrain) log-law.

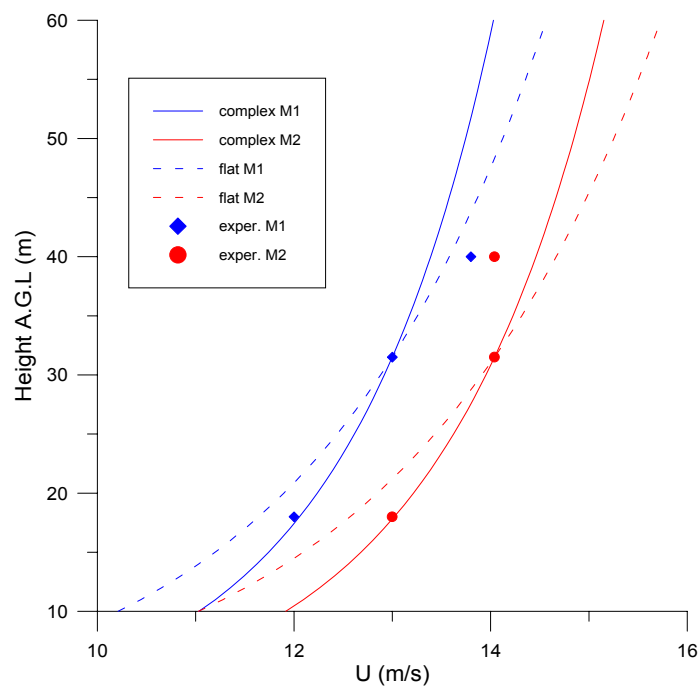


Figure B.1 Application of the Hill Top velocity profile model at Andros

B.4 References

- [B1] D.I. Douvikas, “3D Flow Computations over Complex Terrain - An Integral based Formulation”, CRES report, Oct. 1997.
- [B2] D.I. Douvikas and P.K. Chaviaropoulos, “3D Viscous Computations over Complex Terrain using Integral Boundary Layer Method”, Proc. EWEC 97, Oct. 1997, Dublin, U.K.

Appendix B Theoretical investigation of the Reynolds Stress Tensor in complex terrain [C1]

The terrain influence on turbulence structure is investigated in this Appendix. The presented theoretical approach is based on the non-isotropic Reynolds-Stress-Model proposed by Saffman [C2]. The investigation is limited to 2-D and quasi-3D flows. The emphasis is put on establishing the interrelation between the standard deviation ratios of the wind components with the mean flow gradients.

C.1 Definitions

$(x_i ; i = 1,2,3) \equiv (x, y, z)$	Cartesian coordinates
$(U_i ; i = 1,2,3) \equiv (U, V, W)$	Mean flow velocity components
$(u_i ; i = 1,2,3) \equiv (u, v, w)$	Velocity fluctuation components
$\underline{\underline{R}} : R_{ij} = \overline{u_i u_j} ; i, j = 1,2,3$	Correlation tensor
$\underline{\underline{S}} : S_{ij} = \frac{1}{2} \left(\frac{\partial U_i}{\partial x_j} + \frac{\partial U_j}{\partial x_i} \right)$	Mean strain rate
$\underline{\underline{\Omega}} : \Omega_{ij} = \frac{1}{2} \left(\frac{\partial U_i}{\partial x_j} - \frac{\partial U_j}{\partial x_i} \right)$	Rotation
$k = \frac{1}{2} (R_{11} + R_{22} + R_{33})$	Kinetic energy of turbulence
$\omega = \varepsilon / k$	Specific dissipation rate

C.2 A Second order expression for Reynolds Stresses

Following ref. [C2], the following non-isotropic turbulence model is introduced.

$$\frac{1}{k} \underline{\underline{R}} = \frac{2}{3} \underline{\underline{I}} - \frac{2}{\omega} \underline{\underline{S}} + D \frac{1}{\omega^2} [\underline{\underline{S}} \underline{\underline{\Omega}} - \underline{\underline{\Omega}} \underline{\underline{S}}] \quad ; \quad D \text{ is a constant to be defined}$$

C.3 Application in 2-D flows

The following assumptions / definitions are introduced for 2-D flows

$$V = 0, \quad \frac{\partial()}{\partial y} = 0 \quad ; \quad s = \frac{\partial U}{\partial z}, \quad \lambda = \frac{\partial U / \partial x}{\partial U / \partial z}, \quad \mu = \frac{\partial W / \partial x}{\partial U / \partial z}$$

Then, it can be shown that the only non-zero correlation tensor components are:

$$\frac{\sigma_u^2}{k} \equiv \frac{\overline{u^2}}{k} = \frac{2}{3} - 2\left(\frac{s}{\omega}\right)\lambda - \frac{D}{2}\left(\frac{s}{\omega}\right)^2 (1 - \mu^2)$$

$$\frac{\sigma_v^2}{k} \equiv \frac{\overline{v^2}}{k} = \frac{2}{3}$$

$$\frac{\sigma_w^2}{k} \equiv \frac{\overline{w^2}}{k} = \frac{2}{3} + 2\left(\frac{s}{\omega}\right)\lambda + \frac{D}{2}\left(\frac{s}{\omega}\right)^2 (1 - \mu^2)$$

$$\frac{-(\tau / \rho)}{k} \equiv \frac{\overline{uw}}{k} = -\left(\frac{s}{\omega}\right)(1 + \mu) + D\left(\frac{s}{\omega}\right)^2 \lambda(1 - \mu)$$

Consequently, in all 2-D cases, flat or complex

$$\sigma_u^2 + \sigma_w^2 = 2\sigma_v^2 \quad \text{or} \quad \left(\frac{\sigma_u}{\sigma_v}\right)^2 + \left(\frac{\sigma_w}{\sigma_v}\right)^2 = 2$$

Deviations from the above 2-D SDV's formula indicate 3-dimensionality effects

Application in 2-D Flat Terrain. Estimating the D constant

For 2-D flat terrain it can be assumed that

$$\sigma_u : \sigma_v : \sigma_w \equiv 1 : 0.8 : 0.5$$

and, in addition,

$$\lambda, \mu \cong 0$$

$$U = \frac{u_T}{\kappa} \ln\left(\frac{z}{z_0}\right) \Rightarrow s = \frac{u_T}{\kappa z} \quad \text{in the log - layer}$$

$$k = \frac{u_T^2}{A}, \quad \omega = \frac{u_T}{A\kappa z} \Rightarrow \left(\frac{s}{\omega}\right) = A = \text{const.} \cong 0.183$$

where u_T is the friction velocity. Then, the non-zero components of the correlation tensor yield

$$\begin{aligned} \left(\frac{\sigma_u^2}{k} \right)_{Flat} &= \frac{2}{3} - \frac{1}{2} DA^2 \\ \left(\frac{\sigma_v^2}{k} \right)_{Flat} &= \frac{2}{3} \\ \left(\frac{\sigma_w^2}{k} \right)_{Flat} &= \frac{2}{3} + \frac{1}{2} DA^2 \\ \left(\frac{\overline{uw}}{k} \right)_{Flat} &\equiv \frac{-(\tau / \rho)}{k} \equiv -\frac{u_T}{k} = -A \end{aligned}$$

Applying the 1 : 0.8 : 0.5 rule to the above expression D is estimated to be -23.4.

Application in 2-D Complex Terrain

Assuming that the ratio (s/ω) is constant and retains its flat terrain value A, the non-zero entries of the Reynolds stress tensor yield:

$$\begin{aligned} \left(\frac{\sigma_u^2}{k} \right)_{Complex} &= \left(\frac{\sigma_u^2}{k} \right)_{Flat} - 2A\lambda + \frac{1}{2} DA^2 \mu^2 \\ \left(\frac{\sigma_v^2}{k} \right)_{Complex} &= \left(\frac{\sigma_v^2}{k} \right)_{Flat} = \frac{2}{3} \\ \left(\frac{\sigma_w^2}{k} \right)_{Complex} &= \left(\frac{\sigma_w^2}{k} \right)_{Flat} + 2A\lambda - \frac{1}{2} DA^2 \mu^2 \\ \left(\frac{\overline{uw}}{k} \right)_{Complex} &= \left(\frac{\overline{uw}}{k} \right)_{Flat} - A\mu + DA^2 \lambda (1 - \mu) \end{aligned}$$

Following Wilcox [C3] it can be shown that for high Reynolds numbers $(s/\omega)^2 = \text{const.} * P$, where P represents the net production per unit dissipation of the turbulent kinetic energy.

Considering a 2-D hill case and the accelerating part of the flow (upwind from the hill-top) the turbulence kinetic energy is expected to be increased compared to its free-stream (flat terrain) value, while λ takes positive values. As a consequence (and since D is negative), the normalized (by k) u-component variance is decreased in respect to its free-stream value, the w-component normalized variance is accordingly increased while the v-component variance retains its free-stream value. This means that turbulent energy is transferred from the u- to the w- component. In absolute terms both variances of the v- and w-components are increased because of k while no direct conclusion may be stated for the u-component (since k is increased but the normalized variance is decreased).

C.4 Application in 3-D flows

The treatment of the fully 3-D case is beyond the scope of the present work. A simplified 3-D case will be considered instead, which is based on the assumption that all the mean flow partial derivatives in respect to one of the Cartesian directions are negligible. This can simulate the case of a 2-D infinite hill which faces an oblique flow in respect to its axis of symmetry, for instance. In this case one may model the transversal wind component in respect to the longitudinal one using, for example, the Johnston's triangular profile which is applied below. Under these assumptions:

$$\frac{\partial U_i}{\partial y} \equiv 0 \quad ; \quad \forall i=1,2,3 \quad \text{and} \quad V = a(U_e - U)$$

where the subscript e denotes the external (inviscid part) flow and α is the transversal profile parameter which measures the local three-dimensionality of the flow field. Under the above assumptions the non-zero entries of the normalized Reynolds stress tensor yield:

$$\begin{aligned} \left(\frac{\sigma_u^2}{k} \right)_{3D-Complex} &= \left(\frac{\sigma_u^2}{k} \right)_{2D-Complex} + \frac{1}{2} DA^2 a^2 \lambda^2 &< \left(\frac{\sigma_u^2}{k} \right)_{2D-Complex} \\ \left(\frac{\sigma_v^2}{k} \right)_{3D-Complex} &= \left(\frac{\sigma_v^2}{k} \right)_{2D-Complex} - \frac{1}{2} DA^2 a^2 (\lambda^2 + 1) &> \left(\frac{\sigma_v^2}{k} \right)_{2D-Complex} \\ \left(\frac{\sigma_w^2}{k} \right)_{3D-Complex} &= \left(\frac{\sigma_w^2}{k} \right)_{2D-Complex} + \frac{1}{2} DA^2 a^2 &< \left(\frac{\sigma_w^2}{k} \right)_{2D-Complex} \\ \left(\frac{\overline{uv}}{k} \right)_{3D-Complex} &= aA\lambda + \frac{1}{2} DA^2 a(1 + \lambda^2) \\ \left(\frac{\overline{uw}}{k} \right)_{3D-Complex} &= -A(1 + \mu) + DA^2 \lambda \left(1 - \mu + \frac{1}{2} a^2 \right) \end{aligned}$$

implying that the uv correlation does not vanish any more. It is also seen that the diagonal terms satisfy the following non-equality:

$$\begin{aligned} \left(\frac{\sigma_u^2}{k} \right)_{3D-Complex} + \left(\frac{\sigma_w^2}{k} \right)_{3D-Complex} - 2 \left(\frac{\sigma_v^2}{k} \right)_{3D-Complex} &= \frac{3}{2} DA^2 a^2 (1 + \lambda^2) < 0 \quad \text{or} \\ \left(\frac{\sigma_u^2}{k} \right)_{3D-Complex} + \left(\frac{\sigma_w^2}{k} \right)_{3D-Complex} &< 0 \end{aligned}$$

C.5 Conclusions

For the considered cases it has been shown that

$$\left(\frac{\sigma_u}{\sigma_v} \right)^2 + \left(\frac{\sigma_w}{\sigma_v} \right)^2 \leq 2$$

where the equality holds for all 2-D flows. In the accelerating part of a 2-D flow the kinetic energy of turbulence increases, while turbulent energy is transferred from the longitudinal u to the vertical w wind component. This implies that the turbulence in that area becomes more isotropic. This result is in agreement with the available complex terrain experimental data.

C.6 References

- [C1] P.K. Chaviaropoulos, Unpublished work at CRES.
- [C2] P.G. Saffman, "Development of a Complete Model for the Calculation of Turbulent Shear Flows" April 1976 Symposium on Turbulence and Dynamic Systems, Duke Univ., Durham, NC.
- [C3] D.C. Wilcox, Turbulence Modelling for CFD, © 1993 by DCW Industries Inc., ISBN 0-9636051-0-0

Appendix C Tables from measurement-based PI

The application of the multivariate regression analysis to the experimental load data bases of three machines (WXT110, V27 and NTK500) erected at complex terrain sites is presented in this appendix. The theoretical background of the approach is briefly discussed first.

D.1 Theoretical background

To establish the relative importance of the inflow parameters to the equivalent load range, the multiple regression analysis is adopted. The topics that are discussed herein are related to the regression analysis application and assessment [D1] as well as to the parameter identification procedure ([D2] and [D3]).

The multivariate regression analysis is based on least square fitting process as a way to identify the maximum likelihood estimator of the fitted parameters. It is assumed that the measurement errors are independent and normally distributed with constant standard deviation. The scope of the regression is the estimation of the coefficients $\alpha_k, k=1, \dots, M$, for the expression of the dependent variable y as follows:

$$y(x_i) = \sum_{k=1}^M a_k X_k(x_i) + E(x_i), \quad i = 1, \dots, N$$

where $X_k(x_i)$ is the value of the k^{th} independent variable at point x_i and $E(x_i)$ is the associated error at the same point.

Chi-square fitting is applied as the weighted least square fitting process, in which the magnitude χ^2 defined as:

$$\chi^2 = \sum_{i=1}^N \left(\frac{y_i - \hat{y}_i}{\sigma_i} \right)^2, \quad \hat{y}_i = \sum_{k=1}^M a_k X_k(x_i)$$

is minimised. The magnitude σ_i presents the measurement standard error at point $(y(x_i), x_i)$. If the measurement errors are not known (as in the present practice) they are all set equal to unity. The number $v=N-M$ represents the fitting degrees of freedom.

The minimum of χ^2 occurs where its derivatives with respect to parameters $\alpha_k, k=1, \dots, M$ vanish. The resulting linear equations are solved by the Gauss-Jordan elimination technique, yielding the coefficients $\alpha_j, j=1, \dots, M$:

$$a_j = \sum_{k=1}^M C_{jk} \left[\sum_{i=1}^N \frac{y_i X_k(x_i)}{\sigma_i^2} \right], \quad C_{jk} = \left[\sum_{i=1}^N \frac{X_j(x_i) X_k(x_i)}{\sigma_i^2} \right]^{-1}_{jk}, \quad j = 1, \dots, M$$

where the standard deviation related to the estimate of a_j is given by the equation:

$$\sigma(a_j) = \sqrt{\left(\sum_{i=1}^N \sigma_i^2 \left(\frac{\partial a_j}{\partial y_i} \right)^2 \right)} = \sqrt{C_{jj}}$$

D.2 Assessment of the accuracy of the multivariate regression

For the assessment of the accuracy of the regression analysis, the following magnitudes were considered:

a) The total sum of squares (SSY), sum of squares due to error (SSE), sample squared correlation coefficient (R^2) and finally the fitting standard deviation $\sigma_{\hat{y}}$ defined as:

$$SSY = \sum_{i=1}^N (y_i - y_{mean})^2, SSE = \sum_{i=1}^N (y_i - \hat{y}_i)^2, R^2 = \frac{SSY - SSE}{SSY}, \sigma_{\hat{y}} = \sqrt{\frac{SSE}{N - M}}$$

b) F-test statistic, testing the hypothesis, H_0 : there is no significant overall regression using the M independent variables, is defined as follows:

$$F = \frac{SSY - SSE}{SSE} \left(\frac{N - M}{M - 1} \right)$$

Consequently the p-value for the above defined F-test is calculated from Fisher's F sampling distribution with M-1 and N-M degrees of freedom ($p_{F|M-1, N-M}$ 17).

c) For the quantitative assessment of the relation of the dependent variable on each of the independent parameters X_k , various magnitudes were considered, namely the regression coefficients α_k themselves, the relative per sigma dependence coefficient S_k or the t-test statistic for each parameter. The relative per sigma dependence coefficient S_k , is defined as:

$$S_k = a_k \frac{\sigma_{X_k}}{y_{mean}}, \sigma_{X_k} = \sqrt{\frac{\sum_{i=1}^N (X_k(x_i) - \overline{X_k})^2}{N - 1}}$$

The magnitude S_k represents the relative change of the dependent variable induced by the increase of the value of parameter X_k by its standard deviation σ_{X_k} within the regression domain²⁰. Assuming that the probability of that change is expected to be comparable for all independent variables, the relative assessment of the effect of each variable X_k on y can be attained. Although the above assumption is not valid in cases where the distribution of X_k , within the regression domain, differs significantly from normal, still the magnitude S_k offers a valuable means for weighting the dependence of each X_k on the dependent magnitude.

d) The t-test statistic, testing the hypothesis, H_0 : the regression coefficient a_k ²¹ is zero, is defined as follows:

$$t = \frac{a_k}{\sigma(a_k)}$$

Consequently the p-value for the above defined t-test is calculated from Student's t sampling distribution with N-M degrees of freedom ($p_{t|N-M}$ 22).

D.4 Tables

Table D.1 Sensitivity parameter table for WINCON W110XT operating at CRES test station

Fatigue load (1Hz equiv.)	U	Leq	Sensitivity parameter ($\partial Leq/\partial x_i$)				
			U	α_{ws}	σ_u	σ_v/σ_u	σ_w/σ_u
Flapwise b.m. (m=12)	5-8m/s	13,51	0,99	8,31	5,41	1,65	3,41
	8-11m/s	16,44	0,26	12,30	6,67	2,85	4,84
	13-17m/s	27,36	1,60	s.i.	8,77	4,90	14,82
Edgewise b.m. (m=12)	5-8m/s	31,6	0,30	1,40	1,31	0,32	1,13
	8-11m/s	32,96	0,45	2,83	1,90	0,79	1,81
	13-17m/s	39,81	1,30	s.i.	3,12	4,17	3,31
Shaft yaw (m=8)	5-8m/s	12,25	0,67	10,31	6,40	2,46	2,85
	8-11m/s	15,47	0,64	15,09	6,05	3,33	4,84
	13-17m/s	26,35	1,37	16,78	7,97	6,45	13,71
Shaft tilt (m=8)	5-8m/s	16,86	0,77	8,93	8,33	2,61	4,51
	8-11m/s	21,01	0,69	15,56	8,05	4,23	7,38
	13-17m/s	32,88	1,45	11,72	9,29	4,42	18,24
Tower torsion (m=4)	5-8m/s	12,72	0,76	6,52	4,74	1,89	3,75
	8-11m/s	15,91	0,76	18,65	5,56	1,91	6,77
	13-17m/s	29,31	2,03	21,20	8,53	7,63	13,93
Tower bottom (m=4)	5-8m/s	60,41	5,98	s.i.	35,82	9,54	21,24
	8-11m/s	86,68	6,54	66,36	41,56	17,31	42,62
	13-17m/s	163,0	8,98	113,3	36,38	29,27	50,62

s.i. indicates that the specific parameter was rejected by the backward elimination process

Table D.2 Sensitivity parameter table for VESTAS V27 operating at Andros site

Fatigue load (1Hz equiv.)	U	Leq	Sensitivity parameter ($\partial Leq/\partial x_i$)					
			U	α_{ws}	σ_u	σ_θ/TI	Lu	U_{skew}
Flapwise b.m. (m=12)	5-7m/s	16,17	1,32	s.i.	22,0	4,71	-0,0170	0,315
	8-11m/s	25,34	s.i.	s.i.	16,61	8,32	-0,0183	1,53
	13-16m/s	37,21	2,78	-22,9	22,41	11,36	-0,058	s.i.
Edgewise b.m. (m=12)	5-7m/s	51,71	0,25	s.i.	3,06	0,80	-0,004	-0,116
	8-11m/s	54,82	1,03	s.i.	3,08	2,00	-0,0056	0,836
	13-16m/s	64,83	2,40	18,96	2,49	s.i.	-0,014	2,25
Shaft parallel b.m. (m=8)	5-7m/s	31,74	s.i.	-30,2	17,08	4,37	-0,021	s.i.
	8-11m/s	39,45	0,42	-29,7	15,0	8,56	-0,0277	2,12
	13-16m/s	46,42	s.i.	-25,1	11,40	12,64	-0,0247	2,27
Shaft yaw (m=8)	5-7m/s	19,94	1,09	5,92	15,47	4,99	-0,018	s.i.
	8-11m/s	27,83	0,42	4,10	13,23	7,54	-0,0253	1,31
	13-16m/s	35,62	1,50	s.i.	15,56	12,89	-0,0165	1,28
Shaft tilt (m=8)	5-7m/s	19,92	0,90	s.i.	15,35	6,93	-0,0128	-0,342
	8-11m/s	29,21	s.i.	s.i.	15,60	8,21	-0,0275	1,31
	13-16m/s	37,99	2,18	-9,67	16,62	12,54	-0,039	4,038
Tower top (m=4)	5-7m/s	16,15	s.i.	12,21	4,62	3,99	s.i.	0,939
	8-11m/s	25,81	0,68	12,02	11,73	6,46	-0,0165	1,29
	13-16m/s	32,98	1,33	s.i.	14,67	10,86	-0,0288	2,18
Tower bottom (m=4)	5-7m/s	61,28	2,55	s.i.	55,92	17,05	s.i.	1,47
	8-11m/s	99,75	4,14	16,08	67,69	32,44	-0,101	3,01
	13-16m/s	180,5	21,0 4	s.i.	83,72	61,99	-0,254	33,05

s.i. indicates that the specific parameter was rejected by the backward elimination process

Table D.3 Sensitivity parameter table for NORDTANK NTK500/37 operating at Toplou site

Fatigue load (1Hz equiv.)	U	Leq	Sensitivity parameter ($\partial Leq/\partial x_i$)						
			U	α_{ws}	σ_u	σ_φ/Π	Lu	U _{skew}	U _{kurt}
Flapwise b.m. (m=12)	5-7m/s	45,61	-1,29	s.i.	47,99	8,09	-0,13	s.i.	s.i.
	8-11m/s	46,88	-2,26	s.i.	45,3	13,3	-0,10	-2,62	s.i.
	13-16m/s	68,56	4,07	s.i.	28,72	27,43	-0,069	3,49	s.i.
Edgewise b.m. (m=12)	5-7m/s	151,9	s.i.	-7,46	7,83	-1,25	-0,058	s.i.	s.i.
	8-11m/s	157,8	4,25	0,63	9,16	2,8	-2,20	s.i.	s.i.
	13-16m/s	190,3	4,83	2,24	7,51	s.i.	-0,074	s.i.	0,42
Shaft normal b.m. (m=8)	5-7m/s	85,49	2,03	-39,0	30,54	25,25	s.i.	-1,50	0,33
	8-11m/s	98,79	2,51	-1,17	35,44	28,08	-0,14	-5,23	s.i.
	13-16m/s	141,0	7,07	s.i.	37,9	36,9	-0,13	1,49	s.i.
Shaft yaw (m=8)	5-7m/s	44,20	1,43	s.i.	34,47	7,53	-0,10	-1,87	s.i.
	8-11m/s	52,66	0,73	s.i.	32,43	11,87	-0,076	-1,91	1,16
	13-16m/s	77,09	4,65	1,23	24,55	26,0	-0,036	4,58	1,67
Shaft tilt (m=8)	5-7m/s	51,74	1,47	s.i.	35,27	14,48	-0,083	-1,24	s.i.
	8-11m/s	61,65	1,21	-0,71	37,9	18,56	-0,11	-2,83	0,10
	13-16m/s	95,28	5,46	1,07	32,12	32,51	-0,69	1,37	s.i.
Tower torsion (m=4)	5-7m/s	39,62	s.i.	s.i.	24,84	4,84	-0,060	-1,21	0,55
	8-11m/s	46,9	2,08	s.i.	22,62	6,51	-0,048	-1,0	0,71
	13-16m/s	74,3	5,46	1,57	19,66	15,13	-0,036	4,69	1,87
Tower top (m=4)	5-7m/s	56,95	7,59	s.i.	51,78	10,53	-0,16	-1,15	0,36
	8-11m/s	78,62	5,23	-1,73	61,17	22,18	-0,20	-1,64	1,21
	13-16m/s	164,0	18,32	s.i.	77,72	57,01	-0,17	9,75	2,91
Tower bottom (m=4)	5-7m/s	203,3	14,97	s.i.	246,8	55,64	-0,73	-13,1	2,67
	8-11m/s	274,0	17,05	-8,37	267,7	101,8	-0,81	-10,2	6,01
	13-16m/s	594,3	60,15	5,48	277,6	235,8	-0,50	35,83	13,26

s.i. indicates that the specific parameter was rejected by the backward elimination process

D.5 References

- [D1] Kleinbaum K., Kupper L.: “Applied regression analysis and other multivariable methods”, PWS-KENT Publishing Company, Boston, 1985.
- [D2] Mouzakis F., Morfiadakis E., Fragoulis A.: MOUNTURB (JOU2-CT93-0378) Final Report on Complex terrain wind-WT parameter identification and quantification (Wind and WT measurements), Volume II, November 1996.
- [D3] Mouzakis F., Morfiadakis E., Dellaportas P.: “Parameter identification on power performance of wind turbines operating at complex terrain”, 2nd EACWE, Genova, June 1997.

Appendix D Tables from modelling-based PI

The results obtained from the **coarse** and **fine grain** parameter identification procedure are presented in this Appendix. Cumulative Rainflow Counting tables of Equivalent loads $m=4, 8, 12$ are included for the following loads:

RFM : blade root flapping moment

REM : blade root edge moment

TBM_x : tower bottom bending moment (normal to the mean flow)

TBM_y : tower bottom bending moment (parallel to the mean flow)

TTM : tower torsion

DTM : drive train - low speed - torque

Dimensional moments (kNm) are only presented for the reference cases (2F for coarse grain, for instance). These are clearly designated using bold characters. All the other columns represent the ratio of the calculated moments versus the respective reference value.

Although each machine has been modelled by several participants, one set of results per machine is presented here. The name of the participant whose results are presented is marked on the tables.

Tables E.1 to E.7 include the results of the coarse grain PI. The fine grain PI results are shown in tables E.8 and E.9

Complex Terrain and Fatigue Loading

Table E.1 COARSE GRAIN PI RESULTS WXT110 modelled by NTUA

U _{hub} = 10 m/s													
Leq-4	1F	2F	3F	4F	5F	6F	1C	2C	3C	4C	5C	6C	2C+
RFM	0.68	16.8	1.13	1.14	1.04	1.48	0.70	1.03	1.14	1.17	1.07	1.53	1.23
REM	0.97	42.6	0.96	1.00	1.00	1.04	0.97	1.00	0.96	1.00	1.01	1.05	1.03
TBMx	0.62	46.5	0.98	0.99	0.99	1.56	0.71	1.14	1.11	1.13	1.14	1.77	1.34
TBMy	0.59	88.1	1.00	0.98	0.99	1.60	0.67	1.14	1.15	1.12	1.13	1.81	1.26
TTM	0.64	22.0	1.03	1.00	1.00	1.51	0.63	1.00	1.01	0.99	1.00	1.51	1.29
DTM	0.64	9.7	1.01	0.97	1.00	1.45	0.68	1.07	1.09	1.04	1.07	1.56	1.29
Leq-8	1F	2F	3F	4F	5F	6F	1C	2C	3C	4C	5C	6C	2C+
RFM	0.66	17.5	1.14	1.14	1.03	1.49	0.67	1.04	1.16	1.18	1.07	1.55	1.19
REM	0.97	39.4	0.96	1.00	1.01	1.06	0.97	1.00	0.96	1.00	1.01	1.06	1.04
TBMx	0.62	47.5	1.00	0.99	0.99	1.58	0.71	1.13	1.13	1.12	1.12	1.79	1.32
TBMy	0.58	107.	1.07	0.97	1.00	1.63	0.63	1.12	1.23	1.09	1.12	1.82	1.19
TTM	0.62	21.4	1.03	0.99	1.00	1.53	0.63	1.01	1.03	1.00	1.02	1.56	1.29
DTM	0.64	11.9	1.08	0.97	1.01	1.44	0.67	1.07	1.17	1.05	1.08	1.53	1.17
Leq-12	1F	2F	3F	4F	5F	6F	1C	2C	3C	4C	5C	6C	2C+
RFM	0.65	19.5	1.12	1.14	1.02	1.49	0.67	1.05	1.15	1.18	1.06	1.55	1.16
REM	0.96	38.6	0.96	1.00	1.01	1.07	0.96	1.01	0.96	1.00	1.01	1.08	1.04
TBMx	0.63	51.1	1.00	0.99	0.99	1.57	0.71	1.11	1.13	1.11	1.11	1.78	1.31
TBMy	0.57	125.	1.09	0.96	1.00	1.62	0.62	1.12	1.25	1.08	1.11	1.80	1.16
TTM	0.60	23.0	1.03	0.99	1.01	1.54	0.62	1.02	1.03	1.00	1.03	1.59	1.28
DTM	0.64	13.7	1.10	0.99	1.01	1.43	0.67	1.06	1.18	1.04	1.07	1.50	1.12
U _{hub} = 14 m/s													
Leq-4	1F	2F	3F	4F	5F	6F	1C	2C	3C	4C	5C	6C	2C+
RFM	0.67	20.9	1.55	1.02	1.12	1.56	0.69	1.06	1.56	1.08	1.18	1.67	1.22
REM	0.94	45.7	1.01	0.99	1.03	1.09	0.94	1.00	1.01	1.00	1.03	1.09	1.06
TBMx	0.53	77.7	1.11	1.03	1.02	1.69	0.60	1.11	1.21	1.16	1.13	1.88	1.33
TBMy	0.58	129.	1.01	1.06	0.99	1.65	0.66	1.13	1.13	1.20	1.11	1.89	1.27
TTM	0.61	27.0	1.20	1.02	1.01	1.61	0.62	1.03	1.21	1.04	1.03	1.66	1.26
DTM	0.51	12.3	1.24	1.04	1.02	1.76	0.54	1.06	1.28	1.11	1.07	1.83	1.36
Leq-8	1F	2F	3F	4F	5F	6F	1C	2C	3C	4C	5C	6C	2C+
RFM	0.66	20.8	1.56	1.03	1.13	1.53	0.70	1.08	1.58	1.10	1.19	1.68	1.22
REM	0.93	42.6	1.01	0.99	1.03	1.10	0.93	1.00	1.01	1.00	1.03	1.11	1.07
TBMx	0.54	78.4	1.13	1.02	1.01	1.72	0.60	1.13	1.25	1.16	1.15	1.90	1.33
TBMy	0.57	133.	1.03	1.05	0.99	1.66	0.65	1.14	1.17	1.19	1.12	1.94	1.25
TTM	0.60	26.0	1.20	1.02	1.01	1.63	0.63	1.05	1.24	1.07	1.07	1.75	1.25
DTM	0.52	12.4	1.33	1.08	1.02	1.81	0.55	1.06	1.41	1.17	1.07	1.90	1.36
Leq-12	1F	2F	3F	4F	5F	6F	1C	2C	3C	4C	5C	6C	2C+
RFM	0.66	22.2	1.54	1.03	1.11	1.51	0.70	1.08	1.56	1.09	1.18	1.66	1.23
REM	0.92	42.0	1.02	0.99	1.03	1.12	0.92	1.00	1.02	1.00	1.03	1.12	1.08
TBMx	0.54	83.0	1.14	1.01	1.01	1.73	0.60	1.14	1.30	1.17	1.17	1.91	1.33
TBMy	0.57	144.	1.05	1.04	0.99	1.65	0.64	1.14	1.20	1.18	1.11	1.94	1.24
TTM	0.60	27.7	1.18	1.02	1.01	1.64	0.63	1.07	1.25	1.08	1.08	1.78	1.24
DTM	0.53	13.2	1.39	1.10	1.02	1.85	0.56	1.07	1.48	1.20	1.08	1.95	1.37
U _{hub} = 18 m/s													
Leq-4	1F	2F	3F	4F	5F	6F	1C	2C	3C	4C	5C	6C	2C+
RFM	0.64	25.2	1.85	0.99	1.13	1.64	0.67	1.08	1.89	1.08	1.21	1.79	1.30
REM	0.93	47.2	1.10	0.99	1.04	1.14	0.93	1.01	1.10	1.00	1.04	1.15	1.07
TBMx	0.52	108.	1.17	0.99	1.02	1.67	0.57	1.12	1.32	1.12	1.15	1.88	1.38
TBMy	0.55	182.	1.00	0.97	1.00	1.58	0.62	1.12	1.13	1.11	1.13	1.79	1.30
TTM	0.60	32.6	1.26	0.96	1.03	1.71	0.62	1.06	1.31	1.02	1.09	1.83	1.34
DTM	0.50	16.3	1.28	0.98	1.01	1.74	0.53	1.07	1.36	1.06	1.09	1.85	1.39
Leq-8	1F	2F	3F	4F	5F	6F	1C	2C	3C	4C	5C	6C	2C+
RFM	0.63	24.9	1.88	1.00	1.13	1.65	0.67	1.10	1.95	1.12	1.22	1.84	1.30
REM	0.92	44.0	1.11	1.00	1.03	1.16	0.92	1.01	1.12	1.00	1.04	1.18	1.08
TBMx	0.50	113.	1.13	0.95	1.01	1.65	0.56	1.11	1.29	1.09	1.14	1.86	1.35
TBMy	0.54	188.	0.99	0.98	1.01	1.58	0.62	1.11	1.13	1.11	1.13	1.79	1.29
TTM	0.60	30.6	1.33	0.97	1.04	1.74	0.65	1.09	1.42	1.07	1.13	1.92	1.36
DTM	0.49	17.2	1.25	0.95	0.99	1.72	0.53	1.09	1.33	1.02	1.09	1.84	1.32
Leq-12	1F	2F	3F	4F	5F	6F	1C	2C	3C	4C	5C	6C	2C+
RFM	0.62	26.7	1.84	1.00	1.11	1.65	0.66	1.10	1.93	1.13	1.20	1.83	1.31
REM	0.91	43.5	1.13	1.00	1.03	1.18	0.91	1.01	1.14	1.01	1.05	1.20	1.09
TBMx	0.48	124.	1.09	0.91	1.01	1.60	0.54	1.09	1.25	1.06	1.12	1.82	1.32
TBMy	0.54	204.	0.99	0.97	1.02	1.57	0.61	1.10	1.11	1.10	1.12	1.77	1.27
TTM	0.62	31.5	1.38	0.99	1.03	1.76	0.67	1.12	1.50	1.11	1.16	1.99	1.38
DTM	0.48	18.8	1.22	0.94	0.99	1.72	0.53	1.11	1.32	0.99	1.10	1.84	1.27

Table E.2 COARSE GRAIN PI RESULTS V27 modelled by RISO

U _{hub} = 10 m/s													
Leq-4	1F	2F	3F	4F	5F	6F	1C	2C	3C	4C	5C	6C	2C+
RFM	0.60	23.5	1.13	0.99	1.03	1.59	0.77	1.33	1.45	1.32	1.35	2.14	1.56
REM	0.90	58.1	1.00	1.01	0.99	1.05	0.94	1.05	1.05	1.05	1.05	1.11	1.06
TBMx	0.52	64.2	1.14	1.01	1.02	1.58	0.68	1.30	1.49	1.30	1.35	2.04	1.68
TBMy	0.55	148.	1.29	1.01	1.03	1.63	0.69	1.31	1.67	1.29	1.31	2.12	1.50
TTM	0.59	27.6	1.00	1.00	1.01	1.58	0.74	1.31	1.28	1.32	1.31	2.09	1.66
DTM	0.58	11.9	1.01	1.00	0.99	1.54	0.73	1.27	1.26	1.27	1.28	1.97	1.46
Leq-8	1F	2F	3F	4F	5F	6F	1C	2C	3C	4C	5C	6C	2C+
RFM	0.60	29.8	1.12	0.99	1.04	1.56	0.70	1.21	1.36	1.19	1.23	1.95	1.46
REM	0.89	61.7	1.00	1.02	0.99	1.05	0.91	1.03	1.03	1.03	1.03	1.10	1.08
TBMx	0.52	74.5	1.15	1.01	1.05	1.58	0.66	1.26	1.45	1.26	1.31	1.96	1.67
TBMy	0.55	227.	1.31	1.04	1.02	1.68	0.58	1.11	1.39	1.07	1.10	1.77	1.27
TTM	0.56	33.6	1.00	0.99	1.01	1.55	0.71	1.26	1.22	1.27	1.25	1.99	1.67
DTM	0.55	19.6	1.04	1.01	0.98	1.52	0.59	1.06	1.06	1.05	1.06	1.60	1.19
Leq-12	1F	2F	3F	4F	5F	6F	1C	2C	3C	4C	5C	6C	2C+
RFM	0.61	35.7	1.10	1.00	1.05	1.55	0.68	1.17	1.36	1.13	1.18	1.87	1.38
REM	0.88	63.9	1.01	1.02	0.99	1.06	0.89	1.04	1.04	1.03	1.03	1.13	1.09
TBMx	0.51	84.2	1.15	1.01	1.09	1.58	0.66	1.25	1.48	1.26	1.31	1.95	1.67
TBMy	0.55	286.	1.32	1.05	1.03	1.71	0.57	1.09	1.36	1.04	1.07	1.73	1.21
TTM	0.55	38.8	0.99	0.98	1.03	1.54	0.71	1.27	1.23	1.29	1.26	2.01	1.68
DTM	0.55	24.4	1.06	1.01	0.98	1.52	0.60	1.06	1.07	1.05	1.06	1.60	1.15
U _{hub} = 14 m/s													
Leq-4	1F	2F	3F	4F	5F	6F	1C	2C	3C	4C	5C	6C	2C+
RFM	0.62	32.9	1.11	0.99	1.01	1.57	0.72	1.20	1.29	1.17	1.20	1.92	1.53
REM	0.91	61.9	0.99	1.00	0.98	1.11	0.95	1.03	1.03	1.02	1.03	1.18	1.10
TBMx	0.56	113.	1.24	1.00	1.03	1.66	0.68	1.24	1.46	1.23	1.23	2.06	1.68
TBMy	0.58	230.	1.24	1.01	1.03	1.65	0.71	1.23	1.44	1.24	1.26	2.00	1.54
TTM	0.57	40.2	0.99	1.00	1.00	1.62	0.68	1.20	1.18	1.20	1.20	1.99	1.63
DTM	0.58	16.9	1.13	1.01	1.02	1.67	0.68	1.21	1.24	1.19	1.20	2.04	1.63
Leq-8	1F	2F	3F	4F	5F	6F	1C	2C	3C	4C	5C	6C	2C+
RFM	0.61	42.4	1.08	0.98	0.99	1.55	0.70	1.15	1.21	1.13	1.15	1.84	1.45
REM	0.89	66.4	0.99	1.00	0.98	1.13	0.95	1.04	1.03	1.03	1.04	1.20	1.12
TBMx	0.57	130.	1.28	1.01	1.02	1.70	0.67	1.29	1.53	1.28	1.25	2.17	1.74
TBMy	0.61	304.	1.23	0.99	1.00	1.61	0.74	1.22	1.37	1.22	1.23	1.90	1.43
TTM	0.56	49.0	0.96	0.99	0.99	1.60	0.67	1.18	1.15	1.20	1.21	1.99	1.65
DTM	0.54	22.4	1.36	1.02	1.02	1.69	0.64	1.17	1.38	1.15	1.15	1.98	1.51
Leq-12	1F	2F	3F	4F	5F	6F	1C	2C	3C	4C	5C	6C	2C+
RFM	0.61	50.0	1.07	0.97	0.99	1.52	0.69	1.13	1.16	1.10	1.12	1.78	1.44
REM	0.88	69.3	0.99	1.00	0.98	1.14	0.95	1.05	1.04	1.04	1.05	1.23	1.14
TBMx	0.58	145.	1.31	1.00	1.01	1.72	0.68	1.32	1.58	1.31	1.28	2.23	1.76
TBMy	0.62	357.	1.24	0.99	0.99	1.60	0.76	1.24	1.34	1.23	1.23	1.88	1.40
TTM	0.56	56.4	0.95	0.99	0.98	1.59	0.67	1.19	1.14	1.20	1.22	2.01	1.68
DTM	0.53	26.7	1.42	1.03	1.02	1.68	0.63	1.17	1.40	1.15	1.13	1.97	1.45
U _{hub} = 18 m/s													
Leq-4	1F	2F	3F	4F	5F	6F	1C	2C	3C	4C	5C	6C	2C+
RFM	0.63	44.1	1.19	0.99	0.98	1.61	0.74	1.25	1.36	1.25	1.24	2.03	1.61
REM	0.88	64.1	1.02	1.00	0.98	1.25	0.91	1.10	1.09	1.09	1.07	1.42	1.28
TBMx	0.56	223.	1.00	1.00	1.00	1.66	0.72	1.28	1.21	1.28	1.27	2.13	1.69
TBMy	0.54	388.	1.33	1.00	1.03	1.67	0.65	1.22	1.58	1.22	1.26	2.06	1.57
TTM	0.59	54.9	1.06	1.01	1.01	1.63	0.73	1.27	1.27	1.26	1.27	2.09	1.80
DTM	0.59	31.8	0.93	1.00	1.01	1.62	0.71	1.25	1.09	1.25	1.24	1.94	1.65
Leq-8	1F	2F	3F	4F	5F	6F	1C	2C	3C	4C	5C	6C	2C+
RFM	0.61	55.	1.26	0.99	1.00	1.63	0.71	1.23	1.41	1.22	1.22	2.02	1.56
REM	0.86	70.	1.01	1.00	0.98	1.26	0.90	1.11	1.09	1.10	1.07	1.44	1.29
TBMx	0.55	262.	1.00	1.00	1.00	1.69	0.72	1.28	1.21	1.28	1.27	2.14	1.68
TBMy	0.55	489.	1.36	1.00	1.02	1.65	0.64	1.18	1.60	1.20	1.23	1.98	1.49
TTM	0.59	64.4	1.05	1.01	1.03	1.63	0.74	1.33	1.30	1.31	1.33	2.23	1.87
DTM	0.58	41.5	0.95	1.01	1.01	1.65	0.70	1.23	1.11	1.23	1.22	1.94	1.54
Leq-12	1F	2F	3F	4F	5F	6F	1C	2C	3C	4C	5C	6C	2C+
RFM	0.61	63.3	1.31	0.98	1.01	1.62	0.69	1.21	1.45	1.20	1.22	2.02	1.54
REM	0.84	74.3	1.01	0.99	0.98	1.27	0.89	1.11	1.09	1.11	1.08	1.48	1.31
TBMx	0.55	294.	0.99	1.01	1.01	1.74	0.72	1.28	1.21	1.28	1.28	2.15	1.67
TBMy	0.55	566.	1.39	1.01	1.02	1.66	0.64	1.19	1.62	1.20	1.22	1.94	1.45
TTM	0.60	73.	1.04	1.02	1.04	1.62	0.75	1.35	1.33	1.32	1.36	2.30	1.92
DTM	0.58	48.7	0.96	1.01	1.00	1.65	0.70	1.22	1.13	1.22	1.21	1.92	1.51

Complex Terrain and Fatigue Loading

Table E.3 COARSE GRAIN PI RESULTS MADE AE/30 modelled by NTUA

U _{hub} = 10 m/s													
Leq-4	1F	2F	3F	4F	5F	6F	1C	2C	3C	4C	5C	6C	2C+
RFM	0.62	52.8	1.24	1.13	1.01	1.53	0.64	1.04	1.27	1.16	1.06	1.61	1.20
REM	0.97	137.	0.95	1.01	1.01	1.04	0.97	1.00	0.95	1.01	1.01	1.05	1.02
TBMx	0.59	54.1	0.89	1.01	0.99	1.55	0.66	1.15	1.01	1.16	1.14	1.81	1.19
TBMy	0.56	220.	0.99	0.99	1.00	1.56	0.64	1.14	1.15	1.13	1.14	1.77	1.07
TTM	0.61	62.1	1.01	0.98	1.00	1.53	0.61	1.00	1.01	0.98	1.00	1.54	1.25
DTM	0.58	27.3	0.94	1.00	1.00	1.46	0.64	1.09	1.06	1.09	1.09	1.58	0.96
Leq-8	1F	2F	3F	4F	5F	6F	1C	2C	3C	4C	5C	6C	2C+
RFM	0.59	60.9	1.19	1.10	1.00	1.51	0.61	1.02	1.25	1.13	1.04	1.57	1.10
REM	0.97	127.	0.95	1.01	1.01	1.06	0.97	1.00	0.95	1.01	1.01	1.06	1.03
TBMx	0.57	73.0	0.85	1.02	0.99	1.54	0.62	1.11	0.93	1.12	1.10	1.74	1.07
TBMy	0.56	325.	1.00	0.98	1.00	1.53	0.62	1.10	1.14	1.09	1.10	1.68	0.98
TTM	0.60	60.8	1.02	0.98	1.00	1.55	0.61	1.02	1.03	1.00	1.02	1.59	1.25
DTM	0.59	42.1	0.96	1.00	1.00	1.43	0.62	1.05	1.05	1.05	1.05	1.48	0.90
Leq-12	1F	2F	3F	4F	5F	6F	1C	2C	3C	4C	5C	6C	2C+
RFM	0.58	70.6	1.16	1.09	0.99	1.48	0.59	1.00	1.22	1.10	1.02	1.53	1.05
REM	0.96	125.	0.95	1.01	1.01	1.07	0.96	1.00	0.95	1.02	1.01	1.08	1.03
TBMx	0.56	85.4	0.84	1.02	0.99	1.54	0.61	1.10	0.91	1.11	1.09	1.74	1.04
TBMy	0.56	384.	1.00	0.98	1.00	1.51	0.61	1.08	1.14	1.07	1.08	1.64	0.95
TTM	0.60	64.9	1.03	0.98	1.00	1.56	0.61	1.03	1.04	1.00	1.03	1.62	1.25
DTM	0.59	50.2	0.97	1.00	1.00	1.41	0.62	1.04	1.06	1.04	1.04	1.45	0.87
U _{hub} = 14 m/s													
Leq-4	1F	2F	3F	4F	5F	6F	1C	2C	3C	4C	5C	6C	2C+
RFM	0.61	66.2	1.61	1.05	1.06	1.62	0.67	1.12	1.67	1.17	1.17	1.84	1.23
REM	0.96	146.	0.98	1.00	1.03	1.08	0.96	1.01	0.98	1.01	1.04	1.09	1.05
TBMx	0.53	89.3	0.93	0.96	1.01	1.59	0.62	1.17	1.11	1.14	1.18	1.99	1.24
TBMy	0.55	257.	1.02	1.00	0.99	1.68	0.64	1.17	1.19	1.16	1.16	1.99	1.13
TTM	0.61	78.6	1.08	1.01	1.01	1.59	0.63	1.06	1.12	1.07	1.07	1.71	1.25
DTM	0.56	28.7	1.15	0.98	1.01	1.60	0.62	1.09	1.29	1.07	1.10	1.77	1.01
Leq-8	1F	2F	3F	4F	5F	6F	1C	2C	3C	4C	5C	6C	2C+
RFM	0.60	67.3	1.61	1.05	1.06	1.63	0.67	1.15	1.70	1.20	1.19	1.92	1.20
REM	0.95	136.	0.99	1.00	1.03	1.09	0.96	1.01	0.99	1.01	1.04	1.11	1.06
TBMx	0.50	106.	0.86	0.92	1.02	1.61	0.60	1.15	1.03	1.08	1.17	2.23	1.14
TBMy	0.53	335.	1.03	0.99	1.00	1.71	0.60	1.14	1.19	1.12	1.14	1.97	1.03
TTM	0.60	77.3	1.08	1.01	1.01	1.62	0.65	1.10	1.18	1.11	1.12	1.82	1.26
DTM	0.56	41.6	1.16	0.97	1.00	1.60	0.60	1.07	1.28	1.05	1.07	1.72	0.93
Leq-12	1F	2F	3F	4F	5F	6F	1C	2C	3C	4C	5C	6C	2C+
RFM	0.60	72.5	1.59	1.04	1.05	1.62	0.68	1.16	1.69	1.19	1.18	1.96	1.20
REM	0.94	134.	0.99	1.00	1.03	1.11	0.95	1.01	1.00	1.01	1.04	1.13	1.07
TBMx	0.49	122.	0.83	0.90	1.03	1.61	0.58	1.14	1.00	1.05	1.16	2.34	1.10
TBMy	0.53	389.	1.03	1.00	1.00	1.71	0.60	1.13	1.19	1.13	1.13	1.95	0.99
TTM	0.60	83.6	1.06	1.01	1.00	1.63	0.66	1.12	1.22	1.13	1.14	1.85	1.26
DTM	0.56	48.5	1.16	0.97	1.00	1.60	0.59	1.06	1.28	1.04	1.06	1.70	0.91
U _{hub} = 18 m/s													
Leq-4	1F	2F	3F	4F	5F	6F	1C	2C	3C	4C	5C	6C	2C+
RFM	0.59	82.5		1.01	1.09	1.60	0.67	1.17		1.17	1.25	1.88	1.29
REM	0.93	146.		0.99	1.06	1.10	0.94	1.01		1.00	1.07	1.12	1.05
TBMx	0.54	127.		1.01	1.02	1.70	0.62	1.16		1.17	1.16	2.44	1.31
TBMy	0.55	369.		1.00	1.00	1.76	0.64	1.19		1.20	1.18	2.11	1.22
TTM	0.59	96.2		0.99	1.01	1.63	0.64	1.12		1.11	1.14	1.85	1.32
DTM	0.50	26.0		1.02	1.01	2.22	0.53	1.09		1.12	1.10	2.48	1.19
Leq-8	1F	2F	3F	4F	5F	6F	1C	2C	3C	4C	5C	6C	2C+
RFM	0.59	82.2		1.02	1.08	1.62	0.68	1.21		1.20	1.28	1.97	1.29
REM	0.92	136.		0.99	1.06	1.12	0.93	1.01		1.01	1.07	1.15	1.06
TBMx	0.53	140.		1.01	1.03	1.78	0.62	1.17		1.18	1.19	3.02	1.30
TBMy	0.52	439.		1.00	1.00	1.84	0.61	1.15		1.16	1.15	2.17	1.14
TTM	0.58	94.3		1.00	1.01	1.61	0.67	1.19		1.18	1.19	1.93	1.32
DTM	0.45	34.7		1.02	1.02	2.38	0.47	1.09		1.11	1.11	2.61	1.08
Leq-12	1F	2F	3F	4F	5F	6F	1C	2C	3C	4C	5C	6C	2C+
RFM	0.59	86.8		1.03	1.07	1.63	0.68	1.23		1.23	1.29	2.01	1.29
REM	0.91	135.		0.99	1.06	1.13	0.92	1.02		1.01	1.08	1.18	1.06
TBMx	0.53	154.		1.01	1.04	1.82	0.62	1.18		1.18	1.20	3.25	1.31
TBMy	0.51	499.		1.00	1.00	1.83	0.59	1.14		1.15	1.14	2.16	1.11
TTM	0.59	100.		1.00	1.01	1.59	0.68	1.21		1.21	1.22	1.97	1.32
DTM	0.43	40.4		1.02	1.03	2.40	0.46	1.10		1.11	1.13	2.63	1.04

Complex Terrain and Fatigue Loading

Table E.4 COARSE GRAIN PI RESULTS NTK500 modelled by NTUA

U _{hub} = 10 m/s													
Leq-4	1F	2F	3F	4F	5F	6F	1C	2C	3C	4C	5C	6C	2C+
RFM	0.62	72.6	1.28	1.14	1.02	1.54	0.64	1.06	1.32	1.20	1.08	1.65	1.19
REM	0.97	230.	0.95	1.01	1.00	1.05	0.97	1.00	0.95	1.01	1.00	1.05	1.03
TBMx	0.60	122.	0.91	1.00	0.99	1.49	0.68	1.16	1.05	1.16	1.15	1.76	1.23
TBMy	0.57	382.	0.97	0.99	1.00	1.56	0.65	1.15	1.15	1.14	1.15	1.79	1.05
TTM	0.63	105.	1.04	0.99	1.00	1.52	0.64	1.03	1.06	1.01	1.03	1.57	1.24
DTM	0.59	47.9	0.86	0.99	1.00	1.45	0.65	1.10	1.02	1.10	1.10	1.58	1.00
Leq-8	1F	2F	3F	4F	5F	6F	1C	2C	3C	4C	5C	6C	2C+
RFM	0.58	82.5	1.25	1.08	1.02	1.56	0.62	1.07	1.29	1.16	1.09	1.68	1.08
REM	0.96	213.	0.95	1.01	1.00	1.06	0.97	1.00	0.95	1.01	1.01	1.07	1.03
TBMx	0.58	154.	0.88	1.00	0.98	1.46	0.63	1.11	1.00	1.11	1.09	1.66	1.12
TBMy	0.57	554.	0.97	0.99	1.00	1.54	0.63	1.11	1.14	1.10	1.11	1.71	0.96
TTM	0.62	103.	1.04	0.99	1.01	1.53	0.64	1.04	1.08	1.03	1.05	1.63	1.23
DTM	0.59	70.9	0.88	0.99	1.00	1.42	0.63	1.06	1.04	1.06	1.06	1.49	0.92
Leq-12	1F	2F	3F	4F	5F	6F	1C	2C	3C	4C	5C	6C	2C+
RFM	0.57	94.6	1.24	1.05	1.02	1.57	0.60	1.07	1.27	1.13	1.08	1.67	1.04
REM	0.96	209.	0.95	1.01	1.00	1.07	0.96	1.00	0.95	1.01	1.01	1.08	1.03
TBMx	0.57	179.	0.88	0.99	0.97	1.44	0.62	1.10	0.99	1.09	1.07	1.61	1.08
TBMy	0.57	650.	0.88	0.99	1.00	1.53	0.63	1.10	1.14	1.09	1.09	1.69	0.93
TTM	0.61	110.	1.05	0.98	1.01	1.54	0.63	1.05	1.09	1.04	1.07	1.65	1.22
DTM	0.59	83.6	0.90	0.99	1.00	1.41	0.62	1.05	1.05	1.05	1.05	1.46	0.90
U _{hub} = 14 m/s													
Leq-4	1F	2F	3F	4F	5F	6F	1C	2C	3C	4C	5C	6C	2C+
RFM	0.61	92.1	1.81	1.05	1.10	1.62	0.67	1.15	1.85	1.19	1.23	1.88	1.21
REM	0.96	248.	0.98	1.00	1.03	1.08	0.96	1.00	0.99	1.00	1.03	1.09	1.06
TBMx	0.56	195.	0.98	0.97	1.01	1.56	0.66	1.21	1.15	1.17	1.22	1.88	1.24
TBMy	0.55	437.	1.11	0.98	0.99	1.68	0.66	1.19	1.33	1.18	1.19	2.02	1.14
TTM	0.60	134.	1.14	1.01	1.01	1.56	0.65	1.11	1.20	1.11	1.12	1.75	1.24
DTM	0.56	52.8	1.24	0.99	1.02	1.56	0.63	1.11	1.41	1.10	1.12	1.75	1.05
Leq-8	1F	2F	3F	4F	5F	6F	1C	2C	3C	4C	5C	6C	2C+
RFM	0.60	93.0	1.81	1.08	1.08	1.69	0.68	1.19	1.87	1.26	1.25	1.99	1.19
REM	0.95	231.	0.99	1.00	1.03	1.09	0.95	1.00	1.00	1.00	1.03	1.11	1.06
TBMx	0.54	232.	0.85	0.93	1.01	1.45	0.66	1.19	1.01	1.11	1.20	1.75	1.15
TBMy	0.53	569.	1.15	0.94	1.00	1.68	0.61	1.16	1.35	1.12	1.17	1.98	1.04
TTM	0.60	133.	1.13	0.99	1.01	1.57	0.68	1.16	1.23	1.15	1.18	1.82	1.23
DTM	0.56	71.8	1.28	0.98	1.03	1.56	0.61	1.08	1.43	1.08	1.10	1.71	0.96
Leq-12	1F	2F	3F	4F	5F	6F	1C	2C	3C	4C	5C	6C	2C+
RFM	0.59	99.4	1.79	1.10	1.07	1.73	0.67	1.22	1.87	1.32	1.25	2.07	1.18
REM	0.94	228.	1.00	1.00	1.03	1.11	0.94	1.00	1.01	1.01	1.03	1.13	1.07
TBMx	0.53	272.	0.80	0.92	1.00	1.38	0.65	1.18	0.94	1.09	1.18	1.65	1.12
TBMy	0.53	665.	1.15	0.93	1.00	1.67	0.60	1.16	1.35	1.11	1.17	1.95	1.02
TTM	0.61	143.	1.12	0.99	1.01	1.57	0.70	1.19	1.25	1.16	1.22	1.85	1.22
DTM	0.56	82.8	1.30	0.98	1.03	1.56	0.60	1.07	1.45	1.07	1.09	1.70	0.94
U _{hub} = 18 m/s													
Leq-4	1F	2F	3F	4F	5F	6F	1C	2C	3C	4C	5C	6C	2C+
RFM	0.62	121.	2.11	0.99	1.11	1.61	0.71	1.19	2.18	1.17	1.29	1.91	1.29
REM	0.93	257.	1.07	0.99	1.05	1.11	0.93	1.01	1.07	1.00	1.06	1.14	1.07
TBMx	0.61	280.	1.00	0.96	1.03	1.69	0.70	1.19	1.19	1.14	1.21	1.93	1.28
TBMy	0.57	611.	0.99	0.99	0.99	1.77	0.68	1.19	1.21	1.20	1.19	2.10	1.25
TTM	0.62	177.	1.04	0.96	1.01	1.62	0.70	1.16	1.16	1.11	1.17	1.89	1.32
DTM	0.62	53.0	1.34	1.00	1.01	1.83	0.68	1.11	1.51	1.12	1.12	2.02	1.24
Leq-8	1F	2F	3F	4F	5F	6F	1C	2C	3C	4C	5C	6C	2C+
RFM	0.62	121.	2.09	1.00	1.10	1.64	0.72	1.19	2.19	1.19	1.31	1.96	1.29
REM	0.92	241.	1.08	0.98	1.05	1.12	0.92	1.01	1.08	1.00	1.06	1.15	1.08
TBMx	0.61	299.	1.00	0.98	1.04	1.73	0.70	1.21	1.19	1.17	1.24	2.02	1.29
TBMy	0.56	682.	1.03	1.00	0.99	1.88	0.66	1.17	1.23	1.18	1.17	2.18	1.22
TTM	0.61	175.	1.06	0.96	1.02	1.66	0.71	1.20	1.24	1.15	1.22	1.99	1.37
DTM	0.59	58.5	1.49	1.04	1.03	2.04	0.65	1.12	1.71	1.15	1.15	2.26	1.23
Leq-12	1F	2F	3F	4F	5F	6F	1C	2C	3C	4C	5C	6C	2C+
RFM	0.62	129.	2.06	1.00	1.09	1.66	0.72	1.19	2.17	1.19	1.30	1.99	1.29
REM	0.90	240.	1.08	0.98	1.05	1.14	0.91	1.01	1.09	1.00	1.06	1.17	1.09
TBMx	0.60	327.	0.99	1.00	1.05	1.76	0.70	1.22	1.18	1.19	1.26	2.09	1.30
TBMy	0.57	754.	1.05	1.01	0.99	1.93	0.65	1.16	1.25	1.17	1.16	2.20	1.21
TTM	0.61	186.	1.09	0.96	1.02	1.70	0.72	1.22	1.32	1.19	1.25	2.05	1.42
DTM	0.58	64.9	1.53	1.07	1.05	2.12	0.63	1.13	1.76	1.17	1.18	2.35	1.22

Complex Terrain and Fatigue Loading

Table E.5 COARSE GRAIN PI RESULTS DANWIN 180 modelled by TG

U _{hub} = 10 m/s													
Leq-4	1F	2F	3F	4F	5F	6F	1C	2C	3C	4C	5C	6C	2C+
RFM	0.60	21	1.34	1.25	1.02	1.45	0.63	1.07	1.38	1.31	1.08	1.56	1.27
REM	0.95	54	1.02	1.00	1.00	1.07	0.95	1.00	1.02	1.00	1.00	1.06	1.06
TBMx	0.53	210	0.72	0.99	1.00	1.50	0.64	1.21	0.90	1.20	1.19	1.80	1.10
TBMy	0.59	59	1.51	0.99	1.00	1.40	0.72	1.24	1.85	1.25	1.22	1.73	1.29
TTM	0.66	25	1.07	1.00	1.00	1.43	0.67	1.05	1.10	1.05	1.05	1.52	1.33
DTM	0.65	10	0.94	0.98	1.01	1.27	0.69	1.10	1.09	1.09	1.09	1.40	1.03
Leq-8	1F	2F	3F	4F	5F	6F	1C	2C	3C	4C	5C	6C	2C+
RFM	0.59	29	1.18	1.15	1.03	1.41	0.62	1.08	1.24	1.23	1.07	1.52	1.14
REM	0.95	58	1.02	1.00	1.00	1.08	0.95	1.00	1.02	1.00	1.00	1.08	1.07
TBMx	0.53	369	0.66	0.99	0.99	1.46	0.60	1.14	0.84	1.13	1.13	1.67	0.95
TBMy	0.59	94	1.31	0.99	1.00	1.30	0.67	1.15	1.72	1.16	1.14	1.54	1.11
TTM	0.63	30	1.05	1.00	0.98	1.44	0.65	1.03	1.10	1.03	1.03	1.51	1.28
DTM	0.64	18	0.91	0.98	1.00	1.25	0.67	1.07	1.06	1.06	1.06	1.34	0.96
Leq-12	1F	2F	3F	4F	5F	6F	1C	2C	3C	4C	5C	6C	2C+
RFM	0.60	35	1.11	1.11	1.03	1.38	0.62	1.07	1.17	1.18	1.07	1.48	1.09
REM	0.94	59	1.03	1.00	1.00	1.09	0.94	1.00	1.02	1.00	1.00	1.09	1.07
TBMx	0.53	464	0.65	0.98	0.98	1.46	0.59	1.13	0.84	1.12	1.11	1.63	0.92
TBMy	0.59	117	1.27	0.98	1.01	1.25	0.65	1.13	1.70	1.13	1.12	1.48	1.05
TTM	0.61	36	1.01	1.00	0.97	1.44	0.62	1.00	1.07	1.00	1.00	1.46	1.22
DTM	0.64	23	0.90	0.97	1.00	1.24	0.67	1.06	1.05	1.05	1.04	1.31	0.95
U _{hub} = 14 m/s													
Leq-4	1F	2F	3F	4F	5F	6F	1C	2C	3C	4C	5C	6C	2C+
RFM	0.59	28	1.83	1.10	1.09	1.49	0.62	1.10	1.84	1.18	1.18	1.65	1.24
REM	0.93	59	1.01	0.98	1.02	1.09	0.93	1.01	1.02	0.99	1.03	1.10	1.11
TBMx	0.57	251	0.86	1.06	0.97	1.67	0.72	1.35	1.00	1.42	1.37	2.23	1.24
TBMy	0.60	88	1.63	1.19	1.00	1.48	0.69	1.14	1.97	1.37	1.15	1.93	1.35
TTM	0.61	33	1.04	1.06	1.02	1.52	0.65	1.09	1.16	1.16	1.10	1.65	1.33
DTM	0.60	10	0.87	0.98	1.01	1.40	0.63	1.08	1.03	1.04	1.09	1.55	1.01
Leq-8	1F	2F	3F	4F	5F	6F	1C	2C	3C	4C	5C	6C	2C+
RFM	0.57	34	1.76	1.10	1.08	1.51	0.61	1.12	1.78	1.19	1.19	1.65	1.20
REM	0.92	63	1.01	0.98	1.02	1.11	0.93	1.01	1.03	0.99	1.03	1.11	1.12
TBMx	0.53	364	0.74	1.09	1.00	1.68	0.65	1.27	0.91	1.31	1.30	2.14	1.14
TBMy	0.55	121	1.49	1.10	0.98	1.42	0.63	1.07	1.80	1.28	1.09	1.85	1.25
TTM	0.59	38	0.99	1.03	1.03	1.54	0.64	1.12	1.16	1.15	1.13	1.68	1.35
DTM	0.53	17	0.74	0.96	1.00	1.36	0.53	1.02	0.98	0.97	1.04	1.44	0.91
Leq-12	1F	2F	3F	4F	5F	6F	1C	2C	3C	4C	5C	6C	2C+
RFM	0.56	39	1.68	1.09	1.06	1.52	0.59	1.14	1.69	1.20	1.19	1.63	1.17
REM	0.91	65	1.01	0.98	1.03	1.12	0.92	1.01	1.04	0.99	1.03	1.12	1.14
TBMx	0.51	452	0.69	1.10	1.01	1.66	0.61	1.24	0.87	1.26	1.27	2.10	1.12
TBMy	0.52	147	1.44	1.06	0.98	1.38	0.59	1.03	1.71	1.21	1.06	1.80	1.19
TTM	0.59	44	0.96	1.01	1.04	1.56	0.64	1.14	1.17	1.13	1.16	1.70	1.36
DTM	0.53	22	0.71	0.95	1.00	1.33	0.51	0.99	0.94	0.94	1.01	1.36	0.89
U _{hub} = 18 m/s													
Leq-4	1F	2F	3F	4F	5F	6F	1C	2C	3C	4C	5C	6C	2C+
RFM	0.66	36	1.94	1.00	1.11	1.40	0.71	1.10	2.01	1.13	1.23	1.55	1.29
REM	0.92	63	1.04	0.97	1.04	1.11	0.93	1.00	1.05	0.97	1.06	1.12	1.09
TBMx	0.63	387	0.98	1.01	1.01	1.50	0.83	1.27	1.25	1.33	1.26	1.42	1.34
TBMy	0.60	179	1.46	0.88	0.95	1.34	0.69	1.12	1.83	1.08	1.13	1.31	1.21
TTM	0.61	44	1.14	0.99	1.00	1.43	0.66	1.09	1.24	1.08	1.11	1.59	1.33
DTM	0.79	12	0.98	0.96	1.01	1.22	0.85	1.10	1.05	1.03	1.08	1.20	1.13
Leq-8	1F	2F	3F	4F	5F	6F	1C	2C	3C	4C	5C	6C	2C+
RFM	0.65	42	1.94	1.01	1.10	1.44	0.71	1.11	2.03	1.15	1.24	1.56	1.27
REM	0.91	68	1.04	0.97	1.04	1.13	0.91	1.00	1.05	0.97	1.05	1.12	1.09
TBMx	0.62	475	0.94	1.06	1.01	1.59	0.82	1.23	1.18	1.32	1.28	1.42	1.32
TBMy	0.57	237	1.40	0.83	1.00	1.32	0.65	1.13	1.73	1.01	1.17	1.14	1.23
TTM	0.60	50	1.13	0.98	1.03	1.46	0.66	1.13	1.26	1.09	1.14	1.56	1.33
DTM	0.83	18	0.94	0.95	1.01	1.14	0.86	1.05	0.97	0.99	1.04	1.09	1.05
Leq-12	1F	2F	3F	4F	5F	6F	1C	2C	3C	4C	5C	6C	2C+
RFM	0.66	46	1.94	1.03	1.10	1.48	0.71	1.11	2.04	1.18	1.25	1.57	1.27
REM	0.89	71	1.04	0.97	1.03	1.16	0.90	1.00	1.05	0.97	1.05	1.12	1.09
TBMx	0.61	538	0.92	1.08	1.01	1.66	0.81	1.20	1.14	1.32	1.29	1.42	1.31
TBMy	0.57	275	1.38	0.81	1.02	1.31	0.64	1.13	1.69	0.99	1.19	1.07	1.24
TTM	0.59	56	1.12	0.97	1.04	1.48	0.65	1.16	1.27	1.10	1.15	1.50	1.33
DTM	0.85	22	0.95	0.96	1.02	1.12	0.86	1.04	0.97	0.99	1.03	1.05	1.03

Table E.6 COARSE GRAIN PI RESULTS Nassudden II modelled by TG

U _{hub} = 10 m/s													
Leq-4	1F	2F	3F	4F	5F	6F	1C	2C	3C	4C	5C	6C	2C+
RFM	0.59	1141	0.98	1.22	1.00	1.49	0.61	1.04	1.00	1.26	1.05	1.57	1.15
REM	0.95	1930	1.00	1.01	1.00	1.07	0.95	1.00	1.00	1.00	0.99	1.07	1.03
TBMx	0.70	33837	0.87	1.17	0.99	1.41	0.68	0.95	0.86	1.15	0.94	1.33	0.95
TBMy	0.57	38741	1.19	1.91	1.03	1.41	0.60	1.03	1.15	1.94	1.04	1.48	1.00
TTM	0.64	1091	0.99	1.06	1.00	1.26	0.70	1.08	1.10	1.13	1.08	1.32	1.10
DTM	0.55	287	0.88	1.02	0.98	1.49	0.59	1.06	0.85	1.05	1.04	1.55	0.93
Leq-8	1F	2F	3F	4F	5F	6F	1C	2C	3C	4C	5C	6C	2C+
RFM	0.59	1593	1.01	1.20	1.00	1.49	0.60	1.01	0.97	1.22	1.04	1.54	1.04
REM	0.94	2229	1.00	1.01	1.00	1.08	0.94	1.00	1.01	1.00	0.99	1.08	1.03
TBMx	0.66	43535	0.88	1.13	0.99	1.49	0.63	0.95	0.85	1.11	0.94	1.37	0.95
TBMy	0.56	52633	1.10	1.68	1.01	1.38	0.59	1.03	1.02	1.74	1.00	1.48	0.97
TTM	0.68	1359	0.99	1.05	1.00	1.19	0.74	1.05	1.07	1.10	1.06	1.23	1.07
DTM	0.55	514	0.88	1.02	0.98	1.49	0.57	1.03	0.78	1.02	1.00	1.49	0.86
Leq-12	1F	2F	3F	4F	5F	6F	1C	2C	3C	4C	5C	6C	2C+
RFM	0.59	1936	1.02	1.19	1.00	1.50	0.60	1.00	0.95	1.18	1.03	1.52	1.03
REM	0.93	2357	1.00	1.01	1.00	1.10	0.94	1.00	1.01	1.01	1.00	1.10	1.03
TBMx	0.64	49235	0.90	1.12	0.99	1.53	0.61	0.95	0.84	1.09	0.94	1.40	0.95
TBMy	0.55	62702	1.05	1.58	1.00	1.38	0.58	1.03	0.94	1.65	0.98	1.49	0.95
TTM	0.72	1510	1.00	1.04	1.00	1.16	0.78	1.04	1.05	1.08	1.04	1.20	1.06
DTM	0.55	644	0.89	1.02	0.99	1.49	0.56	1.02	0.76	1.01	0.99	1.48	0.86
U _{hub} = 14 m/s													
Leq-4	1F	2F	3F	4F	5F	6F	1C	2C	3C	4C	5C	6C	2C+
RFM	0.62	1580	1.12	1.18	1.02	1.47	0.65	1.05	1.16	1.23	1.07	1.53	1.15
REM	0.92	2058	1.01	1.02	1.00	1.11	0.93	1.02	1.02	1.04	1.01	1.13	1.05
TBMx	0.67	40486	0.96	1.20	0.96	1.40	0.65	0.96	0.85	1.18	0.93	1.34	0.91
TBMy	0.66	52020	1.70	1.68	1.11	1.39	0.66	0.97	1.61	1.67	1.10	1.33	0.94
TTM	0.70	1368	1.04	1.08	1.03	1.19	0.74	1.05	1.07	1.11	1.07	1.19	1.05
DTM	0.55	390	1.08	1.01	1.02	1.50	0.62	1.13	1.22	1.12	1.14	1.69	1.02
Leq-8	1F	2F	3F	4F	5F	6F	1C	2C	3C	4C	5C	6C	2C+
RFM	0.65	2154	1.14	1.15	1.00	1.40	0.67	1.03	1.15	1.19	1.05	1.45	1.06
REM	0.91	2406	1.01	1.03	1.00	1.13	0.92	1.02	1.02	1.04	1.02	1.15	1.05
TBMx	0.66	50574	1.08	1.17	0.97	1.43	0.63	0.95	0.93	1.14	0.94	1.38	0.93
TBMy	0.66	65028	1.62	1.58	1.14	1.39	0.65	0.96	1.54	1.55	1.11	1.34	0.94
TTM	0.75	1585	1.05	1.06	1.02	1.16	0.79	1.04	1.07	1.09	1.05	1.16	1.04
DTM	0.56	636	1.11	1.02	1.04	1.49	0.61	1.10	1.27	1.10	1.13	1.65	0.93
Leq-12	1F	2F	3F	4F	5F	6F	1C	2C	3C	4C	5C	6C	2C+
RFM	0.66	2570	1.15	1.13	0.99	1.38	0.67	1.02	1.14	1.16	1.03	1.41	1.03
REM	0.89	2582	1.01	1.03	1.00	1.15	0.90	1.02	1.02	1.04	1.02	1.18	1.04
TBMx	0.65	57320	1.14	1.16	0.98	1.44	0.63	0.94	0.98	1.11	0.94	1.40	0.94
TBMy	0.66	73405	1.58	1.53	1.14	1.38	0.64	0.95	1.51	1.49	1.11	1.35	0.94
TTM	0.78	1702	1.06	1.06	1.02	1.15	0.81	1.03	1.07	1.08	1.05	1.15	1.04
DTM	0.56	792	1.09	1.02	1.04	1.48	0.59	1.09	1.27	1.09	1.11	1.63	0.91
U _{hub} = 18 m/s													
Leq-4	1F	2F	3F	4F	5F	6F	1C	2C	3C	4C	5C	6C	2C+
RFM	0.54	2118		1.20	0.99	1.47	0.55	1.03		1.22	1.04	1.54	1.05
REM	0.88	2196		1.02	0.99	1.15	0.89	1.02		1.04	1.01	1.17	1.05
TBMx	0.72	328026		1.09	0.95	1.29	0.70	0.96		1.05	0.91	1.24	0.96
TBMy	0.69	356428		1.79	1.05	1.33	0.64	0.96		1.73	0.99	1.28	0.93
TTM	0.74	1499		1.09	1.00	1.13	0.77	1.01		1.10	1.02	1.14	1.02
DTM	0.56	497		1.01	1.00	1.48	0.63	1.14		1.18	1.15	1.76	1.11
Leq-8	1F	2F	3F	4F	5F	6F	1C	2C	3C	4C	5C	6C	2C+
RFM	0.51	2944		1.18	0.99	1.38	0.53	0.98		1.19	1.04	1.46	0.94
REM	0.87	2583		1.02	0.99	1.17	0.88	1.03		1.05	1.02	1.19	1.05
TBMx	0.71	403381		1.10	0.95	1.30	0.68	0.98		1.05	0.94	1.28	0.96
TBMy	0.67	463429		1.64	1.04	1.34	0.62	0.94		1.58	0.99	1.26	0.88
TTM	0.78	1723		1.07	1.00	1.12	0.81	1.01		1.08	1.02	1.14	1.02
DTM	0.56	681		0.99	1.01	1.52	0.63	1.16		1.21	1.18	1.86	1.08
Leq-12	1F	2F	3F	4F	5F	6F	1C	2C	3C	4C	5C	6C	2C+
RFM	0.50	3601		1.18	0.99	1.34	0.52	0.96		1.17	1.06	1.40	0.90
REM	0.85	2778		1.02	0.99	1.19	0.86	1.04		1.06	1.03	1.22	1.06
TBMx	0.70	456212		1.10	0.95	1.31	0.67	0.99		1.05	0.95	1.30	0.97
TBMy	0.65	548896		1.55	1.03	1.33	0.59	0.92		1.50	0.97	1.21	0.83
TTM	0.81	1843		1.06	1.00	1.11	0.83	1.00		1.07	1.01	1.14	1.02
DTM	0.56	800		0.99	1.01	1.55	0.63	1.15		1.20	1.18	1.90	1.07

Complex Terrain and Fatigue Loading

Table E.7 COARSE GRAIN PI RESULTS MAGLARP/WTS3 modelled by TG

U _{hub} = 10 m/s													
Leq-4	1F	2F	3F	4F	5F	6F	1C	2C	3C	4C	5C	6C	2C+
RFM	0.56	693	1.00	1.00	1.00	1.51	0.60	1.07		1.07	1.08	1.61	1.02
REM	0.98	2135	1.00	1.00	0.99	1.03	0.98	0.99		1.00	0.99	1.02	1.01
TBMx	0.51	9353	1.00	1.00	1.00	1.47	0.62	1.17		1.17	1.17	1.76	0.92
TBMy	0.75	1758	1.00	1.03	0.99	1.35	0.84	1.21		1.23	1.20	1.68	1.10
TTM	0.76	105	1.00	1.03	1.01	1.34	0.77	1.03		1.07	1.04	1.41	1.20
DTM	0.54	217	1.00	1.00	1.00	1.50	0.59	1.10		1.09	1.10	1.62	0.85
Leq-8	1F	2F	3F	4F	5F	6F	1C	2C	3C	4C	5C	6C	2C+
RFM	0.55	1183	1.00	1.00	1.00	1.50	0.59	1.07		1.06	1.07	1.58	0.93
REM	0.98	2394	1.00	1.00	0.99	1.03	0.97	1.00		1.00	0.99	1.03	1.01
TBMx	0.51	16985	1.00	1.00	1.00	1.44	0.60	1.14		1.13	1.13	1.68	0.87
TBMy	0.66	2822	1.00	1.01	0.99	1.40	0.77	1.21		1.22	1.19	1.71	1.06
TTM	0.72	120	1.00	1.02	1.01	1.37	0.75	1.07		1.10	1.07	1.50	1.20
DTM	0.54	403	1.00	1.00	1.00	1.50	0.59	1.09		1.09	1.09	1.59	0.83
Leq-12	1F	2F	3F	4F	5F	6F	1C	2C	3C	4C	5C	6C	2C+
RFM	0.55	1471	1.00	1.00	1.00	1.49	0.58	1.06		1.06	1.06	1.57	0.93
REM	0.97	2499	1.00	1.00	0.99	1.04	0.97	1.00		1.00	0.99	1.04	1.01
TBMx	0.51	21271	1.00	1.00	1.00	1.42	0.60	1.13		1.11	1.12	1.65	0.86
TBMy	0.65	3461	1.00	1.01	0.99	1.40	0.76	1.22		1.22	1.20	1.71	1.06
TTM	0.69	134	1.00	1.02	1.01	1.38	0.73	1.08		1.10	1.08	1.53	1.20
DTM	0.54	510	1.00	1.00	1.00	1.50	0.59	1.09		1.09	1.09	1.58	0.82
U _{hub} = 14 m/s													
Leq-4	1F	2F	3F	4F	5F	6F	1C	2C	3C	4C	5C	6C	2C+
RFM	0.81	1150		0.97	0.99	1.27	0.87	1.08		1.06	1.08	1.42	1.01
REM	0.97	2354		1.00	0.99	1.05	0.97	0.99		1.00	0.98	1.04	1.01
TBMx	0.63	13122		1.00	1.00	1.46	0.79	1.32		1.31	1.32	1.98	1.15
TBMy	0.65	2791		1.04	0.98	1.34	0.78	1.27		1.28	1.25	1.70	1.13
TTM	1.02	320		0.90	0.99	1.02	1.01	0.99		0.91	0.99	1.03	0.95
DTM	0.55	293		1.02	1.00	1.44	0.61	1.14		1.16	1.14	1.67	0.91
Leq-8	1F	2F	3F	4F	5F	6F	1C	2C	3C	4C	5C	6C	2C+
RFM	0.79	1775		0.98	0.99	1.24	0.84	1.07		1.08	1.07	1.39	0.97
REM	0.96	2666		1.00	0.99	1.07	0.96	0.99		0.99	0.98	1.05	1.01
TBMx	0.66	21272		1.00	1.00	1.44	0.77	1.27		1.26	1.27	1.85	1.07
TBMy	0.62	4234		1.04	0.98	1.39	0.74	1.22		1.23	1.20	1.65	1.07
TTM	0.94	378		0.89	0.99	1.07	0.95	1.00		0.93	1.02	1.13	0.96
DTM	0.55	535		1.01	1.00	1.42	0.60	1.13		1.15	1.13	1.63	0.89
Leq-12	1F	2F	3F	4F	5F	6F	1C	2C	3C	4C	5C	6C	2C+
RFM	0.79	2164		0.98	0.99	1.23	0.82	1.06		1.07	1.07	1.37	0.97
REM	0.95	2806		1.00	0.99	1.08	0.95	0.99		0.99	0.98	1.07	1.01
TBMx	0.67	25892		1.00	1.00	1.44	0.77	1.26		1.25	1.26	1.84	1.06
TBMy	0.62	5156		1.04	0.98	1.42	0.73	1.21		1.22	1.18	1.63	1.03
TTM	0.90	424		0.89	0.99	1.11	0.91	1.00		0.93	1.03	1.19	0.97
DTM	0.55	667		1.01	1.00	1.41	0.61	1.14		1.16	1.14	1.63	0.90
U _{hub} = 18 m/s													
Leq-4	1F	2F	3F	4F	5F	6F	1C	2C	3C	4C	5C	6C	2C+
RFM	0.76	1536		0.99	1.00	1.27	0.80	1.08		1.07	1.08	1.38	0.98
REM	0.96	2550		1.00	0.99	1.07	0.96	0.99		0.99	0.98	1.05	1.01
TBMx	0.52	19474		1.01	1.00	1.44	0.71	1.36		1.36	1.36	1.98	1.14
TBMy	0.61	3441		1.03	0.98	1.52	0.75	1.30		1.31	1.28	2.10	1.21
TTM	1.03	407		0.92	1.00	1.07	1.03	1.00		0.93	1.00	1.06	0.98
DTM	0.48	289		1.00	0.99	1.61	0.64	1.28		1.28	1.30	2.11	1.12
Leq-8	1F	2F	3F	4F	5F	6F	1C	2C	3C	4C	5C	6C	2C+
RFM	0.66	2427		1.00	1.00	1.22	0.72	1.07		1.07	1.07	1.30	0.89
REM	0.95	2898		1.00	0.99	1.09	0.95	0.99		0.99	0.98	1.07	1.01
TBMx	0.52	31493		1.01	1.00	1.33	0.66	1.27		1.27	1.26	1.76	1.06
TBMy	0.59	5001		1.02	0.98	1.51	0.77	1.34		1.34	1.32	2.15	1.21
TTM	0.96	485		0.93	1.00	1.13	0.96	1.02		0.95	1.01	1.15	1.01
DTM	0.47	456		1.00	1.00	1.68	0.65	1.24		1.24	1.27	2.15	1.12
Leq-12	1F	2F	3F	4F	5F	6F	1C	2C	3C	4C	5C	6C	2C+
RFM	0.65	2949		1.01	1.00	1.22	0.71	1.07		1.07	1.07	1.28	0.89
REM	0.94	3061		1.00	0.99	1.10	0.93	0.99		0.99	0.98	1.09	1.01
TBMx	0.53	38366		1.01	1.00	1.31	0.65	1.24		1.24	1.24	1.70	1.05
TBMy	0.59	5969		1.01	0.97	1.49	0.78	1.37		1.35	1.33	2.19	1.22
TTM	0.91	545		0.94	1.00	1.14	0.92	1.02		0.96	1.01	1.19	1.02
DTM	0.45	558		0.99	1.00	1.70	0.66	1.22		1.22	1.24	2.17	1.13

Table E.8 FINE GRAIN PI RESULTS NTK500 modelled by RISO

U _{hub} = 10 m/s						
Leq-4	No 1	2	3	4	5	6
RFM	23.7	1.01	1.00	1.14	1.02	1.00
REM	170.1	1.00	1.00	1.00	1.00	1.00
TBMx	189.4	1.00	1.00	1.20	0.95	0.99
TBMy	63.0	1.00	1.00	1.20	0.97	1.00
TTM	31.8	1.00	1.00	1.13	1.01	0.99
DTM	85.6	1.00	1.00	1.03	1.01	1.00
Leq-8	No 1	2	3	4	5	6
RFM	30.6	1.01	1.00	1.11	1.02	1.00
REM	185.5	1.00	1.00	1.00	1.00	1.00
TBMx	260.3	1.01	1.00	1.15	0.95	1.00
TBMy	81.6	1.00	1.00	1.16	1.00	0.98
TTM	39.5	1.01	1.00	1.13	1.00	1.01
DTM	96.8	1.00	1.00	1.04	1.01	1.00
Leq-12	No 1	2	3	4	5	6
RFM	36.1	1.00	1.00	1.09	1.01	0.99
REM	191.2	1.00	1.00	1.00	1.00	1.00
TBMx	310.5	1.01	1.00	1.13	0.95	1.00
TBMy	96.3	1.00	1.00	1.13	1.01	0.98
TTM	45.8	1.00	1.00	1.13	1.00	1.02
DTM	103.2	1.00	1.00	1.04	1.00	1.00
U _{hub} = 14 m/s						
Leq-4	No 1	2	3	4	5	6
RFM	39.9	1.01	1.00	1.09	0.99	0.98
REM	179.0	1.00	1.00	1.00	1.00	1.00
TBMx	357.3	1.00	1.00	1.18	0.93	0.99
TBMy	135.8	1.00	1.00	1.20	0.95	0.99
TTM	54.4	0.98	1.00	1.09	0.98	0.96
DTM	104.7	1.00	1.00	1.03	0.99	0.99
Leq-8	No 1	2	3	4	5	6
RFM	49.8	1.02	1.00	1.07	0.99	0.98
REM	195.8	1.00	1.00	1.00	1.00	1.00
TBMx	452.4	1.00	1.00	1.19	0.93	0.99
TBMy	173.0	1.00	1.00	1.20	0.95	0.99
TTM	66.3	0.97	1.00	1.07	0.97	0.95
DTM	122.1	1.01	1.00	1.03	0.99	1.00
Leq-12	No 1	2	3	4	5	6
RFM	57.2	1.02	1.00	1.06	0.98	0.98
REM	202.5	1.00	1.00	1.00	1.00	1.00
TBMx	515.7	1.00	1.00	1.20	0.93	1.00
TBMy	196.3	1.00	1.00	1.20	0.95	0.99
TTM	76.1	0.97	1.00	1.06	0.96	0.94
DTM	132.8	1.01	1.00	1.03	0.99	1.00
U _{hub} = 18 m/s						
Leq-4	No 1	2	3	4	5	6
RFM	67.4	1.02	1.00	1.07	0.97	0.97
REM	178.7	1.00	1.00	1.00	1.00	1.00
TBMx	788.6	1.04	1.00	1.11	0.92	0.98
TBMy	202.7	1.04	1.00	1.11	0.95	0.98
TTM	92.6	0.99	1.00	1.08	0.96	0.96
DTM	138.4	1.02	1.00	1.04	0.98	0.99
Leq-8	No 1	2	3	4	5	6
RFM	78.5	1.02	1.00	1.07	0.97	0.96
REM	195.2	1.00	1.00	1.00	1.00	1.00
TBMx	939.9	1.05	1.00	1.12	0.92	0.98
TBMy	252.1	1.05	1.00	1.12	0.97	0.99
TTM	114.1	0.97	1.00	1.04	0.95	0.95
DTM	167.4	1.02	1.00	1.03	0.98	0.98
Leq-12	No 1	2	3	4	5	6
RFM	86.4	1.02	1.00	1.06	0.97	0.96
REM	201.6	1.00	1.00	1.00	1.00	1.00
TBMx	1041.	1.05	1.00	1.13	0.92	0.98
TBMy	283.6	1.05	1.00	1.13	0.97	0.99
TTM	132.8	0.97	1.00	1.02	0.94	0.94
DTM	186.9	1.03	1.00	1.03	0.98	0.98

Complex Terrain and Fatigue Loading

Table E.9 FINE GRAIN PI RESULTS V39 modelled by RIS0

U _{hub} = 10 m/s						
Leq-4	1	2	3	4	5	6
RFM	72.5	1.02	1.01	1.10	1.02	1.00
REM	162.1	1.00	1.00	1.03	1.00	1.01
TBMx	540.6	1.01	1.01	1.11	0.96	1.02
TBMy	319.0	1.01	1.01	1.18	0.96	0.95
TTM	74.9	1.01	1.01	1.14	1.03	0.98
DTM	48.9	1.00	1.00	1.03	0.97	1.03
Leq-8	1	2	3	4	5	6
RFM	83.4	1.02	1.01	1.07	1.00	1.02
REM	151.0	1.00	1.00	1.03	1.00	1.01
TBMx	711.8	1.01	1.01	1.04	0.96	1.05
TBMy	328.0	1.01	1.01	1.16	0.96	0.93
TTM	78.5	1.01	1.02	1.13	1.03	1.00
DTM	71.9	1.00	1.00	0.98	0.97	1.05
Leq-12	1	2	3	4	5	6
RFM	94.0	1.02	1.01	1.06	1.00	1.03
REM	149.1	1.00	1.00	1.04	1.00	1.02
TBMx	833.0	1.01	1.01	1.02	0.96	1.05
TBMy	359.0	1.01	1.01	1.14	0.97	0.92
TTM	86.2	1.01	1.02	1.12	1.03	1.03
DTM	84.8	1.00	1.00	0.96	0.98	1.06
U _{hub} = 14 m/s						
Leq-4	1	2	3	4	5	6
RFM	105.3	1.02	1.01	1.09	1.03	1.02
REM	187.0	1.00	1.00	1.06	1.01	1.01
TBMx	785.7	1.01	1.01	1.14	0.96	1.04
TBMy	538.8	1.00	1.00	1.22	0.96	1.05
TTM	114.8	1.01	1.02	1.12	1.02	0.95
DTM	78.5	1.00	1.00	1.08	0.97	1.07
Leq-8	1	2	3	4	5	6
RFM	114.1	1.02	1.01	1.06	1.01	1.07
REM	177.8	1.00	1.00	1.07	1.01	1.02
TBMx	906.8	1.01	1.01	1.08	0.95	1.04
TBMy	542.2	1.01	1.00	1.21	0.96	1.11
TTM	121.5	1.01	1.02	1.11	1.01	0.94
DTM	100.0	1.00	1.00	1.07	0.95	1.13
Leq-12	1	2	3	4	5	6
RFM	126.3	1.02	1.01	1.04	1.01	1.10
REM	179.1	1.00	1.00	1.07	1.01	1.03
TBMx	1030.	1.01	1.01	1.06	0.95	1.04
TBMy	583.7	1.01	1.00	1.19	0.97	1.15
TTM	132.5	1.01	1.02	1.10	1.00	0.93
DTM	113.9	1.00	1.00	1.07	0.95	1.16
U _{hub} = 18 m/s						
Leq-4	1	2	3	4	5	6
RFM	158.4	1.01	1.00	1.10	1.02	0.97
REM	209.3	1.00	1.00	1.08	1.02	1.00
TBMx	1278.	1.01	1.00	1.17	0.94	1.01
TBMy	930.6	1.00	1.00	1.20	0.96	1.01
TTM	180.4	1.00	1.00	1.15	1.04	0.95
DTM	144.3	1.00	1.00	1.14	0.98	1.03
Leq-8	1	2	3	4	5	6
RFM	175.4	1.01	1.00	1.07	1.01	0.98
REM	202.5	1.00	1.00	1.08	1.02	0.99
TBMx	1459.	1.01	1.00	1.12	0.95	1.02
TBMy	941.0	1.00	1.00	1.20	0.96	1.03
TTM	193.6	1.00	1.00	1.14	1.03	0.93
DTM	165.9	1.00	1.00	1.12	0.98	1.06
Leq-12	1	2	3	4	5	6
RFM	191.7	1.01	1.00	1.06	1.01	1.00
REM	209.2	1.00	1.00	1.10	1.02	0.98
TBMx	1636.	1.01	1.00	1.10	0.95	1.02
TBMy	996.4	1.00	1.00	1.20	0.96	1.06
TTM	214.7	1.00	1.00	1.13	1.03	0.91
DTM	183.0	1.00	1.00	1.11	0.98	1.07

EUROPEAN WIND TURBINE STANDARDS II
PART 1
LOAD SPECTRA AND EXTREME WIND CONDITIONS
SUB C
EXTREME WIND CLIMATE EVENTS

D. Winkelaar (ed.)	Netherlands Energy Research Foundation ECN
J.W.M. Dekker	Netherlands Energy Research Foundation ECN
P. Chaviaropoulos	CRES
I. Carlén	Teknikgruppen AB
G.C. Larsen	Risø National Laboratory

CONTENTS OF PART 1Sub C

LIST OF SYMBOLS	5
1 INTRODUCTION	9
2 THE DISTRIBUTION OF THE EXTREME WIND SPEED	11
2.1 The cdf of the extreme 10-minute average wind speed	11
2.1.1 Exact extreme distribution based on Weibull parent	11
2.1.2 The FT type-I distribution based on a Weibull parent	11
2.1.3 The Davenport correction	12
2.2 The number of independent events per year	12
2.3 Evaluation of V_{ref} in the IEC 1400-1 standard	13
2.4 The pdf of the 3-second average wind speed	15
2.5 The cdf of the extreme 3-sec average wind speed	17
2.6 Evaluation of V_{e1} and V_{e50} in the IEC 1400-1 standard	18
2.7 Conclusions	19
3 THE DISTRIBUTION OF EXTREME GUSTS	21
3.1 The pdf of single point gusts	21
3.1.1 The correlation function	23
3.1.2 The number of independent events	23
3.2 Results and comparison with IEC	24
4 THE DISTRIBUTION OF EXTREME WIND DIRECTION CHANGE	29
4.1 The pdf of wind direction	29
4.2 The pdf of wind direction change	33
4.3 Results and comparison with the IEC 1400-1 standard	33
5 OTHER EXTREME ATMOSPHERIC EVENTS	39
5.1 Downbursts	39
6 SUMMARY, CONCLUSIONS AND RECOMMENDATIONS	43
A NOTATION AND BACKGROUND	45

A.1	Symbols and Definitions	45
A.1.1	Distribution and density functions	46
A.1.2	Joint statistics	46
A.1.3	Order Statistics from Independent and Identically Distributed Samples	47
A.1.4	Return period	48
A.1.5	Characteristic largest value	48
A.2	The Normal Distribution	49
A.3	The Weibull Distribution	49
A.4	The Gumbel Distribution	50
B	DERIVATION OF GUMBEL DISTRIBUTION	51
B.1	Derivation Based on Order Statistics	51
B.1.1	Order statistics and asymptotic distributions	51
B.1.2	The Gumbel distribution for a Weibull parent	52
B.2	Derivation Based on Exceedance Statistics	53
B.2.1	Exceedance statistics	53
B.2.2	Frequency of maxima	55
	REFERENCES	58

LIST OF SYMBOLS

c_1	Constant defined in Eq. (2.13).
c_2	Constant defined in Eq. (2.14).
$E[\]$	Denotes the ensemble averaged value of the quantity in square brackets.
f	Frequency (Hz).
f_0	Lower cut-off frequency (Hz).
$f(x)$	(First-order) probability density function (pdf).
$f_x(x)$	Marginal probability density function.
$f(x, y)$	Second-order (joint) probability density function.
$f(x y)$	Conditional probability density function for the distribution of x when y is specified.
i_u	Longitudinal signal to noise ratio, $= \frac{U}{\sigma_u}$, or the reciprocal of the longitudinal turbulence intensity.
i_v	Transversal signal to noise ratio $= \frac{V}{\sigma_v}$.
J_n	Jacobian.
k	Shape parameter of the Weibull distribution.
n	Number of independent events.
$n_a^+(T)$	Number of crossings of the level $y = a$ with positive slope in time T for a single member function of the random process $y(t)$.
q_T	Ratio of the standard deviation σ_T to σ .
r	Polar co-ordinate ; probability of exceedance.
t	Time.
u	Longitudinal (x) component of the wind speed.
u_T	Longitudinal component of the wind speed averaged over time interval T .
v	Transversal (y) component of the wind speed.

w	Vertical (z) component of the wind speed.
$y(t)$	Random process composed of an ensemble of member functions each of which is a different function of t .
z	Vertical co-ordinate.
z_0	Surface roughness length (m).
C	Scale parameter of the Weibull distribution.
$F(x)$	(First-order) probability distribution function (cdf).
$F_x(x)$	Marginal probability distribution function.
$F(x, y)$	Joint probability distribution function (cdf) for the random variable x .
I	Identity matrix.
I_{ave}	Annual average turbulence intensity.
L	Integral length scale.
$N_a^+(T)$	Average number of crossings of the level $y = a$ with positive slope in time T for a random process $y(t)$.
Pr	Abbreviation for “probability”.
S_{uu}	Auto-spectral density function of u .
T	Time period ; Averaging time ; Record length.
T_p	Sample period (generally one year, but 20 and 50 years are also used).
T_r	Return period.
U	Ten-minute mean value of the longitudinal component of the wind speed.
V	Ten-minute mean value of the transversal component of the wind speed.
V_{ave}	Annual average wind speed at hub height.
V_{cg}	Maximum coherent gust over the whole rotor swept area.
V_{e1}	Extreme 3-sec. average wind speed at hub height with a 2% probability of being exceeded within a year.

V_{e50}	Extreme 3-sec. average wind speed at hub height with a 2% probability of being exceeded within 50 years.
V_{gust1}	Extreme 3-sec. average gust with a specified starting value and a 2% probability of being exceeded within a year.
V_{gust50}	Extreme 3-sec. average gust with a specified starting value and a 2% probability of being exceeded in 50 years.
V_r	Annual extreme 10-min. average wind speed at hub height with a return period of T_r years.
V_{ref}	Annual extreme 10-min. average wind speed at hub height with a return period of 50 years.
α	Reciprocal value of the dispersion factor of the Gumbel distribution.
β	Modal value of the Gumbel distribution.
γ	Euler's constant = 0.5772156649... ;
δ	Scale parameter of the Gumbel distribution.
θ	Polar co-ordinate.
λ	Location parameter of Gumbel distribution.
μ	Mean of the normal distribution.
ν_a^+	Average frequency of positive slope crossings of the level $y = a$ for a random process $y(t)$.
ν_0^+	Average frequency of positive slope crossings of the zero level.
ν_T	Average frequency of statistically independent events.
ρ_{xy}	Correlation coefficient (normalized covariance) for the random variables x and y .
σ_u	Standard deviation of longitudinal wind speed at hub height.
σ_v	Standard deviation of transversal wind speed at hub height.
σ_T	Part of the standard deviation σ_u which remains after having applied a low pass filter with averaging time T .
τ	Time lag (time difference).
Γ	Gamma function.

1 INTRODUCTION

Critical loads result in responses that exceed the limits beyond which structural damage or irreversible change may be expected. Thus the designer is interested in the number of times, or the probability, that large loads and resulting large responses may occur over the life time of the system.

The IEC 1400-1 standard divides the wind regime for load and safety considerations into normal wind conditions which will occur frequently during normal operation of the wind turbine, and extreme wind conditions which are defined as having a 1 year or 50 year recurrence period. The extreme wind conditions are used to determine critical design loads which the turbine must withstand during its lifetime. These extreme conditions include peak wind speeds due to storms and rapid changes in wind speed and direction.

The purpose of this investigation is to review the models for extremes of the IEC 1400-1 standard. To that end it was decided not to analyse wind speed measurements as for example is done by a revision working group (TC88/WG7) [2]. Although measurements should ultimately be decisive, it is obviously dangerous to infer statistics of extremes from a rather limited set of data. Besides if we would perform exactly the same sort of investigation as the working group TC88/WG7 did, then it would be difficult to validate or invalidate the results of that group.

Inspired by a report by Bergström [1] and papers by Cook [6] and Harris [14] it was decided to adopt a completely different and more theoretical approach, by using Extreme Value Theory. Assuming that the statistics of the wind climate is given (i.e. the Weibull distribution and the turbulence model) it is possible to derive the probability of occurrence of extreme wind climate events. An additional advantage of this mathematical/statistical approach is that the models for extremes and the models for normal turbulence are logically connected, making the results to some extent more “physical.”

Section 2 describes the derivation of the probability density function (pdf) and cumulative distribution function (cdf) of the 10-minute and extreme 3-second average wind speed. These functions are used to compute the survival wind speeds as function of the Weibull shape and scale parameter and the values obtained are compared with the values given by the IEC 1400-1 standard in the so-called Extreme Wind speed Model (EWM).

Section 3 deals with the problem of deriving a pdf and cdf of the extreme 3-second average gust. The resulting distribution function is used to compute extreme gust magnitudes with a probability of occurrence as specified by the IEC standard and the values found are compared with the values given by the IEC in the so-called Extreme Operational Gust model (EOG) and Extreme Coherent Gust model (ECG).

Section 4 is concerned with the derivation of a pdf and cdf of extreme wind direction changes. This problem is not quite solved but an approximate distribution function is given which seems to yield reasonable results.

Section 5 deals with the question whether there are extreme wind events which are not described by the IEC standard but should be included. One rare event is described, a so-called downburst, which may induce extreme loads on a wind turbine.

Section 6 gives a summary, some conclusions and recommendations.

Finally, the Appendices A and B give some background on statistics and extreme value theory, mostly taken from references [3, 8, 14, 17–19, 21].

2 THE DISTRIBUTION OF THE EXTREME WIND SPEED

Two types of statistics are of interest; those relating to the total population of wind speeds and second the properties of the extremes. In the following it is assumed that the statistics of the wind climate at the site of the structure is established and what will be discussed is an attempt to find a relation between these statistics and the properties of extremes. In statistical jargon: we assume that the parent distribution is somehow known and we want to find the extreme value distributions.

Some of the difficulties in finding these limit distributions are addressed. Using these limit distributions we determine extreme wind speeds defined in the Extreme Wind Speed Model (EWM) of the IEC 1400-1 standard and compare them with the values actually given by that standard. Some conclusions are drawn and recommendations given.

2.1 The cdf of the extreme 10-minute average wind speed

2.1.1 Exact extreme distribution based on Weibull parent

Taking the Weibull cdf (A.23) as the parent, the distribution of the yearly extreme 10-minute averages is given by the distribution of the n 'th order statistic:

$$\text{Exact : } F^n(V) = \left[1 - \exp \left\{ - \left(\frac{V}{V_{\text{ave}}} \Gamma \left(1 + \frac{1}{k} \right) \right)^k \right\} \right]^n. \quad (2.1)$$

If V_r is the yearly extreme 10-minute average wind speed with a return period of T_r years then the following relation holds:

$$\frac{1}{1 - F^n(V_r)} = T_r \quad \rightarrow \quad F(V_r) = \exp \left(\frac{\ln(1 - 1/T_r)}{n} \right). \quad (2.2)$$

Combining (2.1) and (2.2) we find after some simple algebra:

$$\frac{V_r}{V_{\text{ave}}} = \frac{1}{\Gamma(1 + 1/k)} \left[-\ln \left\{ 1 - \exp \left(\frac{\ln(1 - 1/T_r)}{n} \right) \right\} \right]^{\frac{1}{k}}. \quad (2.3)$$

2.1.2 The FT type-I distribution based on a Weibull parent

The Fisher-Tippett type-I or Gumbel distribution of the yearly extreme 10-minute average wind speed with the Weibull distribution as a parent, i.e. the asymptotic version of (2.1), is given by :

$$\text{Gumbel : } F_n(V) = \exp [-\exp \{-\alpha (V - \beta)\}], \quad (2.4)$$

where

$$\alpha = \frac{k}{C} (\ln n)^{1 - \frac{1}{k}}, \quad (2.5)$$

$$\beta = C (\ln n)^{\frac{1}{k}}, \quad (2.6)$$

$$C = \frac{V_{\text{ave}}}{\Gamma(1 + 1/k)}. \quad (2.7)$$

For a return period of T_r years we find:

$$\frac{1}{1 - F_n(V_r)} = T_r \quad \rightarrow \quad F_n(V_r) = 1 - 1/T_r. \quad (2.8)$$

Combining (2.4) and (2.8) yields:

$$\frac{V_r}{V_{ave}} = \frac{(\ln n)^{\frac{1}{k}-1}}{k\Gamma(1 + 1/k)} [k \ln n - \ln \{-\ln(1 - 1/T_r)\}]. \quad (2.9)$$

2.1.3 The Davenport correction

Using exceedance statistics, as proposed by Davenport [8], slightly different expressions are found for α and β , see section B.2 :

$$\alpha_{Dav} = \alpha \left\{ 1 - \frac{k-1}{k \ln n} \right\}, \quad (2.10)$$

and

$$\beta_{Dav} = \beta \left\{ 1 + \frac{\ln \left[k\Gamma\left(\frac{1}{k} + 1\right) (\ln n)^{\frac{k-1}{k}} \right]}{k \ln n - (k-1)} \right\}. \quad (2.11)$$

We then find for the ratio of V_r to V_{ave} :

$$\frac{V_r}{V_{ave}} = \frac{(\ln n)^{\frac{1}{k}-1}}{c_1 k\Gamma(1 + 1/k)} [c_1 c_2 k \ln n - \ln \{-\ln(1 - 1/T_r)\}], \quad (2.12)$$

where

$$c_1 = \left\{ 1 - \frac{k-1}{k \ln n} \right\}, \quad (2.13)$$

and

$$c_2 = \left\{ 1 + \frac{\ln \left[k\Gamma\left(\frac{1}{k} + 1\right) (\ln n)^{\frac{k-1}{k}} \right]}{k \ln n - (k-1)} \right\}. \quad (2.14)$$

2.2 The number of independent events per year

In all three expressions (2.3), (2.9) and (2.12) the ratio of V_r to V_{ave} is a function of the Weibull shape parameter k , the number of independent events n and the return period T_r .

Extreme value theory only deals with extremes of samples of n independent and identically distributed observations which originate from a parent population with cumulative distribution function (cdf) $F(x)$. Then the largest value has a probability distribution given by $F^n(x)$. Thus in the case of 10-minute average wind speeds, if the values of each ten minute average were statistically independent of those of neighbouring ten minutes, then it would be expected that the annual largest value of the ten-minute average wind speed would have a probability distribution given by $[F(x)]^{52596}$, where $F(x)$ is the Weibull distribution and 52596 the number of ten minutes in a year. This is not observed in practice, because values of adjacent ten minutes are not independent. More recent studies (see Castillo [3]) have shown that provided the data are statistically stationary, and hence have a finite correlation time, τ , then the

distribution of the largest value is given by $F^n(x)$, where $n \sim T/\tau$ if T is the record length (see Harris [14]).

Following Bergström [1], a relatively simple and convenient way to determine τ is to use the autocorrelation function $\rho(\tau)$, where τ is the time lag over which the correlation is calculated. If we put $\rho = 0.5$ and solve for τ , the solution may be interpreted as a measure of the average time between two 50% correlated values in the time series. The solution of this particular case becomes, using spectral representation (see Rice [20]) :

$$\nu_T = \left[\int_{f_0}^{0.5/T} f^2 S_{uu}(f) df / \int_{f_0}^{0.5/T} S_{uu}(f) df \right]^{1/2}, \tag{2.15}$$

where $S_{uu}(f)$ is the spectral density function, f the frequency and $\nu_T = 1/\tau$ is the sought effective frequency valid for averaging time T . The lower integration limit, f_0 , may be chosen to be about $1/(2 \cdot 3600)$ Hz to eliminate the synoptical part of the spectrum. The number of independent observations, averaged over a period of length T , within a time period T_p , may then be estimated from the relation

$$n = \nu_T \cdot T_p \tag{2.16}$$

Bergström [1] states that the effective frequency is rather insensitive to the specific choice of spectral density function. This is not confirmed by our own calculations, see Table 2.1. The table shows that the estimated effective frequencies, using the IEC Von Kármán spectrum with $L/U = 10$ (see Eq. (3.11)), are roughly four times greater than the corresponding values given by Bergström. It is possible that Bergström actually used a lower correlation. We will use Bergströms values because he finds good agreement between measurements and computation for 1-hour and 10-minute averages, but for shorter averaging times his computed estimates are slightly too high.

Table 2.1 The effective frequency ν_T and the ratio $q_T = \sigma_T/\sigma_u$ for various averaging times T ; according to Bergström [1] and according to present calculations based on the IEC Von Kármán and Kaimal spectrum with $L/U = 10$.

T [s]	ν_{T-B} [s ⁻¹]	ν_{T-VK} [s ⁻¹]	ν_{T-K} [s ⁻¹]	q_{T-B}	q_{T-VK}	q_{T-K}
600	0.00073	0.000526	0.000522	0.18	0.167	0.163
60	0.00100	0.004637	0.004456	0.48	0.541	0.482
10	0.00460	0.019240	0.020772	0.78	0.853	0.775
5	0.00790	0.030721	0.035490	0.85	0.909	0.852
3	0.01000	0.042996	0.051734	0.89	0.936	0.893
1	0.02400	0.088163	0.112265	0.95	0.970	0.948

2.3 Evaluation of V_{ref} in the IEC 1400-1 standard

In the IEC 1400-1 standard [16] the peak values of the wind speed are given in the so-called *Extreme Wind Speed Model (EWM)*. This model must be applied as an ultimate load case at parked conditions. The extreme wind speeds are given as a function of the reference wind speed V_{ref} which is defined as : ‘the extreme 10-minute average wind speed at turbine hub height with a recurrence period of 50 years.’

This definition is here interpreted as : ‘the *annual* extreme 10-minute average wind speed at hub height with a confidence limit of 98%’.

In the IEC 1400-1 standard the ratio of V_{ref} to V_{ave} is constant for wind turbine class I through IV:

$$\frac{V_{\text{ref}}}{V_{\text{ave}}} = 5.$$

The choice of this ratio is based on typical values found in the British building code. This ratio is probably characteristic of mid latitudes because in de Dutch building code the same ratio appears. This value is, to a large extent, based on a Gumbel type analysis of wind speed measurements.

Using the above derived expressions (2.3), (2.9) and (2.12), the ratio of V_r to V_{ave} is computed as a function of the Weibull shape parameter k and presented in Figure 2.1. In this figure the curves based on the ‘exact’ extremal distribution and the Gumbel distribution almost coincide. To determine the number n of independent events in a year, the effective frequency ν_T given by Bergström [1], see Table 2.1, is used :

$$\left. \begin{aligned} \nu_T &= 7.3 \times 10^{-4} \\ T_p &= 3.15576 \times 10^7 \end{aligned} \right\} n = \nu_t \cdot T_p = 23037 \quad (2.17)$$

It should be noted that the computed curves are not very sensitive for the precise choice of effective frequency in Table 2.1: n is always so large that the extreme value curve has practically converged to the limit value curve. For flat terrain sites at mid latitudes the value of the Weibull shape parameter k (for

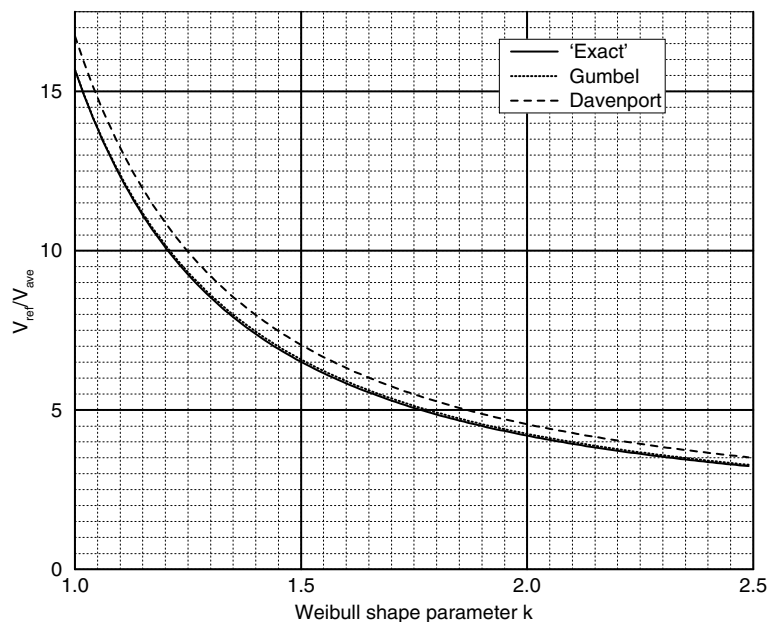


Figure 2.1 The ratio of V_{ref} to V_{ave} as function of the Weibull shape parameter k .

10-minute averages) varies typically between 1.65 inland, 1.9 in coastal areas and 2.1 at sea. Figure 2.1 shows that $V_{\text{ref}}/V_{\text{ave}} \leq 5$ for $k > 1.77$ if we use the ‘exact’ or Gumbel distribution. Hence at mid latitudes the ratio $V_{\text{ref}}/V_{\text{ave}} = 5$ is acceptable for most inland flat terrain sites, and even slightly conservative for

flat terrain coastal areas.

If we take Davenport's correction into account then the range of acceptable flat terrain sites would be smaller unless we increase the ratio to 5.5. Note that Bergström [1] finds a good agreement between long term measurements and extreme value theory, using the Davenport correction.

Figure 2.1 also makes clear that a ratio of 5 is too low for sites in complex terrain, where k -values ≤ 1.5 are found. Taking $k = 1.4$ as a characteristic value for complex terrain then according to Figure 2.1 the ratio $V_{\text{ref}}/V_{\text{ave}}$ should be approximately 7.5. Hence with respect to V_{ref} , an IEC Class I wind turbine is only suitable for complex terrain sites with an annual average wind speed V_{ave} which is lower than 6.7 m/s (at hub height!).

2.4 The pdf of the 3-second average wind speed

So far the extreme value distribution for ten-minute averages has been studied. We would like to have also extreme value distributions for wind speeds averaged over much shorter intervals, e.g. 3 seconds. To that end we first have to derive the parent distribution of the 3-sec average wind speeds.

These short term averages will be denoted by u_T , where T is the averaging time. It will be assumed that u_T is normally distributed around the 10-minute mean value, U , with standard deviation σ_T . Then the conditional pdf of u_T given U is:

$$f(u_T | U) = \frac{1}{\sigma_T \sqrt{2\pi}} \exp \left[-\frac{1}{2} \left(\frac{u_T - U}{\sigma_T} \right)^2 \right]. \quad (2.18)$$

We assume that the distribution of U follows a Weibull function with scale parameter C and shape parameter k :

$$f(U) = \frac{k}{C} \left(\frac{U}{C} \right)^{k-1} \exp \left[- \left(\frac{U}{C} \right)^k \right], \quad (2.19)$$

According to probability theory the conditional density function of Y given X is:

$$f(y | x) \equiv \frac{f(x, y)}{f_x(x)}, \quad (2.20)$$

where $f(x, y)$ is the joint probability density function of X and Y and $f_x(x) = \int_{-\infty}^{\infty} f(x, y) dy$ is the marginal density function of X . Using (2.20) we find

$$f(u_T, U) = f(u_T | U)f(U), \quad (2.21)$$

from which it follows that

$$f(u_T) = \int_0^{\infty} f(u_T, U) dU = \int_0^{\infty} N[u_T; U, \sigma_T(U)] \cdot W[U; C, k] dU, \quad (2.22)$$

where $N[u_T; U, \sigma_T(U)]$ and $W[U; C, k]$ are shorthand notations for the Normal distribution and Weibull distribution respectively, and σ_T is the part of the total standard deviation σ_u which remains after having applied a low pass filter with averaging time T .

The ratio $q_T = \sigma_T / \sigma_u$ can be computed (see Bergström [1]) from :

$$q_T \approx \left[\frac{\int_{f_0}^{0.5/T} S_{uu}(f) df}{\int_{f_0}^{\infty} S_{uu}(f) df} \right]. \quad (2.23)$$

The lower integration limit f_0 can be chosen to be about $1/(2 \cdot 3600)$ Hz, to eliminate the synoptical part of the spectrum, see Table 2.1. The table shows that the values given by Bergström are quite close to the values found with the Kaimal spectrum given by the IEC 1400-1 standard.

The standard deviation, σ_u , is a random variable. Hence we would prefer to use a conditional pdf $f(\sigma_u | U)$ for the standard deviation, but if such a function is not available then we can either use :

$$\sigma_u = \frac{U}{\ln z/z_0} \quad (2.24)$$

or the expression given by the IEC 1400-1 standard :

$$\sigma_u = 1.2I_{\text{ave}}(0.75U + 0.16V_{\text{ave}}) \quad (2.25)$$

Using (2.22) and (2.25), the pdf $f(u_T)$ of the 3-sec average wind speed is computed for IEC wind turbine class I through IV, and presented in Figure 2.2. The figure shows that the distribution of the 3-sec average

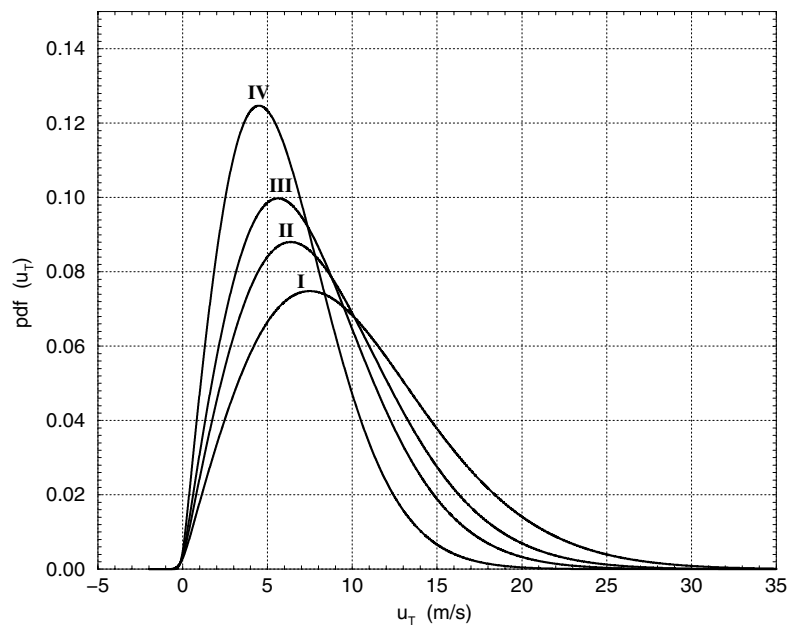


Figure 2.2 The probability density function of the 3-second average wind speed for IEC 1400-1 wind turbine class I through IV.

wind speed resembles a Weibull distribution but is somewhat flatter and has a more pronounced right tail than the underlying Weibull distribution of 10-minute averages. Note, however, that contrary to the Weibull distribution, the left tail in theory extends to $-\infty$.

2.5 The cdf of the extreme 3-sec average wind speed

The cumulative distribution function (cdf) of u_T is given by:

$$F(u_T) = \int_{-\infty}^{u_T} \int_0^{\infty} N[u_T; U, \sigma_T(U)] \cdot W[U; C, k] dU du_T. \tag{2.26}$$

Assuming n independent observations, the extreme value distribution is then given by the distribution of the n 'th order statistic (cf. Appendix A.1.3) :

$$F_{X_{n:n}}(u_T) = F^n(u_T). \tag{2.27}$$

Some examples of $F^n(u_T)$ are presented in Figure 2.3. The value of n is based on the effective frequency given by Bergström in Table 2.1. Unfortunately, the computation of $F(u_T)$ is very time consuming. An alternative, much faster, procedure takes advantage of the fact that two cdf's with the same right tail, the same values for the (0.9,1) range say, and very different values in the (0,0.9) interval have exactly the same (maximum) limit distribution, see Castillo [3][Chapter4.5].

Since $f(u_T)$ resembles a Weibull distribution function, we can fit a Weibull distribution to the right tail of $f(u_T)$. The parameters C and k of this Weibull fit can then be used to obtain the extreme value distribution, by either solving x from Eq. (B.7) or Eq. (B.9). The use of (B.7) is slightly more accurate than (B.9) which introduces some additional error by neglecting the higher order terms in the Taylor expansion (see Appendix B). In practice, good agreement with the 'exact' computation (2.27) is obtained if the right tail in the (0.9,1) range is taken, see Figure 2.4.

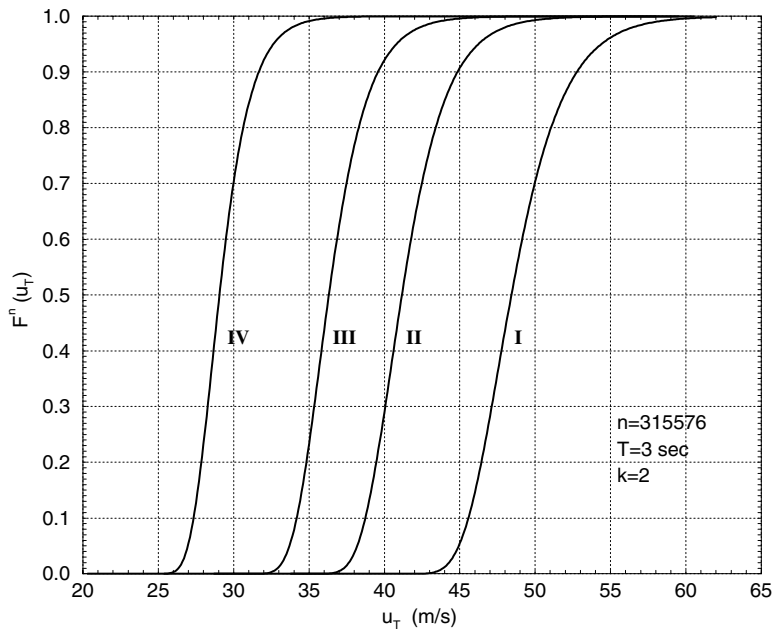


Figure 2.3 The 'exact' cumulative extreme value distributions of the 3-sec average wind speed for the four IEC wind turbine classes.

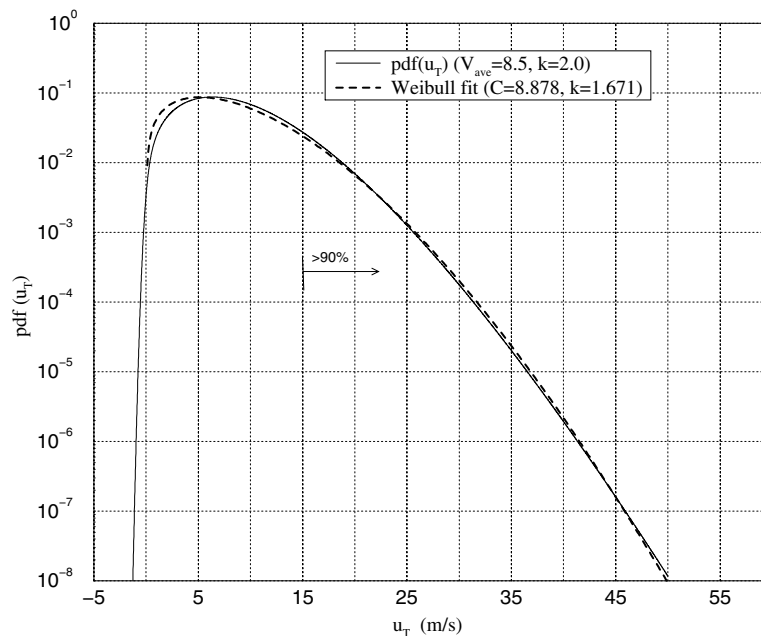


Figure 2.4 The calculated pdf of u_T and a fitted Weibull distribution

2.6 Evaluation of V_{e1} and V_{e50} in the IEC 1400-1 standard

In the IEC 1400-1 standard [16] two extreme 3-second average wind speeds are defined:

1. The 50-year extreme wind speed V_{e50} , which is defined as the extreme 3-seconds average wind speed with a recurrence period of 50 years.
2. The yearly extreme wind speed V_{e1} , which is defined as the extreme 3-seconds average wind speed with a recurrence period of one year.

V_{e1} and V_{e50} are both based on the reference wind speed V_{ref} and have to be computed as a function of height z using the following equations :

$$V_{e50}(z) = 1.4V_{ref}(z/z_{hub})^{0.11}, \quad (2.28)$$

$$V_{e1}(z) = 0.75V_{e50}(z), \quad (2.29)$$

For each of these two extreme wind speeds a recurrence period is specified, so that, in principle, the probability of occurrence is known. Unfortunately the definitions given above are difficult to interpret, especially the definition of V_{e1} seems a bit odd. None of the definitions contain information on the length of the samples, which is essential in order statistics. Assuming that the extremes distribution is based on samples of one year length, a yearly extreme wind speed with a recurrence period of one year has a 100% probability of being exceeded (cf. Section A.1.4). This cannot be intended of course. Therefore we assume that the following definitions should be employed for V_{e50} and V_{e1} :

- V_{e50} is the annual extreme 3-second average wind speed with a 2% probability of being exceeded in a year. In other words V_{e50} has a return period of 50 years.

- V_{e1} is the yearly characteristic largest 3-second average wind speed. This value gives an idea of the central location of the possible largest values, and corresponds to a confidence level of approximately 63.21%, cf. Section A.1.5.

To verify whether the values given by the IEC standard correspond to the definitions as we assume they should be, V_{e1} and V_{e50} have been computed for various values of V_{ave} and k . The results are shown in Figures 2.5 and 2.6. For the purpose of comparison these figures also show the IEC values for the four wind turbine classes. These figures show that the IEC values for V_{e1} and V_{e50} are valid for sites where $k > 1.9$ and $k > 1.7$, respectively. Hence the assumed confidence levels for V_{e50} and V_{e1} are probably correct. That V_{e1} is less conservative than V_{e50} , in terms of k -values, seems appropriate because V_{e1} should also be used in fatigue calculations (DLC 6.2).

It can be concluded that the IEC values of V_{e1} and V_{e50} are acceptable for most flat terrain sites at mid latitudes and certainly valid if the parent distribution is Rayleigh. But, with respect to these values, a Class I wind turbine is only suitable for complex terrain sites ($k \approx 1.4$) where $V_{ave} \leq 7.5$ m/s at hub height.

2.7 Conclusions

In the previous sections the theoretical values of V_{ref} , V_{e1} and V_{e50} have been derived as a function of the annual average wind speed V_{ave} and the Weibull shape parameter k . These theoretical values are compared to the values specified by the IEC 14001-1 standard in the so-called Extreme Wind Speed Model (EWM).

It is shown that according to these theoretical computations the IEC values are acceptable for flat terrain sites at mid latitudes. For sites with a Rayleigh parent distribution the IEC values are conservative. As was to be expected, the IEC values are definitively not valid for complex terrain sites. With respect to the survival wind speeds, V_{e1} and V_{e50} , a IEC Class I wind turbine is only suitable for complex terrain sites ($k \approx 1.4$) with an annual average wind speed which is lower than 7.5 m/s at hub height.

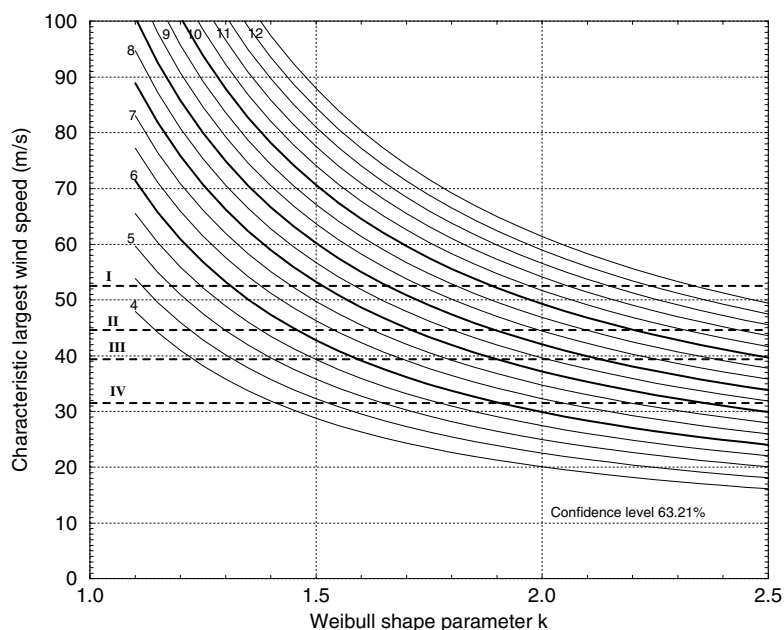


Figure 2.5 The annual characteristic largest 3-sec average wind speed as function of the Weibull shape parameter k and annual average wind speeds V_{ave} varying between 4 m/s and 12.5 m/s. Also shown are the values of V_{e1} for the four IEC wind turbine classes.

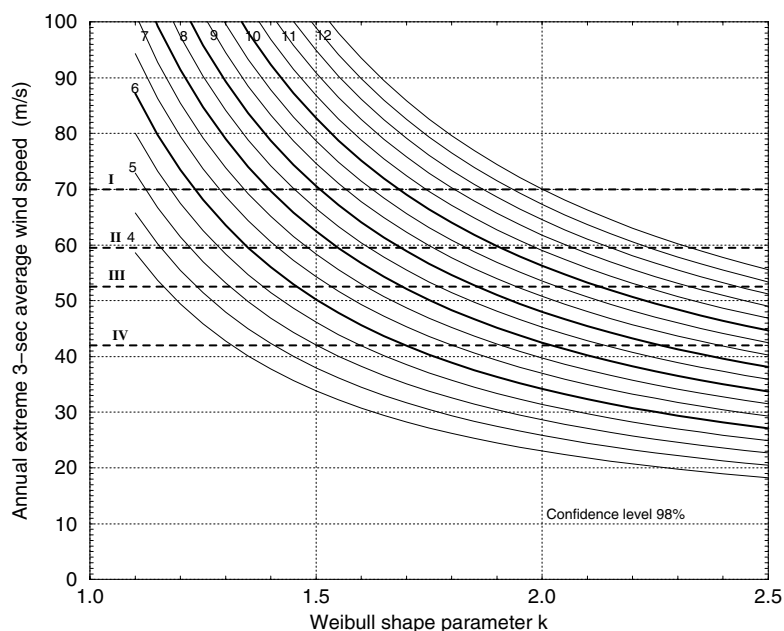


Figure 2.6 The annual extreme 3-sec average wind speed with a confidence level of 98%, as function of the Weibull shape parameter k and annual average wind speeds V_{ave} varying between 4 m/s and 12.5 m/s. Also shown are the values of V_{e50} for the four IEC wind turbine classes.

3 THE DISTRIBUTION OF EXTREME GUSTS

3.1 The pdf of single point gusts

To find the probability density function of gusts we consider the short-term average wind speeds u_{T_1} and u_{T_2} at the same location but at two instants t_1 and t_2 . Let $\tau = t_2 - t_1$ be the time difference and let us assume that u_T is normally distributed around the 10-minute mean value U . Then the conditional pdf $f(x_1, x_2 | U)$ is jointly normal :

$$f(\mathbf{x}) = \frac{1}{(2\pi)^{n/2} |\mathbf{K}_{xx}|^{1/2}} \exp \left[-\frac{1}{2} (\mathbf{x} - \mathbf{m}_x)^T \mathbf{K}_{xx}^{-1} (\mathbf{x} - \mathbf{m}_x) \right], \quad (3.1)$$

with mean vector and covariance matrix

$$\mathbf{m}_x = \{U, U\}^T, \quad \mathbf{K}_{xx} = \sigma_T^2 \begin{pmatrix} 1 & \rho(\tau) \\ \rho(\tau) & 1 \end{pmatrix}, \quad |\rho(\tau)| < 1, \quad (3.2)$$

and where $\rho(\tau) = \sigma_{x_1 x_2} / \sigma_{x_1} \sigma_{x_2}$ is the so-called correlation coefficient which depends on the time difference τ . To evaluate gust amplitudes we need to determine the conditional pdf $f(x_2 - x_1 | x_1)$, expressing the difference $x_2 - x_1$ for a given 'starting' wind speed x_1 . This pdf is derived by following the steps :

(i) Introduce a linear transformation of random variables :

$$Y_1 = X_1, \quad Y_2 = X_2 - X_1;$$

(ii) Evaluate the conditional $f((y_1, y_2) | U)$ according to the transformation rule :

$$f(\mathbf{y}) \equiv f((y_1, y_2) | U) = f(\mathbf{g}(\mathbf{x})) |J_n| \quad (3.3)$$

where J_n is the Jacobean of the inverse transformation :

$$J_n = \det \left[\frac{\partial(x_1, x_2, \dots, x_n)}{\partial(y_1, y_2, \dots, y_n)} \right] \quad (3.4)$$

Using (3.3) and (3.4) we find:

$$f(\mathbf{y}) = \frac{1}{2\pi\sigma^2\sqrt{1-\rho^2}} \exp \left\{ -\frac{1}{2(1-\rho^2)} \left[\frac{(y_1 - \mu_1)^2}{\sigma^2} - 2\rho \frac{(y_1 - \mu_1)(y_2 - \mu_2)}{\sigma^2} + \frac{(y_2 - \mu_2)^2}{\sigma^2} \right] \right\}, \quad (3.5)$$

where

$$\mu_1 = U \quad \text{and} \quad \mu_2 = U - y_1 = U - x_1. \quad (3.6)$$

(iii) Using

$$f(x_1, x_2, \dots, x_m | x_{m+1}, \dots, x_n) = \frac{g(x_1, x_2, \dots, x_n)}{h(x_{m+1}, \dots, x_n)}, \quad (3.7)$$

it can be shown that

$$f((y_2 | y_1), U) = \frac{f((y_2, y_1) | U) \cdot f_U(U)}{f_1(y_1)}, \quad (3.8)$$

where $f(y_1) \equiv f_1(y_1 | U)$ is the marginal density function of y_1 and which is equal to $N[y_1; U, \sigma_T(U)]$, see section 2.4 for the notation.

(iv) Evaluation of (3.8) results in :

$$f((y_2 | y_1), U) = N[y_2; (U - y_1)(1 - \rho), \sigma_T(1 - (\rho^2)^{1/2})] \cdot W[U; C, k].$$

(v) Hence the pdf of y_2 given y_1 is :

$$f(y_2 | y_1) = \int_0^\infty f((y_2 | y_1), U) dU = \int_0^\infty N[y_2; (U - y_1)(1 - \rho), \sigma_T(1 - (\rho^2)^{1/2})] \cdot W[U; C, k] dU. \quad (3.9)$$

In other words, $f(y_2 | y_1)$ is the product of a normal distribution with mean $(U - y_1)(1 - \rho)$ and standard deviation $\sigma_T(1 - \rho^2)^{1/2}$ and a Weibull distribution with parameters C and k . The resulting pdf provides the probability of a wind increase $y_2 = x_2 - x_1$ in a given time interval τ and a starting wind speed $y_1 = x_1$. It should be noted that the pdf depends on the correlation function ρ which is not only a function of τ but also of L/U (see section 3.1.1). As a consequence ρ cannot be entered as a constant in (3.9), as was incorrectly done in [4]. The discussion on σ_T held in the previous section applies here as well. A typical plot of $f(y_2 | y_1)$ is presented in Figure 3.1. This figure shows that for decreasing annual average

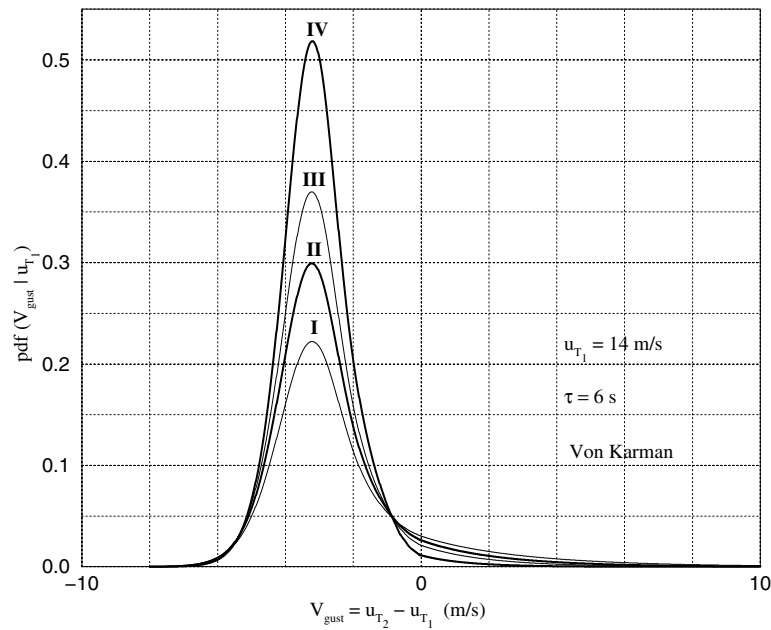


Figure 3.1 Pdf of $(u_{T_2} - u_{T_1} | u_{T_1})$ with $T = 3$ sec, $u_{T_1} = 14$ m/s, and external conditions according to IEC wind turbine class I - IV.

wind speed the negative gust portion increases and vice versa. It can also be shown that when τ decreases (more correlation) the width of $f(y_2 | y_1)$ is reduced and the peak becomes higher, sharper and more symmetrically centered around zero. When the starting value u_{T_1} increases, the peak of the distribution shifts to the left, indicating that the probability of finding large (positive) gusts becomes smaller.

Using (3.9) we can for example find that the probability of Y_2 being between c and d given that $y_1 < Y_1 < y_1 + dy_1$ is

$$\Pr(c < Y_2 < d | y_1 < Y_1 < y_1 + dy_1) = \int_c^d f(y_2 | y_1) dy_2, \quad (3.10)$$

hence $\Pr(Y_2 \geq y_2) = 1 - \Pr(-\infty < Y_2 < y_2 \mid y_1 < Y_1 < y_1 + dy_1)$.

3.1.1 The correlation function

Under stationary conditions, one may obtain the dependence of the correlation coefficient on the time interval τ from the power spectrum of the longitudinal component. Assuming ergodicity it can be shown that the correlation function is the inverse Fourier transform of the non-dimensional spectrum S_{uu}/σ_u^2 , where u is the wind speed component in longitudinal direction. For a Von Kármán-type spectrum :

$$\frac{S_{uu}}{\sigma_u^2} = 4 \frac{L}{U} \frac{1}{(1 + 70.78(fL/U)^2)^{5/6}} \tag{3.11}$$

it is evident that the correlation function will not only be a function of τ but also of the ratio L/U , which is equal to the integral time scale when Taylor’s hypothesis of frozen turbulence applies. The positive-time part of $\rho(\tau)$ is shown in Figure 3.2. Note that for a given time lag τ the correlation will be

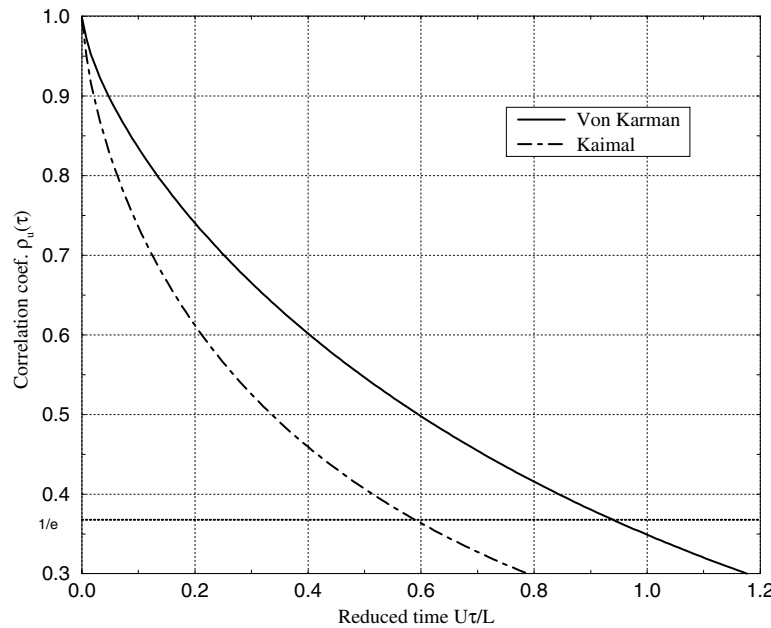


Figure 3.2 The correlation coefficient as function of dimensionless time $\tau/(L/U)$.

higher according to Kaimal than according to Von Kármán, due to the much larger integral length scale L in the Kaimal spectrum.

3.1.2 The number of independent events

To find the number of independent events n for the extreme gusts, we introduce four jointly normal random variables X_1, X_2, X_3, X_4 , corresponding to longitudinal wind component ensembles at $t = 0, t = \tau, t = a$ and $t = \tau + a$. Let the process be stationary and ergodic and let U be the ten-minute mean and

σ the standard deviation of each individual random variable. Then, the jointly normal $f(x_1, x_2, x_3, x_4)$ will be characterized by the mean vector $\{U, U, U, U\}^T$ and the correlation matrix :

$$K_{xx} = \sigma^2 \begin{bmatrix} 1 & \rho_\tau & \rho_a & \rho_{\tau+a} \\ & 1 & \rho_{\tau-a} & \rho_a \\ & & 1 & \rho_\tau \\ \text{symm} & & & 1 \end{bmatrix} \quad (3.12)$$

Performing the necessary calculus to express $f(x_3 - x_1, x_4 - x_2 | x_1, x_2)$ it is shown that this is a jointly normal pdf with correlation matrix

$$K = \sigma^2 \left(2\gamma + \frac{\gamma^2 - \delta}{1 - \rho_\tau^2} \right) \begin{bmatrix} 1 & \rho_\tau \\ \rho_\tau & 1 \end{bmatrix}, \quad (3.13)$$

where

$$\gamma = 1 - \rho_a \quad \text{and} \quad \delta = (\rho_{\tau+a} - \rho_\tau)(\rho_{\tau-a} - \rho_\tau). \quad (3.14)$$

This denotes that the correlation coefficient of the gust pdf is equal to the correlation coefficient ρ_τ of the two jointly normal wind speed variables (X_1, X_2) placed at time distance τ . In other words, wind speed variables and gust variables have the same correlation coefficient and, consequently, one can apply the earlier derived effective frequency values for extreme wind speeds to extreme gust computations as well.

3.2 Results and comparison with IEC

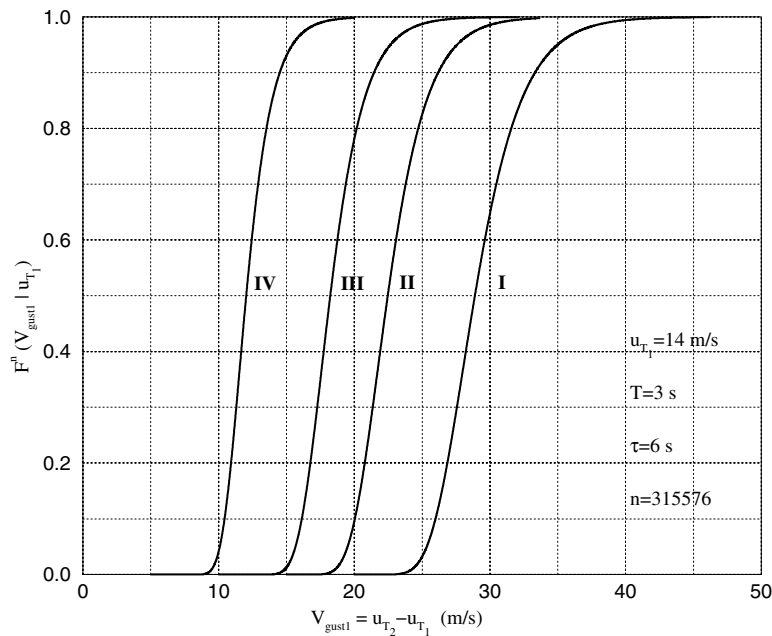


Figure 3.3 The limit distributions of the extreme operational gust (EOG) as prescribed by the IEC

Using Eq. (3.9), the magnitude of the extreme operating gusts is computed, assuming the same confidence levels as for the extreme 3-second average wind speeds, i.e. 63.2% for V_{gust1} and 98% for V_{gust50} . For

the long term wind conditions we take the conditions according to IEC Class I to IV. According to the list of load cases prescribed by the IEC standard, the starting wind speeds should be either $V_{rmmrated}$ or V_{out} . We assume that $V_{rated} = 14$ m/s and $V_{out} = 25$ m/s. The results are presented in Table 3.1.

The table also contains the magnitude of the extreme coherent gust V_{cg} . The IEC does not specify a recurrence period for this gust and therefore it is assumed that the confidence level of this gust magnitude corresponds to that of the characteristic largest value. Hence V_{gust1} and V_{cg} have the same assumed probability of occurrence, only the time lag is different ($\tau = 6$ s and $\tau = 10$ s, respectively).

In all computations the correlation function is the inverse FFT of Von Kármán’s auto power spectrum of the longitudinal wind speed component, see Eq. (3.11). It should be noted that the correlation function based on Kaimal’s expression for the longitudinal turbulence spectrum results in lower gust values.

Figure 3.4 shows that, at least in the range considered, there is a linear correspondence between the gust magnitude and the annual average wind speed. For a given probability, the gust values are lower at a starting wind speed of 25 m/s than at 14 m/s. The difference between V_{gust1} and V_{cg} is small considering the relatively large difference in time lag τ (6 s and 10 s, respectively). This is due to the correlation function which does not change very much when the time lag τ is greater than the integral time scale L/U , see Figure 3.2. The results presented in Table 3.1 clearly show that the computed values are significantly

Table 3.1 The extreme operational gust and extreme coherent gust for a starting wind speed $u_{T_1} = 14$ m/s and 25 m/s and external conditions according to the IEC wind turbine class I – IV.

IEC class	IEC (EOG, ECG)			$u_{T_1} = 14$ m/s			$u_{T_1} = 25$ m/s		IEC rev. 2		
	V_{gust1} (m/s)	V_{gust50} (m/s)	V_{cg} (m/s)	V_{gust1} (m/s)	V_{gust50} (m/s)	V_{cg} (m/s)	V_{gust1} (m/s)	V_{gust50} (m/s)	V_{gust1} (m/s)	V_{gust50} (m/s)	V_{cg} (m/s)
I	15.6	20.8	15.0	29.9	37.1	31.0	19.7	26.7	18.7	25.0	15.0
II	15.4	20.5	15.0	23.3	29.3	24.5	13.4	19.3	18.7	25.0	15.0
III	15.3	20.3	15.0	18.9	24.2	20.1	9.4	14.4	18.7	25.0	15.0
IV	15.1	20.1	15.0	12.6	16.6	13.4	3.6	7.4	18.7	25.0	15.0

different from the values specified by the IEC standard, both in trend and magnitude. At a starting wind speed of 14 m/s most computed gust amplitudes are much higher than those specified by the IEC. At 25 m/s the values are comparable for Class I and II but for Class III and IV the IEC values are much higher. All computed gust amplitudes have a clear dependence on the annual average wind speed (see Figure 3.4), while no such dependence is evident in the IEC specification.

There are, however, a few remarks to be made here :

1. Experience using the IEC standard has shown that the Normal Turbulence Model (NTM) leads in most cases to higher loads than the extreme operating gust, indicating that the EOG model is too benign with respect to actual external conditions.
2. New analysis of the extreme operating gust, performed by a working group of the IEC (TC88/WG7) [2], based on measurements from the German lowland and Californian sites, shows a ratio of gust magnitude (V_{gust1}) to standard deviation (σ_1) of about 4.8. For V_{gust50} the ratio is estimated at 6.4. They also observe that this ratio is more or less independent of the turbulence intensity of the site. Based on this analysis the working group has proposed a new model for the extreme operating

gusts. The corresponding gust amplitudes are presented in Table 3.1 under the heading IEC rev. 2. The new values are closer to our predicted values for class I and II, in good agreement for class III and higher for class IV.

3. The reason that our computed gust magnitudes for Class III and IV are so low has to do with the fact that we assumed the same rated and cut-out wind speed for all IEC classes, viz. 14 m/s and 25 m/s, respectively. In practice an IEC Class III or IV wind turbine will have a lower rated and cut-out wind speed. For example, considering a Class IV wind turbine with $V_{\text{rated}} = 8$ m/s and $V_{\text{out}} = 20$ m/s, we find that $V_{\text{gust}1} = 17.5$ m/s and $V_{\text{gust}50} = 21.7$ m/s at a starting wind speed of 8 m/s, and $V_{\text{gust}1} = 7.7$ m/s and $V_{\text{gust}50} = 11.6$ m/s at a starting wind speed of 20 m/s.
4. The IEC should make a distinction between the gust amplitudes at different starting wind speeds. A starting wind speed equal to V_{rated} is generally much more likely than a starting wind speed at V_{out} . Consequently a gust with an amplitude of 25 m/s has a much lower probability to start at V_{out} than to start at V_{rated} , everything else being equal.
5. The IEC standard (and the proposed revision) is unclear about how to compute the standard deviation in the EOG model. It must be made clear that in all cases σ_1 should be computed for $V_{\text{hub}} = V_{\text{out}}$, but this is nowhere stated.
6. The extreme values computed here may seem very high, but they are based on all possible mean values of the 10-minute average U . Obviously the largest gust values will be found during a period of high mean wind speed. For example when $U = 25$ m/s then a drop to 14 m/s and a consequent increase to 36 m/s is not exceptional. What makes it exceptional is that this wind speed change takes place within 6 seconds and the high mean wind speed itself.
7. The gust magnitude is very sensitive for the Weibull shape parameter k . For example, for a Class III wind turbine, with $k = 1.7$ and $V_{\text{rated}} = 10.5$ m/s, we find that $V_{\text{gust}1} = 29$ m/s at a starting wind speed of 10.5 m/s.
8. The computed values should be considered with some caution. Because the gusts should be applied with the turbine in operation it would be better to restrict the range of U and to compute the extreme gusts using the density function $f((y_2 | y_1) | U \leq V_{\text{out}})$. This will reduce the computed gust values.
9. The gusts considered here are single point gusts, i.e. wind speed changes as they would be measured by a single anemometer. It is obvious that coherent gusts will have a smaller magnitude if we assume the same confidence limit. This so-called rotor averaging effect can be taken into account by means of a spatial correlation function. The gust magnitude will then also be a function of the rotor diameter.
10. The above derived gust distribution function (3.9) may be used to construct gust time histories, because the pdf and cdf depend on the time lag τ . One could think of some kind of Markov chain simulation (random walk).
11. We are not so much interested in extreme gusts but in gusts which cause extreme loads in the various components of the wind turbine. It is quite possible that the extreme gust values found here do not induce the highest loads, simply because the wind turbine does not have time to respond to such large and rapid wind speed changes. The extreme values given in Table 3.1 should serve as an upper limit, we do not need to evaluate larger gusts. When the gust is found that induces

the highest loads (this may vary with the design and the cross section that is considered) the above presented theory can be used to compute the number of occurrences.

12. Due to their physically unrealistic nature, sinusoidal gust are not the most reliable means to compute extreme loads, see Winkelaar [23]. It is recommended to use several realisations of a wind field which somehow contains the gust to compute the (hopefully) extreme loads.

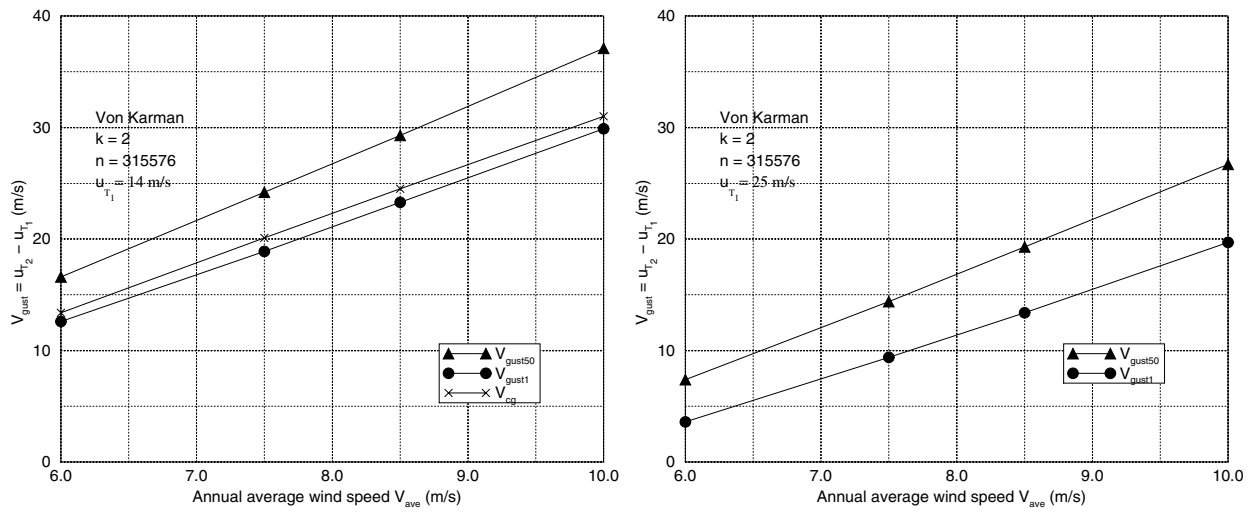


Figure 3.4 The extreme 3-sec average gust as a function of the annual average wind speed for two starting wind speeds (14 m/s and 25 m/s), two confidence levels (63.2% and 98%) and two time lags (6 s and 10 s).

4 THE DISTRIBUTION OF EXTREME WIND DIRECTION CHANGE

4.1 The pdf of wind direction

There are several ways to approach the problem of deriving the pdf of the horizontal wind direction. The easiest way is to use the streamwise coordinate system x, y, z , and the corresponding velocity components u, v, w . These velocities can be separated into a mean component, here denoted by capital letters and an eddy component denoted by a prime :

$$u_T = U + u'_T, \quad (4.1)$$

$$v_T = V + v'_T, \quad (4.2)$$

$$w_T = W + w'_T. \quad (4.3)$$

By definition, we have $\overline{u'_T} = \overline{v'_T} = \overline{w'_T} = 0$. If the x axis is defined in the direction of the mean flow, $V = W = 0$. Over flat, level, homogeneous terrain, we take x and y to be horizontal and z to be vertical and positive upwards.

To construct the joint pdf of u_T and v_T we assume that both wind components are normally distributed

$$f_u(u_T | U) = \frac{1}{\sigma_{u_T} \sqrt{2\pi}} \exp \left[-\frac{1}{2} \left(\frac{u_T - U}{\sigma_{u_T}} \right)^2 \right], \quad (4.4)$$

$$f_v(v_T | U) = \frac{1}{\sigma_{v_T} \sqrt{2\pi}} \exp \left[-\frac{1}{2} \left(\frac{v_T}{\sigma_{v_T}} \right)^2 \right], \quad (4.5)$$

where it is assumed that U has a Weibull distribution and σ_{u_T} and σ_{v_T} are functions of U .

If we assume that u_T and v_T are jointly normal and uncorrelated then the joint distribution function $f_{uvU}(u_T, v_T, U)$ is given by

$$f(u_T, v_T, U) = f_u(u_T | U) \cdot f_v(v_T | U) \cdot f_U(U). \quad (4.6)$$

To construct the pdf of wind direction we transform to polar coordinates and consider the random variables :

$$r = \sqrt{u_T^2 + v_T^2} \quad \theta = \arctan v_T/u_T \quad (4.7)$$

where we assume that $r > 0$ and $-\pi < \theta \leq \pi$. With this assumption the system has a single solution

$$u_T = r \cos \theta \quad v_T = r \sin \theta \quad \text{for} \quad r > 0. \quad (4.8)$$

Since

$$J(u_T, v_T) = \begin{vmatrix} \cos \theta & \sin \theta \\ -r \sin \theta & r \cos \theta \end{vmatrix}^{-1} = \frac{1}{r} \quad (4.9)$$

we conclude from (3.3) that

$$f(r, \theta, U) = r f(u_T, v_T, U) = \frac{r}{2\pi\sigma_u\sigma_v} \exp \left[-\frac{1}{2} \left\{ \left(\frac{r \cos \theta - U}{\sigma_u} \right)^2 + \left(\frac{r \sin \theta}{\sigma_v} \right)^2 \right\} \right] \cdot W[U; C, k] \quad (4.10)$$

for $r > 0$ and zero for $r \leq 0$.

The pdf of wind direction is then given by

$$f_{\Theta}(\theta) = \int_0^{\infty} \int_0^{\infty} \frac{r}{2\pi\sigma_u\sigma_v} \exp\left[-\frac{1}{2}\left\{\left(\frac{r\cos\theta - U}{\sigma_u}\right)^2 + \left(\frac{r\sin\theta}{\sigma_v}\right)^2\right\}\right] \cdot W[U; C, k] dr dU. \quad (4.11)$$

Now $f_{\Theta}(\theta)$ is not computed for a given U and σ but computed for all possible mean wind speeds between zero and infinity. In reality only mean wind speeds up to V_{out} are of importance, so we are actually interested in $f_{\Theta}(\theta | U \leq V_{\text{out}})$. Clearly the numerical evaluation of these multidimensional integrals is computationally expensive. Therefore we seek a simpler approach, assuming that U , σ_{u_T} and σ_{v_T} are given (chosen) values.

If we again assume that u_T and v_T are normally distributed

$$f_u(u_T) = \frac{1}{\sigma_u\sqrt{2\pi}} \exp\left[-\frac{1}{2}\left(\frac{u_T - U}{\sigma_u}\right)^2\right], \quad (4.12)$$

$$f_v(v_T) = \frac{1}{\sigma_v\sqrt{2\pi}} \exp\left[-\frac{1}{2}\left(\frac{v_T}{\sigma_v}\right)^2\right], \quad (4.13)$$

and if we also assume that these wind speed components are statistically independent, then the joint density function is given by :

$$f(u_T, v_T) = f_u(u_T) \cdot f_v(v_T) = \frac{1}{2\pi\sigma_u\sigma_v} \exp\left[-\frac{1}{2}\left\{\left(\frac{u_T - U}{\sigma_u}\right)^2 + \left(\frac{v_T}{\sigma_v}\right)^2\right\}\right]. \quad (4.14)$$

To find the pdf of wind direction we transform to polar coordinates :

$$f(r, \theta) = r f(u_T, v_T) = \frac{r}{2\pi\sigma_u\sigma_v} \exp\left[-\frac{1}{2}\left\{\left(\frac{r\cos\theta - U}{\sigma_u}\right)^2 + \left(\frac{r\sin\theta}{\sigma_v}\right)^2\right\}\right] \quad r > 0 \quad (4.15)$$

and zero for $r \leq 0$.

We then find for the pdf of θ :

$$f_{\Theta}(\theta) = \int_0^{\infty} f(r, \theta) dr = \int_0^{\infty} \frac{r}{2\pi\sigma_u\sigma_v} \exp\left[-\frac{1}{2}\left\{\left(\frac{r\cos\theta - U}{\sigma_u}\right)^2 + \left(\frac{r\sin\theta}{\sigma_v}\right)^2\right\}\right] dr. \quad (4.16)$$

The same pdf can be derived by starting with an arbitrary Cartesian coordinate system x and y and assuming that the velocity components u_x and u_y are jointly normal distributed with mean $\{\mu_x, \mu_y\}^T$ and covariance matrix

$$\mathbf{K} = \begin{pmatrix} \sigma_x^2 & \sigma_{xy}^2 \\ \sigma_{xy}^2 & \sigma_y^2 \end{pmatrix}.$$

Following Ibarra [15] one can always define a transformation $(u_x, u_y) \rightarrow (u, v)$ that diagonalizes the covariance matrix. In tensorial terms, the entire process is reduced to finding the eigenvalues and principal directions of \mathbf{K} . The principal directions are those of an ellipse, the eigenvalues σ_u^2, σ_v^2 are given by

$$\sigma_u^2, \sigma_v^2 = \frac{I}{2} \pm \left[\left(\frac{I}{2}\right)^2 - |\mathbf{K}| \right]^{1/2}, \quad (4.17)$$

where $I = \sigma_x^2 + \sigma_y^2$, and the principal directions are determined by :

$$\tan 2\alpha = \frac{2\sigma_{xy}}{\sigma_x^2 - \sigma_y^2}, \quad (4.18)$$

where α is the angle formed by the Cartesian co-ordinate system and the principal directions. In flat terrain this procedure is identical to finding the ‘streamlined’ co-ordinate system (longitudinal, transversal) where

$$U = \mu_x \cos \alpha + \mu_y \sin \alpha, \quad (4.19)$$

$$V = 0, \quad (4.20)$$

and $\sigma_u : \sigma_v = 1 : 0.8$ and $\sigma_{uv} = 0$. In general, however, the new jointly normal random variables will have a mean vector $\{U, V\}^T$ with $V \neq 0$.

To obtain the pdf of the horizontal wind direction we proceed in the same way as before by a transformation to polar coordinates :

$$f(r, \theta) = \frac{r}{2\pi\sigma_u\sigma_v} \exp \left\{ -\frac{1}{2} \left[r^2 \left(\frac{\cos^2 \theta}{\sigma_u^2} + \frac{\sin^2 \theta}{\sigma_v^2} \right) - 2r \left(\frac{\cos \theta}{\sigma_u} i_u + \frac{\sin \theta}{\sigma_v} i_v \right) + (i_u^2 + i_v^2) \right] \right\}, \quad (4.21)$$

where

$$i_u = \frac{U}{\sigma_u} \quad \text{and} \quad i_v = \frac{V}{\sigma_v}. \quad (4.22)$$

This expression is clearly the same as (4.15) for $i_v = 0$.

The pdf of wind direction is again found by integrating $f(r, \theta)$ for r in $[0, \infty]$. The integral can be cast into closed form, see Gradshteyn and Ryzhik [12] :

$$f_{\Theta}(\theta) = \frac{\exp(-\gamma)}{2\pi\sigma_u\sigma_v} \left\{ \frac{1}{2a} - \frac{\sqrt{\pi}}{2a} \frac{\beta}{\sqrt{a}} \exp \left[\left(\frac{\beta}{\sqrt{a}} \right)^2 \right] \operatorname{erfc} \left[\frac{\beta}{\sqrt{a}} \right] \right\}, \quad (4.23)$$

where

$$a = \frac{1}{2} \left(\frac{\cos^2 \theta}{\sigma_u^2} + \frac{\sin^2 \theta}{\sigma_v^2} \right), \beta = -\frac{1}{2} \left(\frac{\cos \theta}{\sigma_u} i_u + \frac{\sin \theta}{\sigma_v} i_v \right), \gamma = \frac{1}{2} (i_u^2 + i_v^2). \quad (4.24)$$

It can be shown that $f_{\Theta}(\theta)$ does not depend on the actual values of σ_u and σ_v (or U and V) but only on the non-dimensional ratios $\lambda = \sigma_v : \sigma_u$, i_u and i_v , the latter two are the reciprocal of the ‘directional’ turbulent intensities. Evidently this is also true for the standard deviation of $f_{\Theta}(\theta)$, which is denoted by σ_{θ}

$$\sigma_{\theta}^2 = \int_{-\pi}^{\pi} \theta^2 f_{\Theta}(\theta) d\theta \quad (4.25)$$

A similar analysis is presented by Weber [22]. For $\lambda = 1$ and $i_v = 0$ the relation of the standard deviation of θ and the turbulence intensity (TI) of the longitudinal component is given in table 4.1. It can be shown that, under extremely calm conditions ($i_u = i_v = 0$), $f_{\Theta}(\theta)$ is uniformly distributed in the interval $[-\pi, \pi]$. For larger values of i a symmetric bell-type distribution with zero mean is obtained.

For values of the turbulence intensity we are interested in, $f_{\Theta}(\theta)$ does not resemble a Gaussian pdf. To demonstrate this, a logarithmic plot of $f_{\Theta}(\theta)$ along with the corresponding Gaussian pdf (which has the same mean and variance as $f_{\Theta}(\theta)$) is presented in Figure 4.1 for $\lambda = 1$, $i_v = 0$ and TI=15%. It is seen that the tails of the distribution – which are very important for extreme value considerations – are not

Table 4.1 σ_θ versus turbulence intensity TI

TI	5%	10%	15%	20%	25%	30%
σ_θ (deg)	2.88	5.76	8.70	11.71	14.88	18.30

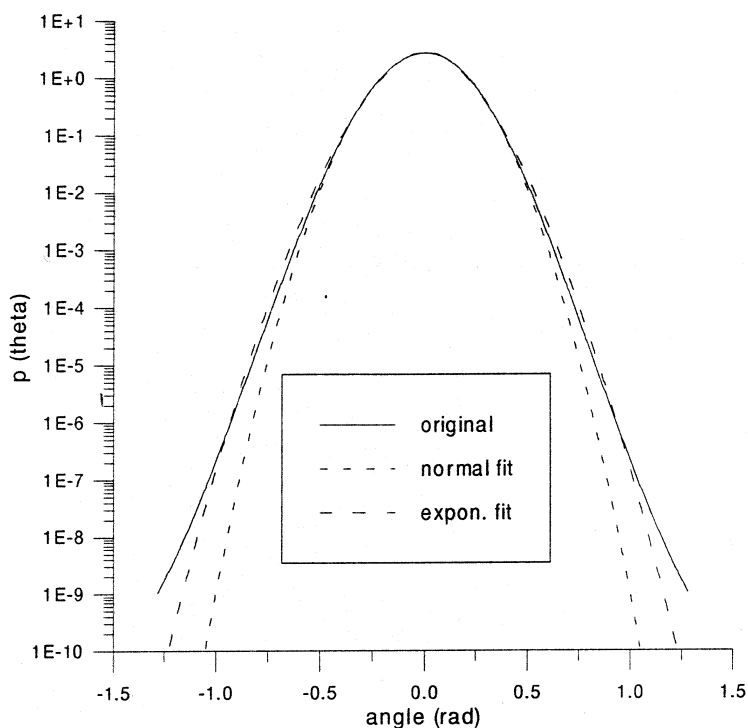


Figure 4.1 The pdf of wind direction and two fits.

well predicted by the Gaussian fit. This creates some difficulties in applying the theory of section 3 to wind direction changes; we cannot assume that $f_{\Theta_1\Theta_2}(\theta_1, \theta_2)$ is jointly normal. A better tail-fit can be obtained by introducing the following symmetric pdf :

$$f(x) = \frac{1}{2} \frac{\exp \left[-(x - \mu/C)^k \right]}{C\Gamma(1 + 1/k)}, \quad (4.26)$$

with

$$\mu = E[x],$$

and

$$\sigma^2 = E[(x - \mu)^2] = C^2 \frac{\Gamma(3/k)}{\Gamma(1/k)}. \quad (4.27)$$

It is seen that for given standard deviation the introduced pdf has only one free parameter, the shape parameter k (for $k = 2$ the pdf (4.26) becomes the normal pdf). For $k = 1.73$ a curve is obtained, called the exponential fit in Figure 4.1, which represents the tail distribution of $f_\Theta(\theta)$ in a much better way than the Gaussian fit.

4.2 The pdf of wind direction change

Due to the non-Gaussian tail of $f_{\ominus}(\theta)$ the gusts theory presented in section 3 cannot be applied directly to wind direction changes. To circumvent this, it was first tried to introduce four jointly normal (U_1, V_1, U_2, V_2) variables representing the Cartesian components of the horizontal wind speed vector at two locations (1) and (2) with given correlation coefficient (or given time lag). A transformation of variables from Cartesian to polar co-ordinates would then provide $f(r_1, r_2, \theta_1, \theta_2)$. Integrating twice with respect to r_1 and r_2 would then give $f(\theta_1, \theta_2)$ and the procedure of section 3 could then be followed. Unfortunately, the double integral cannot be cast into closed form while numerical integration is too costly. To face this problem an alternative, approximate, technique is proposed, based on the following assumptions :

1. The sought $f(\theta_2 - \theta_1 | \theta_1)$, for a given longitudinal turbulence intensity, respects the mean and variance of the ‘equivalent Gaussian problem’ discussed in section 3. In other words it is assumed that :

$$m[(\theta_2 - \theta_1) | \theta_1] = -\theta_1(1 - \rho),$$

and

$$\sigma[(\theta_2 - \theta_1) | \theta_1] = \sigma_{\theta}(1 - \rho^2)^{1/2},$$

where ρ is the corresponding correlation coefficient.

2. The new pdf retains the shape parameter k of the corresponding wind direction distribution.

Under these assumptions $f((\theta_2 - \theta_1) | \theta_1)$ will have the form of Eq. (4.26) with $\mu = -\theta_1(1 - \rho)$ and a scale parameter C which corresponds to the ‘modified’ standard deviation $\sigma_{\theta}(1 - \rho^2)^{1/2}$ through Eq. (4.27). The relation of the time distance between station (1) and (2) and the correlation coefficient can be obtained by applying an inverse FFT to a typical wind direction spectrum. It is recalled that $f_{\ominus}(\theta)$ and consequently $f((\theta_2 - \theta_1) | \theta_1)$, does not depend on the mean wind speed or the standard deviation of any wind component, but depends on the non-dimensional values $\lambda = \sigma_v : \sigma_u, i_u$ and i_v which can be considered to be site dependent constants.

4.3 Results and comparison with the IEC 1400-1 standard

Figures 4.2 to 4.4 present contour plots for various Weibull parameters and turbulence intensities. The driving parameter here is the turbulence intensity and the three plots correspond to 10%, 15% and 20% turbulence intensity. The calculated extremes correspond to $\gamma = 1$ (complex terrain oriented) and $i_v = 0$. It is clearly seen that the extreme values increase rapidly as the turbulence intensity increases. Although not exact in this case, the correlation \rightarrow time transformation is again performed by means of the longitudinal wind component spectral properties. As already discussed a typical wind direction spectrum should be used in this case to provide the ‘exact’ $\rho(\tau)$ curve.

Note that if we had used the expression (4.10) as starting point, then the correlation function would be a function of τ and of L/U and the results would not only be different, it would also be impossible to present them the way they are presented now.

Projecting all the extreme values of a $\theta_1 = \text{const.}$ line on the time axis the time history of an extreme wind direction change is synthesized. Time histories of the extreme wind direction change (IEC code name

EDC) are presented in Figure 4.5. Comparing amplitudes and rise times it is seen that the IEC values are in good agreement with the present values obtained with $\theta_1 = -90$ deg. (the most severe case). It is also worth noting that both the IEC model and the present are based on a single site parameter, the turbulence intensity. The IEC curve is computed for $TI = 18\%$, while the present curves correspond to the contour plot of Figure 4.3 ($TI = 15\%$). It is seen that the present model predicts large direction changes at early times.

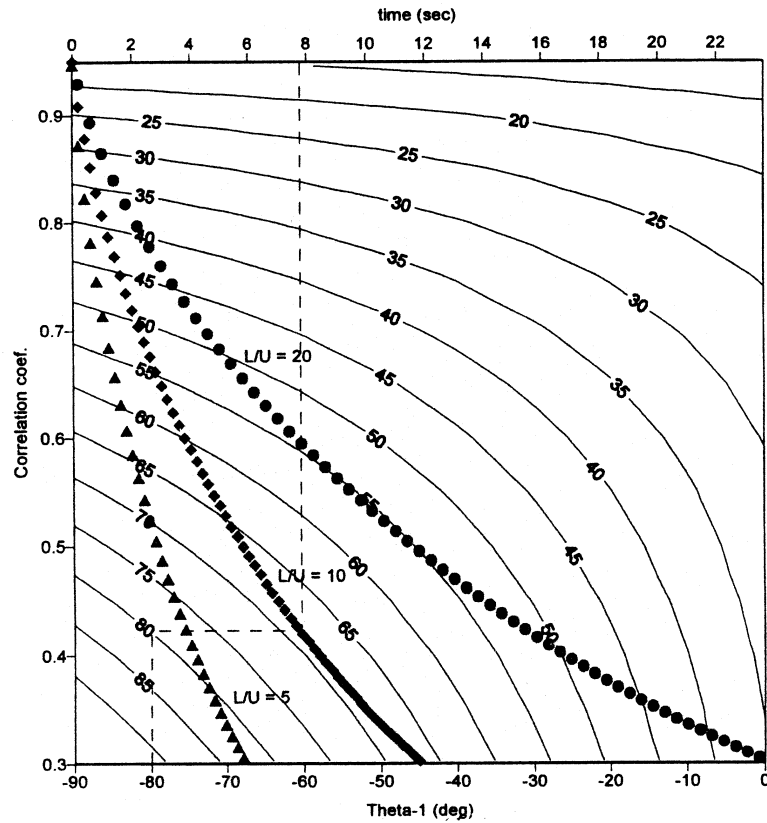


Figure 4.2 Extreme 50-year wind direction change. 10% turbulence intensity and 95% confidence level

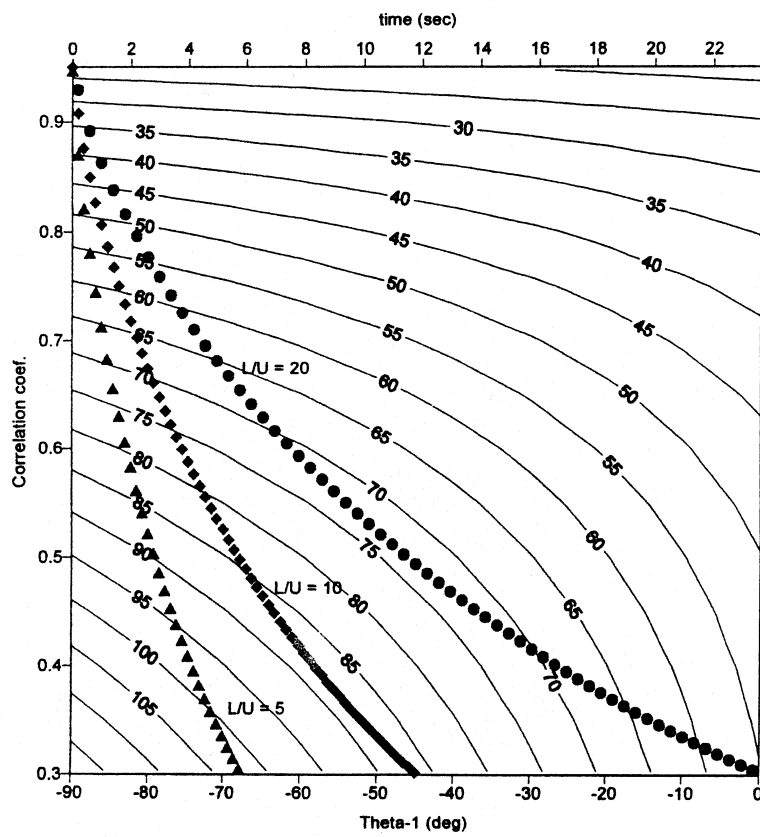


Figure 4.3 Extreme 50-year wind direction change. 15% turbulence intensity and 95% confidence level

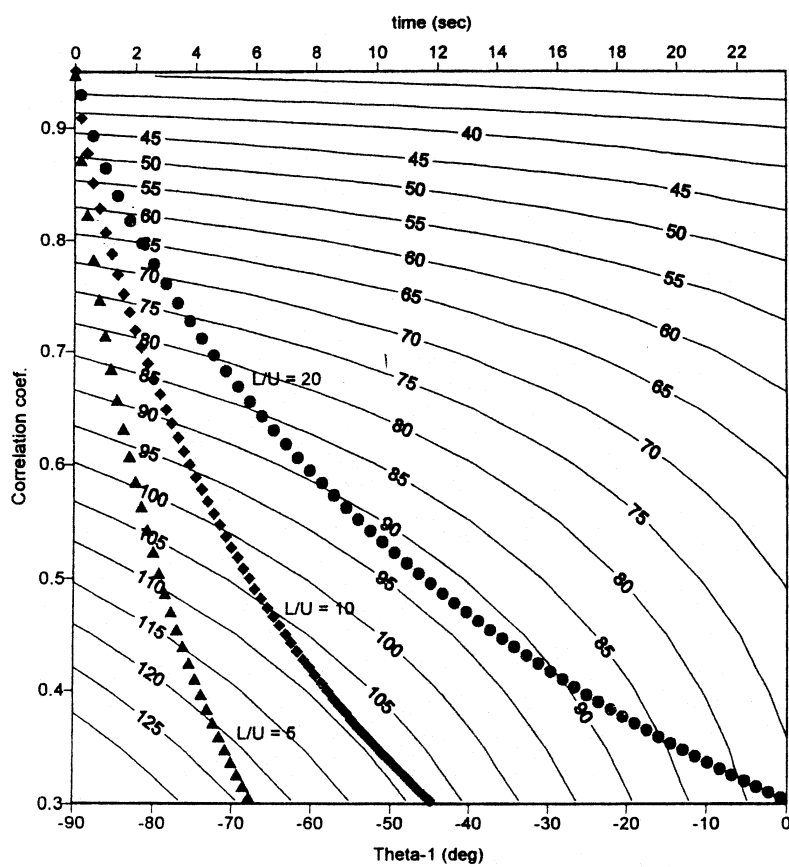


Figure 4.4 Extreme 50-year wind direction change. 20% turbulence intensity and 95% confidence level

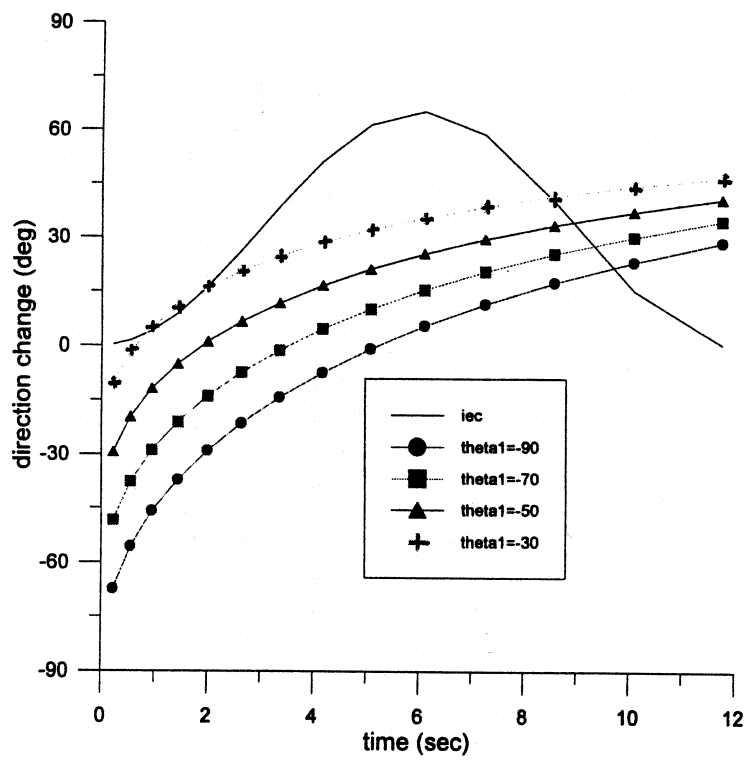


Figure 4.5 Extreme 50-year wind direction change time history. Present (Figure 4.3, $L/U=10$) versus IEC standard.

5 OTHER EXTREME ATMOSPHERIC EVENTS

At most sites, wind speed arises from a variety of physically distinct meteorological mechanisms, such as depressions, thunderstorms, tropical cyclones, etc. In the previous sections it is assumed, however, that all large wind speeds are produced by only one of these mechanisms. For sites at temperate latitudes, such as most sites in Europe, this is a reasonable assumption, the dominant mechanism being depressions.

In meteorological terms it is assumed that when the highest gust speeds and the highest average (over 10 min or 1 h) wind speed occur near the ground (say at 10 m) the lower boundary layer is neutrally stratified and the gusts are caused solely by the vertical shear of the wind and the resistance of the rough ground. This condition of the boundary layer is usually defined (in meteorology) by the criterion that $|h/L_{MO}| \leq 0.1$, where h is the height above the boundary layer depth (typically 500–1000 m) and L_{MO} is the Monin-Obukhov length. Typically in temperate climates this criterion is satisfied if the wind speed at 10 m above the ground U_{10} is greater than 10 m/s.

However, even for mid-latitudes, where tropical cyclones do not occur, it has been recognized that there are exceptional meteorological situations when mechanisms quite different to shear turbulence cause very high wind speeds. In particular, tornadoes are associated with high swirl velocities (≤ 100 m/s) and vertical upward motion, while downdrafts, produced by cold air formed in deep clouds well above the boundary layer, descend and spread out rapidly on hitting the ground giving rise to typical gust speeds ≤ 30 m/s [11]. Although both these phenomena are most frequent in continental climates and the tropics, they are occasionally observed even in temperate climates, such as those of North Western Europe, and need to be included in the statistics of extreme winds, see Collier et al. [5].

In this section we will not concern ourselves with tornadoes. To date, most tornado study is a post-disaster analysis of structures which were victims of the storm, with the damage assessed by calculating the upper limit of the failure load due to a straight line wind approximated as 140 m/s. Judging from the survival wind speeds specified in the IEC standard (70 m/s at the most) a wind turbine does not have to survive a tornado.

Although it is sometimes difficult to distinguish a downburst from a tornado the associated wind speeds are generally not that high. Two large measurement campaigns (NIMROD and JAWS) in the USA (Fujita [11]) recorded gust speeds up to 30 m/s and showed that intense downbursts can leave a trail of damage, like uprooted trees etc. For these reasons and the assumption that downbursts probably happen much more often than tornadoes it seems a good idea to study the phenomenon more closely, to see whether it should be included as a load case in the IEC standard.

5.1 Downbursts

The following is taken from Fujita [11]. A downburst is a localized, intense downdraft that may be dry or may be driven by cooling when the water vapour in falling moist air evaporates. The vertical velocity is defined to be more than 3.6 m/s at 91 m above ground level. Damaging winds, either straight or curved, are highly divergent. The sizes of downbursts vary from less than one kilometer to tens of kilometers. Downbursts are subdivided into macrobursts and microbursts according to their horizontal scale of damaging winds.

MACROBURST : A large downburst with its outburst winds extending in excess of 4 km in horizontal dimension. An intense macroburst often causes widespread, tornado-like damage. Damaging winds, lasting 5 to 30 minutes, could be as high as 60 m/s.

MICROBURST : A small downburst with its outburst, damaging winds extending only 4 km or less. In spite of its small horizontal scale an intense microburst could induce damaging winds as high as 75 m/s.

Not all microbursts are alike; some are accompanied by heavy rain, while others form beneath small virga, see Figure 5.1. The parents clouds which induce microbursts are not always thunderstorms.

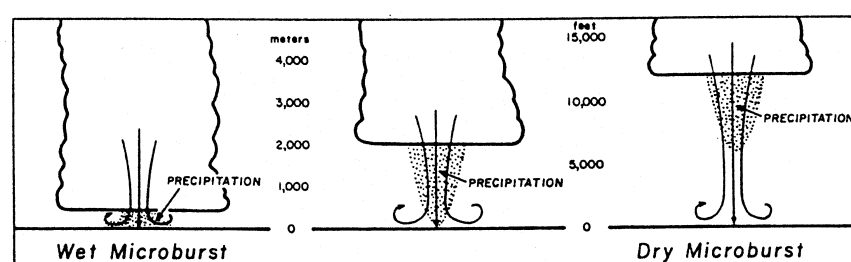


Figure 5.1 Three types of microburst clouds confirmed by radar observation (Courtesy Ref. [11]).

Often, isolated rainshowers spawn relatively strong microbursts which endanger aircraft operations at low altitude.

By virtue of its small size and its short life of less than 10 minutes, a microburst often escapes detection by non-Doppler radars or ground-based anemometers. Consequently a wind turbine could encounter a microburst unexpectedly. A small but very strong microburst often causes a starburst-shaped tree damage. If we assume a 25 m/s outburst wind along a circle of 100 m radius from the microburst center, the mean divergence inside the circle is as large as 0.5 per second. In order to induce such a large divergence at the near-ground level, the downflow speed will have to be 5m/s at 10 m AGL and 10 m/s at 20 m AGL. In other words the downward current at the starburst center is very strong even at the tree-top level.

The maximum wind speed in a microburst measured in the NIMROD experiment was 31.3 m/s and in JAWS was 32.6 m/s. However, most wind speeds were in the range of 12 to 14 m/s. A Gumbel type of analysis reveals that extreme wind speeds with a very low probability of occurrence could be as high as 75 m/s.

In contrast to the very strong outburst winds inside a microburst, its boundary propagates outward rather slowly. Photographic evidence of the microburst winds made visible by flying dust often shows a vortex with a horizontal axis. When the horizontal vortex encircles the downflow center, forming a vortex ring, the outbursting winds beneath the vortex ring are accelerated continuously as the ring expands and stretches, see Figure 5.2. The ring vortex keeps stretching as a surface microburst gets older, until reaching a stretching limit. Thereafter the vortex is cut into several pieces of roll vortices, each with a horizontal axis. Some of these vortex rolls run away from their source region, inducing bands of high winds, lasting two or three minutes.

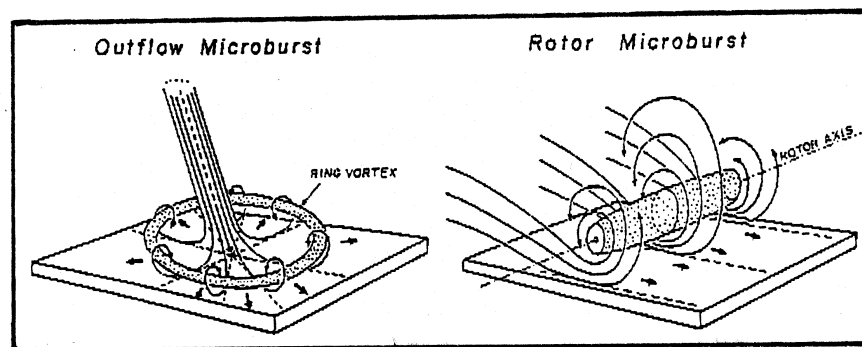


Figure 5.2 Outflow microburst are the most commonly observed type. Some rotorbursts develop inside macrobursts behind their gust fronts (Courtesy Ref. [11]).

6 SUMMARY, CONCLUSIONS AND RECOMMENDATIONS

Using extreme value theory it is shown that, given a certain knowledge of the climatology, it is possible to derive statistical characteristics of extreme wind conditions which are believed to be important for wind turbine design, e.g. the survival wind speed, extreme gusts and extreme wind direction changes. In the present report the limit distributions of these extreme wind conditions have been investigated, assuming that the design external conditions (i.e. the climatology) is defined by the IEC 1400-1 standard wind turbine classes I–IV.

With the assumptions given above the derivation of the probability density function (pdf) and cumulative distribution function (cdf) for the 10-minute average and 3-second average extreme wind speeds is straightforward. It is shown that, given a certain confidence level or return period, the magnitude of the extreme wind speed strongly depends on the shape (k) and scale (C) parameters of the parent Weibull distribution. Smaller shape parameters lead to higher extreme values and vice versa. The influence of k becomes pronounced when $k < 1.8$.

Comparison with the IEC values shows that the reference wind speed V_{ref} is acceptable for sites with $k \geq 1.77$, i.e. for most flat terrain sites in Western Europe. This is also the case for the extreme 3-second average wind speeds V_{e1} and V_{e50} (the so-called ‘survival wind speeds’) given in the IEC Extreme Wind speed Model (EWM). But it should be noted that the annual extreme 3-second average wind speed with a recurrence period of one year, V_{e1} , has been redefined to the “*annual characteristic largest 3-second average wind speed.*”

If a wind turbine has to be designed for complex terrain ($1.4 \leq k \leq 1.5$), it is recommended to increase the ratio of the reference wind to the annual average wind speed to

$$\frac{V_{\text{ref}}}{V_{\text{ave}}} = 6.6.$$

In that case, the equations for V_{e1} and V_{e50} , given by the IEC, still hold.

Assuming longitudinal wind speed fluctuations u_{T_1} and u_{T_2} at the same location but at different instants t_1 and t_2 to be jointly normal, the conditional pdf $f(u_{T_2} - u_{T_1} | u_{T_1})$ is derived and the limit distribution function computed through numerical integration. For extreme gusts not only a strong dependence on the parameters of the parent Weibull distribution is found but also on the assumed turbulence model, viz. Von Kármán or Kaimal, which determines the temporal correlation as function of the time lag $\tau = t_2 - t_1$ and the integral time scale, which is equal to L/U when Taylor’s hypothesis of frozen turbulence applies. The magnitude of the extreme gust shows the same dependence on the Weibull parameters as the extreme wind speed. The gust speed increases for increasing time lag τ until the time lag is greater than the integral time scale, from that point on the the gusts speed does not change very much. Given the same confidence level, gust values are greater for a starting wind speed at V_{rated} than at V_{out} .

The values found for the extreme 3-sec average gusts with a confidence level of 98% are much larger than the values specified by the IEC 1400-1 standard. This was to be expected because experience using the IEC standard has shown that the Normal Turbulence Model (NTM) leads in most cases to higher loads than the extreme operating gust, indicating that the extreme operational gust model is too benign with respect to actual external conditions¹.

New analysis of the extreme operating gust, performed by a working group of the IEC (TC88/WG7), based on measurements from the German lowland and from Californian sites, shows a ratio of gust

¹Assuming that extreme sinusoidal gusts induce extreme loads.

magnitude ($V_{\text{gust}1}$) to standard deviation (σ_1) of about 4.8, indicating that ‘real’ extremes (which are generally not measured) will yield higher ratios, closer to values found in the present project, which are estimated to vary between 4.4 for wind turbine class IV and 7 for wind turbine class I.

The analysis presented here could be refined in two ways. Firstly we should replace the single point gust by a so-called coherent gust. To compute the distribution function of coherent gust we have to take into account the spatial correlation function. Secondly the 10-minute average wind speed should be restricted to $U \leq V_{\text{out}}$. In the present computations U varies in theory between zero and infinity, but in practice machine accuracy limits that range to much lower values. Both refinements will lead to lower gust values. The gust values presented here should be regarded as upper limits; in design calculations we do not need to evaluate larger gusts. When the gust is found that induces the highest loads, the distribution function could be used to compute the number of occurrences.

It is shown that there are several approaches to derive the pdf of wind direction change which will not yield the same results.² The derivation of $f_{\Theta}(\theta)$ that is given here can be found in the literature. It can be shown that this angular pdf only depends on the reciprocal value of the turbulence intensities and the non-dimensional ratio of the standard deviation of the u and v component of the wind (a measure of the anisotropy of the fluctuations). This pdf allows for the calculation of the standard deviation of the wind direction fluctuations as function of the turbulence intensity.

Because of the non-Gaussian tail of $f_{\Theta}(\theta)$ it cannot be assumed that the density function $f(\theta_1, \theta_2)$ is jointly normal and it turns out to be impossible to derive, from first principles, this density function in closed form. Numerical integration proved to be too costly.

To circumvent this problem an exponential type density function is fitted to $f_{\Theta}(\theta)$ and the extreme value analysis is performed in much the same way as for the extreme gusts. This approach, however, requires the presently unknown PSD of wind direction fluctuations in order to compute the correlation function. Given the uncertainties in the analysis the comparison with the IEC values is very limited. Computations are performed assuming that with good approximation the correlation function of the longitudinal component can be used instead.

The present approach allows for a very simple construction of time histories of wind direction change. It turns out that the computations for a turbulence intensity of 15%, a confidence limit of 95% and an integral time scale $L/U = 10$ results in amplitudes and rise times which are in good agreement with the IEC values if a starting value $\theta_1 = 90$ deg. is taken.

The expression derived here for the distribution function of the wind direction change is not quite satisfactory however. It is recommended to look into this problem once again.

Finally some attention is given to some rare meteorological phenomena – tornadoes and downbursts – which quite likely will induce extreme wind loads, but which are not included in the extreme climate events described by the IEC standard. Given the high price it takes, it is questionable whether wind turbines should be designed to survive a tornado, but it seems likely that they should be designed to withstand an intense microburst.

One of the main reasons for this assumption is that, although microbursts are sometimes difficult to distinguish from tornadoes, they are probably less rare and the associated wind speeds compare quite well with the extreme gust speeds established here. In addition it seems quite likely that this phenomenon induces extreme loads due to the combination of a strong vertical wind speed, high gust speeds in all directions and a vortex with a horizontal axis. It is therefore recommended to study this phenomenon in more detail, both physically and statistically, and to determine what its impact on a wind turbine could be.

²Actually the same remark applies to the pdf of gusts

A NOTATION AND BACKGROUND

A.1 Symbols and Definitions

For the definitions and notation we follow Castillo [3], Papoulis [18], and Spiegel [21].

$f(x)$	(First-order) probability density function (pdf).
$f(x, y)$	Second-order (joint) probability density function.
$f_x(x), f_y(y)$	Marginal probability density functions.
k	Shape parameter of the Weibull distribution.
n	Number of independent observations in a sample.
r	Probability of exceedance (risk).
x	Possible value of the random variable X .
C	Scale parameter of the Weibull distribution.
$F(x)$	(First-order) probability distribution function (cdf).
$F(x, y)$	Joint probability distribution function.
$F_x(x), F_y(y)$	Marginal probability distribution function.
$F_{X_n}(x)$	Extreme value distribution for the largest values of X .
Pr	Abbreviation for “probability”.
T_p	Sample period (generally one year, but 20 and 50 years are also used).
T_r	Return period.
X	Random variable.
γ	Euler’s constant = 0.5772156649...
δ	Scale parameter of the Gumbel distribution.
λ	Location parameter of Gumbel distribution.
μ	Mean of the normal distribution.

σ Standard deviation of normal distribution.

Γ Gamma function.

A.1.1 Distribution and density functions

A random variable (abbreviation : RV) is a number $X(x)$ assigned to every outcome x of an experiment. All random variables will be written in capital letters. The elements of the set \mathcal{S} that are contained in the event $\{X \leq x\}$ change as the number x takes various values. The probability $\Pr\{X \leq x\}$ of the event $\{X \leq x\}$ is therefor a number that depends on x . This number is denoted $F(x)$ and is called the (*cumulative*) *distribution function* (abbreviation : cdf) of the RV X .

Definition A.1 (Distribution function) *The distribution function of the RV X is the function*

$$F(x) = \Pr\{X \leq x\} \quad (\text{A.1})$$

defined for every x from $-\infty$ to ∞ .

The derivative

$$f(x) = \frac{dF(x)}{dx} \quad (\text{A.2})$$

of $F(x)$ is called the (*probability*) *density function* (abbreviation : pdf) of the RV X . From the monotonicity of $F(x)$ it follows that

$$f(x) \geq 0 \quad (\text{A.3})$$

Integrating (A.2) from $-\infty$ to x and using the fact that $F(-\infty) = 0$, we obtain

$$F(x) = \int_{-\infty}^x f(\xi) d\xi. \quad (\text{A.4})$$

From (A.4) it follows that

$$F(x_2) - F(x_1) = \int_{x_1}^{x_2} f(x) dx. \quad (\text{A.5})$$

Hence

$$\Pr\{x_1 < X \leq x_2\} = \int_{x_1}^{x_2} f(x) dx. \quad (\text{A.6})$$

At points of continuity of $f(x)$, the \leq in (A.6) can be replaced by $<$ if desired.

A.1.2 Joint statistics

The joint distribution $F(x, y)$ of two RVs X and Y is the probability of the event

$$\{X \leq x, Y \leq y\} = \{(X, Y) \in D\}$$

where x and y are two arbitrary real numbers and D a specified region :

$$F(x, y) = \Pr\{X \leq x, Y \leq y\} \quad (\text{A.7})$$

The function $F(x, y)$ is such that

$$F(-\infty, y) = 0 \quad F(x, -\infty) = 0 \quad F(\infty, \infty) = 1 \quad (\text{A.8})$$

The joint density of X and Y is by definition

$$f(x, y) = \frac{\partial^2 F(x, y)}{\partial x \partial y} \quad (\text{A.9})$$

From this property it follows that

$$F(x, y) = \int_{-\infty}^x \int_{-\infty}^y f(\alpha, \beta) \, d\alpha \, d\beta \quad (\text{A.10})$$

and

$$\Pr\{X \leq x\} = F_x(x) = \int_{-\infty}^x \int_{-\infty}^{\infty} f(\alpha, \beta) \, d\alpha \, d\beta \quad (\text{A.11})$$

$$\Pr\{Y \leq y\} = F_y(y) = \int_{-\infty}^{\infty} \int_{-\infty}^y f(\alpha, \beta) \, d\alpha \, d\beta \quad (\text{A.12})$$

We call $F_x(x)$ and $F_y(y)$ the marginal distribution functions (or simply the distribution functions) of X and Y respectively. The derivatives of (A.11) and (A.12) with respect to x and y are then called the marginal density functions (or simply density functions) of X and Y . We maintain that

$$\begin{aligned} F_x(x) &= F(x, \infty) & F_y(y) &= F(\infty, y) \\ f_x(x) &= \int_{-\infty}^{\infty} f(x, y) \, dy & f_y(y) &= \int_{-\infty}^{\infty} f(x, y) \, dx \end{aligned} \quad (\text{A.13})$$

Cf. Papoulis [18] and Spiegel [21].

A.1.3 Order Statistics from Independent and Identically Distributed Samples

Consider a series of independent observations belonging to the same population and divided into samples each containing n observations.

Definition A.2 (Order statistic) *Let (X_1, X_2, \dots, X_n) be a sample from a given population. If the values of the sequence X_1, X_2, \dots, X_n are rearranged in an increasing order $X_{1:n} \leq X_{2:n} \leq \dots \leq X_{n:n}$ of magnitude, then the r -th sample of this new sequence is called the r -th order statistic of the sample.*

Note that the sample size n is included in the notation $X_{r:n}$ and that any order statistics must have an associated sample size.

The two important members of the sample

$$X_{1:n} = \min(X_1, X_2, \dots, X_n)$$

and

$$X_{n:n} = \max(X_1, X_2, \dots, X_n)$$

are called extremes of the random variable X and play an essential role in applications.

Now suppose that the members X_1, X_2, \dots, X_n of the sample are independent and identically distributed and that they come from a parent population of samples with cumulative distribution function (cdf) $F(x)$. If we fit separate distributions for the smallest values of the samples only and for the largest values of the samples only the resulting distributions, $F_{X_1}(x)$ and $F_{X_n}(x)$ are called the extreme value distributions for the smallest and largest values of X , respectively. It is possible to express the extreme value distributions $F_{X_1}(x)$ and $F_{X_n}(x)$ in terms of the parent distribution $F_X(x)$.

To find the distribution of the largest value X_n , we use the relation

$$\begin{aligned} F_{X_n}(x) &= \Pr\{X_n \leq x\} = \Pr\{\text{all } X_i \leq x\} \\ &= \Pr\{X_1 \leq x\} \Pr\{X_2 \leq x\} \cdots \Pr\{X_n \leq x\}, \end{aligned} \quad (\text{A.14})$$

if all X_i are independent. This means that the probability of realizing X_n less than equal to x is the same as the probability of realizing all $X_i, i = 1, 2, \dots, n$ to be less than or equal to x . If the X_i is identically distributed with the distribution function $F_X(x)$,

$$F_{X_n}(x) = [F_X(x)]^n. \quad (\text{A.15})$$

Cf. Castillo [3] and Rao [19].

A.1.4 Return period

The return period is defined as the average elapsed time between occurrences of an event with a specified magnitude or greater. If an exceedance occurs every 50 years, on the average, then the probability that the event occurs in any given year is $1/50 = 0.02$ or 2 percent. Thus the return period T_r and the probability of occurrence are related as

$$T_r = \frac{1}{1 - F(x)} \quad (\text{A.16})$$

The use of this term can lead to dangerous misunderstanding when one is not aware of the fact that T_r is only the *average* value of the length of the time interval between two consecutive crossings. After the occurrence of an exceedance there is a big chance, that before T_r has past, there is at least one more exceedance. Rather than choosing a return period it is better to state the risk r one considers acceptable that a certain value, x_{limit} say, is exceeded within T_p years. The corresponding return period T_r then follows from the relation

$$1 - r = \left(1 - \frac{1}{T_r}\right)^{T_p}. \quad (\text{A.17})$$

Note that the risk r that x_{limit} is exceeded within 20 years is 33.2%, when a return period of 50 years is specified Note also that a return period of one year (as the IEC 1400-1 standard in some cases specifies) is rather difficult to understand unless we assume that the parent distribution and the limit distribution are based on a sample length which is shorter than one year. Cf. Castillo [3], Rao [19], Wieringa [9].

A.1.5 Characteristic largest value

The particular value of the random variable X , denoted x_n , is called the *characteristic largest value* for a period of n units if the mean value of the number of exceedances of x_n is unity. The characteristic largest

value gives an idea of the central location of the possible largest value. By definition the characteristic largest value is given by the relation

$$n [1 - F(x_n)] = 1 \quad (\text{A.18})$$

If we consider n time periods, the distribution of the largest value of x_n is given by

$$F_{X_n}(x_n) = [F(x_n)]^n = \left(1 - \frac{1}{n}\right)^n \quad (\text{A.19})$$

Thus the probability of exceeding the characteristic largest value in n time periods will be

$$1 - F_{X_n}(x_n) = 1 - \left(1 - \frac{1}{n}\right)^n \quad (\text{A.20})$$

As n tends to infinity, Eq. (A.20) converges to the value $1 - e^{-1} \approx 0.6321$. Cf. Castillo [3] and Rao [19].

A.2 The Normal Distribution

The normal cumulative distribution function (cdf) is given by

$$\Pr\{X \leq x\} \equiv F(x) = \int_{-\infty}^x \frac{1}{\sigma\sqrt{2\pi}} \exp\left[-\frac{1}{2}\left(\frac{t-\mu}{\sigma}\right)^2\right] dt; \quad -\infty < x < \infty, \quad (\text{A.21})$$

where σ is the standard deviation and μ the arithmetical mean. The associated probability density function (pdf) is

$$f(x) = \frac{1}{\sigma\sqrt{2\pi}} \exp\left[-\frac{1}{2}\left(\frac{x-\mu}{\sigma}\right)^2\right]; \quad -\infty < x < \infty. \quad (\text{A.22})$$

The main parameters of the normal distribution are summarised in table A.1.

A.3 The Weibull Distribution

The Weibull cdf is given by

$$F(x) = 1 - \exp\left[-\left(\frac{x}{C}\right)^k\right]; \quad 0 < x < \infty; C > 0; k > 0, \quad (\text{A.23})$$

where C and k are constants known as the scale and shape parameters, respectively. The associated pdf is

$$f(x) = \frac{k}{C} \left(\frac{x}{C}\right)^{k-1} \exp\left[-\left(\frac{x}{C}\right)^k\right]; \quad 0 < x < \infty; C > 0; k > 0. \quad (\text{A.24})$$

The main parameters of the Weibull distribution are summarised in table A.1. For $k = 2$ the well known Rayleigh distribution is found.

A.4 The Gumbel Distribution

The Gumbel or Fisher-Tippett type-I cdf of maxima is given by

$$F(x) = \exp \left[- \exp \left(\frac{-(x - \lambda)}{\delta} \right) \right]; \quad -\infty < x < \infty; \delta > 0, \quad (\text{A.25})$$

where λ and δ are constants known as the location and scale parameters, respectively. The associated pdf is

$$f(x) = \frac{\exp \left(\frac{-(\lambda-x)}{\delta} \right) \exp \left[- \exp \left(\frac{-(x-\lambda)}{\delta} \right) \right]}{\delta}; \quad -\infty < x < \infty. \quad (\text{A.26})$$

The main parameters of the Gumbel distribution are summarised in table A.1.

Table A.1 Some parameters of the Weibull, Gumbel and Normal distribution

	Weibull	Gumbel	Normal
Mean	$C\Gamma \left(1 + \frac{1}{k} \right)$	$\lambda + \gamma\delta$	μ
Median	$C(\ln 2)^{1/k}$	$\lambda - \ln(\ln(2))\delta$	
Mode		λ	
Variance	$C^2 \left[\Gamma \left(1 + \frac{2}{k} \right) - \Gamma^2 \left(1 + \frac{1}{k} \right) \right]$	$\frac{\pi^2\delta^2}{6}$	σ^2
Kurtosis		1.1396	
Euler's constant		$\gamma = 0.5772156649..$	

B DERIVATION OF GUMBEL DISTRIBUTION

The importance of the Gumbel distribution is due to its extreme value behaviour. It has been applied as the parent distribution or as an asymptotic approximation, to describe extreme wind speeds, sea wave heights, floods, rainfall, air pollution, geologic problems, etc. , see Castillo [3][Ch. 5.2].

For a derivation of the Gumbel distribution, based on order statistics, we follow Harris [14] who in turn based his text on a derivation by Cramer [7]. This derivation is given in section B.1.

An alternative derivation is given by Davenport [8]. He uses exceedance statistics to derive an asymptotic distribution and casts this Poisson distribution into a Gumbel-like form for a Rayleigh parent distribution. In section B.2 we will derive the same asymptotic distribution based on exceedance statistics, showing the underlying assumptions, and then cast this distribution into a Gumbel-like form for the more general Weibull parent distribution. Davenport claims that his version of the Gumbel distribution (for a Rayleigh parent) is more exact than the one based on order statistics. We doubt that. In both derivations assumptions are made which are not entirely met in reality.

B.1 Derivation Based on Order Statistics

B.1.1 Order statistics and asymptotic distributions

The distribution function of the extreme value X_1 and X_n becomes increasingly insensitive to the exact shape of the common distribution function $F_X(x)$ as n tends to infinity. The limiting forms as $n \rightarrow \infty$ are known as asymptotic distributions. The asymptotic distributions often describe the behaviour of the random variable X_1 or X_n reasonable well even when the exact shape of the parent distribution is not known precisely. The asymptotic distributions are classified into three types based on the general features of the tail part of the distribution of the random variable X see e.g. Fisher & Tippett [10] and Gumbel [13]. Different types of asymptotic distributions have been used for different engineering applications.

The Gumbel or Fisher-Tippitt type-I asymptotic distribution for the maximum values is useful whenever the right tail of the parent distribution $F_X(x)$ is unbounded ($x \rightarrow \infty$) and is of an exponential type. In such a case we can express $F_X(x)$ as

$$F_X(x) = 1 - e^{-h(x)} \quad (\text{B.1})$$

where $h(x)$ increases with x monotonically. The distributions such as normal, lognormal and Weibull distributions belong to this category. If $F_X(x)$ is of the form given by Eq. (B.1) the asymptotic distribution function of the largest value can be found as follows. If we assume that the observations in a sample are independent and identically distributed then the exact distribution of the largest value is

$$F_{X_{n:n}}(x) = [F(x)]^n = \{1 - \exp[-h(x)]\}^n. \quad (\text{B.2})$$

To investigate what happens when $n \rightarrow \infty$ we have to introduce the so-called characteristic largest value, denoted by x_n , cf. A.1.5. The characteristic largest value, x_n , is defined by the relation

$$1 - F(x_n) = 1/n = \exp[-h(x_n)]. \quad (\text{B.3})$$

Thus

$$F_{X_{n:n}}(x) = \left(1 - \frac{\exp[h(x_n) - h(x)]}{n}\right)^n. \quad (\text{B.4})$$

Now since $h(x)$ is a positive and increasing function of x , as x increases beyond x_n , $\exp[h(x_n) - h(x)] \ll 1$. A well-known result for the exponential function originally due to Cauchy is

$$\lim_{n \rightarrow \infty} \left(1 - \frac{\epsilon}{n}\right)^n = \exp(-\epsilon) \quad (\text{B.5})$$

and the convergence of this expression to the limit is such that if ϵ is small and n is large, the exponential limit is a good approximation to the left hand side, the leading term being $\epsilon^2/2n$. Thus applying this result to (B.4) gives

$$F_{X_{n:n}}(x) \simeq \exp\{-\exp[h(x_n) - h(x)]\}. \quad (\text{B.6})$$

Note that apart from the Cauchy formula, (B.6) is exact—it contains no other approximations. Taking logarithms twice gives

$$-\ln\{-\ln[F_{X_{n:n}}(x)]\} \simeq h(x) - h(x_n) = h(x) - \ln(n). \quad (\text{B.7})$$

The right-hand side of (B.7) is now expanded in a Taylor series about $x = x_n$ and gives

$$-\ln\{-\ln[F_{X_{n:n}}(x)]\} = (x - x_n) \frac{h'(x_n)}{1!} + (x - x_n)^2 \frac{h''(x_n)}{2!} + \dots \quad (\text{B.8})$$

The familiar Fisher-Tippett type-I asymptotic formula is obtained by truncating the Taylor series at the first term, and thus

$$-\ln\{-\ln[F_n(x)]\} \simeq \alpha(x - x_n), \quad (\text{B.9})$$

where $F_n(x)$ is used to denote the asymptotic form of $F_{X_{n:n}}(x)$ and

$$\alpha = h'(x_n) = n(dF/dx)_{x=x_n}. \quad (\text{B.10})$$

Comparing (B.9) with (A.25) shows that

$$\alpha = \frac{1}{\delta} \quad (\text{B.11})$$

B.1.2 The Gumbel distribution for a Weibull parent

To find the shape and scale parameter of the Gumbel distribution for a Weibull parent we make use of the fact that $h(x) = \left(\frac{x}{C}\right)^k$. Hence

$$\alpha = h'(x_n) = \frac{k}{C} \left(\frac{x_n}{C}\right)^{k-1}. \quad (\text{B.12})$$

Because of (B.3) we find

$$n = \exp[h(x_n)] \quad (\text{B.13})$$

and

$$\beta = x_n = C(\ln n)^{\frac{1}{k}}. \quad (\text{B.14})$$

Substituting (B.14) in (B.12) gives:

$$\alpha = \frac{k}{C} (\ln n)^{1-\frac{1}{k}}. \quad (\text{B.15})$$

B.2 Derivation Based on Exceedance Statistics

A series of independent and identically distributed observations will only yield a set of maxima that conform to an asymptotic extreme value distribution if the maxima have been drawn from infinitely large samples. In practice this is never achieved. If we take hourly averages for example, then there are 8766 observations per year³ and moreover these observations are not independent. It can be shown that for hourly averages the number of independent observations is approximately 800. With such a small number, the question arises whether extreme value theory is satisfied within acceptable limits. It depends of course on how fast the extreme value distributions approach their limiting form.

To avoid these problems Davenport [8] uses exceedance statistics to derive a limit distribution for extremes, which he casts into a Gumbel distribution for a Rayleigh parent. By doing so he finds alternative expressions for the shape factor and the scale parameter of the Gumbel distribution.

B.2.1 Exceedance statistics

Critical wind speeds result in responses that exceed the limits beyond which structural damage may be expected. We would like to know the frequency with which the wind speed exceeds the critical value V . The statistical function ν_V^+ is defined to be the number of times per second that the process passes with positive slope through the value V (see Figure B.1), and the associated concepts are known as the theory of exceedance statistics.

Crossing analysis

Suppose that we could consider a sample of length T of the one-hour or 10-min. average wind speed U as a sine wave of varying amplitude and phase, i.e. a narrow-band random process, see Fig. B.1. Suppose

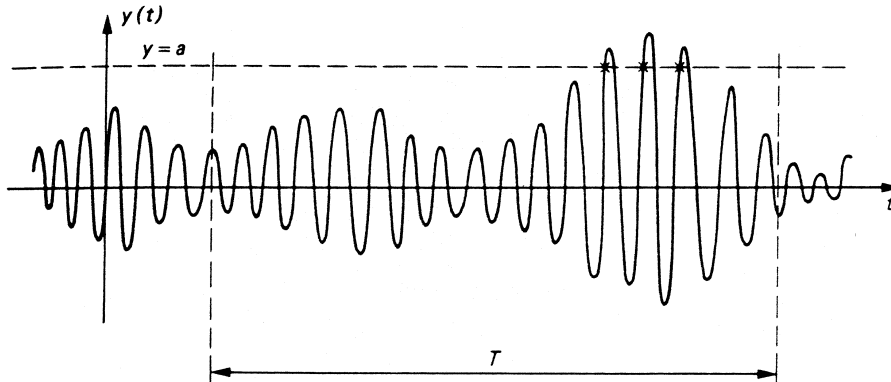


Figure B.1 Typical sample of a narrow band process (Courtesy Ref. [17]).

that we enquire how many ‘cycles’ of $U(t)$ have amplitudes greater than the level $U = V$ during the time period T . Let $n_V^+(T)$ denote the number of positive slope crossings of $U = V$ in time T for a typical sample and let the mean value for all samples be $N_V^+(T)$ where

$$N_V^+(T) = E[n_V^+(T)]. \tag{B.16}$$

³We assume that a year has on average 365.25 days.

Since the process is stationary, if we take a second interval of duration T immediately following the first we shall therefore obtain

$$N_V^+(2T) = 2N_V^+(T)$$

from which it follows that the average number of crossings is proportional to the time interval T . Hence

$$N_V^+(T) \propto T$$

or

$$N_V^+(T) = \nu_V^+ T \tag{B.17}$$

where ν_V^+ is the average frequency of positive slope crossings of the level $U = V$. We now consider how the frequency parameter ν_V^+ can be deduced from the underlying probability distribution for $U(t)$.

Consider a small length of duration Δt of a typical sample function. Suppose that $U < V$ at the beginning of the interval, time t . There is a minimum slope at time t if the level $U = V$ is to be crossed in time Δt depending on the value of U at time t , see Fig. B.2. This is

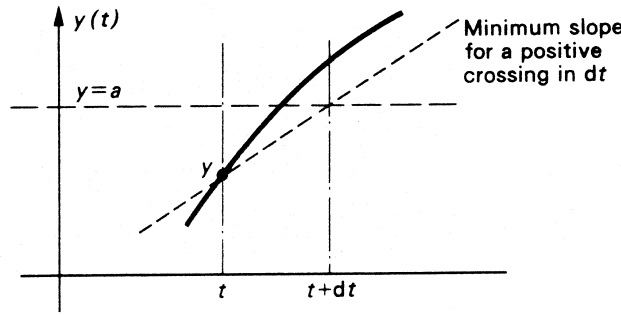


Figure B.2 Conditions for a positive slope crossing of $U = V$ in time interval Δt (Courtesy Ref. [17]).

$$\frac{V - U}{\Delta t}$$

and so there will be a (high probability of a) positive slope crossing of $U = V$ in the next time interval Δt if, at time t ,

$$U < V \quad \text{and} \quad \frac{dU}{dt} > \frac{V - U}{\Delta t}. \tag{B.18}$$

The probability that both conditions are satisfied can be calculated from the joint probability density function $p(U, \dot{U})$, hence

$$\Pr \left\{ \begin{array}{l} \text{Positive slope crossing} \\ \text{of } U = V \text{ in time } \Delta t \end{array} \right\} = P_{\Delta t} = \int_0^\infty d\dot{U} \int_{V - \dot{U}\Delta t}^V p(U, \dot{U}) dU \tag{B.19}$$

and thus it follows that

$$P(V) = \lim_{\Delta t \rightarrow 0} \frac{P_{\Delta t}}{\Delta t} = \int_0^\infty \dot{U} p(V, \dot{U}) d\dot{U}, \tag{B.20}$$

when the term $p(V, \dot{U})$ is understood to mean the joint probability density function $p(U, \dot{U})$ evaluated at $U = V$, see Newland [17] [Ch. 8].

Now let ΔT be the time within a total period T which U spends in the domain ($V - \dot{U}\Delta t \leq U \leq V, \dot{U} > 0$) in (U, \dot{U}) space. Then $\Delta T/\Delta t$ is the average number of crossings of the interval $V - \dot{U}\Delta t \leq U \leq V$, because we assume that $\dot{U}\Delta t$ is small and the process $U(t)$ is smooth so occupation of the interval is equivalent to crossing it in Δt .

By definition, $P_{\Delta t} = \Delta T/T$, and so $P_{\Delta t}/\Delta t = (\Delta T/\Delta t)/T$ is the average number of crossings of V in unit time. Thus

$$\nu_V^+ = \int_0^\infty \dot{U} p(V, \dot{U}) d\dot{U} \quad (\text{B.21})$$

This is a general result which applies for any probability distribution.

In order to calculate the exceedance curve ν_V^+ we must know the joint probability density function of U and \dot{U} . It is a property of any stationary random process $x(t)$ that x and its derivative \dot{x} are uncorrelated

$$E[x\dot{x}] = 0.$$

Hence we can write

$$p(U, \dot{U}) = p(U)p(\dot{U}). \quad (\text{B.22})$$

Substituting (B.22) in (B.21) yields

$$\nu_V^+ = p(V) \int_0^\infty \dot{U} p(\dot{U}) d\dot{U} \quad (\text{B.23})$$

Cf. Newland [17][Ch. 8].

B.2.2 Frequency of maxima

Our analysis of peaks is based on the assumption that the narrow band process resembles a sine wave of varying amplitude and phase. If ν_V^+ is the average number of exceedances per unit time, then $\nu_V^+ T$ is the average number of exceedances per time interval T .

Now divide such a time interval into n subintervals with length $\Delta T = T/n$. In such an interval there can be one or more exceedances or no exceedance at all. We assume however

1. Δt is so small, hence n so large, that exceedance can only happen once⁴
2. the probability p of exceedance is equal for all subintervals.
3. the exceedances are independent.

In this case the stochastic variable $N_V^+(T)$, which is the number of exceedances in time T , has a binomial distribution. If we now let $n \rightarrow \infty, p \rightarrow 0$ while $pn = \nu_V^+ T$, we find the well known Poisson limit for the binomial distribution.

$$\Pr \{N_V^+(T) = N\} = \frac{(\nu_V^+ T)^N}{N!} e^{-\nu_V^+ T} \quad \text{for } N = 0, 1, 2, \dots, \quad (\text{B.24})$$

where $N_V^+(T)$ is the number of exceedances in time interval T . The probability that there will be no crossings of the level $U = V$ in the time interval T is

$$\Pr \{N_V^+(T) = 0\} = e^{-\nu_V^+ T} \quad \text{for } T \geq 0 \quad (\text{B.25})$$

⁴In the sense that the probability of exceedance twice or more is extremely small.

Hence, the probability that there will be one or more crossings in time T is then simply

$$\Pr \{N_V^+(T) > 0\} = \Pr \{U > V\} = 1 - e^{-\nu_V^+ T} \quad (\text{B.26})$$

Because $\Pr \{U > V\} = 1 - F(V)$ we find that the cdf $F(V)$ is

$$F(V) = e^{-\nu_V^+ T} \quad (\text{B.27})$$

Limit distribution for a Weibull parent

Suppose that the one-hour or ten-minute average wind speed U is Weibull distributed with shape factor k and scale parameter C and suppose that the derivative of U is also Weibull distributed with the same shape factor k and a different scale parameter C' . Hence

$$p(U) = \frac{k}{C} \left(\frac{U}{C}\right)^{k-1} \exp \left[- \left(\frac{U}{C}\right)^k \right] \quad (\text{B.28})$$

and

$$p(\dot{U}) = \frac{k}{C'} \left(\frac{\dot{U}}{C'}\right)^{k-1} \exp \left[- \left(\frac{\dot{U}}{C'}\right)^k \right] \quad (\text{B.29})$$

Substituting (B.28) and (B.29) in (B.23) yields

$$\begin{aligned} \nu_V^+ &= \frac{k}{C} \left(\frac{V}{C}\right)^{k-1} \exp \left[- \left(\frac{V}{C}\right)^k \right] C' \int_0^\infty k \left(\frac{\dot{U}}{C'}\right)^k \exp \left[- \left(\frac{\dot{U}}{C'}\right)^k \right] \frac{d\dot{U}}{C'} \\ &= \Gamma \left(\frac{1}{k} + 1 \right) k \frac{C'}{C} \left(\frac{V}{C}\right)^{k-1} \exp \left[- \left(\frac{V}{C}\right)^k \right] \end{aligned} \quad (\text{B.30})$$

Put

$$\frac{C'}{C} = \frac{\sigma_{\dot{U}}}{\sigma_U} = \nu \quad (\text{B.31})$$

and note that ν is a frequency. We will call ν the effective frequency and if $\sigma_{\dot{U}}$ and σ_U are not known we can find ν alternatively from:

$$\nu = \left[\frac{\int_0^\infty f^2 S_{UU}(f) df}{\int_0^\infty S_{UU}(f) df} \right]^{1/2}, \quad (\text{B.32})$$

because the spectral density of \dot{U} is just f^2 times the spectral density of the original process U . Substitution of (B.30) in (B.27) and noting that $\nu T = n$ gives

$$F(> V) = \exp \left[- \exp \left\{ - \left(\frac{V}{C}\right)^k + \ln \left(n k \Gamma \left(\frac{1}{k} + 1 \right) \left(\frac{V}{C}\right)^{k-1} \right) \right\} \right] \quad (\text{B.33})$$

To cast this expression into a Gumbel-like form we apply the same procedure as in the previous section. Put $h(x) = \left(\frac{V}{C}\right)^k$. Then taking logarithms twice gives:

$$- \ln \{ - \ln [F(> V)] \} = h(x) - \ln \left\{ n k \Gamma \left(\frac{1}{k} + 1 \right) \right\} - \ln \{ h(x)^{-1} \} \quad (\text{B.34})$$

Expanding the right hand side in a Taylor series about $x = x_n$ and truncating at the first term and some rearranging gives

$$-\ln \{-\ln [F(> V)]\} \simeq -h'(x_n) \left(1 - \frac{k-1}{k} \frac{1}{\ln n}\right) \left[x - x_n \left\{ 1 + \frac{\ln \left[k \Gamma \left(\frac{1}{k} + 1 \right) (\ln n)^{\frac{k-1}{k}} \right]}{k \ln n - (k-1)} \right\} \right] \quad (\text{B.35})$$

Comparing (B.36) with (B.9) shows that

$$\alpha_{\text{Dav}} = \alpha \left\{ 1 - \frac{k-1}{k} \frac{1}{\ln n} \right\} \quad (\text{B.36})$$

and

$$\beta_{\text{Dav}} = \beta \left\{ 1 + \frac{\ln \left[k \Gamma \left(\frac{1}{k} + 1 \right) (\ln n)^{\frac{k-1}{k}} \right]}{k \ln n - (k-1)} \right\} \quad (\text{B.37})$$

Typically, for $k = 2$, α_{Dav} is about 5% greater than α and β_{Dav} is about 10% greater than β . The increase becomes smaller for decreasing k .

References

- [1] Bergström, H. “Distribution of Extreme Wind Speed”. Wind Energy Report WE 92:2, Uppsala University, Department of Meteorology, Uppsala, Sweden, 1992.
- [2] Butterfield, S., B. Holley, P. Hauge Madsen, and C. Stork. “Report on 88/69/CD–Wind Turbine Generator Systems Part 1: Safety Requirements, 2nd edition”. unpublished report, 1996.
- [3] Castillo, E. *Extreme Value Theory in Engineering*. Academic Press, Inc., 1988.
- [4] Chaviaropoulos, P.K. “Probabilistic Analysis of Extreme Wind Events”. *Wind Engineering*, 20(3):139–159, 1997.
- [5] Collier, C.G., J. Dixon, M.S.J. Harrison, J.C.R. Hunt, J.F.B. Mitchell, and D.S. Richardson. “Extreme surface winds in mid-latitude storms: forecasting and changes in climatology”. *J. Wind Eng. Ind. Aerodyn.*, 52(Complete):1–27, 1994.
- [6] Cook, N.J. “Towards better estimation of extreme winds”. *J. Wind Eng. Ind. Aerodyn.*, 9:295–323, 1982.
- [7] Cramer, H. In Gumbel, E.J., editor, “*Statistics of Extremes*”, page 170. Columbia Univ. Press, New York, 1958.
- [8] Davenport, A.G. “The Dependence of Wind Loads on Meteorological Parameters”. In *Proc. Int. Res. Seminar*, pages 19–82, Ottawa, 1967. University of Toronto Press. Wind effects on buildings and structures.
- [9] Wieringa, J en P.J. Rijkoort. “*Windklimaat van Nederland*”. Staatsuitgeverij ’s-Gravenhage, 1983.
- [10] Fisher, R.A. and L.H.C. Tippett. “Limiting Forms of the Frequency Distributions of the Largest or Smallest Member of a Sample”. *Proc. Cambridge Philos. Soc.*, 24:180–190, 1928.
- [11] Fujita, T.T. “The downburst”. SMRP Research Paper Number 210, Department of the Geophysical Sciences, The University of Chicago, Chicago, Illinois 60637, 1985. Published by Satellite and Mesometeorology Research Project (SMRP).
- [12] Gradshteyn, I.S. and I.M. Ryzhik. *Table of Integrals, Series and Products*. Academic Press, Inc., 1980.
- [13] Gumbel, E.J. *Statistics of Extremes*. Columbia Univ. Press, New York, 1958.
- [14] Harris, R.I. “Gumbel re-visited – a new look at extreme value statistics applied to wind speeds”. *J. Wind Eng. Ind. Aerodyn.*, 59(1):1–22, 1996.
- [15] Ibarra, J.I. “A New Approach to the Determination of Horizontal Wind Direction Fluctuations”. *J. of Applied Meteorology*, 34:1942–1949, 1995.
- [16] International Electrotechnical Commission. “*International Standard IEC 1400-1; Wind turbine generator systems – Part 1: Safety requirements*”, first edition, 1994.
- [17] Newland, D.E. *Random Vibrations and Spectral Analysis*. Longman, Inc., New York, second edition, 1984.

- [18] Papoulis, A. *Probability, Random Variables, and Stochastic Processes*. Electrical Engineering Series. McGraw-Hill, Inc., second edition, 1984.
- [19] Rao, S.S. *Reliability-based design*. McGraw-Hill, Inc., 1992.
- [20] Rice, S.O. “Mathematical Analysis of Random Noise”. *Bell System Tech. J.*, 23:282–332, 1944, and 24:46–156, 1945. both of which are reprinted in N. Wax (ed.), *Selected Papers on Noise and Stochastic Processes*, Dover, New York, 1954.
- [21] Spiegel, M.R. *Probability and Statistics*. Schaum’s Outline Series in Mathematics. McGraw-Hill, Inc., 1975.
- [22] Weber, R. “Estimator of the Standard Deviation of Wind Direction Based Moments of the Cartesian Components”. *J. of Applied Meteorology*, 30:1341–1353, 1995.
- [23] Winkelaar, D. “Some Ideas on the Modelling of Atmospheric Turbulence”. In *IEA Joint Action on Wind Conditions for Wind Turbine Design; 1st Symposium*, Hamburg, Germany, June 1994.

EUROPEAN WIND TURBINE STANDARDS II
PART 2
QUANTIFICATION OF FAILURE PROBABILITIES

H. Braam (editor)
A.J. Seebregts
M.W. Jensen
P. Christensen
C.J.C. Christensen
E. Hinrichsen

Netherlands Energy Research Foundation ECN
Netherlands Energy Research Foundation ECN
RISØ National Laboratory
RISØ National Laboratory
RISØ National Laboratory
Germanischer Lloyd

CONTENTS OF PART 2

1. INTRODUCTION.....	5
1.1 Background.....	5
1.2 Objectives.....	5
1.3 Methodology.....	6
2. SCOPE AND FIELD OF APPLICATION.....	7
3. DEFINITIONS.....	9
4. SYMBOLS AND ABBREVIATIONS.....	11
5. RELIABILITY OF LOAD CARRYING COMPONENTS.....	13
5.1 Target values for structural reliability.....	13
5.1.1 Introduction.....	13
5.1.2 Reliability Methods.....	13
5.1.3 Target Reliability's in Structural Design Codes.....	14
5.2 Partial safety coefficients.....	14
5.2.1 The Limit State - Probabilistic Design Requirement.....	14
5.2.2 Evaluating the failure probability.....	15
5.2.3 Partial coefficient method.....	17
5.2.4 Calibration of partial coefficients.....	17
5.2.5 Target reliability and probabilistic safety calculations.....	18
6. RISK CRITERIA AND RISK TARGET VALUES.....	19
6.1 Recommendations for risk criteria and risk target values to be used for wind turbines.....	19
6.2 Example mortality rate calculation for wind turbines.....	20
7. DATA COLLECTION AND PARAMETER ESTIMATION.....	23
7.1 Introduction.....	23
7.2 Design specific failure data.....	24
7.3 Generic wind turbine failure data.....	24
7.4 Generic Failure Data from Other Industries.....	26
7.5 Summary of Guidelines.....	27
8. QUANTIFICATION OF MODELS (BENCHMARK STUDY).....	29
8.1 Outline of Benchmark.....	29
8.2 Benchmark results.....	29
8.3 Conclusions and recommendations.....	34
9. CONCLUSIONS AND RECOMMENDATIONS.....	35
10. REFERENCES.....	39
Appendix A. REVIEW OF SAFETY AND RISK CRITERIA.....	41
Appendix A.1 Target reliability's in various countries and in various branches of industries.....	43
Appendix A.2 Risk criteria in the various countries.....	49
Appendix A.3 Mortality rates observed.....	52
Appendix A.4 Wind turbine failure data.....	52
Appendix B. MORTALITY RATE CALCULATION.....	55
Appendix B.1 Assumptions.....	55
Appendix B.2 Calculational procedure.....	55
Appendix B.3 Reference.....	56

Appendix C. BENCHMARK ON DATA COLLECTION AND PARAMETER ESTIMATION	57
Appendix C.1 Guidance for benchmark exercise	57
Appendix C.1.1 List of Basic Events (BEs) from EWTS-I case study.....	57
Appendix C.1.2 Information needed for each BE	58
Appendix C.1.3 Sources of information.....	58
Appendix C.1.4 Failure type model.....	58
Appendix C.1.5 Example of data to be provided for each BE:	59
Appendix C.2 Overall approach ECN.....	59
Appendix C.3 Overall approach RISØ	61
Appendix C.4 Data and results	65
Appendix D. DERIVATION OF FAILURE RATES FROM REPORTED FAILURES	69

1. INTRODUCTION

1.1 Background

Presently, wind turbines are being designed in accordance with deterministic design rules embedded in standards like the IEC 1400-1 [1.1] and various national standards and certification criteria. These rules concern the design of the load carrying components and the design of safety and control systems.

Design of load carrying components and partial safety factors

For a safe design of load carrying components a margin is introduced between the design value of the strength and the characteristic value of the load. Over the years various methods to define safety margins have been used, but nowadays the concept of the partial safety factors is commonly embodied in the structural design codes. These partial safety factors ensure that there is a safety margin both on the load side and on the strength side. The magnitude of the partial safety factors has to reflect the required safety level and likewise the uncertainty in the load and the strength should be taken into account. This means that the partial safety factor for wind loads has a larger value than for well defined static loads, like the self-weight. The determination of the magnitude of the partial safety factors can be done empirically. However, a probabilistic approach is preferred, because in this way uncertainties in the load and the strength can be considered in a more rational manner. This probabilistic method has been applied already in other branches of industry like offshore and civil engineering, but is not introduced in the wind energy branch yet. As the concept of probabilistic calibration of partial safety factors is fairly new in the wind turbine community the principles behind the method were examined as part of the EWTS-I subproject “Calibration of Safety Factors” [1.2]. To calibrate partial safety factors based on a probabilistic method target values for the structural reliability of load carrying components have to be drawn up. This aspect was not considered in the EWTS-I project.

Control and safety systems, beyond design situations

Generally, the control systems have to keep the wind turbine within its design limits during normal operation and to ensure that electrical energy is generated and supplied to the grid in an efficient manner. In case of a failure or in case of abnormal external conditions, the control systems in combination with the safety systems have also to keep the turbine within its design envelope to prevent damage or unsafe operation. As a consequence of a failure of a safety system the wind turbine can run into overspeed and is operating beyond design conditions. This can lead to catastrophic failures like blade rupture. Scenarios how a wind turbine can run into overspeed or failed operation can be derived by means of a qualitative Probabilistic Safety Assessment (PSA). With a quantitative PSA it is also possible to calculate the frequency of occurrence of for example overspeed. PSA’s for wind turbines have been carried out successfully in various countries (e.g., see [1.3]). Because it is expected that PSA’s will be used more and more the guidelines developed in the various countries should be harmonised to obtain unified assumptions and comparable results. For this reason guidelines or recommended practices were formulated as part of the EWTS-I subproject “Assessment of Wind Turbine Safety; Recommended Practices” [1.2]. To illustrate the method a limited case study was performed for a ‘postulated’ design, but with similar characteristics to the AOC 15/50 [1.4]. The results of that case study are given in part 4 of [1.2]. However the development of guidelines for the derivation of data for the quantification was beyond the scope of the EWTS-I project.

Risks to the public

As mentioned above failure of the safety system might lead to catastrophic failures like blade rupture, which can cause risks to the public. In that way it is of great interest for e.g. authorities, especially in densely populated areas. To judge whether a risk is unacceptable limits have to be indicated above which the risks become unacceptable (maximum permissible levels).

1.2 Objectives

The objectives of the 2nd EWTS-II subproject “Quantification of Failure Probabilities” are two-fold, viz.:

- derivation of target values for structural reliability and for risk criteria on which the designer should aim and which the certifying bodies can use as a criterion;
- preparation of guidelines to collect data and to estimate parameters to be used for quantitative safety and

reliability analyses (PSA's).

1.3 Methodology

The approach taken was a literature study to obtain target values, followed by a limited case study to obtain guidelines for data collection.

Target values

The literature study included references from various countries and branches of industries and resulted in an overview of:

- target reliability's (screening of available codes for building and construction to establish reliability levels for the design of load carrying components);
- risk criteria and risk figures used and observed (review of national and international regulations on risk limits and references for observed risk figures, e.g., mortality rates);
- wind turbine failure data (review of national and international generic data on wind turbine failures, e.g., actual frequency of occurrence of catastrophic blade failures, failure of main components or safety systems).

In appendix A of this report the references used are listed together with the corresponding summaries. From these reviews conclusions and recommendations for target values are derived.

Chapter 5 presents the recommendations for target values for structural reliability. In addition, it presents an outline how these target values can be used to calibrate partial safety factors.

Chapter 6 presents the conclusions and recommendations for risk criteria and mortality rates. Fatalities of the 'public' as a result of wind turbine accidents are not known. Only personnel was involved in such cases, which is a labour safety item and outside the scope of this project. The 'public' mortality rate for wind turbines can therefore only be assessed by means of an analysis. To illustrate the possibilities and the limitations of such a mortality rate analysis, a simple calculation example is presented in appendix B.

Guidelines for data collection and parameter estimation

Guidelines to collect data for quantitative safety and reliability analyses were formulated based on a limited benchmark study (essentially with the same design and with the same scope as in the EWTS-I subproject 'Assessment of Wind Turbine Safety: Recommended Practices'). ECN and Risø participated in the benchmark study.

Chapter 7 first presents an overview of the various data sources that are available and finally the resulting set of practical guidelines for collecting data and estimating parameters for quantitative safety analyses.

Chapter 8 summarises the results of the benchmark study. Based on this study, appendix C provides more detailed guidelines for data collection and parameter estimation, and it describes the results in more detail. The guidelines formulated are based on previous experience present at ECN (seven quantitative wind turbine safety and reliability studies) and the experience obtained within this project (jointly by ECN, GL, and Risø).

2. SCOPE AND FIELD OF APPLICATION

The target values for structural reliability are primarily meant for the calibration of partial safety factors using a probabilistic method. As part of the EWTS-I project a procedure for this calibration was already developed, however the target values itself were not considered at that time.

The risk of a wind turbine can be assessed by means of a quantitative Probabilistic Safety Assessment (PSA). As part of the EWTS-I project guidelines and recommendations were defined to perform such a PSA. However, these recommendations were applied to a limited extend only. In the current report the applicability of these recommendations was considered by performing a case study for a postulated although realistic design of a wind turbine. With the results of this case study the recommended practices from the EWTS-I project were adjusted and extended.

Risk is defined in this project as: Risk to the public, and to be more precise as the probability of dying as a result of a wind turbine incident or accident. Risk to personnel (labour safety) or economic risk or the risk of loosing the structural integrity of the wind turbine is not considered here.

The target values for the reliability and safety of wind turbines are strongly related to the requirements in national and international standards and European directives. The recommended target values can serve as a starting point for standardisation in this field.

The recommendations for quantitative safety and reliability analyses together with the guidelines for data collection and parameter estimation can be used by manufactures and designers to assess the reliability of advanced protection systems and to identify critical components or weak spots in the design.

3. DEFINITIONS

Environmental

- Impact Statement : Study and report in which the environmental impacts of an (industrial) activity are outlined and shown below acceptable levels.
- Risk : Risk is defined as the unwanted consequence of a particular activity in relation to the likelihood that this may occur.
- Risk to the public : Risk posed to the group of people outside the premises of the installation, the consequence here referring to death.
- Group risk : The likelihood per year that a group of at least a certain size will all be victim of a single accident at one and the same time. The group risk should indicate the probability that a certain group of people outside a facility will die due to an accident caused by the facility. As such, this risk takes account of the surrounding area. Group risk does not involve the calculation of the individual risk but rather the risk of a number of deaths. In addition, the group has to be a fixed and identifiable group of persons, viz. the group of persons actually living at/near the corresponding site.
- Individual risk : The likelihood that a person will suffer a given detrimental effect (here: death) as a result of exposure to an agent (expressed in probability units per year or related to an average concentration per year).
The IR is calculated for the person who runs the greatest risk at a given location. In practice, this normally refers to an individual who is present at a particular place in the vicinity of an industrial site 24 hours per day.
- Mortality rate : Number of deaths per year for a given population.
- Risk criteria : A measure of risk, e.g., group risk or individual risk.
- Risk targets : A level for the risk value which is aimed at not to exceed.
- Risk limits : A strict level for the risk value which is not to be exceeded, e.g., in the Netherlands the limit for individual risk is $1e-6$ /yr.
- Target reliability : Maximum failure probability prescribed in a code.

4. SYMBOLS AND ABBREVIATIONS

ALARP:	As Low As Reasonable Practicable
BE :	Basic Event
ET :	Event Tree
FT :	Fault Tree
FORM :	First order reliability method
HSE :	UK Health and Safety Executive
PSA :	Probabilistic Safety Assessment
QRA :	Quantitative Risk Assessment
WTB :	Wind Turbine
β :	Reliability index

5. RELIABILITY OF LOAD CARRYING COMPONENTS

5.1 Target values for structural reliability

5.1.1 Introduction

Structures are generally designed with design codes or building codes, which are prescribed by the relevant national legislation. To obtain a certain level of safety against uncertainties and tolerances in the material properties and the loading, safety factors are included in the design formulas of these codes.

Traditionally this has been a single, global safety factor to account for all uncertainties. Modern design codes apply the so called partial safety factor method, which uses separate safety factors for the material properties and the loading. The advantage is that uncertainties, especially in environmental loads, can be better accounted for. The disadvantage is, that it requires more work. A further problem is that these partial safety factors need to be calibrated, to ensure that the desired safety level is met. This calibration is done through a probabilistic method based on a certain target reliability.

Following a brief outline of structural reliability methods is given, in order to have a better understanding of the concepts and terms used, see also [5.1] for this purpose. Then an overview is given of target reliability's as used in design codes in different countries and different industries. This is based on the summaries of references contained in appendix A. This may then be used by regulatory bodies to define target reliability values for wind turbines, since this is outside the scope of this sub-project.

5.1.2 Reliability Methods

System Reliability

In ISO 2394 [5.3] this is defined as: 'The reliability of a structural system which has more than one relevant failure mode or the reliability of a system of more than one relevant structural element'. Although this is relevant to wind turbines, especially if one considers the safety and control systems, there are to our knowledge, no national codes available that specify target values for system reliability. We found two general references that would give target values for control systems, one for safety systems of nuclear power plants and one for the safety system of a wind turbine.

Structural Reliability

The term structural reliability may be defined as follows: 'The probability that the loading of a structure does not exceed its strength for a specified period of time' [5.2]. In order to be able to determine this probability, a set of so called 'limit states' for the loading (L) and the resistance R of the structure in question must be formulated. Then the probability that (L-R) is positive can be calculated and compared to a predefined target value. It should be noted that the limit state of a structural element may be exceeded by ultimate loads or through fatigue damage, both must be considered. This is also the key principle of the proposed revision of ISO 2394 [5.3], which defines structural performance as follows: 'The structural performance of a whole structure or part of it should be described with reference to a specified set of limit states beyond which the structure no longer satisfies the design requirements'. A distinction is made between 'ultimate' and 'serviceability' limit states. Ultimate limit states correspond to the maximum load carrying capacity of the structure, whereas serviceability limit states concern the normal use of the structure, see [5.3] for examples. For complex structures it is normally not feasible to solve the limit state function exactly, due to the excessive computation times required for the numerical integration. Typically these functions are solved by applying FORM (First Order Reliability Methods), which means approximation and simplification of the complex integrals involved. A commonly used presentation of the failure probability is the reliability index, β . The failure probability, P_F , and the reliability index are related through the standardised normal distribution, Φ , by

$$\beta = \Phi^{-1}(P_F)$$

5.1.3 Target Reliability's in Structural Design Codes

An extensive literature review has been performed with the aim to find target reliability's from different industries and different countries, see appendix A. It became obvious that, although most of the current design codes reviewed were using partial safety factors to a varying degree, and some also mentioned that these have been calibrated through probabilistic methods, but they are very reluctant to mention an explicit value for target reliability. Following is a summary of what was found

Target Values for System Reliability

In Ref. (A1.2) in appendix A it is stated that the unavailability of the safety system of a nuclear power plant shall be less than $1E-3$ to $1E-4$ per demand. In Ref. (A1.12) and (A1.13) in appendix A it is mentioned that the unavailability of the safety system of a wind turbine shall be less than $2E-4$ per demand.

Target Values for Structural Reliability

In order to be able to compare the different figures, we shall give all target values in the form of the safety index β . Furthermore we shall consider only the safety indices that correspond to the ultimate limit states and not to the serviceability limit states, since those will not result in a risk to the public.

Ref. (A1.1), Netherlands Building Codes:

Here the average safety level of the former Dutch building code was determined to arrive at a target reliability with which the partial safety factors of a new code were then calibrated. The result was an average β of 3.8, based on a reference period of 50 years.

Ref. (A1.3), NEN 6700:

This reference actually defines a target safety level. Thereby three Safety Classes, depending on the consequences in terms of personnel injury, are defined. The safety indices are given as 2.3, 2.4 and 2.6 resp. for the three safety classes for wind load and as 3.2, 3.4 and 3.6 for other loads. The indices are based on the service life of the structures.

Ref. (A1.5), NKB Nordic Committee for Building Regulations:

Here also three safety classes and a target reliability are defined, similar to the previous reference. The safety indices are given as 3.71, 4.26 and 4.75 for the three safety classes. The reference period is one year.

Ref. (A1.10), Eurocode 1:

This gives a yearly target reliability of 4.7, corresponding to the NKB safety class 'high'.

5.2 Partial safety coefficients

The target reliability level is a central concept for the partial coefficient method normally used for evaluating the safety and reliability of a structure. In this chapter we shall give a short review of the use of target reliability levels for calibrating partial coefficients in the partial coefficient method. A more comprehensive discussion was given in *European wind turbine standards*, EUR 16898, part 2 (1996). Here a short overview is given with a mind to bringing out the rationale in treating structural reliability in the context of probabilistic safety calculations. It should be remarked that in this section the mathematical symbols are chosen as normally used in structural reliability. This means that f denotes the resistance rather than a probability function.

5.2.1 The Limit State - Probabilistic Design Requirement

A key element of the reliability or safety evaluation for load carrying structures is the *limit state*. According to ISO 2394 [5.3], structural performance is defined by

The structural performance of a whole structure or part of it should be described with reference to a specified set of limit states beyond which the structure no longer satisfies the design requirements.

The specification of one particular limit state out of the set calls for the following definitions:

- *Failure type for limit state*
The failure type can be subdivided into different types of rupture, plastic deformations, loss of stability etc.
- *Cause of failure*
Failure may happen for different reasons, each of which requires a separate evaluation of safety, e.g.
 - *ultimate (extreme) load failure caused by extreme loads that only appear few times in the life time of a wind turbine (e.g. caused by a 50 yr. extreme wind speed)*
 - *fatigue induced failure caused by many repeated changes of loads, often mainly during normal operating conditions (e.g. every day power production, routine stops and starts)*
- *Design Requirement*
The purpose of design calculations or prototype testing is to keep the probability of a limit state being reached below a certain value prescribed for the type of structure in question (ISO 2394).

The probability of a limit state being reached is often called the failure probability, P_F , whereas the maximum allowed value, P_L , is typically defined as the complement of the target reliability, P_T . Thus the design requirement can be written as

$$P_F \leq P_L$$

or

$$P_F \leq 1 - P_T \tag{5.1}$$

5.2.2 Evaluating the failure probability

For the evaluation of the design requirement, a probabilistic formulation of the limit state condition is set up as follows. To describe the structure, a *set of stochastic basic variables*, X_n , is selected, including, e.g. its strength, stiffness, geometry, and (possibly several types of) loading. The n basic variables selected are grouped into one vector \mathbf{X} .

For the limit state under consideration, a so-called *limit state function* $g(\mathbf{X})$ (also called performance function or reliability function) is defined as a relation between the basic variables X_n with the following properties

$$g(\mathbf{X}) = \begin{cases} R > 0 & \text{for } \mathbf{X} \text{ in the safe set} \\ S = 0 & \text{for } \mathbf{X} \text{ on the limit state surface} \\ T < 0 & \text{for } \mathbf{X} \text{ in the failure set} \end{cases} \tag{5.2}$$

$g(\mathbf{X})=0$ can be seen as an equation determining the *limit state surface* in an n -dimensional space spanned by vectors, each vector corresponding to one of the basic variables.

The limit state surface in (5.2) separates the possible realisations of \mathbf{X} (i.e. the different value sets of X_1, X_2, \dots, X_n) into two sets; the set for which the structure will be safe, and the set for which the structure will fail.

The limit state surface can be seen as a sharply defined limit of safety in the sense that we can assume that, if the values of the basic variables were accurately known, an infinitesimal change of \mathbf{X} from the limit state surface into the failure region would mean assured failure. This is, however, an overly simplified mathematical abstraction. The basic variables are only known with a certain uncertainty, i.e. they are stochastic variables. Therefore we can not talk about assured failure or survival, but must evaluate the *probability of failure*.

Using the limit state function, (5.2), the probability of failure can be regarded as the probability that the limit state function takes on negative values and should be calculated as the probability of the system being in the failure set (the failure probability):

$$P_F = P[g(\mathbf{X}) \leq 0] = \int_{g(\mathbf{X}) \leq 0} f_{\mathbf{X}}(\mathbf{x}) d\mathbf{x} \tag{5.3}$$

where $f_{\mathbf{X}}(\mathbf{x})$ is the *joint probability density function* for \mathbf{X} . The integral extends over the part of the n -dimensional

space defined by the n basic variables, where $g(\mathbf{X}) < 0$.

The calculation of the probability of failure is in principle simple, in practice often very difficult. The difficulties are concerned with, e.g., picking the relevant basic variables, deciding on the distribution functions for these variables (the description of the low probability tails is important and complicated), doing the probabilistic integral in (5.3).

As the very simplest example with one load and one resistance variable, take $(X_1, X_2) = (F, f)$:

$$g(\mathbf{X}) \equiv f - F \tag{5.4}$$

F is the load variable, and f is the resistance variable. The variables are both stochastic variables which are characterised by their distribution functions (shown full drawn) in Fig. 5.1.

The distribution function shown at high loads is the strength distribution, at lower loads the load distribution. For both distributions the mean values are shown dashed. The 3rd dashed line between the two mean values the design value for both load and resistance, which are identical in the limit state. The two dotted lines are the so-called characteristic values, see next section, equation (5.5). The condition for failure according to (5.4) inserted in (5.2) is then $g(\mathbf{X}) = f - F < 0$ or $f < F$, i.e., resistance smaller than load. $g(\mathbf{X})$ can also be seen as a derived stochastic variable $Z = f - F$, often called the safety margin. The failure probability can then be found from the distribution function for this Z function, which is also shown in Fig. (5.1) as the dot-dash curve. In this simple case, where we assume that f and F are both normal distributions, it is simple to find the distribution of the difference, which will also be normal. The mean value will be the difference between the mean values of the two, and the variance will be the sum of the variances of the two elements.

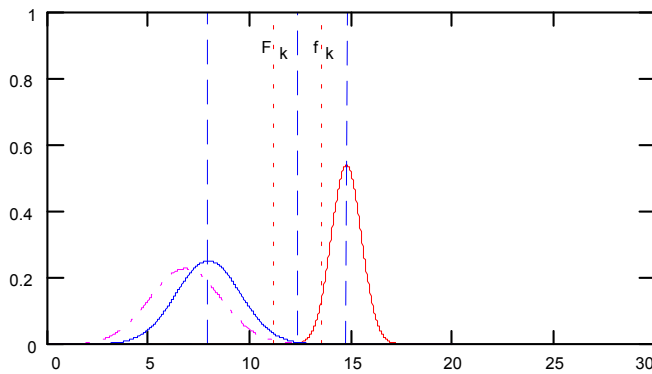


Figure 5.1 Distribution functions for load and resistance, probability per unit load vs. load.

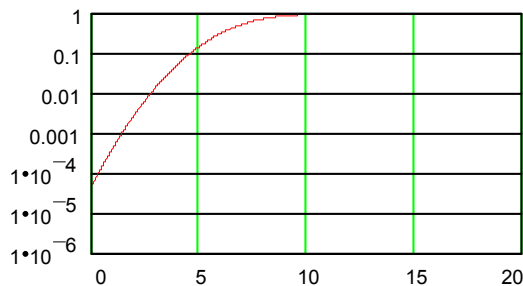


Figure 5.2 Safety margin distribution, cumulative and logarithmic.

Fig. 5.2 shows the cumulative distribution corresponding to the differential safety margin distribution in fig. 5.1.

The cumulative distribution gives the probability, that Z is less that the abscissa value, thus it is seen that $Z < 0$ with a probability of 0.00005 in the case illustrated.

5.2.3 Partial coefficient method

For practical design calculations, simple approximation methods have been developed, e.g. the partial coefficient method.

According to this method the design requirement for the limit state can in the very simplest cases be expressed by the *design inequality*

$$f_d = f_k / \gamma_m \geq F_k \gamma_f = F_d \quad (5.5)$$

f and F designate values of resistance and load, respectively, index k indicates characteristic values and index d design values. The γ 's are partial safety factors for load (γ_f) and for resistance (γ_m). Very simply stated the design inequality, (5.5), expresses that the design value of the resistance function of a component should be stronger than that of the load. The inequality (5.5) is turned into the *design equation* for the limit state by replacing the \geq -sign with =.

This design equation (5.5) is an approximate simplification of the basic limit state equation (5.2) in the simplest case with $g(\mathbf{X})$ defined as in (5.4).

The design equation in the partial coefficient method is constructed such that when used in a (broad) region of the variables, the target reliability is approximately obtained without doing the probabilistic calculations. The partial coefficients will typically be available from existing standards for structural safety.

In the partial coefficient method, the stochastic parameters are described by means of characteristic values. These values should be chosen as quantiles for the stochastic variables, resistance and load. Thus a typical characteristic value for resistance is a 5% quantile. The meaning of this characteristic value is that out of 100 samples produced, approximately 5 will not be as strong as indicated by the characteristic value.

The partial safety factors used in the design equation together with the chosen quantiles regulates the failure probability obtained through the use of the design equation. In 5.2.1 the characteristic values are shown. Also the design values derived by application of partial safety factors the characteristic values are shown. As the distributions are chosen such that the design equation is valid, the two design values merges into one as shown.

The simple equation (5.5) is often not sufficient. In building codes, e.g., one could wish to treat several loads which can interact

$$F_d = F_k / \gamma_m \geq f_{p,k} \gamma_{p,f} + f_{v,k} \gamma_{v,k} = f_d \quad (5.6)$$

Here it is assumed, that the two forces are a permanent force (e.g. gravity) and a variable force with their natural uncertainties. The statistical properties of these two forces are very different, but if they are well defined, the partial coefficients also serves to allow to add the characteristic values with suitable weights so that the combined action represents the statistical combination of the two different forces.

5.2.4 Calibration of partial coefficients

The calibration of partial coefficients basically is the process of deciding on the partial coefficients such that the target reliability wished is obtained. There are several ways to do that. For a probabilistic treatment, the process contains a calculation of the failure probability, and adjusting the partial coefficients so that the wanted target reliability is found. In Fig. 5.3 such a calibration is illustrated using the equation

$$P_f = \int_0^{\infty} (1 - \Phi_f(x)) \cdot \varphi_F(x) dx \quad (5.7)$$

Here the probability of failure is calculated as follows. A failure could happen at any value of the resistance x , if the load happens to get larger than x . The probability of the resistance being around x if $\varphi_F(x)dx$. The probability that the load surpasses can be found from the cumulative strength distribution $(1 - \Phi_f(x))$. Multiplying these two probabilities the probability of a certain value of the resistance combined with the load surpassing the resistance is obtained. Integrating this product over x gives the wanted failure probability. In each figure in Fig. 5.3 the resistance

distribution and the cumulative load distribution are shown full-drawn. Their characteristic values are shown dotted as is the integrand of (5.7).

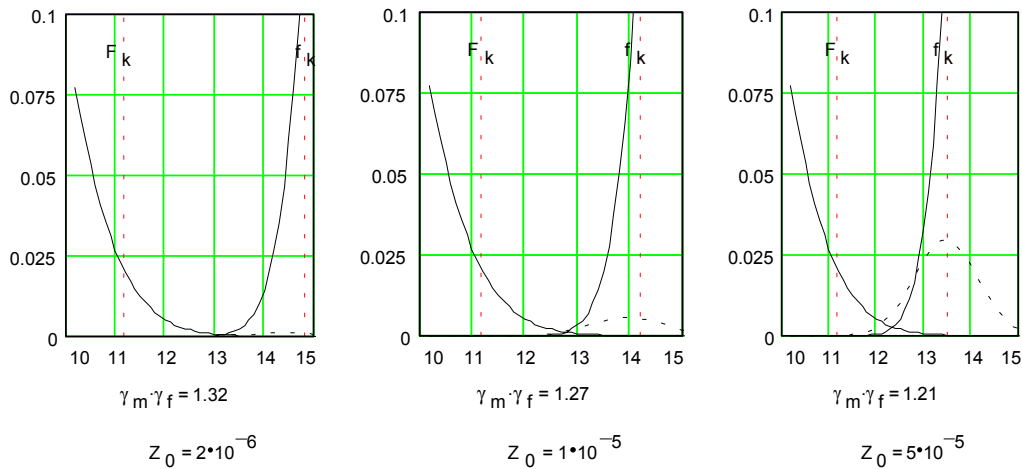


Figure 5.3 Illustration of the effect of decreasing the partial coefficients.

The product of the partial coefficients is varied (decreased) by 5% for each figure. The failure probability ($P[Z < 0] = z_0$) was calculated in each case. If a target reliability corresponding to a failure probability (P_L) of $1 \cdot 10^{-5}$ is prescribed, the centre situation in Fig. 5.3 is the result.

5.2.5 Target reliability and probabilistic safety calculations

It should be stressed that it is often said in codes that the failure probability we have talked about here is only a formal mathematical abstraction. This is mainly because of the many difficulties and approximations involved in the calibration process, but also because the limit state concept is specifically developed for use in structural reliability. Often a structural failure can happen in many ways, that all have to be considered. This should, however, not prevent us from using the concept also in our probabilistic safety analyses.

This has two reasons. First, a structural failure can very well be imagined as initiating event before a major accident. Secondly, the process that leads us to using the probabilistic concepts in structural reliability analysis is so clearly geared towards calculating the probability of failure, that there seems to be no other way. Therefore the amalgamation of structural failure probability and other probabilistic safety calculations is absolutely natural, as long as the necessary caution in using the structural failure concept is shown. It is, however, deemed to be outside reach in this project to go into further examination of the peculiar problems when amalgamating these fields.

6. RISK CRITERIA AND RISK TARGET VALUES

The safety of a construction operating within the design limits can be checked by means of design codes. However, situations might occur such that the construction is operating beyond the design limits. This can be caused by the failure of the safety system or by loadings not foreseen in the design. Ultimately, this may lead to catastrophic failures like blade rupture which can cause risks to the public. Such risks are of great interest for, e.g., authorities, especially in densely populated areas. To judge whether a risk is acceptable limits have to be indicated above which the risks become unacceptable (maximum permissible levels).

Section 6.1 provides recommendations for risk criteria and risk targets to be used for wind turbines. Such risks are calculated for, e.g., an Environmental Impact Statement (in Dutch: MER) of a wind turbine park. These risk figures can also be used in the design phase of a wind turbine, e.g., to assess whether the conditional probability of a catastrophic blade failure in an accidental situation is acceptable or not.

In addition, Section 6.2 summarises a simple mortality rate calculation made on request of the EWTS Project Steering Committee (PSC). This calculated mortality rate can be used for comparison purposes with mortality rates observed in other branches of industry and from other activities.

6.1 Recommendations for risk criteria and risk target values to be used for wind turbines

Various sources of literature on risks and risk criteria have been reviewed. Appendix A presents a list of references followed by a brief summary of each of them. This material formed the basis for the EWTS-II sub 2 project group to draw conclusions on risk criteria and risk target values to be used for wind turbines.

Risk Criteria

Risk criteria applicable for wind turbines are the individual risk and the group risk (as defined in the official Dutch premises for risk management [6.1]). The risk limits for these two criteria as used in the Netherlands are rather stringent. To our knowledge, there is no other country that adheres to such strict limits. In some countries, similar criteria are used, but the levels are set higher and they are also mere target levels. An example is the United Kingdom [6.2].

Risk Target Values

We recommend the use of the individual risk with a risk target level of 10^{-5} /year (which is 10 times higher than the Dutch risk limit of 10^{-6} /year, see Fig. 6.1). The individual risk is independent of the site of the wind turbine (park) and can be calculated without knowing the exact location of the installation. Note that we do not use the term 'risk limit'; we prefer to use the term 'risk target', because risk limits are not commonly used in all EU countries.

The individual risk can be used for design purposes. Suppose we have a generic value of 10^{-3} - 10^{-2} /year for blade failure frequency. Then the conditional probability of being lethally hit by such a failed blade (part) thrown away should be less than 10^{-2} (10^{-3} failure frequency) or than 10^{-3} (10^{-2} failure frequency) in order to get below the risk target for individual risk. This is based on the assumption that the combined effect of more than one wind turbine at the same site is negligible. In practice, this may not always be the case.

Studies¹ performed by ECN as support of an Environmental Impact Statement (in Dutch: MER) indicate that the conditional probability mentioned above is not higher than about 10^{-4} based on a modern 500 kWe wind turbine design.

Although the limits for group risk in The Netherlands are rather stringent, we do not foresee problems of any wind turbine not complying with the limit for group risk as defined in the Netherlands. Hence, the target values recommended for the group risk is equal to the Dutch risk limits. The target value is that the likelihood of an

¹ Unfortunately, these risk studies are confidential and contain proprietary information. Therefore, no references are given.

accident with 10 deaths occurring should not exceed one in every hundred thousand years (10^{-5} /year). The aim of setting target values for group risk is to prevent social disruption (the death of a group of people all at once). Accidents with even more serious consequences lead to correspondingly greater degrees of disruption. It is therefore assumed that an n -times larger impact than 10 deaths should correspond with an n -squared smaller probability of such an accident occurring (see Fig. 6.2, so-called f - n curve). The actual group risk is expressed as a so-called Complementary Cumulative Distribution Function (CCDF).

Although accident scenarios can be thought of in which a group of people can be killed (e.g., a bus with 30 people is hit by a blade and subsequently drives into the Noordhollands Canal and 20 people are drowned; however, such a group is not within the definition of the Dutch group risk), we do not anticipate any problems with compliance with the group risk. The probability of such scenarios seem negligible (but needs additional investigation).

The project group could not reach a conclusion on whether the risk criteria and target values should be used for an individual turbine, or, for a park as well. This remains an open item.

6.2 Example mortality rate calculation for wind turbines

In the Netherlands, a number of risk studies for wind turbine parks have been performed (e.g., by ECN). These risk studies indicated that the acceptable limit (of 10^{-6} /year) for individual risk (as defined in the Netherlands) may be exceeded. It should be noted that the results of such studies depend strongly on the specific wind turbine design, the site of the park and the population in the vicinity of the parks into account.

When we relate this risk to a given population (e.g., all wind turbines in operation in the Netherlands), the risk of each individual wind turbine can be combined to calculate the mortality rate. This rate is defined as the number of deaths per year (due to a specified activity) for a given population. The Dutch premises for risk management [6.1] present a table of such observed mortality rates in the Netherlands, see Table 6.1.

The PSC of the EWTS-II project asked for a generic type of mortality rate calculation for the total number of wind turbines in the Netherlands and to take the type of population in the vicinity of the parks into account. This mortality rate could then also be compared with mortality rates of other activities (e.g., as displayed in Table 6.1).

Given the available resources in this project (and because this calculation was not part of the original work programme), such calculation could only be generic and guided by simplifying assumptions. Appendix B presents the details of these assumptions and of the calculational procedure.

Table 6.1 Annual mortality rate associated with certain occurrences and activities in the Netherlands ([6.1])

Activity/Occurrence	Annual mortality rate	
Drowning as a result of a dike collapse	10^{-7}	1 in 10 million
Bee sting	$2 \cdot 10^{-7}$	1 in 5.5 million
Being struck by lightning	$5 \cdot 10^{-7}$	1 in 2 million
Flying	$1.2 \cdot 10^{-6}$	1 in 814,000
Walking	$1.85 \cdot 10^{-5}$	1 in 54,000
Cycling	$3.85 \cdot 10^{-5}$	1 in 26,000
Driving a car	$1.75 \cdot 10^{-4}$	1 in 5,700
Riding a moped	$2 \cdot 10^{-4}$	1 in 5,000
Riding a motorcycle	$1 \cdot 10^{-3}$	1 in 1,000
Smoking cigarettes (1 packet a day)	$5 \cdot 10^{-3}$	1 in 200

Table 6.2 presents the results of the calculations (spreadsheet). The most conservative calculation results in $2E-4$ /yr, which is comparable to riding a moped (Sens. 1). A more realistic value seems $1.2E-6$ /yr, which is comparable to flying (Sens. 6). The last value seems still larger than the actual fatality statistics. To our knowledge, not a single person (from the public, not personnel) has ever been killed by a electricity-generating wind turbine. Many people have been killed as a result of flying. We expect that a realistically calculated value would be of the order of the mortality rate due to being struck by lightning ($1E-7$ /yr).

Conclusion

Although based on rather simplified assumptions (mainly conservative ones) and a simple calculational procedure, a 'best-estimate' of the mortality rate in the Netherlands due to an overspeed accident and consequential blade failure is of the order of the mortality rate of being struck by lightning.

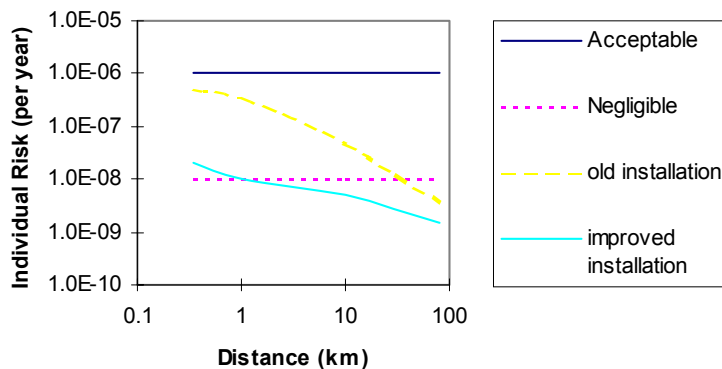


Figure 6.1 Example of individual risk limit and result for an installation

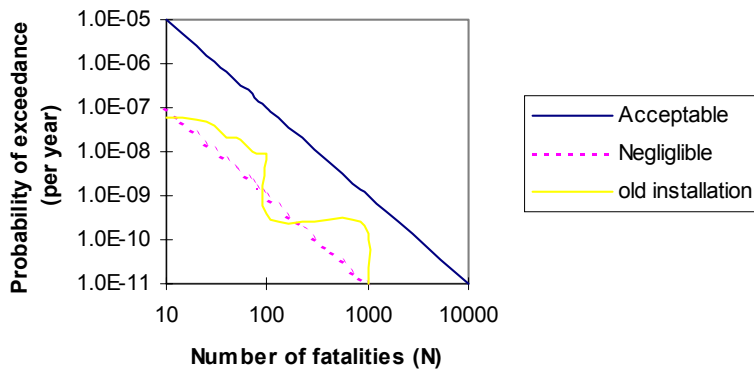


Figure 6.2 Example of group risk limits and a CCDF for an installation

Table 6.2 Results of example mortality rate calculations for wind turbines in the Netherlands

Example Mortality Rate Calculation EWTS-Ilsub2 74228.01.12							
(Assumptions given in accompanying text)							
	Base Case	Sens. 1	Sens. 2	Sens. 3	Sens. 4	Sens. 5	Sens. 6
Parameter description/Value Calculated		High BFF (Most conservative)	Medium EF	Low EF	High BFF, Medium EF	High BFF, Medium EF	Medium BFF, Low EF (most realistic)
Blade failure frequency (BFF)	1.0E-03	5.0E-03	1.0E-03	1.0E-03	5.0E-03	5.0E-03	3.0E-03
Max. conditional probability of being hit assuming 24 hour exposure (MCP - 1m)	1.0E-04	1.0E-04	1.0E-04	1.0E-04	1.0E-04	1.0E-04	1.0E-04
Exposure fraction (EF)	1.00	1.00	0.33	0.01	0.33	0.33	0.01
Number of wind turbines (NWTB)	400	400	400	400	400	400	400
<i>Dutch IR per WTB</i>	1.0E-07	5.0E-07	3.3E-08	1.0E-09	1.7E-07	1.7E-07	3.0E-09
<i>MR for all sites</i>	4.0E-05	2.0E-04	1.3E-05	4.0E-07	6.6E-05	6.6E-05	1.2E-06
Note: exposure fraction can also be used as measure for 'rare' situations, e.g., a group visit to the WTB							

7. DATA COLLECTION AND PARAMETER ESTIMATION

7.1 Introduction²

The practices (guidelines) from the previous EWTS subproject were not applied in the case study (excluded from the scope). These guidelines were:

Recommended Practices from EWTS subproject 'Assessment of Wind Turbine Safety'

1. For initial quantification purposes, generic data/engineering judgement should be used (order of magnitude values). Specific wind turbine failure data should be collected and used in the next phases if the scope of the study or the preliminary results ask for more detailed and more accurate data.
2. The analyst should provide a discussion why certain data is valid for the specific design.
3. The analyst should provide the procedure how key failure data is derived from the data used. This includes both the methodology and the actual calculations.

It is the objective of the current EWTS subproject to apply these guidelines to the same case, learn from the experience, and update or extend the guidelines.

Data collection and parameter estimation process

Data are necessary to feed the quantification process. The steps of the data collection and parameter estimation are outlined in Fig. 7.1 (based on [7.2]).

For safety and reliability purposes, the following types of data have to be collected:

- *maintenance and failure data*, which includes not only periodical maintenance and inspection but also failure and incident registration (unplanned maintenance). Examples are the instances of the events, possible causes, conditions under which events take place, detection and restoration times, affected components, performed actions, etc.;
- *wind turbine modes data*, which includes the times and duration the wind turbine is in a certain operational mode, and the frequencies of alarm signals and transitional modes; and
- *external conditions* under which events take place, mainly data concerning the wind but also other climatological data and grid behaviour.

² The material in this chapter is largely based on the the previous EWTS subproject 'Assessment of Wind Turbine Safety' [7.1] and the ECN Study [7.2] (Chapter 5 and appendix A that deals with the systematic collection and analysis of operational and failure data of wind turbines). For completeness and to be self-contained, some of the material is repeated here. More details can be found in, e.g., [7.2, 7.3].

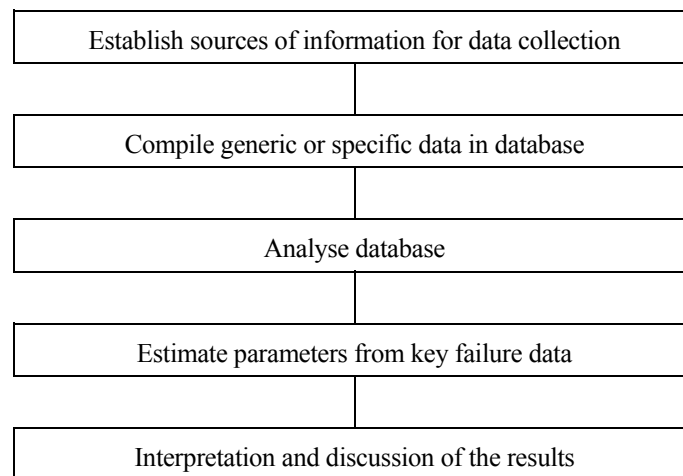


Figure 7.1 Steps in the Data Collection and Parameter Estimation Process

The above mentioned types of data originate from various sources, e.g., *design specific sources* like failure registration forms of the manufacturer, maintenance sheets, monitoring systems, logbooks, and the owner's operating experiences. Since collecting wind turbine data for quantification purposes is at present not common practice, many data have to be derived from *generic sources*, which may be from the wind turbine industry, or from other industries.

The next section discusses briefly the collection of design specific data and parameter estimation.

Section 7.3 presents an overview of generic wind turbine databases and of generic data on external conditions (e.g., grid loss and lightning).

Section 7.4. gives an overview of generic databases from other industries or contained in reliability handbooks.

Finally, Section 7.5 summarises the guidelines.

7.2 Design specific failure data

Details of the collection of design specific failure data and parameter estimation can be found in [7.2] and [7.3]. In particular, the recommendations set out in [7.2.] can be used as guidelines for design specific failure data. These will not be repeated here. In addition, there is sufficient literature (in the form a reliability handbooks) on this topic. The recommendations set out in [7.2] and [7.3] can be used for design specific data collection and parameter estimation.

7.3 Generic wind turbine failure data

Some attempts have been made to collect wind turbine data on a national or even European level, e.g., WindStats in Denmark, the EUROWIN database, the database on accidents and incidents, and the EPRI database, see the Table 7.1. Unfortunately, the information that can be derived from these generic wind turbine databases often appear to be of very limited use for quantification. Details like failure causes, effects and external conditions are missing. In addition, only main components are included.

Table 7.1 Examples of generic wind turbine failure databases

Database	Year	Industry	Reference
EUROWIN	1991	Wind	Schmid, J., and Klein, H.P: 'Performance of European Wind Turbines - A Statistical Evaluation from the European Wind Turbine Database EUROWIN', Fraunhofer Institute for Solar Energy Systems, Freiburg, July 1991.
Accidents and Incidents	1990	Wind	W.J. Stam, et al.: 'Collection of Data on Accidents and Incidents of Wind Turbines for Updating of Safety Criteria', ECN-C--90-017, May 1990.
EPRI	1989	Wind	Electric Power Research Institute: 'Assessment of Wind Power Station Performance and Reliability', EPRI GS-6256, Project 1590-10, Final Report, March 1989.
Windstats	-	Wind	WindStats Newsletter, Spring 1992, Vol. 5, No. 2, ISSN-0903-5648 WindStats Newsletter: Vrinners Hoved, Dk-8420 Knebel, Denmark, or: PO Box 496007, Ste 2170, Redding, California 96099-6007, USA.

External Conditions

Some information was received from ISET who report results of the German '250 MW Wind' Programme [7.4] .

a. General Downtime

The following data is from an earlier report on the 250 MW Project [7.5]. All participants in the program have to report downtimes due to maintenance and due to failures. The report must contain the reason for the downtime and the length and cost of the necessary repair work.

More than 800 wind turbines were included in this study, of which 43% were located in the coastal region, 36% were located in the northern lowlands and 21% were located in the mountain areas of central Germany. The following table is the result of this study:

Region	Grid loss	Lightning	Ice	Storm
Coast (43%)	69%	22%	16%	24%
N. Germ (36%)	8%	21%	19%	29%
Mount. (21%)	23%	57%	65%	47%

This shows that in the mountain areas failures due to lightning and ice are 2 to 4 times more often than in the other areas. The high proportion of grid losses in the coastal areas is due to the high density of wind turbines, so that many turbines are affected if part of the grid is lost.

b. Failure Cause Lightning Strikes

Ref. [7.4] and is based on 393 reports from 1992 to 1995, 269 indirect strikes and 124 direct strikes were reported. The wind turbine locations were the same as before.

	Coast	Lowlands	Highlands	Total
No. of WECS	605	531	335	1471
Oper. time (a)	1827	1445	786	4058
No. Events	116	110	167	393
Direct Strikes	43	33	48	124
Events per WECS Year	6%	8%	21%	10%
Direct Strikes per WECS Year	2.4%	2.3%	6.1%	3.1%

This shows that lightning strikes are about three times more likely for turbines in mountain areas due to the higher frequency of thunder storms there. A map published by the German weather service indicates less than 20 thunderstorms per year for coastal regions and 20 to 35 for mountainous regions. Most thunderstorms occur in the period from May to September.

Mean repair costs for all direct lightning strikes were DM 50000 to DM 60000. If all three rotor blades were damaged, they did amount to more than DM 100000.

7.4 Generic Failure Data from Other Industries

This section presents an overview of some generic databases outside the wind turbine industry. Such generic databases may be the only available source of information. In general, these sources provide more details than the generic wind turbine databases.

The overview as displayed in the next table lists publicly available generic databases, based on a review of [7.6], [7.7], [7.8]. Most of these sources are in the form of a report. Some of them may also be available as a computerised database.

Case studies by ECN indicate that such generic sources can be used, certainly to obtain order of magnitude numbers for failure rates for generic categories of component and failure modes. Also, some sources provide error factors for these numbers. However, the use of engineering judgement is often involved in combining data from different sources and in declaring generic data valid to be used for a specific design.

Table 7.2 : Overview of generic reliability databases from other industries

Database	Year	Industry	Reference
Engineering Reliability	1959	Aerospace	Procedure and Data for Estimating Reliability and Maintainability, Engineering Reliability, Martin, M-M-P-59-21, 1959
Reliability Technology	1972	All	Green, A.E. and Bourne, A.J.: Reliability Technology, Wiley, London, 1972
WASH-1400	1974	Nuclear	
IEEE Std 500-1984	1984	Nuclear	IEEE, IEEE Guide to the Collection and Presentation of Electrical, Electronic, Sensing Component, and Mechanical Equipment Reliability Data for Nuclear-Power Generating Stations, IEEE Std 500-1984, IEEE, Inc., New York, 1983.
IAEA-TECDOC-478	1988	Nuclear	IAEA: Component Reliability Data for Use in Probabilistic Safety Assessment, IAEA-TECDOC-478, Vienna, 1998
Davidson	1988		J. Davidson (ed.): The Reliability of Mechanical Systems, The Institution of Mechanical Engineers, 1988.
American Institute of Chemical Engineers	1989	Chemical	Guidelines for Process Equipment Reliability Data, Center for Chemical Process Safety of the American Institute of Chemical Engineers, New York, 1989

Table 7.2 : Overview of generic reliability databases from other industries

MIL-HDBK-217F	1991	Military	Military Handbook: reliability prediction of electronic equipment, MIL-HDBK-217F, Griffiss Air Force Base, Rome, New York, 1991
EIRADA	1991	All	European Industry Reliability Data Handbook, CEC-JRC/ISEI 21020, Ispra (Varese) Italy, EDF - DER/SPT 93206 Saint Denis (Paris), France, 1991
RAC	1991	Military	Reliability Analysis Center: 'Nonelectronic Parts Reliability Data 1991', RAC, P.O.Box 4700, Rome, NY 13440-8200, 1991.
T-Book	1995	Nuclear	T-book, reliability of components in Nordic Nuclear Power Plants, 4rd edition, 1995
OREDA	1992	Offshore	OREDA Participation Offshore Reliability Data, OREDA-92, P.O.Box DNV Technica, N-1322, Hovik, Norway, 1992 OREDA, Guideline for Data Collection, 6 th edition, prepared by SINTEF on behalf of OREDA, 1995 H.A. Sandtorv: Practical experiences with a data collection project: the OREDA project. <i>Reliability Engineering and System Safety</i> 51 (1996) 159-167.

7.5 Summary of Guidelines

The recommended practices from the EWTS-I project can be extended by the following, more detailed guidelines:

- 1 The recommendations set out in [7.2] and [7.3] can be used for design of specific data collection and parameter estimation. Also, recommendations in [7.2] on the use of generic data are still valid.
- 2 Preferably, use should be made of standard, proven methods as laid down in reliability handbooks. Preferably, computerised versions of (generic) databases and existing software for reliability data analysis should be used.
- 3 Generic wind turbine data sources can be used if no specific data is available or if there are no time or resources available to collect design specific data.
- 4 Generic wind turbine data sources can be used to provide data on a high level, e.g., an estimate of blade failure frequency to be used in risk studies, or for frequencies of certain initiating events, e.g., grid loss.
- 5 If generic data is used to estimate a particular parameter (e.g., a failure rate), the following should be clearly documented for each parameter estimated:
 - *reference(s) to the source(s) used;*
 - *discussion why the source is considered valid or why the source is used;*
 - *the calculation procedure to arrive at the final estimate if multiple sources are used.*
- 6 If engineering judgement is used to provide an estimate, the reason for this should be indicated. Engineering judgement should be used to provide an estimate if design specific or generic sources do not provide an adequate answer.

8. QUANTIFICATION OF MODELS (BENCHMARK STUDY)

This chapter summarises the results of the benchmark study. It was used to support the development of guidelines for the collection of data and for the estimation of parameters, to be used for quantitative safety and reliability analyses of wind turbines.

8.1 Outline of Benchmark

The preliminary guidelines set out in Chapter 7 were finalised and extended on the basis of the benchmark results. The benchmark case consisted of a model of a hypothetical design, as defined and used in a previous EWTS-I subproject ‘Assessment of Wind Turbine Safety: Recommended Practices’ [8.1]. The model includes only one initiating event potentially leading to (catastrophic) overspeed of the wind turbine. The accident sequences were modelled with 3 event trees, 4 fault trees, and about 30 component failure modes (so-called basic events).

Two of the three partners in the subproject, ECN and Risø, participated in the benchmark. The benchmark exercise was performed following the next steps:

- formulate preliminary guidelines;
- define the benchmark PSA model and establish the types of data to be collected;
- first iteration: collect data independently and quantify model;
- compare results and explain differences in quantification results;
- second iteration: adjust data after having removed misunderstandings and unrealistic data, and re-quantify model;
- calculate importance measures and rank the component failure modes;
- learn from the benchmark results and finalise guidelines.

The necessity of the second iteration clearly demonstrated the difficulties in the quantification even with the same model available to the participants (e.g., also observed in [8.7]).

8.2 Benchmark results

Preliminary guidelines

Based on previous ECN case studies and experience [8.2-8.6], preliminary guidelines were formulated prior to collecting data and estimating parameters. The guidelines covered:

- the list of basic events for which to collect data;
- a list of failure mode types based on event tree/fault tree analysis software used (NUPRA [8.8]);
- depending on the failure mode selected, a list of parameters to be collected (e.g., failure rates, time factors);
- reporting formats to submit the data.

Appendix C presents the final guidelines. The relationship of the data to be collected, their sources, and the parameters to be estimated is displayed in Figure 8.1.

The guidelines were restricted to the use of generic sources of data (e.g., from literature).

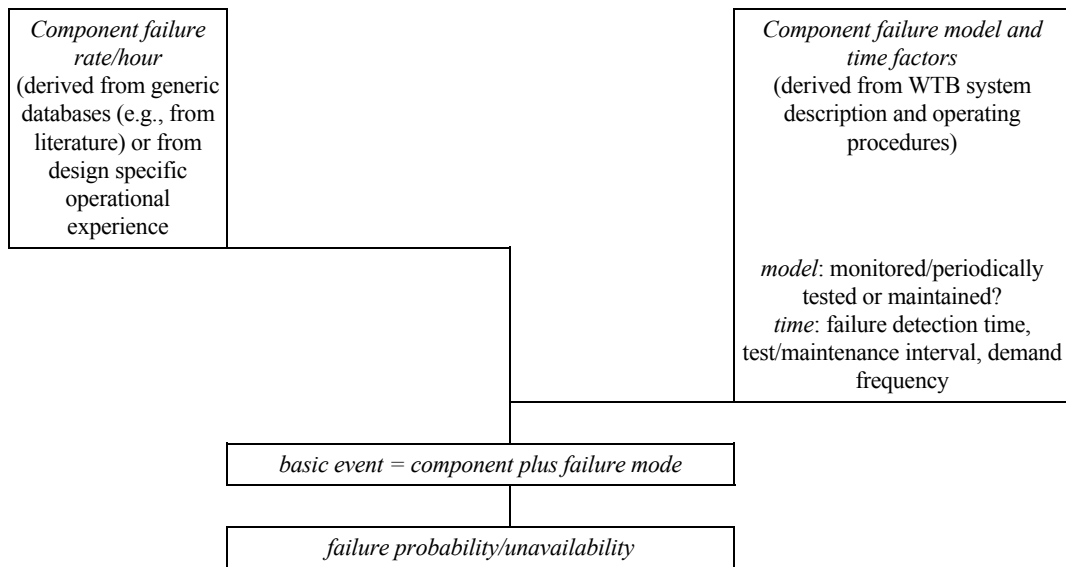


Figure 8.1 Relationship between data to be collected, data sources and parameters to be estimated

Model and data to be collected

The case concerns a hypothetical design but with similar characteristics to the AOC 15/50 turbine [8.2]. It was selected because it was previously used in the EWTS-I project [8.1]. As a result, the qualitative part of the case was documented extensively. The case model consisted of only one initiating event potentially leading to (catastrophic) overspeed of the wind turbine. The accident sequences were modelled with 3 event trees, 4 fault trees, and about 30 component failure modes (so-called basic events).

The first event tree described the event sequences emerging from the initiating event (Too high an inverter temperature). Some of the sequences transferred into two other event trees which were developed for a fast shutdown and an overspeed situation. The last one is presented in Figure 8.2. Note that the frequencies of the sequences are not simply the product of the nonavailabilities/failure probabilities of the individual events displayed in the heading of the event tree, e.g., see sequence S05. The product equals $1.07e-8$ ($2.02e-5 * 2.83e-2 * 2.49e-2 * 7.55e-1$), while the frequency of SEQ S05 equals $2.01e-5$. This shows how the fault tree linking approach takes account of the intersystem dependencies and of events already failed.

Fault trees were made for the Detection System, Tip Brake System, Mechanical Brake System, and the Generator Disconnection. The actuation/operation of these systems follow more or less the chronology of the various events.

From the various end states of these sequences, only the end state ‘Catastrophic overspeed’ was selected for this benchmark exercise. Other end states (e.g., failed operation without any safety implications or successful shutdowns) were not investigated further.

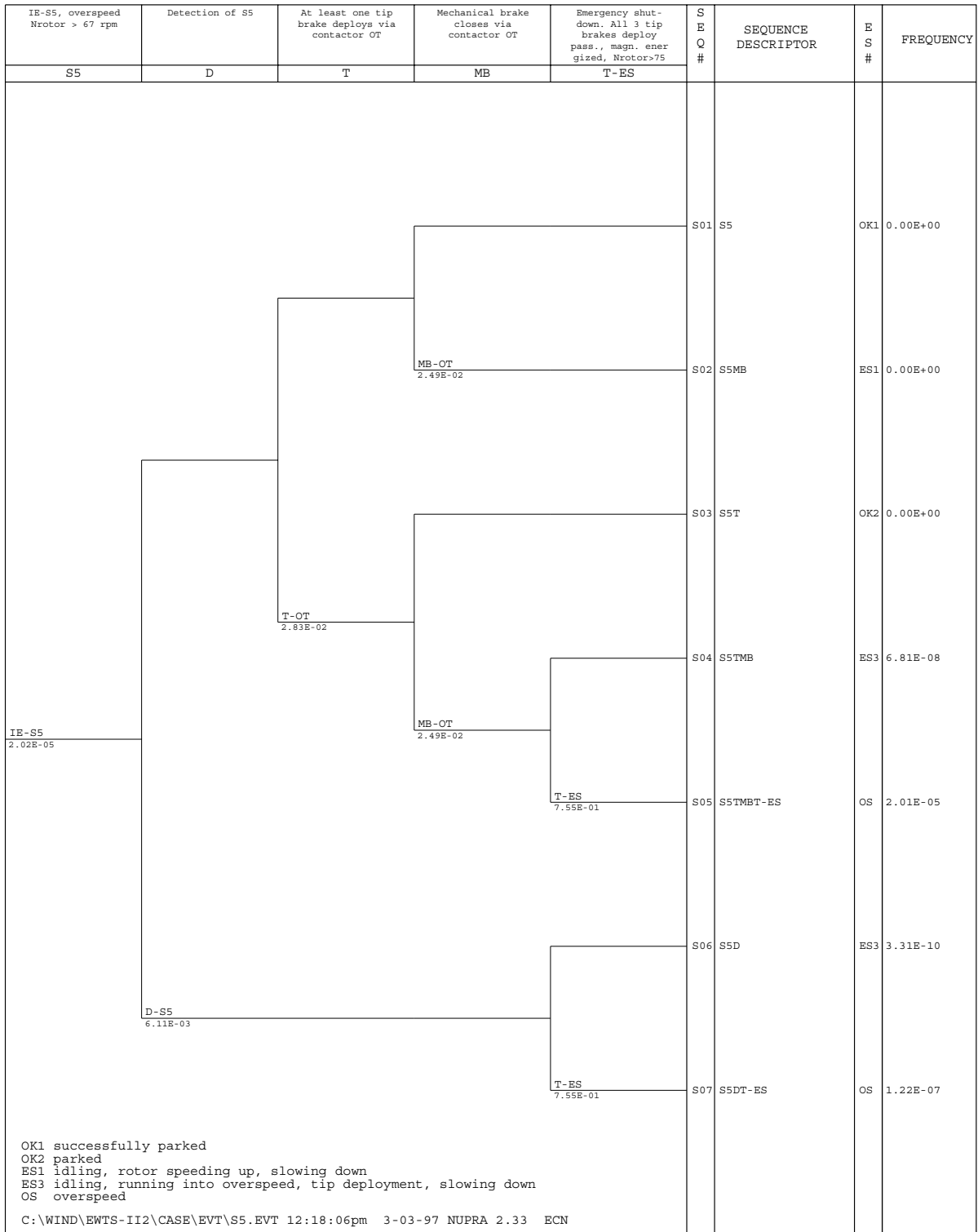


Figure 8.2 Event tree depicting sequences leading to overspeed

First data collection, parameter estimation, and quantification

The sources were restricted to generic data (generic wind turbine data as well as average data from other types of industry). It should be noted that design specific data are normally the preferred source of data. However, specific data are often not available or only at the Expense or too much time and resources. Moreover, the case model concerns a hypothetical turbine for which of course no specific data is available.

ECN and Risø started a first iteration with the same set of documentation on the system description (as laid down in [8.1]), and with the same preliminary guidelines. This resulted in two data sets comprising for each basic event: component failure model (e.g., periodically tested, monitored i.e. self-annunciating failures), failure rate, time factors (e.g., test intervals, detection time) and some rationale on how the data was derived.

Comparison of first results

ECN used a combination of generic wind turbine data (from previous ECN safety and reliability studies on wind turbines, e.g., LW 15/75, AOC 15/50, NEWECS45), industry average data (as collected and used in a recent ECN reliability study of the NEDWIND40), and engineering judgement. Risø used one commercial reliability database (FARADIP.THREE), data of one 150 kW wind turbine of Nordic design, and engineering judgement.

Direct comparison of the two data sets revealed large differences, which showed up more strikingly after quantification of the model. The resulting frequency of occurrence of overspeed, OS Freq, and the conditional probability of overspeed (given the occurrence of the initiating event), Cond. Prob., differed by more than four orders of magnitude (see Table 8.1), while the failure rates differed no more than one to two orders of magnitude. The results of Risø seemed to be unrealistically low, in particularly when looking at the resulting conditional probability of overspeed and the common cause failure involved.

Table 8.1 Overall results, first and second iteration: frequencies of the initiating event (IEF) and of overspeed (OS) and conditional probability of overspeed given the initiating event

	First iteration			Second iteration		
	IEF [/yr]	OS Freq [/yr]	Cond. Prob. [-]	IEF [/yr]	OS Freq [/yr]	Cond. Prob. [-]
ECN	3.8 e-2	2.0 e-5	5.3 e-4	3.8 e-2	2.0 e-5	5.3 e-4
Risø	8.4 e-6	7.1 e-15	8.5 e-10	3.1 e-3	8.3 e-8	2.7 e-5
Factor ECN/Risø	4.5 e+3	2.8 e+9	6.3 e+5	12	242	20

The differences in data were explained by the following factors:

1. Initiating event frequency.
The initiating event frequency (IEF) was about 4500 times higher in the ECN case (ECN: 3.8e-2; Risø 8.4e-6), which directly affects the frequency of a catastrophic overspeed (OS Freq).
2. Failure rates.
In general, ECN used higher failure rates resulting in higher nonavailabilities (one to two orders of magnitude higher).
3. Failure model.
ECN used mostly a periodically tested component model, except for the CPU and the initiating event (IE-S7), with intervals of 730, 1750 or 8760 hours. Risø used mostly a monitored component model, with a detection/repair time of 24 hours. This had a great impact on the resulting nonavailabilities (ECN higher than Risø). There was probably a difference in the understanding of the wind turbine system operation, although the same information was used.
4. Time factors.
ECN took the demand frequency into account resulting in smaller intervals than one year for the periodically tested components (and hence smaller nonavailabilities). However, the effects of using higher failure rates (see 2.) and other failure models were larger.
5. Common Cause Failure (CCF).
The CCF unavailability of the tip brakes was very small in the Risø case (three orders of magnitude smaller than

the corresponding independent failure modes), which might be too different from reality. Risø had modelled a functional dependency, viz. loss of grid, as common cause. If sufficient details were available, such dependent failures should however be modelled in the logic of the fault trees, not at the basic event level. ECN used a so-called 'beta factor' of 0.1, based on engineering judgement and because such value is considered relatively conservative, according to the reliability literature. This means that 10 % of the failures involve a (residual) common cause.

Adjustment of Risø data and re-quantification

After having explained the differences, the Risø data were adjusted. Basically, only the failure models and time factors were changed. The full details of the fault tree analysis software was not available to Risø. Because of that, some difficulties with understanding the different meanings of failure models were encountered. In addition, the CCF failure rate was adjusted.

Comparison of second results and calculation of importance measures

With the new Risø data, the overall ECN and Risø results appeared to be better in agreement, see Table 8.1. The differences in results were less significant, e.g., the conditional probability differed by a factor 20 (in stead of $6e+5$ in the first iteration). The still persisting differences were within the line of expectation, since ECN and Risø used different (generic) data sources. If (the same) design specific operational experience was used as data source, the results would certainly be very close.

The new results were considered suitable to compare also the relative, qualitative results, as expressed in the importance measures, e.g., of the component failure modes contributing to the overspeed frequency.

The importance's are displayed in Table 8.2 for the component failure modes contributing 1% or more to the end state 'Catastrophic overspeed'. The columns 'Relative Importance' (The relative importance of the component failure mode as contributing to the frequency of catastrophic overspeed) and 'Rank' are the ones which are interesting. In both cases, the Tip Brake (TB) and Mechanical Brake (MB) systems appeared to be very important. The Electrical System (EL) is relatively unimportant. The CCF of the Tip Brakes was important in both cases (ranked 1 and 2, respectively). Broken down to the individual components or even failure modes, there were still some differences between the ECN and Risø results.

These were explained by two factors:

1. in general, ECN used higher failure rates, which lead to higher component nonavailabilities;
2. in general, ECN used smaller test/maintenance intervals by taking into account the average demand frequency of certain standby components, in case this frequency is higher than the usual test/maintenance frequency: this lead to lower component nonavailabilities.

The effect of 1. appeared to be more important than the effect of 2.

Lessons learned from the exercise and final guidelines

Additional guidelines were formulated in order to prevent the misunderstandings observed in the first iteration of the exercise. The lessons learned were used to adjust the preliminary guidelines set out before. In particular, additional guidance was given on the selection of failure model and associated time factors.

Table 8.2 Ranking of the most component failure modes (based on second iteration)

System, component failure mode	ECN			Risø		
	Unavaila- bility	Relative Importance	Rank	Unavaila- bility	Relative Importance	Rank
MB, cylinder stuck	1.9e-2	79%	1	6.1e-4	20%	2
TB, common cause failure	1.1e-2	41%	2	8.7e-3	96%	1
TB, hinge 1/2/3	8.3e-2	19%	3	1.6e-2	1%	6
TB, damper 1/2/3	8.3e-2	19%	3	4.4e-3	0%	9
TB, catch plate 1/2/3	8.3e-2	19%	3	1.5e-2	1%	7
MB, spring loss of function	4.5e-3	19%	4	6.1e-4	20%	2
MB, valve Y2 stuck	1.3e-2	1%	5	3.1e-3	1%	4
EL, contactor KM fails to open	3.6e-4	1%	6	3.1e-3	4%	3
MB, throttle valve blocked	1.3e-2	1%	7	1.2e-2	1%	5
MB, valve Y1 stuck	1.3e-2	1%	7	3.1e-3	0%	8
MB, filter unit blocked	7.3e-6	0%	8	6.1e-4	20%	2
MB, disk fracture	7.3e-6	0%	8	6.1e-4	20%	2
MB, brake pad wear out	7.3e-6	0%	8	6.1e-4	20%	2

8.3 Conclusions and recommendations

The following is concluded from the benchmark study:

- The main differences in the results after the first iteration of the data collection and parameter estimation were caused by different understanding of the system operation. E.g., this resulted in the assignment of different failure models and associated time factors for the basic events. Therefore, the guidelines were extended such that the analyst will make less mistakes in assigning either a monitored or periodically tested failure model, and a better detection time and test interval, respectively.
- After the second iteration in the benchmark exercise, the qualitative results were more or less similar, e.g., with respect to the two most important systems and to the most important individual component failure modes.
- The results of the benchmark show the strength of such quantitative reliability analysis, even in case of a lack of data. E.g., lack of design specific data should not be an excuse for not performing quantitative reliability or safety studies.

The following is recommended based on the findings of the study:

- The guidelines formulated as part of this EWTS-II subproject can be an aid to collect data and to use it wisely for the purpose of safety and reliability studies of wind turbine designs.
- Qualitative safety and reliability are recommended very strongly as a minimum, as these studies result often in the identification of design errors (e.g., no or too less redundancy, no defence for certain events). Quantification, even with only the use of generic data sources, often results in a good ranking of the important event sequences, component failure modes, and systems. A combination of generic data and engineering judgement can always be used, although the reliability analyst should be aware of the limitations. In this way, a design can be made (more) balanced.
- Quantitative safety and reliability studies should be used primarily for the 'relative' (qualitative) purposes outlined above. The use of absolute figures and absolute criteria should be avoided.
- It would be interesting to conduct a similar benchmark on an existing design rather than a hypothetical one. For this existing design, specific data and operational experience should preferably be available in maintenance records, logbooks, etc. If not already available, collection of the data should be possible with limited effort. Our experience learns that this is feasible if such an effort gets the support and involvement of the owners and developer/manufacturer of the design.

9. CONCLUSIONS AND RECOMMENDATIONS

The two objectives of the EWTS-II subproject ‘Quantification of Failure Probabilities’ are:

- derivation of target values for structural reliability and for risk criteria at which the designer should aim and which the certifying bodies can use as a criterion; risk is here meant as risk to the public;
- preparation of guidelines to collect data and to estimate parameters to be used for quantitative safety and reliability analyses (or PSA’s).

To meet these objectives, the subproject was divided into two parts:

- a literature study to obtain target values for structural reliability and risk criteria;
- a limited benchmark exercise to obtain guidelines for data collection and parameter estimation.

Target values for structural reliability

From the literature study (as reported in Chapter 5), it is concluded that:

- The Scandinavian countries and The Netherlands seem to be leading in the application of structural reliability methods.
- The code which is not local to a country, but shall be applied Europe-wide, is the Eurocode 1.

Therefore, it is recommended to apply the safety level of the Eurocode to wind turbines, which would mean a yearly safety index of 4.7, corresponding to a failure probability of 10^{-6} /year.

Risk criteria and target values

From the literature study (as reported in Chapter 6), it is concluded that:

- Risk criteria related to the risk to the public that are applicable for wind turbines are the individual risk and the group risk (as defined in the official Dutch premises for risk management).

For these two criteria, the following target values are recommended:

Individual risk

For the use of the individual risk a risk target level of 10^{-5} /year is recommended. The individual risk is independent of the site of the wind turbine (park) and can be calculated without knowing the exact location of the installation. Note that the term ‘risk limit’ is not used but instead the term ‘risk target’, because risk limits are not commonly used in all EU countries.

Group risk

The target value for the group risk is that the likelihood of an accident with 10 deaths occurring should not exceed one in every hundred thousand years (10^{-5} /year). The aim of setting target values for group risk is to prevent social disruption (the death of a group of people all at once). Accidents with even more serious consequences lead to correspondingly greater degrees of disruption. It is therefore assumed that an n -times larger impact than 10 deaths should correspond with an n -squared smaller probability of such an accident occurring. The actual group risk is expressed as a so-called Complementary Cumulative Distribution Function (CCDF).

Mortality rate calculation

On a special request by the Project Steering Committee, a generic type of mortality rate calculation for the total number of wind turbines in the Netherlands was performed. This mortality rate was compared with mortality rates of other activities. Although based on rather simplified assumptions (mainly conservative ones) and a simple calculational procedure, a ‘best-estimate’ of the mortality rate in The Netherlands due to an overspeed accident and consequential blade failure is of the order of the mortality rate of being struck by lightning.

Guidelines for data collection and parameter estimation

As guidelines for data collection and parameter estimation, it is recommended to use as starting basis:

1. the guidelines as outlined in the LW 15/75 and NEWECs-45 studies reports; and
2. the recommended practices from the EWTS-I project.

In addition to these reports, the following is recommended:

1. The recommendations set out in the LW15/75 and NEWECS-45 studies can be used for design of specific data collection and parameter estimation. Also, the recommendations of the LW 15/75 study on the use of generic data are still valid.
2. Preferably, use should be made of standard, proven methods as laid down in reliability handbooks. Preferably, computerised versions of (generic) databases and existing software for reliability data analysis should be used.
3. Generic wind turbine data sources can be used if no specific data is available or if there are no time or resources available to collect design specific data.
4. Generic wind turbine data sources can be used to provide data on a high level, e.g., an estimate of blade failure frequency to be used in risk studies, or for frequencies of certain initiating events, e.g., grid loss.
5. If generic data is used to estimate a particular parameter (e.g., a failure rate), the following should be clearly documented for each parameter estimated:
 - *reference(s) to the source(s) used;*
 - *discussion why the source is considered valid or why the source is used;*
 - *the calculation procedure to arrive at the final estimate if multiple sources are used.*
6. If engineering judgement is used to provide an estimate, the reason for this should be indicated. Engineering judgement should be used to provide an estimate if design specific or generic sources do not provide an adequate answer.

Benchmark study

A benchmark study by ECN and Risø was used to test and extend the initial guidelines. The study was performed in two. In addition, the following was concluded from the benchmark study:

1. The main differences in the results after the first iteration of the data collection and parameter estimation were caused by different understanding of the system operation. E.g., this resulted in the assignment of different failure models and associated time factors for the basic events. Therefore, the guidelines were extended such that the analyst will make less mistakes in assigning either a monitored or periodically tested failure model, and a better detection time and test interval, respectively.
2. After the second iteration in the benchmark exercise, the qualitative results were more or less similar, e.g., with respect to the two most important systems and to the most important individual component failure modes.
3. The results of the benchmark show the strength of such quantitative reliability analysis, even in case of a lack of data. E.g., lack of design specific data should not be an excuse for not performing quantitative reliability or safety studies.

It would be interesting to conduct a similar benchmark on an existing design rather than a hypothetical one. For this existing design, specific data and operational experience should preferably be available in maintenance records, logbooks, etc. If not already available, collection of the data should be possible with limited effort. Our experience learns that this is feasible if such an effort gets the support and involvement of the owners and developer/manufacturer of the design.

Final recommendations

The following summarises the main recommendations that result from this EWTS-II subproject:

1. The guidelines formulated as part of this EWTS-II subproject can be an aid to collect data and to use it wisely for the purpose of safety and reliability studies of wind turbine designs.
2. Qualitative safety and reliability studies are recommended very strongly as a minimum, as these studies result often in the identification of design errors (e.g., no or too less redundancy, no defence for certain events). Quantification, even with only the use of generic data sources, often results in a good ranking of the important event sequences, component failure modes, and systems. A combination of generic data and engineering judgement can always be used, although the reliability analyst should be aware of the limitations. In this way, a design can be made (more) balanced.
3. Quantitative safety and reliability studies should be used primarily for the 'relative' (qualitative) purposes outlined above. The use of absolute figures and absolute criteria should be avoided.

10. REFERENCES

- [1.1] IEC 1400-1, *Wind Turbine Generator Systems -Part 1: Safety Requirements*, ed. 2, 1997
- [1.2] European Commission, 'European Wind Turbine Standards - Project Results', Part 3: Assessment of Wind Turbine Safety: Recommended Practices and Part 4: Assessment of Wind Turbine Safety: Case Study, Contract JOU2-CT93-0387, Final Report, EUR 16898 EN, 1996.
- [1.3] A.J. Seebregts, L.W.M.M. Rademakers, B.A. van den Horn, 'Reliability Analysis in Wind Turbine Engineering', *Microelectron. Reliab.*, Vol. 35, Nos 9-10, pp. 1285-1307, 1995.
- [1.4] Rademakers, L.W.M.M. and Carter, J., 'Reliability Analysis of the AOC 15/50 Wind Turbine Generator', ECN-C--94-057, Petten, The Netherlands, November 1994.
- [5.1] Calibration of Safety Factors, Joule II, Volume 4, JOU2-CT93-0387, ECN, Petten
- [5.2] Structural Reliability Analysis for Horizontal Axis Wind Turbines Components, B. A. van den Horn, L. W. M. M. Rademakers, T. W. Verbrüggen, ECN-RX_94-097, 1994.
- [5.3] *General principles on reliability for structures*, ISO-2394, 2nd edition, Okt. 1985
- [6.1] Ministry of Housing, Physical Planning and Environment (VROM): *Premises for Risk Management - Risk Limits in the Context of Environmental Policy*, Annex to the Dutch National Environmental Policy Plan "Kiezen of Verliezen" (to Choose or to Loose) Second Chamber of the States General, session 1988-1989, 21 137, no 5, The Netherlands.
- [6.2] F.R. Allen et al.: *The Management of Risk to Society From Potential Accidents*, Elsevier Science Publishers LTD, ISBN 1-85166-892-6, 1992.
- [7.1] L. Rademakers, et al.: *European Wind Turbine Standards. Vol. 4 Assessment of Wind Turbine Safety*, EUREC-Agency, JOULE-II Programme, Contr.: JOU2-CT93-0387, 1996.
- [7.2] L.W.M.M. Rademakers, A.J. Seebregts, B.A. van den Horn, J.N.T. Jehee, B.M. Blok: *Methodology for PSA for Wind Turbines - Demonstrated by a Case Study of the LAGERWEIJ 15/75 Design*. ECN-C--93-010, Petten, The Netherlands, March 1993.
- [7.3] L.W.M.M. Rademakers, A.J. Seebregts, T.W. Verbrüggen, R. Disseldorp: *Reliability Analysis and Design Review of the NEWECs-45, Part 1: Feedback of Operational Experience*, ECN-C--94-066, September 1994.
- [7.4] M. Durstewitz, C. Ensslin, M. Hoppe-Kilpper, K. Rohrig: *External Conditions for wind turbine operation, Results from the German '250 MW Wind' Programme*, EU Wind Energy Conf., Goteborg, May 20-24, 1996.
- [7.5] German 250 MW Project, presented at 3rd Austrian Wind Energy Symposium, St. Pölten, 26.-28.4.95.
- [7.6] Cooke, R.M. et al: *Design of Reliability Data Bases for Aerospace Applications*, Report 93-110, Delft University of Technology, ISSN 0922-5641, 1993.
- [7.7] J.R. Fragola: Reliability and risk analysis data base development: an historical perspective. *Reliability Engineering and System Safety* **51** (1996) 125-136.
- [7.8] R.M. Cooke: The design of reliability data bases, part I: review of standard design concepts. *Reliability Engineering and System Safety* **51** (1996) 136-146.
- [7.9] H.A. Sandtorv: Practical experiences with a data collection project: the OREDA project. *Reliability Engineering and System Safety* **51** (1996) 159-167.
- [8.1] European Commission, 'European Wind Turbine Standards - Project Results', Part 3: Assessment of Wind Turbine Safety: Recommended Practices and Part 4: Assessment of Wind Turbine Safety: Case Study, Contract JOU2-CT93-0387, Final Report, EUR 16898 EN, 1996.
- [8.2] Rademakers, L.W.M.M. and Carter, J., 'Reliability Analysis of the AOC 15/50 Wind Turbine Generator', ECN-C--94-057, Petten, The Netherlands, November 1994.
- [8.3] L.W.M.M. Rademakers, A.J. Seebregts, B.A. van den Horn, J.N.T. Jehee, B.M. Blok, 'Methodology for PSA for Wind Turbines - Demonstrated by a Case Study of the Lagerweij 15/75 Design', ECN-C--93-010, March 1993.
- [8.4] L.W.M.M. Rademakers, A.J. Seebregts, T.W. Verbrüggen, R. Disseldorp, 'Reliability Analysis and Design Review of the NEWECs-45, Part 1: Feedback of Operational Experience', ECN-C--94-066, September 1994.
- [8.5] L.W.M.M. Rademakers, A.J. Seebregts, and T.W. Verbrüggen, 'Applications of Reliability Analysis Methods for Wind Turbines', Proceedings EWEC'94 Conference, Thessaloniki, Greece, 10-14 October 1994, Vol. 1, pp. 640-646.

- [8.6] A.J. Seebregts, L.W.M.M. Rademakers, B.A. van den Horn, 'Reliability Analysis in Wind Turbine Engineering', *Microelectron. Reliab.*, Vol. 35, Nos 9-10, pp. 1285-1307, 1995.
- [8.7] Contini, S., Amendola, A. and Ziomas, I. 'Benchmark exercise on major hazard analysis', Volume I: Description of the project, discussion of the results and conclusions, CEC/JRC-Ispra EUR 13386 EN, 1991.
- [8.8] Halliburton NUS, 'NUPRA User's Manual', Version 2.31 Supplement, Gaithersburg, Maryland 208878, August 1995.

APPENDIX A. REVIEW OF SAFETY AND RISK CRITERIA

For the derivation of target values for structural reliability and for risk criteria on which the designer should aim and which the certifying bodies can use as a criterion, a number of references are reviewed and summarized. This appendix contains a list with the references considered (Table A.1) and the corresponding summaries. The conclusions are part of the main report. In chapter 5 of the report recommendation for target values for structural reliability are presented. The conclusions and recommendations for risk criteria and mortality rates are given in chapter 6 of the report. The wind turbine failure data are incorporated in chapter 7 of the report.

The references and summaries are grouped into the following categories:

- Target reliability's in various countries and in various branches of industries,
- Risk criteria in the various countries,
- Mortality rates observed, and
- Wind turbine failure data.

Table A.1 List of references

Nr.	Reference
A.1	Target reliability's in various countries and in various branches of industries
[A1.1]	Vrouwenvelder, A.C.W.M. and Siemes, A.J.M.: <i>Probabilistic calibration procedure for the derivation of partial safety factors for the Netherlands building codes</i> .
[A1.2]	IAEA: <i>General Design Safety Principles for Nuclear Power Plants - A Safety Guide</i> , IAEA Safety Series Report No. 50-SG-D11, Vienna, 1986.
[A1.3]	<i>Technische Grondslagen voor de berekening van Bouwconstructies</i> (in Dutch, Technical basis for the design of building constructions).
[A1.4]	ASME/USNRC: <i>Risk-Based Inspection - Development of Guidelines</i> , General Document, NUREG/CR-0005, CRTD-Vol.20-1, R5, RG, February 1992.
[A1.5]	Nordisk Komite for bygningstemmelse: <i>Guidelines for loading and safety regulations</i> , NKB-rapport No 55 (Danish) +55E (English translation), juni 1987, available from Danish Standards.
[A1.6]	DS409, <i>The Safety of Structures</i> and DS-410, <i>Loads for the Design of Structures</i> , English translation, NP-157-T of 'Normstyrelsens publikationer', N-157-N, June 1982, Teknisk Forlag, Copenhagen.
[A1.7]	DS 412: <i>Code of Practice for the Structural Use of Steel (NP-163-N)</i> in Danish, NP-163-T: English translation, Teknisk Forlag, Copenhagen, April 1983, translation March 1984.
[A1.8]	DS 456: <i>Constructions made of Glass-fibre reinforced unsaturated polyester</i> , 1 st edition, Teknisk Forlag NP-178-N, Copenhagen, 1985.
[A1.9]	DS 472 (DIF-norm): <i>Last og sikkerhed for vindmøllekonstruktioner, 1. udgave 1992</i> (In Danish, Loads and Safety of Wind Turbine Construction, first edition), Teknisk Forlag.
[A1.10]	EUROCODE no. 1: <i>Basis of Design and Actions</i> ; part 1: <i>Basis of Design</i> , European Commission, CEN/TC 250/SC 1, in preparation.
[A1.11]	ISO 2394: <i>General Principles on Reliability for Structures</i> , 1986.

- [A1.12] *Teknisk Grundlag for typegodkendelse og certificering af vindmøller* (In Danish, Technical Criteria for type approval and certification of wind turbines), November 1994; Energistyrelsen, Risø-I-943.
- [A1.13] *Rekommendation til opfyldelse af krav i Teknisk Grundlag* (In Danish, Recommendation Compliance with Requirement Technical Basis for the Type Approval and Certification of Wind Turbines In Denmark), 1. July 1992, Energistyrelsen.
- [A1.14] BS 8100, part 2: 1986, *Lattice Towers and Masts*.
- [A1.15] DIN 18800.
- [A1.16] API RP 2A - LRFD, Planning, Designing and Constructing Fixed Offshore Platforms - Load Resistance Factor Design, 1993.

A.2 Risk criteria in the various countries

- [A2.1] Ministry of Housing, Physical Planning and Environment (VROM): *Premises for Risk Management - Risk Limits in the Context of Environmental Policy*, Annex to the Dutch National Environmental Policy Plan “Kiezen of Verliezen” (to Choose or to Loose) Second Chamber of the States General, session 1988-1989, 21 137, no 5, The Netherlands.
- [A2.2] Vrijling, J.K., Hengel, W. van, Houben, R.J.: *A Framework for Risk Evaluation*, Journal of Hazardous Materials **43** (1995) 245-261.
- [A2.3] Vrijling, J.K., Hengel, W. van, Maanen, S.E. van: *The application of the concept of societal risk to various activities in the Netherlands*, Proc. ESREL’96/PSAM-III Int. Conf. on Probabilistic Safety Assessment and Management, June 24-30, 1996, Crete, Greece, pp. 960-966.
- [A2.4] Sprent, P.: *Taking Risks - The Science of Uncertainty*, London, Penguin, 1988 (Chapter 11) (Dutch translation: *Risico’s - Zekerheden over onzekerheid*, Bloemendaal, Aramith, 1990).
- [A2.5] IPO (Interprovinciaal Overleg): *Handleiding voor het opstellen en beoordelen van een extern veiligheidsrapport (EVR) (In Dutch) (Manual to draft and to review an external safety report)*, IPO-publikatienummer 54, The Hague, The Netherlands, April 1994.
- [A2.6] *SI 1992/2885: Offshore Installations (Safety Case) Regulations 1992 and Relevant Guidelines*.
- [A2.7] F.R. Allen et al.: *The Management of Risk to Society From Potential Accidents*, Elsevier Science Publishers LTD, ISBN 1-85166-892-6, 1992.

A.3 Mortality rates observed

- [A3.1] Sprent, P.: *Taking Risks - The Science of Uncertainty*, London, Penguin, 1988 (Chapter 11) (Dutch translation: *Risico’s - Zekerheden over onzekerheid*, Bloemendaal, Aramith, 1990).
- [A3.2] Danmarks Statistik: *Statistical Year Book 1995*.

A.4 Wind turbine failure data

- [A4.1] Schmid, J., and Klein, H.P.: *Performance of European Wind Turbines - A Statistical Evaluation from the European Wind Turbine Database EUROWIN*, Fraunhofer Institute for Solar Energy Systems, Freiburg, July 1991.
- [A4.2] Goezinne, F. en Veldkamp, H.F.: *'Veiligheidsanalyse Windparken Noord-Groningen'*, (In Dutch, Safety and Risk Analysis Wind Parks in the North of Groningen) Goezinne & Veldkamp, Enschede, september 1993.
- [A4.3] *WindStats Newsletter*: Vrinners Hoved, DK-8420 Knebel, Denmark, or: PO Box 496007, Ste 2170, Redding, California 96099-6007, USA.
- [A4.4] Curvers, A. and Schuurman, J.J.: *'Bedrijfsgegevens van IPW-windturbineprojecten: eerste fase' (Operating experience of IPW wind turbine projects: first phase)*, ECN-C--91-041, June 1991.
- [A4.5] W.J. Stam, et al.: *'Collection of Data on Accidents and Incidents of Wind Turbines for Updating of Safety Criteria'*, ECN-C--90-017, May 1990.
-

Appendix A.1 Target reliability's in various countries and in various branches of industries

[A1.1]

The paper describes the procedure how partial safety factors in the Netherlands building code were calibrated with a probabilistic calibration procedure. First many types of components of various materials were designed in accordance with the Netherlands building code (beams, columns, T-joints, etc.). Next, these elements were subjected to a FORM reliability analysis in order to determine the safety level. In this way an idea was obtained of the average safety level and of the scatter with respect to it. The types of distributions and their parameters to describe the stochastic variables (loads and resistance) were obtained from an extensive literature survey. The purpose of the project was so to derive partial safety factors that this scatter would, in the future code, be reduced while the average remained approximately unchanged. The following was concluded from the reliability analysis.

- The value of the safety index β for the limit state "ultimate load" ranges between 2.2 and 6.1 with an average of 3.8 (failure probability $\approx 7 \cdot 10^{-5}$) and a standard deviation of 1.4.
- For the serviceability limit states, an average value for β was found to be 1.7 (failure probability $\approx 5 \cdot 10^{-2}$) and a standard deviation of 1.2.

It should be noted here that the reference time was 50 years so the failure probability per year is approximately $1.4 \cdot 10^{-6}/\text{yr}$ for the ultimate limit state and 10^{-3} for the serviceability limit state. The general trend was that a high reliability index was obtained for loading cases comprising a relatively high proportion of self-weight. The low values were found for loading cases for which the variable loads dominate. The variable loads have a higher coefficient of variation and therefore need a higher safety factor.

[A1.2]

With respect to reliability design, this reference discusses (qualitatively) the following echelons of defense: redundancy, diversity, independence, fail-safe design, and auxiliary services. However, no quantitative target reliability values are provided for each line of defense.

A Dutch amendment to this Safety Guide does include some quantitative reliability requirement:

- a non-diverse safety system should have an unavailability of less than 10^{-4} - 10^{-3} per initiating event (per demand).

[A1.3]

NEN 6700 “TGB 1990 - General Principles” gives general requirements for reliability (safety and serviceability) on a fundamental level. These requirements have to be fulfilled for all building structures independent of the materials used in these structures. In NEN 6700, which has become operational in 1991 the deterministic approach used in the preceding norm (NEN 3850: 1972) is replaced by a probabilistic approach. The target values for the safety index β as specified in this norm are presented in Table A.2. These target values are determined such that the reliability level of a building structure designed according to NEN 6700 is on average equal to the reliability level for the design based on the preceding norm (NEN 3850: 1972). For this reason distinction had to be made between wind loadings and other loadings. Three safety classes are distinguished depending on the consequences of failure. In [A1.1] the procedure for determination the safety index and the corresponding partial safety factors is outlined.

Table A.2 Safety index β

Safety class	Safety index		
	ultimate load		serviceability
	wind load	other loads	
1: negligible personnel injury, small public loss	2.3	3.2	1.8
2: some personnel injury, significant public loss	2.4 ¹⁾	3.4 ²⁾	1.8
3: extensive personnel injury, significant public loss	2.6	3.6	1.8

¹⁾ reference period $t \geq 15$ years; for $t < 15$ years, $\beta = 3.1 - 0.60 \log t$
²⁾ reference period $t \geq 15$ years; for $t < 15$ years, $\beta = 3.6 - 0.85 \log t$

From an economical point of view the safety index is kept constant, independent of the design lifetime of the building structure. This implies that the failure probability per year will be higher for building structures with a shorter design lifetime.

The general requirements of NEN 6700 are elaborated in more detail with respect to the determination of the characteristic loading and with respect to the specification of the partial safety factors in NEN 6702 (TGB 1990 - Loadings and Deformations, December 1990). For a number of building structures the safety class and reference period is specified. Wind turbines are not mentioned, but building structures for electric power stations are classified as class 3 with a reference period of 50 years. Special applications of NEN 6702 are given in NEN 6706 for bridges and in NEN 6707 for roofs.

The determination of the resistance of a building construction against the applied load is elaborated in the following material specific norms:

- NEN 6710 for aluminium construction;
- NEN 6720 for concrete construction;
- NEN 6740 for geotechnics;
- NEN 6750 for lumber construction;
- NEN 6770 for steel construction;
- NEN 6790 for bricks.

These material specific norms, which always have to be used in connection with NEN 6702, provide characteristic material properties and partial safety factors. Also rules are specified which can be used to check whether the requirements of NEN 6700 are fulfilled. The framework of this series of TGB norms is such that in case the requirements of the material specific norms in connection with NEN 6702 are fulfilled, the general requirements of NEN 6700 are satisfied automatically.

Besides, in NEN 6701 (TGB 1990 - Names and symbols and quantities) names and symbols are defined for a number of quantities.

[A1.4]

Although the title focuses on inspection, this report presents a variety of target reliability values and approaches in several industries: nuclear, fossil, aircraft, civil engineering and marine structures, industrial insurance. However no relevant information for this project is presented.

[A1.5]

NKB, or Nordic Committee for building regulations, is a co-operative formed by the Nordic building authorities. The NKB is responsible for harmonizing the Nordic building regulations. All Nordic countries are members (Denmark, Finland, Iceland, Norway, and Sweden).

The NKB report details the partial coefficient code format to be used in Nordic codes. For establishing the code format, the NKB states, that close contact with the international ‘Joint Committee on Structural Safety’ has been maintained. Furthermore it says that the concept of ‘safety’ is equivalent to the concept reliability in ISO 2394 [A1.11]. The NKB report also outlines the Nordic probabilistic code calibration project that forms the basis for the Nordic safety evaluation.

In this report, the safety requirement is expressed in terms of the safety index and is also given as an equivalent ‘formal yearly probability of failure’, which is the target reliability. Nordic codes distinguish between different ‘safety classes’ which are defined to depend on the ‘consequences-of-failure’. Thus the ‘consequences-of-failure’ partial coefficient as defined in the ISO-2394 is closely related to Nordic safety class concept. The NKB report specifies the target reliability as shown in Table A.3 for the three safety classes in the form of both safety index and formal probability of failure.

The connection between safety class and consequences-of-failure is given in Table A.4 from NKB-55E.

Table A.3 Stipulated values of the safety index and the formal failure probability for the ultimate limit state for ductile failure without safety reserve capacity. Corresponding consequences-of-failure materials partial coefficient γ_n .

Safety Class	Safety Index	Target reliability (failure probability per year)	γ_n
Low	3.71	10^{-4}	0.9
Normal	4.26	10^{-5}	1.0
High	4.75	10^{-6}	1.1

Table A.4 Safety classes vs. consequences of failure

Consequences of failure	Safety class
Slight personnel injury and insignificant public loss	Low
Some personal injury or significant public loss	Normal
Extensive personal injury or very significant public loss	High

Table A.3 also shows the consequence-of-failure partial coefficient γ_n . The implication of $\gamma_n = 1$ for the normal class is, that the basic target failure probability for normal class constructions and for ductile failure is put at 10^{-5} per year. In another safety class one modifies the design by changing the safety-class dependent materials partial coefficients up or down by 10% for high or low safety class, respectively. This in turn will decrease or increase, respectively, the failure probability by a factor of 10 as also seen in the table in the particular safety check under study. For completeness, it should be mentioned that γ_n depends on both safety class and type of failure in the materials part of DS 409 and the (old) NKB 35. In the new NKB 55, these two variables are split into two separate (materials) safety factors.

[A1.6]-[A1.9]

The Danish code system consists of the following:

- The basic Danish code DS-409 [A1.6],
- A load detailing code DS-410 [A1.6],
- A number of material codes for separate materials (e.g. DS-412 for steel [A1.7], DS-456 for GRP materials [A1.8]),
- A number of codes for specialised structures (e.g. off shore constructions, or wind turbines (DS-472 [a1.9])). These codes may specify both loads and resistance either by reference to the relevant specialised loads or materials codes, or in some cases by defining deviations from these codes when such deviations are needed.

[A1.6]

The basic safety code DS-409 does not explicitly mention a target reliability as the partial coefficients method for practical use is formulated largely without reference to probabilistic methods.

DS-409 prescribes the use of the partial coefficient method and gives definitions for:

- The loading system to be assumed with building structures ;1 permanent load + 1 variable load
- Within this loading system, the characteristic values to be used and partial coefficients and possible reduction factors are given
- An annex (DS 409, annex 1) specifies rules for further material codes in the Danish code system. Here it suggests partial coefficients to account for uncertainties of different variables. They are given as a function of percentile used for characteristic values and of the coefficient of variation for the materials strength.

Hereby, the target reliability is fixed without actually referencing the target reliability value. For details and for the general philosophy of the partial coefficient method to be used, DS-409 does refer to and is generally in accordance with NKB-report 35: Guidelines for loading- and safety regulations for structural design. Now superseded by report 55 + 55E, same title [A1.5].

[A1.10]

The basic Eurocode 1 is ENV 1991-1, part 1¹⁾ is the European equivalent of ISO 2394. Compared to Danish codes it covers partly NKB 55 plus DIS 409. In Eurocode 1, informative Annex 1 on partial factor design, “Table A.2” specifies an indicative value for the target reliability index for the ultimate limit state of $\beta = 4.7$ corresponding to a failure probability of 10^{-6} per year corresponding to Danish safety class ‘high’.

The table is shown here as Table A.5.

Table A.5 Target reliability as defined in Eurocode 1 (informative)

Limit state	Target reliability index (design working live)	Target reliability index (1 year)
Ultimate	3.8	4.7
Fatigue	1.5 to 3.8	-
Serviceability (irreversible)	1.5	3.0

Depends on degree of inspectability, reparability and damage tolerance²⁾

¹⁾ ENV 1991-1- part 1: Basis of design and actions on structures-Basis of design, CEN, Bruxelles, 1994

²⁾ IEC 2394-1986: General principles on reliability for structures. Switzerland 1986.

The Eurocodes do not contain safety classes. They do, however, in several places indicate that in some cases one may wish to choose a different reliability level for other types of failure or for other consequences of failure. This can in turn be done by adding or subtracting 0.5 - 1 to the target index. This seems to indicate, that the basic target reliability is 10^{-6} . The Eurocodes, however, have in most cases not been probabilistically calibrated. Therefore the connection between the partial coefficient requirements and target reliability stated is maybe not quite good. We have compared Eurocodes and the Danish codes and found that they agree reasonably well when considering the use of partial coefficients.

[A1.11]

The ISO 2394 code does not state a target reliability or any partial coefficient values and consequently it has no target reliability (or safety level) but is mainly a systematising the partial coefficient method. It should be remarked that the ISO code does suggest the use of a safety factor for consequences-of-failure and for failure type which is not present in the Eurocodes.

[A1.12],[A1.13]

Section 4.2.4 Page 18: “The target for the reliability of the safety system must be so great that the probability of a failure of the safety system combined with the probability of a critical fault requiring the engagement of the safety system is less than $2 \cdot 10^{-4}$ per year.”

[A1.14]

This is the British Standard for the design of lattice towers and masts. Part 2 in particular is a guide for Part1, which is “ Code of Practice for Loading”. It talks about reliability theory and the probability of failure of towers and masts. The actual strength calculations are performed through application of partial safety factor methods. Target reliability’s are not given.

[A1.15]

The main code for the design of steel structures in Germany is DIN 18800. This applies a partial safety factor method for the loads and for the material/resistance to account for uncertainties and imperfections. In the introduction to this code it is mentioned that characteristic values for load and resistance shall be

derived from the distribution of these values by calculating p -quantiles. The characteristic values together with the desired target reliability can then be used to determine partial safety factors. But due to practical reasons the partial safety factors used in the code have been determined beforehand, based on a global calibration and experience. Furthermore we received the information that there are currently no plans to define a target reliability for civil structures and re-calibrate the safety factors.

Other relevant civil codes are DIN 4228, Concrete Masts and DIN 4133, Chimneys. Both use partial safety factors for the wind loads.

The requirements of the German authorities for the approval of wind turbines is described in Appendix 1 of the GL Rules for Certification of Wind Turbines.

[A1.16]

This recommended practice shall replace API RP 2A - WSD, Working Stress Design, which was using one global safety factor to account for uncertainties in loading and resistance of offshore platforms. It has been developed for the Gulf of Mexico and forms the basis of ISO/DIS 13819 Part 2, which is currently developed for world-wide application.

API sponsored research revealed that the WSD method does not provide structures with consistent component reliability. Therefore the LRFD code was developed and the load and resistance factors have been matched to their respective uncertainties in order to reduce the reliability variations. The factors have been calibrated using a reliability model and design experience. LRFD principles have been applied to several other US structural codes as well, like ACI (reinforced concrete), AASHTO (bridges) and AISC (steel structures). The reliability model used for establishing the load and resistance factors is based on the safety index method.

In order to maintain the safety level from the old code, β values of components of existing platforms were determined with structural reliability methods. From there target β values were determined. LRFD will be more conservative than WSD for environmental loads and less conservative for gravity loads. This reflects the greater uncertainty that is present in environmental loads.

Appendix A.2 Risk criteria in the various countries

[A2.1]

This first reference will be treated in more detail, because it also provides useful definitions and general notions of risks.

The Dutch concept of risk assessment was first introduced into environmental policy in the 1986-1990 Multi-year Programme for Environmental Management. Limits are indicated above which the risks become unacceptable (maximum permissible levels) and for establishing levels below which they are negligible.

Risks from the following categories are discussed:

- major accidents;
- substances;
- genetically modified organisms;
- radiation;
- noise; and
- unpleasant odours.

The risk category relevant for wind turbine safety are (major) accidents. The risk associated with such accidents are known as external safety risks and are established by means of quantitative risk analysis techniques. Detrimental effects can therefore be expressed in mortality terms, taking account of the fact that lethal accidents will also result in a number of less seriously injured casualties. The parameters in such risk analyses refer specifically to individual risk (IR) and group risks (GR). The definitions are:

Individual Risk (IR), the likelihood that a person will suffer a given detrimental effect (here: death) as a result of exposure to an agent (expressed in probability units per year or related to an average concentration per year)

The IR is calculated for the person who runs the greatest risk at a given location. In practice, this normally refers to an individual who is present at a particular place in the vicinity of an industrial site 24 hours per day. The IR is generally displayed in the form of iso-risk contours. The *maximum acceptable level* is defined as 10^{-6} /year. The *negligible level* is defined as 10^{-8} /year.

In the Netherlands, the following societal risk is defined:

Group Risk (GR), the likelihood per year that a group of at least a certain size will all be victim of a single accident at one and the same time

The GR should indicate the probability that a certain group of people outside a facility will die due to an accident caused by the facility. As such, this risk takes account of the surrounding area. GR does not involve the calculation of the individual risk but rather the risk of a number of deaths. In addition, the group has to be a fixed and identifiable group of persons, viz. the group of persons actually living at/near the corresponding site.

The limits chosen for the GR specify that the likelihood of an accident with 10 deaths occurring shall not exceed one in every hundred thousand years and aim to prevent social disruption (the death of a group of people all at once). Accidents with even more serious consequences lead to correspondingly greater degrees of disruption. It is therefore assumed that an n -times larger impact than 10 deaths should correspond with an n -squared smaller probability of such an accident occurring .

E.g., the *maximum permissible levels* are defined as 10^{-5} /year for $n = 10$ or more deaths and 10^{-7} /year for $n=100$ or more deaths. The corresponding *negligible levels* are defined as 10^{-7} /year for $n=10$ or more deaths and 10^{-9} /year for $n=100$ or more deaths.

In estimation of GR and IR, acute deleterious risks are determined on the basis of death up to two or three weeks after exposure. Exposure is often of short duration, up to a few hours at most.

In contrast to the GR, the IR refers to the degree of danger in the vicinity of the facility irrespective of the surroundings. In assessing the individual risk at a particular place, it does not matter whether for instance, a house or a stadium is situated there. However, this information would be relevant when estimating the group risk.

The levels below which the risks to man as well as to ecosystems can be regarded as negligible have been defined in principle as 1% of the maximum permissible values wherever possible. This approach has been adopted to take account of factors such as multiple exposures (additivity of risks and synergism), uncertainties in the estimates (limited testing and specific sensitivity) and to leave a sufficient margin to distinguish between maximum permissible levels and the values below which the risks involved become negligible.

When comparing perceived risks with the limits, a distinction is generally made between existing and new activities. In the case of existing activities that give rise to situations in which the specified limits are exceeded, social considerations are often of importance when determining the period over which these hazards should be curbed. New activities, however, must comply with the specified limits immediately.

[A2.2], [A2.3]

These two references discuss the Dutch group risk in a more general framework that includes a policy factor β in the societal risk criterion. This enables relative voluntariness and economic benefits to be included and gives greater flexibility than the original VROM criterion and level (in [A2.1]). The framework was tested on: (1) the extension of the national airport Schiphol (Amsterdam), (2) transport of dangerous chemicals over water, (3) flooding of polders, (4) car traffic, (5) chemical plants, and (6) operation of modern wind turbines in housing areas. Examples for (1) - (4) are given, but unfortunately not for (6).

[A2.4] (Ref. [A2.4] also occurs as [A3.1] (Mortality rates observed)

This reference is interesting because it also discusses aspects like risk perception, voluntary versus involuntary risks, and the different bases on which to calculate and to compare risks. Generally, external safety risks are expressed in probabilities of death per year (see [A2.1]), but also other bases are possible. E.g., for energy producing installations, one could also calculate the probability of death per energy output generated (/MWe*year). This reference also presents a variety of observed risk figures (mortality rates, number of accidents, etc.) of different industries and activities.

[A2.5]

Most important part of this reference for the EWTS-II sub II project is the way GR can be calculated. E.g., ref. [A2.4] allows the use of factors correcting for the probability of people living in the vicinity of the installation. However, both ref. [A2.1] and [A2.4] explicitly state that for IR a 24 hour per day exposure to the risk should be assumed.

[A2.6]

Following the Piper Alpha Disaster in 1989, in which 167 lives were lost on a UK Offshore Installation, the UK Government commissioned an enquiry about offshore safety, which was led by Lord Cullen. Based on the report of Lord Cullen a whole new set of offshore legislation for the UK Continental Shelf was originated. The aim was to move from prescriptive legislation to a goal setting legislation, through application of the ALARP principle, meaning that the duty holder has to demonstrate that risk associated with his installation is "As Low As Reasonable Practicable". One of the means to demonstrate ALARP shall be through the application of QRA.

The Safety Case Regulations are part of this legislation and in the guidance to those the UK Health and Safety Executive (HSE) requires in Para. 117 a demonstration that "the frequency with which accidental

events will result in loss of integrity of the Temporary Refuge, within a minimum endurance time, which needs to be determined for the actual installation, does not exceed the order of 1 in 1000 a year". The demonstration shall be by QRA techniques, where the HSE will make proper allowance for the uncertainties in QRA.

[A2.7]

This report describes the nature and definitions of risks and discusses risk targets and goals in various countries. It appears that only the Netherlands and the USA have limits for individual risk and societal risk, with the Netherlands as being the most stringent ($1E-6/yr$ for individual risk). The UK uses the concept of tolerable risk, with $1E-4/yr$ as just tolerable level for the public and $1E-6/yr$ as broadly acceptable. Denmark and France use as acceptable levels $1E-6/yr$, but they are more a guide than mandatory.

Appendix A.3 Mortality rates observed

[A2.1]

Ref. [A2.1] also contains relevant material for part 3 “Mortality rates observed”. E.g., the next table shows observed annual mortality rates in the Netherlands.

Table A.6 Annual mortality rate associated with certain occurrences and activities in the Netherlands

Activity/Occurrence	Annual mortality rate	
Drowning as a result of a dike collapse	10^{-7}	1 in 10 million
Bee sting	$2 \cdot 10^{-7}$	1 in 5.5 million
Being struck by lightning	$5 \cdot 10^{-7}$	1 in 2 million
Flying	$1.2 \cdot 10^{-6}$	1 in 814,000
Walking	$1.85 \cdot 10^{-5}$	1 in 54,000
Cycling	$3.85 \cdot 10^{-5}$	1 in 26,000
Driving a car	$1.75 \cdot 10^{-4}$	1 in 5,700
Riding a moped	$2 \cdot 10^{-4}$	1 in 5,000
Riding a motorcycle	$1 \cdot 10^{-3}$	1 in 1,000
Smoking cigarettes (1 packet a day)	$5 \cdot 10^{-3}$	1 in 200

[A3.1]

Ref. [A3.1] also occurs as Ref. [A2.4]

[A3.2]

Railway casualties in Denmark (population 5 million):

	1992	1993
Passengers	26	30
of whom killed	6	1
Employees	3	32
of whom killed	1	1

Fatal casualties in road traffic accidents (1993): 596 ($\approx 3 \cdot 10^{-4}$)

Appendix A.4 Wind turbine failure data

[A4.1] No relevant information.

[A4.2]

Based on figures and statistics in WindPower Monthly, the following values were derived for blade

failures (loss of blade).

Table A.7 Probability of loss of blade per year per turbine

Year	Probability of blade loss	Reference
1987	$3 \cdot 10^{-2}$ (500 years of operation)	Dutch data *
1987 - 1989	$2 \cdot 10^{-3}$ - $5 \cdot 10^{-3}$	Danish data *
1987 - 1989	$3 \cdot 10^{-3}$ (22000 years of operation)	American data *
1991 - 1992	$5 \cdot 10^{-3}$ (4000 years of operation)	Wind Power Monthly

* The data was based on an earlier investigation “De Vries et al *Vooronderzoek omgevingsveiligheid wind turbines* (In Dutch, Pre investigation on safety of wind turbine surroundings), 1989”.)

[A4.3]

The results of an analysis of reported blade failures are given in Table A.8.

Table A.8: Number of (reported) turbines with a blade failure

	1990 apr may jun	1990 jul aug sep	1990 oct nov dec	1991 jan feb mar	1991 apr may jun	1991 jul aug sep	1991 oct nov dec	1992 jan feb mar	1992 apr may jun	1992 jul aug sep	1992 oct nov dec	1993 jan feb mar	To- tal
BLADES													
1. Overspeed				1		1		1				1	4
2. Cracks, Storm	1		3	3								2	8
3. Lightning, Others		1				1	1	2		1	1	3	10
Total no. of Turbines	1829	1831	1873	1964	1988	1915	2146	2034	2092	2113	2187	2241	

Total number of years of operation: ≈ 6000 yr

$$P_{\text{overspeed}} = 4/6000 = 6.7 \cdot 10^{-4} / \text{yr}$$

$$P_{\text{normal operation}} = 8/6000 = 1.3 \cdot 10^{-3} / \text{yr}$$

$$P_{\text{lightning}} = 10/6000 = 1.7 \cdot 10^{-3} / \text{yr}$$

[A4.4] No relevant information.

[A4.5] No relevant information.

APPENDIX B. MORTALITY RATE CALCULATION

This appendix presents the details of the assumptions for the mortality rate calculation and the details of the calculational procedure. Section 6.2 of the main report provides the background, results and the conclusion of this calculation.

Appendix B.1 Assumptions

- Only one accident scenario, viz. overspeed with given number of revolutions/min with one blade failure frequency (BFF);
- All wind turbines are of equal design, viz. the 3-bladed 500 kW, pitch controlled design, with a diameter of 40 m from the ECN/TNO risk study from September 1993 [B1]);
- No park effects, i.e. the risk of n WTB's in a park is n * the risk of the individual WTB;
- The individual risk (IR) will be used to calculate the mortality rate (MR);
- The base case calculation will take the figures from the aforementioned ECN/TNO study:
BFF = 1E-3/yr (generic value: 1E-3 to 5E-3/yr);
Max. 'conditional' IR from one WTB = 1E-4 at 1 m; 1E-5 at 20 m and 1E-6 at 80 m; as a rule of thumb, a conditional IR of 1E-6 at 2 * diameter is suggested;
The ECN/TNO study revealed that the combined effect of more than 1 WTB on the IR is negligible;
- The number of WTBs is equal to 400;
- No more than one fatality per accident.

The actual risk is dependent on:

- design (height tower, blades)
- location (site) of WTB, incl. wind regime at the site, population and activities around WTB (determines exposure fraction), (site also determines BFF!)
- blade failure frequency (BFF)
- number of WTB's
- exposure fraction

The boldfaced parameters are included in the calculation. The other ones are neglected or are implicitly included in other parameters.

Sensitivity analyses may be performed to change some of the other figures.

Appendix B.2 Calculational procedure

The calculation will be performed as a spreadsheet calculation. This facilitates sensitivity analyses.

Parameters:

- Blade failure frequency (normally derived from a design and site-specific analysis);
- Number of wind turbines;
- Conditional probability of being hit assuming 24 hour exposure (normally derived from a design and site-specific analysis);
- Exposure fraction (to differentiate between different locations; normally derived from a design and site-specific analysis).

Exposure fractions:

- corresponding to and in accordance with the definition of Dutch IR (very conservative);
- corresponding for a farmer working 8 hours a day without shielding (less conservative);
- more realistic value, but still estimated to be conservative.

Appendix B.3 Reference

[B1] 'A. Vrouwenfelder, L. Rademakers: *Risico-analyse voor het windplan nabij de Roompotsluizen*, 93-CON-R1055, TNO, ECN, September 1993 (In Dutch, Confidential report)

APPENDIX C. BENCHMARK ON DATA COLLECTION AND PARAMETER ESTIMATION

This appendix presents the details of the benchmark study. In addition, it provides also more practical and detailed guidance for the data collection and parameter estimation.

Appendix C.1 Guidance for benchmark exercise

Appendix C.1.1 List of Basic Events (BEs) from EWTS-I case study

This list is given in Appendix A of Volume 4B of the EWTS-I project:

<i>NUPRA 2.2 Property of ECN File: EWT.BED</i>				<i>Page 1</i>
<i>Created: Mon Sep 25 16:41:18 1995 Printed: Mon Sep 25 16:41:33 1995</i>				
Basic Event	Id	Point Est	Description	
DE-CPU-----	ERR	1.00E-003	CPU-failure	
-				
DE-SEN-----	LF	1.00E-003	Failure of overspeed relay	
DE-SEN-HISPS-	LF	1.00E-003	SENsor on HIGH SP. Shaft loses func. (LF)	
-				
DE-TC-----	LF	1.00E-003	Thermo couple fails	
-				
EL-CON-H-----	FTO	1.00E-003	Contactator H fails to open.	
-				
EL-CON-K1-----	FTO	1.00E-003	Contactator K1 fails to open.	
EL-CON-K2-----	FTO	1.00E-003	Contactator K2 fails to open.	
EL-CON-K3-----	FTO	1.00E-003	Contactator K3 fails to open.	
EL-CON-K4-----	FTO	1.00E-003	Contactator K4 fails to open	
EL-CON-K6-----	FTO	1.00E-003	Contactator K6 fails to open.	
EL-CON-KM----	FTO	1.00E-003	Contactator KM fails to open	
-				
EL-CON-OT-----	FTO	1.00E-003	Contactator OT fails to open	
-				
IE-S7		2.00E+000	Generator temp. over 150 C AND wind speed over 5 m	
MB-BP-----	WEA	1.00E-002	Too much wear of brake pads.	
-				
MB-CYL-----	STU	1.00E-002	Cylinder stuck.	
MB-DIS-----	FRA	1.00E-002	Fracture of disk or shaft.	
MB-FU-----	BLK	1.00E-002	Filter unit blocked	
MB-SPR-----	LF	1.00E-002	Insufficient spring force.	
-				
MB-TVA-----	BLK	1.00E-002	Throttle valve blocked.	
-				
MB-VAL-Y1-----	STU	1.00E-002	Valve Y1 stucked.	
MB-VAL-Y2-----	STU	1.00E-002	Valve Y2 stucked.	

TB-CP--1-----	STU	1.00E-002	Catchplate stucked to magnet.
-			
TB-CP--2-----	STU	1.00E-002	Catchplate stucked to magnet.
-			
TB-CP--3-----	STU	1.00E-002	Catchplate stucked to magnet.
TB-DAM-1---	STU	1.00E-002	Damper stucked.
TB-DAM-2---	STU	1.00E-002	Damper stucked.
TB-DAM-3---	STU	1.00E-002	Damper stucked.
TB-HIN-1----	BST	1.00E-002	Hinge broken or stucked.
TB-HIN-2----	BST	1.00E-002	Hinge broken or stucked.
TB-HIN-3----	BST	1.00E-002	Hinge plate broken or stucked.
TBXTIP-123---	FTD	1.00E-003	Common cause failure of three tip brakes.

Appendix C.1.2 Information needed for each BE

For each of the basic events, one has to specify:

1. The component failure mode type, i.e.:
 - i. repairable, monitored component (failure ‘directly’ detected, after which repair follows; the component is unavailable during the detection and repair time).
 - ii. periodically tested component;
 - iii. constant unavailability/frequency type; or
2. Depending on type, the following parameters have to be provided:
 - i. a failure rate plus ‘repair time’, with the repair time here detection time plus logistic plus actual repair time;
 - ii. a failure rate plus a test interval;
 - iii. an unavailability or frequency;

Moreover, for failure rates and unavailability’s, error factors should be provided.
3. For each of the selected types, the reasons and source(s) of information;
4. For each of the parameters, the reasons, source(s) of information.

Appendix C.1.3 Sources of information

In general, for a quantitative safety and reliability analysis, the following sources of information for the failure data may be used:

- turbine specific data (not available here!);
- generic wind turbine failure data, e.g. from generic wind turbine databases, from existing case studies or from tests of involved components;
- generic industry-averaged failure data; and
- engineering judgment.

If more sources are used for one particular parameter, the way these sources of data are combined to obtain one estimate, should be described.

Appendix C.1.4 Failure type model

(referred to as ‘component types’ in EWTS-I report, see Table 10.1, Vol. 4A)

After having identified the sources of information, the following has to be done for each basic event:

1. define component type (constant unavailability/frequency, periodically tested, repairable (monitored));
2. dependent of type, data has to be collected.

NUPRA supports 5 mathematical models for deriving point estimates of BEs, viz.

Repairable, Type 1:

represents monitored event whose failure is revealed and repaired during operation. A linear approximation is used to give the average unavailability $U = \lambda \cdot \theta$ (failure rate \cdot mean time to repair). If the component cannot be repaired during operation (which is the case for wind turbines, the repair time can be viewed as detection time).

Periodically tested, Type 2:

used to model standby components whose failure is detected on test or on demand.

$U = (\lambda \cdot T - 1 + \exp(-\lambda \cdot T))/(\lambda \cdot T)$, where T = mean time between tests. This expression approximately equals $\frac{1}{2} \lambda \cdot T$ for $\lambda \cdot T \ll 0.1$.

Failure on demand, type 3:

models average probability of failure on demand of a component. It is also usable in cases where the probability of failure is known but the event type is not, and for initiating event frequencies. Other types of events can be temporarily changed to type 3 to allow editing the unavailability if the need arises.

Running failure, type 4:

models a component with a constant failure rate during its mission. It is usable for components known to be available at the start of the mission and which have to stay unavailable during the mission time (e.g., up to a moment the installation has been brought to a safe condition).

$U = 1 - \exp(-\lambda \cdot T_m)$, where T_m equals the mission time.

Module, type 5:

not used in this study.

Appendix C.1.5 Example of data to be provided for each BE:

As an example of the way the data should be provided to ECN, the BE DE-SEN-HISPS-LF is given:

DE-SEN-HISPS-LF Sensor on High SP. Shaft loses func. (LF)

7e-6/hr based on NEDWIND40 case which used for this component generic data contained in [Denson, IEEE]. It is not yet clear if the value represents an average or if the two references provide the same value.

Basic Event Id	Failure Model	Un'av'ty	Fail Rate	Time Factor
DE-SEN-HISPS-LF	Type 2-Periodical	3.00E-002	7.00E-000	8.76E+003

So, a failure rate of 7e-6/hr. The component is periodically tested once a year ($T=8760$ hours), according to the description in the EWTS-I report. Failure of the component is not directly detected (may be dormant). It is not clear if this sensor is demanded more frequently than once per year. If such information is known, the average demand period could be taken less than one year.

Appendix C.2 Overall approach ECN

For this benchmark, use was made of the most recent (confidential) ECN wind turbine case study (November 1996, referred to as further as 'LAST'). For this LAST study, 6 generic databases (from other than the wind turbine industry) were consulted. For the EWTS-II benchmark study, these individual generic databases (reports) were not consulted again. Rather, the information was directly taken from the

LAST study. The information taken were failure rates (per hour), for a particular component and failure mode.

One problem was that in the LAST report, no details were given on how data from more than one generic source were combined. The impression is that the average failure rates were presented.

This information was supplemented with experience from other wind turbine case studies (mainly LW15/75 and NEW ECS-45) and engineering judgment.

The design information was taken from the EWTS-I report. This applied to the type of components (whether it was a monitored one with self-annunciating features of its failure, whether it was a standby periodically tested component) and test interval parameters (a test interval of one year was mentioned).

Additional assumptions had to be made on parameters like detection, repair times, test intervals, the frequency of normal shutdowns, and the frequency of visits to the wind turbine.

Test intervals of standby components

The turbine is tested/maintained once a year, so this gives an upperbound of the test interval. It is assumed that test/maintenance will reveal any dormant failure contained in the basic event list. For certain components, actual demands occur more frequently than this yearly interval. In that case, the test interval could be set to the average interval between two demands on that component. This applies in particular to the components involved in the normal shutdowns.

However, for this demonstration case, such information is not available, but an assumption could be made on the number of normal shutdowns per year.

The components demanded in a normal shutdown are:

K1, K3, K4, and CPU.

Investigation of the FTs shows that the following components/BEs are also ‘demanded’ in these cases, i.e., failure of them would be identified if the normal shutdown should fail:

Via K1: all MB BEs; Via K3: KM and the CCF of the TB; Via K4: K6.

In addition, a potential overspeed situation is also assumed to occur relatively frequently. (E.g, 5 times per year). The following components are demanded in such cases:

Overspeed relay; OT, H, KM and all MB BEs; All independent TB BEs.

Frequency of visits and detection times

(Engineering Judgment, for a real case this can easily be derived from design specific information sources) It is assumed that the wind turbine is at least visited once per day. So, for the monitored components the detection time is no more than 24 hours and failure of such a component in an operating wind turbine will not last longer than this 24 hours.

Frequency of a normal shutdown

(Engineering Judgment, for a real case this can easily be derived from design specific information sources)

The frequency of a normal shutdown is estimated as once per month, so T is set to 730 hours.

Frequency of overspeed

(Engineering Judgment, for a real case this can easily be derived from design specific information sources)

The frequency of a potential overspeed situation is estimated as five times per year, so T is set 1752 hours.

Summary of data and rationale

The data for the failure rates and rationale are listed below.

BASIC EVENT ID DESCRIPTION/RATIONALE FOR FAILURE RATE/FREQUENCY/ETC.

DE-CPU-----ERR CPU-failure
 NEWECS-45 study showed no CPU failures in contrast to electrical/hydraulic/mechanical failures: therefore, a factor of 10-100 compared to, e.g., electrical failures see also page 47, 2-nd bullet, ECN-C--94-066 So, take the least failure rate, divide by 10

DE-SEN-----LF Failure of overspeed relay
 7e-6/hr based on NEDWIND40 (Denson, IEEE). Not clear if it represents an average or if all references provide the same value. Note T taken as average recurrence time of an overspeed alarm

DE-SEN-HISPS-LF SENSor on High SP. Shaft loses func. (LF)
 7e-6/hr based on NEDWIND40 (Denson, IEEE). Not clear if it represents an average or if all references provide the same value. Note T taken as average recurrence time of an overspeed alarm

DE-TC-----LF Thermo couple fails
 35E-6/hr based on NEDWIND40 (Cremer, Green). Not clear if it represents an average or if all references provide the same value.

EL-CON-H-----FTO Contactor H fails to open
 EL-CON-K1----FTO Contactor K1 fails to open
 EL-CON-K2----FTO Contactor K2 fails to open
 EL-CON-K3----FTO Contactor K3 fails to open
 EL-CON-K4----FTO Contactor K4 fails to open
 EL-CON-K6----FTO Contactor K6 fails to open
 EL-CON-KM----FTO Contactor KM fails to open
 EL-CON-OT----FTO Contactor OT fails to open
 For all contactors, a generic failure rate of 1E-6/hr is used. Such value is referenced in more than one generic source, according to the NEDWIND40 study (Denson, Davidson, Dummer, IEEE)

IE-S7 Generator temp. over 150 C AND wind speed over 5 m
 LW15/75 study: 0.038/year (unconditional of wind speed)

MB-BP-----WEA Too much wear of brake pads.
 Least of all other failure rates has been used (Engineering Judgment)

MB-CYL-----STU Cylinder stuck.
 53E-6/hr based on NEDWIND40 (Green, Denson, Davidson, IEEE). Not clear if it represents an average or if all references provide the same value.

MB-DIS-----FRA Fracture of disk or shaft.
 0.02E-6/hr based on NEDWIND40 (Green)

MB-FU-----BLK Filter unit blocked
 Least of all other failure rates has been used (Engineering Judgement)

MB-SPR-----LF Insufficient spring force.
 12.5E-6/hr based on NEDWIND40 (Green, Denson). Not clear if it represents an average or if both references provide the same value.

MB-TVA-----BLK Throttle valve blocked.
 Used value 37E-6/hr, based on NEDWIND40 (Cremer, Green, Denson, Davidson, IEEE). It is not clear if this value was the average of these 5 references For the throttle valve, the same value is used (Engineering Judgment)

MB-VAL-Y1----STU Valve Y1 stucked.
 Used value 37E-6/hr, based on NEDWIND40 (Cremer, Green, Denson, Davidson, IEEE). It is not clear if this value was the average of these 5 references For the throttle valve, the same value is used (Engineering Judgement)

MB-VAL-Y2----STU Valve Y2 stucked.
 Used value 37E-6/hr, based on NEDWIND40 (Cremer, Green, Denson, Davidson, IEEE). It is not clear if this value was the average of these 5 references For the throttle valve, the same value is used (Engineering Judgment)

TB-CP--1-----STU Catchplate stucked to magnet.
 TB-CP--2-----STU Catchplate stucked to magnet.
 TB-CP--3-----STU Catchplate stucked to magnet.
 Use similar value as for hinge

TB-DAM-1-----STU Damper stucked.
 TB-DAM-2-----STU Damper stucked.
 TB-DAM-3-----STU Damper stucked.
 Use similar value as for hinge
 TB-HIN-1-----BST Hinge broken or stucked.
 TB-HIN-2-----BST Hinge broken or stucked.
 TB-HIN-3-----BST Hinge plate broken or stucked.
 For hinge, 1E-4/hr based on NEDWIND40 (Denson1988).
 TBXTIP-123---FTD Common cause failure of three tip brakes.
 CCF unavailability takes into account independent failure rate, the number of
 tip brakes (3), and CCF parameters for CCF involving 2 and 3 tip brakes; A
 generic beta factor of 0.1 is taken, hence CCF is 0.1 of independent failure,
 hence 3*0.1*1E-4

Appendix C.3 Overall approach RISØ

Risø used three types of data sources:

- “Nordic generic”: a pseudonym for a Scandinavian manufacturer. Risø got the permission to use this “real” failure data for a 150 kW turbine on the condition that the real name would remain confidential;
- FARADIP.THREE database: an English database for component reliabilities. It can be bought from TECHNIS, 26 Orchard Drive, Tonbridge, Kent TN10 4LG, UK. Risø has had it here for some years, and has used it a good deal.
- Engineering judgment: Rise considers the design method as follows: Such components are designed with a 20 years life expectancy and it is allowed that 5 percent of the items designed that way may fail before 20 years have passed. If you assume (which the design rules do) that the life expectancy of such a mechanical component has a normal distribution, and at the same time you take (as the design rules state, too) , 0.2 as parameter for the normal distribution, it is possible to calculate the mean life expectancy of the items, whereby you end up with 29 years (if only 5 percent are allowed to fail before 20 years). The mean time between failures at 29 years correspond to a failure rate of 3.8e-6/hr.

The data and rationale for the first iteration is presented below. The data for the second iteration is presented in Appendix C.4.

DE-CPU-ERR CPU-failure

Data are “Nordic generic”, 0.7e-6/hr

Basic event Id	Failure model	Un'av'ty	Fail rate	Time factor
DE-CPU-ERR	Type 1-repairable		0.7e-6	*)

*) = 24 hours

DE-SEN-LF

Data are “Nordic generic”, 0.7e-6/hr

Basic event Id	Failure model	Un'av'ty	Fail rate	Time factor
DE- SEN-LF	Type 1-repairable		0.7e-6	*)

DE-SEN-HISPS-LF

Data are “Nordic generic”, 0.7e-6/hr

Basic event Id	Failure model	Un'av'ty	Fail rate	Time factor
DE- SEN-HISPS-LF	Type 1-repairable		0.7e-6	*)

DE-TC-LF

Data from FARADIP data base, average value

Basic event Id	Failure model	Un'av'ty	Fail rate	Time factor
DE-TC-LF	Type 1-repairable		10e-6	*)

EL-CON-H-FTO

Data are “Nordic generic”, 0.7e-6/hr

Basic event Id	Failure model	Un'av'ty	Fail rate	Time factor
EL-CON-H-FTO	Type 1-repairable		0.7e-6	*)

EL-CON-K1-FTO

Data are “Nordic generic”, 0.7e-6/hr

Basic event Id	Failure model	Un'av'ty	Fail rate	Time factor
EL-CON-K1-FTO	Type 1-repairable		0.7e-6	*)

EL-CON-K2-FTO

Data are “Nordic generic”, 0.7e-6/hr

Basic event Id	Failure model	Un'av'ty	Fail rate	Time factor
EL-CON-K2-FTO	Type 1-repairable		0.7e-6	*)

EL-CON-K3-FTO

Data are “Nordic generic”, 0.7e-6/hr

Basic event Id	Failure model	Un'av'ty	Fail rate	Time factor
EL-CON-K3-FTO	Type 1-repairable		0.7e-6	*)

EL-CON-K4-FTO

Data are “Nordic generic”, 0.7e-6/hr

Basic event Id	Failure model	Un'av'ty	Fail rate	Time factor
EL-CON-K4-FTO	Type 1-repairable		0.7e-6	*)

EL-CON-K5-FTO

Data are “Nordic generic”, 0.7e-6/hr

Basic event Id	Failure model	Un'av'ty	Fail rate	Time factor
EL-CON-K5-FTO	Type 1-repairable		0.7e-6	*)

EL-CON-K6-FTO

Data are “Nordic generic”, 0.7e-6/hr

Basic event Id	Failure model	Un'av'ty	Fail rate	Time factor
EL-CON-K6-FTO	Type 1-repairable		0.7e-6	*)

EL-CON-KM-FTO

Data are “Nordic generic”, 0.7e-6/hr

Basic event Id	Failure model	Un'av'ty	Fail rate	Time factor
EL-CON-KM-FTO	Type 1-repairable		0.7e-6	*)

EL-CON-OT-FTO

Data are “Nordic generic”, 0.7e-6/hr

Basic event Id	Failure model	Un'av'ty	Fail rate	Time factor
EL-CON-OT-FTO	Type 1-repairable		0.7e-6	*)

IE-S7

Data for generator 0.7e-6 are “Nordic generic”, while it is assumed that the probability of a wind speed > 5m/s is 0.5. The resulting rate is calculated as the product of these 2 values, i.e. 0.35e-6/hr.

Basic event Id	Failure model	Un'av'ty	Fail rate	Time factor
IE-S7			0.35e-6	

MB-BP-WEA

“Nordic generic data” has a total value for MB-BP-WEA, MB-CYL-STU, MB-DIS-FRA, MB-FU-BLK and MB-SPR-LF as a system, so 1/5 of the value is taken as the value for each. It is not known, whether this division in equal values is correct.

Basic event Id	Failure model	Un'av'ty	Fail rate	Time factor
MB-BP-WEA	Type 1-repairable		0.14e-6	*)

MB-CYL-STU

“Nordic generic data” has a total value for MB-BP-WEA, MB-CYL-STU, MB-DIS-FRA, MB-FU-BLK and MB-SPR-LF as a system, so 1/5 of the value is taken as the value for each. It is not known, whether this division in equal values is correct.

Basic event Id	Failure model	Un'av'ty	Fail rate	Time factor
MB- CYL-STU	Type 1-repairable		0.14e-6	*)

MB-DIS-FRA

“Nordic generic data” has a total value for MB-BP-WEA, MB-CYL-STU, MB-DIS-FRA, MB-FU-BLK and MB-SPR-LF as a system, so 1/5 of the value is taken as the value for each. It is not known, whether this division in equal values is correct.

Basic event Id	Failure model	Un'av'ty	Fail rate	Time factor
MB- DIS-FRA	Type 1-repairable		0.14e-6	*)

MB-FU-BLK

“Nordic generic data” has a total value for MB-BP-WEA, MB-CYL-STU, MB-DIS-FRA, MB-FU-BLK and MB-SPR-LF as a system, so 1/5 of the value is taken as the value for each. It is not known, whether this division in equal values is correct.

Basic event Id	Failure model	Un'av'ty	Fail rate	Time factor
MB-FU-BLK	Type 1-repairable		0.14e-6	*)

MB-SPR-LF

“Nordic generic data” has a total value for MB-BP-WEA, MB-CYL-STU, MB-DIS-FRA, MB-FU-BLK and MB-SPR-LF as a system, so 1/5 of the value is taken as the value for each. It is not known, whether this division in equal values is correct.

Basic event Id	Failure model	Un'av'ty	Fail rate	Time factor
MB- SPR-LF	Type 1-repairable		0.14e-6	*)

MB-TVA-BLK

Data are “Nordic generic”, 2.8e-6/hr

Basic event Id	Failure model	Un'av'ty	Fail rate	Time factor
MB-TVA-BLK	Type 1-repairable		2.8e-6	*)

MB-VAL-Y1-STU

Data are “Nordic generic”, 0.7e-6/hr

Basic event Id	Failure model	Un'av'ty	Fail rate	Time factor
MB-VAL-Y1-STU	Type 1-repairable		0.7e-6	*)

MB-VAL-Y2-STU

Data are “Nordic generic”, 0.7e-6/hr

Basic event Id	Failure model	Un'av'ty	Fail rate	Time factor
MB-VAL-Y2-STU	Type 1-repairable		0.7e-6	*)

TB-CP-1-STU

Data are average for heavy duty magnets taken from the FARADIP database.

Basic event Id	Failure model	Un'av'ty	Fail rate	Time factor
TB-CP-1-STU	Type2-periodical		3.5e-6	8760

TB-CP-2-STU

Data are average for heavy duty magnets taken from the FARADIP database.

Basic event Id	Failure model	Un'av'ty	Fail rate	Time factor
TB-CP-2-STU	Type2-periodical		3.5e-6	8760

TB-CP-3-STU

Data used are average values for heavy duty magnets, taken from the FARADIP database.

Basic event Id	Failure model	Un'av'ty	Fail rate	Time factor
TB-CP-3-STU	Type2-periodical		3.5e-6	8760

TB-DAM-1-STU

Data used are for hydraulic pistons, taken from the FARADIP database

Basic event Id	Failure model	Un'av'ty	Fail rate	Time factor
TB- DAM-1-STU	Type2-periodical		1e-6	8760

TB-DAM-2-STU

Data used are for hydraulic pistons, taken from the FARADIP database

Basic event Id	Failure model	Un'av'ty	Fail rate	Time factor
TB- DAM-2-STU	Type2-periodical		1e-6	8760

TB-DAM-3-STU

Data used are for hydraulic pistons, taken from the FARADIP database

Basic event Id	Failure model	Un'av'ty	Fail rate	Time factor
TB- DAM-3-STU	Type2-periodical		1e-6	8760

TB-HIN-1-STU

Data are engineering judgement based on a design to last for 20 years with a 5 percent fractile of a normal distribution (= 0.2).

Basic event Id	Failure model	Un'av'ty	Fail rate	Time factor
TB- DAM-3-STU	Type2-periodical		3.8e-6	8760

TB-HIN-2-STU

Data are engineering judgement based on a design to last for 20 years with a 5 percent fractile of a normal distribution (= 0.2).

Basic event Id	Failure model	Un'av'ty	Fail rate	Time factor
TB- HIN-2-STU	Type2-periodical		3.8e-6	8760

TB-HIN-3-STU

Data are engineering judgement based on a design to last for 20 years with a 5 percent fractile of a normal distribution (= 0.2).

Basic event Id	Failure model	Un'av'ty	Fail rate	Time factor
TB- HIN-3-STU	Type2-periodical		3.8e-6	8760

TBXTIP-123-FTD

Failure assumed to be 24 V AC failure, i.e. transformer failure, data from FARADIP database

Common cause event	Failure model	Un'av'ty	Fail rate	Time factor
TBXTIP-123-FTD	Type 1-repairable		0.4e-6	

Appendix C.4 Data and results

The data used and the results are summarised in the following spreadsheets. RISØ2 stands for the second iteration data of Risø.

The total operational time should be assessed according to the formula;

$$T_{\text{total}} = (t_{\text{Now}} - t_{\text{Past}}) N_{\text{WTB}} - \sum_{i=1}^{N^f} (t_{\text{Now}} - t_f^i) - \sum_{i=1}^{N^s} (t_i^s - t_{\text{Past}})$$

where t_{Past} is defined as the date of reporting the first failure in the database, N_{WTB} is the number of wind turbines under observation, N^f is the number of wind turbines removed from operation within the interval $[t_{\text{Past}}, t_{\text{Now}}]$, N^s is the number of wind turbines put into operation within the interval $[t_{\text{Past}}, t_{\text{Now}}]$. The remaining variables are shown in Fig. D1

Data for case study EWTS-2

Basic Event Id	Failure Model			U _h /a/ty			Fail Rate			RISO2
	ECN	RISO	RISO2	ECN	RISO	RISO2	ECN	RISO		
DE-CPU—ERR	Type 1	Type 1	Type 1	4.8e-8	1.7e-5	1.7e-5	2.0e-9	7.0e-7		
DE-SEN—LF	Type 2	Type 1	Type 2	6.1e-3	1.7e-5	3.1e-3	7.0e-6	7.0e-7		
DE-SEN-HSPS-LF	Type 2	Type 1	Type 2	3.0e-2	1.7e-5	3.1e-3	7.0e-6	7.0e-7		
DE-TC—LF	Type 2	Type 1	Type 2	1.4e-1	2.4e-4	4.3e-2	3.5e-5	1.0e-5		
EL-CONH—FTO	Type 2	Type 1	Type 2	8.8e-4	1.7e-5	3.1e-3	1.0e-6	7.0e-7		
EL-CONK1—FTO	Type 2	Type 1	Type 2	3.7e-4	1.7e-5	3.1e-3	1.0e-6	7.0e-7		
EL-CONK2—FTO	Type 2	Type 1	Type 2	4.4e-3	1.7e-5	3.1e-3	1.0e-6	7.0e-7		
EL-CONK3—FTO	Type 2	Type 1	Type 2	3.7e-4	1.7e-5	3.1e-3	1.0e-6	7.0e-7		
EL-CONK4—FTO	Type 2	Type 1	Type 2	3.7e-4	1.7e-5	3.1e-3	1.0e-6	7.0e-7		
EL-CONK6—FTO	Type 2	Type 1	Type 2	3.7e-4	1.7e-5	3.1e-3	1.0e-6	7.0e-7		
EL-CONKM—FTO	Type 2	Type 1	Type 2	3.7e-4	1.7e-5	3.1e-3	1.0e-6	7.0e-7		
EL-CONOT—FTO	Type 2	Type 1	Type 2	8.8e-4	1.7e-5	3.1e-3	1.0e-6	7.0e-7		
IES7	Type 3	Type 1	Type 1	3.8e-2	8.4e-6	3.1e-3		3.5e-7		
MB-BP—WEA	Type 2	Type 1	Type 2	7.3e-6	3.4e-6	6.1e-4	2.0e-8	1.4e-7		
MB-CYL—STU	Type 2	Type 1	Type 2	1.9e-2	3.4e-6	6.1e-4	5.3e-5	1.4e-7		
MB-DIS—FRA	Type 2	Type 1	Type 2	7.3e-6	3.4e-6	6.1e-4	2.0e-8	1.4e-7		
MB-FU—BLK	Type 2	Type 1	Type 2	7.3e-6	3.4e-6	6.1e-4	2.0e-8	1.4e-7		
MB-SFR—LF	Type 2	Type 1	Type 2	4.6e-3	3.4e-6	6.1e-4	1.3e-5	1.4e-7		
MB-TVA—BLK	Type 2	Type 1	Type 2	1.3e-2	6.7e-5	1.2e-2	3.7e-5	2.8e-6		
MB-VAL-Y1—STU	Type 2	Type 1	Type 2	1.3e-2	1.7e-5	3.1e-3	3.7e-5	7.0e-7		
MB-VAL-Y2—STU	Type 2	Type 1	Type 2	1.3e-2	1.7e-5	3.1e-3	3.7e-5	7.0e-7		
TB-CP-1—STU	Type 2	Type 2	Type 2	8.3e-2	1.5e-2	1.5e-2	1.0e-4	3.5e-6		
TB-CP-2—STU	Type 2	Type 2	Type 2	8.3e-2	1.5e-2	1.5e-2	1.0e-4	3.5e-6		
TB-CP-3—STU	Type 2	Type 2	Type 2	8.3e-2	1.5e-2	1.5e-2	1.0e-4	3.5e-6		
TB-DAM1—STU	Type 2	Type 2	Type 2	8.3e-2	4.4e-3	4.4e-3	1.0e-4	1.0e-6		
TB-DAM2—STU	Type 2	Type 2	Type 2	8.3e-2	4.4e-3	4.4e-3	1.0e-4	1.0e-6		
TB-DAM3—STU	Type 2	Type 2	Type 2	8.3e-2	4.4e-3	4.4e-3	1.0e-4	1.0e-6		
TB-HIN1—BST	Type 2	Type 2	Type 2	8.3e-2	1.7e-2	1.7e-2	1.0e-4	3.8e-6		
TB-HIN2—BST	Type 2	Type 2	Type 2	8.3e-2	1.7e-2	1.7e-2	1.0e-4	3.8e-6		
TB-HIN3—BST	Type 2	Type 2	Type 2	8.3e-2	1.7e-2	1.7e-2	1.0e-4	3.8e-6		
TBXTIP-123—FTD	Type 2	Type 1	Type 2	1.1e-2	2.0e-6	8.7e-3	3.0e-5	1.0e-6	2.0e-6	

Time Factor Ratio U_h/a/ty Ratio Fail R Ratio Time f New value for sensitivity
 ECN RISO RISO2 ECN/RISO ECN/RISO ECN/RISO Sens. 1 Sens. 2

DE-CPU—ERR	24	24	24	0.003	0.003	1	4.8e-8		
DE-SEN—LF	1750	24	8760	363.7	10.0	72.9	1.7e-4		
DE-SEN-HSPS-LF	8760	24	8760	1785.7	10.0	365.0	1.7e-4		
DE-TC—LF	8760	24	8760	579.2	3.5	365.0	8.4e-4		
EL-CONH—FTO	1750	24	8760	52.1	1.4	72.9	2.4e-5		
EL-CONK1—FTO	730	24	8760	21.7	1.4	30.4	2.4e-5		
EL-CONK2—FTO	8760	24	8760	260.1	1.4	365.0	2.4e-5		
EL-CONK3—FTO	730	24	8760	21.7	1.4	30.4	2.4e-5		
EL-CONK4—FTO	730	24	8760	21.7	1.4	30.4	2.4e-5		
EL-CONK6—FTO	730	24	8760	21.7	1.4	30.4	2.4e-5		
EL-CONKM—FTO	730	24	8760	21.7	1.4	30.4	2.4e-5		
EL-CONOT—FTO	1750	24	8760	52.1	1.4	72.9	2.4e-5		
IES7		24	8760	4523.8	na	na		3.8e-2	
MB-BP—WEA	730	24	8760	2.2	0.1	30.4	4.8e-7		
MB-CYL—STU	730	24	8760	5684.5	378.6	30.4	1.3e-3		
MB-DIS—FRA	730	24	8760	2.2	0.1	30.4	4.8e-7		
MB-FU—BLK	730	24	8760	2.2	0.1	30.4	4.8e-7		
MB-SFR—LF	730	24	8760	1354.2	89.3	30.4	3.0e-4		
MB-TVA—BLK	730	24	8760	199.4	13.2	30.4	8.9e-4		
MB-VAL-Y1—STU	730	24	8760	797.6	52.9	30.4	8.9e-4		
MB-VAL-Y2—STU	730	24	8760	797.6	52.9	30.4	8.9e-4		
TB-CP-1—STU	1750	8760	8760	5.4	28.6	0.2	4.3e-1		
TB-CP-2—STU	1750	8760	8760	5.4	28.6	0.2	4.3e-1		
TB-CP-3—STU	1750	8760	8760	5.4	28.6	0.2	4.3e-1		
TB-DAM1—STU	1750	8760	8760	18.9	100.0	0.2	4.4e-1		
TB-DAM2—STU	1750	8760	8760	18.9	100.0	0.2	4.4e-1		
TB-DAM3—STU	1750	8760	8760	18.9	100.0	0.2	4.4e-1		
TB-HIN1—BST	1750	8760	8760	5.0	26.3	0.2	4.3e-1		
TB-HIN2—BST	1750	8760	8760	5.0	26.3	0.2	4.3e-1		
TB-HIN3—BST	1750	8760	8760	5.0	26.3	0.2	4.3e-1		
TBXTIP-123—FTD	730	2	8760	5450.0	30.0	365.0	6.0e-5		

Results case study EWTS-2

Comparison ECN and Riso results; based on importances and on totals
2-nd (final) iteration

Importances ECN

Rank	EVEN POINT EST.	F-V IMPORT	RSK ACMT	RISK RED	Corr. rank
4 MB-CYL----	1.9e-2	79%	41.8	4.9	1
5 TBXTIP-12;	1.1e-2	41%	38.5	1.7	2
6 TB-HIN-1/2/	8.3e-2	19%	3.2	1.2	3
9 TB-DAM-1/2/3-----STU					
12 TB-CP--1/2/3-----STU					
15 MB-SPR---	4.5e-3	19%	42.4	1.2	4
16 MB-VAL-Y	1.3e-2	1%	2.1	1.0	5
17 EL-CON-K	3.6e-4	1%	29.1	1.0	6
18 MB-TVA---	1.3e-2	1%	1.6	1.0	7
19 MB-VAL-Y	1.3e-2	1%	1.6	1.0	7
20 MB-FU-----	7.3e-6	0%	42.2	1.0	8
21 MB-DIS----	7.3e-6	0%	42.2	1.0	8
22 MB-BP-----	7.3e-6	0%	42.2	1.0	8

Note: IEF and XCOM have been deleted from the lists (no component failure modes)

Importances RISO

Rank	EVEN POINT EST.	F-V IMPORT	RSK ACMT	RISK RED	Corr. rank
4 MB-CYL----	6.1e-4	20%	322.2	1.2	2
3 TBXTIP-12;	8.7e-3	96%	110.1	24.1	1
12 TB-HIN-1/;	1.6e-2	1%	1.5	1.0	6
19 TB-DAM-1	4.4e-3	0%	1.5	1.0	9
15 TB-CP--1/;	1.5e-2	1%	1.5	1.0	7
5 MB-SPR---	6.1e-4	20%	322.2	1.2	2
10 MB-VAL-Y	3.1e-3	1%	5.9	1.0	4
9 EL-CON-KM	3.1e-3	4%	12.9	1.0	3
11 MB-TVA---	1.2e-2	1%	2.0	1.0	5
18 MB-VAL-Y	3.1e-3	0%	2.0	1.0	8
6 MB-FU-----	6.1e-4	20%	322.2	1.2	2
7 MB-DIS----	6.1e-4	20%	322.2	1.2	2
8 MB-BP-----	6.1e-4	20%	322.2	1.2	2

Totals

	IEF S7	OS Freq	Cond. prob
ECN	3.8e-2	2.0e-5	5.3e-4
RISO	8.4e-6	7.1e-15	8.5e-10
RISO2	3.1e-3	8.3e-8	2.7e-5

Difference

ECN/RISO	4523.8	2.8e+9	6.3e+5	first iteration
ECN/RISO2	12.4	242.2	19.6	second iteration

APPENDIX D. DERIVATION OF FAILURE RATES FROM REPORTED FAILURES

The general formula for assessing the failure rate of the i th basic event, λ_{BE_i} , (h^{-1}) is as follows:

$$\lambda_{BE_i} = \frac{\sum_{j=1}^k n_{ij}}{m_i T_{total}}$$

where n_{ij} is the number of occurrences of the i th basic event for the j th WTB; m_i is the number of similar components on one WTB; k - the number of wind turbines of a given type; T_{total} (h) -total operational repair time for all k WTBs. To understand the link between a basic event and a component, it is enough to say that a basic event is completely defined by the system, component, and the failure mode, i.e. the same component can belong to different basic events.

The parameter T_{total} can be calculated in different ways depending on particularities of the data collecting. So, if failure data are collected from all wind turbines in operation, then $T_{total} = \sum^k t_j$ where t_j is the total time of operation of the j th wind turbine of a given type. In case the failure data are collected from a fixed time in the past t_{past} we have to take into account five different wind turbines life lines (see Fig. D.1)

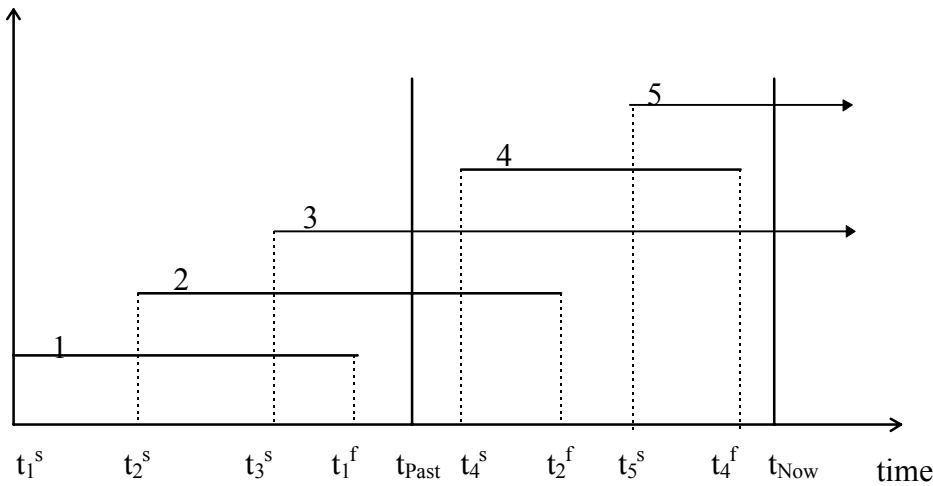


Figure D.1 Possible life lines of wind turbines; t_i^s is the time of the start of the i th wind turbine, t_i^f is the stop of the operation, t_{past} is the time of the beginning of the data collection, and t_{Now} is the present time.

EUROPEAN WIND TURBINE STANDARDS II
PART 3
INTEGRATION OF BLADE TEST IN DESIGN

B.H. Bulder (ed.)	Netherlands Energy Research Foundation ECN
P. Vionis	Centre of Renewable Energy Research CRES
F. Arias Vega	Centro de Energeticas Investigaciones Medioambientales y Technologicas
J.C. Sanz-Martín	idem
M.W. Jensen	Risø National Laboratory
Chr. Brokopf	Germanischer Lloyd

CONTENTS OF PART 3

1	INTRODUCTION	7
1.1	General	7
1.2	Project work	8
2	DISCUSSION ON THE VALUE OF TESTING OF ROTOR BLADES FOR DESIGNERS	9
2.1	General	9
2.2	Property tests	9
2.2.1	Static tests	9
2.2.2	Natural vibration tests	10
2.3	Fatigue tests	11
2.3.1	Introduction	11
2.3.2	Damage equivalent testing	11
3	CONCLUSION	15
3.1	General	15
3.2	Rotor blade property tests	15
3.3	Stiffness/static strength tests	15
3.4	Fatigue strength tests	15
	REFERENCES	17
A	CURRENT TEST PRACTICES	19
A.1	General	19
A.2	Background	19
A.3	Test Principles or Approaches	20
A.3.1	Tests giving statistic information	20
A.3.2	“Empiric” tests	20
A.3.3	Tests based on a probabilistic approach	20
A.4	Material and component tests	21
A.5	Full scale strength tests	21
A.5.1	Ultimate strength tests	22
A.5.2	Fatigue strength test	22
A.6	Full scale blade property tests	23
A.6.1	General	23
A.6.2	Deflection	23
A.6.3	Natural frequencies	23
A.6.4	Mass distribution	23
A.6.5	Stiffness distribution	23

A.6.6	Mode shapes	24
A.6.7	Strain distribution measurements	24
A.6.8	Damping	24
A.6.9	Creep	24
A.6.10	Other non destructive testing	25
A.6.11	Blade sectioning	25
B	CURRENT STANDARDS AND INFORMATION FROM PREVIOUS PROJECTS	27
B.1	Introduction	27
B.2	Standards and Codes	27
B.2.1	Wind turbine engineering related standards	27
B.2.2	Non wind turbine engineering standards	27
B.3	Research information for verification/validation test	29
B.3.1	Strength and Fatigue of Large Size Wind Turbine Rotors S&FAT	29
B.3.2	European Wind Turbine Testing Procedure Development	29
B.3.3	PRObability FATigue Reliability	29
C	GUIDELINES FOR TESTS TO VERIFY ENGINEERING MODELS	31
C.1	Overview	31
C.2	Full scale tests	31
C.2.1	Purpose of tests	31
C.2.2	Design requirements (elements of design principles) (design methodology)	32
C.2.3	Types of testing	32
C.2.4	Aeroelastic model verification	34
C.2.5	Structural model verification	34
C.2.6	Sensitivity analysis	35
C.2.7	Required accuracy	35
D	GUIDELINES TO INTERPRET RESULTS OF MECHANICAL TEST	37
D.1	Introduction	37
D.2	Need of tests	37
D.3	Causes of the differences between the blade theoretical calculations and the tests results	37
D.4	Classification of static tests	39
D.5	Blade identification measurements	40
D.6	Natural Vibration Test (eigenfrequencies)	41
D.6.1	Natural Blade Frequencies	41
D.6.2	Damping	41
D.7	Elastic test	41
D.7.1	Equivalent stiffness test	42

D.7.2	Influence coefficient test	43
D.8	Static loads strength test	44
D.8.1	Limit load strength test	44
D.8.2	Ultimate load test	46
E	CRUSHING¹	49

1 INTRODUCTION

1.1 General

The general aim of the project European Wind Turbine Standards II is to remove vital constraints and bottle necks in the technical harmonisation of the European wind turbine market.

Concerning sub project 3: Integration of Blade Test in Design, this objective can be met when a recommended methodology is developed to include full-scale blade tests in the wind turbine design process. The project will be performed along the following activities:

1. an evaluation of the known test practices,
2. evaluation of existing standards,
3. specification of guidelines which items have to be taken into account,
4. specification of guidelines how to interpret the test results with respect to the design criteria,
5. investigation of potential valuation of a static and fatigue strength test.

Full scale blade tests, as they are performed nowadays, are performed to demonstrate adequate safety margin and verify design calculations. Actual test and measurement procedures do not need to be addressed here, especially because they are in development under the coordination of a working group of IEC TC-88WG8.

During the performance of the work a continuing discussion has been held whether the general objective, the deliverables and the to be performed activities are in compliances with each other.

The performance of mechanical tests on rotor blades is already a fact today, although the tests are usually performed at the end of the design process. Consequently the test results are not used to upgrade the design, unless the experiments showed that the design criteria are not met. These test are performed to demonstrate, to a reasonable level of certainty, that the rotor blade's, when produced according to certain specifications, specified limit states are not reached. In other words that the rotor blade will survive the design load spectrum. The usefulness of these test for the designer to improve the design is discussed in section 2.

Due to the fact that the conditions during the test, specifically for the strength and fatigue test, are different than in real service, and that the test has to be performed in a limited time period, implies that the test load spectrum is not equal to the design load spectrum. This makes full-scale testing, definition according to [3]:

both the test specimen and the loading spectrum, including sequence should be representative of actual service conditions

in fact not possible.

The full-scale tests which are performed nowadays usually have the objective to show that the construction and manufacturing is sound and has no flaws in them which would result is a catastrophic failure during its design life. However it is not possible to determine the actual margins of the individual failure mechanism let alone the combination of all failure mechanism. The results can also be used to verify whether the proper quantities have been used in the design analysis, e.g. whether the eigen frequencies of the blade assumed in the aero-elastic calculations is close to the measured ones.

To make a procedure where the tests should be incorporated in the design process at an earlier stage is not that simple because it is not possible to test a blade before the prototype is build. In fact only procedures what to do with the tests results can be developed while it is the decision of the designer whether he wants to redesign his rotor blade using the results of the tests. However the trend in most technologies is to reduce the time to market, which implies for rotor blade manufacturers that rotor blades are produced already in series before the testing is complete. Thus design alterations are only performed when there is a necessity.

In view of the above the authors assigned to this sub project, found it not possible to come up with a recommended methodology to include full-scale blade test in the wind turbine design process.

This part of the project describes the value of full-scale and component testing for designers. Components are included because they are usually tested at a much earlier stage in the design process. Especially when a new kind of construction is applied there is a need to have an engineering model, to dimension this part. These models can be based on a physical relation or empirical relations. The engineering model is usually verified with a number of test. These test are designed and analysed by the designers.

1.2 Project work

In this sub project we will come up with recommendations how to perform model verification tests of structural details or the full scale rotor blade and how to interpret the measured results.

Material characterisation and damage models are left out of this project. Material characterisation test are well defined in a number of ISO/DIN/ASTM test standards. Fatigue damage models are probably of such a fundamental level, and the cost to update the used models will probably be so high that it can not be expected that research funds available for wind energy industry will be directed to this area.

Test which are meant here are test to verify engineering models of e.g. blade root connections or shear web – shell connections. One could also think of buckling load test of parts of the rotor blade, with a realistic ratio between the bending moments and the shearing forces.

The engineering models verified by mechanical tests are models to determine the static strength, stiffness, fatigue life and stability of structural details which are common to modern large rotor blades.

The deliverables of the work as reported should contain information concerning recommended methodologies to include blade tests in the wind turbine design process in order to:

1. demonstrate adequate safety margin;
2. verify design calculations

All tests are split up in (blade) property tests, strength tests, and fatigue tests. For the activities 1 and 2, see previous page, use can be made of the reports and guidelines of the S&FAT [1] and IEC-TC88 WG8 [2] documents or any other document or standard which is directed to material and or structural testing.

2 DISCUSSION ON THE VALUE OF TESTING OF ROTOR BLADES FOR DESIGNERS

2.1 General

The objective to perform full-scale tests on rotor blades is usually to show that the blade has the properties which are assumed in the design calculations and that the strength, stability and fatigue design are sufficient. These tests convince customers and the certification authority that the blade design and manufacturing meets the design requirements.

These test do not prove that the design will not fail during service because the tests are designed with Design load spectrum as input and not with the Service load spectrum, see figure 2-1.

Other reasons, more aimed at improving the design process, to perform full-scale tests are, validation of computer programs or the model behind the program and determination of the weakest spot or section.

These full scale tests are normally not used to modify or optimize the design when all tests results are satisfactorily. When one or more tests show that the blade does not meet the design targets, and resulting in a blade not fit for purpose, it will be modified.

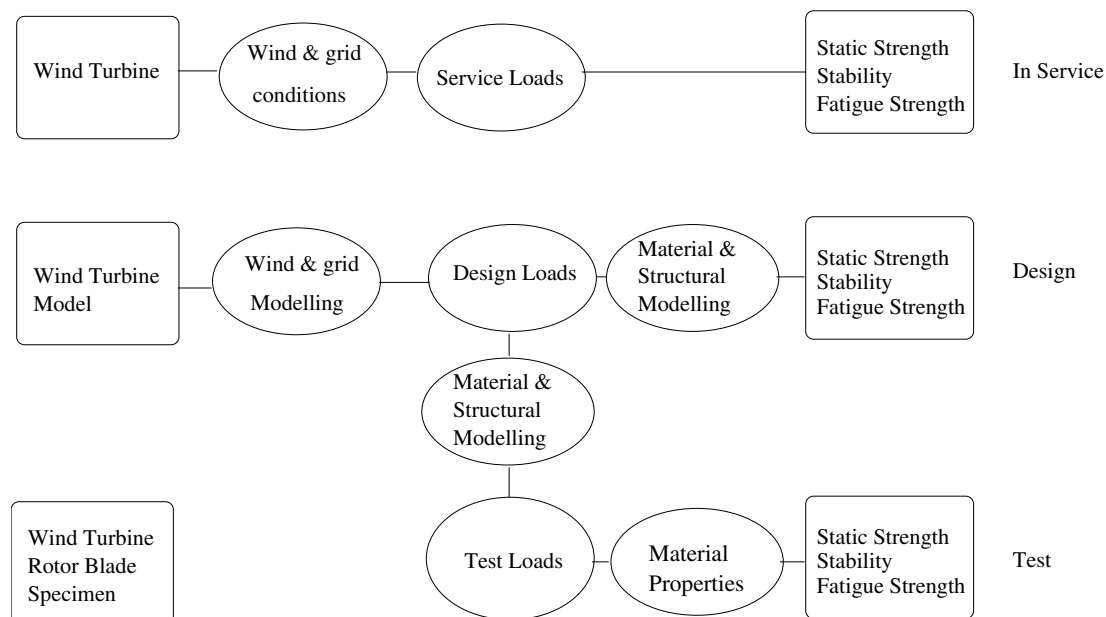


Figure 2.1 The scope of mechanical test for rotor blades

2.2 Property tests

2.2.1 Static tests

For strength/stiffness tests one can quite easily show that when the stress/strain distribution that is measured differs from the calculated or assumed distributions one has to go back to the design calculations. One has to check whether the measured blade properties are within the design margins for all failure phenomena, like strength, fatigue or stability. Also the reason behind the difference between the measured

and predicted stress/strain distributions should be determined. This is however not a simple problem since there are many factors that could influence the results. The differences can occur due to a bad engineering model or due to differences in the test w.r.t. the design load or due to differences between the design specification and the manufactured rotor blade. The differences due to bad engineering model are of most interest for this project. Differences due to the fact that the test loading is different from the design loading, e.g. shearing forces during the test are usually higher than the design loads due to concentrated load application, are not very interesting for the design – test evaluation. However analysis of a failure should include the possibility of such effects. When the origin of the difference is found one can update the design analysis procedure and could even optimize the blade when the error is larger than expected or required and it is attractive for cost saving to change the design.

Determination of the actual strength margins is more difficult, especially when the blade specimen also has to be used for the fatigue test. However even when it is allowed to destroy the blade one has to choose the loading situation for which the margin is determined. See for this problem figure 2-2 from the S&FAT report [1].

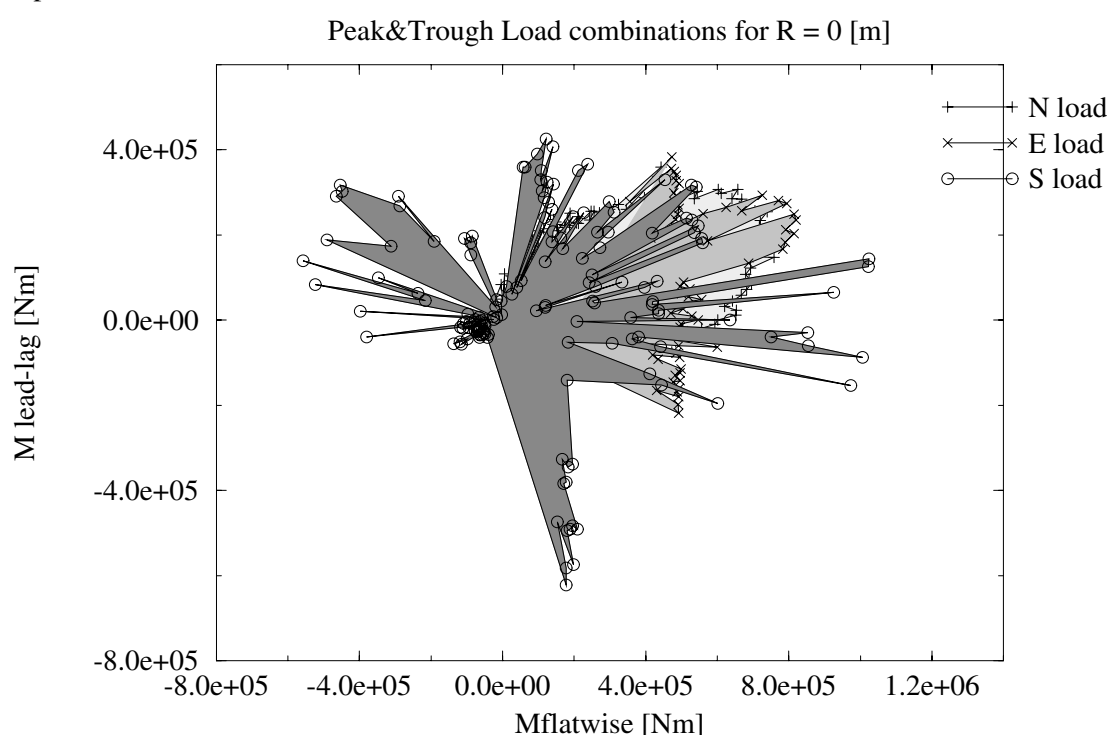


Figure 2.2 Binned peak&trough bending moments at rotor blade "F1" cross section 0.00 [m], excluding PLF_{lim} .

2.2.2 Natural vibration tests

The same reasoning holds for natural vibration tests, when large discrepancies are found w.r.t. the used or calculated eigenfrequencies in the design analysis, the designer has to repeat (some of) the aero-elastic calculations to determine the sensitivity of the response of the wind turbine towards the eigenfrequencies for the given external conditions and determine the loads on the rotor blades. If the sensitivity is large the design analysis has to be repeated with the measured values. It is also interesting to find the reason why

the eigen frequency is so much different than predicted. This could lead to better prediction methods for future designs.

2.3 Fatigue tests

2.3.1 Introduction

The reasoning for the fatigue test differs from the blade property tests. This is due to a number of reasons:

- Experimental fatigue results have a much larger scatter in life (or number of cycles): *it is assumed that for coupons the test life is between 0.3 – 3.0 times the design life* [3] than the scatter in static strength.
- The used allowable material properties in the fatigue analysis are very conservative. The characteristic values which are used are not less than 95 % survival probabilities with 95 % confidence limits, assuming a normal distribution of test results of these parameters thus normally fatigue failure will not occur.
- These allowable material parameters values are reduced by uncertainty factors which are assumed in the design analysis, e.g. for environmental effects (moisture, UV etc.), which are not present in the tests.
- Another major difference of fatigue tests w.r.t. strength tests is that one has to modify the design load spectrum to a test load spectrum. *A test has to be performed in a relatively short time, say between 3 and 6 month while the design life is in the order of 20 – 30 years.* This means that one has to modify the design load spectrum by relying, or on the basis of, the fatigue damage formulation used in the design analysis. This is in fact very awkward, because one of the objectives of performing full-scale fatigue test is to check whether the fatigue damage formulation is also correct for a complete rotor blade.

The conversion method between a design load spectrum to a test load spectrum is based on the following general procedure. One omits a large number of small load variations of which the fatigue damage is small or negligible, increase the load application rate and increases the range of a number of the remaining load cycles with a TLF (test load factor) to compensate for the cycles that are omitted.

- One other factor, of unknown magnitude, which could be included in the test load, a factor to compensate for testing only one blade. Due to scatter in (fatigue) strength and the possibility that the blade which is tested is of better quality than an average production blade one has to increase the loading to make sure that when a blade resists the test one can assume that a large majority of blades of the same type can resist the loading.

2.3.2 Damage equivalent testing

To do a meaningful (realistic) test, where the test fatigue damage is determined using the appropriate factors, see the design criteria of IEC 1400-1, for the test conditions and the test fatigue damage is at least equal to the design fatigue damage. The total load factor, the ratio between test loads and design loads, can be quite high resulting in fatigue loads higher than the maximum loads for a static strength test.

In formula form this comes down to the following simple equation:

$$D_{test} \geq D_{design} \quad (2.1)$$

In which the D stands for theoretical determined fatigue damage.

For the result of the fatigue analysis it doesn't matter whether one assumes partial load/material factors on the loads or on the allowable material values. According to ISO 2394 [4], the design values of the loads are given by the equation

$$F_d = \gamma_f F_r \quad (2.2)$$

and the design (allowable) values for the material is given by the equation

$$f_d = f_k \gamma_m \quad (2.3)$$

The γ_f and γ_m are functions which represent a number of effects. Especially for the material factor some effects are sometimes present in service but not in the more benign laboratory conditions. Which in the end means that the factor γ_m reduces and consequently the loads have to be increased to make sure that the theoretical fatigue damage in the test equals the theoretical fatigue damage in the design analysis.

Then there are also the factors

C which describes acceptable deformations, accelerations, crack widths with respect to the serviceability limit state;

a_d characteristic values of geometrical parameters;

γ_n which is a coefficient by which the importance of the structure and the consequence of failure are (is) taken into account;

γ_d which is a coefficient related to model uncertainties or other circumstances which is not yet taken into account by other γ values.

For practical design application the above results in

$$\gamma_n S(F_d, a_d, \gamma_{sd}) \leq R(f_d, a_d, C, \gamma_{Rd}) \quad (2.4)$$

or in

$$\gamma_n \gamma_{sd} S(F_d, a_d) \leq \frac{1}{\gamma_{Rd}} R(f_d, a_d, C) \quad (2.5)$$

In which γ_d has been split into a part for the load (S) and an part for the resistance (R) side of the analysis.

On paper it doesn't matter much where, on the loads or on the resistance side of the equation, an effect is taken into account. For testing however it does matter. All factors which one has applied in the design analysis on the resistance side but do not need to be applied in the test analysis e.g. the factor for humidity - in a laboratory environment the humidity is usually low - does not need to be applied in the fatigue test analysis. As a result the loads will need to be multiplied with the factor to reach the design fatigue damage. This can result in a test load spectrum which can be close to or even above the maximum design loads expected in the life of a wind turbine. This is not acceptable because other (non-linear) failure mechanisms can or will than become dominant and destroy the rotor blade which in reality would not occur.

In the IEC-TC88 WG8 guidelines test are divided into strength based and load based test. The load based test are not very useful to determine margins in the structure and the strength based test could be useful when one assume that failure of a cross section or spot in a construction is a one or two dimensional effect.

A simple example of non-linear effects on stresses in rotor blades is the crushing load. These loads work on the shear beam and are quadratic with the bending moment, see appendix E. A more serious non-linear effect is buckling which is an actual design driver for large size rotor blades. In the worst case buckling appears as a bifurcation phenomena, leading to a drastic reduction in stiffness and severe damage due to secondary bending.

One has also to be careful with applying loads higher than 1.35 times the normal design loads. The load factor which has to be applied in the design for the extreme loads is 1.35. For a well designed blade the extreme loads will have almost the same magnitude as the maximum loads in the so called fatigue load cases. This is especially true in the flapwise direction. The fatigue phenomena which are active can change due to the much higher stress levels and result into fatigue failures which are not realistic.

Taking the above consideration into account one cannot say anything about the actual fatigue design margins of a blade which doesn't show major fatigue damage after the test. Damage occurring in the start of a test usually means that the blade has a serious fatigue problem.

These considerations on fatigue testing do however not mean that one can say that full-scale fatigue testing is not necessary (useful). Most tests which were performed resulted in modifications of the design. A favourable effect of the highly non-linear fatigue process is that (small) errors in the design analysis show already early in the test that something is not designed or manufactured in accordance with the specifications. These results protect the wind turbine and rotor blade manufacturers from early failures and large cost associated with re-fitting the wind turbines with new blades or repair of the existing blades.

3 CONCLUSION

3.1 General

The value of full scale blade test, that is rotor blade property, strength and fatigue tests, is high for designers however not all test are of equal weight. This is due to the used method and the position in time of the design process that they are performed. Usually these kind of tests are performed for certification to show that the construction “contains” sufficient margin and not to determine the actual static strength and fatigue life margins. This implies that only a failure during the test gives information about the margin to the required static/fatigue strength. However due to common practice nowadays, to use the same rotor blade for the static and fatigue test implies that it is normal not to go to failure in the static test. Thus the static strength margin is not determined. The fatigue test is less valuable for designers due to the fact that the test load spectrum is determined from the design load spectrum using the same models as used in the design analysis. So it is impossible to make solid conclusions about the true margin of the fatigue life for the structure under the design load spectrum.

Model verification test are valuable for designers. In the end all engineering models have to be validated and or verified by these kind of test. The result of these test can be used to improve or “tune” the engineering model and after a while, when already many products have been produced which are dimensioned with the (engineering) model a designer relies on these models. Testing of that part is then not required any more.

However, usually the need for cheaper and or lighter construction lead the designer to other, more advanced, structural details which need more and other test to derive and validate/verify engineering models.

3.2 Rotor blade property tests

The rotor blade property test is most valuable for the designer. The properties determined here are mass (distribution, centre of gravity, eigenfrequencies possibly including the mode shapes, damping etc.

With the results of this test the designer can get confidence that the assumption made in the design analysis, mainly the aero-elastic load calculations, are good or good enough. This implies that the design load spectrum is well determined. This is the basis for continuation of the tests. When the difference between test results and assumption, is too large the assumed design load spectrum is probably not correct and continuation of the test, no matter what the result is, can not be used to prove that the rotor blade is fit for purpose.

3.3 Stiffness/static strength tests

This test is also valuable for designers, the test results can be used to improve the (engineering) model to determine the strains and subsequent determine the static and fatigue strength margins. It is also useful to check the actual stiffness distribution, especially when the mode shapes are not measured in the property test.

3.4 Fatigue strength tests

The fatigue strength test is less valuable for the designer, due to the fact that the test load spectrum differs quite a lot with the design load spectrum.

However, fatigue test are still the only way to get sufficient confidence that the structure, design and manufacturing, is sound. It still happens that rotor blades fail during the fatigue test while the static strength or property test did not show large differences with the design analysis. Detailed analysis of the failure usually leads to the conclusion of a design error or something which is not taken into account in the design analysis.

References

- [1] Grof, H.J. Van. "STRENGTH AND FATIGUE TESTING OF LARGE SIZE WIND TURBINE ROTORS; Volume I: Rationale and directions.". ECN 95-C-052, ECN, December 1995.
- [2] Ann. "Draft Standard of the International Electrical Commity Wind Turbine Generator Systems IEC 1400-1, Part; Full scale structural testing of rotor blades for WTGS's". Draft, IEC-TC88-WG8, September 1997.
- [3] Collins, J.A. *Failure of materials in mechanical design. Analyses - Prediction - Prevention*. John Wiley & Sons, 1981.
- [4] Ann. "General principles on reliability for structures". Technical Report ISO 2394, International Standardisation Organisation, 1986.
- [5] Smet B.J. de and P.W. Bach. "Lifetime predictions of glass fibre reinforced polyester with the database FACT.". -C- 94-044, ECN, April 1994.
- [6] Smet B.J. de and P.W. Bach. "DATABASE FACT FATigue of Composites for wind Turbines.". -C- 94-045, ECN, April 1994.
- [7] Jooose P.A. and B.J. de Smet P.W. Bach, B.H. Bulder. "Emperical Fatigue Formulation for GRP, discussion paper in Workshop on Fatigue, 10 April 1994". Technical report, SPE, April 1994.
- [8] Delft van D.R.V., G.D. de Winkel, and P.A. Jooose. "Fatigue behaviour fo fibreglass Wind Turbine Blade Material under variable amplitude loading.". In *Proceedings of the 4th IEA expert meeting on wind turbine fatigue*, pages 55-62, February 1996.
- [9] Reifsnider, K.L., editor. *Fatigue of Composite Materials*. Elsevier Amsterdam, 1991.
- [10] Hartog J.P. "*Strength of Materials*". Dover Publications Inc., New York, 1977.
- [11] Delft D.R.V. van and J.L. van Leeuwen. "Full scale fatigue testing wind turbine rotor blades". In *Proceedings of the EWEC Conf. Thessaloniki 1994*, pages -, October 1994.
- [12] Delft van D.R.V., G.D. de Winkel, and P.A. Jooose. "IEC TC88 WG 8 Testing of Rotor Blades.". In *Proceedings of the 4th IEA expert meeting on wind turbine fatigue*, pages 55-62, February 1996.
- [13] Musial W.D., M.E. Clark, N. Egging, and M.D. Zuteck. "Comparison of Strength and Load Based Methods for Testing Wind Turbine Blades". In Walt Musial and Dale Berg, editors, *A collectin of the 1997 ASME Wind Energy Symposium Technical Papers - at the - 35th AIAA Aerospace Sciences Meeting and Exhibition*, pages 97-0957, January 1997.
- [14] Philipidis Th. and P. Vionis. "Rotor blade design verification by means of full scale testing.". In *Proceedings of the ECWEC conference held at Dublin 1997*, pages ?? - ??, October 1994.
- [15] Mandell J.F., D.D. Samborsky, and D.S..Cairns. "Avanced wind turbine blade structures development program at Montana State University". paper 97-0952, AIAA, 1997.
- [16] Musial W.D. and C. Butterfield. "Using Partial Safety Factors in Wind Turbine Design and Testing". In *Proceedings of the Windpower '97, Austin, Texas*, page ??, June 1997.

- [17] Madsen P.H. et al. “*Recommended practices for wind turbine testing and evaluation*”; 3. *FATIGUE LOADS*. International Energy Agency, 2 edition, 1990.
- [18] Vega F. A. and E.S. Lascorz. “STRENGTH AND FATIGUE TESTING OF LARGE SIZE WIND TURBINE ROTORS; Volume II: Full size natural vibration and static strength test; a reference case.”. REFCIE - 43D21/02, CIEMAT, July 1996.
- [19] Gere J.M. and S.P. Timoshenko. “*Mechanics of Materials*”. Van Nostrand Reinhold (U.K.) Co. Ltd, 2 edition, 1987.
- [20] Bruhn E.F. and et al. “*Analyses and Design of Flight Vehicle Structures*”. Tri-State Offset Company, USA, 1973.

A CURRENT TEST PRACTICES

A.1 General

This appendix contains a short description of full scale tests as they have been performed until now including static and fatigue strength tests as well as blade property tests (strain/stress distributions, mode shapes, damping etc.). Further tests performed to determine material and component characteristics will be mentioned briefly. A more detailed description of especially test methods and procedures is given in the draft technical IEC report CDV IEC-61400-23 "Full Scale Structural Testing of Rotor Blades for WTGS's".

A.2 Background

Normally blades are designed according to some national or international standards or codes such as IEC 61400-1 "Wind Turbine Generator Systems - Part 1: Safety Requirements" which uses the principles of ISO 2394 defining the limit states and partial coefficients, which have to be applied to obtain the corresponding design values.

The reason to perform full scale tests is basically to verify or demonstrate to a reasonable level of certainty that the tested item - here the wind turbine blade - when manufactured according to a certain set of specifications has the prescribed strength and/or safety margins with reference to specific limit states and has the assumed blade properties as e.g. stiffness or natural frequencies. I.e. that the blade therefore possesses the strength, service life and other properties provided for in the design. The partial coefficients given in most material standards reflect uncertainties and are chosen in order to keep the probability of a limit state being reached below a certain value prescribed for the structure.

The need for tests will depend on the level of uncertainty in the design assessment due to the use of new design concepts, new materials, new production processes etc. and the possible impact on the structural integrity. Normally full scale tests are only performed on a very limited number of samples. Because of the costs only one or two blades of a given design are tested, so no statistical distribution of production blade strength or other properties can be obtained.

A variety of different tests and test methods for wind turbine blades is (and has been) in use world wide. Full scale tests but also component tests and material tests are and have been performed in relation to the development, documentation and verification of wind turbine blades. Roughly the used tests can be divided into three main groups defined by the methods/approaches they are based on:

- Tests giving statistic information
- "Empiric" tests
- Tests based on a probabilistic approach.

These approaches are described in the following section.

In Europe most full scale blade tests are performed in connection with certification, but also tests supporting the design process are performed.

A.3 Test Principles or Approaches

A.3.1 Tests giving statistic information

Full scale tests on series of blades giving statistic information as mean values and standard deviations are more or less unknown. The costs for such a kind of investigation have until now been judged as too high compared with the profits. A few full scale statistical investigations on strain distribution, stiffness and deflections and geometrical variations have been performed, but only to a very limited level.

But for material characterisation the statistical approach is the current practice when performing tests on coupons. Series of tests on a lot of different materials have been performed in many years to obtain specifications of static strength, fatigue strength (normally defined as S-N curves) including investigations on the influence of R-ratios, stiffness etc. (see paragraph A.4).

Also on some wind turbine details as glued in bolts and studs the statistical approach has been used determining these values (see section 2.4).

A.3.2 "Empiric" tests

Most full scale blade tests performed until now are performed in accordance with procedures and methods defined either by the blade manufacturer himself or by national standards, recommendations or guidelines.

Only one or a few blades are tested and the methods and procedures are more based on "thumb rules" defining reasonable empiric test factors than on straight statistic or probabilistic approaches to the testing. That means that the test factors are more based on values origin from a "best guess" based on reasonable reasons and experience than on scientific investigations.

A.3.3 Tests based on a probabilistic approach

As described above it remains to investigate and formulate how tests on one or a few blades can be used to draw conclusions about the strength and other properties of a series of blades of the same kind.

The determination of the actual margins to the limit states is desirable because such margins can provide a measure of the actual safety obtained for the resistance of the test blade. Interpretation of such values is not straightforward and presumable probabilistic methods have to be applied. It can be done combining the ultimate limit states and probability density functions for e.g. load and resistance.

The principles can be explained with reference to figure A-3 The probability density functions for load and resistance $f(L)$ and $f(R)$ are shown and the characteristic values for the same two functions are denoted L_c and R_c . These two values usually correspond to 5

The probability density function of the load is nowadays more or less well known as defined in e.g. the IEC 61400-1 standard. The problem is that the full resistance density function (including e.g. the pure material values, scaling and shape factors, environmental influences, blade to blade variations, influences of the chosen test method etc.) is not known yet. For some materials as glass fibre reinforced polyester the pure material characteristics are known, but not the full resistance density function for the whole blade.

More running projects as the EU subsidized SMT-project "Blade Test Methods and Techniques" and the JOULE-project PROFAR have the goal to investigate some of the unknown aspects.

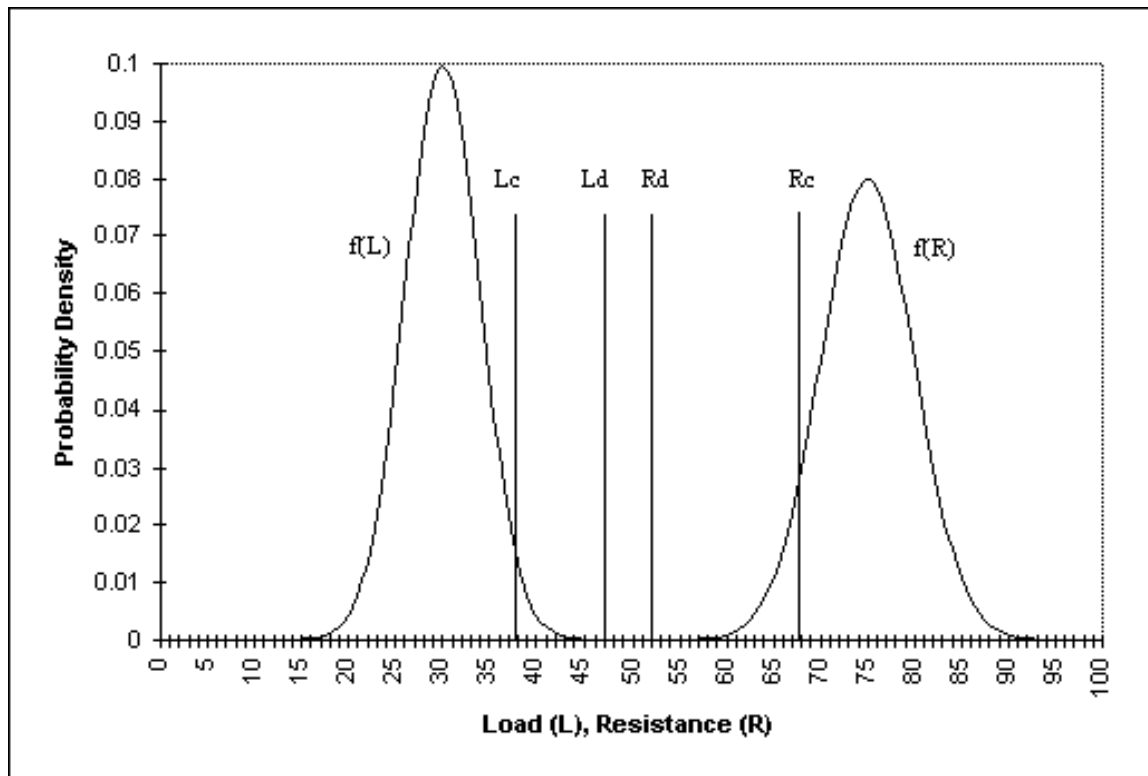


Figure A-1 Load- and resistance-functions and characteristic and design values for load and resistance.

A.4 Material and component tests

Material tests are normally performed to derive material properties and strength formulations from series of tests using statistic methods. This type of tests is well known and described and forms the basis of most national and international material standards.

As mentioned material tests have been performed for some of the normally used blade materials. A European database for values for fibre reinforced plastics is established in the so called FACT database [5–7] by ECN in the Netherlands.

Component tests are and have been performed e.g. on blade roots, root bolts/studs or special details as e.g. bonded connections. Some of these tests are or have been performed on a larger number of items giving statistical information on the detail (average, standard deviation etc.). Others are only performed on one or a few items just to determine the behaviour of the detail.

Some blade root tests in 2D and 3D have been subsidised by EU.

A.5 Full scale strength tests

A lot of different test methods and procedures has been used until now in different countries (see e.g. CDV IEC 61400-23). They have different advantages and disadvantages, but some problems are general and independent of the chosen method. In full scale testing it is not possible to load the blade with all load components and/or to establish the same conditions as in the design. As no single test can load the whole blade optimally, representative loading should be applied to the areas defined as critical for the

construction. Beyond that fatigue testing must be accelerated by increasing the test load to expose the blade to sufficient fatigue damage within a reasonable period. Other differences from the ideal loading such as increased shear loading and other problems caused by concentrated load application are also general.

The difference between just proving the blade to a prescribed load and finding the actual reserve factor or safety margin leads to two principally different attitudes to full scale strength testing namely load based tests and strength based tests. These two types of tests have been used for different reasons, the load based mainly in connection with certification of blades and mainly in Europe, the strength based mainly in connection with design valuation and mainly in USA.

Using load based testing each design load case has to be defined to allow the test load to be accurately assessed at the critical areas to be tested. If strength based testing is used, the appropriate blade strength at each relevant cross section has to be given.

For both types of tests the assumptions for the design operating conditions must be clearly stated as well as the test environmental conditions. In many cases it may be necessary to modify the test load to account for differences between the test conditions and the environment assumed in the load or strength data sets.

The basis for the load based testing (or design load-envelope testing) is the total collection of design loads. Its purpose is to show that the blade can sustain the intended loads without failure. The test load is generally a reduction of the distributed aerodynamic and inertial blade moments into discrete forces positioned along the span. Testing to destruction is not required.

Strength based testing uses as-manufactured blade strength data as its basis. It is often intended to load the blade to destruction. Strength based testing allows a direct verification of the design methodology and an assessment of ways in which the design computations and the design itself might be improved. This method can be used to find the lowest strength location, relative to expected strength, within a broad region.

A.5.1 Ultimate strength tests

Two main methods are and have been used until now loading the blade either by a surface load (e.g. sand bags) or in one or more concentrated point loads. Using point loading a variety of equipment is and has been in use and both single axis testing methods as well as combined tests are well known.

As mentioned care must be taken that the loading method will not lead to local buckling or excessive shears which were not intended or on the other hand lead to local strengthening of the blade.

A.5.2 Fatigue strength test

Many methods to load a blade in fatigue testing are or have been in use. Also here loads can be applied in a single or more points. The loads can be applied to a single axis or as combined loading. The load can be of constant amplitude and frequency or variable. Each type has advantages and disadvantages. In the CDV IEC 61400-23 more of the normal used methods and procedures are described.

A general problem is to accelerate the fatigue test reaching a reasonable test period. Too high loads can lead to unrealistic failure modes. Besides, the fatigue effects of stress concentrations caused by altered material composition and/or other structural details, which may have little effect in static loading, must be accounted for in the fatigue test.

A.6 Full scale blade property tests

A.6.1 General

In the previous sections only strength related tests are dealt with. However, other tests giving additional information on (other) structural or dynamic properties are important and are also commonly carried out in many countries. These tests can be performed independently of the strength tests, but normally most of them will, due to practical reasons, be performed in connection with the strength tests - especially with the static strength test.

Most of the mentioned blade property tests are used both for verification and as a method to tune the design tools.

A.6.2 Deflection

For the verification the flatwise deflection of the blade has most significance because of the (normal) limited clearance to the wind turbine tower but both flatwise and edgewise deflections are often used also by the designer to check the design tools. During the test both the deflections of the blade and test rig have to be recorded. The number of displacement measurement locations has to be adequate to determine the displacement curve and stiffness for the whole blade.

A.6.3 Natural frequencies

The most important frequencies (normally defined as the first and the second flatwise, the first edgewise and in some cases the first torsion frequency) are normally measured to determine the behaviour of the blade. For most blades these frequencies are well separated and more or less uncoupled. Consequently, they can be measured directly one by one by putting the blade into the desired vibration mode while monitoring signals from e.g. strain gauges or accelerometers representing the vibration mode.

If it is not possible to excite the modes separately, a frequency analysis can be made on signals gained from exciting the blade in free vibration outside its harmonics.

A.6.4 Mass distribution

A rough mass distribution is given by the total mass of the blade and the centre of gravity normally already by the blade manufacturer. More refined methods based on sets of strain gauges and the blade eigenweight have also been used. If necessary the mass distribution can be measured by cutting the blade in small sections and weighing each section.

A.6.5 Stiffness distribution

The blade bending stiffness in given load directions can be derived from the load/strain measurements or from deflection measurements (see above).

The load/strain method is very suitable if a detailed stiffness distribution is required - especially in the root and inner part sections. The strain measurement points have to be chosen carefully and sets of strain gauges on each side of the blade are to be distributed along the blade. Loading the blade tip and measuring the strains on each side of the blade the local curvature can be found. From the curvature and the bending moment the stiffness can be derived.

The torsional stiffness of the blade can be expressed in terms of angular rotation as a function of a rising torque.

A.6.6 Mode shapes

The mode shapes can be derived by putting the blade into the wanted vibration mode with one accelerometer mounted at the tip and a number of other accelerometers well distributed along the blade.

Further, the normal mode shape values can for to lightly damped linear structures with well separated natural frequencies be approximated by the imaginary part of the transfer function (at resonance) relating the force input to the acceleration response at the points where the mode shape values are to be determined.

Flatwise and edgewise measurements can be and have been performed by applying an excitation force (measured by a force transducer at the frequency of concern) at an appropriate point (mostly the tip) of the blade while mounted on a rigid test stand. The resulting acceleration responses have to be monitored in the points of interest. The measurements can then be fed into an analyser which offers the possibility of extracting the modulus as well as the phase of the complex transfer function at the resonance frequency.

A.6.7 Strain distribution measurements

Strain distribution tests for blades have been performed for many years using strain gauges placed in areas of interest. The number of measurement points will normally depend on the blade (size, complexity etc.) and blade strains are then measured on the blade skin, typically at blade locations where geometry transitions and critical design details are present or where the strain level is expected to be high.

Each measurement point can include up to three strain measurements. If the direction of the principal strains is not known, a strain gauge rosette can be used to determine the magnitude and direction of the principal strain values at the measurement points.

In some cases e.g. if only stress concentrations or a certain strain level are of interest, stress coat can be used. Stress coat is a strain sensitive paint with a well defined cracking limit. This method are normally only used as a supplement to strain gauge measurements e.g. in areas where it is difficult to use gauges.

Stresses can also be derived using photo-elastic measurements, but until now this method is only used in a few projects.

A.6.8 Damping

The structural damping are normally recorded for the flatwise and edgewise directions by measuring the logarithmic decrement of an undisturbed oscillation. The amplitude of the oscillation has to be small to avoid influence from aerodynamic damping. The damping can be very dependent of the temperature.

A.6.9 Creep

Some materials used for the wind turbine blade are sensitive to creep (e.g. wood). If that is the case tests can be performed tests to define the creep and recovery characteristics. These test are normally performed for a longer duration of time under static loading. During the test the deflection is measured frequently and the deflection versus the time is recorded. After a period the load is removed and the recovery versus time is again recorded as the blade relaxes.

A.6.10 Other non destructive testing

Non Destructive Testing (NDT) techniques are in some cases used to prove if the blade is built in accordance to the design assumptions and to find manufacturing defects. NDT can be performed in connection with other tests or as a part of the quality assurance during the production of the blade . Some of the methods used are measurements checking the blade geometry and tolerances, coin-tap and ultra-sound to check primarily for delaminations and bondings etc.

A.6.11 Blade sectioning

Blade sectioning can be used to prove if the blade is built in accordance to the design assumptions and to find manufacturing defects. E.g. the mass distribution, the (airfoil) geometry and the build-up of laminates, beams, glued connections etc. can be checked.

Blade sectioning is also used to investigate the failure modes in case of failures during strength tests.

B CURRENT STANDARDS AND INFORMATION FROM PREVIOUS PROJECTS

B.1 Introduction

The current (draft) “Wind Turbine Standards” which are looked at are IEC 1400-1 ed.2 ©IEC:1997 - 1 - 88/CJC/XX *Safety of wind turbine generator systems* and IEC-1400-23©IEC:1997 *Full - scale structural testing of rotor blades for wind turbine generator systems*.

Next to these also some non wind turbine standards, specifically made for material characterisation, are reviewed whether they contain useful information for full scale tests or component/model verification test. These other standards are, ISO 2602 1973 (first edition) *Statistical interpretation of test results – estimation of the mean – confidence interval*, ISO 1922 1982 (second edition) *Cellular Plastics – Determination of shear strength of rigid materials*, ASTM C 297 – 61 (Re-approved 1988) *Standard test method for Tensile Strength of Flat Sandwhich Constructions in Flatwise plane*, ASTM D 3410 – 75 (Re-approved 1982) *Standard test method for Compressive Properties of Unidirectional or Cross-ply Fibre-Resin Composites*, ISO 3268 1978 (first edition) *Plastics – Glass-reinforced materials – Determination of Tensile Properties*, ASTM D 3039 – 76 (Re-approved 1982) *Standard test method for Tensile Properties of Fibre-Resin Composites*, DIN 50 100 1978 *Dauerschwingversuch Begriffe Zeichen Durchföuring Auswertung*, and ISO 2394 *General Principles on Reliability for Structures*.

Finally also volume I - rationale and directions - of the S&FAT project, [1], has been reviewed in view of this work.

B.2 Standards and Codes

B.2.1 Wind turbine engineering related standards

The IEC-1400-1 mentions in the part structural design that *an acceptable safety level shall be ascertained and verified by calculations and or tests to demonstrate that the design loading will not exceed the relevant design resistance*.

So testing of rotor blades is not required to pass a certification approval using the IEC-1400-1 criteria.

The draft guideline produced by Working Group 8 of TC-88 of IEC states that the purpose of the full scale tests which are dealt with in their document is “*to demonstrate, to a reasonable level of certainty, that a blade type, when manufactured according to a certain set of specifications, has the prescribed reliability with reference to specific limit states*”. This means that the test is only used to show that it can withstand the design load envelope and not to evaluate the actual margins to the limit states. It is even stated that the actual margin can not straightforwardly be obtained. It is mentioned that by using probabilistic methods it might be possible to obtain the actual margins to the limit states. The main reason that this is not a practical answer is that for probabilistic methods you need more than one test to produce statistical data and in reality one needs many tests to come up with reliable data.

B.2.2 Non wind turbine engineering standards

Some remarks found in non wind turbine engineering standards are listed here:

Hardware

Testing machines must have a constant rate of traverse, this is also of importance for testing of larger specimen like full scale rotor blades or smaller components. The load application rate should be in the same order of magnitude as is foreseen in actual service.

The grips shall be made so to allow alignment of the specimen axis with the testing machine axis or direction of applied force. This could be read in such a way that one has to take load angle changes due to deformation into account during the test. This item is also mentioned in the draft guideline IEC-1400-23.

The test load must be applied with an accuracy of 1% of the design value. This is also true for full scale or component tests. Especially the fatigue damage formulation is very sensitive to the applied load. 1% change in load can result already a substantial difference in the number of cycles to failure.

Together with the loads also the measurement of strains should be with an accuracy of at least 1%. The measurement devices should not alter the properties of the specimen.

Documentation of tests

Next to what is requested in the TC88WG8 document [2] The test report shall include the following particulars:

- complete identification of specimen(s);
- method of preparation of specimen;
- test conditions like temperature, relative humidity, test speed;
- Test results like maximum strength or maximum force or if applicable force at break, modulus of elasticity;
- statistical information like number of specimen, number of test results. Determine standard deviations and possibly the 95% confidence interval of mean value;
- if there is a number of rejected test motivate why they are rejected.

Other items to take into account

Size effects can reasonably well be taken into account for steel structures, they are already incorporated in the design codes for composite structures. The general effect for metals is that due to larger size/volume the fatigue properties reduce. An explanation for this is that larger specimen have a higher probability of containing a more serious stress concentration or fatigue nucleus. For composite structures it is not sure whether the same explanation holds.

An other effect to take into account is variable – constant amplitude loading. For metals this effect can be quit dramatically, for composite materials this size of this effect is not yet known, although in a recent publication [8] it is indicated that the effect could be large.

Statistical Interpretation of Test Results – Estimation of the Mean – Confidence Interval; ISO 2602

This standard deals with estimation of mean and standard deviation for test results which are *normal distributed*.

The use of this standard for model verification test is limited.

One can not assume that the distribution is normal at fore-hand.

There is also a strong indication that the strength distribution is more like a Weibull distribution, see [9].

B.3 Research information for verification/validation test

B.3.1 Strength and Fatigue of Large Size Wind Turbine Rotors S&FAT

The S&FAT project, [1] dealt a.o. with the same problem as discussed here, how to make use of test results in such a way that this or futures design can be improved. One separate item in this project was the Cost and Benefit question. With a questionnaire the European rotor blade manufactures and wind turbine industries in general were asked to reveal which test the find necessary and how much (money) they are willing to spent on testing for a rotor blade of a 700 kW wind turbine rotor. The result showed that a property and static strength test should always be performed, a fatigue strength test only when commercial series production is foreseen.

An other subject which got quite some attention in the S&FAT project which specimen, i.e. rotor blade, of a series production has to be used for testing. This in view of the fact that the first produced rotor blade will be different to the third and e.g. the tenth rotor blade, due to the fact that manufacturing blades is still to a large extend performed by humans. It is mentioned that it should not be the first but the third or fourth blade. That means the first rotor blades (sh)(c)ould be used for the prototype wind turbine.

B.3.2 European Wind Turbine Testing Procedure Development

Within the European program Standard Measurement and Testing a project is ongoing about test procedures and the influence of different test procedures on the results.

Within this project 5 different institutes perform a property, static and fatigue test on identical rotor blades. At the time this report is written no results are available of this project.

B.3.3 PRObability FATigue Reliability

The PROFAR project, which will start in the near future, has the folowing objectives:

- to determine static and fatigue strength distributions of wind‘ turbine rotor blades;
- To determine the so called blade to blade variation factor which should be applied in a test to compensate for possible scatter;
- to generate data which can be used for a probabilistic design tool.

It is not the intention to use real blades in the project but small blades which are specifically designed to fail in fatigue at load levels which result in fatigue failures below 50 million cycles.

C GUIDELINES FOR TESTS TO VERIFY ENGINEERING MODELS

C.1 Overview

After the loads on an engineering structure have been determined or properly estimated and when from these loads and the chosen dimensions of the structure the stresses have been calculated, the question presents itself of whether the construction is safe or not. Since a structure will always start to fail at one spot (the weakest) first, the question reduces to that of the safety of an element of material subjected to a given stress pattern. During the last 2 centuries a number of assumptions have been made concerning the criterion of failure of such an element, and these assumptions have been honoured with the designation "theory of strength" [10] pp72-73. Full scale testing is used in many countries [1, 11–14] for answering questions such as whether the construction is safe or not (certification) or as a means for verification of the engineering models or assumptions. In particular, for blade constructions made of composite materials using various techniques ranging from hand lay-up in open mould to resin transfer moulding (RTM) the iterative approach design/ materials/manufacturing/laboratory testing/service testing is considered of high importance [15] . Due to the complexity of the structure, the method of fabrication and the material itself, coupon testing or component testing is not considered sufficient for either proof of the blade structural integrity, or verification of the design assumptions. Coupon testing may provide data which deviate significantly from the characteristics of the actual lay-up used in the fabricated blades. In addition, the materials used, including the adhesively bonded joints, still have same uncertainties with respect to their fatigue or strength properties. Moreover structural details such as adhesively bonded joints cannot always be analysed in a manageable way with the available engineering tools. The use of testing, in particular for design verification, is dealt with in the following paragraphs.

C.2 Full scale tests

A guideline of recommended practices for "full scale structural testing of rotor blades for WTGS's", is in preparation by the WG8 of the IEC Technical Committee 88,[2]. This part of IEC 1400 is intended to be used as a guideline for the full-scale structural testing of wind turbine blades and gives guidance for the interpretation or evaluation of results, as a possible part of a design verification of the integrity of the blade. The primary emphasis of this WG effort was to identify commonly accepted practices among the various laboratories and to give guidance in establishing blade test criteria. In the present analysis, the integration of blade testing in the design procedures is in particular addressed.

C.2.1 Purpose of tests

As specified in[2], the fundamental purpose of a wind turbine blade test is to demonstrate to a reasonable level of certainty that a blade type, when manufactured according to a certain set of specifications, has the prescribed safety margin with reference to specific limit states, or, more precisely, to verify that the specified limit states are not reached and the blade therefore possesses the strength and service life provided for in the design. Furthermore, blade testing as considered in the present document can play an important role in helping the designer with the verification of the engineering models used and the design assumptions.

C.2.2 Design requirements (elements of design principles) (design methodology)

Following the requirements of the new edition of IEC 1400-1, the design of the blades of a wind turbine is based on the principles of limit state design as described in the standard ISO 2394 [4]. According to this standard the structural performance of a whole structure or part of it should be described with reference to a specific set of limit states beyond which the structure no longer satisfies the design requirements. All limit states should be considered in design. A calculation model should be established for each specific limit state. This model should incorporate all appropriate variables and also allow for the uncertainties with respect to actions. According to the standard the purpose of design calculations or prototype testing is to keep the probability of a limit state being reached below a certain value prescribed for the type of structure in question. To verify the reliability of the structural design, the format of partial coefficients, is recommended.

In many cases the design procedure consists of

- structural analysis which gives the forces and moments in the cross-sections, and
- analysis of cross-sections, joints etc. which gives their resistance and more generally their behaviour.

According to the standards provisions the analysis of a structure can be made with the aid of calculation, model testing or prototype testing. In some cases a combination of these methods is considered as useful. Calculation models and basic assumptions for the calculation should express the structural response according to the limit state under consideration.

A structure or part of it may be designed on the basis of results from appropriate model testing coupled with the use of model analysis to predict the behaviour of the actual structure. In most cases, model testing is used for structural analysis to verify calculations or as a substitute for them. Conversion of model test results to be compatible for use in the actual structures should be ensured.

Eventually, a structure or part of it may also be designed on the basis of results from testing prototype units relevant to the particular design under consideration. This type of testing is sometimes used as a substitute for calculation to verify the resistance of small units or details. It is important, therefore, that the prototype testing is conducted as nearly as possible under the same conditions and assumptions as for the actual structure regarding strength, dimensions, loading and environmental conditions. If only a few prototype test results are available, statistical uncertainties should be indicated.

As seen in the previous sections, it is of significant importance for the designer both the verification of the aeroelastic codes used for the load determination and the verification of the structural model used for stress and strain calculations (FEM or analytical methods).

C.2.3 Types of testing

There are two characteristic methods of blade test loading that can be applied in an actual blade test, i.e. load based testing and strength based testing. The two methodologies are described in detail in [2]. The former type of testing is performed to demonstrate that the tested blade, within a certain level of confidence, has met the structural design requirements concerning its operating or extreme load conditions. Testing to destruction is neither sought nor required. The basis for the test loads is the entire envelope of blade design loads, derived according to generally accepted standards such as IEC1400-1. A load-based test verifies the blade's ability to withstand a particular load combination, but even after a successful test many areas of the blade may still be under-loaded relative to the blade's ability to carry

the load. For a strength based test, the test load is derived from a span wise distribution of the predicted design strength of the test blade. If the blade is tested to its design strength, the design methodology is verified for all of the load cases encompassed by the strength-based loads, providing that the design strength calculations were correct [13].

The differences between the 2 approaches and the principles of the testing procedures can be further explained in figure C-4, which shows the relationship between the design and test-load factors for the two cases [16]. In the figure the probability density functions of loads and resistance are shown along with the characteristic values for both. These values usually correspond to 2.5-5% fractile values of the involved variables. By applying the appropriate partial coefficients on the variables the corresponding design values are obtained. In the case of the IEC 1400-1, the value of the general material factor accounting for the inherent variability of the strength parameter is prescribed to be not less than 1.1 when applied to characteristic material properties of 95% survival probability, with 95% confidence limit and a coefficient of variation of 10%. For different survival probabilities and/or coefficients of variation the relevant general factor is also given. However to derive the global material factor from this general factor it is necessary to account for scale effects, tolerances degradation due to external actions, i.e. ultraviolet radiation, humidity and defects that would normally be detected. One should note that in the case of load-based test the design partial safety factors and appropriate test load factors (TLF) are applied to the characteristic loads to arrive at the load-based test load. The values of the TLF vary a lot depending on the method of testing etc. [8], [2, 13], therefore, it is presented as a region in the relevant figure.

On the other hand, a strength test is concerned only with the right side of figure C-4. It uses the 95% survival value on the "test blade" distribution to set a proof test load with a high probability of not failing the blade. The remainder between the load based test load and the strength based test load is the reserve strength.

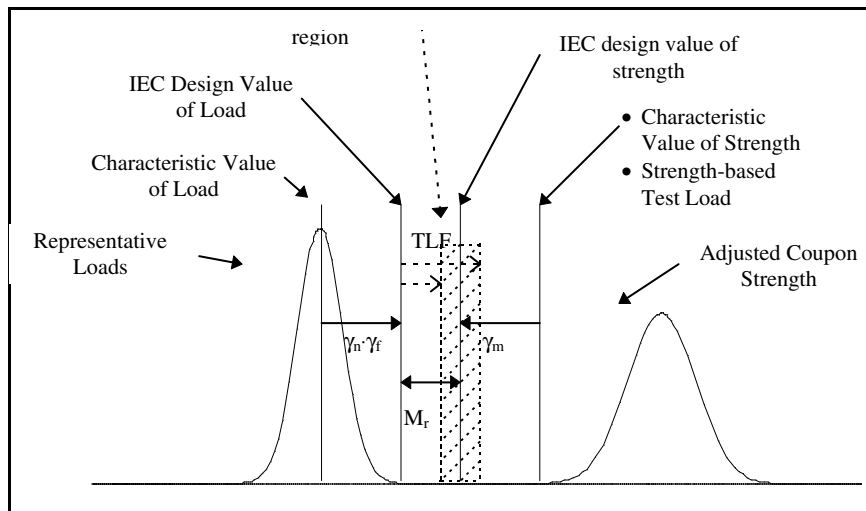


Figure C-1 Application of Load Factors for WT blade testing according to IEC standards.

γ_f : Load uncertainty (1.1 for fatigue and 1.35 for ultimate strength)

γ_n : Consequences of failure (1.15 for fatigue and 1.0 for ultimate strength)

γ_m : Materials Strength Uncertainty (1.1 with 95% survival, 95% confidence, 0.1 COV)

M_r : Reserve Margin

TLF : Test Load Factor (according to[2])

Apparently, load-based test loading is not of direct use for the verification of engineering models, though important for blade certification. As already discussed, the probability of occurrence of any failure when

the blade is subjected to this type of loading is extremely low. Therefore, potential failures indicate insufficient design procedures, manufacturing quality etc. However firm conclusions on the design assumptions and the engineering methods followed by the designer can be drawn only if additional tests have been carried out as discussed in paragraphs C.2.4 and C.2.5. In addition, it should be noted that further information about failure modes, manufacturing quality and reserve strength can be obtained if the testing is continued to blade failure. On the other hand strength based testing allows a direct verification of the design methodology and an assessment of ways in which the design computations, and the resulting design itself, might be improved. This method can be used to find the lowest strength location, relative to expected strength, within a broad region. Strength based testing is particularly useful if the test loading type is desired to be different from that which determined the design, such as if a blade whose design was determined by fatigue operating loads is tested for extreme loading, or vice versa. For such cases, the blade strength distribution will often be quite different from design load cases that did not determine its design. Another purpose might be to assess the strength reduction between bulk material as it exists within the blade and small coupons upon which material strength testing has been performed. Eventually, under a strength based test, a re-evaluation of the load cases can be made without conducting a new test.

C.2.4 Aeroelastic model verification

The role of full-scale testing in the verification of the aeroelastic models used for blade design is detailed in this paragraph. In the design of current WT's according to existing standards, the use of aeroelastic modelling in order to effectively simulate the prescribed design load cases for both ultimate and fatigue loading is more and more common. Aeroelastic modelling has become the most important tool for developing new designs as well as to predict wind turbine loading with increased reliability, therefore leading to design optimisation. Full scale blade testing can provide the designer with the appropriate blade properties for the correct modelling of the blades and the verification of the design assumptions used. In the draft document of WG8 of TC88[2] these tests are described as Other Tests Determining Blade Properties. The blade properties that are important for the verification of the aeroelastic models and should be measured during full scale testing are:

- natural frequencies, at least first two in flap and lead-lag directions;
- mass distribution;
- stiffness distribution;
- damping, as a function of temperature;
- mode shapes;
- profile deformations due to load or manufacturing.

Details on the performance of these tests are included in [2] .

C.2.5 Structural model verification

Detailed FEM techniques or approximate analytical tools are used for the determination of the resistance of the blade structure, which characterises its behaviour. The following properties derived from full scale blade testing are necessary for the verification of the aforementioned models. Details on these tests are also included in chapter Other Tests Determining Blade Properties of [2] :

- strain/stress distribution;
- stress concentrations at certain areas
- mass distribution
- stiffness distribution
- creep
- tip deflection due to tower clearance
- profile deformations due to load or manufacturing.

C.2.6 Sensitivity analysis

The required accuracy for the measurement of the blade properties required for the verification of aeroelastic modelling depends on the specific wind turbine design parameters, the characteristics of the aeroelastic code used by the designer, as well as the safety margin of a certain design. It is recommended that a sensitivity analysis is performed by the designer, prior to setting up the accuracy requirements of the full scale test measurements. The purpose of the sensitivity analysis is to investigate the influence of the identified in paragraph C.2.4 parameters, on the load calculations. The sensitivity analysis should result in creating a "loading influence matrix", depicting the influence on the loading of a specific wt component, by a deviation of the identified parameters by a certain percentage of their nominal values. The influence on the fatigue loading of the wt component can be expressed in terms of the increase of the "equivalent fatigue load" L_{eq} , while for the ultimate loading in terms of the increase of the calculated loads. Once the rainflow spectrum is calculated [17] based on the output of the aeroelastic code, it can be converted to an equivalent load range L_{eq} and an equivalent number of load cycles, by applying the Palmgren-Miner damage rule on various Wöhler curves with different slopes ($1/m$). The equivalent load range is calculated as:

$$L_{eq} = \left(\frac{\sum n_i \cdot L_i^m}{N_{eq}} \right)^{\frac{1}{m}} \quad (C-1)$$

where n_i is the number of cycles in the i^{th} load range, L_i is the maximum value of each load level bin, N_{eq} is the equivalent number of constant amplitude cycles and m the slope of the material S-N curve, which can be assumed to be of the type:

$$N = k \cdot S^{-m} \quad (C-2)$$

Table C-1 shows a typical "Loading influence matrix" for blade flapwise bending moment calculation results. In this table the "Base case" columns represent the calculations with all parameters at their nominal values, while the "Increase" columns depict the percentage increase of the loading for the specified percentage increase of the parameter. Similar "influence matrices" could be established by the designer using different techniques than the presented methodology of equivalent loads based on the design assumptions and the methodology followed.

C.2.7 Required accuracy

It is not suggested to specify particular accuracy levels for the measured blade properties. Based on the results of the sensitivity analysis, and taking into account the relevant design safety margin, the designer

Table C-1 Influence matrix for blade loading

Flapwise blade loading (m= X for fatigue)					
Parameter variation	Fatigue base case L_{eq} (kN)	Increase in L_{eq} (%)	Ult.LC 1 Base case (kN)	Increase in Loading (%)
1st flapwise natural frequency	a	a1	b	b1
etc					

can determine the required accuracy levels for the measurement of the blade properties of interest during full scale testing. In the case of measurement of primary quantities used to determine blade properties, e.g. acceleration measurement used for the calculation of the blade natural frequencies, the required accuracy of the relevant measurement is dependent on the required accuracy of the product quantity of interest, e.g. the blade natural frequencies.

D GUIDELINES TO INTERPRET RESULTS OF MECHANICAL TEST

D.1 Introduction

The objective of this section of the report is:

- to disseminate the experience of CIEMAT towards the interpretation of full scale rotor blade test results and the use of engineering models for rotor blade design.
- a description of by CIEMAT accepted deviations of principal parameters between theoretical design and actual determined values in the tests. The deviation is expressed in a non dimensional form, namely:

$$Error = \frac{M_m - M_t}{M_t} \cdot 100$$

where M_m = measuring magnitude and M_t = theoretical magnitude.

- comments, by CIEMAT, on the IEC-1400-1 partial factors to check whether the test result is acceptable to reach the required safety level.

When the CIEMAT criteria are met, indicated by the test blade error values which should/must be less than the values reflected in this document, the design/blade is adequate for certification.

The error margin, accepted for certification, is adequately adjusted so that the product has a guaranteed quality/reliability, but at the same time the margin is not that low that this makes the product excessively expensive.

D.2 Need of tests

It is well known (see e.g. the S&FAT project, [1, 18]) that wind turbine rotor blades test are performed to compare the measured values with the theoretically determined values. Another objective is to determine the safety level of an individual blade including the effects of (series) fabrication. The answer on the question how representative is the result of one test for the series produced blades depends on the manufacturing process characteristics. This implies that the test is not representative when the manufacturing process is changed throughout the series production.

The reasoning and rules given in this section are based on the fact that the results obtained from a full scale rotor blade test are only valid for a series produced group of blades of which the manufacturing procedure, neither the quality of the materials nor the structural design has changed.

Thus, the validity of the test is based on the validity of the test self, but also on the quality of the manufacturing process of the series production.

VERIFICATION OF BLADE IS ESSENTIAL

D.3 Causes of the differences between the blade theoretical calculations and the tests results

One has to accept that there will always be a difference between measured properties of actual structures and theoretically determined values of those properties.

In this section is shown how to interpret the engineering model verification tests results.

By a test, we can verify several structural parameters of a given structure. However the determination of such parameters is not exact, obviously in every test and measurements some errors are included.

There are many causes of these errors which appear in four fundamental phases of the design (verification) process:

- A) Modelling, in which a engineering model is elaborated.
- B) Manufacturing, in which the blade is fabricated.
- C) Test, in which we carry out a test for the design verification.
- D) Interpretation of test results.

Itemising the causes that contribute to the error(s) we come to the following:

A) **MODELLING PHASE**

- A-1) Codes to calculate the aerodynamic loads and the wind turbines performances.
- A-2) Structural codes, finite elements programs for composite structures
- A-3) Finite elements type selected to model the rotor blade.
- A-4) To model the blade by finite elements means check codes capacity criteria and CPU time. Total number of elements and distribution and fineness of the mesh for these elements along the blade. Boundary conditions.
- A-5) Number load application points (or localised straps) and its distribution along the wingspan, that represent the load envelop, as test loads in order to determine some structural parameters, according to specification test. Localised pulling point in every load section.
- A-6) Knowledge of the used materials and of the aerodynamic parameters and coefficients.

B) **FABRICATION PHASE**

- B-1) Intake and quality control of materials.
- B-2) Factory conditions, Cleanliness, hygiene, air-conditioning in order to fulfil the fabrication processes requirements.
- B-3) Laminate quality, criteria of weight content both in fibre and resin. Possible air inclusion, resin excess.
- B-4) Mold tolerance with regard to the calculations and the blade plans.
- B-5) Laminated adaptation to the mold. Spring bag phenomenon, wrinkled, three-dimensional effects by internal stress in the laminate. Internal dimensions of pieces.
- B-6) Adhesive, in case that exist blade stuck parts.
- B-7) Process repetitiousness. Possibility that in a series production rotor blades are not identical e.g. due to deformations during post-curing.

C) **TEST PHASE**

- C-1) Test bed stiffness.

- C-2) Precision of the loads systems and in associated equipment. Adequate loads aligning.
- C-3) Accuracy of the strain measure systems and in associated equipment.
- C-4) Accuracy of the accelerometers and in the vibrations measure equipment.
- C-5) Loading time. Load profiles versus time.
- C-6) Temperature measures.
- C-7) Selected zones of measure. Stress concentration. Saint Venant principle.
- C-8) Selection and precision of the strain gauges employees and in associated equipment. Strain gauge assembly selection type. Thermal and hygrometric compensation.
- C-9) Precision registering of all data types.

D) INTERPRETATION PHASE

- D-1) Manufacturer to test analysis correct communication about the blade mass, geometric, and elastic characteristics.
- D-2) Mathematical data treatment precision. Numerical analysis.
- D-3) Test analyst experience. Though this characteristic is valid for the others factors also.

As to be expected there are a lot of possible sources of errors. In spite of these possible errors the total effect will remain restricted when the test is performed correctly and the test can be of great use for the manufacturer.

D.4 Classification of static tests

A static test must be complete, i.e. must cover all areas of the structural knowledge. This is based on the experience acquired in projects such as AWEC-60 (WEGA I), S&FAT (Joule), etc. We consider it convenient to divide (or to classify) the static general test activities into the following subtasks (see Table D-2)

Table D-1

STATIC TEST	Natural vibration test	
	Elastic test	Equivalent stiffness
		Influence coefficients
	Static load strength test	Limit load
		Ultimate load

Not shown in table D-2, but before executing the static test, we must perform some geometric and mass measurements on the test specimen. After these measurements are carried out, we will proceed to perform the static test, i.e. all the activities as shown in table D-2.

The first test is the vibrations dynamic test, since the blade has not been loaded and is not deteriorated by any destructive test yet.

The next test is the elasticity test to obtain the elastic and structural blade properties.

The last static tests is the limit load and ultimate load test. During these test the resistance of the blade against the load is measured. During the ultimate load test the blade (local) strains might be above the linear elastic allowable strain, even break the blade.

D.5 Blade identification measurements

As already mentioned, before testing a blade so called specimen identification measurements have to be carried out. The objective of these measurements is to check the conformity of the blade with the design specifications.

In this paragraph the minimum measurements are indicated that must performed before the blade is tested. In table D-3 the measurements are listed including the maximum admissible deviations with the design specifications, according to the criteria of CIEMAT.

The aim of this work is that the given results are valid for any type of blade.

Table D-2 Determined Previous Measures

MEASURE	MAXIMUM ADMISSIBLE DEVIATION	AFFECTED CAUSES
Geometric and mass properties		
Blade wingspan	err. < 0.1 %	- Mold tolerance - Blade compound integration
Chords distribution along the blade span	err. < 0.2 %	-Mold tolerance -End work, finish edge and blade polish
Total twist (absolute) value between the first aerodynamic section and tip	abs. err. < 2°	-Mold tolerance Post-cure twist phenomena
bolt hole diameter tolerance of the blade root connection	abs. err. < ± 0.5 mm	-Commercial drill bits -Cutting speed and erosion
Bolt hole centre location tolerance of blade root connection	abs. err. < ± 1 mm	-Placement drilling machine -Machine tolerance
Blade weight	error < ± 5%	-Blade fabrication processes -Reproduction process not exact
Blade centre of gravity position	error < ± 5%	-Blade fabrication processes -Non exact reproduction process

These are the minimum requirements, on errors of geometric and mass characteristics, to be fulfilled to proceed the test.

Obviously other characteristics like e.g. the blade longitudinal moment of inertia in relation to the rotor shaft etc. could also be specified, but these are of less importance. Due to the fabrication process -lamination of perfectly established layers - the blade weight as well as its centre of gravity position are (usually) very similar to the theoretical values. In the practice the similarity between test and theoretically determined values of the blades longitudinal inertia moment is guaranteed.

D.6 Natural Vibration Test (eigenfrequencies)

Is well known that the objective for the vibration test is to determine the blade's natural frequencies and overall damping.

D.6.1 Natural Blade Frequencies

The objective of the natural frequency test is to determine possible blade resonance problems, e.g. using a Campbell diagram. On the other hand, the stiffness distributions will be determined by subsequent test (elasticity test). In a blade test there is necessary to determine the first two flap and lag frequencies.

Table D-3 Admissible differences between the actual and theoretically determined values of blade frequencies (CIEMAT criteria)

FREQUENCY	PERCENT OF ERROR
1st of flap	< 12 %
2nd of flap	< 13 %
1st of lag	< 18 %
2nd of lag	< 20 %

These tolerances are justified by the stiffness and mass distribution variations, and also by considerations based on the Campbell diagram.

Due to fact that the natural torsion frequencies are (much) higher than the natural bending frequencies, it is not required to obtain this value.

D.6.2 Damping

To determine both damping components, aerodynamic (viscous) and structural, is not an easy task. Also, the results vary quite a lot due to e.g. the test methodology and/or due to the temperature of the blade.

According to the CIEMAT criteria the damping error must be less than 50%

(See S&FAT document, VOL II, [18])

Error < 50 %

D.7 Elastic test

The elastic test is composed of two subtasks:

7-1) Stiffness equivalent test.

7-2) Influence coefficients test.

The objective of these tests is to know the principal elastic and structural blade characteristics. These tests can be execute one after the other or simultaneously.

D.7.1 Equivalent stiffness test

The objective of this test is to obtain the equivalent stiffness, i.e. EI, in several blade sections. The equivalent stiffness can be determined by assuming one or more prismatic cross section(s) ending up with the same behaviour as the real stiffness distribution.

It is difficult to establish criteria in this field because it is related with the blade sections which can vary a lot and due variations of its construction system.

And so, the admissible error in this case is taken conservatively and can therefore be applied to any type of existing blade in the market, because the given value is based in elastic considerations.

When the error, between the design and the test values, exceed this value the difference is considered to be unacceptable.

The maximum error value can be put in the form

$$\frac{\overline{EI}_R - \overline{EI}_T}{\overline{EI}_T} \cdot 100\% < 10\%$$

Where EI_R = actual test stiffness, and EI_T = theoretical stiffness value.

Namely the maximum error value must be less to the 10 %.

Due to the fact that the information recorded by strain gauges is based on a small area, the theoretically calculated stiffnesses, EI_T s, compared to a measured bending moment based on a strain gauge couple may deviate.

Consequently we propose to place several strain gauge couples in each of the interesting sections.

The minimum number of strain gauge couples to determine the equivalent stiffness in a section must be two. And the minimum number of blade sections to check the equivalent stiffness must be four.

The strain gauge couples must be placed between 25 % and 50 % of the profiles chord, counting from the leading edge.

The span wise location to check the stiffness are shown in table D-5.

Table D-4 Span wise locations to measure the equivalent stiffness (in blade wing span percentage)

SECTION	1%	$3\% \leq x \leq 5\%$	35%	70%
---------	----	-----------------------	-----	-----

The location $x = 1\%$ takes into account the characteristic phenomena of stress concentration in the blade-hub zone.

The sections with $(3\% \leq x \leq 5\%)$ takes into account the blades handle (neck) behaviour.

The locations 35% and 70% of the span are distributed along the blade wingspan.

As we can see there are a number of error sources for this test, the errors are associated with:

- the strain gauge itself and its local placement on the blade;
- the determination of the materials characteristics;
- the engineering model.

D.7.2 Influence coefficient test

When it is valid to use the linear elastic theory then the reciprocal-work theorem of Betti/Rayleigh is valid. The reciprocal-work theorem is stated as:

The work done by the forces in the first state of loading when they move through their corresponding displacements in the second state of loading is equal to the work done by the forces in the second state of loading when they move through their corresponding displacements in the first state of loading.

See e.g. a text book by Timoshenko & Gere, [19].

In one dimensional formula form this comes down to

$$P_a u_B = P_B u_A$$

Or also by definition of a coefficient indicating the displacement in direction k at a location j due to a certain load applied at point i in an other direction l . We will symbolise the coefficient by C_{jl}^{ik} .

Generally, the displacement δ_{ik} is due to an arbitrary force F^{jl} , applied in point j in the direction l , in the point i and in the direction k . Mathematically we have:

$$\delta_{ik} = C_{jl}^{ik} \cdot F^{jl} \tag{D-1}$$

For a determined test we could simplify the prior expression for a single load, F , that acts in a given point in a certain prefixed direction, for example in flap direction. The expression D-8 is now:

$$\delta_{ik} = C^{ik} \cdot F \tag{D-2}$$

The criteria of CIEMAT, to get a good indication of the blade production quality, requires only one test. This test is to measure the displacements δ_{ik} resulting of a single load, F , in one point and one direction. This test is assumed to be sufficient and is much more simple than the more general test.

The flap direction is elected, due to the fact that this direction has the lowest stiffness and thus the displacements are larger and, in consequence, the influence coefficient could be measured with a high precision.

For certification the maximum error in the influence coefficients must be less than the 8%.

error < 8%

A maximum error of less than 8% is correct because it implicates a good similarity between the theoretical engineering model and the test results.

Other error sources must also be considered, such as:

- the lack of precision or resolution in the measurement systems. These systems could be as simple as, e.g. threads, rulers, etc..
- the variability of basic material properties, resulting in different laminate properties, or
- the errors in the engineering model.

However, such errors are less than associated with the equivalent stiffness measurement, because in the last case strain gauges are used which detect locally.

Furthermore the closer we get to the blade root, where the deflections are very small, the larger this last type of error becomes. The measurement is not valid when the measurement systems error is of the same magnitude as the error in the deflection to be measured.

Consequently, when the measure systems are simple like e.g. threads, rulers, etc., they should not be used to measure the influence coefficients in those blade zones, whose X coordinate is less than 35 % of the wingspan. In such cases, to guarantee correct measure of the influence coefficients, we recommend the use of laser measurement devices or other with equivalent accuracy, whose inherent errors are less than the mentioned 8 %.

D.8 Static loads strength test

The objective of this test is to put the blade to the limit and ultimate loads to verify its strength and to obtain, furthermore, the safety factor and the design reserve factor.

D.8.1 Limit load strength test

This test is to put the blade to the design limit load, LL_{DES} , which definition is the following:

$$LL_{DES} = PSF_{LIM} * LL_T \quad (D-3)$$

Where PSF_{LIM} is the loads partial safety factor, and LL_T is the theoretical limit load.

Testing the blade at this load, our experience indicated that measuring 3 sections is enough. Certainly 3 sections is not a great number, but it reduces the costs of the test. To test more than 3 sections would make the test unnecessarily expensive or excessively complicated.

These three sections corresponding to 0%, 35%, and 70% of the wing span.

Analogous to this reasoning loading 3 sections is enough to reproduce the bending moments and the shearing forces envelope adequately.

The loads must be introduce in the effective shear centre for each blade section. *The maximum admissible error in shear centre determination must be less than 7% of the local chord.*

$$\mathbf{error} < 7 \%$$

For severity of static load test we think that the relative static strength factor:

$$RSSF = \frac{SSF_{design}}{SF_{test}}$$

should never exceeds 1.2, so this factor will have to be limited to:

$$RSSF < 1.2$$

Stress tolerances

In the opinion of CIEMAT, the admissible error values, test results compared to the pertinent (engineering) models, for a number of phenomena are indicated below:

$$\text{Error tensile-compressive stress} < 5\%$$

Error bending stress < 5%

Error shear stress < 8%

Error buckling stress < 10%

Error post-buckling stress < 16%

Error micro cracking stress < 8%

Safety factors

To palliate certain uncertainties of both, project and test, we utilise the so-called partial safety factors.

The partial safety factor, which is a parameter that corrects theoretical and laboratory values, takes into account the uncertainty or variations, both in the loads and in the materials, in order to make the design reliable and to avoid failure.

A review of the principals safety factors, and the values applied by CIEMAT in comparison with IEC-1401-1, table 3 is given below.

Partial safety factor for loads, ν_F

This factor is defined by following equation

$$F_d = \nu_F \cdot F_t$$

where F_d is the design aerodynamic load, and F_t is the theoretical aerodynamic load.

Load type	ν_F factor
Aerodynamic	1.30
Operational	1.80
Gravity	1.10
Other inertias	1.30

The main discrepancy between the CIEMAT value and the IEC-1400-1 is in the operational load value. The value of 1.45 given by IEC, is assumed to be very low.

For loads related with transport, considering the very complex terrains as in Spain, a $\nu_F(transport)$ is introduced with and estimated value of

$$\nu_F(transport) = 1.7$$

for all load types.

Partial material factor, ν_m

This factor is mathematically defined as follows

$$f_d = \frac{f_k}{\nu_m}$$

where f_d is the design values for material, and f_k is the characteristic values of material property.

Material type		ν_m	
Steel		1.05	
Aluminium		1.12	
GFRP	Hand lay-up	1.30	
	"Pre-pegs"	1.08	
	Un-tempered laminate	1.15	
	Tempered laminate	without thermal slope	1.05
		with thermal slope	1.02
Creep strength		1.6	
GFRP (compaction process)	By vacuum	1.05	
	By pressure with male and nut	1.05 -1.2	
	Pressure cooker	1.02	
Glue		1.20	

Partial factor for failure consequences, ν_n

$$\nu_n \cdot S(F_d) \leq R(f_d)$$

where S is a stress function and R is a material resistance. For static test and all failure consequence types

$$\nu_n = 1.00$$

in agreement with the IEC-1400-1 given value.

Test load scatter factor, ν_{su}

$$\nu_{su} = 1.05$$

When the manufacturing process is correct the value of 1.1, given by IEC-TC88-WG8 (p. 32), could be excessively high.

D.8.2 Ultimate load test

This test is to put the blade to ultimate load, UL , which definition is the following:

$$UL = SF_{DES} * LL_{DES} \tag{D-4}$$

Where SF_{DES} is the design safety factor, and LL_{DES} is the factor defined in equation D-10.

In our opinion should be:

$$SF_{DES} = 1.5$$

The aim of this test is to obtain

$$SF_{DES}^{TEST} = UL^{TEST} / LL_{DES} \tag{D-5}$$

The load applied to the structure through this test is increase step by step, until eventually the ultimate load, UL^{TEST} , that according to our criterion, is the load under the which the structure endured for at least 10 seconds.

From equation D-12 yields SF_{DES}^{TEST} . And this test concludes the blade adequacy if:

$$SF_{DES}^{TEST} SF_{DES}$$

Evidently that implies

$$UL_{TEST} \geq UL$$

We are believing that the SF_{DES} minimum value must be great than 1.5 in order to certify a blade

$$SF_{DES} \geq 1.5$$

According to our criterion the elected sections for both tests, ultimate load and limit load strength one, are equals. Namely, corresponding to the 0%, 35% and 70% of the wingspan.

E CRUSHING¹

As an example of a non linear phenomena which makes test results difficult to interpret when load levels are higher than used in the design analysis.

A slender beam like structures will bend due to a moment M with curvature radius R according to the following formulation:

$$M = \frac{EI}{R} \tag{E-1}$$

The beam will be deformed in a circular shape by the bending moment. The bottom and top skin will now have the tendency to move towards each other. This phenomena is called “crushing”.

Crushing loads will be expressed in a force C per unit of length and are in plane of the shear web. These loads are in fact the loads which bend the upper and lower skins and increase the bending stresses in the skin.

This crushing load is quadratic with the bending moment

$$C = \frac{M^2}{EIh} \tag{E-2}$$

Thus the skin is not only loaded with the so called membrane stresses which are constant over the wall thickness for thin walled structures but also by local bending stresses which are quadratic with the bending moment due to the curvature.

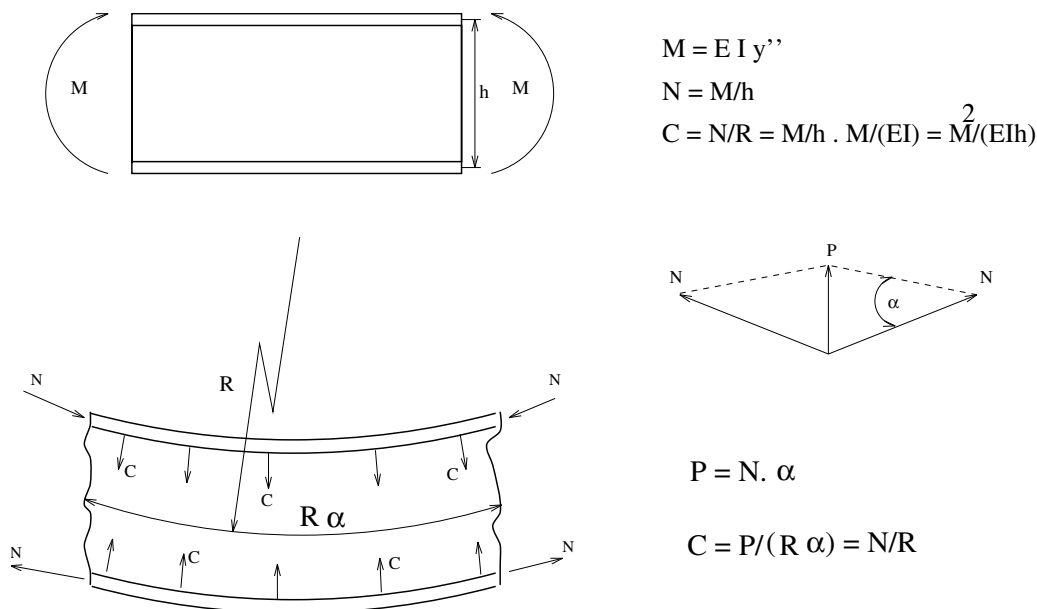


Figure E-1 The loading on a bend slender wing beam

¹Copied from lecture notes of Prof. Ir. J. Ten Asbroek

The load on the shear web is even more complex, it carries the largest share of the shear force, a small part of the bending moment and the crushing loads. The first two are linear with the increase in (test) load but the crushing load is quadratic with the increase in (test) load. The buckling load of the shear web is again determined with the stress ratio or interaction curves first presented by Shanley see e.g. [20].

For combined loadings the general conditions for failure are expressed by Shanley as follows:

$$R_1^x + R_2^y + R_3^z + \dots \geq 1.0 \quad (\text{E-3})$$

In which R is an expression of the stress ratio $\frac{f}{F}$ where f is the applied stress and F the allowable stress. In eq. E-15 the R_i could stand for bending, shear and crushing. The exponents x, y, and z give the relationship for combined stresses. These exponents can be determined for some simpler combined load systems. However, in many cases of combined loading and for particular types of structures the exponents must be determined by making actual failure tests of combined load systems.

EUROPEAN WIND TURBINE STANDARDS II
PART 4
POWER PERFORMANCE IN COMPLEX TERRAIN

E. Morfiadakis

I. Antoniou

A. Cuerva

R. Hunter

F. Mouzakis

N. van der Borg

D. Westermann

CRES

RISØ National Laboratory

CIEMAT

NEL

CRES

Netherlands Energy Research Foundation ECN

DEWI

CONTENTS OF PART 4

1. INTRODUCTION.....	5
1.1 Background.....	5
1.2 Objective.....	5
1.3 Working Method.....	6
1.3.1 Project technical description.....	6
1.3.2 Project scientific and technical performance.....	6
2. SCOPE AND FIELD OF APPLICATION.....	9
3. DEFINITIONS, SYMBOLS AND ABBREVIATIONS.....	11
4. POWER PERFORMANCE MEASUREMENTS.....	13
4.1 Introduction.....	13
4.2 Effect Of Terrain Orography On Wind Field.....	13
4.3 Effect Of Obstacles On Wind Field.....	14
4.3.1 Wind turbines.....	14
4.3.2 Other obstacles.....	14
4.4 Site Calibration.....	15
4.4.1 Wind tunnel simulation.....	15
4.4.2 Numerical modelling.....	15
4.4.3 Field measurements.....	17
4.5 Alternative Methodology For Power Curve Measurements.....	18
4.6 Effects Of Turbulence And Wind Shear On Power Curve.....	19
4.7 Conclusions.....	19
5. EXPERIMENTAL RESEARCH ON WIND TURBINE POWER PERFORMANCE.....	21
5.1 Introduction.....	21
5.2 Review Of Power Performance Campaigns.....	21
5.2.1 WINCON 100XT operating at CRES test station.....	21
5.2.2 VESTAS V27 operating at Andros site.....	23
5.2.3 VESTAS V27 measured by DEWI.....	24
5.2.4 VESTAS V27 measured by WINDTEST.....	25
5.2.5 NORDTANK 500/37 operating at Toplou site.....	25
5.2.6 NORDTANK 500/37 operating at Taff-Ely (turbine A).....	27
5.2.7 NORDTANK 500/37 operating at Taff-Ely (turbine B).....	28
5.2.8 NORDTANK 500/37 operating at Pilsum site.....	29
5.2.9 NORDTANK 500/37 measured by WINDTEST.....	30
5.2.10 MADE AE-30 operating at Fuerteventura and Tarifa.....	30
5.3 Assessment Of Site Calibration Methodologies.....	32
5.3.1 Site calibration for WINCON 110XT.....	32
5.3.2 Site calibration for VESTAS V27.....	32
5.3.3 Site calibration for NORDTANK 500/37.....	33
5.3.4 Conclusions.....	33
5.4 Conclusions.....	33
5.5 Tables.....	35
5.6 Figures.....	41
6. ALTERNATIVE POWER PERFORMANCE METHODOLOGIES.....	59
6.1 Introduction.....	59
6.2 Nacelle Cup Methodology.....	59
6.2.1 Introduction.....	59
6.2.2 Nacelle cup anemometry on 1MW wind turbine.....	59
6.2.3 Nacelle cup anemometry on 500kW wind turbine.....	73
6.2.4 Nacelle cup anemometry on 110kW wind turbine.....	79
6.3 Upwind Rotor Measurements.....	85
6.3.1 Introduction.....	85
6.3.2 Rotor disk measurements on a 110kW wind turbine.....	85
6.3.3 Conclusions.....	86

6.4 Conclusions.....	87
7. PARAMETER IDENTIFICATION OF WIND TURBINE POWER PERFORMANCE	88
7.1 Introduction.....	88
7.2 Parameter Identification Procedure On Experimental Data Bases.....	88
7.2.1 Multivariate regression analysis	88
7.2.2 Assessment of the accuracy of the multivariate regression	90
7.2.3 Parameter identification procedure.....	90
7.3 Identification And Quantification Of Site Related Effects On Power Performance	91
7.3.1 Parameter identification on a 225kW pitch regulated WT	92
7.3.2 Parameter identification on a 110kW stall regulated WT.....	92
7.3.3 Parameter identification on a 500kW stall regulated WT.....	92
7.3.4 Parameter identification on a 300kW stall regulated WT.....	94
7.3.5 Parameter identification on a 3MW pitch controlled WT	94
7.4 Conclusions.....	95
8. ASSESSMENT OF POWER PERFORMANCE PRACTICES	109
8.1 Introduction.....	109
8.2 Review On The Characterization Of Complex Terrain	109
8.3 Critical Points On Existing Recommendations	110
8.3.1 Test site requirements	110
8.3.2 Characterization of wind speed sensors.....	110
8.3.3 Influence of wind mean and turbulent structure	112
8.3.4 Site calibration	112
8.3.5 Response system.....	112
8.3.6 Measurement analysis.....	113
8.3.7 Contractual aspects	113
8.4 Conclusions.....	113
9. PRACTICAL RECOMMENDATIONS	115
9.1 Definition Of Site Complexity	115
9.2 Selection And Characterisation Of Instrument Configuration	115
9.2.1 Definition of reference wind speed	115
9.2.2 Mean wind speed and turbulence structure measurements.....	115
9.2.3 Wind turbine control system response.....	115
9.3 Site Calibration	116
9.4 Normalization Procedure	116
9.5 Uncertainty Estimation Procedure	116
9.6 Power Curve Measurements Of Wind Farms	116
10. REFERENCES.....	123
11. ACKNOWLEDGEMENTS	129

1. INTRODUCTION

1.1 Background

A large and promising portion of the European wind energy market is located in the southern European countries, namely Greece, Spain, South Italy and Portugal. The most suitable sites for wind energy exploitation in these countries, as well as in other northern European countries such as Great Britain, are in the majority of cases located in very complex mountainous terrain. Nevertheless, the influence of such complex terrain on the operation of wind turbines is a major research topic while the research results will significantly influence the market.

EWTS.II-IV contributed significantly to the identification and quantification of the complex terrain effects on the power performance of wind turbines. The program, included extensive review of current power performance measurement practices, wind turbine measurements from such mountainous regions (Greece, Great Britain and Spain) along with evaluation of previous or ongoing similar measurements in flat and complex terrain for stall and pitch regulated wind turbines operating in wind parks of different sizes and ratings.

The present final report of EWTS.II-IV “Power Performance In Complex Terrain”, comprises a review of the project objectives and analysis methodologies related to wind turbine measurements, presentation of literature surveys, detailed presentation of all information regarding the wind turbine experiments and measurement analysis carried out or included within the framework of the project as well as a complete assessment of the results. Finally, the assessment of the existing power performance verification guidelines is presented along with the resulting recommendations for the feasible inclusion of the research results in a power performance practice that will address the wind turbine operation in complex terrain sites.

The assessment of the results is based on the comparison of the performance and the wind characteristics effect of the wind turbines operating at flat and complex terrain. Moreover, the effect of complex terrain on wind turbine operation is quantified by utilising parameter identification analysis.

In the present chapter a review of the project, regarding objectives, technical description and achievements, is presented. In chapter 2 a brief review of the scope and field of application of the status report is given whereas in chapter 3 the used nomenclature is defined. In chapter 4 the literature survey results on the issue of power performance measurements is given. In chapters 5 and 6 the experimental research regarding power performance measurements and alternative methodologies respectively, that were carried out within the framework of the project is presented. In chapter 7 the description of the statistical tool, utilised for the parameter identification purposes, is presented along with the research results. In chapter 8 the assessment of the existing power performance recommendations and standardisation documents is presented. Finally, the technical basis for the development of new recommendations on the issue of power performance in complex terrain resulted from the project results and the assessment of the existing methodologies is summarised in chapter 9.

1.2 Objective

The main objective of the sub-project is the preparation of a status report which will be the technical basis for further standardisation work on power performance determination and verification in complex terrain.

The major achievements of the project are:

- presentation and assessment of various power performance measurements regarding wind turbines of different size and control strategy
- identification and quantification of the terrain induced effects on the power performance of wind turbines
- development of a new procedure of compiling the power performance measurements accounting for terrain effects

- assessment of the existing recommendation and standardisation documents and identification of all inefficiencies that influence the power performance assessment and verification in complex terrain
- construction of the technical basis for the development of a reliable procedure for power performance measurements in complex terrain

1.3 Working Method

1.3.1 Project technical description

The sub-project comprised six tasks with the following objectives:

	Task description/objective
Task 1.	Inventory of existing information on the issue of power performance measurements in complex terrain.
Task 2.	Inventory of power performance measurement campaigns and selection of well documented campaigns suitable for further analysis. Emphasis will be given to cases which claim to use methods yielding better accuracy by applying site calibration.
Task 3.1.	Comparison of different power curve measurements at different sites through annual energy production estimation. Uncertainty estimation for power curve and annual energy production.
Task 3.2.	Power curve evaluation using nacelle anemometers.
Task 3.3.	Parametric analysis of the available power curve measurements for the identification of the site related effects influencing the power performance behaviour.
Task 4.	Assessment of existing guidelines and their validity for complex sites. Identification of drawbacks connected to the application of existing guidelines and recommendations for power performance measurements in complex sites.
Task 5.	Drafting of a status report providing a comprehensive overview of the up to date available information on power performance in complex terrain and of the proposed solutions and results of the parameter identification.
Task 6.	Co-ordination of the sub-project work.

1.3.2 Project scientific and technical performance

The project scientific and technical progress of the sub-project is presented for each task separately.

Task 1

A literature research has been performed, by all participants, in order to gather the available information on power performance measurements in complex terrain. The literature research resulted in many topic-related articles and documents, yet it provided with a limited readily exploitable information for complex terrain measurements. The survey and the resulting conclusions regarded topography effects, effect of obstacles, site calibration practices, alternative power curve measurement procedures and site dependent wind characteristics effect on power curve.

Task 2

The power performance campaigns that have been selected and analysed are listed in table 1.1. The available campaigns cover a wide range of wind turbine size, control techniques, terrain complexity, site calibration methods and nacelle cup practices.

Task 3.1

Summary reports on power performance measurements have been produced for the selected campaigns. The summary reports contained information on the reference measurement procedure, annual energy production and estimated uncertainty, power as well as power coefficient curves. The curves were accompanied by the curve tabulated data list and their basic, within each bin, statistics. CRES contribution included the analysis of the power performance measurements for the V27, WINCON 110XT and NTK500/37 wind turbines. CIEMAT contribution

regarded the measurement analysis for the MADE AE/30 operating at complex terrain (Tarifa site). Attention was paid to the double stall phenomena that were encountered during the operation of the machine. DEWI contribution regarded the analysis of two power performance measurements, one for a NT500/37, operating at Pilsum, and another for V27. NEL contribution regarded the power performance analysis of two NT500/37 wind turbines operating at Taff-Ely wind farm, a complex terrain site located at south Wales. The machines chosen for the analysis were those presenting the least upwind terrain slopes in the direction of the prevailing winds. RIS contribution regarded the power performance measurements for ELKRAFT 1MW wind turbine. Moreover, comparisons of the annual energy production estimation for NT500 and V27, from power curve measurements by WINDTEST, were included. Except from the summary reports for the analysed wind turbines, documentation containing information regarding the wind field structure (i.e. mean wind speed and direction, air density, turbulence and wind shear), the turbine operational characteristics (i.e. power mean and standard deviation, yaw error etc.) as well as the analysis of the uncertainty components estimation, in accordance to IEC (1997) guidelines, was also produced.

In the fields of site calibration different techniques were assessed. The *nacelle cup on standstill wind turbine* practice was applied in all power performance campaigns by CRES (V27, W110XT and NTK500/37) using a cup anemometer that was installed on a mobile mast on the wind turbine nacelle, while the turbine was at standstill in the downwind direction. The measurements from the nacelle cup were correlated to the measurements from the reference mast either directly in cases where the measuring points were at the same elevation or by correcting for wind shear. The *rotor disk averaged wind speed* practice was applied by CRES for the W110XT campaign by the aid of 5 cup measurements spread all over the upwind rotor disk plane. Conventional site calibration with *meteorological mast prior wind turbine erection* was applied in the case of NTK500/37 and comparisons of this approach with the one using the nacelle cup with the parked machine were made. Application of *numerical simulation codes (WA^{SP})* was performed by NEL for the NTK500/37 campaigns.

Table 1.1. Analysed power performance campaigns within EWTS-II, part 4

Wind turbine	Terrain	Institute	Site calibration technique	AEP estimation	Uncertainty estimation	Parameter identification
WINCON 110XT (110kW, stall)	complex	CRES	nacelle cup on running WT nacelle cup on parked WT rotor disk measurements	Yes	Yes	Yes
VESTAS V27 (225kW, pitch)	complex	CRES	nacelle cup on parked WT	Yes	Yes	Yes
	flat	RISØ	reference mast	Yes	Yes	No
	flat	DEWI	reference mast	Yes	Yes	No
	flat	WINDTEST	reference mast	Yes	Yes	No
MADE AE-30	flat	CIEMAT	reference mast	Yes	Yes	Yes
	complex	CIEMAT	reference mast	Yes	Yes	Yes
NORDTANK 500/37 (500kW, stall)	complex	CRES	calibration prior WT erection, nacelle cup on parked WT	Yes	Yes	Yes
	flat	RISØ	reference mast	Yes	Yes	Yes
	complex	NEL	numerical simulation	Yes	Yes	Yes
	complex	NEL	numerical simulation	Yes	Yes	Yes
	flat	DEWI	reference mast	Yes	Yes	Yes
	flat	WINDTEST	reference mast	Yes	Yes	Yes
NEDWIND 500kW	complex	DEWI	nacelle cup on running WT	Yes	Yes	No
ELKRAFT 1MW	flat	RISØ	nacelle cup on running WT	Yes	Yes	No

Task 3.2

The assessment of the nacelle anemometer on running machines was performed by RISØ, DEWI, RISØ and CRES. The performed campaigns regarded a wide range of wind turbine sizes ranging from 110kW up to 1MW machines.

RISØ contributed with the results from the application of the nacelle cup technique for the power performance estimation of the ELKRAFT 1MW wind turbine operating at Avedore Holmen. The objectives of the research were:

- to examine to what extent the nacelle anemometer can be used for the derivation of the power of a turbine after its relation to the mast anemometer has been established via measurements in another turbine situated possibly in another kind of terrain
- ii) to investigate the influence of wake situations and different rotor settings on the nacelle cup calibration. DEWI contributed with the results from the application of the method on a 500kW stall regulated wind turbine, whereas CRES applied the method on a 110kW machine.

Task 3.3

Parametric analyses have been performed for the mean and standard deviation of the power output of the analysed turbines. The analysis was based on a multivariate regression method equipped with a backward parameter elimination technique. The effect of the primary deterministic and stochastic parameters was captured and quantified. The analysed campaigns regarded the VESTAS V27, NORDTANK 500/37 (as measured by different institutes at different sites), WINCON 110XT and MADE AE-30 wind turbines. The selected machines present a variety of size and control strategy. Results from the investigation on the influence of different meteorological conditions, namely turbulence, vertical wind shear and atmospheric stratification on the mean power output of a large wind turbine, namely the AEOLUS II were also presented.

Task 4

The existing guidelines were assessed under the perspective of their applicability and validity for complex sites. The identified drawbacks are discussed and proposals for guidelines and recommendations are made.

2. SCOPE AND FIELD OF APPLICATION

The scope of the present status report is to provide with a comprehensive overview of the up to date available information on power performance in complex terrain and proposed solutions and recommendations for best practice. In more detail, the present document regards the following:

- inventory of existing information on the issue of power performance measurements in complex terrain.
- inventory of power performance measurement campaigns with emphasis on the application of site calibration techniques
- comparison of different power curve measurements at different sites through annual energy production estimation and uncertainty estimation for power curve and annual energy production
- power curve evaluation using nacelle anemometers
- parametric analysis of the available power curve measurements for the identification of the site related effects influencing the power performance behaviour
- assessment of existing guidelines and their validity for complex sites; identification of drawbacks connected to the application of existing guidelines and recommendations for power performance measurements in complex sites

3. DEFINITIONS, SYMBOLS AND ABBREVIATIONS

The symbols that are referenced herein are listed and explained in the following table:

a_k	regression equation coefficient of parameter k
D	spatial distance, rotor diameter (m)
$E(x_i)$	regression error at point x_i
f	frequency (Hz)
G_{asymm}	asymmetric shear factor, i.e. $G_{asymm} = 0.5 \left(\frac{U_{top} - U_{hub}}{H_{top} - H_{hub}} + \frac{U_{hub} - U_{low}}{H_{hub} - H_{low}} \right)$
G_{max}	maximum gust factor, i.e. $G_{max} = \frac{u_{max}}{U}$
G_{min}	minimum gust factor, i.e. $G_{min} = \frac{u_{min}}{U}$
G_{symm}	symmetric shear factor, i.e. $G_{symm} = 0.5 \left(\frac{U_{top} - U_{hub}}{H_{top} - H_{hub}} - \frac{U_{hub} - U_{low}}{H_{hub} - H_{low}} \right)$
k	turbulence kinetic energy, i.e. $k = \frac{\sigma_u^2 + \sigma_v^2 + \sigma_w^2}{2}$
L_u	turbulence length scale of the longitudinal wind speed component (m)
L_v	turbulence length scale of the lateral wind speed component (m)
L_w	turbulence length scale of the vertical wind speed component (m)
N	number of samples within 10 minutes sampling period
S_k	dependence coefficient of parameter X_k , i.e. $S_k = a_k \frac{\sigma_{X_k}}{y_{mean}}$
t	time (sec)
$T.I.$	turbulence intensity, i.e. $T.I. = \frac{\sigma_u}{U}$
U	10min period mean wind speed (m/s)
U_{skew}	skewness of the wind speed distribution, i.e. $U_{skew} = \frac{1}{N} \sum_{i=1}^N \left(\frac{u_i - U}{\sigma_u} \right)^3$
U_{kurt}	kurtosis of the wind speed distribution, i.e. $U_{kurt} = \frac{1}{N} \sum_{i=1}^N \left(\frac{u_i - U}{\sigma_u} \right)^4 - 3$
u_i	instantaneous wind speed (m/s)
$X_k(x_i)$	the value of the k^{th} independent variable at point x_i
y.e.	yaw error ($^\circ$), i.e. nacelle direction - wind direction
y.s.	mean yaw speed of the nacelle ($^\circ \text{sec}^{-1}$)
z	elevation from ground (m)
\hat{y}_i	regression estimation at point x_i , i.e. $\hat{y}_i = \sum_{k=1}^M a_k X_k(x_i)$

Greek symbols

α , w.s.	wind shear exponent based on the power law model, i.e. $\frac{U(z_1)}{U(z_2)} = \left(\frac{z_1}{z_2}\right)^\alpha$
θ , w.i.	wind inclination, i.e. the angle between the wind speed vector and the horizontal direction (°)
σ_p	standard deviation of pitch angle (°)
σ_u	standard deviation of longitudinal wind speed component (m/s)
σ_v	standard deviation of lateral wind speed component (m/s)
σ_w	standard deviation of vertical wind speed component (m/s)
σ_φ	standard deviation of wind speed direction (°)
σ_θ	standard deviation of wind inclination (°)
σ_{X_k}	standard deviation of parameter X_k , i.e. $\sigma_{X_k} = \sqrt{\frac{\sum_{i=1}^N (X_k(x_i) - \overline{X_k})^2}{N-1}}$
χ^2	chi squared estimator, i.e. $\chi^2 = \sum_{i=1}^N \left(\frac{y_i - \hat{y}_i}{\sigma_i} \right)^2$
φ	wind direction (°)

Subscripts

H	at hub height
L	at lower position of the meteorological mast
T	at top position of the meteorological mast

4. POWER PERFORMANCE MEASUREMENTS

4.1 Introduction

The methodology for power curve measurements on wind turbines is elaborated in various studies (Christensen C., 1986, Petersen T., 1993b). The internationally agreed procedure for the measurement and data treatment has been laid down in the draft IEC standard on power performance measurements of wind turbines (IEC, 1997). The methodology is based on the assumption that the statistical wind descriptors (average horizontal speed, average turbulence, average direction) measured at a certain distance from the wind turbine are equal to the descriptors of the wind experienced by the turbine. In complex terrain this assumption will be violated. The draft IEC standard gives a description of the terrain for which the above assumption is considered to be valid. For terrain that do not fit to this description, possible procedures are suggested in the draft IEC standard in order to find the relation of the average wind speed at the anemometer location and the average wind speed experienced by the turbine. This site calibration procedure may be based on field measurements, on physical modelling (wind tunnel measurements) or on numerical modelling. However, very little systematic experience is available on the item of site calibration. At the same time power curve measurements have to be performed at sites in mountainous areas or at sites with obstacles to the wind.

The literature study focused on the following items.

- the influence of orography on local wind speeds over distances up to 100 m
- the influence of obstacles on local wind speeds over the same distances
- methods to quantify the differences in the measured wind speed and the wind speed experienced by the turbine
- alternative methodologies for power curve measurements
- the influence of the site wind characteristics on the power curve of the turbine.

4.2 Effect Of Terrain Orography On Wind Field

Variations in terrain height can cause differences in the average measured wind speed at the anemometer location and the average wind speed experienced by the measured wind turbine. The draft IEC standard describes which slopes and height variations are expected to cause too large differences for a normal power curve measurement.

Various publications are available that give an impression of the possible differences in the average wind speed in mountainous areas between potential positions of a wind turbine and corresponding meteorological mast. Of course the differences are very dependent on the degree of complexity of the site and of the measuring height above ground level. Some examples are:

- At 42m a.g.l. at the AWEC-60 site (Cabo-Villano, Spain) at 250m distance differences in average wind speed occur in the order of 4% (Klug H., 1996).
- At 41 m above sea level (about 30 m a.g.l) in the dune landscape of ECN on the North Sea shore differences in average wind speed occur in the order of 3% over distances of 40 to 120m (Vermeulen P., 1982).
- At 40 m a.g.l. at a site on Andros (Greece) differences in average wind speed occur of 3 to 4 % over a distance of 100m (Morfiadakis E., 1994).
- At the height of the Vestas27 hub and over a distance of 1.5 rotor diameters differences in average wind speed occur of -1 to 5% on Samos (Greece) (Nielsen M., 1994).
- On a rather smooth mountainous site (Altamont Pass, USA) at the hub height of a 33 m turbine and a distance of 63 m differences in average wind speed occur of 30 to 40 % with winds over slopes of approximately 25% (Jamieson P., 1988).
- Around a 30 degrees ramp (height 16 m) differences in average wind speed occur of a factor 2 to 4 over a distance of 100 m (observed at 10 m height) (Courtney M., 1990).
- Smooth terrain variations with a height of 10% of the rotor diameter can cause 4% speed on values at heights equal to the rotor diameter (Pedersen T.F., 1993).

The conclusion is that the orography of wind turbine sites can cause significant to extreme differences between the wind speed at the anemometer and at the turbine, even if the position of the anemometer and the selection of the wind direction are chosen carefully. None of the references contradicts the criteria of the draft IEC standard.

4.3 Effect Of Obstacles On Wind Field

Neighbouring wind turbines and obstacles as buildings and vegetation can cause differences in the average measured wind speed at the anemometer location and the average wind speed experienced by the measured wind turbine. The draft IEC standard describes which wind direction sectors must be excluded to prevent disturbance by running turbines and other obstacles of the wind speed at the anemometer and at the measured turbine. The draft standard regards parked turbine as obstacles. Available information on wind speed effects by running turbines is given in paragraph 4.3.1. The effects of other obstacles (buildings and trees) are discussed in paragraph 4.3.2.

4.3.1 Wind turbines

Wind speed deficits measured up to 8 rotor diameters down wind of turbines have been presented in reference 20. The deficits are for the largest distance (8 diameters) still significant (order of 10 %).

The ratio between the undisturbed wind speed and the wind speed measured inside a wind farm is given, as a function of direction, in the work of Larsen A., 1989. The deficits for distances of about 6 rotor diameters downwind vary from -5% up to 18%.

Wind speed deficits behind a turbine is given in the work of Magnusson M., 1994, for stable and unstable stratification. The wind deficit in percentage of the ambient wind speed at hub height behind a turbine is given by the formula $\Delta U/U=100(X/D)^{-0.8}$ for unstable stratification and $\Delta U/U=150(X/D)^{-0.8}$ for stable stratification. The formulae have been obtained by fitting measured data obtained from three wind farms for down wind distances between about 2 and 10 rotor diameters. Although extrapolation outside this range from 2 to 10 diameters is not really appropriate, an extrapolation to 20 diameters has been made for comparison with the draft IEC standard. This standard considers upwind turbines at larger distances than 20 diameters as non-existing. Extrapolation of the above given formula to 20 diameters and an unstable stratification results in a deficit of 9%.

Some measured and calculated wind speed deficits in wakes from turbines are presented in the work of van der Snoek L., 1989. In the work of Emeis S., 1993, and Frandsen S., 1992, simple models to calculate the wind speed inside a large wind farm or between a large number of obstacles are presented.

The conclusion is that the available data suggest that wind deficits at 20 diameters down wind may be still significant.

4.3.2 Other obstacles

According to Frandsen S., 1994, the distance between an obstacle (of approximate size of the WT) and the WT should minimal be 15-20D or 30-40D, depending of the wind direction, to secure a wind speed difference of less than 1%.

European Wind Atlas (Troen I., 1989), gives some guidance to calculate the effect of obstacles. Using this guidance the wind deficit has been calculated for a building (zero porosity) with height and width equal to D at a distance of 20D and at a height of 1D. The calculated deficit in this example is 2.5%.

In the work of Burger T., 1988, wake measurements made at a distance of 7m behind a house are presented. Measured wind speed deficits behind a row of trees at rather small distances along with the influence of the atmospheric stability on the deficit are included. This influence is rather small for distances of more than twice the obstacle height.

In the work of Nierenberg R. (1993), the effects of trees with a height of 12m on the wind speeds between the trees up to a height of 32m are presented.

The conclusion is that the available data suggest that wind deficits at 20 diameters down wind may be still

significant.

4.4 Site Calibration

If the 10 minutes averaged ratio between the wind speed at the anemometer position and the wind speed as experienced by the turbine is known per wind direction sector, the wind speed measured at the anemometer position can be translated to the wind speed experienced by the turbine during the power curve measurements. In order to determine the 10 minutes averaged values ratio a site calibration has to be performed. It is uncertain how stable the estimated ratio is in time. In the work of Smedman A. (1996) and Magnusson M. (1994) it is shown that terrain effects can depend upon the atmospheric stability.

Site calibration can be done by modeling (physical or numerical) or by field measurements. The draft IEC standard gives the possibility to perform a site calibration by numerical modelling and by field measurements using a temporary meteorological mast. The associated uncertainties (minimum values prescribed by the draft IEC standard) are respectively 50% and 33% of the maximum correction found in the measurement sector. More information found in the literature is presented in the following paragraphs.

4.4.1 Wind tunnel simulation

The site can be calibrated by using a physical model of the site in a wind tunnel. Numerous examples of this approach are found in experimental literature.

In the work of Chien H. (1980) the wind flow field over Kahuku Point has been studied using a wind tunnel and using field measurements. The results have been compared and proved to be satisfactory. In the work of Pearse J. (1982) wind tunnel studies of 3 smooth conical hills with slopes of 0.15, 0.25 and 0.50 have been performed. The results have been compared with similar work on ridges. The effects of the ridges are stronger than the effects of the hills because the flow passes around the hills rather than over it. In the work of Hassan U. (1982) the wind flow field at Burgar Hill has been investigated by means of physical modelling (wind tunnel), numerical modelling, short term field measurement campaigns and long term field measurement campaigns.

In the work of Vermeulen H. (1982) a wind tunnel experiment of a low rise hill (height 100m, slope 10- 20%) has been carried out and the results have been compared with field measurements. The comparison shows good agreements between the wind tunnel results and the field measurement results. Only heights a.g.l. of 3-10m have been considered. In the work of Veenhuizen S. (1987) different methodologies for micro-siting have been discussed: field measurements (using kites), physical models and numerical models. The uncertainties in wind speed resulting from these three different approaches are 10% or higher. In the work of Vermeulen P. (1989) a wind tunnel study has been performed on a scale model of the ECN test station for three heights, six positions and with a wind direction resolution of 15 degrees.

In the work of McCarthy E. (1993) a wind tunnel study has been undertaken to examine the wind flow over hills and ridges, covered with trees. The study involved two dimensional ridges with various heights, slopes and forest configurations. Combination of the various parameter settings resulted in totally 96 different tests. In the work of Sierputowski (1995) wind tunnel experiments have been described for a hill-valley configuration.

The conclusion is that site calibration by physical modelling is considered reliable if the modelling is done properly in terms of orography discretisation, tunnel characteristics and instrumentation.

4.4.2 Numerical modelling

Numerical models have been developed and extensively used for site assessment purposes. A state of the art review is found in the work of Glinou G. (1996). According to the review the available models are categorised as follows:

Kinematic or mass consistent models

The kinematic models are based on the solution of the continuity equation simulating inviscid flow fields. This concept was introduced by Sherman C. (1978) and further developed by Traci R. (1987). Numerous models are in

use today, among which NOABL, AIOLOS and WINDS are well known. Research on the kinematic models has led to improvements related to inclusion of atmospheric stability effects, simulation of the 3D flow field by solving a momentum equation in the vertical direction as well as inclusion of a turbulence model, for instance the two equation k- ϵ model (Croba D., 1996).

Dynamic models

Dynamic models are based on the solution of boundary layer equations. The concept of the linear perturbation theory of Jackson P. (1975) in two dimensions and Mason P. (1979) in three dimensions introduced a two-layer approximation using different perturbation schemes in the inner and outer region of the boundary layer. This concept gave rise to the development of several analytical models (i.e. WA^{SP}, MS3DJH), which have given satisfactory results in geometry's where no flow reversal exists (Walmsley J., 1986). In the work of Mason P. (1985) a review of different models and compared their results against their finite difference model which is effectively identical to the model of Taylor P. (1977). At present analytical models based either on the potential flow theory or on boundary layer parametrisations are used for predicting the wind flow over complex terrain. The WA^{SP} programme capable of generalising a long-term meteorological data series at a (reference) site which may then be used to estimate conditions at other (predicted) sites is nowadays the most extensively used practical tool applied for this purpose. The MS3DJN family of models conserve mass but also attempt to solve momentum equations in an approximate manner by using a constant-density atmosphere. It is assumed that the physics of the flow can be simplified by using a mixing length closure for the turbulent stresses which is only valid for statically stable conditions and that the momentum equations subjected to the thin shear layer approximation can be linearized and then solved using perturbation techniques. In general the models belonging to this category have inherent limitations concerning the terrain slopes and so their validity in complex terrain is not guaranteed.

Time averaged Navier-Stokes equation solutions

The solution of time averaged Navier-Stokes equations have been extensively used in all fluid dynamics applications and specifically to atmospheric flows (Tryfonopoulos D., 1989, Alm L., 1993). In the literature several models have been proposed for closure of the equations such as zero order models, one equation models, two equation models, Reynolds stress models etc. To suppress the computational cost, most Navier-Stokes runs are performed in relatively coarse grids applying law of the wall type boundary conditions. Simulations with more elaborate turbulence models, like the low Reynolds k- ϵ or the algebraic Reynolds stress models, which could better estimate the wind profiles and the Reynolds stress tensor, require large memory and computer time and this renders them cost ineffective. Validation studies have confirmed that the k- ϵ is a good compromise between the simple models and the more complicated ones (Tombrou M., 1993, Bergeles G., 1985).

Meso scale models

All the previous models are unable to account for the influence that local wind systems have on the annual wind conditions especially at a complex terrain site. One important aspect of siting wind converters is a description of the local wind climate with high spatial resolution which is often not available from observations in the atmosphere. The density of operational observation networks is too poor for that purpose so that additional information is required. Therefore methods have to be applied to achieve this information from the large scale state of the atmosphere and topographic parameters by applying mesoscale models. The mesoscale simulation models are able to simulate local wind systems produced by the orography and/or solar radiation, because they incorporate the appropriate physics but also because of their working domain (characteristic dimensions of time and length of the meso scale) which is restricted in the previously mentioned models. Only at this scale where the typical dimension of time lies between a few minutes and a 24hour day and the typical length lies between 2,5km-mountain and valley winds to 2500km-tropical cyclone, local wind systems phenomena occur. All meso scale models calculate the wind field by numerical solving the Navier-Stokes conservation equation for mass, energy, momentum etc. The specific formulation of all equations and the used approximations depend on the specific meso scale model that is selected. Summarising, meso scale models are able to describe the wind field with a high spatial resolution during short episodes in complex terrain. For gaining a wind climatology from simulations with these models available statistical information about the large scale state of the atmosphere have to be scaled down to the required resolution by applying meso scale models, which describe principally the modification of the large scale state by meso scale processes induced by the topography.

A number of meso scale models that are used for site assessment applications are found in the literature, i.e. the HIRLAM model by Danish Meteorological Institute, the KAMM model by University of Karlsruhe, the GESIMA

model by GKSS, the MEMO model by IEH-REG, the UK Meteorological Office model and the meso scale model run by the University of Uppsala (Petersen E., 1996, Landberg L., 1996, Mengelkamp H., 1996, Hojstrup J., 1996). The tremendous computer resource needed for applying these models should be taken into account. Moreover the grid step used in the analysis which can not always be as small as required and the fact that the models require several basic assumptions (i.e. definition and number of episodes, assumed frequency distribution of wind velocity etc.), lead us to believe that at the moment their results are considered to allow for a qualitative description of wind statistics in regions where observations are not available but the accuracy of the absolute values resulting from these procedures is not always ensured.

Hybrid models

Recently, research addressed towards the combination or nesting of models with different spatial resolutions (i.e. WA^{SP} /local scale with KAMM or HIRLAM / meso scale (Petersen E., 1996, Landberg L., 1996) or WA^{SP} with Navier Stokes solvers) and hybrid micro-siting models (Lalas D., 1996) combining the mass consistent methodology with principles of the Navier Stokes approach. During the JOULE I project, contract no. JOUROO67 entitled "Wind measurements and modelling in complex terrain" it was attempted to estimate the possible zones of separating flows based on the topography input and to verify by means of the measurements obtained in the same project. In the European Wind Atlas Vol.II (to be published shortly), the KAMM model able to calculate the resource over hundreds of kilometres was used as a supplement to the WA^{SP} model which in contrast can handle very detailed information on the topography in a radius of approximately five to ten kilometres from the sites. Preliminary results for assessing the wind potential of Ireland are quite promising (Frank H., 1996).

Evidently, depending on its background theory each model has certain possibilities and limitations. Simple models are still in almost exclusive use. Due to their approximate character, calibration procedures (wind tunnel studies, in situ) are often needed. In some cases, additional calculations with more advanced (Navier-Stokes), generalised (meso scale) or even statistical tools (i.e. MOS -Model Output Statistics) seem necessary for improving the prediction accuracy.

Representative site calibration applications with the models BZ- WA^{SP}, NOABL*, MS-MICRO, (NL)MSFD, MASON-KING MODEL D, AVENU and MS3DJH/3R (predecessor of MS-MICRO) are found in the works of Hassan U. (1982), Veenhuizen S. (1987), Troen I. (1989), Walmsley J. (1989), Barnard J. (1990), Botta G. (1992), Kline J. (1993), Weng W. (1994), Watson R. (1994), Sandstrom S. (1994) and Smedman A. (1996).

4.4.3 Field measurements

Prior to or after the actual power curve measurements the relation can be determined between the average wind speed measured by the anemometer on the meteorological mast and the average wind speed experienced by the wind turbine using an anemometer at the location of the turbine.

This anemometer can be supported by a temporary meteorological mast or by the parked turbine. These two possibilities are treated in the following paragraphs.

4.4.3.1 Anemometer on a temporary meteorological mast

This procedure is recommended by the draft IEC standard. The ratio between the average wind speed at the anemometer at the meteorological mast and at an anemometer at the turbine rotor center (placed on a temporary mast) are measured during a certain period. The temporary meteorological mast is positioned at the wind turbine location before the erection or after the dismantling of the turbine. In Klug H. (1996) it is supported that the ratio is rather independent of the wind speed of interest and that the ratio should be measured using wind speeds between 5 and 10 m/s. The ratio has to be determined in wind direction bins of 30 degrees or finer. The recommended minimum duration of the used measurements is 10 to 48 hours per wind direction sector (Klug H., 1996). It is uncertain what the effect of the atmospheric stability on the wind speed distribution is. For this reason it is felt that the duration of 48 hours per sector should be considered as a minimum.

The disadvantage of this procedure is the need to erect a temporary meteorological mast and to delay the erection of the wind turbine (or to remove it).

The conclusion is that the procedure is expected to give reliable results if the measurement duration per wind

direction sector is 48 hours or more.

4.4.3.2 Anemometer on parked wind turbine

To avoid the disadvantage of the use of a temporary meteorological mast the anemometer at turbine location can also be supported by the turbine itself while the turbine is parked. To prevent disturbance of the measured wind speed by the turbine the anemometer cannot be positioned at the exact location of the turbine rotor center. In the work of Nielsen M. (1994) and Jamieson P. (1988) the anemometer is positioned on a vertical boom (length 3 or 4m) attached to the rear end of the nacelle while the turbine rotor automatically remained down wind. In the work of Morfiadakis E. (1994) a procedure has been described with the anemometer mounted on a vertical 10 m mast supported by the nacelle. The effect of wind shear has been accounted for by measuring the wind shear at the permanent meteorological mast. In both cases (with the anemometer displaced horizontally or vertically from the rotor center) an uncertainty is introduced because the site effect is not measured at exactly the position of interest. Furthermore it is not exactly known which distance between the turbine and the nacelle mounted anemometer guarantees an undisturbed wind speed measurement. Information on the disturbance of the measured wind speed by booms and masts in the vicinity of the anemometer can be found in the works of Dahlberg J. (1996) and Pedersen B.M. (1991). The available information shows that the effects in front of or above a nacelle at rather small distances (a few times the nacelle dimension) can certainly not be neglected.

The conclusion is that no simple instruction has been found to position the anemometer in the vicinity of the nacelle with an acceptable 1% wind speed disturbance. On the other hand current experimental and theoretical research is focusing on the issue and the determination of proper position, depending on nacelle geometry and acceptable wind speed disturbance, is feasible.

4.5 Alternative Methodology For Power Curve Measurements

The effects of complex terrain as described in paragraphs 4.2 and 4.3 may cause differences in the measured wind speed and the wind speed as experienced by the turbine. Preventing of or accounting for these effects is difficult and costly in terms of money and time. For this reason an alternative procedure for power curve measurements is highly desirable. In this procedure the undisturbed wind speed at the center of the turbine rotor is obtained from the wind speed reading of an anemometer positioned on the nacelle of the (running) turbine. The anemometer is positioned in such a way that disturbance of the measured wind speed is minimised and that small uncertainties in the positioning do not have significant effects on this disturbance. A suggestion for the position is given in the work of Pedersen T.F. (1994). The relation between the average undisturbed wind speed at a meteorological mast and the average wind speed reading of the nacelle mounted anemometer is measured on a non-complex site (or on a site-calibrated complex site) and is assumed to be applicable for the power curve measurements of another turbine of the same make and model at another site. It is uncertain how good this assumption is.

In the work of Dekker J. (1986) it is shown that the wind speed ratio for the examined wind turbine, with variable rotational speed, and anemometer mounting was wind speed and rpm dependent.

In the work of Nielsen M. (1994) the power curve obtained with a 1.5D meteorological tower and a site calibration as described in 4.4.3.2. compared with the alternatively obtained power curve. The two power curves are identical for wind speeds up to about 11m/s. At higher wind speeds systematic differences are observed. With the alternative procedure the power curves of four nominally identical turbines have been determined. The resulting four potential annual energy production values are identical within 2% for the annual wind speed of Samos island. In the work of Riddle A. (1996) the use of a nacelle mounted anemometer for power curve measurements has been mentioned but limited data are given in order to allow the assessment of the reliability of the method. In the work of Slater J. (1996) two power curves of one turbine of a wind farm on complex site were presented. One power curve has been measured using a meteorological mast and a site calibration (including the measurement of the relation of the nacelle mounted anemometer and the meteorological mast anemometer) and another with the nacelle mounted anemometer. The observed significant differences between the power curves are obscured in the presented AEP because the deviations in the power curves at the low wind speed compensate for the deviations at the high wind speed.

The conclusion is that none of the papers gives a proof that the relation between undisturbed wind speed and the reading of the nacelle mounted anemometer is independent of the power curve itself. As a consequence of this a

power curve measurement cannot be performed using the nacelle mounted anemometer unless it is sure that the power curve of the turbine is equal to the power curve of the turbine with which the relation between undisturbed wind speed and reading of the nacelle mounted anemometer has been determined. In that case there is obviously no need to measure the power curve again. Nevertheless it can be argued that the procedure can be of use for checking whether the power curve of a turbine differs from the power curve of the reference turbine (for which the power curve and the relation between the undisturbed wind speed and nacelle mounted anemometer reading has been measured). If the measured “power curve” of the tested machine is equal to the power curve of the reference turbine, one can conclude that the power curves are indeed equal. The reason of this is that a positive deviation of the power curve from the reference curve will change the wind speed relation to lower ratio’s which will make the measured “power curve” even higher. In the same way a negative deviation will be enhanced in the results. If the measured “power curve” of the turbine deviates from the reference curve one cannot conclude that the power curve of the turbine is equal to the reference power curve and the measured “power curve” has no further meaning.

4.6 Effects Of Turbulence And Wind Shear On Power Curve

The previous paragraphs focused on the effects of complex terrain on the measurement of the power curve. These effects cause uncertainties in the determination of the undisturbed wind speed at the center of the turbine rotor. However complex terrain can also have effects on the power curve itself since the power curve of a turbine is (by definition) basically the relation of the undisturbed wind speed at the center of the turbine rotor and the power output of the turbine. The effects of the turbulence levels and the wind shear on the produced power are not accounted for. This makes the measured power curve to a certain extent dependent on the measurement site.

The possible effects of turbulence on the power are the increase of wind power with increasing turbulence for equal 10-minutes average wind speeds and hysteresis effects around cut-in wind speed, rated wind speed and cut-out wind speed. Since the power of a turbine reflects the rotor disc averaged wind speed rather than the wind speed at the rotor center, effects of wind shear on the measured power curve can also be expected.

In the work of Morfiadakis E. (1994) it is shown the significant importance of the turbulence intensity for the power curve. In the work of Sheimman Y. (1992) an analytical method for taking these effects into account is reported. It is shown that not accounting for the effect of turbulence can lead to errors in predicted annual energy productions at other sites of 10%. Elliot D. (1994) reports significant turbulence and shear effects on the power curves of three 2.5 MW turbines. The effects are correlated as the turbulence conditions are characterised by a strong shear in the lower half of the rotor disk and weak or negative shear in the upper half.

In the work of Jamieson (1988) the reduction of all curvatures in the power curve due to turbulence is reported. Especially in hourly averaged data this effect can be strong. The paper says that many commercial agreements are based on hourly averaged data.

In the work of Riddle A. (1996) it is shown that a significant dependence of the power curve with turbulence but a strong dependence of the power curve with the wind direction, as measured in a complex site. In the work of Pedersen T.F. (1996) it is shown that the response of a cup anemometer to turbulence and 3D winds differs from the response of the turbine, in terms of power output, for these winds. This causes a dependence of the power curve with the wind field. This effect however seems to be rather small. Albers A. (1996) indicates that the power curve of a turbine is influenced by the combination of turbulence, wind shear and atmospheric stability.

The conclusion is that, even if all measurement uncertainties would be eliminated, the power curve of a wind turbine is not site-independent. Expressed in potential annual energy production values the differences can be in the order of 10 %.

4.7 Conclusions

The literature research resulted in many topic-related articles and documents providing however only limited ready-to-use information. The conclusions are summarised below.

Effect of orography

The orography of wind turbine sites can cause significant to extreme differences between the wind speed at the

anemometer and at the turbine, even if the position of the anemometer and the selection of the wind direction sector are chosen carefully. None of the references contradicts the criteria of the draft IEC standard.

Effect of obstacles

The available data suggest that wind deficits at 20 diameters downwind may be still significant. Extension of the 20D range of the draft IEC standard should be considered.

Site calibration

- Site calibration by physical modelling is considered to be reliable if the modelling is done properly, in terms of orography discretisation, wind tunnel and instrumentation characteristics.
- Site calibration by numerical modelling may result to increased uncertainty. On the other hand, systematic research is being performed on the issue indicating that numerical modelling should be considered as a candidate methodology.
- Site calibration by field measurements:
 - When the anemometer at the turbine location is supported by a temporary meteo-mast the site calibration is expected to give reliable results if the measurement period per wind direction sector is 48 hours or more.
 - When the anemometer at the turbine location is supported by the parked turbine a procedure is needed to find an “undisturbed” location for the anemometer. The experimental research performed within the project as well as on-going experimental and theoretical research indicate that procedures for location selection may be defined.

Alternative power curve measurement procedure.

The alternative power curve measurement procedure is based on the use of an anemometer mounted on the nacelle of the running turbine. The relation between the reading of this anemometer and the undisturbed wind speed is measured on another (nominal identical) reference turbine at another site. Although, it is possible that the wind speed disturbance is power curve dependent and the alternative procedure is expected to introduce uncertainty, the methodology may be used for verifying whether the power curve of a turbine is equal to the power curve of the reference wind turbine.

Site dependency of power curves.

Even if all measurement uncertainties are eliminated the power curve of a wind turbine is site dependent through the wind field characteristics. Expressed in potential annual energy production values the site-induced differences can be in the order of 10% in complex sites.

5. EXPERIMENTAL RESEARCH ON WIND TURBINE POWER PERFORMANCE

5.1 Introduction

Power performance campaigns were selected and analysed focusing on the issues of the procedure that are related to complex terrain as well as to the identification of the terrain related wind characteristics that affect the power performance of wind turbines.

The analysed campaigns regard wind turbines ranging from 100kW up to 1MW operated at different sites at flat or complex terrain. A list of the analysed campaigns is found in table 1.1. In the following paragraphs a review of the performed experimental research is presented.

5.2 Review Of Power Performance Campaigns

5.2.1 WINCON 100XT operating at CRES test station

5.2.1.1 Description of the experimental research

C.R.E.S Test Station is situated about 50 km SE of Athens. The hill on top of which the WT is located and where the measuring campaign was performed, is 120m high above the sea level. The surrounding terrain is fairly complex and includes hills and coastal regions. The ground cover within a 500m radius is isolated trees, bushes and small summer cottages. Winds are mainly from the North, with occasional strong southern winds. To the west of the site at approximately 2-3km there is a cluster of 450m high hills, while on the other three sides lies the sea at distances varying from 2 km east to 5 km towards the north. The roughness length value has been estimated in terms of visual inspection as 0.13 m. Three 40m towers were erected at a distance of 1.5D from the WT and were equipped with five Gill sonic anemometers in a way to form a cross. At the cross intersection point a sonic anemometer is mounted at the hub height (22.4m) of the central tower. Moreover, four couples of cup anemometers and vane resolvers were mounted at the two side towers above and below the hub height, at a radius distance of 9.4m from the hub anemometer of the central tower. This distance corresponds to a 85% of the WT's blade length. Two more cup anemometers were used: one mounted at the cross intersection point and the other mounted at the hub height on the permanent meteorological mast of the Test Station, namely the north mast, at a distance of 2D from the WT. All masts were of lattice type, whereas the central mast was NRG type mast. The distance of the reference meteorological mast, namely the north mast, is 2D from the wind turbine at NNE direction.

The measurements used in site calibration and machine performance analysis are within the $[330^{\circ}-30^{\circ}]$ wind direction sector. The reference mast is within the selected sector which also includes the prevailing wind directions.

5.2.1.2 Site calibration

The anemometer used for the site calibration procedure was installed at 32.4m height at the location of the wind turbine, using a mobile meteorological mast erected on the nacelle of the wind turbine. Data was collected for a period of approximately 2 months. During this period the wind turbine was at stand-still, in the downwind position and the wind speed varied from 2m/s to 14m/s. The measurements from the nacelle cup were compared with the measurements from the main reference mast at hub height.

In figure 5.1 the distribution of the wind direction against wind speed, measured at the reference mast during the calibration session, is presented. In figures 5.2 and 5.3 the distributions of the turbulence intensity and the wind shear exponent (estimated from least square fitting) are shown. Wind shear is estimated from measurements collected from the west, central and east mast, that are located between the reference mast and the wind turbine. The measurements from the nacelle cup, at height 32.4m, are presented versus the relevant measurements from the

reference cup, at hub height, in figures 5.4 and 5.5 for the mean wind speed and the turbulence intensity respectively. The wind speed at the turbine location and at hub height is estimated from the nacelle cup measurement after correction for wind shear. In figure 5.6 the ratio of the estimated wind speed at wind turbine location at hub over the reference value is presented for the 5-10m/s wind speed range.

The correction factors to be applied to the measured reference wind speed were estimated by applying linear regression, with no intercept, of the estimated wind speed values at wind turbine location at hub height against the measured reference wind speed. The results are summarised below:

Wind direction bin	Correction factor U_{wt}/U_{ref}	Max. correction %
330°-340°	1.018	9%
340°-350°	1.017	6%
350°-360°	1.019	6%
0°-10°	1.014	4%
10°-20°	1.014	4%
20°-30°	1.018	4%

5.2.1.3 Power performance measurements and analysis

Detailed presentation of the wind and turbine measurements are found in the work of Morfiadakis E. (1996d). Data from the 60° wind direction sector from 330° to 30° were analysed. The reference wind speed and direction were measured by the north mast at hub height. In figure 5.7 the wind direction versus wind speed is presented. For the selected wind direction sector the turbulence intensity versus wind speed and wind direction are presented in figures 5.8-9. In figure 5.10 the estimated air density as a function of wind speed is presented.

The power output, mean and extreme values, of the WT110XT as a function of the wind speed is presented in figure 5.11. The standard deviation of the power output and the power coefficient, estimated for the 346m² rotor swept area, as a function of wind speed are given in figures 5.12 and 5.13, respectively. The bin averaged power curve and the power coefficient of the tested wind turbine are given in figure 5.14.

The uncertainty estimation of the measured magnitudes follows IEC (1997) recommendations. In table 5.1 the summary of the uncertainty components for the W110XT is given.

In order to assess the effect of reference wind speed correction and wind direction bin selection on power performance, AEP calculations were performed (based on Rayleigh wind speed distributions) for various power curve estimation cases.

Mean annual wind speed [m/s]	AEP estimations for general applications (Rayleigh distribution)			
	AEP Measured Power curve	Uncertainty		AEP Extrapolated Power Curve
	[MWh]	[MWh]	[%]	[MWh]
5	112,63	4,11	3,65	112,63
6	188,03	5,87	3,12	188,10
7	264,27	7,13	2,70	265,09
8	333,55	7,94	2,38	337,54
9	390,49	8,38	2,15	401,86
10	432,40	8,54	1,97	455,72
11	459,21	8,50	1,85	497,73

5.2.2 VESTAS V27 operating at Andros site

5.2.2.1 Description of the experimental research

Andros is a typical mountainous Cycladic island, situated in the southern Aegean sea. The total area of the island is approximately 400km², measuring 40km in length and 16km maximum width. The wind farm, with the tested machine, is situated near the Kalyvari village at the northernmost part of the island on top of a small ridge with NE to SW orientation. The altitude of the ridge varies between 330 and 320m ASL. The ridge is about 2.5 Km from the closest coast and overlooks the Strait of Euboea to the NNW, i.e. the 10km wide channel separating Andros from the island of Euboea. To the N & NNE the sea extends uninterrupted for over 50 Km. To the south of the wind farm and at a distance of 10km lies the Agioi Saranda ridge (714m ASL) with a NE to SW orientation. The landscape in the vicinity of the wind farm is bare with sparse and low lying vegetation and small rocks. Some low loose-stone built huts serving the local shepherds are found near the wind farm but they can hardly be considered as obstacles because of their low height (less than 3m) and the fact that they are integrated in the overall topography. The typical roughness length has been estimated at a value of $z_0=0.10$ that corresponds with farmland with close appearance. The distance of the reference meteo mast (mast M2) is approximately 1.6D from WT at a east-northeast direction. The measurement sector, used in site calibration and machine measurement campaign as well, is confined in the range [340°-15°], so that no shadowing effects either on WT operation or wind measurements are present. This sector includes the prevailing wind directions.

5.2.2.2 Site calibration

The anemometer used for the site calibration procedure was installed at 40m height at the location of the wind turbine, using a mobile meteorological mast erected on the nacelle of the wind turbine. Data was collected for a period of approximately 30 hours. During this period the wind turbine was at stand-still, in the downwind position and the wind speed varied from 5m/s to 14m/s. The measurements from the nacelle cup were compared with the measurements from the main reference mast (i.e. mast M2), at the same height. Full account of the experiment can be found in the work of Morfiadakis E. (1994a).

The ratio of the mean velocity measured at the WT location over the mean wind speed at M2, for the same height of 40m, was found to have an average of 1.015. Taking into account that mast M2 has been installed on the top of the ridge close to the wind turbine, and the fact that the wind sector used for the analysis corresponds to directions perpendicular to the main axis of the ridge, the hypothesis of equal velocity gradient at both mast and wind turbine locations is quite satisfactory. With this hypothesis, the correlation coefficient calculated for the anemometers at 40m is applied also to the anemometers mounted at 31.5m height. Using the above mentioned correlation coefficient the power curve referred to the undisturbed wind speed at the WT location is calculated.

In this application a 3% standard uncertainty for wind speed measurements due to the terrain effects, is applied when no corrections for the reference wind speed are considered. When the reference wind speed is corrected in order to take into account any terrain induced effects a 1% standard uncertainty is utilised as an indicative approximation, justified by the complex terrain.

5.2.2.3 Power performance measurements and analysis

Detailed presentation of the wind and turbine measurements are found in the work of Morfiadakis E. (1996c). Data from the 35° wind direction sector from 340° to 15° were analysed. In figure 5.15 the wind direction versus wind speed is presented. For the selected wind direction sector the turbulence intensity versus wind speed is presented in figure 5.16. The mean turbulence intensity level is about 10% varying from 5% to 15%. In figure 5.17 the wind shear exponent as a function of wind speed is presented. The wind shear exponent calculated, via least square fitting, from wind speed measured at three different heights varies from -0.05 to 0.15. Finally in figure 5.18 the air density as calculated from the temperature and pressure measurements is presented. In figures 5.19 and 5.20 the power output and its standard deviation are given as functions of mean wind speed. The power coefficient is presented in figure 5.21 whereas in figures 5.22 and 5.23 the pitch angle and its standard deviation are given.

The uncertainty estimation of the measured magnitudes follows IEC (1997) recommendations. In table 5.2 the summary of the uncertainty components for the V27 is given.

The estimation of annual energy production is based on representative Weibull distributions (corresponding to the test site conditions) and on Rayleigh type distributions with mean wind speed ranging from 5 to 11m/s. The former estimations are suitable for Greek applications whereas the latter for general applications. The results are given in the following table.

Mean annual wind speed [m/s]	AEP estimations for general applications (Rayleigh distribution)			
	AEP Measured Power curve [MWh]	Uncertainty [MWh] [%]		AEP Extrapolated Power Curve [MWh]
5	272,81	10,95	4,01	272,83
6	438,06	15,01	3,43	438,88
7	603,55	17,98	2,98	609,93
8	747,74	19,76	2,64	771,50
9	857,19	20,54	2,40	914,36
10	928,31	20,57	2,22	1032,74
11	964,59	20,09	2,08	1123,73

The following observations are made:

- the differences found between the “uncorrected” and the “nacelle cup corrected” power curves are within the uncertainty limit bounds of the relative AEP estimation; this is due to the limited magnitude of the correction factor
- the differences encountered when using different wind direction sectors for power curve estimation, present significant differences (up to 12%) that can not be attributed only to measurement uncertainty;

5.2.3 VESTAS V27 measured by DEWI

5.2.3.1 Power performance measurements and analysis

The power performance experiment was taken place during the period of 12/10-15/4/94. The experiment followed the recommendations of IEA (1990). No site calibration was performed. The reported data refer to a valid wind direction sector of 135°-225°.

The accuracy of the used instruments was as follows:

- cup anemometer (after calibration): 0.1m/s
- power transformer: 1.5kW
- temperature sensor: 1.0°C
- pressure sensor: 2.0hPa

In figure 5.24 the bin averaged power curve and power coefficient are presented.

5.2.4 VESTAS V27 measured by WINDTEST

5.2.4.1 Power performance measurements and analysis

The measurement campaign has been performed during the period 10/3-16/3/94 according to the IEA (1990).

The uncertainty of the instrumentation was as follows:

- wind speed: ± 0.2 m/s
- power transformer: $\pm 0.5\%$ at the nominal power of 300 kW
- air density estimation $\pm 0.25\%$

The bin averaged power curve is presented in figure 5.25. AEP estimations for general applications are presented in the following table:

Mean annual wind speed [m/s]	AEP estimations for general applications (Rayleigh distribution)				AEP Extrapolated Power Curve [MWh]
	AEP Measured Power curve [MWh]	Uncertainty			
		[MWh]	[%]		
5	271,40	12,04	4,44		271,65
6	432,99	20,00	3,96		936,81
7	588,81	16,66	2,83		608,95
8	713,98	17,23	2,91		772,15
9	797,86	17,03	2,13		916,44
10	892,20	16,34	1,94		1035,80
11	854,51	15,39	1,80		1127,36

5.2.5 NORDTANK 500/37 operating at Toplou site

5.2.5.1 Description of the experimental research

Toplou is located at the eastern part of the Crete island. Crete is the largest island in Greece situated at the southern Aegean sea. The total area of the island is approximately 8500 km², measuring 250 km in length and 60 km maximum width. The eastern part of Crete is characterised by complex topography with many hills and ridges of various slopes from 3 to 5° (smooth) to 20°+ (very steep). Toplou site is a very complex terrain site. The landscape in the vicinity of the wind turbine is bare with sparse, low lying vegetation and small rocks. The typical roughness length has been estimated by means of visual inspection at about 0.10m. The distance of the reference meteorological mast is approximately 2D from WT at a SSW direction. The measurements, used in site calibration and machine performance analysis as well, are within the [275°-350°] wind direction sector, so that no shadowing effects either on WT operation or wind measurements are present. This sector includes the prevailing wind direction.

5.2.5.2 Site calibration

Prior to the installation of the wind turbine a meteorological mast was erected at the location of the WT. The mast was equipped with cups and vane resolvers at three heights, i.e. 16.5m, 35m and 39m. Data was collected for a period of 13 days (15 to 28/12/1994). The measured wind speed at WT location at hub height was compared with the corresponding measurement from the reference mast.

In figures 5.26 and 5.27 the distribution of the wind direction and turbulence intensity versus wind speed at hub height for the reference mast are shown. In figure 5.28 the wind speed measured at the reference mast is shown against the one measured at WT location, for all wind directions. In figure 5.29 the bin averaged data for the wind speed ratio (WT over ref. measurement) is presented against wind direction measured at the reference mast. The wind speed range was set to 5-15m/s in order to increase the available data and minimise the uncertainty of estimating the average wind speed ratio.

By using 10° wind direction bins, for the wind speed range of 5-15m/s the estimated correction factors (average and maximum correction) are summarised in the following table:

Wind direction bin	Correction factor U_{wt}/U_{ref}	Max. correction %
-280°	0.976	9%
280°-290°	1.000	9%
290°-300°	0.970	8%
300°-310°	1.000	11%
310°-320°	0.977	10%
320°-330°	0.969	9%
330°+	0.990	9%

In this application a 3.67% standard uncertainty corresponding to one third of the maximum correction encountered (i.e. 11%), for wind speed measurements due to the terrain effects, is applied when no corrections for the reference wind speed are considered. When the reference wind speed is corrected in order to take into account any terrain induced effects a 1% standard uncertainty is utilised as an indicative approximation, justified by the complex terrain.

5.2.5.3 Power performance measurements and analysis

Detailed presentation of the wind and turbine measurements are found in the work of Morfiadakis E. (1996b). Data from the 75° wind direction sector from 275° to 350° were analysed. In figure 5.30 the wind direction versus wind speed is presented. For the selected wind direction sector the turbulence intensity versus wind speed is presented in figure 5.31. The mean turbulence intensity level is about 10% varying from 5% to 15%. Extreme values of about 20% are also present for wind speeds of 8 m/sec. In figure 5.32 the wind shear exponent as a function of wind speed is presented. The wind shear exponent calculated from the three wind speed at different heights varies from -0.5 to +0.40. Finally in figure 5.33 the air density as calculated from the temperature and pressure measurements is presented. In figures 5.34 to 5.36 the power output, its standard deviation and the power coefficient are presented as functions of mean wind speed (measuring period from 7/12/95 to 1/6/1996).

The uncertainty estimation of the measured magnitudes follows IEC (1997) recommendations. In table 5.3 the summary of the uncertainty components for the NT500 is given.

The estimation of annual energy production is based either on representative Weibull distributions (corresponding to the test site conditions) or on Rayleigh distributions with mean wind speed ranging from 5 to 11m/s. The former estimations are suitable for Greek applications whereas the latter for general applications.

The following tables for AEP estimation present the calculations based on the corrected data (i.e. corrected reference wind speed according to site calibration findings) for the whole wind direction sector.

Mean annual wind speed [m/s]	AEP estimations for general applications (Rayleigh distribution)			
	AEP Measured Power curve [MWh]	Uncertainty [MWh] [%]		AEP Extrapolated Power Curve [MWh]
5	539,44	21,00	3,89	539,43
6	887,33	29,88	3,37	887,37
7	1254,71	36,54	2,91	1255,39
8	1604,85	40,78	2,54	1609,10
9	1910,07	42,99	2,25	1924,35
10	2153,13	43,71	2,03	2185,80
11	2327,72	43,38	1,86	2386,00

The following observations are made:

- the differences found between the “uncorrected” and the “nacelle cup corrected” power curves are within the uncertainty limit bounds of the relative AEP estimation; this is due to the small magnitude of the correction factors (up to 3%)
- the differences encountered when using different wind direction sectors for power curve estimation, present significant differences that can not be attributed only to measurement uncertainty; the available data in each wind direction sector may be not adequate to describe consistently the power curve

5.2.6 NORDTANK 500/37 operating at Taff-Ely (turbine A)

5.2.6.1 Description of experimental research

The evaluation was carried out in the wind farm of 20 NTK500/37 turbines located in a complex terrain at an elevation of 300 meters above sea level. The evaluation was conducted by NEL as an independent assessor acting within a purchase and sale contract between the turbine manufacturer and the wind farm developer. IEA (1990) recommendations were prescribed as being the reference procedural standard. The machines chosen for the analysis, herein noted as turbine A and B, were those which had the smoothest incident wind flows (i.e. least steep slopes in the direction of the prevailing south westerly winds). One met mast was used for both turbines being assessed. Turbine A measured tip angles were found to be -2.1° , -2.1° and -2.0° .

5.2.6.2 Site calibration

To avoid interference from other turbines on both the mast and the turbine under test, only data measured in the sector $164^\circ - 259^\circ$ N were used in the power curve determination. The site does not meet the requirements of the IEC procedure with regard to the slopes of the surrounding terrain and therefore a site calibration exercise had to be carried out to determine the wind speed-up between the meteorological mast and the turbine under test. The site calibration was carried out using WA^{SP}. Consequently it was found that site calibration using WA^{SP} was not straightforward in a contractual context because of the sensitivity of results to grid resolution. Agreement was finally reached that all parties would accept the results of an analysis using the Big WA^{SP} code based on a contour resolution of 2m within 200m and a contour resolution of 10m within a 5km domain. In the event it was only possible to access 5m resolution data for the inner domain, but this was extended to a 1600m radius. Although internal calculation in WA^{SP} is believed to be carried out at 5 or 6 degree direction intervals, the data is only available for output in 30 degree sectors. However the analysis can be run with any initial directional offset. To determine directional dependent speed up factors (i.e. site calibrations), the model was run many times, with initial directional offsets being increased by 5 degrees for each run. Linear interpolation was then used to determine the appropriate wind speed correction for each valid data record. The maximum correction applied was 4.7 per cent. The results for turbine A are presented in table 5.4. Each entry in the 'relative to mast' column shows the 30 degree averaged speed up centered on the stated direction. Changing the direction by 5 degrees is seen in some cases to change the averaged correction factor by up to 1.5 percentage implying that the real directional dependent fluctuations in correction factor will probably be very significant. According to the site calibration results there are implications that very small directional sectors should be used in experimental calibration.

5.2.6.3 Power performance measurements and analysis

The measurements and analyses were carried out according to IEC TC88/1400-12/Ed.1 (CDV), dated May 1996. Modifications adopted at the TC88 Meeting, Tokyo in October 1996 have also been applied. The measurement period lasted 7 months. The power curve was corrected to a reference air density of 1.225 kg/m^3 . Data recorded during dry and wet (i.e. rain) conditions were used in this analysis. Topographic corrections were applied to the wind speed data used in this analysis. Mean power output and power coefficient data are presented in figures 5.37 and 5.38 respectively. The bin average power curve is presented in figure 5.39.

At the time of analysis, the IEC guidance on directional rejection criteria was not fully evolved, particularly with regard to wakes from adjacent turbines, therefore an approach was adopted whereby data were split into narrow direction sectors and the consistency in the resulting adjacent power curves was used as the selection/rejection criteria.

The annual energy production was derived from the measured power curve and from the power curve extrapolated to the cut-out wind speed of 25m/s. The measured power curve includes wind speeds up to 23.5 m/s in 0.5 m/s intervals with at least 30 minutes worth of data in each bin. The extrapolated curve assumes that the mean power in the last bin with at least 30 minutes of data (24.5 m/s in this case) is sustained to the cut-out wind speed. A Rayleigh distribution has been assumed, with annual mean wind speeds of 4 to 11 m/s in 1m/s intervals. The standard uncertainty of the energy yields has also been calculated.

Mean annual wind speed [m/s]	AEP estimations for general applications (Rayleigh distribution)			
	AEP Measured Power curve [MWh]	Uncertainty		AEP Extrapolated Power Curve [MWh]
		[MWh]	[%]	
4	203	66	33	203
5	458	99	22	458
6	777	129	17	777
7	1125	152	14	1125
8	1469 inc.	168	11	1470
9	1785 inc.	176	10	1787
10	2053 inc.	180	9	2058
11	2262 inc.	181	8	2273

There were problems in agreeing whether or not the warranted power curves had been attained because of lack of a contractual prescription defining the interpretation of the derived uncertainty figures.

5.2.7 NORDTANK 500/37 operating at Taff-Ely (turbine B)

5.2.7.1 Description of the experimental research

The evaluation was carried out in the wind farm of 20 NTK500/37 turbines located in a complex terrain at an elevation of 300m above sea level. The evaluation was conducted by NEL as an independent assessor acting within a purchase and sale contract between the turbine manufacturer and the wind farm developer. IEA recommendations were prescribed as being the reference procedural standard. The machines chosen for the analysis, herein noted as turbine A and B, were those which had the smoothest incident wind flows (i.e. least steep slopes in the direction of the prevailing south westerly winds). One met mast was used for both turbines being assessed. Turbine A measured tip angles were found to be -2.2° , -2.2° and -2.1° .

5.2.7.2 Site calibration

To avoid interference from other turbines on both the mast and the turbine under test, only data measured in the sector $190^\circ - 262^\circ$ were used in the power curve determination. The site does not meet the requirements of the IEC procedure with regard to the slopes of the surrounding terrain and therefore a site calibration exercise had to be carried out to determine the wind speed-up between the meteorological mast and the turbine under test. The site calibration was carried out using WA^{SP}. Speed-up factors were determined for each 5° sector within the bulk of the valid measurement sector, although on the periphery of the valid sector, 30° increments were used. The corrections are tabulated in table 5.5. Linear interpolation was then used to determine the appropriate wind speed correction for each valid data record. The maximum correction applied was 1.5 per cent.

5.2.7.3 Power performance measurements and analysis

The measurement period lasted 7 months. The power curve was corrected to a reference air density of 1.225 kg/m^3 . Data recorded during dry and wet (i.e. rain) conditions were used in this analysis. Topographic corrections derived using the WA^{SP} wind flow modelling package were applied to the wind speed data used in this analysis. Mean power output and power coefficient data are presented in figures 5.40 and 5.41 respectively. The bin average power curve is presented in figure 5.42.

The annual energy production was derived from the measured power curve and from the power curve extrapolated to the cut-out wind speed of 25 m/s. In this case the measured and extrapolated curves are the same. The measured power curve includes wind speeds up to 25 m/s in 0.5 m/s intervals with at least 30 minutes worth of data in each bin. The extrapolated curve assumes that the mean power in the last bin with at least 30 minutes of data (24 m/s in this case) is sustained to the cut-out wind speed. A Rayleigh distribution has been assumed, with annual mean wind speeds of 4 to 11 m/s in 1m/s intervals. The standard uncertainty of the energy yields has also been calculated.

Mean annual wind speed [m/s]	AEP estimations for general applications (Rayleigh distribution)			
	AEP Measured Power curve [MWh]	Uncertainty		AEP Extrapolated Power Curve [MWh]
		[MWh]	[%]	
4	230	52	23	230
5	495	72	15	495
6	822	88	11	822
7	1171	99	8	1171
8	1510 inc.	106	7	1511
9	1814 inc.	110	6	1818
10	2067 inc.	112	5	2077
11	2261 inc.	112	5	2279

5.2.8 NORDTANK 500/37 operating at Pilsum site

5.2.8.1 Power performance measurements and analysis

The test was performed at Pilsum, Krummhörn, Lower Saxony, Germany. The site is located nearly 1.5 km east of the coast of the North Sea. The ground has only low differences in height. The average turbulence intensity of the measuring sector is nearly 8 % at hub height. The measurement was done following IEA (1990) recommendations. The measurement sector was 120°-225°. The anemometers were calibrated in the wind tunnel of the university of Oldenburg. Measurement period was three months. The measured power curve was adjusted to a reference air density of 1.225 kg/m³. The blade pitch angle was -1.7°.

In figures 5.43 the power and power coefficient curves are given. In table 5.44 the bin averaged curves are also presented. Annual energy production estimations were made under the assumption of 100% availability. The estimations were performed Rayleigh distributions with annual average wind speeds from 5 to 11 m/s at hub height (35.0 m) for general applications.

The absolute uncertainties of the measured wind speed, electrical power and air density are tabulated below:

- wind speed: 0.1m/s
- power: 5kW
- air density: 0.01kg/m³

The estimated annual energy production, based on a Rayleigh distribution is given in the following table:

Mean annual wind speed [m/s]	AEP estimations for general applications (Rayleigh distribution)			
	AEP Measured Power curve [MWh]	Uncertainty		AEP Extrapolated Power Curve [MWh]
		[MWh]	[%]	
5	495	41	8	-
6	831	50	6	-
7	1195	56	5	-
8	1550	61	4	-
9	1869	65	4	-
10	2134	68	3	-
11	2337	69	3	-

5.2.9 NORDTANK 500/37 measured by WINDTEST

5.2.9.1 Power performance measurements and analysis

The measurement campaign has been performed during the period 22/12/93-2/2/94 according to the IEA (1990) recommendations.

The uncertainty of the instrumentation was taken as follows:

- *wind speed: ± 0.2 m/s*
- *power transformer: ± 0.5 % at the nominal power of 750kW*
- *air density estimation ± 0.25 %*

The measured power curve is presented in figure 5.45., whereas the annual energy estimations are presented in the following table:

Mean annual wind speed [m/s]	AEP estimations for general applications (Rayleigh distribution)			
	AEP Measured Power curve [MWh]	Uncertainty		AEP Extrapolated Power Curve [MWh]
		[MWh]	[%]	
5	990,59	23,31	4,75	990,78
6	821,96	30,31	3,69	826,01
7	1163,77	39,89	2,99	1189,30
8	1462,93	37,20	2,54	1595,09
9	1685,55	37,73	2,24	1866,82
10	1826,02	37,12	2,03	2136,88
11	1893,30	35,74	1,89	2346,09

5.2.10 MADE AE-30 operating at Fuerteventura and Tarifa

5.2.10.1 Description of experimental research

The scope of the research on MADE AE-30 turbines was the comparison of the power performance of two identical machines operating at Monteahumada on the Tarifa complex terrain area and at Cañada de la Barca in Fuerteventura island flat terrain site. The characteristics of the MADE AE-30, the monitoring system and the two sites are found in the work of Cuerva A. (1996a-c). MADE AE-30 is a three bladed, horizontal axis, stall controlled wind turbine with 330kW nominal power output. In both cases, the reference wind speed was taken from properly situated meteorological masts without performing any corrections for terrain induced effects.

5.2.10.2 Power performance measurements and analysis

Four cases for complex terrain as well as a reference one in flat terrain have been considered. These four cases are split in two different wind directions and two different turbulence intensity ranges in order to identify their influence on the power output.

A sector within the East wind direction ranged from 56.25° to 123.75° was considered. The general data base for this sector presented the double stall effect which has been included in the study. By stratifying the total measurement set by the turbulence intensity level it was revealed that turbulence plays a significant role on the appearance of this phenomenon. In figures 5.46-47 the power curve measurements, normalised for standard atmospheric conditions, for the low (less than 10%) and high (higher than 10%) turbulence intensities are presented. A sector within the West wind direction ranging from 236.25° to 258.75° was also considered. On the contrary that in the case of the measurements from East direction, double stall effects were not identifiable. In figures 5.48-49 the power curve measurements are presented for the two turbulence ranges.

The comparison of the measured power curves for all the examined cases is presented in figures 5.50-51. Three of the four curves in complex terrain present similar behaviour. Only the one corresponding to the East wind direction and a range of turbulence intensity values up to 10% features lesser values than the other. The reason for this is, as can be checked in the scatter plots, the machine operating with wind from this specific and turbulence intensity range was affected by double stall effect. In relation to the Power curve for flat terrain it can be realised the same way to go into the aerodynamic stall state that in the complex terrain cases which are not featuring double stall effect. Slight deviations of these values occur for wind speeds greater than 15 m/s, these ones reach a maximum difference of 11.4 % at 16.5 m/s (West T.I. >10%-Flat reference). These two curves have been chosen to make the previous statement, since they are the only ones which present real values (No extrapolated) of power up to this wind speed value.

Annual energy production estimations are presented in the following table for all the examined cases, whereas the comparison of the AEP estimations with respect to the reference case of flat terrain are presented in figure 5.52.

Mean wind speed [m/s]	AEP estimation [MWh/year]				
	Flat terrain	Eastern dir. (56.25° - 123.72°)		Western dir. (236.25° - 258.75°)	
		T.I. < 10%	T.I. > 10%	T.I. < 10%	T.I. > 10%
4	160.7	167.9	172.4	145.9	157.8
5	356.5	362.4	371.3	335.6	352.2
6	592.9	589.8	607.5	573.3	590.7
7	827.1	808.6	841.3	815.8	830.1
8	1023.6	987.9	1038.9	1024.5	1033.3
9	1164.5	1113.5	1181.9	1178.1	1180.9
10	1248.5	1185.8	1268.2	1273.2	1270.5
11	1283.8	1213.7	1305.9	1317.2	1310.1

It can be seen that the production for the case of East wind direction, turbulence intensity values lesser than 10% is always lesser than the others, including the flat terrain reference, when the site mean wind speed is greater than 7 m/s must be remembered that the machine presented double stall behaviour in this situation. The differences in this case can reach values up to 6 % (diminution) in relation to the reference or even 8 % if it is compared to the value at 11 m/s in the case of West direction for turbulence intensity ranges up to 10 %. Slight differences in the linear zone of the power curves (bin method) lead to considerable differences in all the AEP cases, between them and in relation to the reference for site mean wind speeds up to 8 m/s since this part of the curve is highly weighed up during the integration of the AEP. therefore, if we were in situation to take advantage of sites with low mean wind speed this could mean big differences in the production estimation depending on the direction and the turbulence intensity range. When the mean wind speed goes over 7m/s at 30m high (more less limit of profitability for constant speed technology) curves always present differences lesser than 3 % between them and in relation to the reference, but in the case of East sector with turbulence intensity up to 10% (double stall effect) already commented. Hence for this range of mean wind speed, direction and turbulence intensity do not seem to be a differential factor for the AEP estimation, whenever double stall effect does not appear.

In order to illustrate the way the AEP estimation can be affected by disturbed measurements of the wind speed due

to the wake of other machines for instance (this is the case) data from a sector within which it occurs is enclosed. In the previous analysis a West wind direction ranging from 236.25° to 258.75° is considered; this is a clean sector but if we take into account measurements for a wind direction greater than 258° and up to 348° the result for the AEP estimation is as follows. The comparison is done presenting the same results for the East sectors and results for a West direction between 236.25° to 348.75° . In figure 5.53 the AEP estimations are compared to the flat terrain case. It can be realised that the differences due to the disturbance effects (West T.I $>10\%$) reach more than 25% in relation to the reference values (flat terrain) surpassing strongly the differences due to double stall effect. The curve in the case of West for T.I $<10\%$ was only slightly affected by the disturbance.

The estimated uncertainties for the AEP calculations are presented in figure 5.54.

5.3 Assessment Of Site Calibration Methodologies

5.3.1 Site calibration for WINCON 110XT

The anemometer used for the site calibration procedure was installed at 32.4m height at the location of the wind turbine, using a mobile meteorological mast erected on the nacelle of the wind turbine. Data was collected for a period of approximately 2 months. During this period the wind turbine was at stand-still, in the downwind position and the wind speed varied from 2m/s to 14m/s. Wind shear was estimated from measurements collected from the upwind erected masts (Morfiadakis E. 1996d). The wind speed at the turbine location and at hub height is estimated from the nacelle cup measurement after correction for wind shear. The correction factors to be applied to the measured reference wind speed were estimated by applying linear regression, with no intercept, of the estimated wind speed values at wind turbine location at hub height against the measured reference wind speed. AEP estimations for two cases, namely with and without correction at upwind reference are presented in table 5.7

The main conclusions are the following:

- due to the small correction factors the differences between AEP estimations based either on corrected or on uncorrected data are less than 3%
- the use of the rotor averaged wind speed leads to estimations close to those without any correction; this is attributed to the fact that wind shear on the turbine location is flat and therefore the rotor centre wind speed value is close to the averaged one
- insignificant differences, less that 2% were found to exist for AEP estimations for different wind direction sectors

5.3.2 Site calibration for VESTAS V27

The procedure was reported in the work of Morfiadakis E. (1994a). The anemometer used for the site calibration procedure was installed at 40m height at the location of the wind turbine, using a mobile meteorological mast erected on the nacelle of the wind turbine. The correlation coefficient calculated for the anemometers at 40m, on the reference mast and the nacelle, was applied also to the anemometers mounted at 31.5m height, under the assumption that wind shear deformations are not sensitive to wind direction. Using a 5-15m/s wind speed bin for the whole wind direction sector the average and the maximum correction factor was found equal to 1.015 for the used wind direction sector. The reference mast was erected side to the turbine at 1.6D distance. Furthermore, the usage of an upwind located reference mast, at a distance of 4D was also assessed. AEP estimations for two cases, namely with and without correction at upwind reference are presented in table 5.7

The main observations are the following:

- the differences between AEP estimations based either on corrected or on uncorrected data are less than 5%
- the reference mast selection (erected side to the turbine) led to small correction factor; if the upwind mast was used the resulting AEP differences would exceed 30%
- the differences encountered in AEP estimations for different wind direction sectors indicate the need for using correction factors for narrower wind direction sectors; this was apparent for the side reference mast whereas the differences when using the upwind mast were lesser

5.3.3 Site calibration for NORDTANK 500/37

Prior to the installation of the wind turbine a meteorological mast was erected at the location of the WT. The mast was equipped with cups and vanes at three heights, i.e. 16.5m, 35m and 39m. Data was collected for a period of 13 days (15 to 28/12/1994). The measured wind speed at the wt location at hub height was compared with the corresponding measurement from the reference mast. The correction factors were estimated using 10° wind direction bins, for the wind speed range of 5-15m/s.

In addition, a brief site calibration with a mobile mast placed on the wind turbine nacelle while the machine was at stand still has been performed. Wind speed measurements were collected for a short period of two days from the nacelle cup as well as from the reference mast. With the applied technique the correlation between the wind speed at the wind turbine location at a height of 43.5m agl and the one measured at the hub height (35m agl) at the reference mast was measured. The calculation of the correlation at the same height, was feasible through the wind shear estimation. AEP estimations for two cases, namely with and without correction at upwind reference are presented in table 5.8. In figure 5.55 the comparison of the results from the two site calibration techniques is presented. Although applied for a short period the alternative site calibration technique yields results which are in fairly good agreement with these of the conventional site calibration.

5.3.4 Conclusions

Different site calibration techniques have been experimentally assessed. When AEP estimation was used as a tool for the assessment all the differences encountered were well within the uncertainty limits of the measurements. The site calibration technique using a mobile meteorological mast placed on the nacelle while the machine is at stand still when applied on a NTK500kW at Toplou yielded results which were in fairly good agreement with these of the conventional site calibration.

The main conclusions are:

- the position of the reference masts are quite suitable as the mean corrections applied to reference wind speeds were limited (up to 3%)
- the maximum observed speed-up within a wind direction bin reached 9% to 11%
- the only case where significant corrections would have been applied is in the case of V27 operating at Andros site, if the upwind mast is chosen as the reference one (the mean bin corrections well exceed 5%)
- the site calibration technique using a mobile meteorological mast placed on the wt nacelle while the machine is at stand still was validated and fairly good agreement found with these of the conventional site calibration
- although the wind speed corrections are of limited magnitude the turbulent characteristics may present significant variation between the reference point and the turbine location.

5.4 Conclusions

Several power performance campaigns have been analysed in order to assess the recommended procedures regarding site calibration, power curve determination and annual energy production uncertainty estimation. The analysed data regarded wind turbines of different size and control strategy operating at different sites.

In the fields of site calibration different techniques were assessed:

Nacelle cup at downwind parked turbine

This practice was applied in all power performance campaigns by CRES. In the case of V27 the site calibration was performed by the aid of a cup anemometer that was installed at 8.5m above the wind turbine nacelle, using a mobile meteorological mast, while the turbine was at standstill in the downwind direction. The measurements from the nacelle cup were correlated to the measurements from the reference mast at the same height. Under the assumption that the wind shear as measured at the reference mast holds at the turbine location too, the correlation factor found was used for the correction of the reference wind speed at hub height. In the case of WT110XT and NTK500/37 the nacelle cup measurements were corrected to hub height by using the wind shear as it was estimated from the upwind reference mast measurements. The correlation between the hub height undisturbed wind speed and the reference one is found using a 10° wind direction bin.

Meteorological mast prior wind turbine erection

In the case of NTK500/37, a meteorological mast was erected at the location of the wind turbine prior to the turbine installation. The measured wind speed at WT hub height was correlated to the corresponding measurements from the reference mast. Wind direction effects were counted for, as the wind direction bin was set to 10°. A comparison of this approach and the one using the nacelle cup yielded results which were in fairly good agreement.

Usage of numerical simulation code (WASP)

This practice was applied by NEL for the NTK500/37 campaigns. The estimated correlation showed significant sensitivity to small wind direction changes.

5.5 Tables

Table 5.1 Uncertainty components for W110XT power performance testing.

Measured parameter	Uncertainty component	Uncertainty limit	Notes
Electric power	current transformers	$\pm 0.35\%$ at 20% load	2 of class 0.2
	voltage transformers		
	power transducer	$\pm 0.5\% \times 170\text{kW}$	1 of class 0.5, nominal power 170kW
	signal transmission (DAS)	$\pm 0.1\%$ of the power	
Wind speed	digitisation (DAS)	$\pm 575/4096$	slope 57.5kW/volt
	anemometer calibration	$\pm 1\%$ of the velocity	
	operational characteristics	$\pm 1\%$ of the velocity	
	mounting effects		
	flow distortion due to terrain	3% of the velocity 1% of the velocity	no site calibration with site calibration corrections
	signal transmission (DAS)	$\pm 1\%$ of the velocity	
Air temperature	digitisation (DAS)	$\pm 94/4096$	slope 9.4m/sec/Volt
	temper. Sensor calibration	$\pm 0.50\text{ }^\circ\text{C}$	
	radiation shielding	$\pm 0.80\text{ }^\circ\text{C}$	
	mounting effects	$0.09\text{ }^\circ\text{C}$	the uncertainty is $(1/3)/10 \times$ (Hub-sensor height)
	signal transmission (DAS)	$\pm 0.07\text{ }^\circ\text{C}$	
Air pressure	digitisation (DAS)	$\pm 250/4096$	slope $25\text{ }^\circ\text{C/Volt}$
	pressure sensor calibration	$\pm 2\text{hPa}$	
	mounting effects	0.25hPa	10% of the applied correction
	signal transmission (DAS)		
	digitisation (DAS)	$\pm 520/4096$	slope 52hPa/Volt

Table 5.2 Uncertainty components for V27 power performance testing.

Measured parameter	Uncertainty component	Uncertainty limit	Notes
Electric power	current transformers	±0.35% at 20% load	2 of class 0.2
	voltage transformers		
	power transducer	±0.5% x 300kW	1 of class 0.5, nominal power 300kW
Wind speed	signal transmission (DAS)	±0.1% of the power	slope 150kW/volt
	digitisation (DAS)	10/4096	
	anemometer calibration	±1% of the velocity	ref. wind speed corrected no corrections applied
	operational characteristics	±1% of the velocity	
	mounting effects		
	flow distortion due to terrain	1% of the velocity 3% of the velocity	
	signal transmission (DAS)	±1% of the velocity	slope 9.4m/sec/Volt
digitisation (DAS)	10/4096		
Air temperature	temper. sensor calibration	±0.50 °C	the uncertainty is (1/3)/10 x (Hub-sensor height) + 1
	radiation shielding	±0.80 °C	
	mounting effects		
Air pressure	signal transmission (DAS)	±0.07 °C	slope 25°C/Volt
	digitisation (DAS)	10/4096	
	pressure sensor calibration	±2hPa	for a height difference of 33.5m the correction is 4.03hPa
	mounting effects	±0.4hPa	
	signal transmission (DAS)		
digitisation (DAS)	10/4096	slope 52hPa/Volt	

Table 5.3 Uncertainty components for NTK500/37 power performance testing.

Measured parameter	Uncertainty component	Uncertainty limit	Notes
Electric power	current transformers	$\pm 0.35\%$ of current at 20% load	2 of class 0.2
	voltage transformers	$\pm 0.20\%$ of voltage at all loads	2 of class 0.2
	power transducer signal transmission (DAS)	$\pm 0.25\% \times 1000\text{kW}$ $\pm 0.1\%$ of the power	1 of class 0.25, nominal power 1000kW
Wind speed	digitisation (DAS)	$\pm 1500/4096$	slope 150kW/volt
	anemometer calibration	$\pm 1\%$ of the velocity	
	operational characteristics mounting effects	$\pm 1\%$ of the velocity	
	flow distortion due to terrain	1% of the velocity 3.67% of the velocity	ref. wind speed corrected no corrections applied
Air temperature	signal transmission (DAS)	$\pm 1\%$ of the velocity	
	digitisation (DAS)	$\pm 61/4096$	slope 6.1m/sec/Volt
	temper. sensor calibration	$\pm 0.50\text{ }^\circ\text{C}$	
	radiation shielding mounting effects	$\pm 0.80\text{ }^\circ\text{C}$	the uncertainty is $(1/3)/10 \times$ (Hub-sensor height)
Air pressure	signal transmission (DAS)	$\pm 0.07\text{ }^\circ\text{C}$	
	digitisation (DAS)	$\pm 250/4096$	slope 25°C/Volt
	pressure sensor calibration	$\pm 1\text{hPa}$	
	mounting effects	$\pm 0.4\text{hPa}$	for a height difference of 33.5m the correction is 4.03hPa
	signal transmission (DAS)		
	digitisation (DAS)	$\pm 520/4096$	slope 52hPa/Volt

Table 5.4 *WASP* orography corrections for NTK500/37(A) at Taff Elly.

Direction (°N)	<i>WASP</i> Orography corrections				Running average
	Absolute (%)		Speed up factor		
	Mast	Turbine A	Mast	Turbine A	
165	22,36	18,17	1,224	1,182	-3,42%
170	25,25	20,56	1,253	1,206	-3,74%
175	28,00	23,10	1,280	1,231	-3,83%
180	30,60	25,50	1,306	1,255	-3,91%
185	32,97	27,72	1,330	1,277	-3,95%
190	34,90	28,58	1,349	1,286	-4,68%
195	36,29	31,75	1,363	1,318	-3,33%
200	36,39	33,75	1,364	1,338	-1,94%
205	35,09	34,83	1,351	1,348	-0,19%
210	33,46	33,73	1,335	1,337	0,20%
215	31,50	32,25	1,315	1,323	0,57%
220	29,28	30,45	1,293	1,305	0,91%
225	27,07	27,21	1,271	1,272	0,11%
230	24,85	25,94	1,249	1,259	0,87%
235	22,57	23,57	1,226	1,236	0,82%

Table 5.5 *WASP* orography corrections for NTK500/37(B) at Taff Elly.

Direction (°N)	<i>WASP</i> Orography corrections				Running average
	Absolute (%)		Speed up factor		
	Mast	Turbine B	Mast	Turbine B	
249	14,07	14,29	1,141	1,143	0,19%
254	11,56	11,82	1,116	1,118	0,23%
259	9,99	9,72	1,100	1,097	-0,25%
264	8,79	7,97	1,088	1,080	-0,75%
269	7,88	6,65	1,079	1,067	-1,14%
274	7,43	5,61	1,074	1,056	-1,69%
279	7,12	4,92	1,071	1,049	-2,05%
284	7,21	4,52	1,072	1,045	-2,51%

Table 5.6 Site calibration assessment via AEP estimations for W110XT (CRES test station).

AEP estimation with corrected reference wind speed			
Mean annual wind speed	Annual Energy Production (Uncertainty) [MWh]		
	Wind direction sector		
[m/s]	330°-30°	350°-10°	10°-30°
5	112,6 (4,11)	111,93 (4,12)	113,89 (4,12)
7	264,3 (7,13)	263,30 (7,15)	265,97 (7,23)
9	390,5 (8,38)	389,55 (8,40)	392,10 (8,66)
11	459,2 (8,50)	458,50 (8,49)	460,48 (8,92)

AEP estimation without correction for reference wind speed			
Mean annual wind speed	Annual Energy Production (Uncertainty) [MWh]		
	Wind direction sector		
[m/s]	330°-30°	350°-10°	10°-30°
5	116,22 (8,35)	115,32 (8,56)	117,21 (7,85)
7	270,00 (14,49)	268,86 (14,68)	271,26 (14,37)
9	396,36 (16,59)	395,07 (16,69)	397,40 (17,24)
11	464,47 (16,32)	462,98 (16,34)	465,20 (17,56)

Table 5.7 Site calibration assessment via AEP estimations for V27 (Andros site).

AEP estimation with corrected reference wind speed			
Mean annual wind speed	Annual Energy Production (Uncertainty) [MWh]		
	Wind direction sector		
[m/s]	345°-15°	345°-360°	0°-15°
5	272,81 (10,95)	270,98 (10,95)	295,69 (11,06)
7	603,55 (17,98)	603,58 (18,12)	619,78 (17,98)
9	857,19 (20,54)	859,54 (20,76)	867,49 (20,48)
11	964,59 (20,09)	968,17 (20,32)	971,06 (20,02)

AEP estimation without correction for reference wind speed			
Mean annual wind speed	Annual Energy Production (Uncertainty) [MWh]		
	Wind direction sector		
[m/s]	345°-15°	345°-360°	0°-15°
5	303,63 (15,88)	281,69 (15,95)	307,18 (15,96)
7	634,49 (25,86)	620,24 (26,19)	637,14 (25,76)
9	884,78 (28,83)	876,68 (29,35)	885,86 (28,65)
11	987,89 (27,56)	983,45 (28,14)	987,92 (27,38)

Table 5.8 Site calibration assessment via AEP estimations for NTK500/37 (Toplou site).

AEP estimation with corrected reference wind speed				
Mean annual wind speed	Annual Energy Production (Uncertainty) [MWh]			
	Wind direction sector			
[m/s]	275°-350°	300°-310°	310°-320°	320°-330°
5	539,44 (21,0)	509,76 (21,0)	564,89 (21,7)	539,94 (20,7)
7	1254,71 (36,5)	1212,29 (36,6)	1301,56 (37,5)	1236,72 (35,6)
9	1910,07 (43,0)	1866,20 (43,9)	1962,62 (44,4)	1878,40 (42,0)
11	2327,72 (43,4)	2290,40 (45,0)	2375,71 (45,5)	2291,42 (42,7)

AEP estimation without correction for reference wind speed				
Mean annual wind speed	Annual Energy Production (Uncertainty) [MWh]			
	Wind direction sector			
[m/s]	275°-350°	300°-310°	310°-320°	320°-330°
5	515,7 (51,7)	509,8 (52,0)	530,0 (50,7)	503,5 (48,8)
7	1217,6 (92,1)	1212,3 (91,9)	1251,5 (92,1)	1171,4 (88,2)
9	1870,2 (108,3)	1866,7 (109,6)	1914,1 (105,5)	1802,1 (105,9)
11	2292,2 (108,4)	2291,9 (111,3)	2336,9 (112,4)	2218,1 (107,8)

5.6 Figures

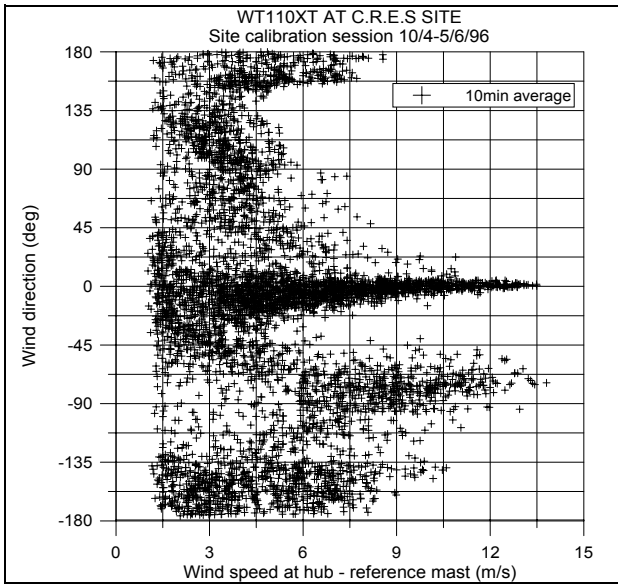


Figure 5.1 Wind direction distribution.

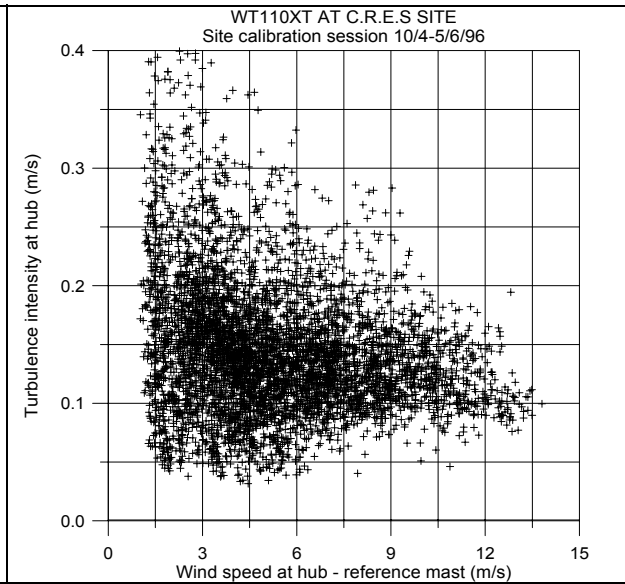


Figure 5.2 Turbulence intensity vs wind speed at hub.

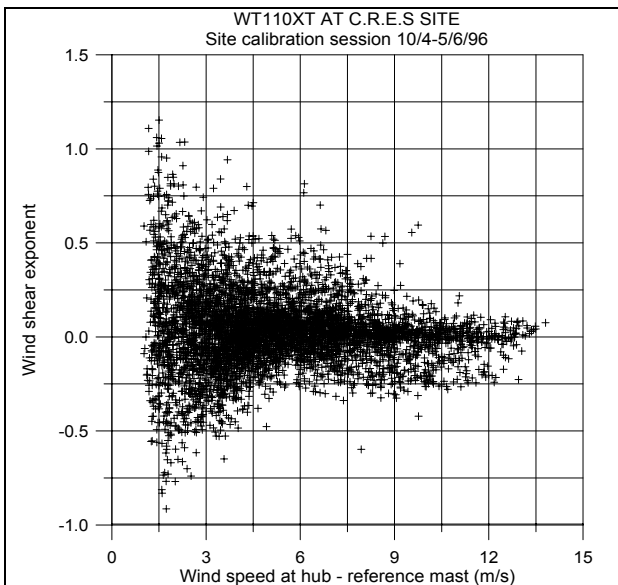


Figure 5.3 Wind shear exponent.

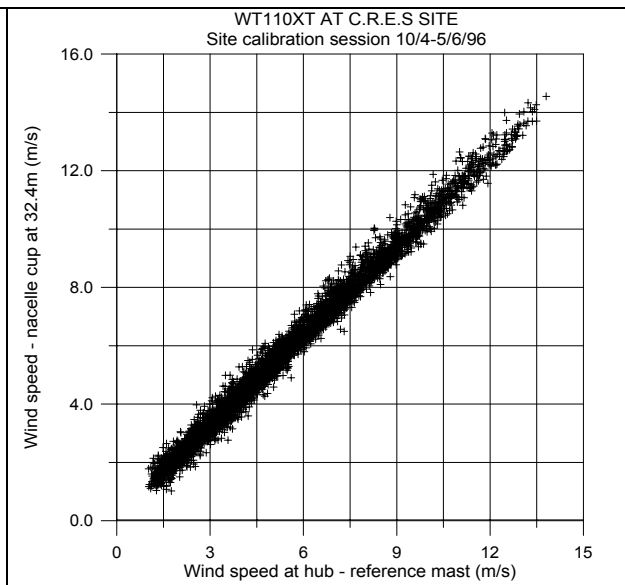


Figure 5.4 Wind speed at nacelle cup vs reference.

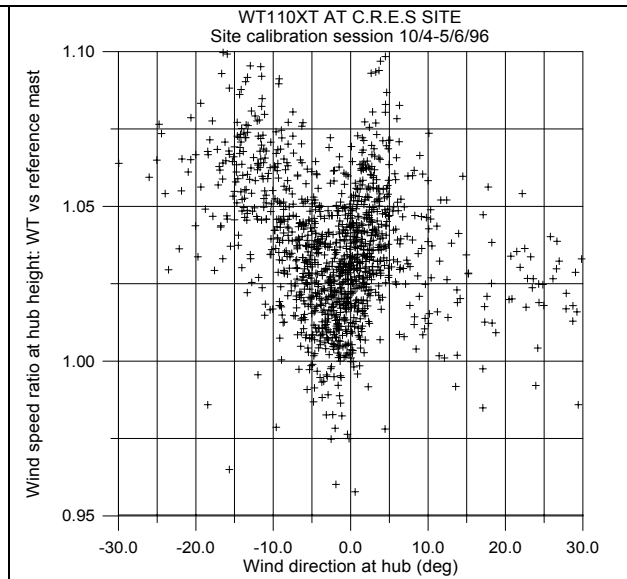
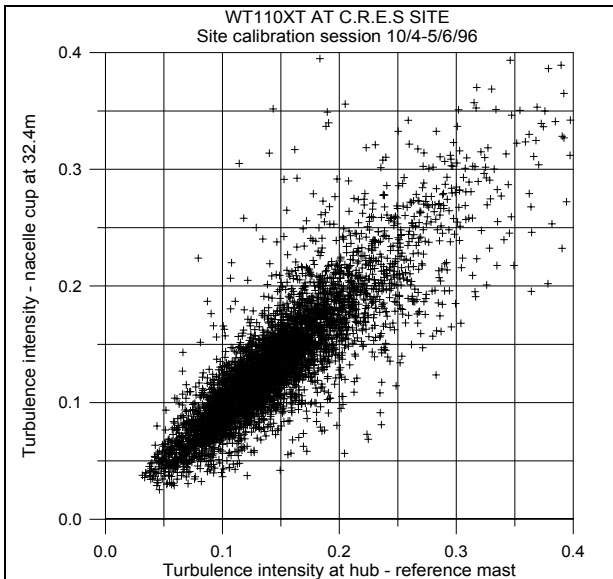


Figure 5.5 Turbulence intensity at nacelle cup vs reference.

Figure 5.6 Wind speed ratio vs reference.

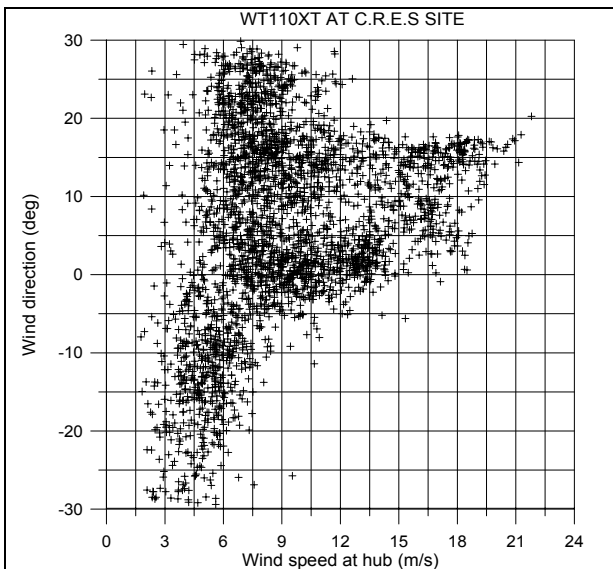


Figure 5.7 Wind direction vs wind speed.

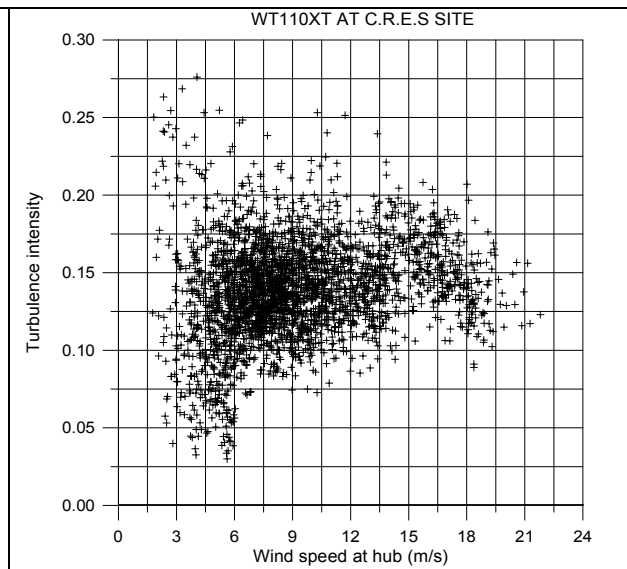


Figure 5.8 Turbulence intensity vs wind speed.

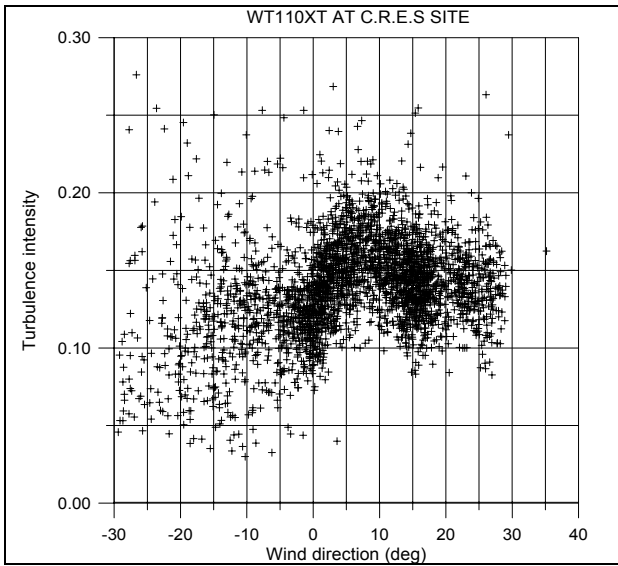


Figure 5.9 Turbulence intensity vs wind direction.

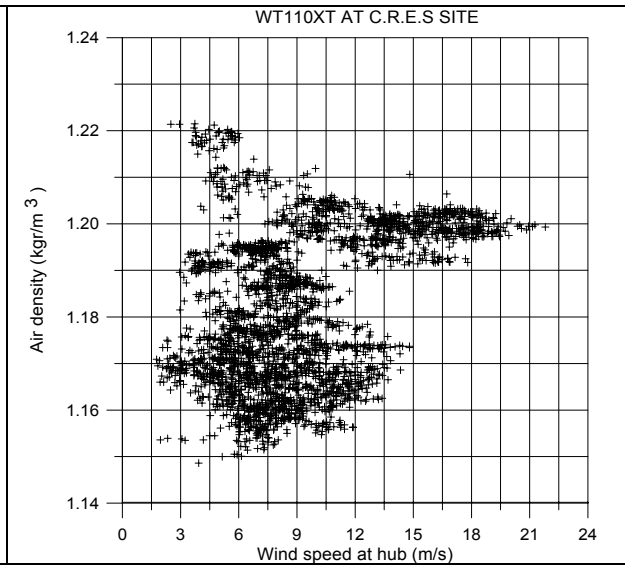


Figure 5.10 Air density vs mean wind speed.

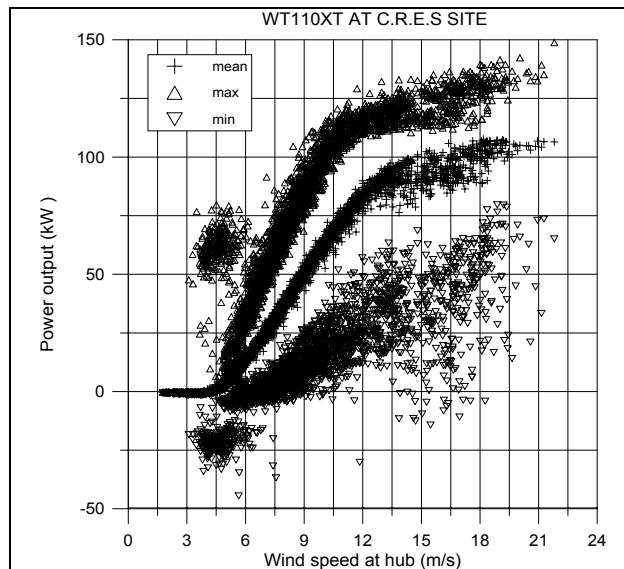


Figure 5.11 Active power vs wind speed at hub.

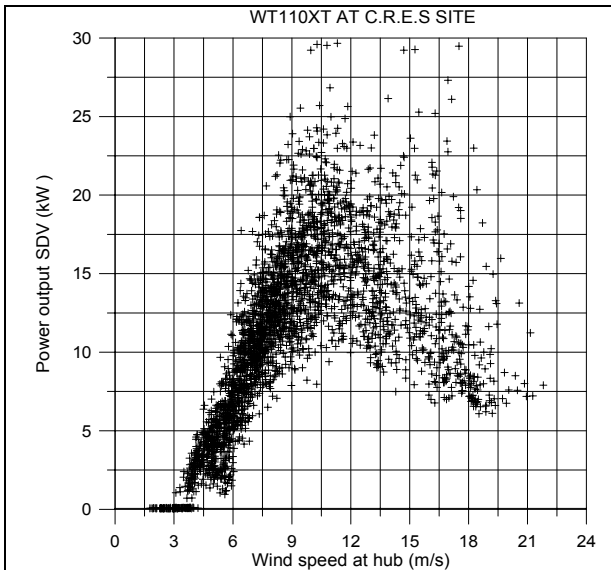


Figure 5.12 SDV power vs wind speed.

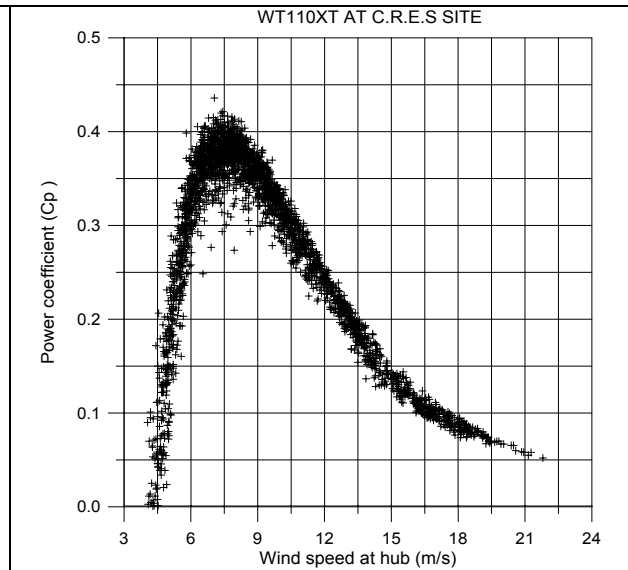


Figure 5.13 Power coefficient vs wind speed.

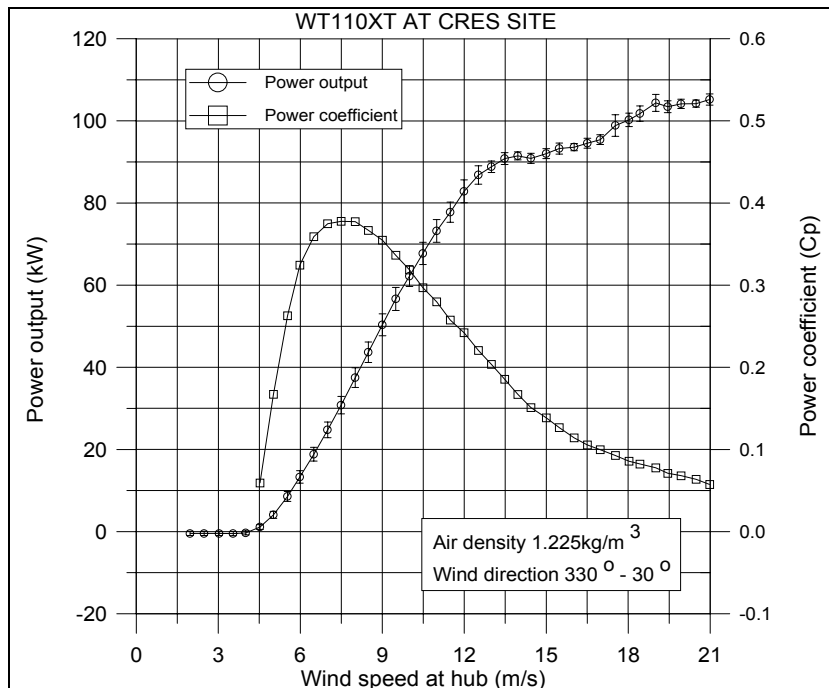


Figure 5.14 Power curve and power coefficient of W110XT.

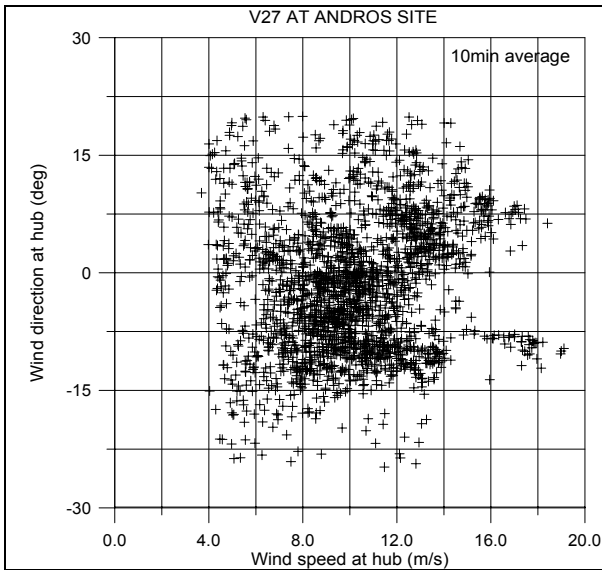


Figure 5.15 Wind direction distribution.

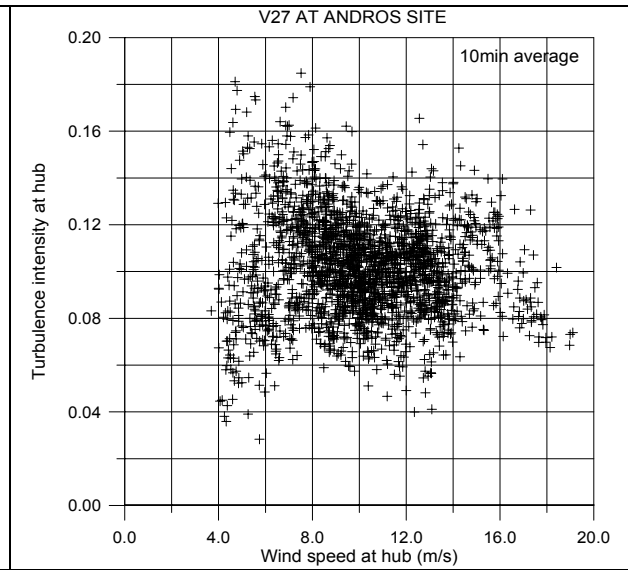


Figure 5.16 Turbulence intensity distribution.

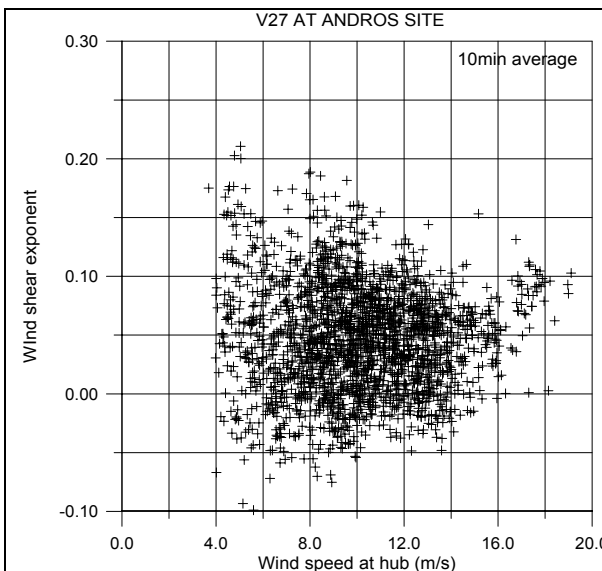


Figure 5.17 Wind shear exponent distribution.

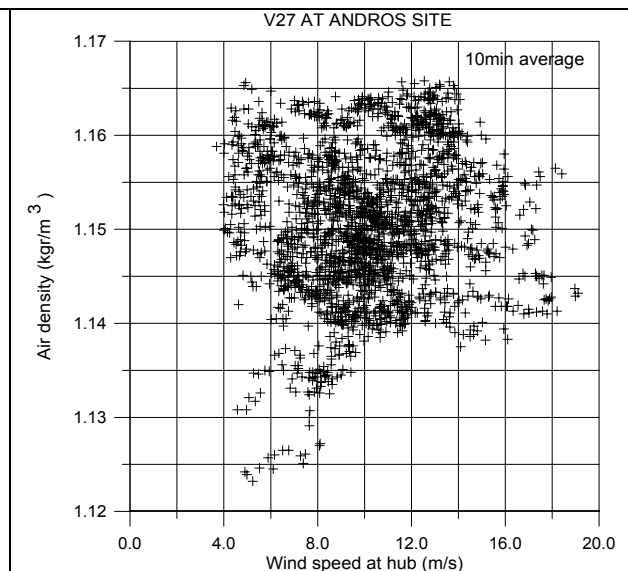


Figure 5.18 Air density distribution.

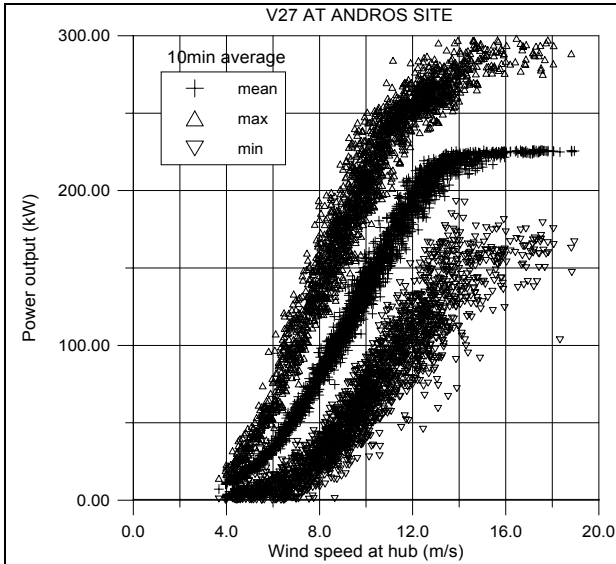


Figure 5.19 Power output of V27.

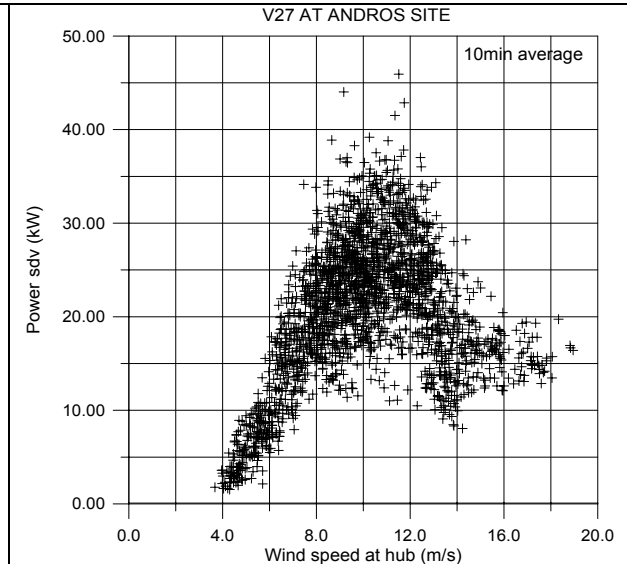


Figure 5.20 Standard deviation of power output.

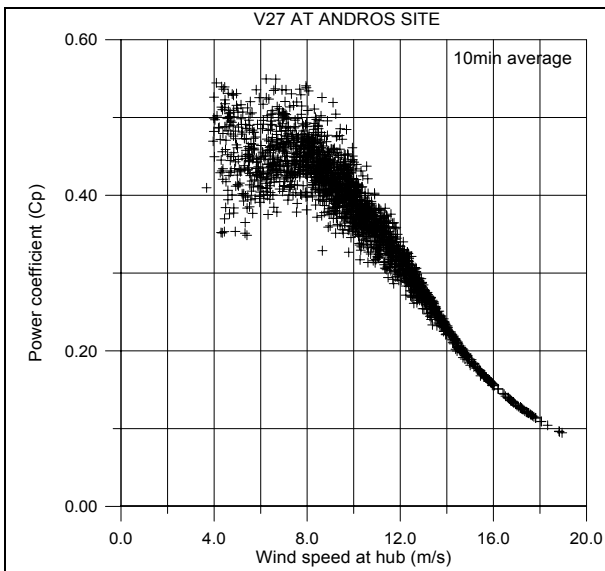


Figure 5.21 Power output of V27.

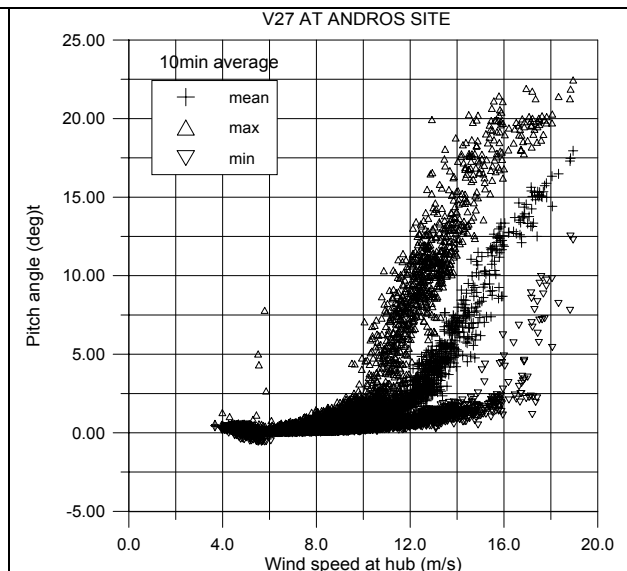


Figure 5.22 Pitch angle vs mean wind speed.

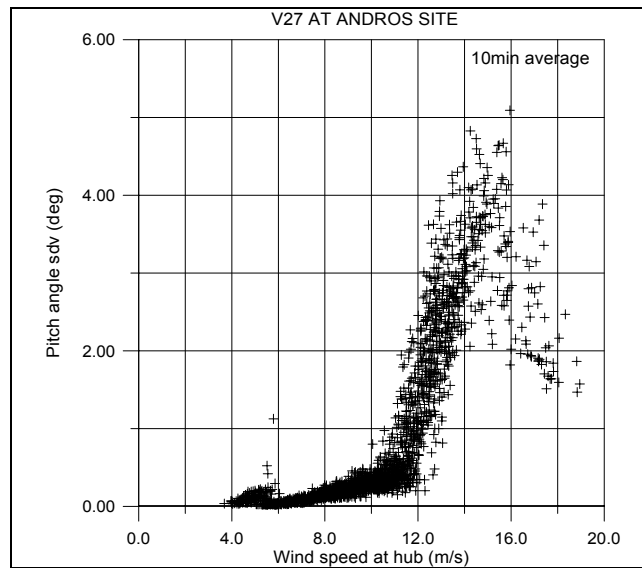


Figure 5.23 Standard deviation of pitch angle.

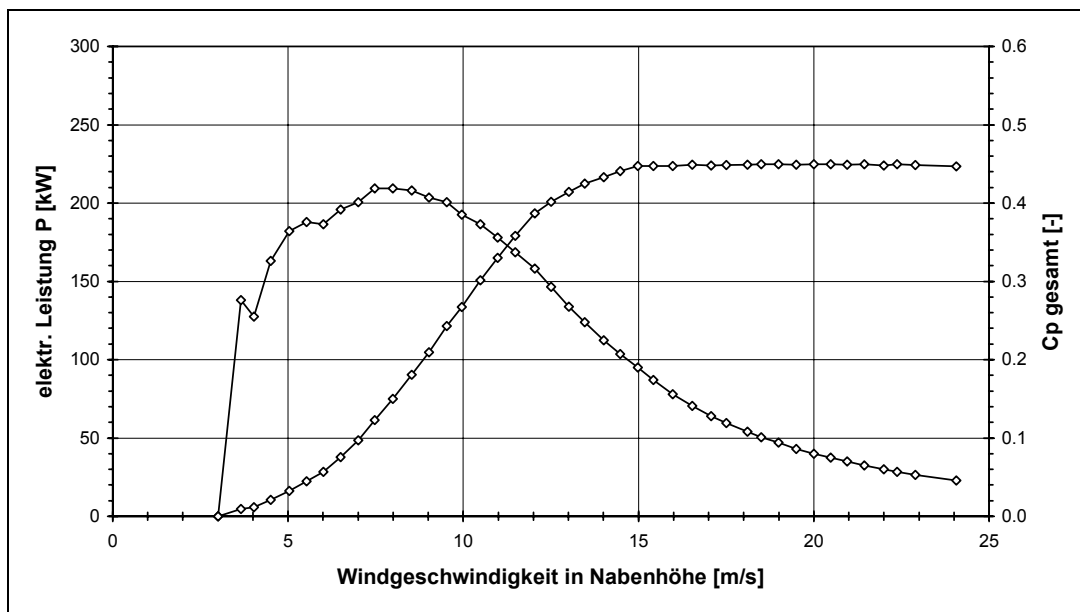


Figure 5.24 Power output and power coefficient for V27 as measured by DEWI.

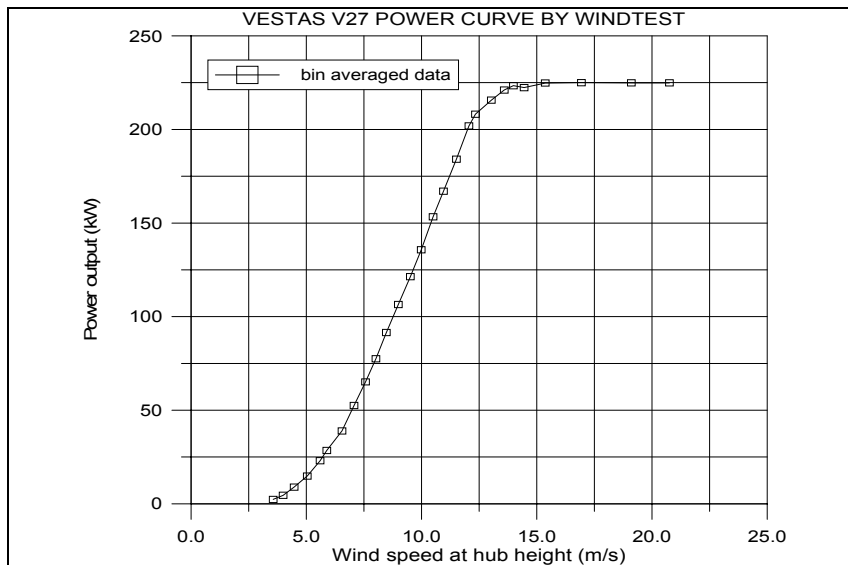


Figure 5.25 Bin averaged power curve for V27 by WINDTEST.

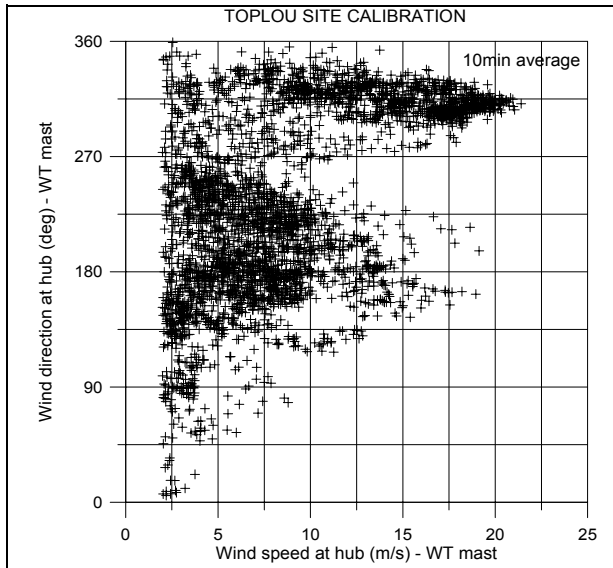


Figure 5.26 Wind direction vs wind speed at hub.

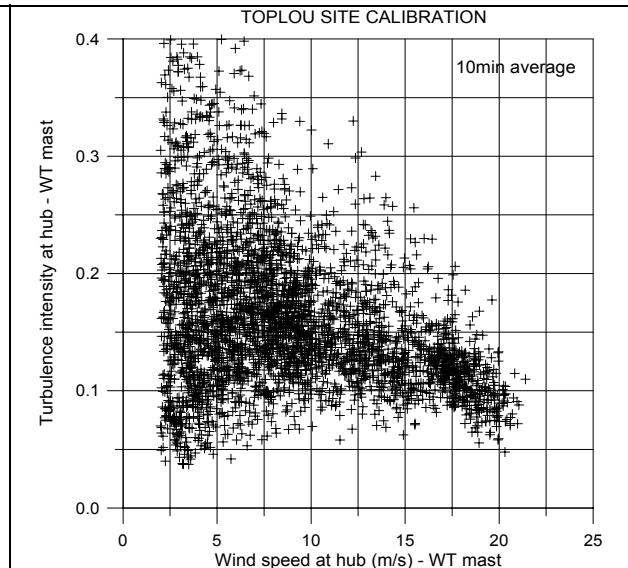


Figure 5.27 Turbulence intensity vs wind speed.

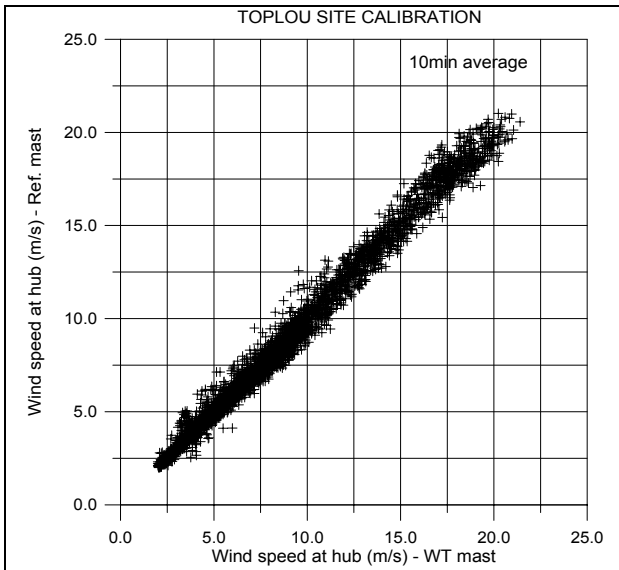


Figure 5.28 Wind speed at reference vs wind speed at WT location.

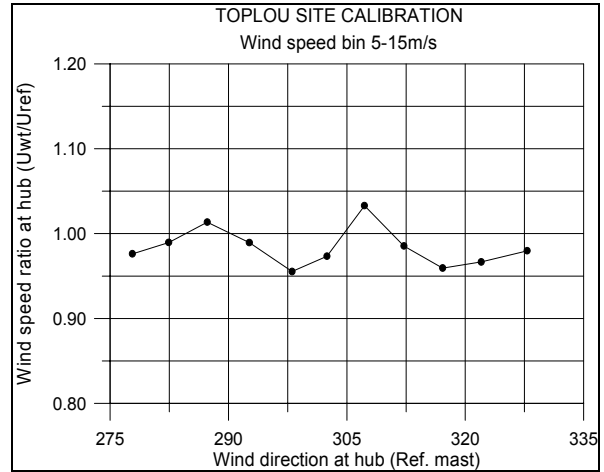


Figure 5.29 Bin averaged wind speed ratio vs wind direction at reference.

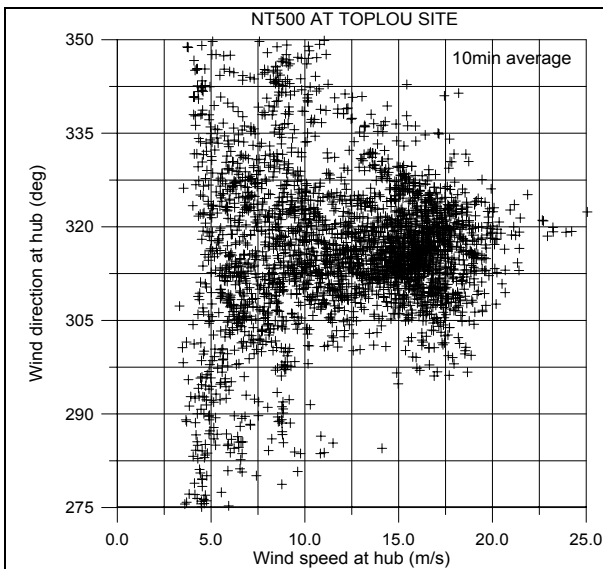


Figure 5.30 Wind direction vs wind speed at hub.

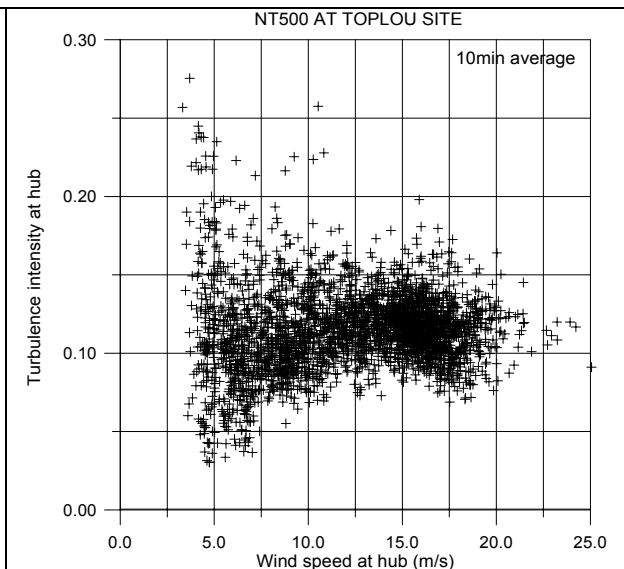


Figure 5.31 Turbulence intensity vs wind speed.

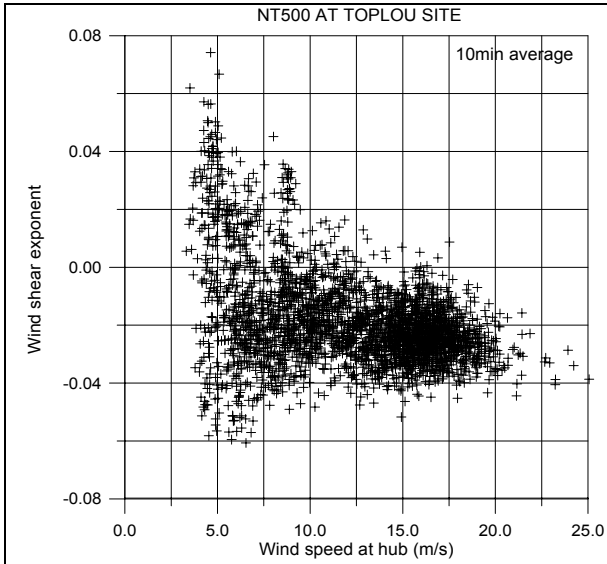


Figure 5.32 Wind shear vs wind speed.

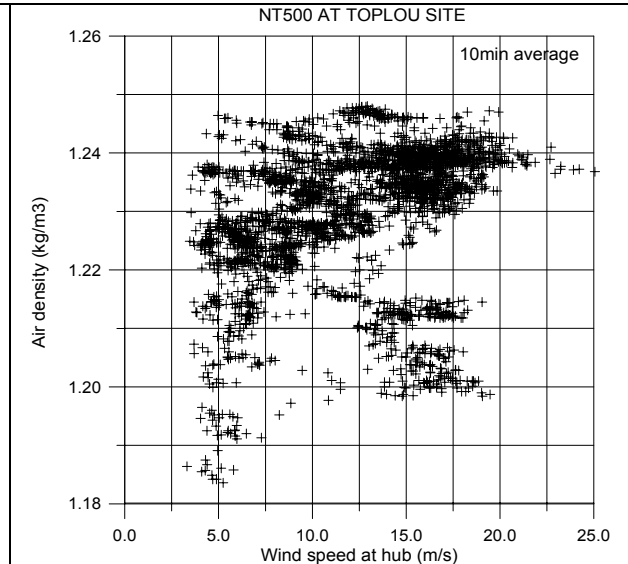


Figure 5.33 Air density vs wind speed at hub.

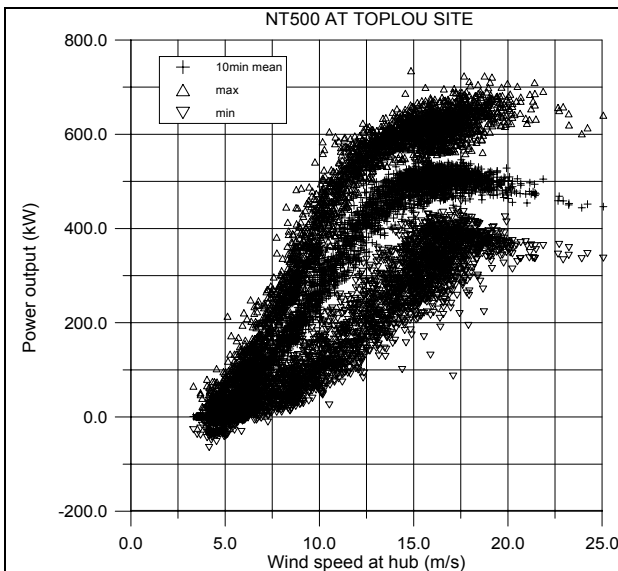


Figure 5.34 Power output of NTK500/37.

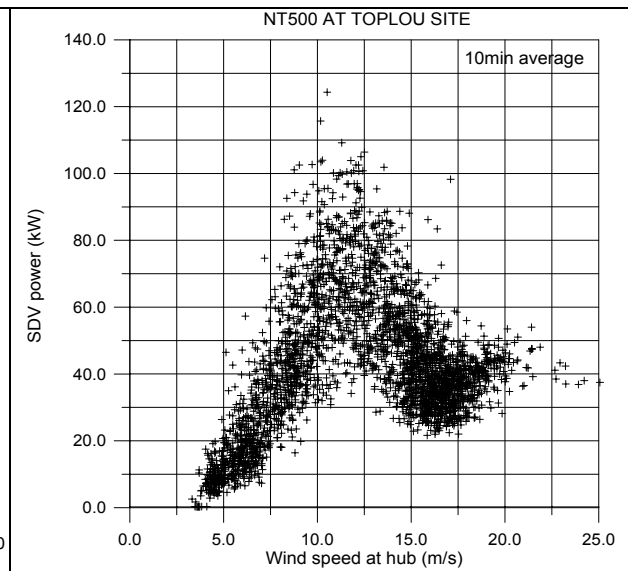


Figure 5.35 Standard deviation of power output.

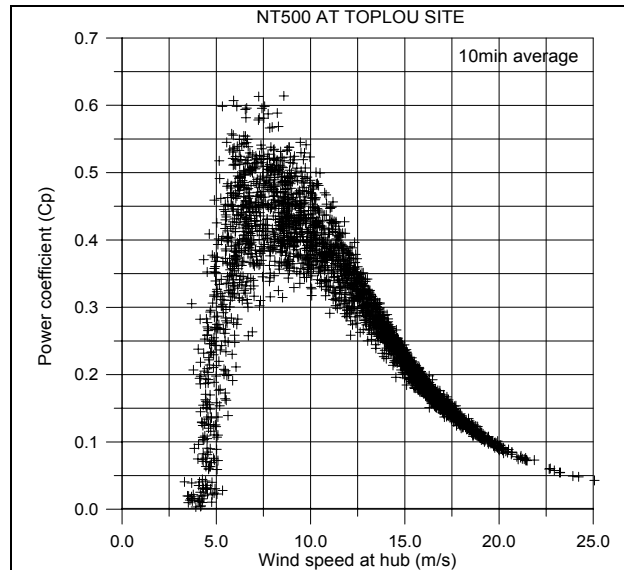


Figure 5.36 Power coefficient for NTK500/37.

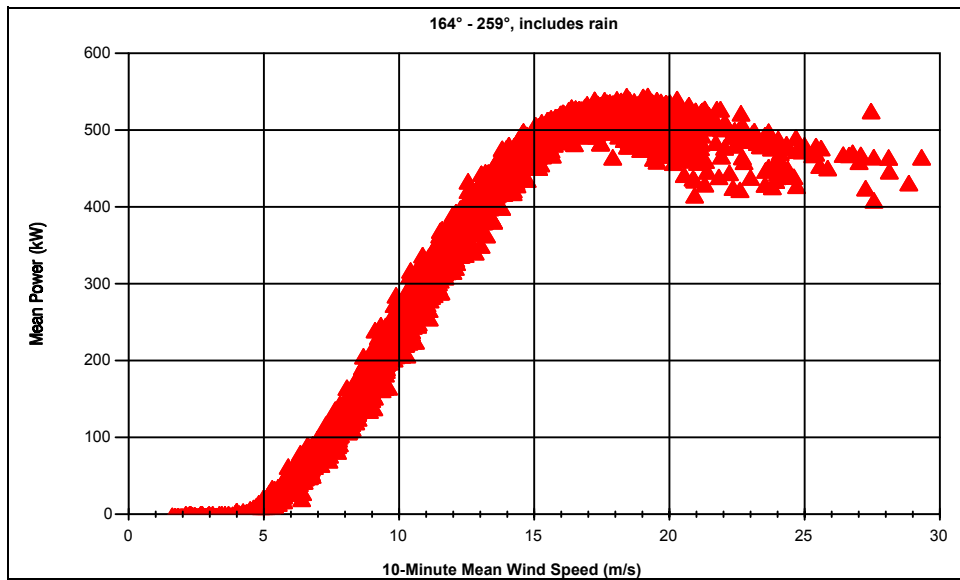


Figure 5.37 Power output of NTK500/37 at Taff-Ely (turbine A).

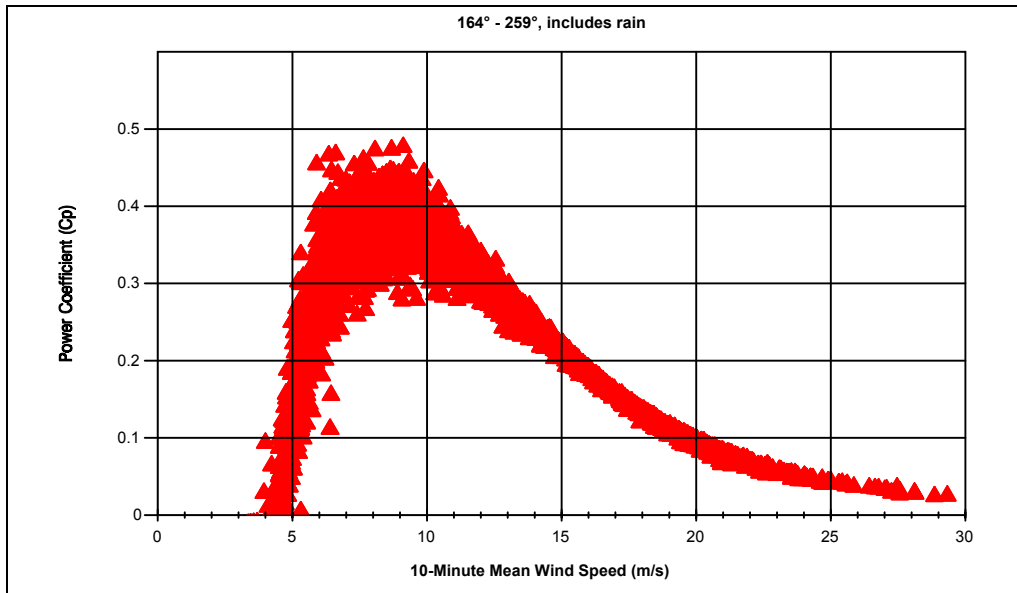


Figure 5.38 Power coefficient of NTK500/37 at Taff-Ely (turbine A).

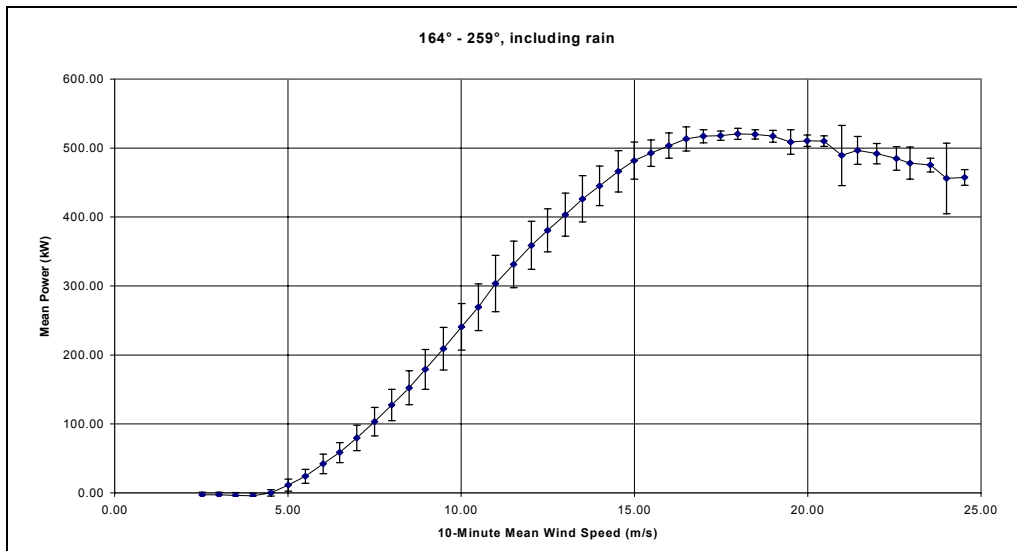


Figure 5.39 Power curve of NTK500/37 at Taff-Ely (turbine A)

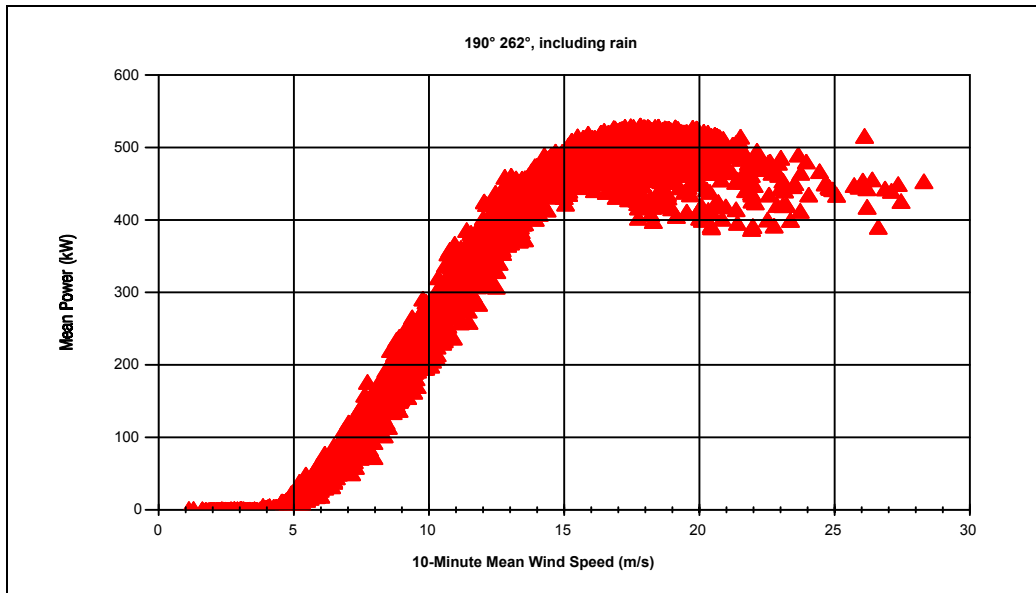


Figure 5.40 Power output of NTK500/37 at Taff-Ely (turbine B).

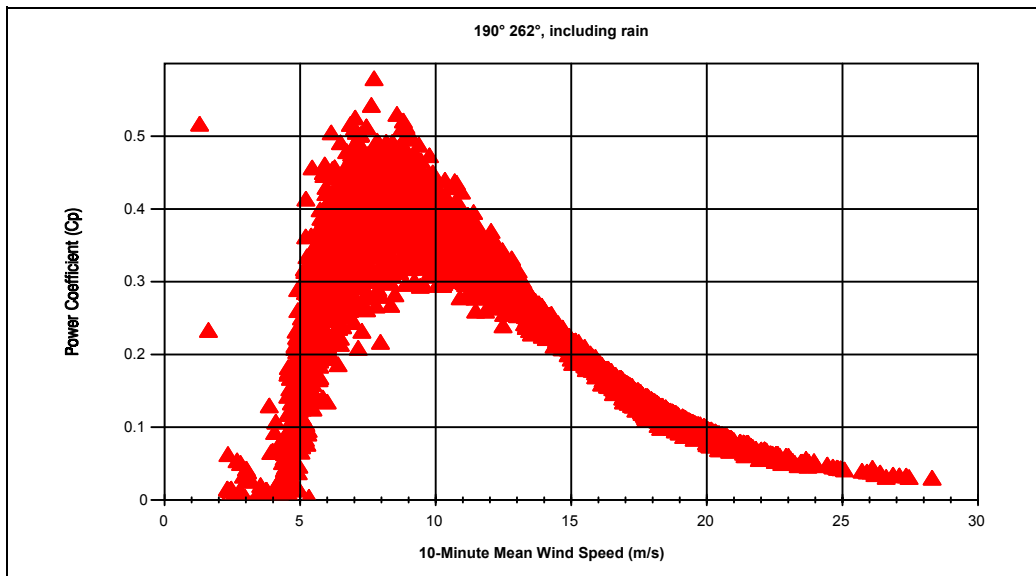


Figure 5.41 Power coefficient of NTK500/37 at Taff-Ely (turbine B).

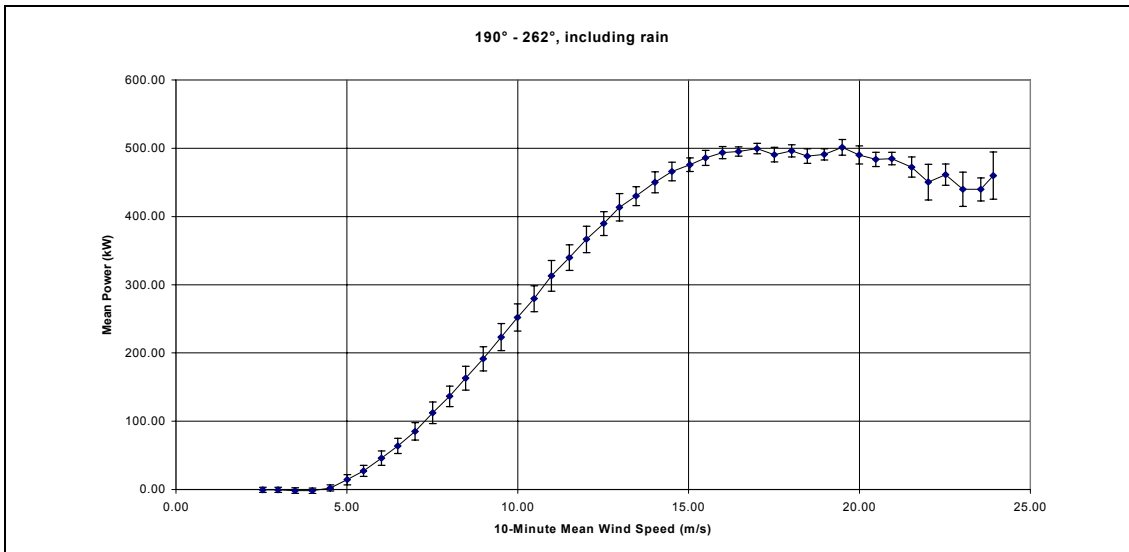


Figure 5.42 Power curve of NTK500/37 at Taff-Ely (turbine B).

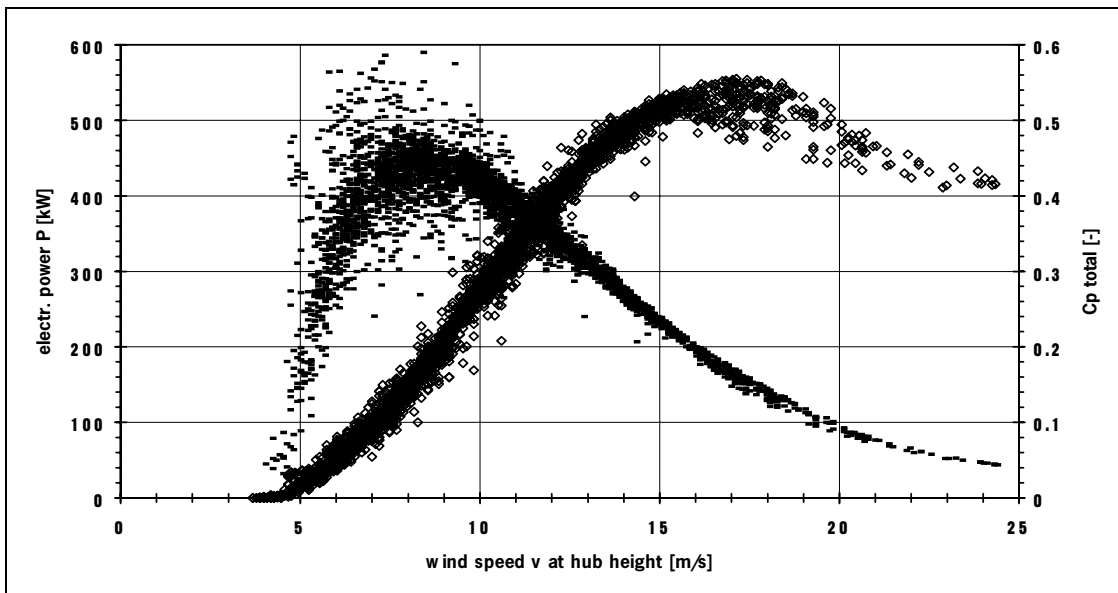


Figure 5.43 Mean power and power coefficient for NTK500/37 measured by DEWI

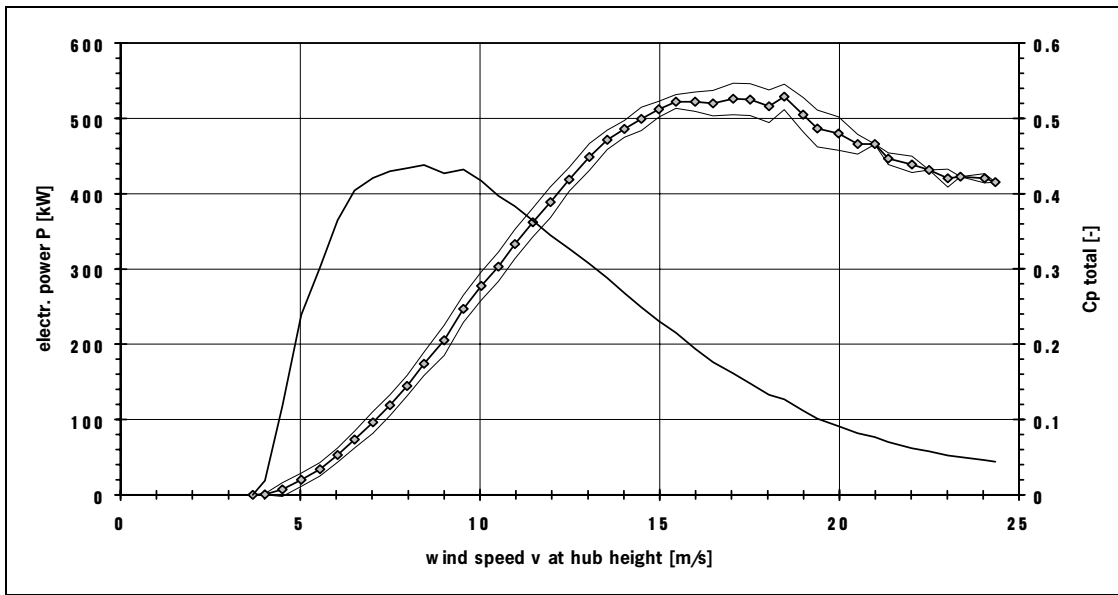


Figure 5.44 Bin averaged power and power coefficient curves for NTK500/37.

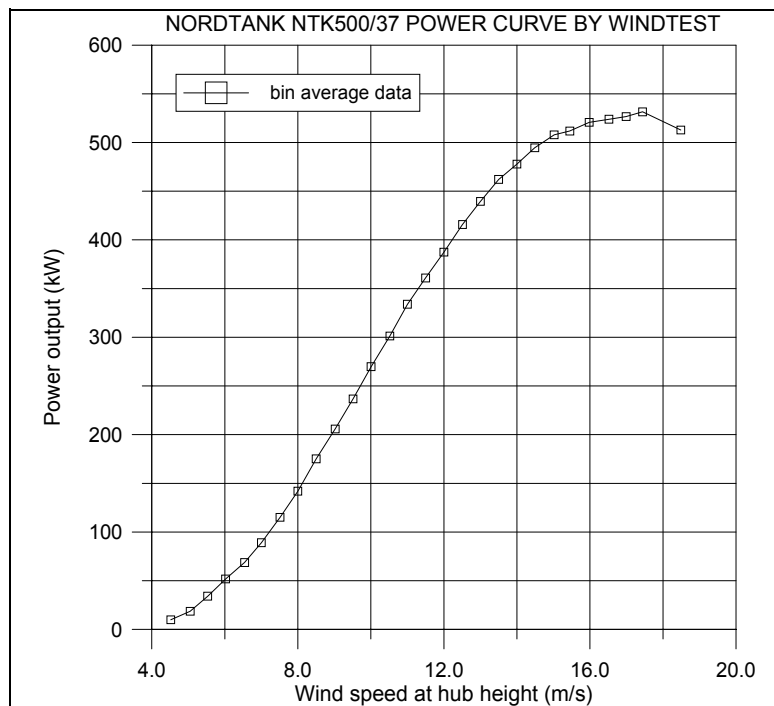


Figure 5.45 Bin averaged power curve for NTK500/37 by WINDTEST.

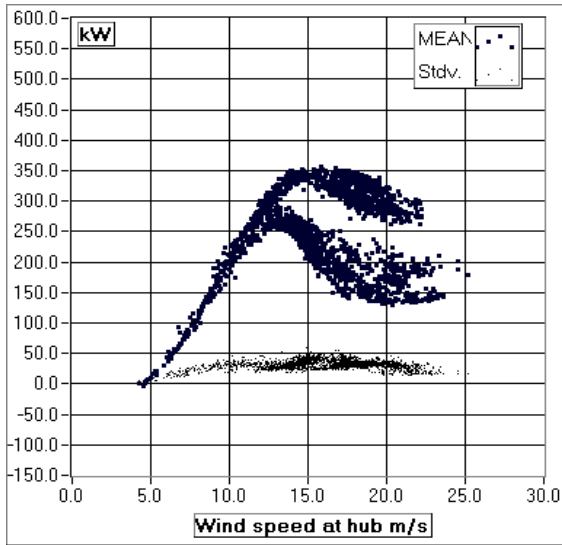


Figure 5.46 Power output for MADE AE-30 (wind direction: 56.25°-123.75°, turbulence intensity <10%)

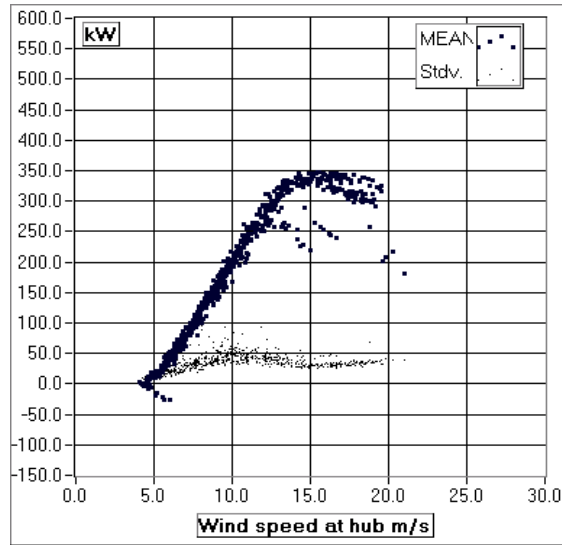


Figure 5.47 Power output for MADE AE-30 (wind direction: 56.25°-123.75°, turbulence intensity >10%).

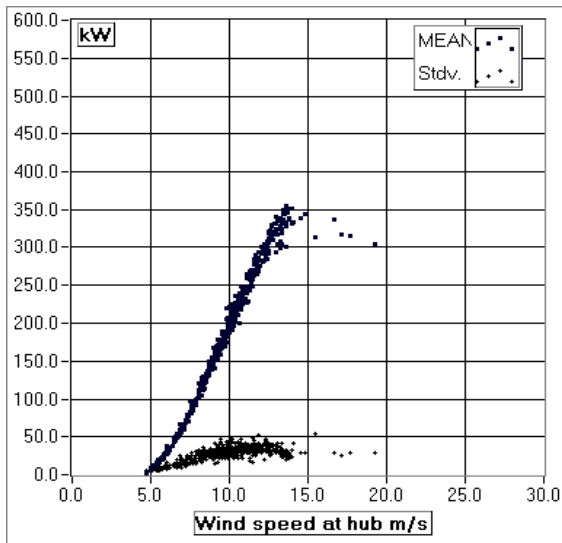


Figure 5.48 Power output for MADE AE-30 (wind direction: 236.25°-258.75°, turbulence intensity <10%).

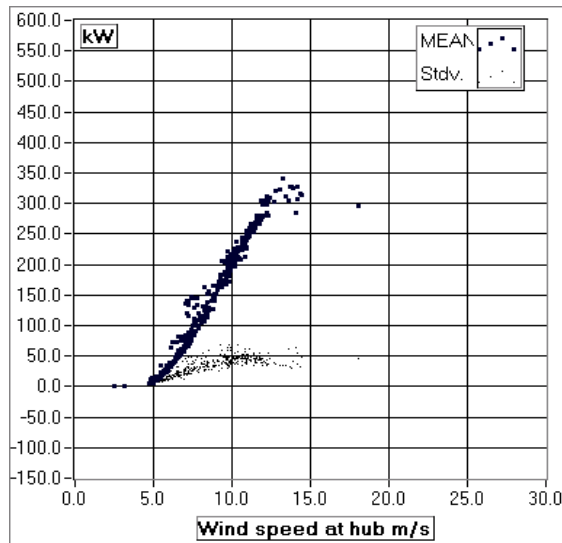


Figure 5.49 Power output for MADE AE-30 (wind direction: 236.25°-258.75°, turbulence intensity >10%).

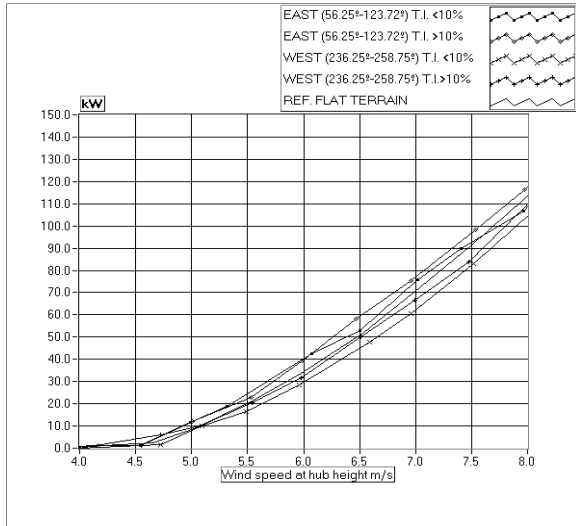


Figure 5.50 Power curve comparison at linear part.

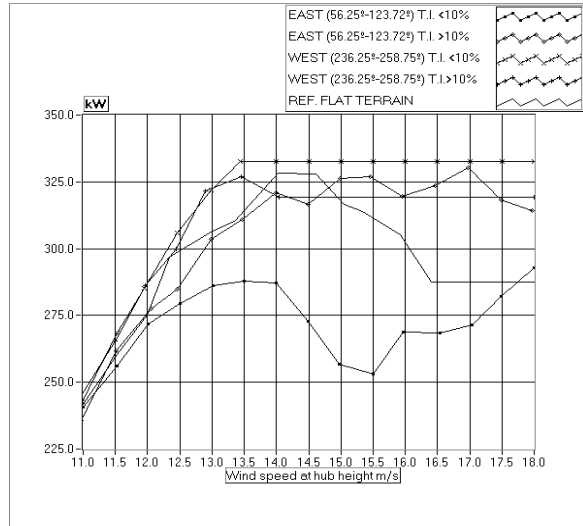


Figure 5.51 Power curve comparison at stall region.

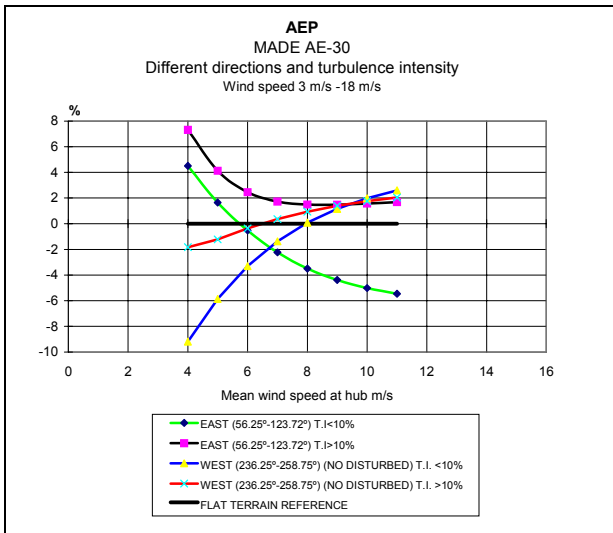


Figure 5.52 AEP comparison (flat terrain as reference).

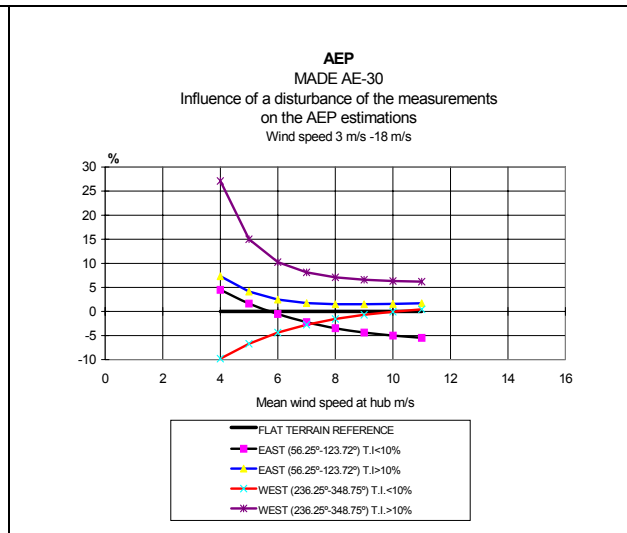


Figure 5.53 AEP comparisons including wake measurements.

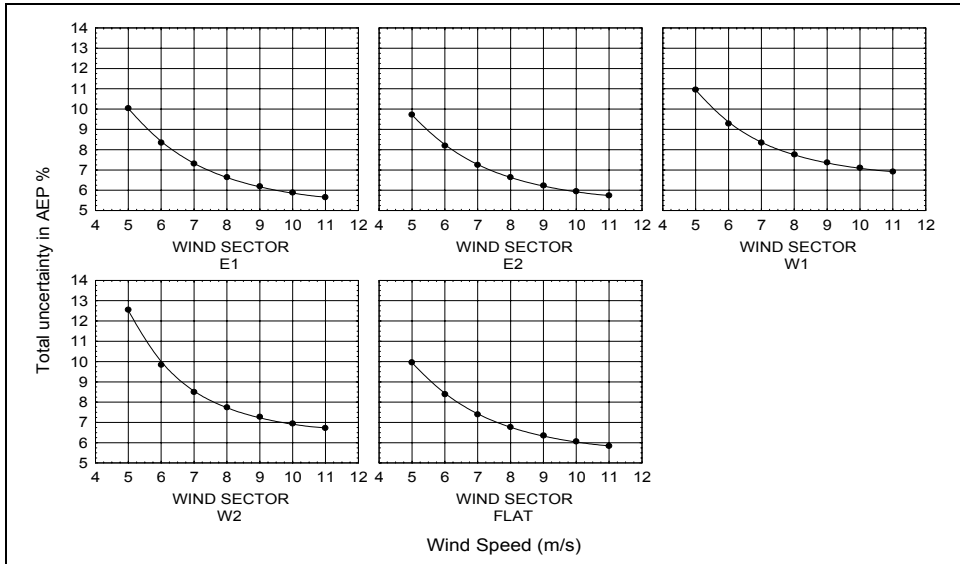


Figure 5.54 AEP estimation uncertainty for MADE AE-30.

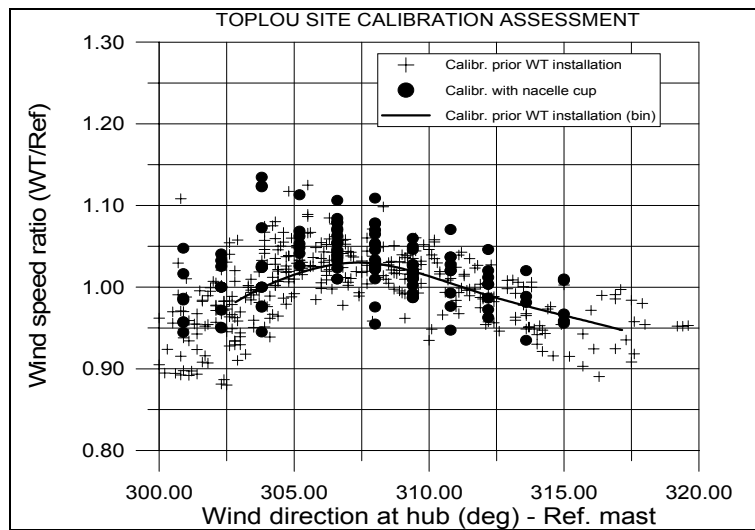


Figure 5.55 Comparison of calibration practices for NTK500/37.

6. ALTERNATIVE POWER PERFORMANCE METHODOLOGIES

6.1 Introduction

In the present chapter the alternative power performance assessment and verification procedures that have been recently developed and experimentally tested are examined. The considered methods regard the use of a nacelle cup behind the running wind turbine rotor and the use of the rotor mean wind speed, yielded from detailed rotor upwind measurements, as the reference wind speed.

6.2 Nacelle Cup Methodology

6.2.1 Introduction

The basic prerequisite for measuring the power curve of a wind turbine is the use of a cup anemometer mounted on a meteorological mast, preferably at a distance of 2.5 rotor diameters upwind of the turbine. However, in the occasions where the installation of the meteorological mast is unsuitable the use of the nacelle anemometer has been suggested for verification of individual turbine power curve. The relation between the response of the nacelle and the mast anemometer should be established during the power curve measurements in terrain where site effects are known. Then the question to be answered is whether this relation can be used to verify another turbine power curve which is installed elsewhere, alone or within a wind park. It is understood that the turbine should be of the same make and type. For the turbine manufacturer or the wind park developer this method has an obvious economic interest as it reduces the costs involved with the assessment of the turbine power curve and the related guaranteed annual energy production.

The wind speed registered by the nacelle anemometer and thus its relation to the mast anemometer is mainly expected to be influenced by two factors, the placement of the anemometer on the nacelle and the retardation of the flow due to the power extracted from the wind. Mounting instructions for the placement of the anemometer on the nacelle are found in the work of Pedersen T. (1994). The presence of the nacelle influences the flow and can easily result in either an acceleration or retardation of the wind speed at the position where the cup anemometer is mounted. The retardation on the other hand of the flow due to the energy extraction is a function of the wind speed (provided that the rotor settings and operational characteristics remain unchanged). Since this relation is not linear, it is expected that neither is the relation between the mast and nacelle anemometer. In the work of Petersen S. (1994b) a linear relation was found whereas in the work of Slater J. (1996) the relation is partly below and partly above unity. The above experimental research show clearly the degree of complexity of the flow around the nacelle

Three power performance campaigns are analyzed for the assessment of the application of nacelle cup anemometer regarding the ELKRAFT 1MW, a 500kW stall and the WINCON XT110XT wind turbines.

6.2.2 Nacelle cup anemometry on 1MW wind turbine

6.2.2.1 Description of experimental research

The research is based on the results of the power curve measurements that have been carried out on the ELKRAFT 1MW stall-regulated wind turbine. The main objectives of the research were the following:

- to investigate whether for the same rotor settings the relation between the nacelle and the mast anemometer (established with data from the 90° power curve measurement sector) is also valid for other sectors. This is equivalent to examining whether the power curve (as a function of the corrected nacelle anemometer) can be reproduced for other sectors and different data sets. It gives also evidence whether the nacelle-mast relation defined within a measurement sector in flat terrain is still valid and thus transferable to another terrain type
- to investigate whether and how the relation between the mast and the nacelle anemometer is influenced by the specific position of the nacelle anemometer.
- to investigate whether different rotor settings affect the relation between the nacelle and the mast anemometer and if so how the use of a wrong relation would affect the correct presentation of the power curve and the evaluation of the annual energy production.

Data collected from three phases of operation and two nacelle anemometer height positions. The varying parameters are tabulated in the following table for the characterization of each phase.

Measurement phase	1	2	3a	3b
Pitch settings	+0.5°	+0.5°	-1.0°	-1.0°
Nacelle anemometer height	1.2m	1.2m	1.2m	3.m
Yaw error at 10m/s	+12	+7	+7	+7
Vortex generators on the blades	no	no	yes	yes

The technical specifications of the wind turbine are found in Antoniou I. (1997).

The sector used for the power curve measurements is from 181.5° to 271.5° for the first and the second phase data and from 175° to 265° for the third phase data. The direction defined by the met mast and the turbine is 270°→90° with the mast located west for the turbine. The distance between the mast and the turbine is 2.56D. The measurement sector selection has been performed according to Pedersen T. (1993b). The terrain around the turbine is flat and in the measurement sector there are no roughness elements of importance except for a wave brake of stones into the sea with an estimated height of one to two meters. In the north of the measurement sector and up to 330° some big obstacles are found, namely a ship dock, a crane and ships of varying size, the Avedøre power plant, high banks of coal, a big fuel tanks and deposits of cinder. From 330° and up to 15°, the terrain becomes more uniform with smaller irregularities. From 15° to 180° the turbine neighbors to the sea and at a distance of some hundred meters there is a recreation rural area without any big terrain irregularities. The area is only a few meters higher than sea level. It should also be mentioned that the ground where the power plant and hence the turbine is located is reclaimed at a later moment from the neighboring ground to the north and therefore this ground is at a higher level relative to the neighboring one.

6.2.2.2 Comparison of data

Data form the sectors between 181.5° and 271.5° (first and second phase) and between 175° and 265° (third phase). These sectors are used for the original power curve measurements and are open water sectors with land present at a longer distance from the turbine. The slight translation of the measurement sector in the third phase is due to the temporary formation of a cinder bank between the turbine and the met. mast and is not consider to have any influence on the results. The cinder is now removed.

The power curve as function of the corrected response of the nacelle anemometer is, except for the above sectors, shown also for the sectors

- 271.5° to 331.5° (turbine in the wake of the power plant)
- 330° to 360° (sector with a different roughness length)
- 110° to 180° (open water and uniform low elevation land).

For all selected runs the two generators of the turbine were connected to the grid. Moreover, all turbulence intensities were included and no rain weather data filtering was performed.

6.2.2.3 Results of the measurement program

Measured operational and performance characteristics

The power curves of the turbine for all the three measurement phases are given as a function of the mast anemometer at 55m height (hub height). The curves are presented as the mean bin data values of ten - minutes periods, corrected for temperature and pressure ($T=15^{\circ}\text{C}$ and $P=1013.3\text{ hPa}$). In figure 6.1 the turbine mean yaw error is shown for the three phases.

In order to correct the initial yaw error, the turbine's wind vane was turned 12° in the anti-clockwise direction. This resulted in a reduction in the yaw error by approximately 7° . Referring still to figure 6.1, the data from phase2 and phase3a follow well each other up to 12m/s after which deviations are observed. It is not clear whether these are due to scatter because of the limited data available or to the modifications of the flow field behind the rotor hub caused by the presence of the vortex generators.

In figure 6.2 the turbine power curves, for the three phases, are shown together with the design power curve calculated for a pitch angle equal to -1.0° (Petersen S., 1994b). The power curves from phase1 and phase2 show good agreement between them up to 7m/s and are in fact slightly better than the design power curve. Between 7m/s and 12m/s the phase2 power curve is better than the phase1 one, which can be attributed to the lower yaw error. At higher wind speeds the two power curves agree well although the phase2 curve shows a higher scatter due to the limited amount of data. The two curves are well below the design curve (result of theoretical calculations) for wind speeds between 8m/s and 17m/s. An explanation of the reduced performance of the rotor relative to the expected design curve under this configuration is that early separation of the flow occurs in the thick inner sections of the blades. Therefore it was decided to install vortex generators on these parts of the blades. The vortex generators were designed by LM which also decided their positioning on the blades.

Regarding the phase3 curve and the design curve, good agreement exists between them up to 8m/s with the phase3 curve being slightly higher than the design one. At wind speeds above 8m/s the two curves follow well each other with the design curve being higher than phase3. The lack of high westerly winds has hindered the completion of the power curve of this phase.

The power coefficients C_p for the three phases are shown in figure 6.3. Below 7m/s the phase3 curve lies lower, while at higher wind speeds it reaches higher values than the two others. In line with the above results from the power curves, it is seen that the phase2 curve is above the phase1 curve between 7m/s and 12m/s.

Relation between the mast- and the non-corrected nacelle anemometer power curves (nacelle anemometer at 1.2m. or 3m. Height)

In figure 6.4, the power curves for the phase1 data are shown both for the mast and the nacelle anemometer (not corrected, placed 1.2m above the nacelle and behind the non-profiled part of the blade). The difference (distance) between the two power curves, in other words the deficit of the wind speed recorded by the nacelle anemometer relative to the mast anemometer, is minimized for very low and very high wind speeds, where extraction of energy from the wind is minimum according to figure 6.3, while it reaches a maximum at values around the maximum C_p . Therefore it may be argued that there is a direct relation between the curves in figures 6.2 and 6.3, as increased power extraction from the incoming wind results in higher retardation of the air coming through the turbine rotor. This is illustrated in figure 6.4 where, for wind speeds around maximum C_p , the nacelle anemometer records a much lower wind speed as compared to the mast anemometer. This is also an indication that the relation between the two cup anemometers is not as a rule linear.

In figure 6.3 the power curve from phase3a is presented as a function of the nacelle and the mast anemometer with the nacelle anemometer at 1.2m height from the roof and behind the non-profiled part of the rotor. When comparing figure 6.4 and figure 6.5, the gap between the corresponding power curves is seen to be more narrow for the phase3a data. The two power curves approach again each other at higher wind speeds but the rate in the case of phase3a data is lower and the two curves have a tendency to run almost parallel with each other. Thus the relation between the nacelle and the mast anemometer is now different when compared to figure 6.4. The presence of the vortex generators, the modification of the yaw, and the modification of the pitch angle has influenced the flow field around the rotor and the relation between the mast and the nacelle anemometer.

In figure 6.6, the relation between the nacelle and the mast anemometer is presented for the phase3b data when the nacelle anemometer is at 3m. height above the roof and behind the profiled part of the blade. Before proceeding with the analysis of the figure it should be mentioned that the data points which deviate from the main body of the power curves respond to an icing situation which occurred during the measurement period. The two power curves are again close to each other at low wind speeds while at higher speeds, contrary to the previous results, the deficit in wind speed as recorded by the nacelle anemometer remain almost constant, also beyond stall. By comparing figures 6.5 and 6.6 it is seen that the wind speed recorded by the nacelle anemometer in phase3b at 3m height is lower compared to the phase3a data recorded at 1.2m height. The higher retardation is probably a result of the larger amount of energy extracted by the profiled part of the blades in front of the anemometer. This conclusion is however different than the one reached after analyzing figures 6.3 and 6.4 as here the behavior of the flow recorded by the nacelle anemometer seems to be influenced more by the flow condition of the blade segment in front. The extraction of any further conclusions is nevertheless hindered by the lack of knowledge of the behavior of the surface flow in the presence of vortex generators.

This is in accordance with the results presented in figure 6.7 where a direct comparison of the bin power curves as a function of the non-corrected nacelle anemometer at 1.2m height and for two rotor conditions is presented. It is evident that the non-corrected nacelle anemometer cannot be used for a comparison of the power curves of a turbine after rotor modifications have taken place. In fact in the figure, the phase3a power curve lies well below the phase1 curve up to 10m/s which should lead to the wrong conclusion that the modifications had a negative effect.

The main conclusions from the above results is that the relation between the mast and the nacelle anemometer depends both on the position of the nacelle anemometer and the characteristics of the rotor. The relation changes as soon as one or both of these factors are modified. Therefore it seems to be of less importance where the cup anemometer is placed on the nacelle as long as the relation between the mast and the nacelle anemometer is determined. The non corrected nacelle anemometer cannot be used to draw any conclusions concerning the turbine's power curve once modifications have taken place.

Relation between the mast and the nacelle anemometer (turbine in operation)

In figure 6.8, the relation between the mast and the nacelle anemometer is shown with the help of raw data from phase1, their bin values and a polynomial curve fitted on the bin values. The relation is not linear and the points have in this case been approximated by a 5th order polynomial curve. When trying to establish the relation between the nacelle and the mast anemometer it is a common practice that the sector used around the mast-turbine direction should be as narrow as possible (e.g. $\pm 20^\circ$). In the present case, since the terrain in the sector used is flat and homogeneous (water), a wider sector has been used due to the lack of high wind speeds within a more narrow sector. This however has not taken place at the cost of the accuracy of the correlation at low speeds as can be verified from the following figure 6.9, where the bin data are presented for two different sectors (10° and 90° wide). The agreement is good at lower wind speeds but becomes poorer at higher wind speeds due to the lack of an adequate number of data points in the narrow sector.

In figure 6.10 the reproduction of the power curve as a function of the corrected nacelle anemometer (via the 5th degree polynomial) for the case of the phase1 data is shown together with the mast power curve (bin values). The data are from the sector 181.5° to 271.5°. The two power curves are as expected practically identical. This means that, once the relation between the mast and the nacelle anemometer is established, it is possible to use the nacelle anemometer instead of the mast anemometer and correctly describe the turbine's power curve. Similar relations as the one shown in figure 6.10 can be established for all the data sets for the different measurement phases.

Relation between the mast and the nacelle anemometer (turbine stopped)

Next the relation between the mast and the nacelle anemometer is presented when the turbine is stopped. WA^SP calculations, not presented here, have confirmed the absence of any site effects within the sector 181.5° to 271.5° and therefore any influence is due to the presence of the nacelle. The way the nacelle presence influences the cup anemometer is really of not great importance as it is by "default" included in the relation derived when the turbine is in operation.

The relation is presented in figure 6.11 and 6.12. In the case of figure 6.11, the data have been filtered with respect to the position of the blades and the yaw error of the turbine. Thus the stopped turbine is oriented towards the mast and one of the blades is always oriented around the vertical and downwards. With the exception of a few data points, the relation between the two anemometers is linear and the flow above the nacelle at the anemometer position is accelerated. In figure 6.12 the raw data for the two heights of the nacelle anemometer are shown. It is interesting to observe that in this case the acceleration of the flow at 3m height is higher relative to the 1.2m. The acceleration of the flow explains why the relation of the nacelle to the mast anemometer is sometimes, as e.g. in the work of Petersen S. (1994b), larger than unity.

As the presence of the nacelle is seen to influence the response of the anemometer, it can be argued that the relation mast-nacelle anemometer is influenced also by the shape of the nacelle and therefore the relation derived for specific rotor settings and a specific nacelle is not necessarily valid for the same rotor settings and a different nacelle shape.

The power curve as a function of the corrected nacelle anemometer (same rotor settings - different sectors)

The conclusion from the above chapters is that once the relation between the nacelle and the mast anemometer is established, then the nacelle anemometer can be used for the verification of the turbine's power curve within the same sector. When using the same sector then by default the same data are used for the power curve as a function of the mast or the corrected nacelle anemometer and therefore the result may be considered as biased. An extension of the above work is to show whether and under which conditions the relation between the nacelle and the mast anemometer is valid for different data sets and for different sectors. For that purpose the turbine's bin power curves from the sector 181.5° to 271.5° (phase1 data) or 165° to 275°(phase3a data) will be compared to the bin power curves derived as a function of the "corrected" nacelle anemometer from other sectors. The sectors used are shown in the following table together with a sort description of the terrain roughness within the sector.

Table 6.1 Description of the terrain within the sectors used.

Sector	Terrain description
181.5°→271.5°	Fetch above land and sea
271.5°→330°	Fetch above land, from 4D to 13D dominated by the power plant, coal banks, oil tanks and cinder deposits
330°→360°	Fetch above land, urban conditions
0°→90°	Fetch above land and sea
100°→180°	Fetch above land and sea

In figure 6.13, the power curve from the sector 181.5° to 271.5° is given as a function of the mast anemometer and it is compared to the power curve from the sector 100° to 180° which is presented as a function of the corrected nacelle anemometer. The surface roughness is the same for the two sectors and the power curves are identical, the minor differences at higher wind speeds being attributed to the limited number of data points in the corresponding bins.

The same good agreement is observed in the case the phase3a data shown in figure 6.14 where the power curve from the sector 175° to 265° is given as a function of the mast anemometer and it is compared to the power curve from three other sectors which are presented as a function of the corrected nacelle anemometer. It is only the sector 330° to 360° which has a bigger surface roughness compared to the rest. For this sector theoretical calculations, not presented here, show that minor differences to the design power curve should be observed at around the nominal power.

Finally in figure 6.15, the power curve as a function of the mast anemometer from the sector 181.5° to 271.5° is compared to the power curve as a function of the corrected nacelle anemometer from the sector 271.5° to 330°. The last one is the sector where the turbine operates in the wake of the power plant and the coal bunks. Unlike the previous cases, the two power curves do not coincide with the one from the sector 271.5° to 330° laying systematically below.

The reason for the lack of coincidence is seen in figure 6.16 where the 5th order polynomial line fitted to the results from the sector 181.5° to 271.5° is presented together with raw data from the sector 271.5° to 330°. The correlation mast-nacelle anemometer is poor compared to the data of the sector 181.5° to 271.5°. This is expected since the mast anemometer is not within the 271.5° to 330° sector and it therefore “sees” another part of the complex terrain in front, compare to the nacelle anemometer. That the relation depends strongly on the wind direction is shown in figure 6.16 as considerable level differences in the measured wind speeds. As a result it is concluded that the presence of the obstacles which generates another terrain type modifies the wind speed profile relative to the flat terrain measurement sector and thereby modifies the relation between the mast and the nacelle anemometer.

The wind shear through the rotor plane and for the two sectors, here defined as the difference in the speed registered by the cup anemometers at 75m and 35m, is presented as a function of the anemometer at hub height (55m) in figure 6.17. The slope is seen to be bigger in the case of the 271.5° to 330° sector. This means that, within the rotor area, the speed deficit of the wind profile, with descending height, is higher in the case of the sector 271.5° to 330° compared to the sector 181.5° to 271.5°. The flow within this sector resembles the flow behind a fence where the wind speed suffers a deficit when compared to the inlet profile. A result of this deficit is the reason for the lower energy produced by the turbine. We examine now how much this difference in the power curves means to the annual energy production (AEP) of the turbine.

The AEP and the related uncertainties for the two power curves are shown in table 6.3 (power curve as a

function of the mast anemometer) and table 6.4 (power curve as a function of the corrected nacelle anemometer). The same sources of uncertainty have been considered for both power curves except for the case a form factor of two table 6.4. There the second uncertainty column is calculated with an additional 1% calibration uncertainty. The mean AEP values, shown in table 6.2, agree with the mean AEP values shown in table 6.3 within the stated uncertainties however the deviations are large.

Table 6.2. The annual energy production, power curve vs. the mast anemometer, phase I data

AEP-measured and related uncertainty [MWh], sector 181.5° to 271.5°										
Wind speed	Form factor									
	1.50		1.75		2.00		2.25		2.50	
4	607.8	82.8	497.6	80.1	414.0	77.0	350.8	74.0	302.6	71.4
5	1120.4	106.0	997.8	107.1	893.5	106.8	808.0	105.6	738.6	104.1
6	1690.8	124.4	1594.5	129.9	1497.6	133.5	1410.8	135.7	1335.6	136.9
7	2254.9	137.3	2222.4	146.5	2160.8	153.6	2094.9	159.2	2032.7	163.6
8	2766.2	145.4	2827.4	157.3	2827.0	166.9	2800.9	174.9	2767.2	181.7
9	3197.9	149.5	3368.4	163.0	3451.5	174.3	3483.1	183.8	3489.9	191.9
10	3540.3	150.7	3819.0	164.9	3998.4	177.0	4104.7	187.2	4165.0	196.0
11	3795.7	149.7	4168.4	163.8	4443.5	176.0	4634.7	186.4	4762.1	195.3

Table 6.3. The annual energy production, power curve vs. the corrected nacelle anemometer, phase I data

AEP-measured and related uncertainty [MWh], sector 271.5° to 330°											
Wind speed	Form factor										
	1.5		1.75		2		2.25		2.5		
4	567.8	80.7	457.3	77.6	374.2	74.1	76.3	312.0	70.8	265.0	68.0
5	1065.9	103.7	940.3	104.7	833.4	104.0	108.2	746.1	102.4	675.6	100.4
6	1624.4	121.4	1524.8	127.5	1423.7	131.2	137.5	1332.6	133.2	1253.8	134.0
7	2177.4	133.0	2142.9	143.4	2078.0	151.4	159.3	2007.7	157.5	1940.6	161.9
8	2677.9	139.3	2738.1	152.4	2736.7	163.5	172.5	2708.5	172.9	2671.2	180.6
9	3099.3	141.7	3268.4	155.9	3352.2	168.6	178.1	3384.6	179.8	3391.3	189.6
10	3432.7	141.1	3708.2	155.5	3888.2	168.4	178.1	3997.0	180.1	4060.2	190.6
11	3680.5	138.6	4047.6	152.3	4321.5	164.6	174.1	4514.8	175.7	4646.3	185.8

These discrepancies in the power curves and the AEP, shown in figure 6.15 and the above tables would certainly be smoothed out if a wider sector was chosen and it would thus be wrongly argued that the nacelle-mast relation is still well applicable. Therefore if the verification of a power curve is wanted and the relation of the mast-nacelle anemometer is known care should be taken to apply this relation in mutually alike sectors.

The presence of the obstacles in the sector 271.5° to 330° simulates in many ways complex terrain conditions for the turbine and the conclusion is that the relation between the mast and the nacelle anemometer derived at one location and under the influence of specific site conditions is not transferable at another location where different conditions prevail. The task of transferring the relation between different terrain types is however not easy as procedures on this subject are not yet agreed. The second important conclusion from figure 6.17 is that since the turbine power curve depends on the shape of the wind profile, then in the presence of site effects the correct relation between the two anemometers at a hub

height is necessary but may be not sufficient for the description of the power curve under complex terrain conditions as it does not give any information on the wind profile shape.

Power curve as a function of the corrected nacelle anemometer: (different rotor settings - same sector)

We now proceed to examine the effect of the changes of the rotor settings on the relation between the nacelle and the mast anemometer for the three phases of the measurement program, for the same position of the nacelle anemometer and for the same sector. Following this we will apply two different nacelle-mast anemometer relations corresponding to two different rotor settings on the same data set.

The results of the relation nacelle-mast anemometer are shown in figure 6.18. By comparing the curves from the first and the second measurement phase differences are observed. This means that the relation between the mast and the nacelle anemometer depends not only on the rotor settings but also on the yaw settings of the turbine. Once the settings have changed a new relation should be established. The differences become even more pronounced between the phase1 and the phase3a data. We proceed now to investigate to what extent these differences can affect the power curve presentation and the AEP since this cannot be estimated from the figure.

In figure 6.19 the power curve from the phase3a data is presented as a function of the corrected nacelle anemometer using both the relation derived during the phase1 (wrong) and the phase3a (correct) measurements.

The use of the wrong relation produces a wrong power curve which in this case is overestimated but the opposite might as well be true. The most important observation is that the differences between the two power curves are in this case systematic, which means that a bias error will be introduced in the AEP calculations which cannot be in any way detected. Therefore if a derived relation, between the mast and the nacelle anemometer in one turbine, should be used in another turbine of the same type and make, care should be taken that the rotor settings, the yaw error and the placement of the nacelle anemometer remain unchanged.

6.2.2.4 Conclusions

The power curves measured as a function of the nacelle anemometer were compared with the power curves measured as a function of the mast anemometer for the same wind turbine settings. It was found generally, that with the nacelle anemometer in the blade cylinder wake region there was very high wind speed deficit in the max. C_p region, whereas this deficit was reduced at low and high wind speeds. With the nacelle anemometer in the profiled blade wake region the wind speed deficit seemed much more constant for medium to high wind speeds. Thus the response of the nacelle anemometer is a function of its location on top of the nacelle. From the comparison it can also be concluded that the modifications on the wind turbine rotor settings, which results in changes of the power curves seen as a function of the mast anemometer, does also change the power curves seen as a function of the nacelle anemometer, but not in a consistent way. This is due to the three dimensional nature of the flow through the rotor and the fact that the wind speed registered by the cup anemometer is of local nature and only representative of that measurement point. In other words, it was found that the nacelle anemometer power curves cannot be used to draw any conclusions concerning the changes of the power curve of the wind turbine due to the modifications made. The main conclusion is thus, that the power curves, using the nacelle anemometer, are dependent on both the position of the nacelle anemometer on the nacelle and the characteristics of the rotor.

The relations between the mast anemometer and the nacelle anemometer were not linear in this study, but they could be fitted well with a 5th order polynomial curve in the case where the cup anemometer is behind the non profiled part of the blade. For the same wind turbine settings a very good agreement was found between the measured power curve (phase 1 data) measured from an open sea sector 181.5° to 271.5° and a power curve, derived from combining the relation between the mast and nacelle anemometers and the

measured power curve using the nacelle anemometer with data from same sector. The same very good agreement was found when combining the relation between the mast and nacelle anemometers and measured power curves from another open sea sector (100° to 180°). The same very good agreement was also found with power curve data from phase 3a (175° to 265°) when combining the relation between the mast and nacelle anemometers and measured power curves from other sectors: a mix of sea and flat land 0° to 90° (low roughness) and an industrial area 330° to 360° (high roughness). On this basis it can be concluded that the nacelle anemometer can be used to verify the same power curve with winds from different terrain roughness'. It was not possible, though, to find good agreement when using wind data (phase 1) from the sector in the wake of a huge power plant (271.5° to 330°). The cause of this is found to be due to the disturbed wind profile which results from the presence of site effects.

For the same measurement sector (about 180° to about 270°) and different wind turbine settings (phase 1, 2 and 3) the relation between the mast anemometer and the nacelle anemometer was quite varying. Therefore, if the wind turbine settings are changed not only the power output changes, but also the nacelle anemometer readings are changed.

With the wind turbine stopped it was found that the nacelle anemometer measured 20-30% higher wind speeds than the mast anemometer, which means that the nacelle presence influences the flow around the nacelle. The wind speed 3m above the roof was higher than at 1.2m. This shows that the induced flow around the nacelle extends quite far from the nacelle, which indicates that the nacelle design has a substantial influence on the reading of the nacelle anemometer.

In conclusion, it can be said that provided the following factors remain unchanged:

- the wind turbine rotor settings
- the wind turbine's yaw error
- the anemometer's position on the nacelle
- the terrain is flat

then the relation mast-nacelle anemometer can be transferred between wind turbines of the same make and type. Under these conditions the "corrected" nacelle anemometer can be used for the verification of the turbine's power curve and the AEP.

Whether and under which conditions this relation is transferable from one kind of terrain to another (e.g. from flat to complex) remains to be investigated as the lack of data on this subject prevents us from drawing any conclusions.

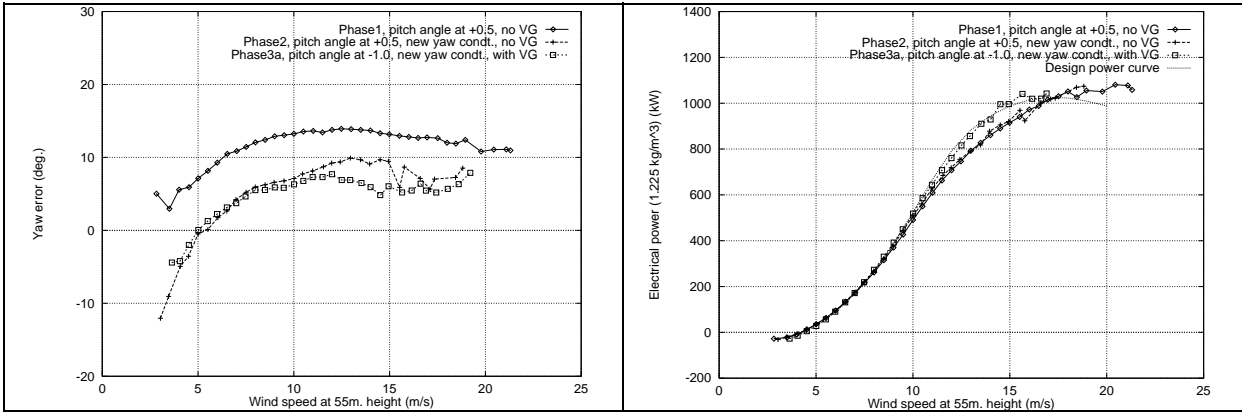


Figure 6.1 The yaw error for the three power curves. Figure 6.2 Power curves for the three phases against design curve.

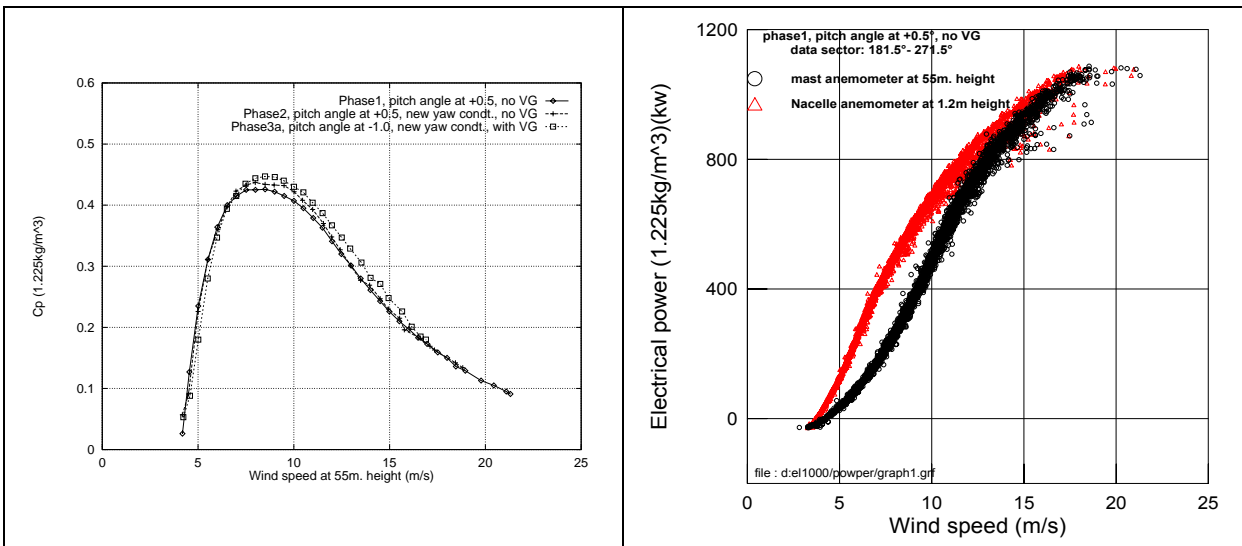


Figure 6.3 The power coefficients for the three phases. Figure 6.4 Phase1, the power curve as a function of the mast and the non-corrected nacelle anemometer

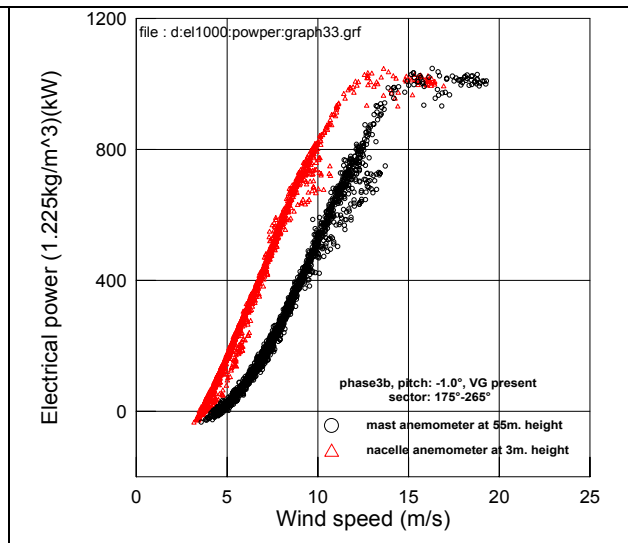
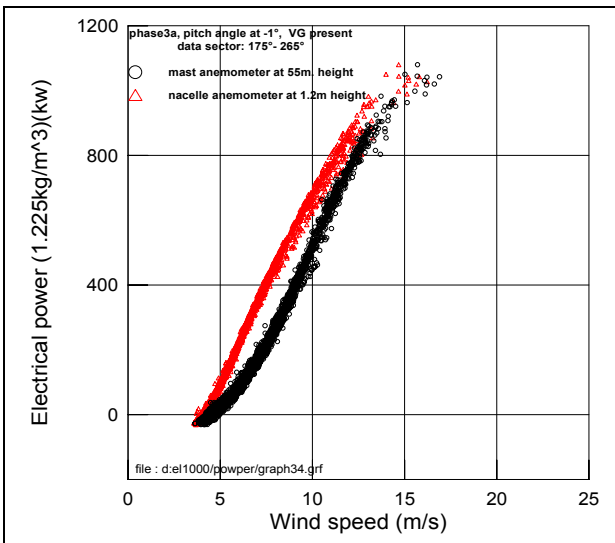


Figure 6.5 Phase3a, the power curve as a function of the mast and the non-corrected nacelle anemometer.

Figure 6.6 Phase3b, the power curve as a function of the mast and the non-corrected nacelle anemometer.

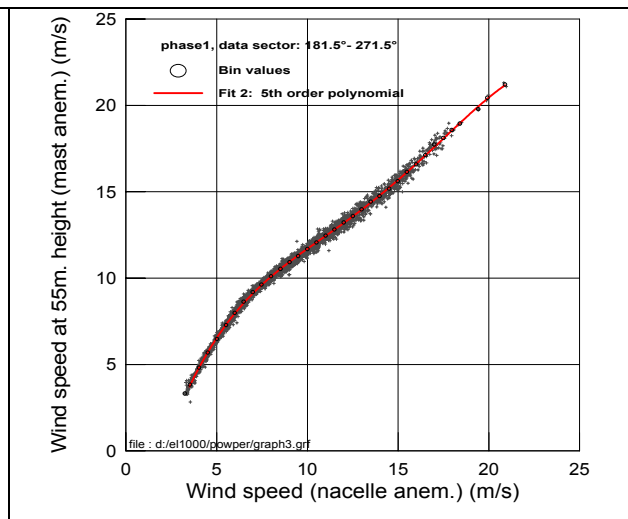
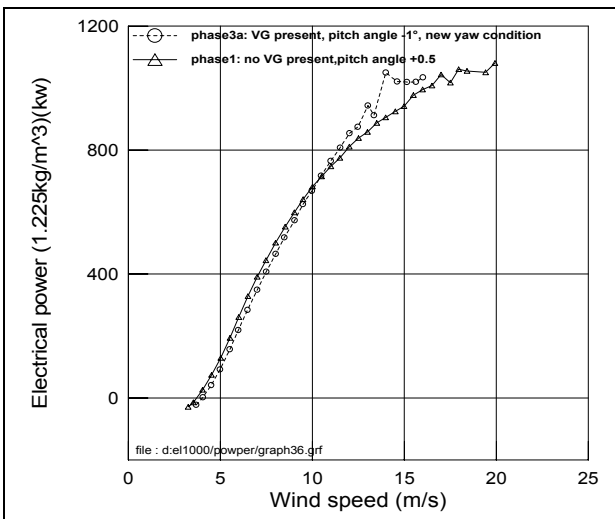


Figure 6.7 The power curve as a function of the nacelle anemometer at 1.2m height above the roof.

Figure 6.8 Relation between the nacelle and the mast anemometers for the phase1 data.

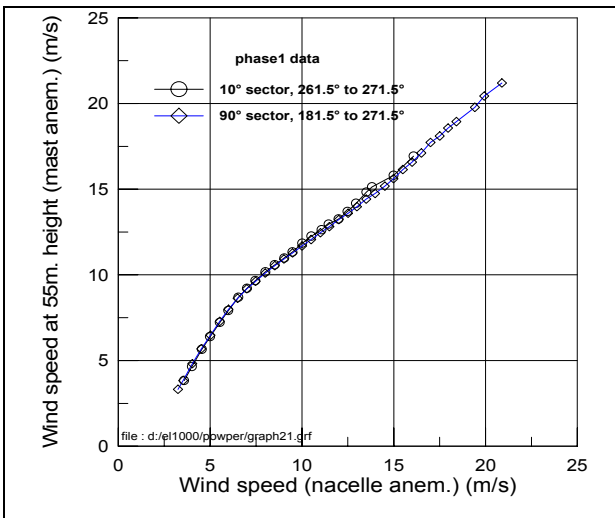


Figure 6.9 Relation between the mast and the nacelle anemometer for the phase1 data (two function of the mast and nacelle corrected different sectors).

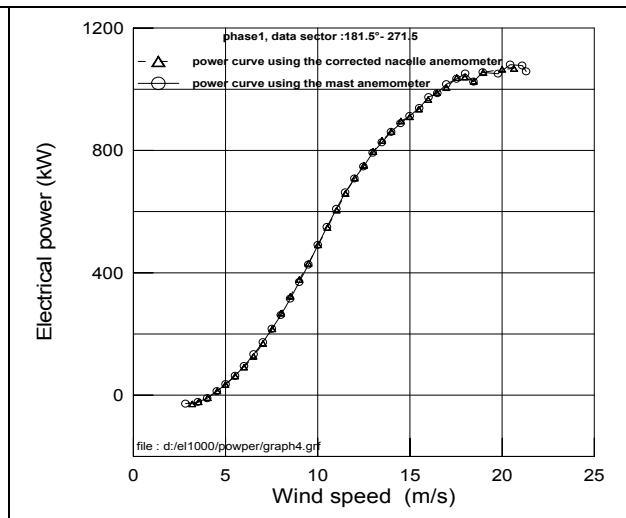


Figure 6.10 Bin averaged power curve as a function of the mast and nacelle corrected anemometer (phase 1).

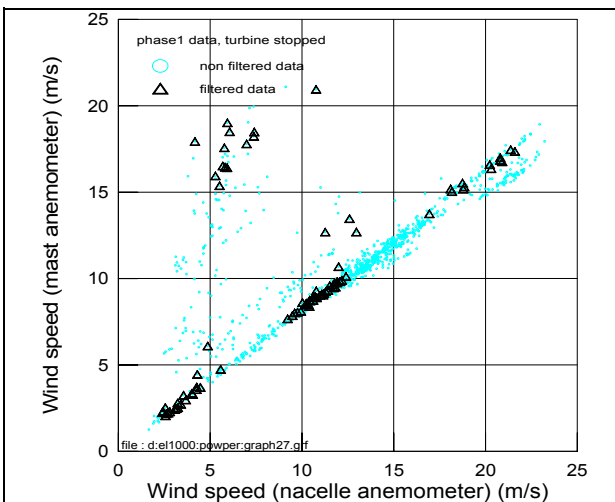


Figure 6.11 Relation between the mast and the nacelle anemometer at 1.2m height with the nacelle anemometer at 1.2m and 3m height, turbine stopped

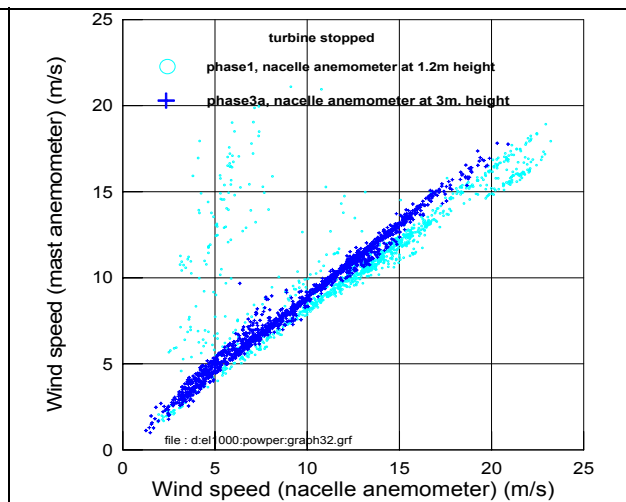


Figure 6.12 Relation between the mast and the nacelle anemometer at 1.2m and 3m height, turbine stopped

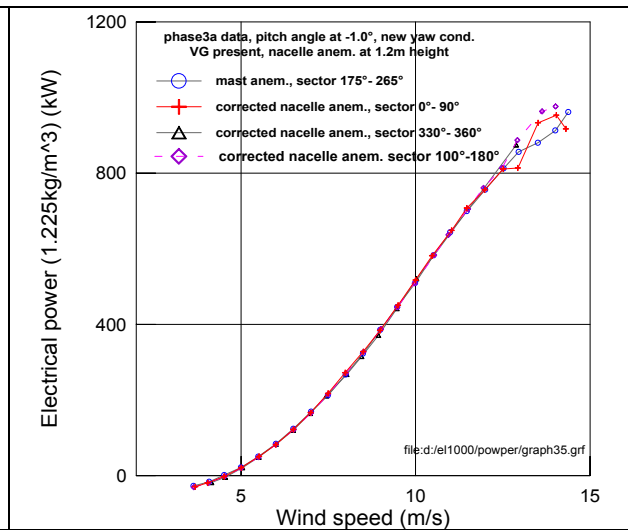
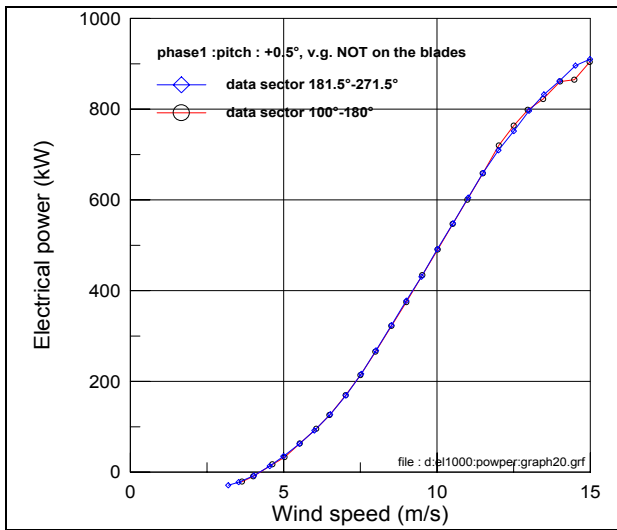


Figure 6.13 Power curve as a function of the mast and the corrected nacelle anemometer (two sectors). Figure 6.14 Power curve as a function of the mast and the corrected nacelle anemometer (four sectors).

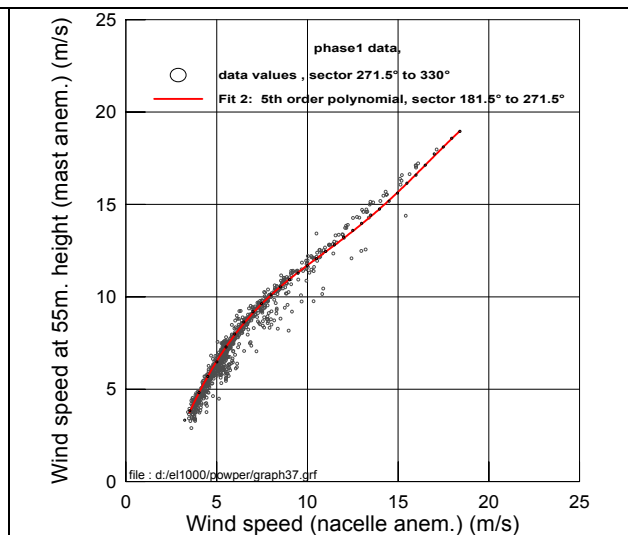
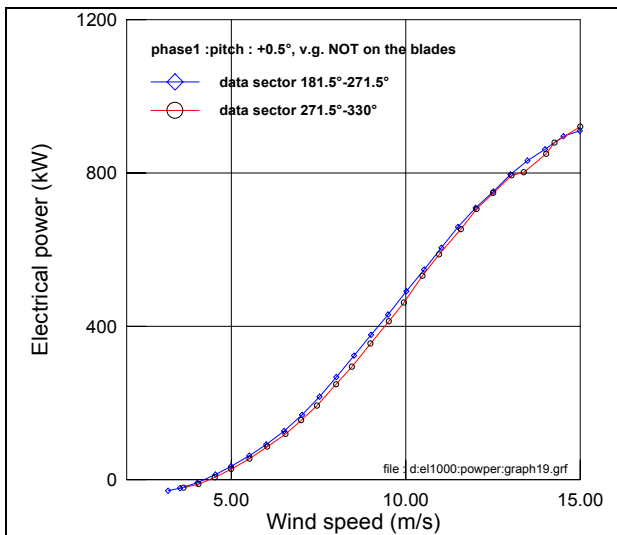


Figure 6.15 Power curve as a function of the mast and the corrected nacelle anemometer (two sectors). Figure 6.16 Comparison between the nacelle and the mast anemometer (phase 1, two sectors).

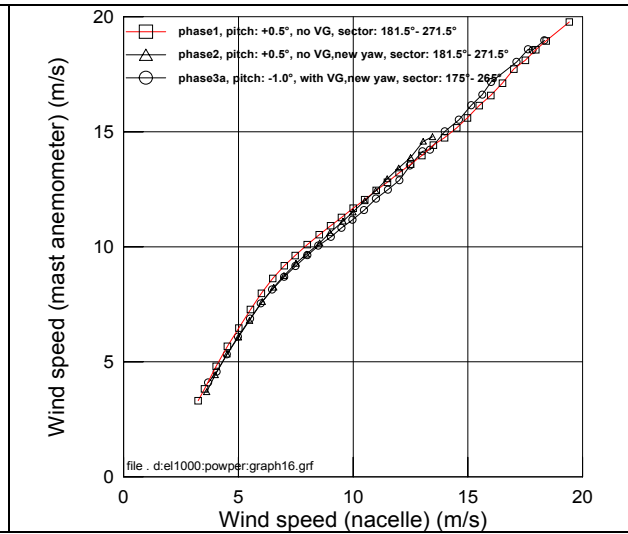
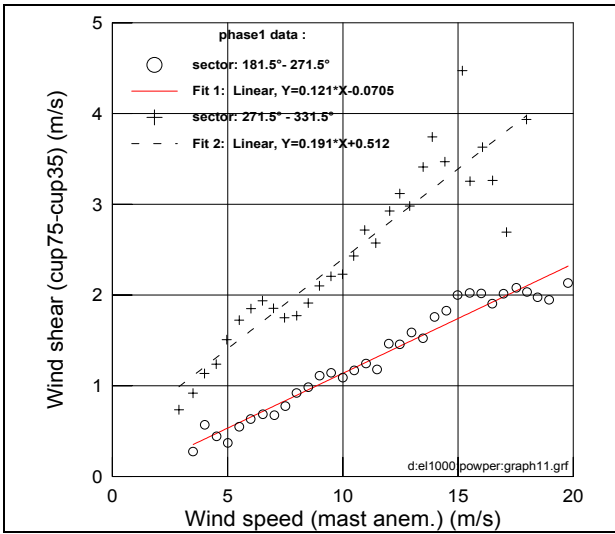


Figure 6.17 The wind shear for the two sectors (phase1).

Figure 6.18 Relation between the nacelle and the mast anemometer for three different rotor settings

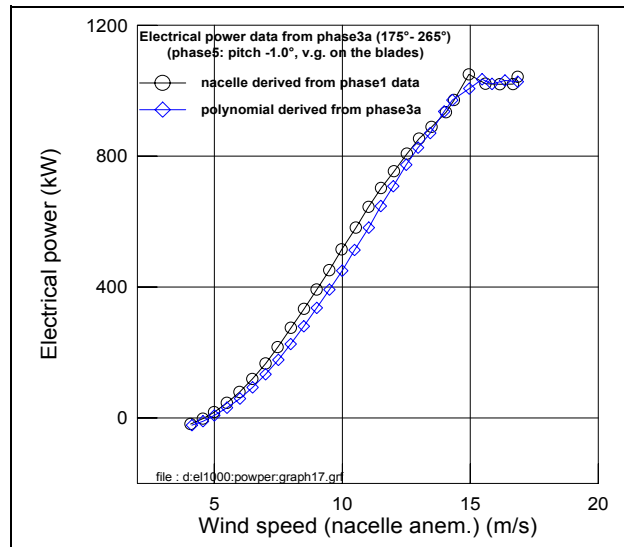


Figure 6.19 Power curve of the turbine when using different corrections for the nacelle anemometer (the stall points are not confirmed by later results).

6.2.3 Nacelle cup anemometry on 500kW wind turbine

6.2.3.1 Description of experimental research

Experimental research was performed on a 500 kW active stall controlled wind turbine for the assessment of power performance evaluation through the utilization of nacelle cup anemometry. Details on the experimental setup and analysis procedures are found in Hinsch C. (1996b).

6.2.3.2 Calibration of the nacelle anemometer

The correlation of the wind speed measured on the nacelle and meteorological mast was approximated by linear formula (figure 6.20). The effects of the nacelle induced boundary layer and flow structure behind the running rotor are approximately canceled out, for the selected location of the nacelle cup. In figure 6.21 the regression of the wind speed ratio, that is the wind speed measured at reference mast over the nacelle value is presented. Differences that exceed 10% of the reference values are encountered. The correlation of the reference and nacelle measured wind speeds in the case where the wind turbine is parked is presented in figure 6.22. It is seen that the nacelle cup measurements are influenced by the nacelle induced boundary layer and lower wind speed values are recorded.

6.2.3.3 Comparison of power curves

In figures 6.23 and 6.24 the power curve data are presented as function of the reference wind speed and the nacelle cup corrected values, respectively. The comparison of the power curves, by means of bin averaged values, is presented in figure 6.25. In figure 6.26 the relationship between power curves measured with corrected nacelle wind speed and with the reference wind speed, for the 240°-340° wind direction sector, is presented. The differences between the power values are less than 7% with the higher values at low wind speeds. The site calibration results, used for determining the reference wind speed, are presented in figure 6.27.

The assessment of the feasibility of the method is attained by comparing the different power curves measured with corrected nacelle wind speed and with the reference wind speed for two different wind direction sectors, namely 190°-210° and 240° - 340°. The above sectors present significantly different terrain effects, as these were captured by the site calibration process (figure 6.27), while the former sector was taken as the reference sector. The results of the comparison are presented in figure 6.28. The use of nacelle cup measurements decreases the encountered differences from 20% down to 7% of the reference power curve values.

6.2.3.4 Conclusions

The experimental research on nacelle anemometry as it was applied on a 500kW wind turbine, resulted in the following:

- lower scatter of the measured power curve is attained by the use of the nacelle cup measurements; this results to clear capture of the switching point between generators
- the use of nacelle cup measurements may decrease significantly the error induced by site calibration, in cases that large discrepancies are encountered between the measured and reference wind speed.

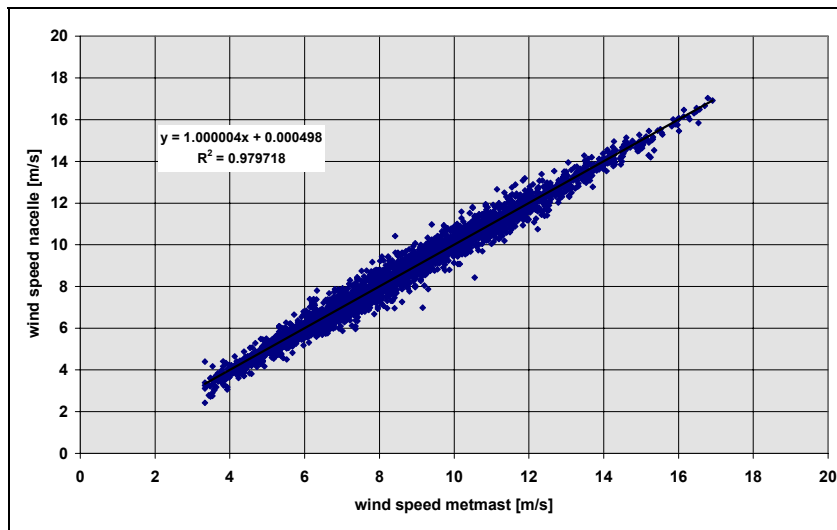


Figure 6.20 Correlation between the anemometer on the metmast and the nacelle.

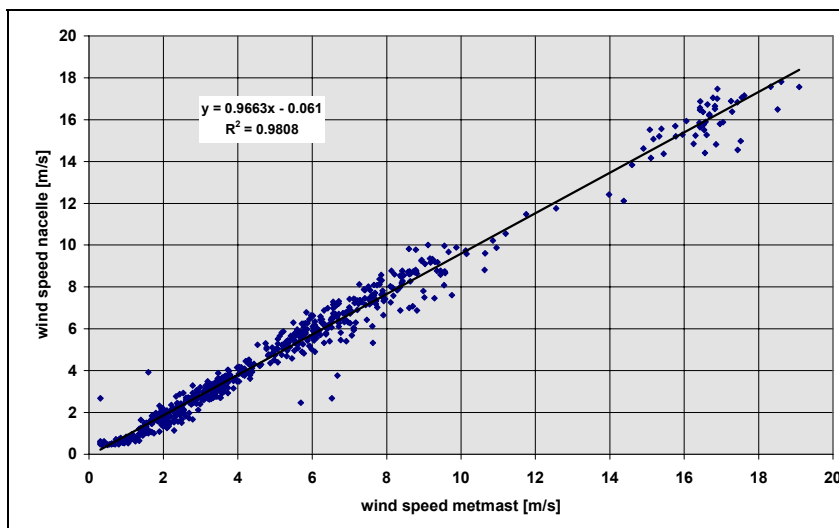


Figure 6.21 Correlation between the anemometer on the met. mast and the nacelle (WEC stopped).

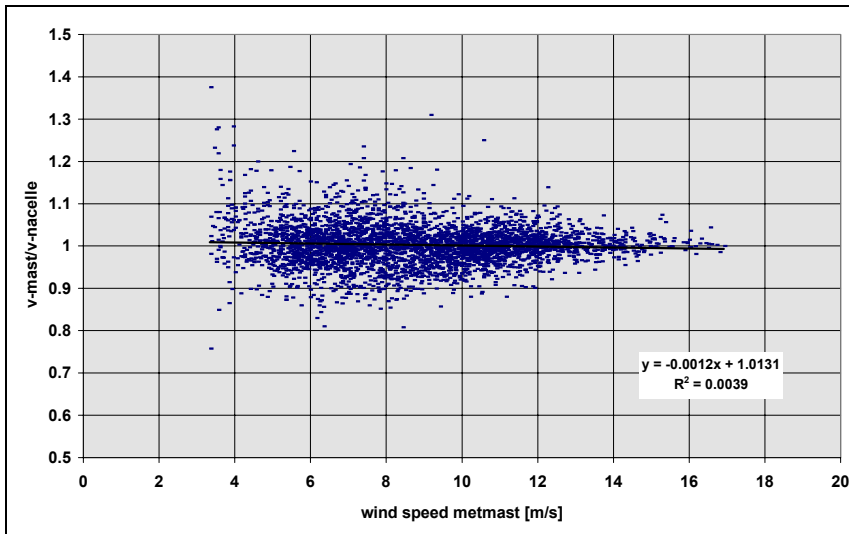


Figure 6.22 Relationship between wind speed on the nacelle and the wind speed on the met. mast.

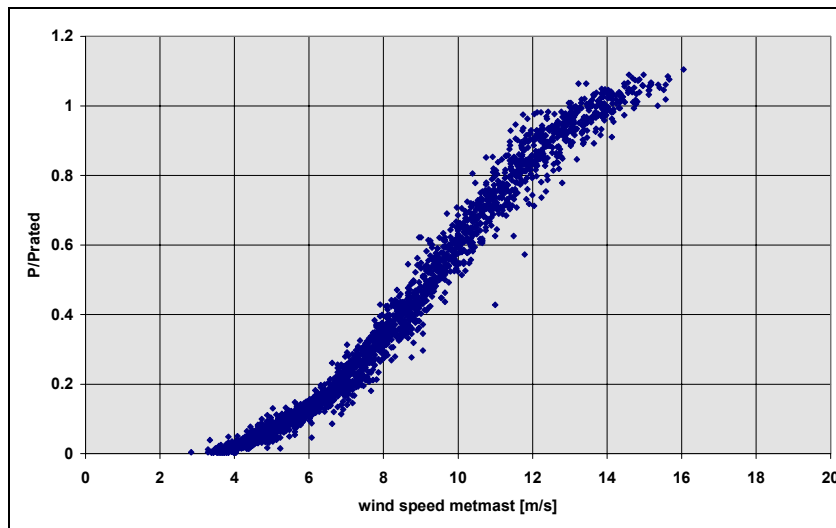


Figure 6.23 Power curve with anemometer on measuring mast

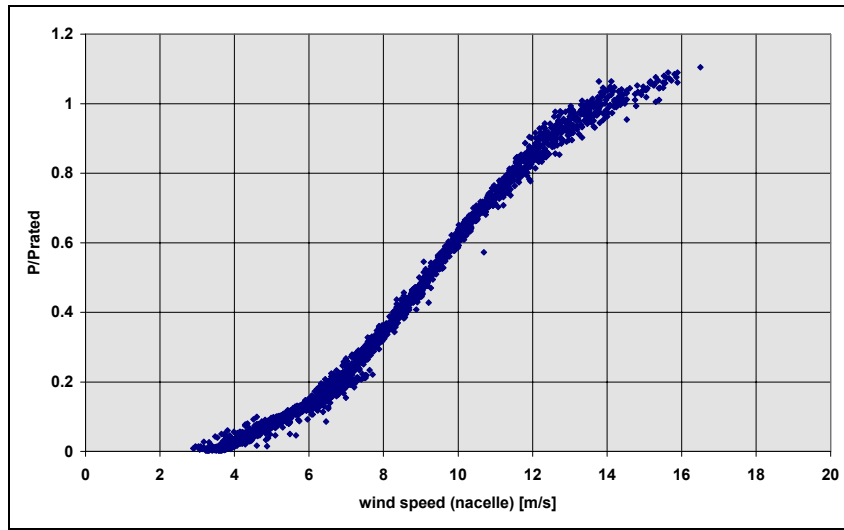


Figure 6.24 Power curve with anemometer on nacelle

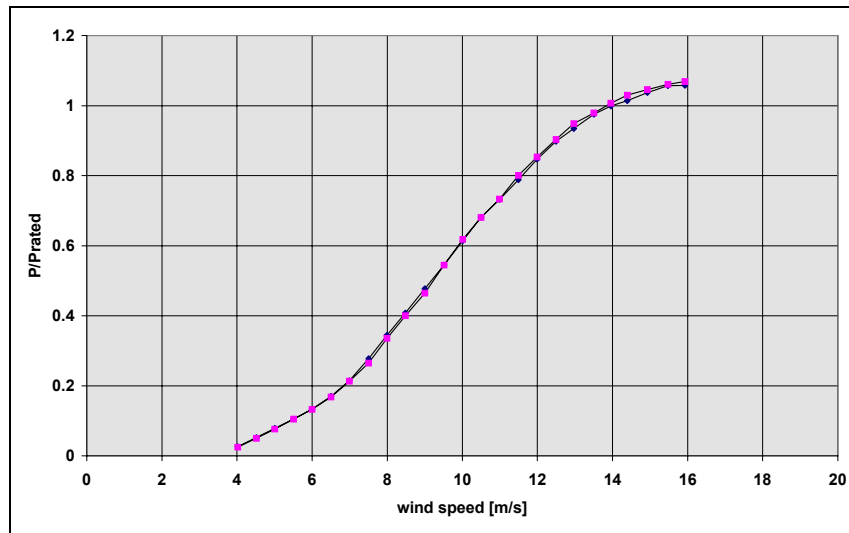


Figure 6.25 Bin-averaged power curves

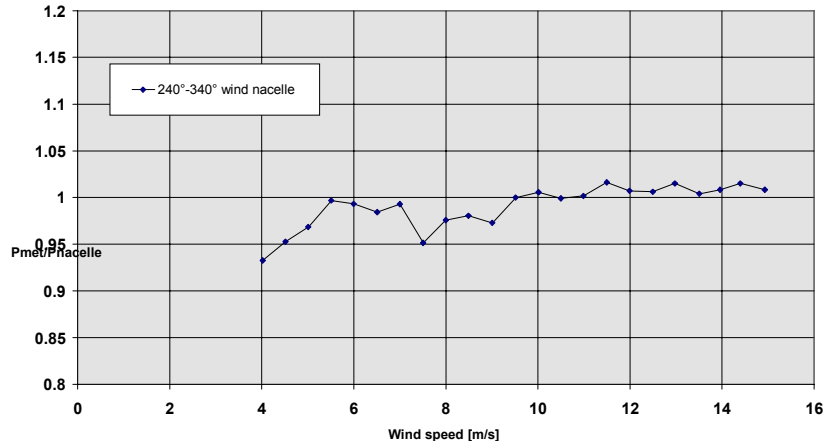


Figure 6.26 Relationship between different power curves measured with wind speed on the nacelle and the wind speed on the metmast

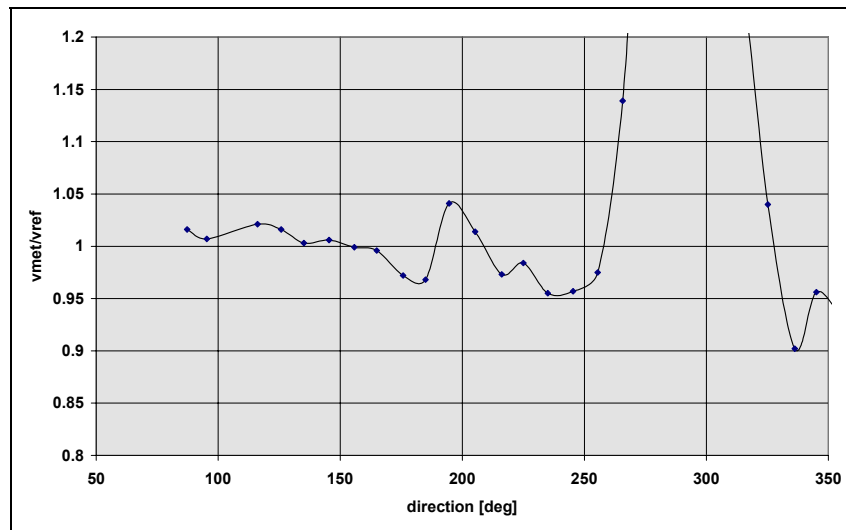


Figure 6.27 Result of the site calibration (wind speed 5-10m/s).

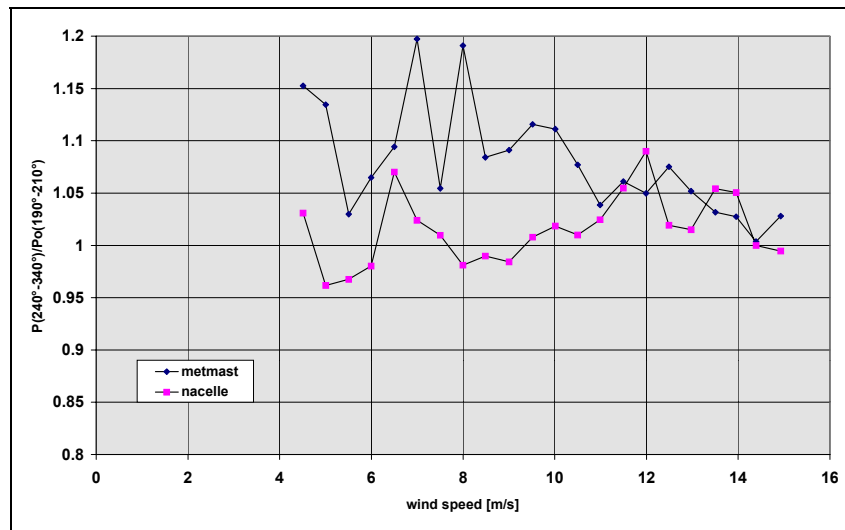


Figure 6.28 Relationship between different power curves measured with wind speed on the nacelle and the wind speed on the met. mast for sector 190°-210° compared to the measured power curve from 240° - 340°.

6.2.4 Nacelle cup anemometry on 110kW wind turbine

6.2.4.1 Description of experimental research

The experimental research performed on WINCON 110XT wind turbine aimed to the assessment of the nacelle anemometer method for power performance purposes.

A cup anemometer was placed on the nacelle according to the practice found in Pedersen T. (1994). The horizontal distance of the cup from the blade root was 2.5 times the blade root diameter while the vertical distance from the nacelle was set to 1m. The experiment lasted one month (from 1/10 to 30/10). Details about the experimental setup and analysis procedures are found in Morfiadakis E. (1996a). In parallel with the nacelle cup measurements the rotor disk experiment at the test station was running, thus giving detailed information about the wind structure. The cup and vane resolver measurements from the central mast at low, hub and top position were used within the present analysis.

In figure 6.29 the measured data from the reference mast are presented by means of wind speed statistics, including the third and fourth order statistics, the length scale as well as the wind shear parameters (referred as gust symmetric and asymmetric factors, Bergstrom H., 1995). In figure 6.30 the nacelle cup measurements are presented against the reference mast measurements. Finally in figure 6.31 the power measurements are given along with the operational characteristics of the machine.

6.2.4.2 Estimation of nacelle cup correlation and assessment

In order to assess the performance of nacelle anemometer technique the whole data set was divided to two wind direction sectors, i.e. 315° - 360° and 0° - 45° . Moreover, the correlation of nacelle cup measurement against the reference cup were estimated for both sectors. Finally, the power curves for each sector using the corrected nacelle cup measurements from the correlation provided from the other sector measurements are drawn. The results of the procedure are shown in figure 6.32.

The assessment of the site calibration technique was performed via annual energy production estimations. The AEP estimations are made for the power curves calculated from the following data sets:

- total data set (i.e. sector 315° - 45°)
- western directions (i.e. sector 315° - 360°), reference cup measurements
- eastern directions (i.e. sector 0° - 45°), reference cup measurements
- western directions (i.e. sector 315° - 360°), nacelle cup (correlation from eastern directions)
- eastern directions (i.e. sector 0° - 45°), nacelle cup (correlation from western directions)

The results are given in table 6.4

Table 6.4 AEP estimations for different wind direction sectors using nacelle cup calibration.

Method	Sector	AEP estimation [MWh] (Rayleigh distribution, power curve 4-14m/s)		
		$U_{\text{mean}}=6\text{m/s}$	$U_{\text{mean}}=8\text{m/s}$	$U_{\text{mean}}=10\text{m/s}$
Ref. wind speed (reference case)	315° - 360°	184.1	260.5	271.1
Ref. wind speed	0° - 45°	184.8	260.8	271.3
Ref. wind speed	315° - 45°	184.3	260.4	270.9
Nacelle cup (correlation from data)	315° - 360°	187.7	264.3	273.9

within 0°-45° sector) Nacelle cup (correlation from data within 315°-360° sector)	0°-45°	180.9	254.9	264.9
---	--------	-------	-------	-------

It is seen that although the AEP estimations are almost identical for the three cases based on the reference mast measurements in the case of nacelle cup based estimations differences are depicted. The differences, that are within the uncertainty of measurement procedure, are attributed to the statistical error induced to the power curve calculations from the nacelle cup correlation as well as to the sensitivity of the correlation to parameters that are not seen by the wind turbine as far as the mean power output is regarded.

In order to depict the effect of the influencing parameters a parameter identification was performed for the nacelle cup wind speed against the reference wind speed and some of the primary wind and wind turbine operational characteristics (details of the method are found in paragraph 7.2). The identification regarded the mean wind speed as well as its standard deviation and the results by means of the dependence coefficients are given in figure 6.33. The dependence coefficients represent the percent change of the dependent parameter (in this case the nacelle cup readings) when each one of the causative wind and wind turbine parameters is increased by one standard deviation of the parameter variability within the regression domain. The effect of the wind turbulent magnitudes (for the lower wind speed ranges) and the wind shear factors and the yaw error (for all wind speed ranges) is captured, though limited. On the other hand, if a nacelle cup calibration formula is to be applied in a site that compared to the site where the calibration took place presents different wind structure and consequent wind turbine response, then the dependencies on the secondary parameters may act in an additive way resulting in higher uncertainty in estimating the power curve.

6.2.4.3 Conclusions

The experimental research, performed on a 110kW stall regulated turbine, resulted to the following conclusions:

- the introduction of the nacelle cup calibration formula introduces a statistical error that should be taken into account in the uncertainty estimation
- the dependency of the calibration formula to the wind and wind turbine parameters was found to be limited; on the other hand these effects are expected to be magnified in cases where the wind structure and wind turbine response is quite different in the calibration and the testing site.

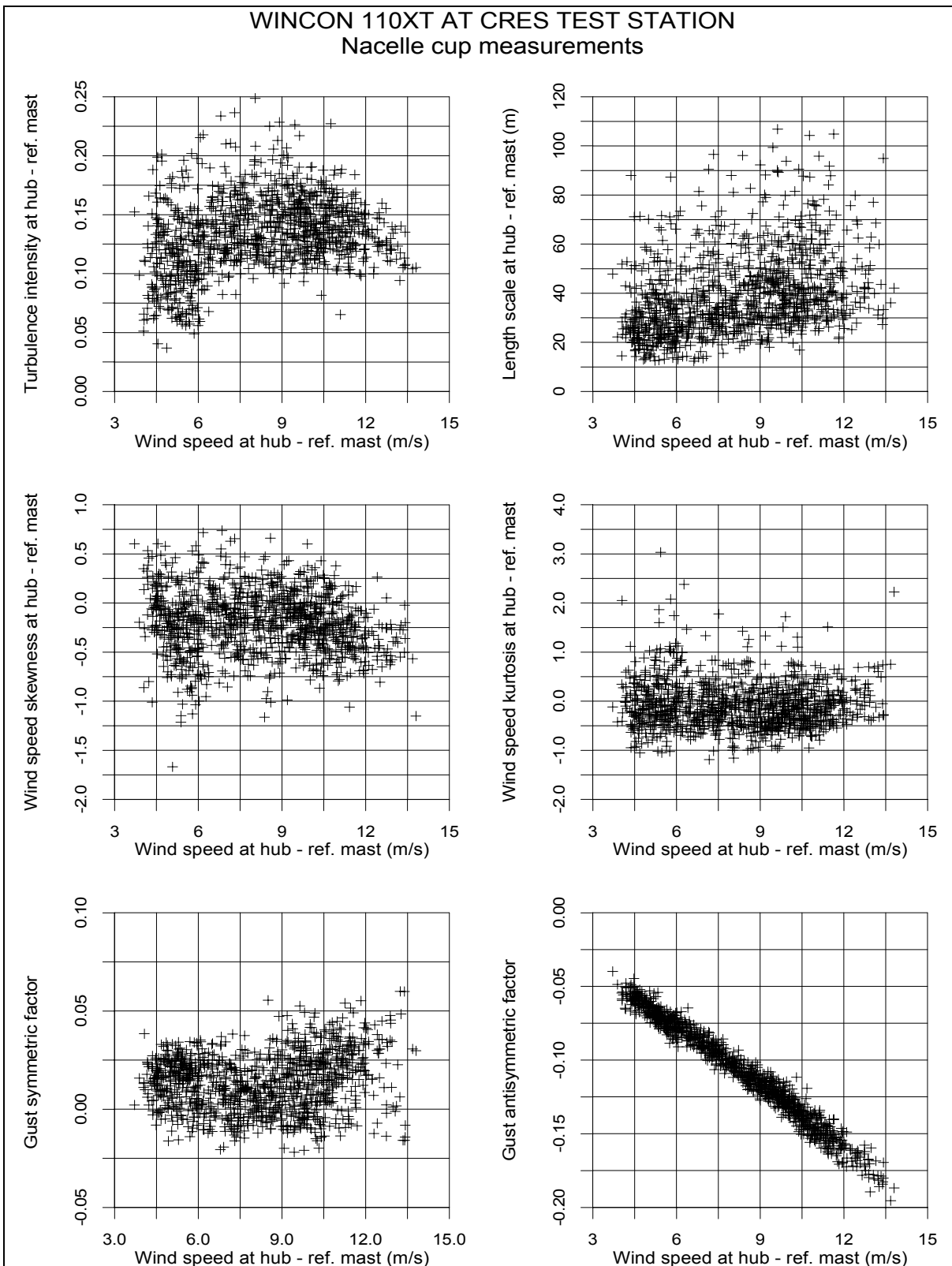


Figure 6.29 Wind statistics from reference mast (wind direction sector 315° - 45°).

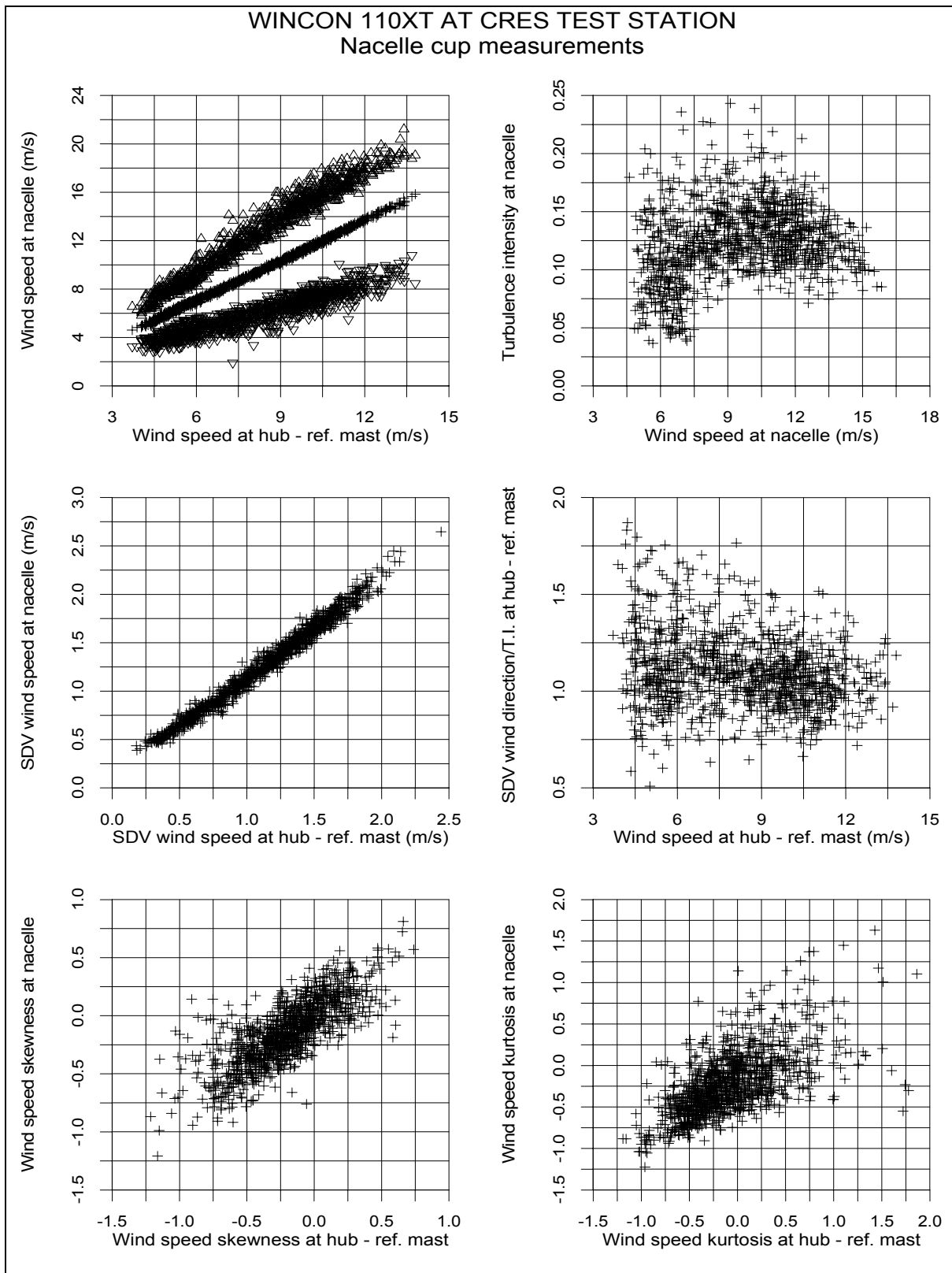


Figure 6.30 Nacelle cup measurements (wind direction sector 315°-45°).

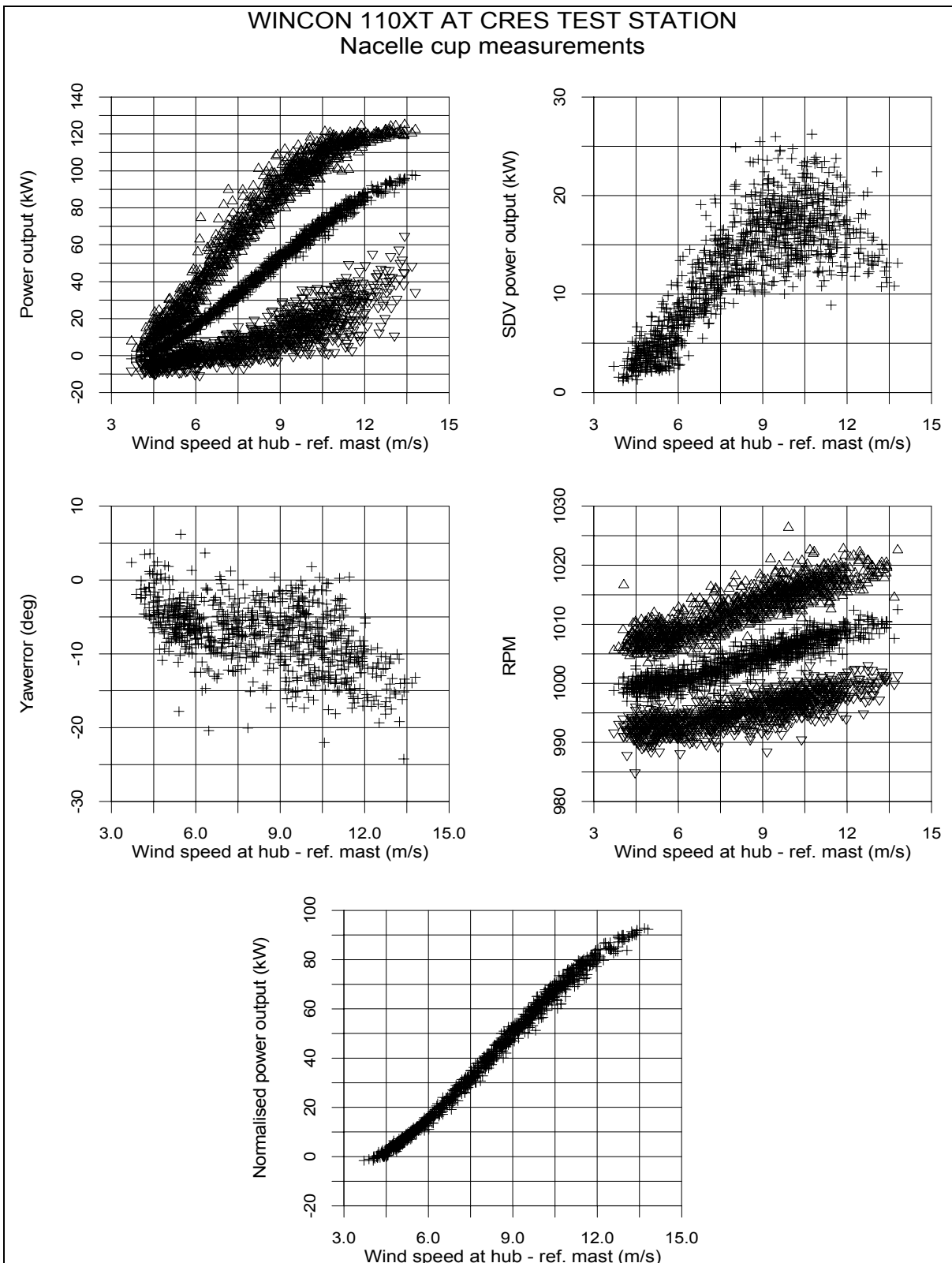


Figure 6.31 Performance measurements for WINCON 110XT WT (wind direction sector 315°-45°).

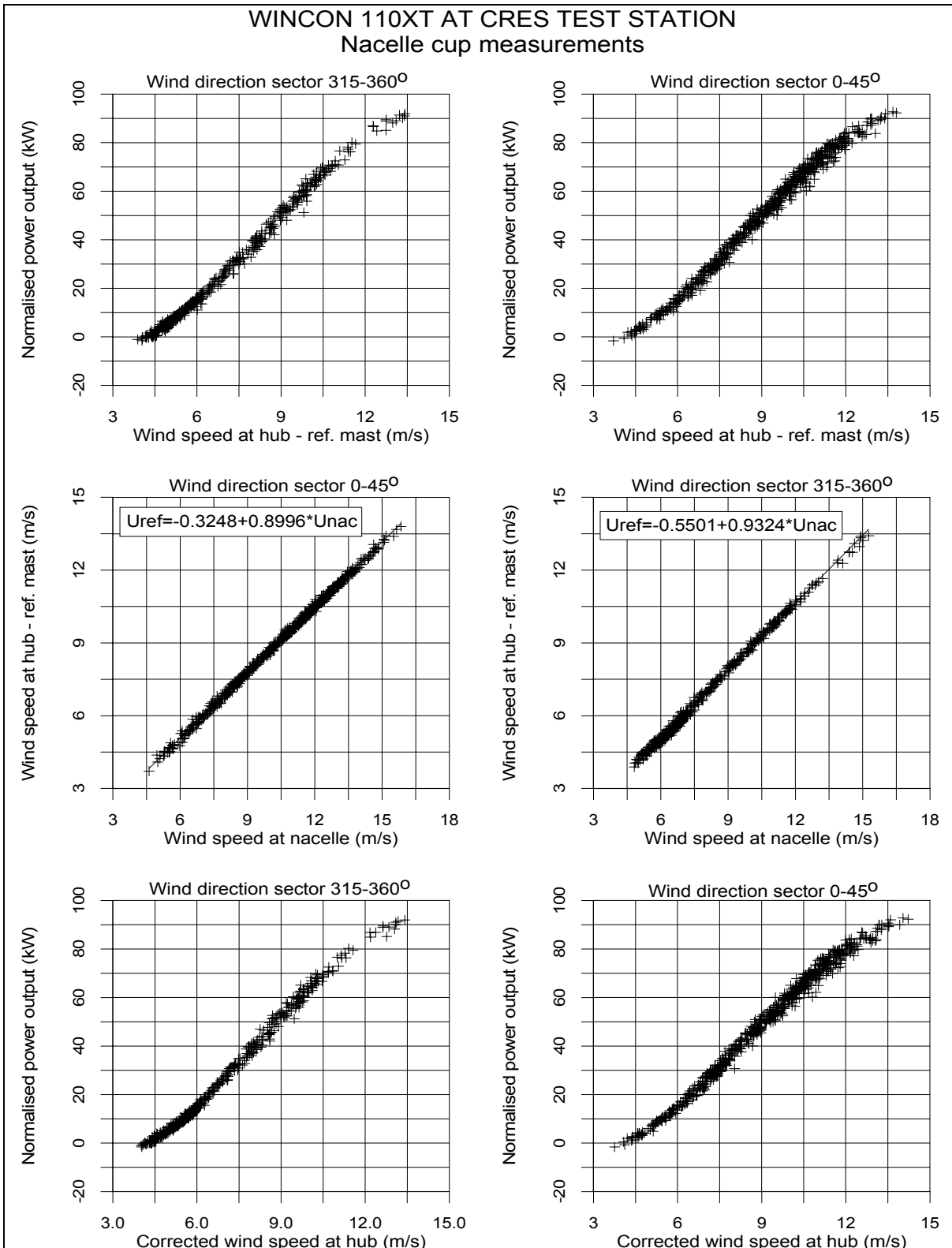


Figure 6.32 Assessment of nacelle cup anemometry for W110XT power curves.

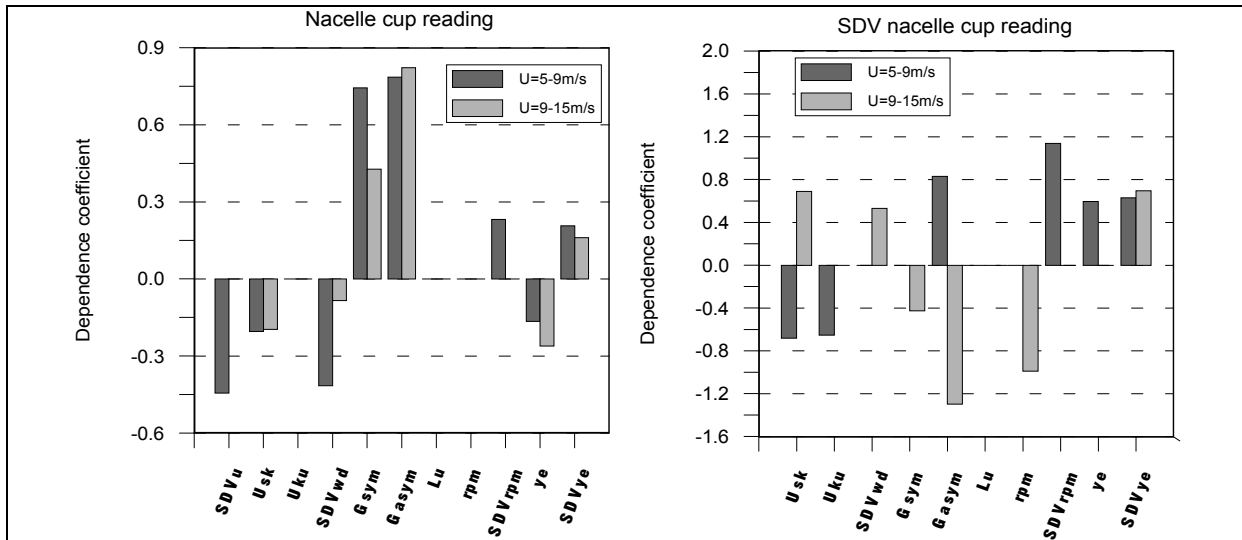


Figure 6.33 Dependency of nacelle cup wind speed and standard deviation on secondary wind and wind turbine operational parameters.

6.3 Upwind Rotor Measurements

6.3.1 Introduction

A large scale experiment was set at CRES test station allowing for assessing the use of the upwind rotor mean wind speed as the reference wind speed. Three 40m towers, forming a straight line, were erected upwind to the WINCON 110XT wind turbine and equipped as follows:

- four couples of cup anemometers and vane resolvers mounted at the two side towers above and below the hub height, at a radius distance of 9.4m from the hub anemometer of the central tower; the distance corresponds to a 85% of the blade length
- one cup mounted at hub height, on the central mast

6.3.2 Rotor disk measurements on a 110kW wind turbine

The rotor mean wind speed is estimated as the average of the five cup readings. The ratio of the rotor mean value over the hub height value is presented in figure 6.34. Due to the fact that on top of the hill, where the meteorological masts and the turbine are erected, the wind shear is rather flat, the resulting ratios are close to unity. The assessment of the method is attained by comparing the estimated annual energy production for the two cases, namely using the rotor mean and the hub height wind speed values; the latter comprises the reference case. The results are given in the following table:

AEP estimation with rotor mean reference wind speed

Mean annual wind speed [m/s]	AEP (Uncertainty) [Difference from reference] [MWh]		
	Wind direction sector 330°-30°	Wind direction sector 350°-10°	Wind direction sector 10°-30°
5	117,3 (8,57) [1,1]	116,3 (8,54) [1,0]	118,6 (8,57) [1,4]
7	271,8 (14,70) [1,8]	270,6 (14,67) [1,1]	273,6 (14,83) [2,3]
9	398,4 (16,79) [2,0]	397,2 (16,75) [2,1]	400,4 (17,20) [3,0]
11	466,5 (16,54) [2,0]	465,4 (16,47) [2,4]	468,3 (17,18) [3,1]

6.3.3 Conclusions

The experimental research on the utilization of the rotor mean wind speed as the reference wind speed for defining the power curve resulted to the following conclusions:

- the procedure is feasible for experimental research purposes; the complexity of the experimental setup makes the procedure unsuitable for large scale power performance evaluations
- in cases where flat wind shear shapes are found the utilization of the rotor mean wind speed does not necessarily results to higher accuracy compared to the estimations based on the hub height measurements; the differences encountered in the present application are significantly smaller than the estimated uncertainty
- the size of the tested wind turbine is one of the parameters that affect the feasibility of the method; larger rotors may present higher sensitivity to wind shear

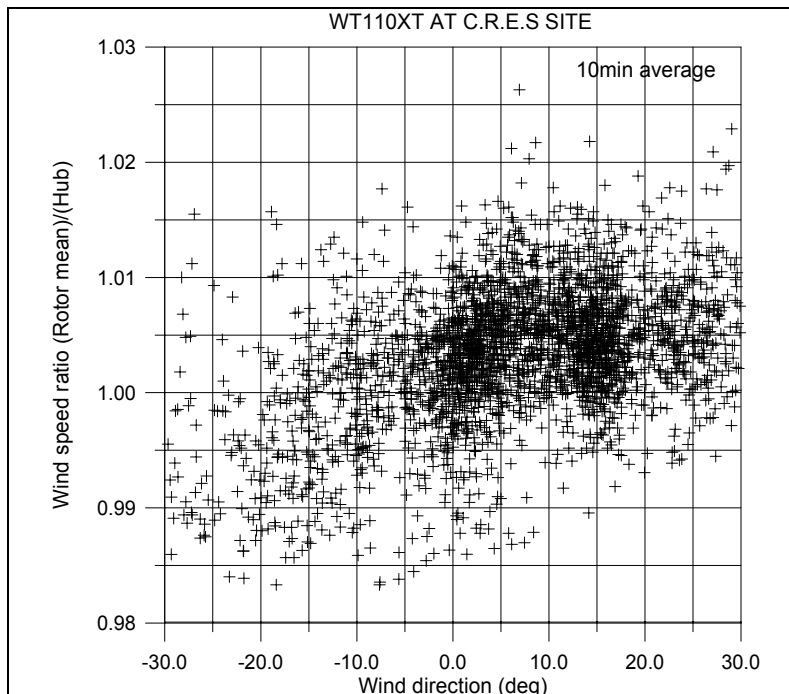


Figure 6.34 Wind speed ratio (rotor mean over reference at hub height) vs wind direction.

6.4 Conclusions

Extensive experimental research carried out on three wind turbines of different size, ranging from 110kW up to 1MW, in order to clarify the feasibility and applicability of the utilization of the nacelle cup anemometer for power performance evaluation purposes. Although the research on the topic is continuing, at this stage several critical conclusions regarding the application field of the method are drawn as follows:

- the cup anemometer is preferably installed behind the non profiled part of the rotor blade
- in several cases the calibration formula was found to be linear; for the large machine a 5th order polynomial curve was used in order to account for the pronounced wind speed deficit in wind speed range corresponding to higher values of power coefficient
- the introduction of the calibration formula should be accompanied by a proper uncertainty estimation, based on the fitting statistics
- the use of nacelle cup measurements may decrease significantly the error induced by site calibration, in cases where large discrepancies are encountered between the measured and reference wind speed
- lower scatter of the measured power curve is attained by the use of the nacelle cup measurements; in cases where two generators are used the switching point is clearly recognizable
- the nacelle cup calibration formula is strongly dependent on the rotor settings and the position of the nacelle cup anemometer; these parameters should be unchanged when transferring the calibration formula
- the calibration formula can be used for sites where the topography is the same with the calibration site, allowing only for surface roughness deviations; on the other hand wind shear changes may introduce significant effect on the calibration formula
- the dependency of the calibration formula to the wind (wind shear and turbulence) and wind turbine parameters (rotational speed, yaw error) was identified for a 110kW turbine. The quantified effects were found to be of limited magnitude, yet these effects are expected to be magnified in cases where the wind structure and wind turbine response is quite different in the calibration and the testing site
- the nacelle anemometer power curves cannot be used to draw any conclusions concerning the changes of the power curve of the wind turbine due to any modifications
- the transfer of the calibration formula for verification purposes presupposes that wind turbine rotor settings, control operation, anemometer position on the nacelle as well as terrain flatness are kept strictly unchanged
- the application of the nacelle cup anemometry in complex terrain proved successful. On the other hand the transfer of the calibration formula to complex terrain, either from flat or from complex terrain, may introduce significant uncertainty on the power curve determination. The same holds in case where the method is to be applied on a wind turbine operating within wakes (wind farm case).

The utilization of rotor mean wind speed as the reference wind speed is feasible only for experimental research purposes due to the complexity of the experimental setup. In cases where flat wind shear shapes are found, and depending on rotor size, the method does not necessarily result to higher accuracy compared to the estimations based on the hub height measurements.

7. PARAMETER IDENTIFICATION OF WIND TURBINE POWER PERFORMANCE

7.1 Introduction

Parameter identification of wind turbine power performance regards the quantification of the dependency of power characteristics, namely mean value and standard deviation, on the wind deterministic and stochastic characteristics.

The scope of performing a parameter identification procedure on different wind turbines operating at different sites is the clarification of the following issues:

- identification of the wind parameters that affect power performance and quantification of their effect
- assessment of the sensitivity of power characteristics of wind turbines of different size and control system
- assessment of the sensitivity of power characteristics of the same wind turbine type when operated in different sites
- assessment of the causative parameters in relation to complex terrain characteristics
- assessment of power curve normalizing procedure based on parameter identification results

7.2 Parameter Identification Procedure On Experimental Data Bases

The scope of a parameter identification procedure is to identify the statistically significant parameters and to quantify their composed effect. Multivariate regression analysis methods present significant advantages, under the restriction of the availability of adequate amount of data, when the goal is to capture the effect of different parameters that are not supposed and most importantly do not need to be uncorrelated. The topics that are discussed herein are related to the regression analysis application and assessment as well as to the parameter identification procedure. Detailed description of the method and sample applications are found in Kleinbaum K. (1985), Morfiadakis E. (1996e), Mouzakis F. (1996).

7.2.1 Multivariate regression analysis

The used multivariate regression analysis is based on least square fitting process as a maximum likelihood estimator of the fitted parameters. It is assumed that the measurement errors are independent and normally distributed with constant standard deviation.

The scope of the regression is the estimation of the coefficients $(a_k, k=1, M)$, for the expression of the dependent variable (y) as follows:

$$y(x_i) = \sum_{k=1}^M a_k X_k(x_i) + E(x_i), \quad i = 1, N \quad (1)$$

where $X_k(x_i)$ is the value of the k^{th} independent variable at point x_i and $E(x_i)$ is the associated error at the same point.

Chi-square fitting is applied as the weighted least square fitting process, in which the magnitude χ^2 is defined as:

$$\chi^2 = \sum_{i=1}^N \left(\frac{y_i - \hat{y}_i}{\sigma_i} \right)^2, \quad \hat{y}_i = \sum_{k=1}^M a_k X_k(x_i) \quad (2)$$

is minimized. The magnitude σ_i presents the measurement standard error at point $(y(x_i), x_i)$. If the measurement errors are not known (as in the present practice) they are all set equal to unity. The number $(n=N-M)$ represents the fitting degrees of freedom.

The minimum of χ^2 occurs where its derivatives with respect to parameters $(a_k, k=1, M)$ vanish. The resulting linear equations are solved by the Gauss-Jordan elimination technique, yielding the coefficients $(a_j, j=1, M)$:

$$a_j = \sum_{k=1}^M C_{jk} \left[\sum_{i=1}^N \frac{y_i X_k(x_i)}{\sigma_i^2} \right], \quad C_{jk} = \left[\sum_{i=1}^N \frac{X_j(x_i) X_k(x_i)}{\sigma_i^2} \right]^{-1}, \quad j = 1, M \quad (3)$$

where the standard deviation related to the estimate of a_j is given by the equation:

$$\sigma(a_j) = \sqrt{\left(\sum_{i=1}^N \sigma_i^2 \left(\frac{\partial a_j}{\partial y_i} \right)^2 \right)} = \sqrt{C_{jj}} \quad (4)$$

7.2.2 Assessment of the accuracy of the multivariate regression

For the assessment of the accuracy of the regression analysis, the following magnitudes were considered:

- a) total sum of squares SSY , sum of squares due to error SSE , sample squared correlation coefficient R^2 as well as fitting standard deviation $\sigma_{\hat{y}}$, defined as follows:

$$SSY = \sum_{i=1}^N (y_i - y_{mean})^2, \quad SSE = \sum_{i=1}^N (y_i - \hat{y}_i)^2, \quad R^2 = \frac{SSY - SSE}{SSY}, \quad \sigma_{\hat{y}} = \sqrt{\frac{\sum_{i=1}^N (y_i - \hat{y}_i)^2}{N - M}} \quad (5)$$

- b) F-test statistic, describing the hypothesis “ H_0 : there is no significant overall regression using the M independent variables”, is defined as follows:

$$F = \frac{SSY - SSE}{SSE} \left(\frac{N - M}{M - 1} \right) \quad (6)$$

Consequently the p-value for the above defined F-test is calculated from Fisher’s F sampling distribution with $M-1$ and $N-M$ degrees of freedom ($p_{F/M-1, N-M}$).

- c) The t-test statistic, describing the hypothesis “ H_0 : the regression coefficient a_k is zero”, is defined as $t = a_k / \sigma(a_k)$ and consequently the p-value for the above defined t-test is calculated from Student’s t sampling distribution with $N-M$ degrees of freedom ($p_{t/N-M}$).
- d) For the quantitative assessment of the relation of the dependent variable on each of the independent parameters X_k , various magnitudes were considered, namely the regression coefficients a_k themselves, the relative per sigma dependence coefficient S_k or the t-test statistic for each parameter. The relative per sigma dependence or dependence coefficient S_k , is defined as:

$$S_k = a_k \frac{\sigma_{X_k}}{y_{mean}}, \quad \sigma_{X_k} = \sqrt{\frac{\sum_{i=1}^N (X_k(x_i) - \overline{X_k})^2}{N-1}} \quad (7)$$

The magnitude S_k represents the relative change of the dependent variable induced by the increase of the value of parameter X_k by its standard deviation σ_{X_k} , within the regression domain²². Assuming that the probability of that change is expected to be comparable for all independent variables, the relativistic assessment of the effect of each variable X_k on y can be attained. Although the above assumption is not valid in cases where the distribution of X_k , within the regression domain, differs significantly from normal, still the magnitude S_k offers a valuable means for weighting the dependence of each X_k on the dependent magnitude.

Another option for assessing the regression results is by means of the *beta* coefficients, defined as:

$$\beta_k = a_k \sigma_{X_k}$$

Beta coefficients are the regression coefficients for the transformed variables in normal distribution (zero mean and unity standard deviation), and are linearly dependent to dependence coefficients.

7.2.3 Parameter identification procedure

The introduced procedure comprises the following phases:

I. Identification of potential causative processes: The deterministic wind characteristics, wind turbulence and the wind speed distribution are regarded as the main causative processes as far as wind turbine power performance is considered.

II. Determination of candidate independent variables for each process: Upon recognition of the potential causative processes, a set of independent variables are selected in order to describe each process. The term independent is used according to the regression analysis nomenclature and does not imply that the predictive variables should be uncorrelated. For the present application, for instance, the deterministic wind characteristics are described by the mean wind speed, the air density, the shape of the wind shear and the wind mean inclination.

III. Application of the full model: The regression analysis is performed for the selected full model as described in the above paragraphs.

IV. Iterative application of evaluation criteria and model reforming: The evaluation criterion is based on the p-values of the t-ratios of each independent variable. Large values for the p-value indicate that the rejection of the hypothesis “ H_0 : the regression coefficient a_k ²³ is zero” is questionable, and consequently the parameter is rejected from the model and the regression analysis is performed again. The rejection threshold, set to 5%, is defined after numerical experimentation.

V. Final selection and assessment: After the completion of the iterative process, the assessment of the regression findings is attained through descriptive magnitudes namely the dependence coefficients.

7.3 Identification And Quantification Of Site Related Effects On Power Performance

The parameter identification procedure, as described in paragraph 7.2 has been applied to the following cases:

- 225kW pitch regulated

- 110kW stall regulated
- 300kW stall regulated
- 500kW stall regulated

In the case of the NTK500/37 the procedure has been applied for all the campaigns that have been performed by the participants. The results of the procedure are assessed either by the dependence coefficients or directly by the sensitivity factors of the regression formula.

Moreover, investigation on the sensitivity of power performance on turbulence, wind shear and atmospheric stability has been performed on a 3MW wind turbine.

7.3.1 Parameter identification on a 225kW pitch regulated WT

The parameter identification for the V27 wind turbine regarded the power mean and standard deviation as well as the mean pitch angle and standard deviation. The independent variables characterize the wind deterministic (mean wind speed, air density and wind shear), stochastic (standard deviation of wind speed and wind direction, turbulence length scale) as well as the distribution characteristics (higher moments of wind speed). The tabulated statistics, namely mean values and standard deviation, of the independent parameters, for the different wind speed ranges where the parameter identification was performed are presented in table 7.1. The regression results, by means of the dependence coefficients are presented in figure 7.1.

The following are observed:

For the mean power output:

- the predominant parameter for all wind speed ranges is the mean wind speed; the results follow the power curve slope
- the standard deviation of wind speed induces a positive effect under 13m/s and an adverse effect for higher wind speed ranges
- the wind direction standard deviation has an adverse effect more pronounced under 13m/s
- wind speed distribution skewness has a limited positive effect for the upper ranges
- air density effect is insignificant due to the small variation of the parameter

For the power standard deviation:

- the predominant parameters for all wind speed ranges are the turbulent components namely the standard deviations of wind speed and wind direction
- wind speed effect is positive in lower wind speeds and adverse in higher ranges
- wind speed distribution skewness has a significant adverse effect in high wind speed ranges
- the limited air density positive effect is present within the middle wind speed ranges

For the mean pitch angle (control system response):

- the predominant parameter for all wind speed ranges is the mean wind speed
- the standard deviation of wind speed and wind skewness induce a positive effect; the opposite holds for the standard deviation of wind direction
- the turbulence length scale induces an adverse effect in the 11-13m/s range

For the standard deviation of pitch angle (control system response):

- the predominant parameters for all wind speed ranges are the mean and the standard deviation of wind speed
- the positive effects of air density, standard deviation of wind direction and wind speed distribution skewness are detected in nearly all ranges
- the turbulence length scale induces an adverse effect in middle wind speed ranges

7.3.2 Parameter identification on a 110kW stall regulated WT

The parameter identification for the WINCON 110XT wind turbine regarded the power mean and standard deviation. The independent variables characterize the wind deterministic (mean wind speed, air density, wind shear and wind inclination angle), stochastic (standard deviation of wind speed components and turbulence length scale) as well as the distribution characteristics (higher moments of wind speed). The tabulated statistics, namely mean values and standard deviation, of the independent parameters, for the different wind speed ranges where the parameter identification was performed are presented in table 7.2. The regression results, by means of the dependence coefficients are presented in figure 7.2. The following are observed:

For the mean power output:

- the predominant parameter for all wind speed ranges is the mean wind speed; the results follow the power curve slope
- air density positive effect is captured for all ranges; this is due to the fact that the parameter values covered a significant domain within the data base
- the standard deviations of the wind speed components are inducing an adverse effect for all wind speed ranges
- wind speed inclination induces an adverse effect that is present for all wind speed ranges

For the power standard deviation:

- the predominant parameter for all wind speed ranges is the standard deviation of longitudinal wind speed component
- wind speed effect is positive in lower wind speeds and adverse in the higher ranges
- standard deviation of the vertical wind speed component is significant and positive for the upper ranges whereas the lateral component effect is present in the higher wind speed range
- wind inclination effect is positive and pronounced in higher wind speed ranges whereas wind shear effect is insignificant
- air density effect is positive in all ranges
- wind speed distribution estimators have adverse effect; skewness effect is pronounced in higher wind speed ranges

7.3.3 Parameter identification on a 500kW stall regulated WT

The parameter identification for the NTK500/37 wind turbine regarded the power mean and standard deviation as well as the mean pitch angle and standard deviation. The independent variables characterize the wind deterministic (mean wind speed, air density and wind shear), stochastic (standard deviation of wind speed and wind direction, turbulence length scale) as well as the distribution characteristics (higher moments of wind speed). The tabulated statistics, namely mean values and standard deviation, of the independent parameters, for the different wind speed ranges where the parameter identification was performed are presented in table 7.3. The regression results, by means of the dependence coefficients are presented in figure 7.3. The following are observed:

For the mean power output:

- the predominant parameter for all wind speed ranges is the mean wind speed; the results follow the power curve slope
- the longitudinal component of turbulence induces a significant positive effect under 11m/s
- the wind direction standard deviation has an adverse effect more pronounced under 11m/s
- wind speed distribution skewness has a positive effect pronounced in the lower wind speed ranges
- the adverse effect of wind shear is significant in the lower wind speed range
- air density effect is insignificant
- turbulent length scale effect is limited and adverse

For the power standard deviation:

- the predominant parameters for all wind speed ranges are the turbulent components namely the standard deviations of wind speed and wind direction
- wind speed effect is positive in lower wind speeds and adverse in higher ranges
- wind speed distribution skewness effect is positive for the lower ranges whereas adverse for the high range
- the air density effect is positive in 8-11 m/s range and adverse in the high wind range

7.3.3.1 Analysis on combined data bases

In order to assess the sensitivity of the power characteristics of one specific wind turbine type in different sites, flat and complex, several power performance campaigns, performed by the participants, were collected and analyzed by means of the parameter identification procedure described in 7.2. The power curve measurements for the NTK500/37 wind turbine were performed by the following institutes:

Institute	Site	Type of site
RISO	RISO	flat
DEWI	Pilsum	flat
WINDTEST	-	flat
NEL (data for 2 WT)	Taff Ely	complex
CRES	Toplou	complex

A brief overview of the data base structure is presented in table 7.4. In figure 7.4 the power data scatter plots are presented for all campaigns. Moreover, in figures 7.5 to 7.7 the basic wind characteristics, namely turbulence intensity, standard deviation of wind direction and wind shear ratio, that were observed during the power performance campaigns are also presented. The bin averaged power curve of each measuring campaign along with AEP estimations for several annual wind speed cases, for Rayleigh distribution, are given in figures 7.8 and 7.9 respectively. The AEP estimations are based for power curves limited in the range 4-14 m/s in order to maintain a common basis for AEP comparisons.

The parameter identification regarded the air density corrected power mean and standard deviation. The independent variables characterize the wind deterministic (mean wind speed and wind shear ratio) and stochastic characteristics (standard deviation of wind speed and wind direction). The regression results, by means of the sensitivity factors are presented in tables 7.5 and 7.6 for mean power and standard deviation, respectively.

The following are observed:

- the captured effects are representative for the specific site with the specific instrumentation used; an uncertainty of limited importance is introduced in the comparison as each instrumentation may respond differently in a turbulent wind field
- the dependency of mean power output on mean wind speed presented differences between the measurements at the different sites. The differences are in accordance with the figure 7.8.
- the effect of wind shear, as described by the ratio of wind speed at two different heights (U_{35m}/U_{18m}), presented different behavior in flat and complex sites. In the former case it affected power output in a positive way whereas in the latter presented an adverse effect
- turbulence effects, as captured by the wind speed standard deviation, presented significant variation for the different sites. In general, positive effects were identified in lower wind speed ranges and negative in higher ranges.
- standard deviation of wind direction introduce in general an adverse effect; at higher wind speed ranges the effect is positive

- standard deviation of power output is strongly dependent on wind speed standard deviation; secondary effects are captured by mean wind speed, wind shear ratio and wind direction standard deviation. In all campaigns the captured effects are quantitatively comparable.

7.3.4 Parameter identification on a 300kW stall regulated WT

The parameter identification for the MADE 300kW wind turbine regarded the power mean and standard deviation. Three groups of data have been utilized regarding operation in flat and complex terrain as follows:

Group	Terrain type	Wind direction
EAST	Complex	56.25°-123.75°
WEST	Complex	236.25°-258.75°
FLAT	Flat	-

The independent variables characterize the wind deterministic (mean wind speed and wind shear factor) and stochastic characteristics (standard deviation of wind speed and wind direction). The data base has been split into wind speed intervals, namely 6-8m/s, 8-11m/s, 11-13m/s and 13-16m/s. The regression analysis tool, in accordance to paragraph 7.2, followed the forward stepwise processing and the regression results are presented by means of the beta coefficients for the variables that have been considered as statistically significant by the method in figures 7.10 and 7.11 for mean power and standard deviation, respectively.

In the case of mean power, wind speed is the principal factor. The non-linear behavior of the power curve at low wind speeds and at wind speeds close to the stall region is also detected in the beta coefficient for this parameter, which is lesser for 6-8m/s wind speed interval for all cases and 13-16m/s for complex EAST case, and even negative for 13-16m/s for complex WEST and FLAT cases. In the three cases, beta coefficient for wind speed presents higher values for the linear region of power curve. When examining standard deviation of wind speed, power performance seems more influenced by this parameter in complex terrain than in flat one. It should be remembered that all variables were transformed into normal distribution and therefore beta coefficient means sensibility, it does not matter the range of variation of the independent variable. Taking this into account, one can interpret this as a different behavior of the wind turbine power performance before the same level of turbulence, depending on the complexity of the terrain. This last fact can be provoked only by a different pattern of the turbulence spatial distribution. For standard deviation of wind direction it is seen that in complex terrain there is more influence of this parameter than in flat terrain. Standard deviation of wind direction is a stochastic parameter which has to do with turbulence pattern of the flow. In complex terrain, specially for WEST direction it is an important negative parameter. This may be attributed to nacelle orientation characteristics. Shear factor does not present a common pattern of influence for the three cases. Only for complex WEST and FLAT this dependence is similar. Moreover the influence appears only in few wind speed intervals. It should be considered that in complex terrain vertical profiles are quite flat, and therefore, shear estimation by means of logarithmic fitting (this was the kind of fitting used here) in these sites is not the most appropriated.

Finally, standard deviation of power is primarily influenced by standard deviation of wind speed for all three cases.

7.3.5 Parameter identification on a 3MW pitch controlled WT

The tendency towards larger wind turbines leads to an increasing interest in the relation between meteorological conditions and the power performance of these systems. The rotor of a MW-scale wind turbine covers a height range of about 50-100 m in which strong vertical wind speed gradients can occur.

In that sense the experimental investigation on the relations between the power performance of the Aeolus II and vertical wind shear, turbulence intensity and atmospheric stability are representative and presented herein.

Aeolus II is a variable speed, pitch controlled wind turbine with a nominal power output of 3MW. The rotor diameter is 80.5m whereas the hub height reaches 92m.

The recorded data at the Aeolus II were classified according to the turbulence intensity. For each turbulence class a power coefficient curve was evaluated, presented in figure 7.12. The resulting annual energy estimations are presented in figure 7.13. When evaluating a power curve the measured power and wind speed is averaged over a period of usually 10 minutes. Because of the wind speed fluctuations and the non linearity of the power curve this time averaging process leads to an increase of the evaluated power curve where the power curve is concave and to a decrease of the evaluated power curve where the power curve is convex. This effect is evident from figures 7.13 and 7.14 and will grow with increasing turbulence intensity.

From the wind speed measurements at the heights 32m, 62m, 92m and 126m a wind gradient weighted with its contribution to the rotor disk area was calculated and served as classification criteria for the recorded data at the Aeolus II. For each class of wind gradient a power curves were calculated and the resulting AEP estimations are presented in figure 7.15. Obviously for the applied wind speed distribution an increase of wind gradient leads to an increase of the AEP. This effect can be generally understood from the observations concerning the influence of turbulence intensity on the power performance discussed before: high wind gradients correspond to high spatial variations of wind speed over the rotor height. The spatial averaging effect of the rotor together with the nearly cubic increase of the power with wind speed result in a higher annual energy production similar to the effect of high turbulence.

At the Aeolus II information about the actual atmospheric stability is derived from measurements of the vertical temperature gradient, i. e. temperature measured at 90 m and 2.5 m. A positive difference of the so called potential temperature $d\theta = \theta(90.0\text{m}) - \theta(2.5\text{m})$ corresponds to a stable layer. A potential temperature difference around 0K indicates a neutral layer and a negative $d\theta$ correspond to an unstable layer. For each class of $d\theta$ a power curve was evaluated. The resulting AEP estimations have the tendency to decrease with increasing stability, as shown in figure 7.16.

The atmospheric stability strongly influences the turbulence intensity and the vertical wind gradient, as it is presented in figure 7.17. Unstable conditions correspond to higher turbulence levels and relative low wind gradients, while lower turbulence and high wind gradients usually occur during stable conditions. Because the turbulence as well as the vertical wind gradient effect the power performance, the observed dependence of the power curve on the stratification can probably be interpreted as an interference of both influences.

7.4 Conclusions

An analytic method is introduced covering parameter identification tasks in power performance measurements. The developed tool is based on multivariate regression analysis with a backward parameter elimination technique in order to count for the statistically insignificant parameters. The method is applied for the parameter identification of the power performance of wind turbines operating at different sites, both flat and complex. The parameters chosen to comprise the model set describe the deterministic part of the wind, the main turbulent characteristics, the turbulence length scale as well as the wind speed distribution. The examined dependent variables were the mean power output, the standard deviation of the power output and in the case of pitch controlled machine the response of the control system. The effect of the above parameters was captured and quantified. It was revealed that except from the mean wind speed

other parameters, related to the deterministic as well to the stochastic wind characteristics are affecting the power performance of the turbine and should be considered within power performance assessment procedures.

More specifically, the following are the concluding remarks:

- air density effects, as they were captured by the parameter identification procedure, were of limited magnitude due to the narrow variation of air density. On the other hand the capture dependency was found to be in accordance with the theoretical linear corrections
- turbulence effects on mean power output it is mainly governed by the averaging effects that result to higher power output at lower wind speed ranges and the reverse at higher wind speed ranges close to power control region. On the other hand it was found that the averaging effect is not the only mechanism that governs the turbulence effect as different sensitivities were found for the same turbine operated at different sites. Moreover, for the case of a small sized stall regulated wind turbine the turbulence effects, captured by the standard deviations of the three wind speed components, were found to be adverse for all wind speed ranges.
- wind shear effect is more pronounced in large wind turbines; the effect is not systematic and depends on the definition of the wind shear descriptor. The different effects that are captured for the same machine at different test sites strongly indicates that the one parameter description of wind shear is inadequate for describing the spatial variations of wind speed upwind to the rotor plane.
- wind inclination impose an adverse effect on mean power output; the effect is pronounced at lower wind speed ranges
- wind speed higher order statistics introduce a secondary effect. Distribution skewness, that is linearly dependent on the mean value of cubed wind speed, impose a positive effect on mean power output that is significant for large wind turbines.
- significant influence of the atmospheric stability, vertical wind shear and the turbulence intensity on the power performance of the 3MW wind turbine was found. The influence of such effects on the predicted AEP is in the range of 4% and should be reflected in the recommendations for power curve measurements for large systems.
- the results of the parameter identification indicate that wind inflow characteristics should be measured and reported in more detail including the 3D structure of mean wind speed and turbulence. This would allow for estimation of sensitivity factors and the optional normalization of the power performance measurements to specified conditions

Table 7.1 Independent parameter variation for the V27 data base.

Wind speed bin Parameter	U=6-8m/s		U=8-11m/s		U=11-13m/s		U=13-16m/s	
	mean	SDV	mean	SDV	mean	SDV	mean	SDV
Mean wind speed - U (m/s)	7.1	0.57	9.53	0.83	12.0	0.578	14.1	0.84
Air density - ρ (kgm ⁻³)	1.15	0.008	1.15	0.007	1.15	0.007	1.15	0.007
Wind shear exponent - α	0.04	0.049	0.048	0.047	0.043	0.038	0.039	0.033
SDV wind speed - σ_u (m/s)	0.785	0.192	0.964	0.178	1.21	0.221	1.42	0.302
SDV wind direction - σ_φ (deg)	6.69	2.29	5.98	1.48	5.67	1.2	5.33	0.986
Wind speed skewness - U_{sk}	-0.045	0.253	-0.046	0.268	-0.063	0.292	-0.136	0.286
Wind speed kurtosis - U_{ku}	-0.192	0.366	-0.123	0.404	-0.157	0.443	-0.22	0.346
Turbulent length scale - L_u (m)	65.29	32.31	58.37	25.37	55.2	21.8	57.6	20.0

Table 7.2 Independent parameter variation for the W110XT data base.

Wind speed bin Parameter	U=6-8m/s		U=8-11m/s		U=11-13m/s		U=13-16m/s	
	mean	SDV	mean	SDV	mean	SDV	mean	SDV
Mean wind speed - U (m/s)	7.23	0.514	9.33	0.82	11.9	0.59	14.2	0.82
Air density - ρ (kgm ⁻³)	1.19	0.027	1.19	0.029	1.18	0.020	1.19	0.018
Wind shear exponent - α	0.029	0.034	0.023	0.028	0.024	0.027	0.03	0.024
Wind inclination - θ (deg)	3.45	1.38	3.49	1.26	3.14	0.984	3.5	0.90
SDV wind speed - σ_u (m/s)	0.97	0.196	1.33	0.27	1.64	0.299	2.07	0.397
Lateral turbulence component σ_v	0.95	0.25	1.21	0.28	1.40	0.30	1.69	0.34
Vertical turbulence component σ_w	0.78	0.20	1.01	0.22	1.16	0.19	1.39	0.24
Wind speed skewness - U_{sk}	-0.087	0.289	-0.13	0.30	-0.255	0.295	-0.20	0.295
Wind speed kurtosis - U_{ku}	-0.054	0.53	-0.071	0.47	-0.025	0.466	-0.063	0.448
Turbulent length scale - L_u (m)	35.7	16.6	40.1	16.3	46.4	18.4	50.6	17.9

Table 7.3 Independent parameter variation for the NTK500/37 data base.

Wind speed bin Parameter	U=6-8m/s		U=8-11m/s		U=11-13m/s		U=13-16m/s	
	mean	SDV	mean	SDV	mean	SDV	mean	SDV
Mean wind speed - U (m/s)	6.97	0.59	9.41	0.845	12.0	0.587	14.7	0.85
Air density - ρ (kgm ⁻³)	1.23	0.009	1.23	0.007	1.23	0.009	1.23	0.011
Wind shear exponent - α	-0.017	0.019	-0.015	0.016	-0.019	0.011	-0.024	0.009
SDV wind speed - σ_u (m/s)	0.739	0.219	1.06	0.273	1.43	0.234	1.76	2.47
SDV wind direction - σ_φ (deg)	5.56	2.14	6.25	1.92	6.22	1.37	6.19	0.99
Wind speed skewness - U_{sk}	0.094	0.315	-0.053	0.269	-0.026	0.26	-0.039	0.22
Wind speed kurtosis - U_{ku}	0.388	1.22	-0.152	0.498	-0.343	0.299	-0.42	0.27
Turbulent length scale - L_u (m)	29.9	14.1	36.1	18.6	45.2	21.2	50.0	21.2

TABLE 7.4 Parameters involved in identification procedure.

Model parameter set	RISO	DEWI	WINDTEST	NEL (#A)	NEL (#B)	CRES
Wind speed	x	x	x	x	x	x
SDV wind speed	x	x	x	x	x	x
Wind speed min/max		x	x			x
Wind speed skewness						x
Wind speed kurtosis						x
Wind shear ratio		x		x	x	x
SDV wind direction		x	x	x	x	x
Power mean (norm.)	x	x	x	x	x	x
SDV power (norm.)		x	x	x	x	x

Table 7.5 Sensitivity factors for mean power output for NORDTANK 500/37 measured at different sites.

MEAN POWER SENSITIVITY FACTOR FOR MEAN WIND SPEED ($\partial\bar{P}/\partial\bar{U}$)						
Wind speed	RISO	DEWI	WINDTEST	NEL (#A)	NEL (#B)	CRES
6m/s	41.5	39.5	35.4	33.7	35.2	39.5
8m/s	57.8	56.9	59.6	48.5	50.7	58.9
10m/s	66.7	63.2	64.1	59.7	59.2	60.3
12m/s	50.0	52.5	52.9	52.1	49.9	51.9
14m/s	39.1	35.9	38.5	39.5	31.7	21.1
16m/s	-	4.3	-	18.6	11.6	4.5
18m/s	-	-1.0	-	0.3	-0.2	-4.5
20m/s	-	-	-	-11.7	-9.9	-
22m/s	-	-	-	-11.6	-16.8	-
MEAN POWER SENSITIVITY FACTOR FOR WIND SHEAR RATIO ($\partial\bar{P}/\partial\bar{w}_{sr}$)						
Wind speed	RISO	DEWI	WINDTEST	NEL (#A)	NEL (#B)	CRES
6m/s	-	105.4	-	.3	-22.7	-202.6
8m/s	-	3.2	-	-7.3	-61.5	-303.0
10m/s	-	18.8	-	-48.9	-124.9	-565.8
12m/s	-	330.0	-	1.4	-131.4	-617.8
14m/s	-	230.0	-	-83.6	-154.3	-269.1
16m/s	-	95.2	-	-55.7	-131.3	-269.8
18m/s	-	849.3	-	-43.6	-112.6	-464.5
20m/s	-	-	-	-185.7	-155.1	-
22m/s	-	-	-	-210.3	110.9	-
MEAN POWER SENSITIVITY FACTOR FOR WIND DIRECTION SDV ($\partial\bar{P}/\partial\sigma_v$)						
Wind speed	RISO	DEWI	WINDTEST	NEL (#A)	NEL (#B)	CRES
6m/s	10.9	4.8	4.2	9.62	4.24	5.52
8m/s	7.3	6.2	-2.2	9.41	6.02	8.53
10m/s	-5.1	-4.7	2.98	9.50	4.24	20.23
12m/s	-17.0	4.93	5.43	-6.26	4.33	3.05
14m/s	-35.1	1.41	13.36	-6.64	-5.03	14.79
16m/s	-	-7.2	-	-4.74	-8.50	-7.08
18m/s	-	-9.7	-	-13.98	-20.57	-9.22
20m/s	-	-	-	-27.18	-14.47	-
22m/s	-	-	-	-5.44	-14.05	-
MEAN POWER SENSITIVITY FACTOR FOR WIND DIRECTION SDV ($\partial\bar{P}/\partial\sigma_\phi$)						
Wind speed	RISO	DEWI	WINDTEST	NEL (#A)	NEL (#B)	CRES
6m/s	-	-	-0.13	-0.27	-0.34	-0.71
8m/s	-	-	1.02	-1.07	-1.75	-2.06
10m/s	-	-	0.03	-1.67	-1.19	-3.10
12m/s	-	-	4.06	-0.45	-2.09	-7.81
14m/s	-	-	3.80	-0.60	-3.37	-0.38
16m/s	-	-	-	-1.18	-0.35	-0.04
18m/s	-	-	-	0.85	-0.91	-0.14
20m/s	-	-	-	3.35	-6.97	-
22m/s	-	-	-	3.78	34.46	-

Table 7.6 Sensitivity factors for power standard deviation for NORDTANK 500/37 measured at different sites.

POWER SDV SENSITIVITY FACTOR FOR MEAN WIND SPEED ($\partial\sigma_p/\partial\bar{U}$)						
Wind speed	RISO	DEWI	WINDTEST	NEL (#A)	NEL (#B)	CRES
6m/s	-	3.46	3.93	4.36	4.71	4.56
8m/s	-	4.50	4.31	4.30	5.22	4.84
10m/s	-	-0.89	1.89	1.90	2.47	5.19
12m/s	-	-2.47	-3.39	-2.52	-3.30	-5.74
14m/s	-	-7.78	-1.89	-6.35	-8.05	-9.70
16m/s	-	0.40	-	-6.09	-3.48	-3.65
18m/s	-	3.09	-	1.23	1.13	1.35
20m/s	-	-	-	2.14	1.13	-
22m/s	-	-	-	-0.58	0.45	-

POWER SDV SENSITIVITY FACTOR FOR WIND SHEAR RATIO ($\partial\sigma_p/\partial\overline{wsr}$)						
Wind speed	RISO	DEWI	WINDTEST	NEL (#A)	NEL (#B)	CRES
6m/s	-	-19.13	-	-7.94	-12.77	-9.76
8m/s	-	-51.43	-	-18.01	-22.58	-18.61
10m/s	-	-56.58	-	-47.79	-60.16	-20.13
12m/s	-	130.8	-	-27.12	-37.67	68.19
14m/s	-	98.2	-	-7.22	16.84	85.26
16m/s	-	51.1	-	-5.91	7.00	15.69
18m/s	-	-100.1	-	9.72	24.71	-40.50
20m/s	-	-	-	97.74	14.30	-
22m/s	-	-	-	87.88	63.45	-

POWER SDV SENSITIVITY FACTOR FOR WIND DIRECTION SDV ($\partial\sigma_p/\partial\sigma_U$)						
Wind speed	RISO	DEWI	WINDTEST	NEL (#A)	NEL (#B)	CRES
6m/s	-	27.48	24.53	26.88	25.57	27.69
8m/s	-	42.55	38.62	40.13	34.98	32.45
10m/s	-	50.58	35.74	37.17	28.27	23.59
12m/s	-	27.20	26.54	19.34	10.46	18.89
14m/s	-	14.25	11.75	16.1	11.37	3.76
16m/s	-	10.59	-	6.98	5.51	4.79
18m/s	-	6.23	-	7.46	5.26	5.11
20m/s	-	-	-	11.6	6.05	-
22m/s	-	-	-	4.47	0.73	-

POWER SDV SENSITIVITY FACTOR FOR WIND DIRECTION SDV ($\partial\sigma_p/\partial\sigma_\phi$)						
Wind speed	RISO	DEWI	WINDTEST	NEL (#A)	NEL (#B)	CRES
6m/s	-	-	1.34	0.41	0.27	0.76
8m/s	-	-	2.06	0.48	1.00	1.92
10m/s	-	-	2.85	1.76	1.98	3.47
12m/s	-	-	2.56	3.62	4.45	1.44
14m/s	-	-	4.57	1.68	3.24	-0.05
16m/s	-	-	-	2.05	1.74	-1.17
18m/s	-	-	-	0.41	2.72	1.63
20m/s	-	-	-	1.93	3.07	-
22m/s	-	-	-	0.41	0.86	-

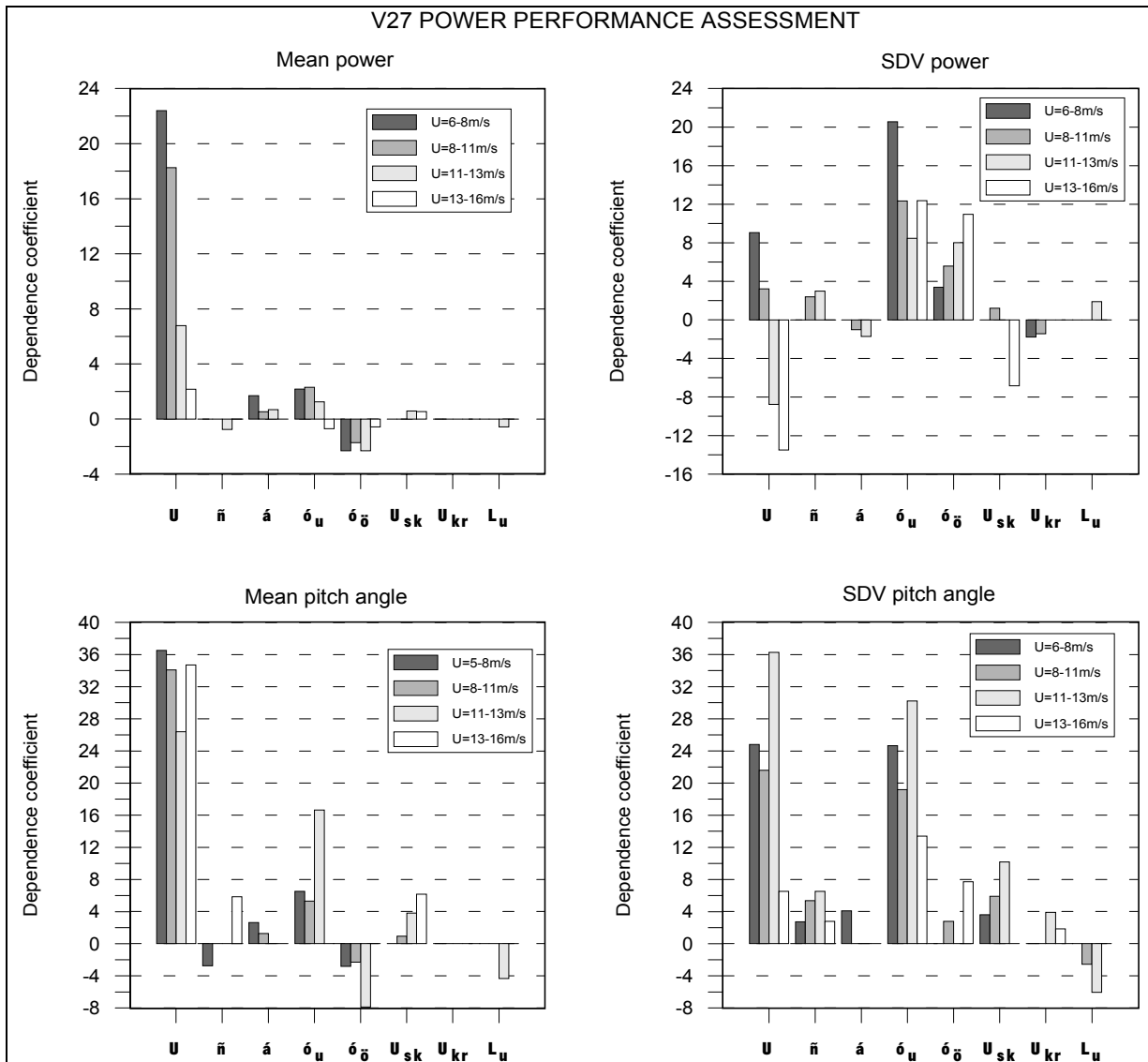


Figure 7.1 Dependence coefficient charts for V27 at Andros power performance.

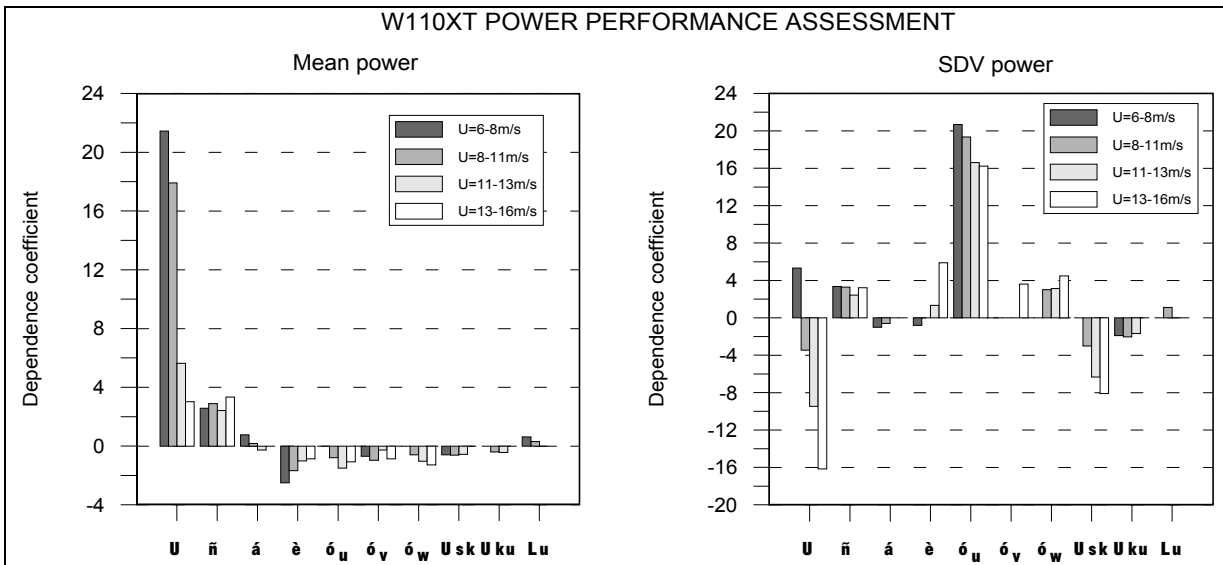


Figure 7.2 Dependence coefficient charts for W110XT at Lavrio power performance.

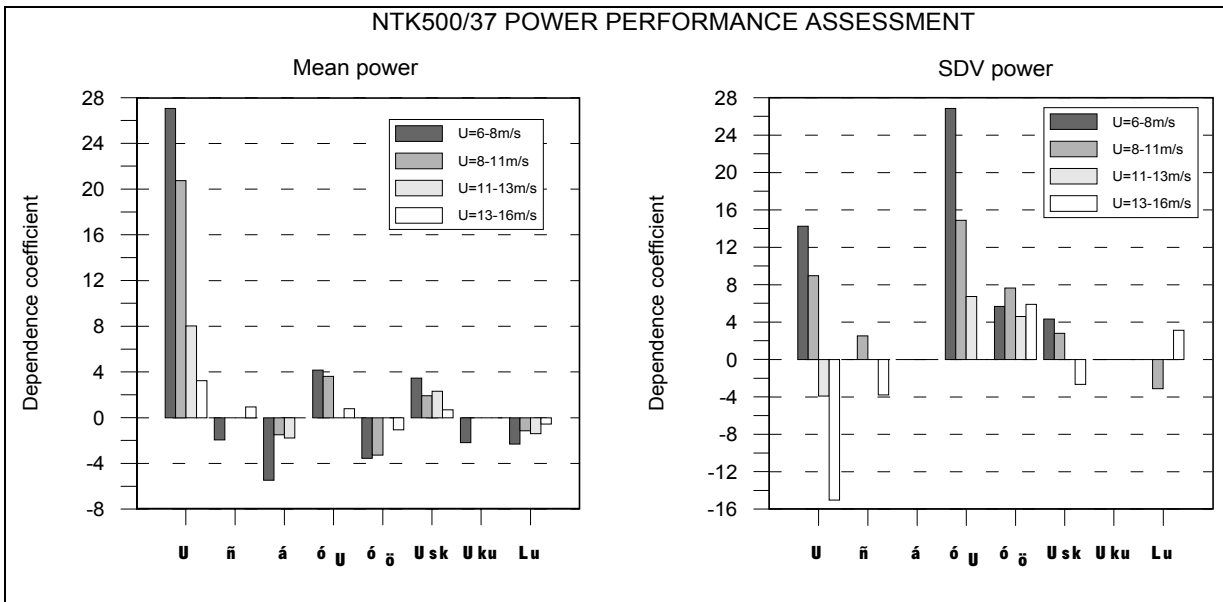


Figure 7.3 Dependence coefficient charts for NTK500/37 at Toplou power performance.

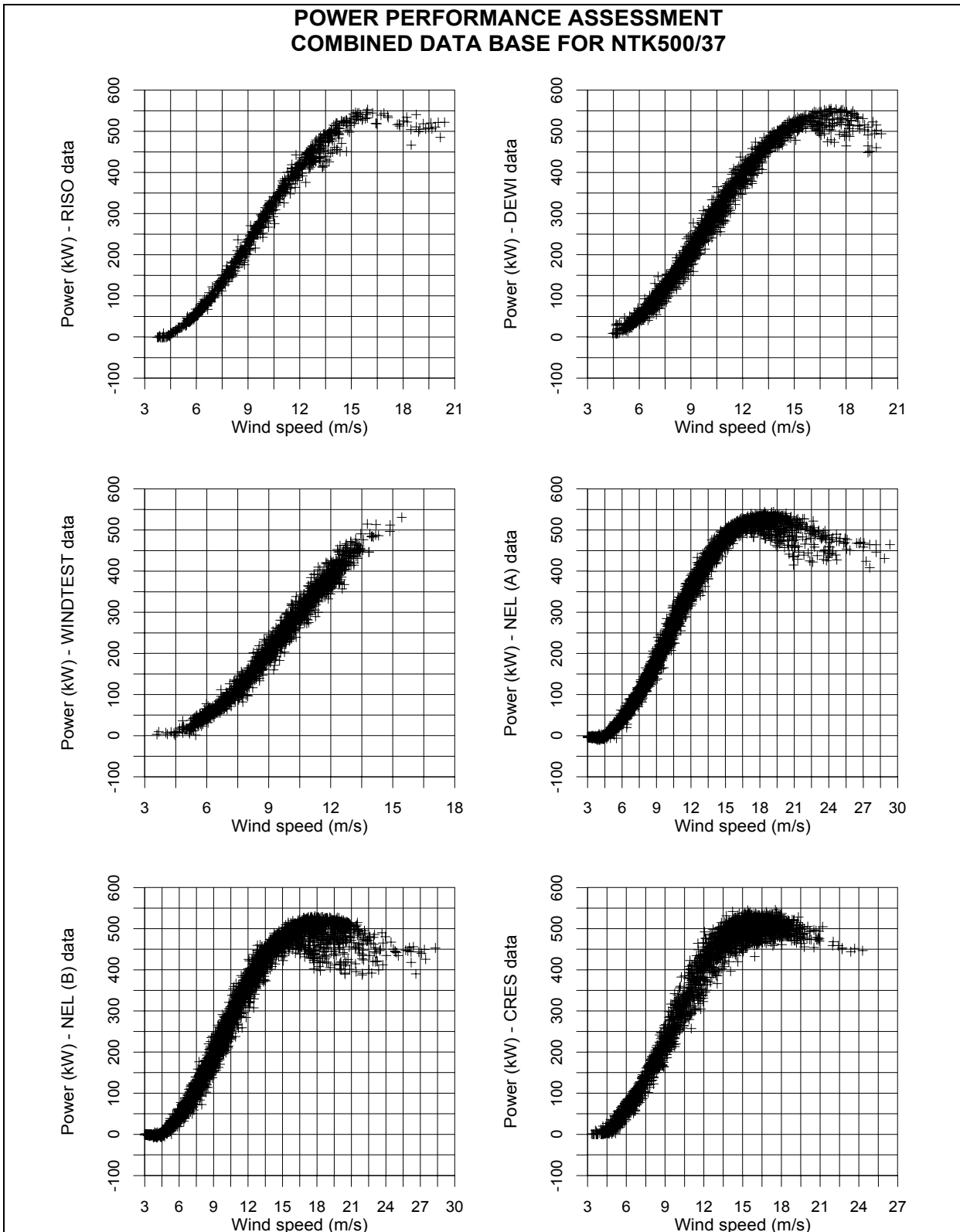


Figure 7.4 Power output for NTK500/37 measured at different sites.

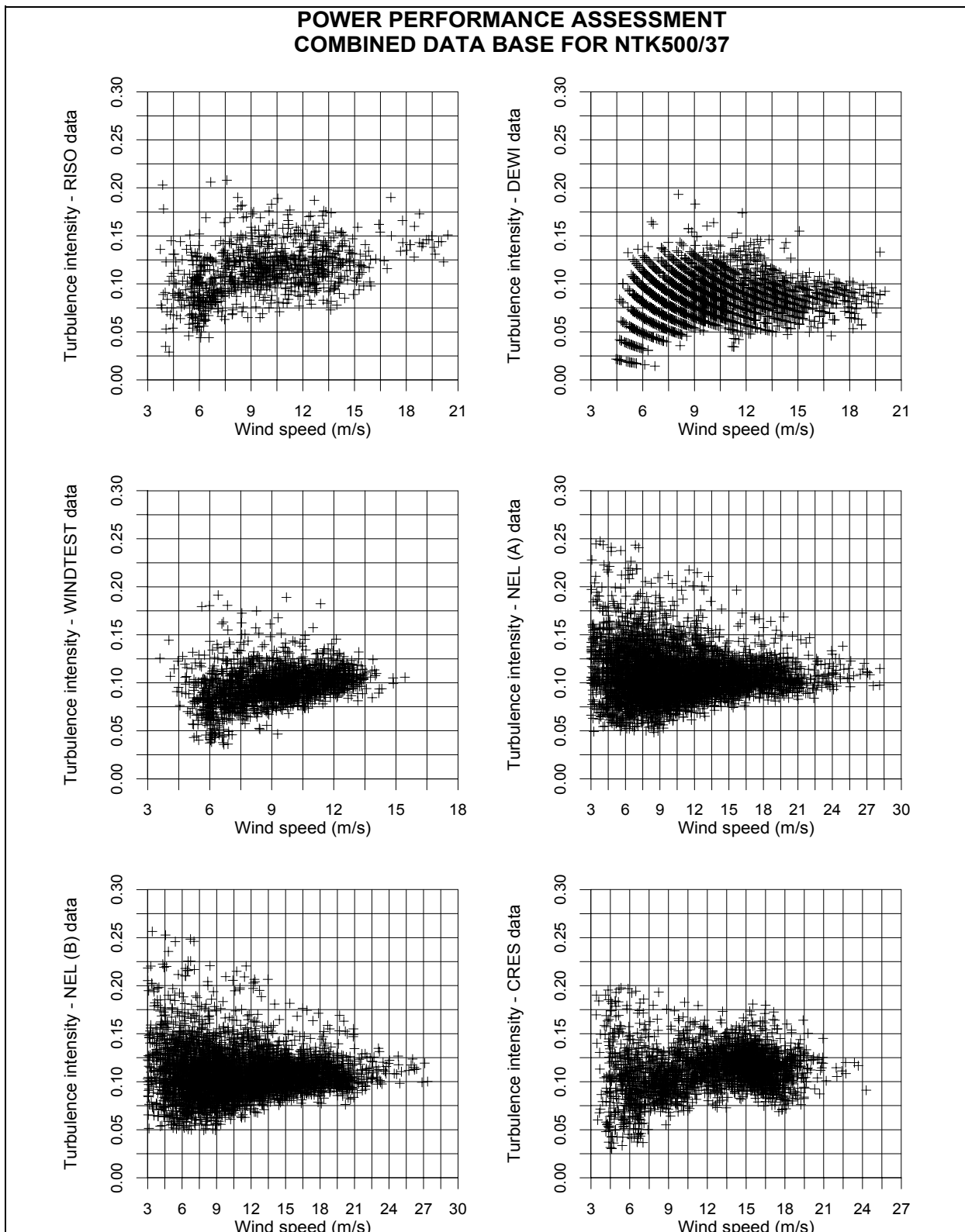


Figure 7.5 Turbulence intensity distributions at NTK500/37 sites.

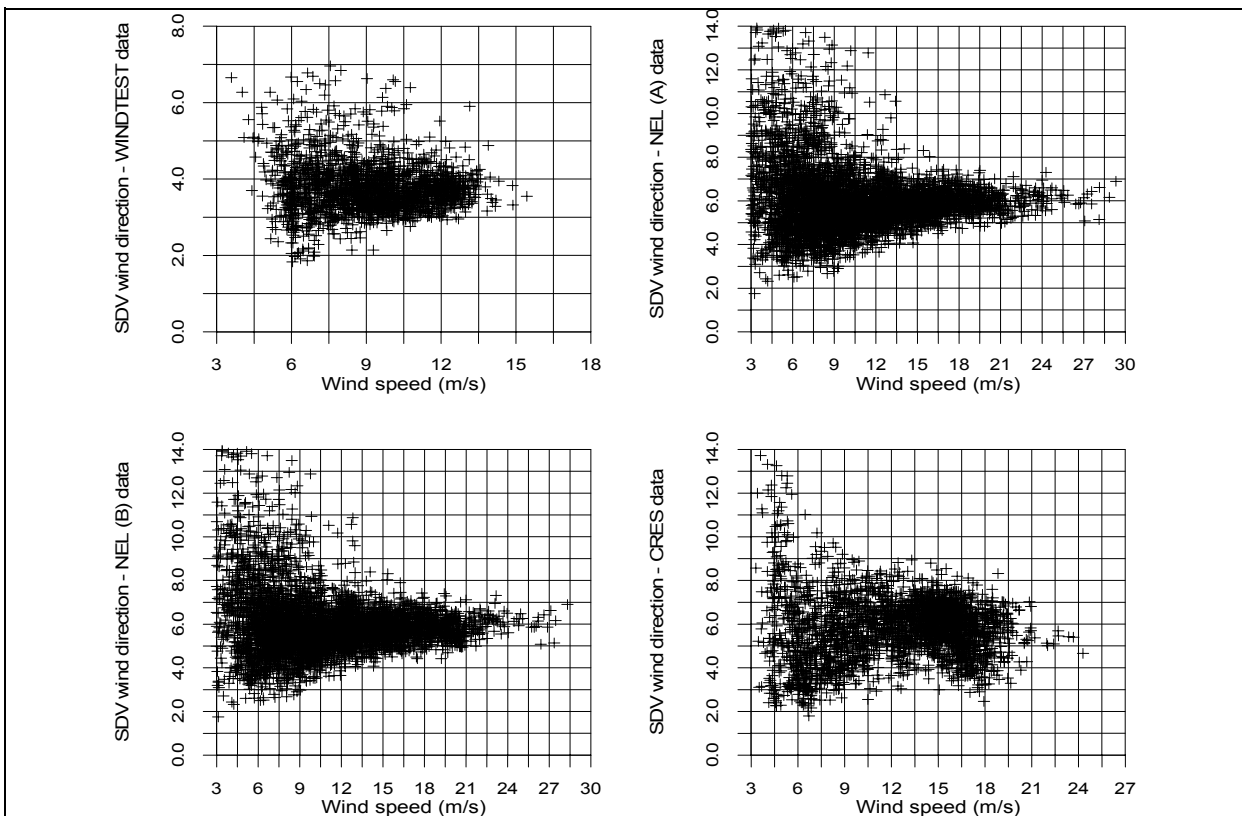


Figure 7.6 Standard deviation of wind direction at NTK500/37 sites.

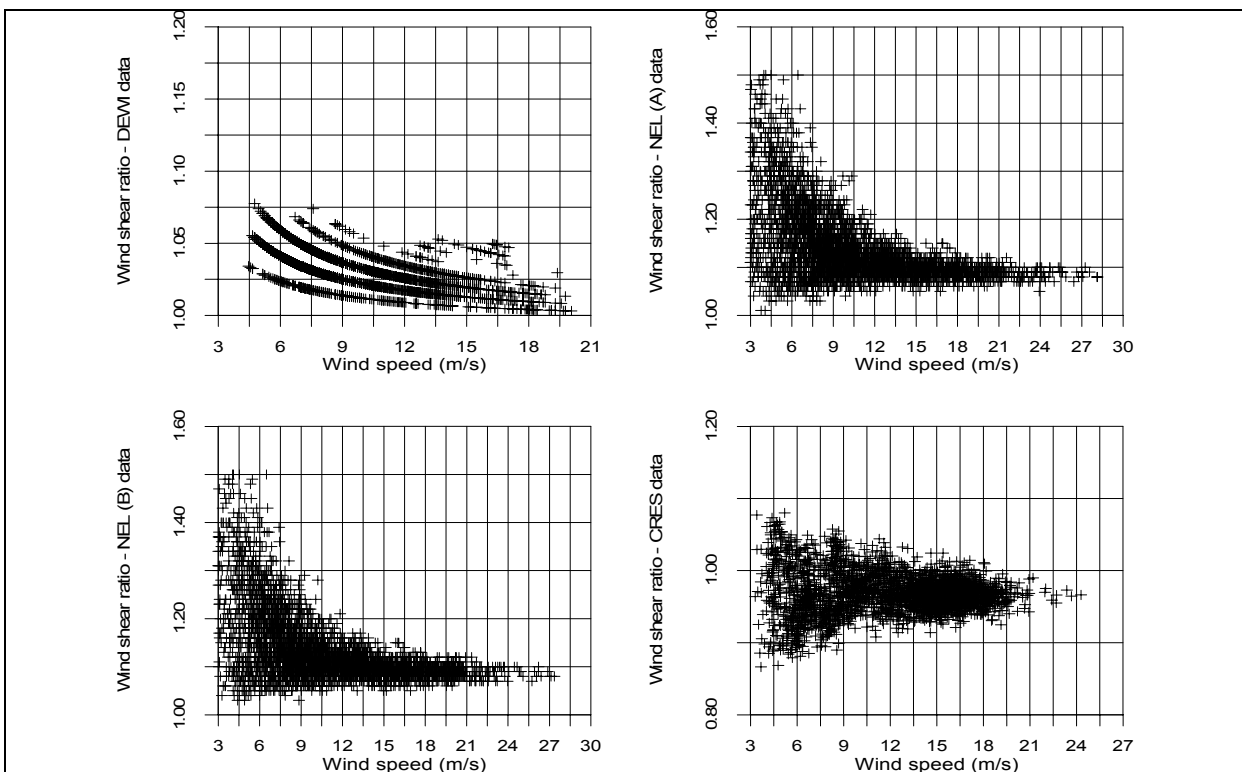


Figure 7.7 Wind shear ratio (U_{35m}/U_{18m}) at NTK500/37 sites.

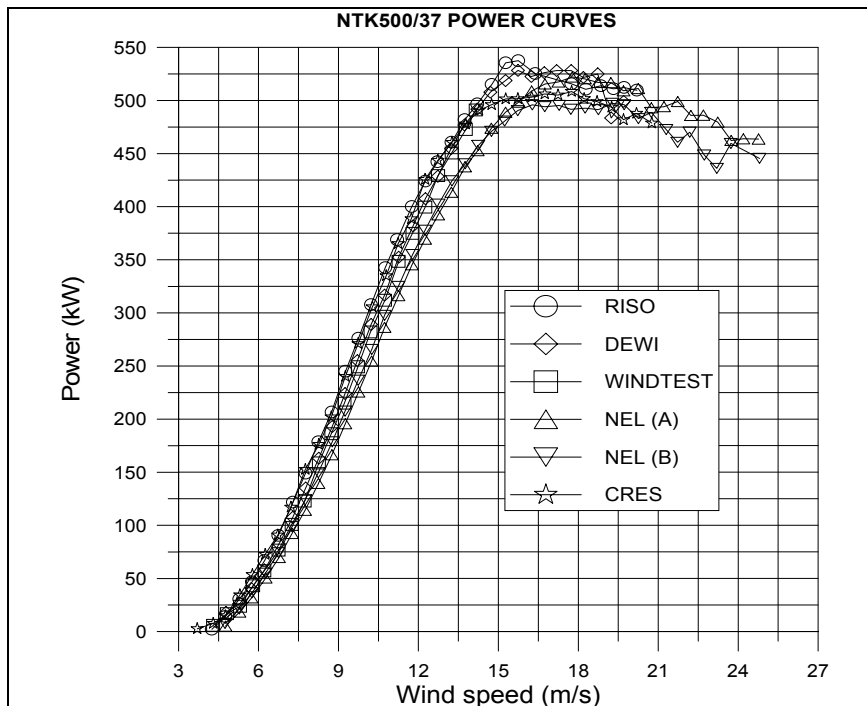


Figure 7.8 Power curves for NTK500/37 measured at different sites.

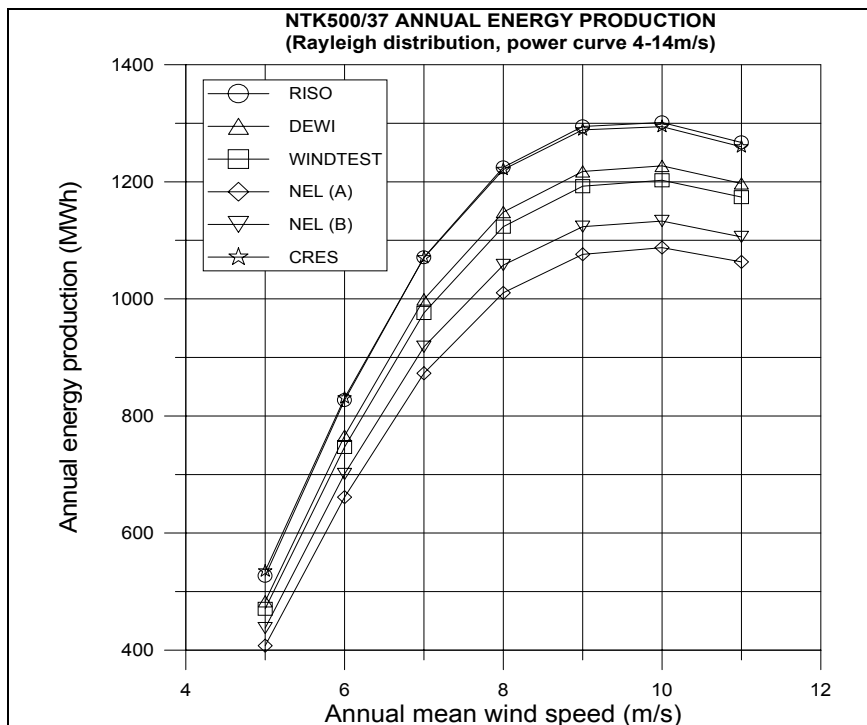


Figure 7.9 Annual energy production estimations for NTK500/37 for different sites.

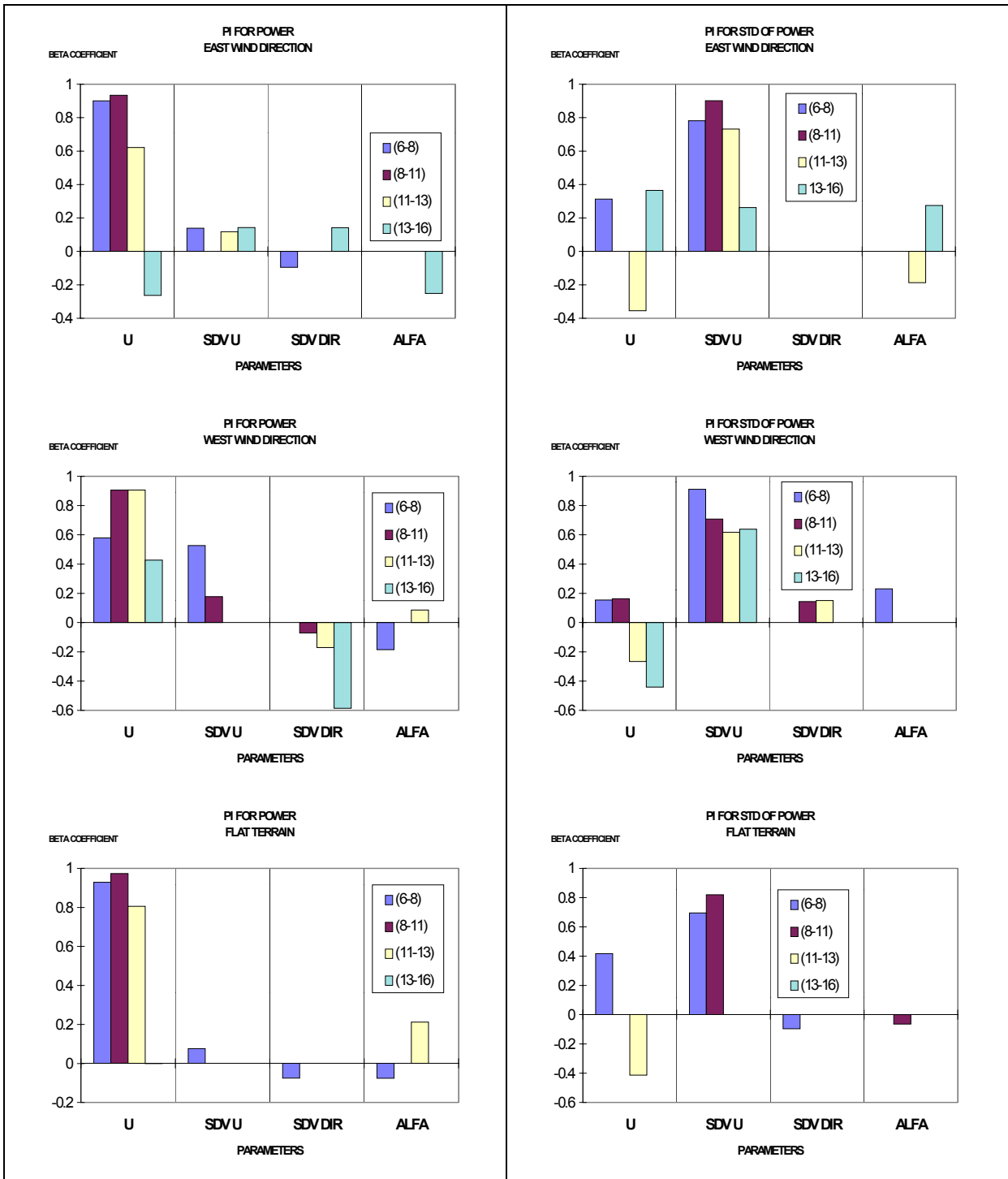


Figure 7.10 Beta coefficients for power mean.

Figure 7.11 Beta coefficients for power SDV.

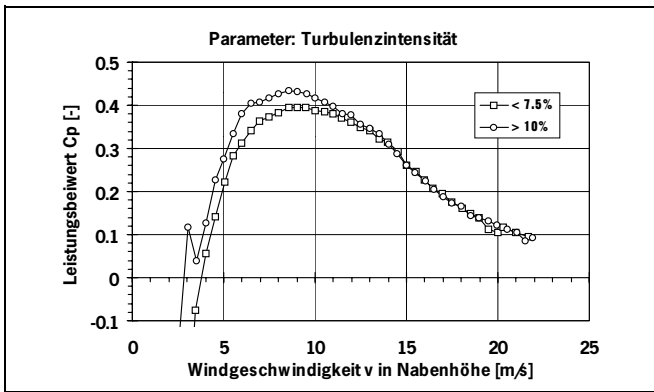


Figure 7.12 C_p -curves of the Aeolus II for different turbulence intensities.

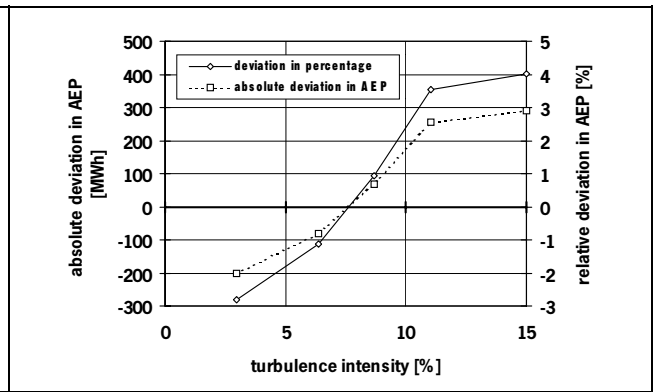


Figure 7.13 Deviations of calculated AEP's of the Aeolus II for different turbulence intensities from average value. Base: measured Weibull distribution at hub height of the Aeolus II.

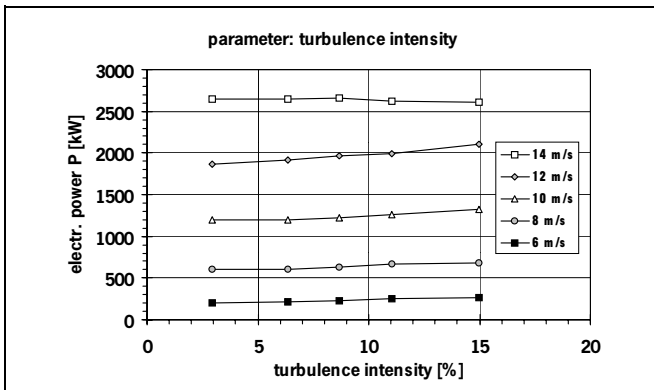


Figure 7.14 Electrical power of the Aeolus II as function of turbulence intensity for different wind speeds.

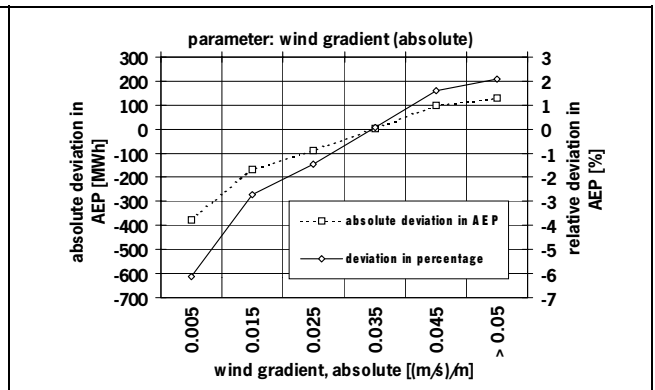


Figure 7.15 Deviations of calculated AEP's of the Aeolus II for different vertical wind gradients from average value. Base: Weibull distribution at hub height of the Aeolus II.

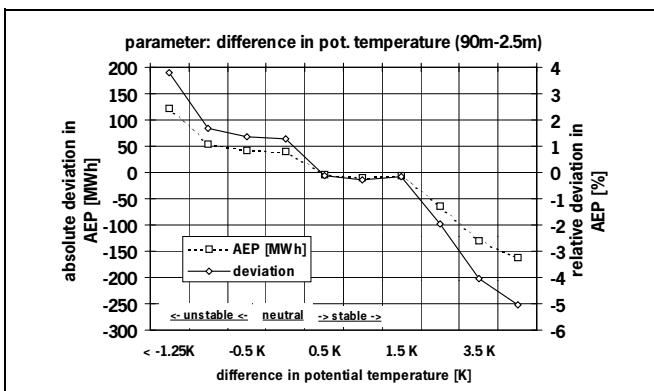


Figure 7.16 Deviations of calculated AEP's of the Aeolus II for different atmospheric stability from average value. Base: Weibull distribution at hub height of the Aeolus II.

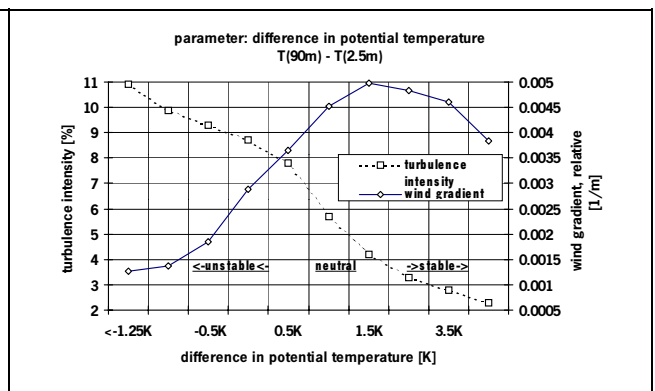


Figure 7.17 Turbulence intensity and wind gradient versus difference in potential temperature. Plotted is the relative vertical wind speed gradient, i. e. the wind speed gradient normalised by the average wind speed over the height.

8. ASSESSMENT OF POWER PERFORMANCE PRACTICES

8.1 Introduction

The assessment is focused on the recommendations of IEC 1400-12. Certain inefficiencies, related to site calibration and uncertainty estimation procedures, were identified.

The assessment of the existing standards and recommendations focused on the following issues:

- status of wind turbine power performance assessment and verification (existing standards, EU project results, contractual matters, market needs etc.)
 - review of characteristics of complex terrain and their effect to power performance
 - points that are not adequately described by the present IEC 1400-12 document, particularly in relation to complex terrain (site calibration, uncertainty estimation etc.)
 - recommendations for performing power performance assessment and verification in complex terrain.
- Only IEC 1400-12 is referenced. Other previously used documents (as IEA and ECN217) have no relevance anymore.

8.2 Review On The Characterization Of Complex Terrain

Complex terrain induces significant deterministic and stochastic variations of the wind field structure. The main characteristics are summarized below:

Deterministic characteristics:

- vertical wind shear is by no means following flat terrain descriptions (i.e. logarithmic)
- wind profile is clearly affected by upwind terrain features inducing local speed-up regions which vary with wind direction
- mean wind speed vector inclination follows the upwind terrain
- upwind terrain induces distortion effects in the transversal component in the vertical direction

Stochastic characteristics:

- significantly higher turbulence kinetic energy levels are encountered in complex sites
- the energy distribution mechanism differs from flat terrain; longitudinal component energy is transferred to the vertical
- increased values of turbulence ratios i.e. σ_v/σ_u , σ_w/σ_u
- spectral density distribution of wind speed deviates from flat terrain descriptions (i.e. low frequency spectral gap)
- smaller turbulence length scales are seen in complex sites
- non Gaussian character of wind speed distribution

The main effects that complex terrain induces to power performance are related to:

- uncertainty of wind speed measurement via cup anemometers
- uncertainty of determination of reference wind speed (i.e. large spatial variation of wind speed)
- effect of turbulence, shear deformations and wind speed distribution
- response of control systems

8.3 Critical Points On Existing Recommendations

The identified critical points regard the test site requirements, the characterization of the wind speed sensors, the influence of mean wind and turbulence structure, site calibration and measurement analysis.

8.3.1 Test site requirements

The document gives an assessment procedure of the test site in Annex A. In this annex upwind obstacles and upwind neighboring wind turbines at a distance of 20 equivalent diameters or more are considered as virtually non-existing. The literature review results (Van de Borg N., 1997) indicate that this could be non-conservative. Furthermore the annex does not take into account the hub height of the WTG under test, which seems to be unrealistic.

Moreover, the test site assessment procedure is quite sensitive to its way of application. Different procedures for mapping, slope computing or wind direction sectoring may lead to different assessment for the same site.

8.3.2 Characterization of wind speed sensors

The existing standard indicates that the measurement of the wind speed must be done by using cup anemometers with some specific characteristics. Cup anemometers present deficiencies that have an important influence on the measure of power curve in complex terrain. The deficiencies are related to the fact that the sensors can not detect some properties of the flow that have a proved influence on the power performance of the machine as well as that they misread the wind speed vector. All these deviations from the real measurement, can be included as uncertainties in power performance due to wind speed, once the response of the sensor is experimentally investigated and the level of the disturbing factors are determined in field. Yet, the magnitude of the resulting uncertainty indicates that the systematic usage of more accurate methods is justified.

In complex terrain significant variations of the wind inclination angle are commonly encountered. In the work of Glocker S. (WindTest), 1996a, 1997, an experimental research on the sensitivity of cup anemometers to inclined flow was performed. The results, shown in figures 8.1 and 8.2, revealed the significant deviation of the cup anemometer recording from the theoretical “cosine” response. From the results it is clear that the anemometers may be classified according to how well their measurements match the “cosine” or the constant response.

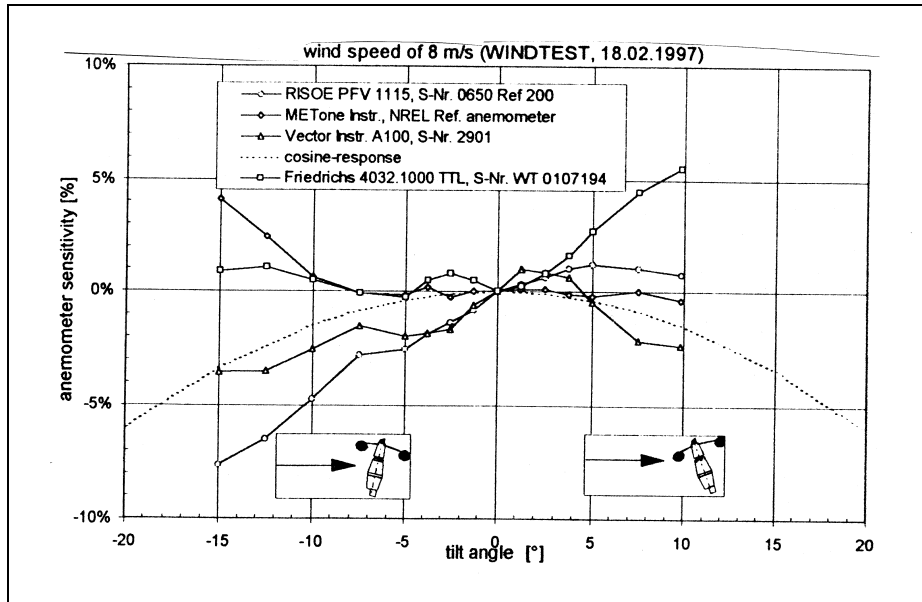


Figure 8.1 Sensitivity of cup anemometers to inclined flow.

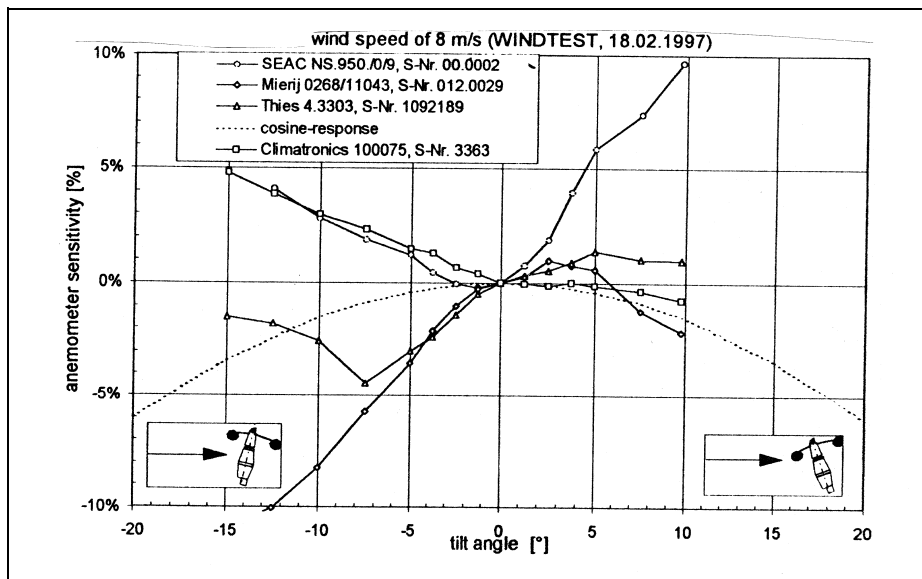


Figure 8.2 Sensitivity of cup anemometers to inclined flow.

8.3.3 Influence of wind mean and turbulent structure

The power curve is defined by the IEC-document as the relation between the undisturbed wind speed at the rotor center and the electrical power, corrected to standard air densities. The document does not take into account the influence of the following parameters:

Turbulence

The IEC-document prescribes the measurement of the turbulence but it does not recommend any corrections. As it was shown from the results of the parameter identification process the effect of turbulence can be identified and quantified. The magnitude of the effect depends on the wind turbine size and control type as well as on the specific site characteristics.

Wind shear

The power of a turbine is related to the wind speed structure all over the rotor plane rather than to the wind speed at the rotor center. For this reason wind shear is expected to influence the power curve of a turbine. As it was shown from the results of the parameter identification process the effect of wind shear can be identified and quantified. Again, the magnitude of the effect depends on the wind turbine size and control type as well as on the specific site characteristics.

Inclined flow

The IEC-document prescribes the use of a cup-anemometer and assumes implicitly that the response of a cup-anemometer and the response of a turbine to inclined flows are identical. Recent experimental research proved that the response of cup anemometers may deviate significantly from the expected “cosine” response”, thus inclined flows may degrade the power curve of a wind turbine.

Since these parameters are dependent on the complexity of the test site it is expected that the power curve of a wind turbine on a complex site may present significant variations from the power curve of the same type turbine operated in a different site (flat or complex).

8.3.4 Site calibration

Sites that do not fulfill the requirements of the IEC (1997) can be calibrated to determine the relation of the measured wind speed at the meteorological mast and the undisturbed wind speed at the turbine location. The experimental site calibration is described in the IEC (1997) in such a way that it allows for personal interpretation, which is also valid for the estimation of the uncertainties associated with the site calibration.

The document gives the possibility to perform site calibration by numerical modeling. The results from the literature survey suggest that numerical modeling may be not applied in a strict and systematic way. On the other hand, great research effort is being spend on the development and validation of numerical codes capable of dealing with atmospheric flows. Although the accuracy requirements of site calibration are high, it is considered that the use of numerical modeling will comprise an alternative to experimental calibration.

The major drawback of IEC (1997) is that no consideration of experimental site calibration in case of an erected wind turbine is made.

8.3.5 Response system

In power performance verification studies it is often found that a specific behavior, such as lower power output, double stall curves etc., of the wind turbine under test is not described properly from the wind measurements. The monitoring and reporting of certain operational characteristics, such as yaw error or

pitch angle, would facilitate the interpretation of those phenomena.

8.3.6 Measurement analysis

The normalization procedure described in IEC (1997) regards air density. The results of the parameter identification, in the cases where the air density variation was significant, are compatible with the theoretical formulae. On the other hand, it was also proved that the effects of wind deterministic and stochastic characteristics may present higher influence on the power curve determination. In that sense the comparison of different power curves, though referenced at the same air density, may inhibit uncertainty related to the above mentioned wind structure effects.

8.3.7 Contractual aspects

Current recommendation documents do not include references on contractual aspects. The primary point is related to the determination of feasible magnitudes of accuracy for assessment and verification purposes.

8.4 Conclusions

The assessment of the applicability of current recommendations for power performance of wind turbine in complex terrain is based on the characteristics of the wind structure as well as on the experience of performing power performance measurements in those sites. The critical points of IEC (1997) are related to test site requirements, characterization of the sensors, description of site calibration, identification of the influence of secondary effects as well as to the data analysis procedures.

9. PRACTICAL RECOMMENDATIONS

The practical recommendations for power performance assessment in complex terrain regard the identified inefficiencies of the IEC (1997). The recommendations regard test site requirements, characterization of the sensors, description of site calibration, identification of the influence of secondary effects as well as to the data analysis procedures.

9.1 Definition Of Site Complexity

The current regulations for site characterization should be kept, after the inclusion of recommendations for mapping scaling and resolution, in order to identify a flat site in a strict way. The usage of purely geographical characteristics is not feasible for classification of any terrain type that does not meet the above mentioned requirements, and consequently it should be considered as complex.

9.2 Selection And Characterisation Of Instrument Configuration

9.2.1 Definition of reference wind speed

Current knowledge does not justify the selection of other than the horizontal wind component referenced at hub height. Results from experiments regarding rotor averaged wind speed values do not justify, in terms of accuracy and cost efficiency, this practice. In cases of large wind turbines, extrapolation techniques may be utilized if their proved accuracy meets specified constraints.

9.2.2 Mean wind speed and turbulence structure measurements

It is recommended that wind measurements for power performance assessment and verification in complex terrain should be more sophisticated in terms of instrumentation and methodology. Complex terrain induced effects on power performance are associated to various deterministic and stochastic wind parameters that should be measured and documented.

The problems of mounting effects, steady state calibration and dynamic response are extensively investigated and guidance, supplementary to IEC (1997) can be given.

The use of 3D wind measurement devices is recommended either in order to produce directly the needed wind speed component or in order to magnify the wind inclination angle. Given the characteristics of the available cup and 3D measuring device characteristics the wind measurement strategy should be straightforward in terms of accuracy. The experimental research support that turbulence and wind shear affect the power curve. Given the fact that the above mentioned effect depends on the wind turbine and the site it is supported that the measuring campaign should include wind shear and turbulence measurements that are to be reported along with power curve. A typical setup that would allow for these measurements include cup anemometers at three heights and one 3D anemometer at hub height.

9.2.3 Wind turbine control system response

The measurement and reporting of specific operational characteristics of the wind turbine would allow the interpretation of power performance deviations from guaranteed curves.

9.3 Site Calibration

Site calibration should also be considered for the cases where the wind turbine under assessment or verification is already erected. It is supported that alternative site calibration procedures should be described and applied under specified ranges of accuracy. The latter should be the only restriction, thus allowing for future improvements.

The recommendations should clarify the following:

- in cases where the site calibration can be performed without the presence of the wind turbine the use of a temporary mast should be preferred
- procedure details, i.e. regression type, amount of data, sectoring procedure etc.
- flow distortion correction factors should be established for each wind direction sector, by regressing the wind data generated from the above procedure (on site measurements prior to the installation of wt or nacelle measurements and assumed wind velocity gradient), referring to the hub height wind speed at wind turbine location, on the measured wind data from the reference mast
- alternative site calibration of a test site may well be performed by placing an anemometer above the nacelle of the wind turbine at a separation distance carefully selected with respect to the nacelle cross section so that the disturbance caused by the presence of it does not exceed 1% of the free stream wind speed. This should be verified by means of physical or theoretical modeling of the flow field around the nacelle of the wt. Any additional corrections which are applied to account for the spatial and vertical variation of the wind speed measured at the wt location and the wind speed driving the wt have to be reported clearly and the associated uncertainty has to be taken into account
- the application of nacelle cup anemometer calibration, on a running wind turbine, is to be applied for identical wind turbines in sites that are in accordance with the calibration site in terms of wind field and turbulence structure
- the application of the numerical site calibration should include specific articles that will ensure that the physics of the wind field over complex terrain are properly simulated. The recommendations should refer to equation set to be solved, the turbulence model, the grid independent solution requirements as well as the validation of the tool against typical validation cases.

9.4 Normalization Procedure

The current normalization procedure, that regards air density, is conserved. It is recommended that for verification purposes the influence of wind parameters that affect power curve should be documented. A practice for quantifying the wind characteristics effect on a specific wind turbine power performance in a specific site is described as parameter identification procedure. From the existing analyses, the magnitude of the wind characteristics effect can be assessed and guidelines for specifying the ranges within which the power curve is to be estimated can be defined. Moreover, the results of the sensitivity analysis facilitate the normalization procedure that will result in a power curve defined at a specific condition. The specific condition point is defined according to the measurements, and represents the mean site condition.

9.5 Uncertainty Estimation Procedure

The uncertainty estimation procedures should be revised, keeping the already existing concepts, in order to account for the additionally needed measurements. Specifically, for the site calibration procedures, proper uncertainty estimation should be prescribed for all applied calibration formulae.

9.6 Power Curve Measurements Of Wind Farms

The technical background is adequate for establishing the framework of power performance assessment

and verification in complex terrain for a specific wind turbine, operating either as stand alone or within a wind farm. Although, recommendations for evaluation techniques for complete wind farms are under development and refinement basic guidelines are given (Hunter R., 1996).

Performance assessment of wind turbine systems may be required for a number of reasons. The interested party might be a manufacturer, a purchaser/developer, a financier or an academic, and in each case the scope of interest might be different. A financier for instance might wish to check that a complete development is performing as predicted by a technical assessor during a due diligence audit, a developer might wish to confirm that every machine in a farm is performing as wanted even when subject to wakes from other machines, whilst a manufacturer may wish to benchmark performance in clean wind so that a basis for setting warranties or for confirming design expectations is established.

The different requirements are not adequately covered by the existing IEC (1997) which deals only with performance of single machines in winds which are undisturbed by adjacent turbines.

The three levels of performance assessment are summarized in the following table:

	IEC 1400-12	Wind Farm Embedded Wind Turbines	Wind Farm
Application	Isolated, single turbine	Individual turbines within a wind farm	Complete wind farm
Nature of 'valid' wind during test	Undisturbed by adjacent machines or obstacles	All wind directions valid, including those during which machine is in the wake of others	All conditions valid, no rejection criteria
Loss mechanism included	None	None	Wake and on-site electrical losses are reflected in the measured performance
Typical purpose of test	Verification of design	Verification of product	Verification of system
Typical interested commissioning party	Manufacturer (supplier)	Developer (purchaser)	Financier

The aim is to define the real not idealized performance by including data from all operational conditions. Unlike the standard method for performance determination of individual wind turbines, the proposed method does not reject data when machines are in the wakes of others, when the wind comes from certain directions or when particular climatic effects are present. The method looks at the wind farm energy delivery at the point of common coupling with the grid therefore deals with energy production net of electrical losses in the in-site electrical collection system.

The procedure is of use to those who wish to determine or verify the overall performance of a wind farm rather than the performance of individual machines. A wind farm developer or financier for example may wish to apply it to verify modeling assumptions made at the wind farm planning stage.

The method does not specify accuracy requirements but does require a thorough uncertainty analysis to be conducted to supplement the results. In figure 9.1 the comparison methodology for real and expected wind farm performance is presented.

In a typical wind farm in complex terrain, wind speed, wind direction and density will have a spatial dependency and what is required will be the relevant values at a reference site. This reference position may not be one at which measurements are possible once the wind farm is operational, and correlation will have to be established prior to the development to allow appropriate corrections to be applied. In figure

9.2 the required setup is presented. Mast M1 is a permanent meteorological mast, probably some considerable distance away from the wind farm site which has a long term wind data archive available. Mast M2 is a meteorological mast which is erected at the wind turbine site near to erection of the wind farm. It has probably been used to establish a short term data archive, of say 6 months from which long term predictions of wind climate have been made using correlations with M1 and the long term data archive from M1. M2 is probably removed shortly before construction of the wind farm. Masts M3 and M4 (the supplementary masts) are deployed prior to construction of the wind farm specifically as part of the procedure described in this document, and data from them during this period are correlated with simultaneous data from mast M2. After construction of the wind farm M3 and M4 are left on site and are used to supply data from which estimates can be made of the wind speed, wind direction and air density that would have been present at M2 had the wind farm not been in place.

The function served by M2 in this example (i.e. providing measurement data for the reference position during the pre-construction, site calibration phase) may equally be served by either M3 or M4, if their positions are deemed suitable as reference in subsequent energy yield tests. In this example, two permanent masts M3 and M4 have been suggested. In practice any number of masts could be used, the requirement being that at all times at least one mast must experience winds which are undisturbed by the wind farm.

An analysis should be conducted for each supplementary meteorological mast position. Each analysis uses data from the relevant supplementary mast and data from the reference mast. The ten minute averaged wind speed data should be sorted according to ten degree sectors, the direction being as indicated by the data set from the reference mast.

The data set for each directional interval can be regarded as being complete if:

- the mean wind speed of all the collected data is representative of what is expected during the subsequent performance evaluation
- the statistical uncertainty of the inferred reference wind speed at this wind speed from the regression factors is below 2%.

A brief overview of the calibration of test site, regarding wind speed and wind direction data, is presented in figures 9.3 and 9.4.

The aim of the measurement procedure is to collect a database of sufficient quantity and quality to determine to the desired level of accuracy what the power production capabilities of the wind farm are for individual directional sectors. These power production capabilities are expressed in terms of the wind speeds experienced and the prevailing air densities. The collected database shall cover the complete operational range of the wind farm both in terms of wind speed and wind direction. This range should be specified prior to initiation of the test campaign.

For each directional sector, the ten minute mean wind speeds should be sorted according to the method of bins into 0.5m/s intervals (figure 9.5). Finally, annual energy production of the wind farm can be carried out if reference wind speed distributions are available for each directional sector and if the probability distribution of wind direction is also specified. For each sector the energy production should be derived according to the procedures contained in IEC (1997). The overall energy production should be estimated by summation of the individual directionally weighted contributions.

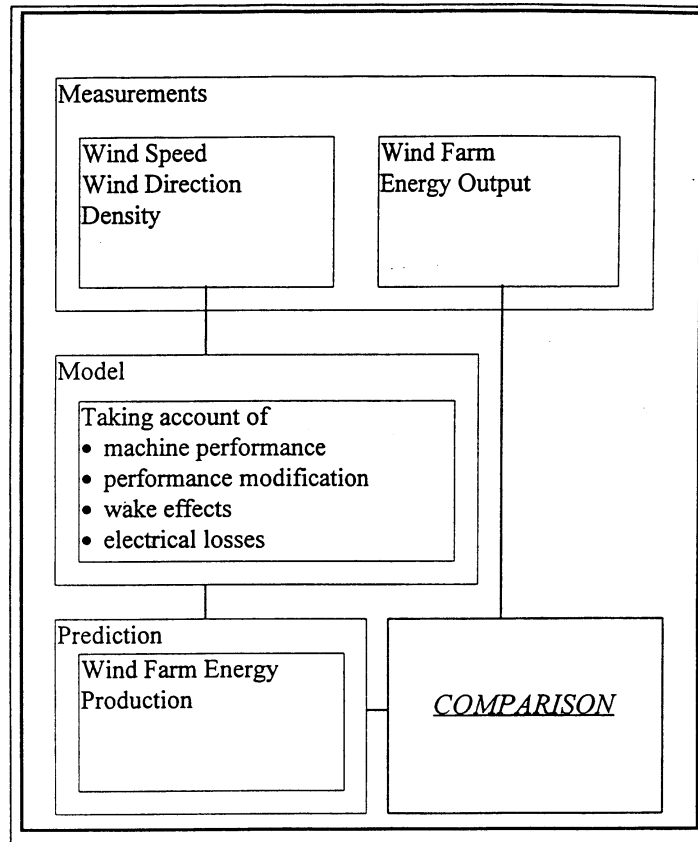


Figure 9.1 Comparison methodology for real and expected wind farm performance.

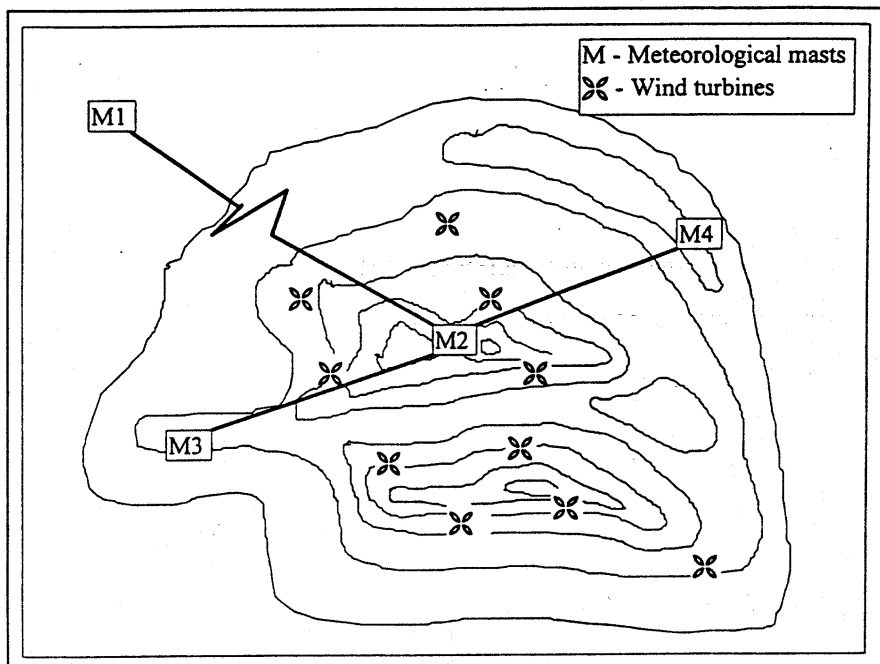


Figure 9.2 Correlation required for determining wind climate at a reference position.

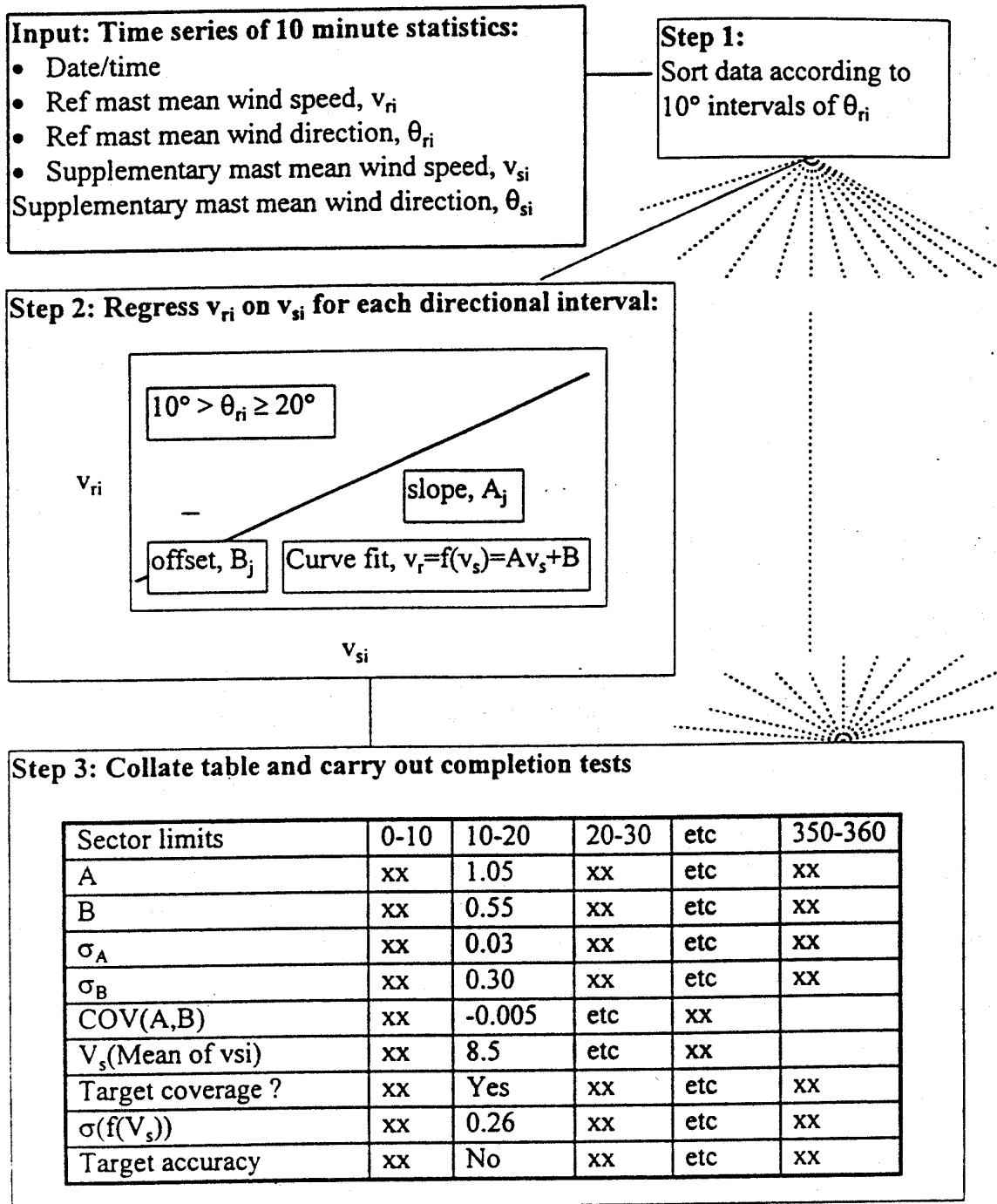


Figure 9.3 Analysis procedure for calibration of test site.

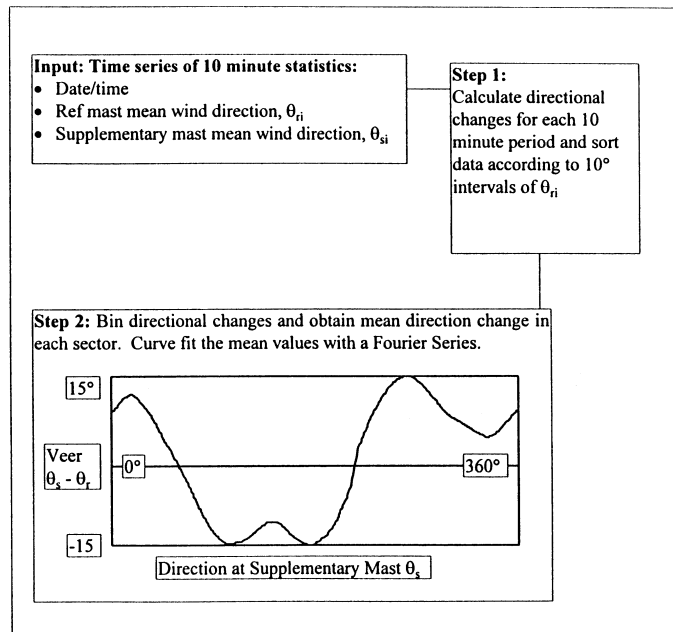


Figure 9.4 Analysis procedure for wind direction data.

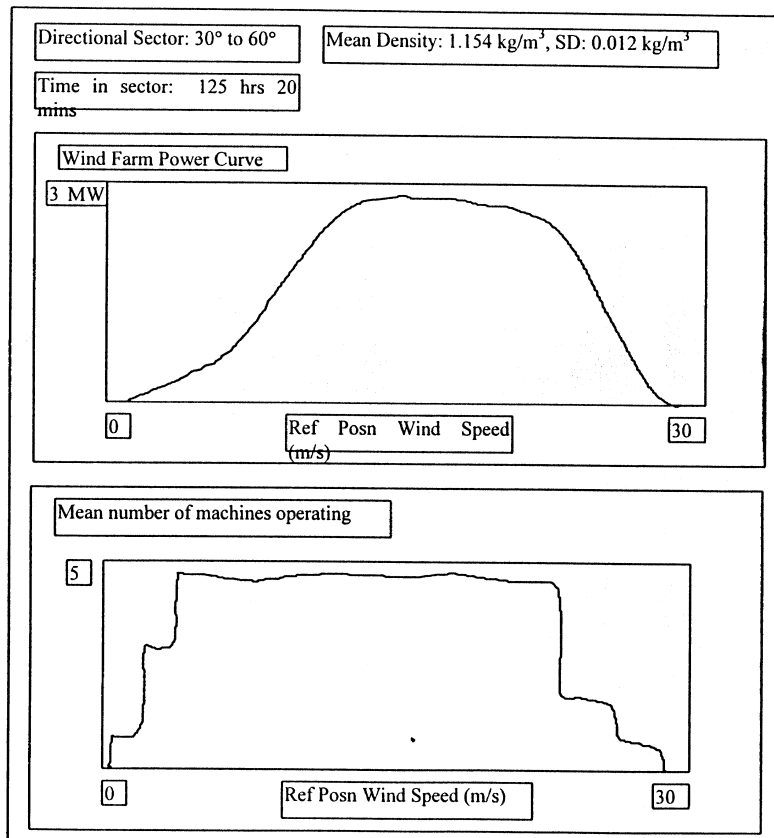


Figure 9.5 Wind farm directional power curve.

10. REFERENCES

- Albers A., Hinsch C., Gabriel J., Klug H., Ronsten G., Simonssen B. (1996): “Comparison of power performance and noise between AEOLUS II and NASUDDEN II”, Proc. EWEC’96, Goteborg Sweden, pp.804.
- Alm L.K., Nygaard T.A. (1993): “Flow over complex terrain estimated by a general purpose Navier-Stokes solver”, Proc. EWEC’93, Travemunde, Germany, pp.591.
- Antoniou I., Pedersen T.F. (1997): “Nacelle anemometer on a 1MW wind turbine”, RISO-R-941(EN).
- Antoniou I., Petersen S.M. (1995): “Wind Turbine Test: Structural Loads ELKRAFT 1MW (Stall Regulated Operation)”, Risø-I-865(EN).
- Barnard J.C. (1990): “An evaluation of three models designed for siting wind turbines in areas of complex terrain”, Report PNL—7357, 6/90.
- Bergeles G. C. (1985): “Numerical calculation of turbulent flow around two dimensional hills”, J. Wind Eng. and Ind. Aerod., Vol.21, pp.307-320.
- Bergstrom H. (1995): “Wind measurements at Lyse wind power station”, Wind Energy report WE95:2, Department of Meteorology, Uppsala University.
- Botta G, Castagna R., Borghetti I., Mantegna D. (1992): “Wind analysis on complex terrain: The case of Acqua Spruzza”, J. of Wind Eng. and Ind. Aero., v.39, pp.357-366.
- Burger, Franke J., Tetzlaff G. (1988): “Wind measurements in the wake of obstacles”, EWEC’88, Herning.
- Chien H., Meroney R.N., Sandborn V.A. (1980): “Sites for wind power installations: Physical modeling of the wind field over Kahuku Point, Oahu, Hawaii”, Wind Energy Systems 1980, pp.75-90.
- Christensen C.J., Dragt J.B. (1986): “Accuracy of power curve measurements”, RISO-M-2632, November.
- Courtney M., Hoestrup M., Jensen I. (1990): “The Hjardem escarpment experiment”, EWEC’90, Madrid, pp.71-75.
- Croba D. et al. (1996): “Improving techniques for statistical and physical modelling of wind resources in complex terrain”, Proc. ECWEC’96, Goteborg, Sweden, pp.514.
- Cuerva A. (1996a): “Multivariable analysis of power in complex terrain (MADE AE-30 wind turbine at Monteahumada wind farm at Tarifa)”, CIEMAT/43E11-96/014.
- Cuerva A. (1996b): “Multivariable analysis of power in flat terrain (MADE AE-30 wind turbine at Cañada de la Barca wind farm at Fuerteventura)”, CIEMAT/43E11-96/013.
- Cuerva A. (1996c): “Studies on the power output of a MADE AE-30 operating on complex terrain. Annual energy production estimation and multivariable analysis”, CIEMAT/43E22-96/001.
- Cuerva A. (1997): “Some preliminary results on uncertainties in AEP for the same machine operating in complex and flat terrain (EWTS-II.IV 3rd meeting)”, CIEMAT/43E22/, 2/97.
- Cuerva A., Benzdenejnykh N., Perales J.M., Sanz A. (1997): “Assessment of performances of ultrasonic anemometers as one step ahead in wind measurements of energy production of a wind turbine”, EWEC’97, Dublin.
- Curvers A., Pedersen T.F. (1989): “Recommendations for a European Wind Turbine Standard on Performance Determination, ECN-217, 7/89.
- Dahlberg J. (1996): “Mast, boom and velocity gradient effects on cup anemometers”, FFA report FFAP-V-009, 2/96.
- Dekker J., de Groot C.M. (1986): “Measurement program for the 45m horizontal axis wind turbine”, ECN-86-149 (EWEC’86).
- Elliot D.L. (1990): “Effects of wind shear and turbulence on wind turbine power curves”, European Community Wind Energy Conference ‘90, Madrid, pp.79 - 83.

- Emeis S., Frandsen S. (1993): “Reduction of horizontal wind speed in a boundary layer with obstacles”, *Boundary Layer Meteorology*, v.64, pp.297-305.
- EWTS (1996a): “Wind speed measurement and site calibration”, JOU2-CT93-0387 Final report, vol.5.
- EWTS (1996b): “Electrical power quality measurement procedure”, JOU2-CT93-0387 Final report, vol.7.
- Foussekis D. (1996): “Characterization of WINCON 110XT wind turbine operating at CRES test station”, MOUNTURB report, CRES.
- Frandsen S. (1992): “On the wind speed reduction in the center of large clusters of wind turbines”, *J. of Wind Eng. and Ind. Aero.*, v.39, pp.211-265.
- Frandsen S. (1994): “Uncertainties on power performance testing related to obstacles around test site”, *Windpower’94 Minneapolis*, pp.523 - 531.
- Frank H.P., Landberg L. (1996): “Modeling the wind climate over Ireland”, *Proc.ECWEC’96, Goteborg, Sweden*, pp.631.
- Fulsang P. (1996): “Separationsmønsteret for et LM19.1 Blad”, *Resultatblad AED_RB_2, Risø*.
- Glinou G. (1996): “Wind flow modeling: A literature review”, CRES internal report.
- Glinou G., Morfiadakis E., Koulouvari M. (1996): “Analysis of full scale measurements for the investigation of the turbulence structure acting on a rotor disk over complex terrain”, *Proc. EWEC’96, Goteborg Sweden*, pp.639.
- Glocker S. (1996a): “Sensitivity of cup anemometer to tilt angle, results and consequences”, Presentation at MEASNET expert group meeting on 2-3/12/96, WINDTEST report.
- Glocker S. (1996b): “Summary report on power performance of Nordtank NT500/37 and Vestas V27 data”, EWTS-II.IV WINDTEST technical note.
- Glocker S. (1997): “Sensitivity to tilt angle of the reference anemometers of the MEASNET Institutes”, Presentation at MEASNET expert group meeting on 6-7/3/97, WINDTEST report.
- Hansen M., Pedersen M.B. (1990): “Influence of the meteorology mast on a cup anemometer”, Technical University of Denmark, internal document.
- Hassan U., Lindley D. (1982): “Preliminary results of a survey of the Burgar Hill, Orkney, wind turbine site”, *Wind Energy Systems 1982, Stockholm*, pp.217-227.
- Hauf T., Hauf G. (1982): “The turbulent wind flow over an embankment”, *Boundary Layer Meteorology*, v.24, pp.357-369.
- Hinsch C., Westermann D. (1996a): “Comparison of different power curve measurements at different sites through AEP estimation for NTK500/37 and V27”, EWTS-II/4 Technical note, DEWI report, 8/96.
- Hinsch C., Westermann D. (1996b): “Power Performance Measurement by means of an anemometer located on the nacelle”, DEWI Technical Note 19/8/96.
- Hojstrup J. et al. (1996): “Wind resources in the Baltic Sea”, *Proc. ECWEC 96* “, Goteborg, Sweden, pp.510.
- Hunter R. (1996): “Outline procedure for performance evaluation of wind farms”, IEC TC88 WG6 report, 5/96.
- Hunter R. (1996a): “Measurement summary on Nordtank NTK500/37 (Turbine A) power curve measurement”, NEL report, version 3, 12/96.
- Hunter R. (1996b): “Measurement summary on Nordtank NTK500/37 (Turbine B) power curve measurement”, NEL report, version 2, 12/96.
- Hunter R. (1996c): “Parameter identification on Nordtank NTK500/37 power performance”, NEL technical note, 12/96.
- IEA (1990): “Recommended Practices for Wind Turbine Testing and Evaluation, 1. Power Performance Testing”, 2nd Edition, Risø National Laboratory.
- IEC (1997): “Wind turbine generator systems. Part 12: Wind turbine power performance testing”, 88/FDIS, 1400-12 Edition 1.
- Jackson P.S., Hunt J.C.R. (1975): “Turbulent wind flow over a low hill” *Q.J.R. Meteorol. Soc.*, vol.101, pp.929-955.
- Jamieson N., Anderson C.G. (1988): “Power performance measurement on the HOWDEN 33m wind turbine”, *Wind Energy Conversion ‘88 (BWEA, London, 22-24 March 1988)*, pp.75-79.

- Kleinbaum K., Kupper L. (1985): "Applied regression analysis and other multivariate methods", PWS-KENT Publishing Company, Boston.
- Kline J.B., Mikhail A. (1993): "Recent experience with the NOABL model in highly complex terrain", Windpower'93, San Francisco, pp.226-233.
- Klug H. et al. (1996): "Wind speed measurement and site calibration", Final report European Wind Turbine Standards, JOULE-II project J0U2- CT93-0387, 2/96.
- Lalas D.P. et al. (1994): "A hybrid micrositing model for wind flow simulation over complex topographies", Proc. ECWEC'94, Thessaloniki, Greece.
- Landberg L. (1996): "Implementing prediction of power from wind farms at Utilities", Proc.1996, Goteborg, Sweden, pp.592, EWTS II-V reference 35.
- Larsen A., Oort H. (1989): "Wind turbine wake interference: A validation study", Report DMI--89836.
- Liu et al. (1987): "Field investigation of a wake structure downwind of a VAWT in a wind farm array", Flow Research Report no.427, 10/87.
- Magnusson M. (1994): "Full scale wake measurements at Alsvik wind farm", EWEC'94, pp.472-477.
- Mason P.J., King J.C. (1985): "Measurements and prediction of flow and turbulence over an isolated hill of moderate slope", Q.J.R. Meteorol. Soc., vol.111, pp.617-640.
- Mason P.J., Sykes R.I. (1979), Q.J.R Meteorol. Soc., vol.105, pp.383-395.
- McCarthy E., Meroney R., Neff D.E. (1993): "Elevation and vegetation considerations on wind power availability: A wind tunnel study", Windpower'93, San Francisco, pp.213-217.
- Mengelkamp H.T. et al. (1996): "Regional and local wind climatologies over heterogeneous terrain", Proc. ECWEC'96, Goteborg, Sweden, pp.506.
- Morfiadakis E. et al. (1997): "Assessment of power performance in complex terrain", EWEC'97, Dublin, 10/97.
- Morfiadakis E., Glinou G., Stefanatos N. (1994a): "Power performance evaluation of a wind turbine operating in a complex terrain wind farm", Proc. EWEC'94, Thessaloniki Greece, pp.906.
- Morfiadakis E., Mouzakis F. (1996b): "Nacelle cup anemometry for WINCON 110XT operating at CRES test site", CRES report, 2/96.
- Morfiadakis E., Mouzakis F. (1996c): "Power performance of NORDTANK NT500 operating at Toplou site", CRES report.
- Morfiadakis E., Mouzakis F. (1996d): "Power performance of VESTAS V27 operating at Andros site", CRES report.
- Morfiadakis E., Mouzakis F. (1996e): "Power performance of WINCON 110 XT operating at CRES site", CRES report.
- Morfiadakis E., Mouzakis F. (1997a): "Power performance parameter identification for NTK500/37", CRES report, 2/97.
- Morfiadakis E., Mouzakis F. (1997b): "Toplou site calibration assessment", CRES report, 2/97.
- Morfiadakis E., Mouzakis F., Dellaportas P. (1996a): "Parameter identification of fatigue loading of a wind turbine operating in complex terrain", CRES report.
- Mouzakis F., Bergeles G. (1991): "Numerical prediction of turbulent flow over a two-dimensional ridge", Int. J. for Num. Meth. in Fluids, v.12, pp.287-296.
- Mouzakis F., Morfiadakis E. (1996): "Parameter identification practice", CRES report.
- Mouzakis F., Stefanatos N., Glinou G. (1997): "Assessment of site calibration techniques for complex terrain", EWEC'97, Dublin, 10/97.
- Nielsen M.A. (1994): "Performance testing in inhomogeneous terrain", EWEC'94 Thessaloniki, pp.911-915.
- Nierenberg A. (1993): "Detailed measurements on the effects of trees on wind speed, energy, vertical wind shear and turbulence", Windpower.
- Pearse J.R. (1982): "Wind flow over conical hills in a simulated atmospheric boundary layer", J. of Wind Eng. and Ind. Aero., v.10, pp.303-313.

- Pedersen M.B., Hansen K., Oye S., Brinch M., Fabian O. (1991): "Some experimental investigations on the influence of the mounting arrangements on the accuracy of cup anemometer measurements", EWEC'91.
- Pedersen T. (1993a): "A parametric study on terrain effects in relation to power performance testing", RISO-I-728(EN), 9/93.
- Pedersen T. (1993b): "Recommendation for Wind Turbine Power Curve Measurements", (ed.), Risø-I-745(EN), 11/93.
- Pedersen T. (1994): "Trends in power performance measurement standards", Windpower'94, Minneapolis.
- Pedersen T., Petersen S.M., Volund P. (1996): "Description and measurements of the wind that drives the power performance and mean loads of wind turbines", EWEC'96.
- Petersen E.L. et al. (1996): "Measurements and modelling in complex terrain" .
- Petersen S.M. (1993): "Vindmolleafproving: Nordtank NTK 500/37 Maling af effektkurve", RISO-I-731(DA), 9/93.
- Petersen S.M. (1994a): "Konceptundersøgelse: Nordtank NTK 500/41 Maling af effektkurve", RISO-I-799(DA), 12/94.
- Petersen S.M. (1994b): "Konceptundersøgelse NORDTANK NTK500/41, Strukturelle laster - Tårnbøjning", Risø-I-786(DA).
- Petersen S.M. (1994c): "Vindmolleafproving: Vestas V39 Maling af effektkurve", RISO-I-754(DA), 2/94.
- Petersen S.M., Pedersen T.F., Paulsen U.S., Morfiadakis E., Koulouvari M., Mouzakis F. (1996a): "Comparison of performance and load characteristics of two V27-225 operating in different complex terrain sites", Proc. EWEC'96, Goteborg Sweden, pp.995.
- Petersen S.M., Pedersen T.F., Paulsen U.S., Morfiadakis E., Koulouvari M., Mouzakis F. (1996b): "Comparison of performance and load characteristics of two V27-225kW operating in different complex terrain sites", EW EC'96.
- Riddle A., Warren J., Hoskin R., Musgrove P., Lindley D. (1996): "The influence of complex terrain on the performance of windfarms", EWEC'96, Goteborg, pp.1077.
- Ronsten G., Dahlberg J. (1996): "Calibration of anemometers in FFA-L2 wind tunnel including twin calibration and tests of sensitivity to wind velocity gradient and tilt", FFA TN 1996-51.
- Sandstrom S. (1994): "WA^SP A comparison between model and measurements", EWEC'94.
- Sheinman O., Rose A. (1992): "A dynamic model of the influence of turbulence on the power output of a wind turbine", J. of Wind Eng. and Ind. Aero., vol.39, pp.329 - 341.
- Sherman C. (1978): "A mass-consistent model for wind fields in complex terrain", J. Appl. Meteorol., vol.17, pp.312.
- Sierputowski, Ostrowski, Cenedese (1995): "Experimental study of wind flow over the model of a valley", J. of Wind Eng. and Ind. Aero., v.57, pp.127-136.
- Slater J.T.D. (1996): "Power Performance Measurement Techniques for Wind Farms", , RES Document 500/RES/1117.
- Smedman A., Bergstrom H., Hogstrom U. (1996): "Measured and modeled local wind field in mountainous terrain", EWEC'96.
- Taylor G.I. (1991): "Wake measurements over complex terrain", BWEA '91, Swansea.
- Taylor P.A. (1977): "Numerical studies of neutrally stratified planetary boundary layer flow above gentle topography. Two dimensional cases", Bound. Layer Meteorol., vol.12, pp.47-60.
- Tombrou M. et al. (1993): "Tests of prediction effectiveness of wind energy computer models in complex terrain", Proc. ECWEC'93, Travemunde, Germany, pp599.
- Traci R.M. (1977): "Development of a wind energy site selection methodology", US Dept. of Energy Rept. RLO/2440-11, pp.205.
- Troen I., Petersen L. (1989): "European wind atlas", ISBN 87-550-1428-8.
- Tryfonopoulos D.A. et al. (1989), Wind Engineering, vol.13, pp.324-337, 1989.

- Van der Borg N. (1996): “Inventory of existing information on the issue of power performance measurements in complex terrain”, ECN-C—96-083, 10/96.
- Van der Snoek L. (1990): “Wake effects in wind farms and behind obstacles”, ECN report.
- Veenhuizen S.D., Lin J.T. (1987): “Wind turbine micro-siting status”, Windpower’87.
- Vermeulen F. (1982): “A wind tunnel study of the flow field over the “SWECS” test site at ECN Petten”, ECN-report 82-014908, 11/82.
- Vermeulen H. McLean I.R., Flay R. (1982), Wind Energy Systems ‘82, Stockholm, pp.195-216.
- Wade J.E., Walker S.N. (1987): “The effects of local terrain on wind characteristics and turbine performance”, Windpower’87, pp.398 - 401.
- Walmsley J.L. et al. (1986), Bound. Layer Meteorol., vol.36, pp.157-186.
- Walmsley J.L., Troen I., Lalas D., Mason N. (1989): “An inter-comparison of models for wind flow in complex terrain and data from the Blashaval experiment”, EWEC’89.
- Watson R. (1994): “Wind measurement and modeling in the republic of Ireland”, EWEC’94.
- Wendel L., Barnard J.C., Morris V.R. (1994): “A proposed wind measurement and analysis approach for evaluating a prospective wind plant site”, Windpower’94.
- Weng W., Walmsley J.L., Karpik R.S., Xu D., Taylor P.A., Ayotte K., Salmon J.R. (1994): “Application of the MSFD and NLMSFD models to airflow over Askervein Hill”, EWEC ‘94.

11. ACKNOWLEDGEMENTS

The participants of the project are indebted to DGXII for cofunding the project, and to the WT manufacturers and operators for their help during the WT measurements. CRES is indebted to the GSRT for cofunding the project and to PPC/DEME for the provision of its WTs for the Greek measurement programs. The coordinator expresses his gratitude to the institutions that participated in this project and the project leaders and to all members of the scientific teams participating for their commitment to the project and their invaluable contributions.

EUROPEAN WIND TURBINE STANDARDS II
PART 5
SITE EVALUATION

Alan Derrick (Editor)
Ioannis Antoniou
Arno Brand
Sten Frandsen
Georgia Glinou
Thomas Pahlke
Ignacio Marti Pérez
Ian Ravey
Bärbel Schwenk

NEL
RISØ National Laboratory
ECN
RISØ National Laboratory
CRES
DEWI
CIEMAT
NEL
DEWI

CONTENTS OF PART 5

1. INTRODUCTION	5
1.1 What is Meant by “Site Assessment/Evaluation”	5
1.2 Relationship to Standards	5
2. SURVEY OF EUROPEAN CONSULTANTS	7
2.1 Purpose of Survey	7
2.2 Implementation	7
2.3 Results of Assessment Technique Survey	7
2.3.1 Denmark	7
2.3.2 Germany	8
2.3.3 Greece	8
2.3.4 Netherlands	9
2.3.5 Spain	9
2.3.6 United Kingdom	10
2.3.7 Overall	11
2.4 Results of Input Data Survey	12
2.4.1 Denmark	12
2.4.2 Germany	13
2.4.3 Greece	13
2.4.4 Netherlands	13
2.4.5 Spain	13
2.4.6 United Kingdom	14
2.4.7 Overall	14
3. MEAN WIND SPEED ASSESSMENT	15
3.1 Wind Flow Modelling	15
3.1.1 Technology Status Review	15
3.1.2 WAsP	17
3.2 Measurement based techniques	22
3.2.1 Status Review	22
3.2.2 MCP	24
3.3 Assessment of Uncertainty	25
3.3.1 Definition of extended (long-distance) site calibration	26
3.3.2 Test parameters	26
3.3.3 Uncertainty components	27
3.3.4 Additional Uncertainties due to Long-Term Climate Variability	30
3.3.5 Conclusions on Uncertainty	33
4. OTHER PARAMETERS	34
4.1 Reference Wind Speed	34
4.1.1 Description of Parameter	34
4.1.2 Methods of Assessment	34
4.1.3 Instrument requirements	38
4.1.4 Further Reading	38

4.2 Reference Turbulence Intensity	39
4.2.1 Description of Parameter	39
4.2.2 Methods of Assessment	39
4.2.3 Measurement Requirements	41
4.2.4 Further Reading	43
4.3 Wind Speed Distribution	43
4.3.1 Description of Parameter	43
4.3.2 Methods of Assessment	44
4.3.3 Measurement Requirements	50
4.3.4 Further Reading	51
4.4 Normal Wind Profile	51
4.4.1 Description of Parameter	51
4.4.2 Methods of Assessment	52
4.4.3 Measurement Requirements	53
4.4.4 Method to Determine which Profile Gives the Higher Loading	53
4.4.5 Further Reading	55
4.5 Wind Direction Distribution	55
4.6 “Other” Parameters	55
4.6.1 Overview	55
4.6.2 Turbulence Length Scale	56
4.6.3 Coherence	57
4.6.4 Standard Deviation Ratios	57
4.6.5 Negative Gust	58
4.6.6 Instrumentation Requirements	59
4.6.7 Special Instrumentation: The Ultrasonic Anemometer	59
4.7 Clarification of Standard	62
5. REFERENCES	64
Appendix A Assessment Of Other Parameters - Mathematical Details	68
Appendix B Use Of Sonic Anemometer	72

1. INTRODUCTION

1.1 What is Meant by “Site Assessment/Evaluation”

Over the ten to fifteen years that commercial wind farm development has been a reality throughout Europe, the term “site assessment” or “site evaluation” has generally tended to be associated with the prediction of the energy yield potential of a site prior to the installation of wind turbines. Hence, historically, the evaluation has primarily been restricted to the assessment of the site annual average wind speed and wind speed distribution. The method and thoroughness of the assessment has varied from country to country depending to a certain extent on the requirements of national subsidy schemes and the uncertainty inherent in the evaluation due for instance to the nature of the terrain and wind regime. However, as the economic and design margins on wind turbines and wind farms become tighter, the need to quantify and minimise risk has become more important. The site evaluation is at the core of this risk evaluation process and consequently the site evaluation needs to consider more than just energy yield potential if other aspects such as turbine integrity are to be assessed.

1.2 Relationship to Standards

Whether or not the prediction of the annual energy yield potential for a proposed wind farm site is a valid subject for standards is a debatable point, however the safety, structural integrity and fitness-for-purpose issues associated with specifying or designing specific wind turbines for a site most certainly are important subjects for standards to address. In that context, the IEC has recently revised their wind turbine safety standard [1] to (amongst other things) consider such issues more thoroughly.

In the terminology of the original IEC standard [1], the site evaluation contributes to the specification of the external conditions. The external conditions are categorised into four pre-defined wind turbine classes each of which is characterised by three basic parameters. A class I turbine is designed for more severe external conditions than a class II turbine and so on down to class IV (an additional special class exists for external conditions specified by the designer). The three basic parameters defining the external conditions in the original version of the standard were:

- reference (extreme) wind speed (V_{ref})
- annual average wind speed (V_{ave})
- annual average turbulence intensity (I_{ave})

Of those parameters, a minimal site evaluation for the purpose of determining energy yield potential would only yield information on the annual average wind speed. The onus to provide a more comprehensive site evaluation is inherent in the following statement extracted from the standard [1]:

“It is the responsibility of the project engineer or the equipment owner to verify that conditions at the actual installation site, including the increased turbulence within turbine arrays, are more benign than those prescribed for the given turbine class”.

The three basic parameters are used to derive a number of additional external condition parameters which allow the structure of the wind to be defined in more detail. These derived parameters may also form part of a site evaluation. However, no guidance is given in the standard on how this or any other part of the site evaluation should be accomplished.

A greater emphasis has been placed on site evaluation in the latest edition of the IEC safety standard [2] with a complete chapter (Chapter 7 Assessment of External Conditions) now added. The following statement introduces that chapter,

“It shall be assessed that the environmental, electrical and soil properties are more benign than those assumed for the design of the WTGS. If the site conditions are more severe than those assumed, the engineering integrity shall be demonstrated”.

As a minimum the three basic parameters have to be assessed by measurement, long term records or local codes or standards. The three basic parameters in this edition [2] of the standard are:

- reference (extreme) wind speed (V_{ref})
- annual average wind speed (V_{ave})
- characteristic turbulence intensity ($I_{1.5}$)

Note that the turbulence intensity parameter is different to that specified in the earlier version of the standard.

The following additional recommendations are made in the standard:

- at least 6 months of reliable data shall be used for the evaluation.
- where seasonal effects on wind conditions are significant, the monitoring period shall include these effects.
- particular care shall be taken in evaluating the characteristic turbulence intensity such that only wind speeds greater than 10 m/s shall be used, low frequency trends must be removed and appropriate anemometers, sampling rates and averaging times shall be used.
- for complex terrain, the assessment must be based on measurements.

However, except in the case of the characteristic turbulence intensity, no detailed guidance is given on how the assessment should be carried out.

This report aims to give guidance on how such an assessment can be carried out in a consistent manner. The task has been restricted to the assessment of wind conditions, reflecting the expertise of the participants in the project and concentrating on that aspect which is particularly important to wind turbine design and which is not likely to be well covered in codes associated with other fields of engineering. Consideration to the effects of wakes from other wind turbines has not been given as this is dealt with in another part of the EWTS 2 project.

2. SURVEY OF EUROPEAN CONSULTANTS

2.1 Purpose of Survey

All of the European nations presently involved in major commercial wind farm development were represented on the project (Denmark, Germany, Greece, Netherlands, Spain and United Kingdom). Even within the project participants, it was apparent that site assessments of varying extent and methodology were in use in each country. Besides the project participants it was recognized that there were many other organizations involved in site assessment and consequently it was decided to carry out a country-by-country survey by questionnaire to obtain a more complete overview of site assessment techniques in use. The first part of the data collection exercise was aimed at identifying the range of techniques that are used in each of the countries participating in this project.

A second aspect was to investigate the sources and availability of input data for use with the site assessment techniques. Both the measurement and modeling based techniques which are used for site (annual average wind speed) assessment require some form of third party input data but it was expected that the quality and range of data readily available would vary from country to country. The intended outcome of this part of the survey was an indication of the “lowest-common-denominator” of available input data which could be recommended for use with each assessment technique.

2.2 Implementation

To encourage a good response, most of the questionnaires were completed by telephone interview with each organization rather than by post. In most if not all cases, only organizations involved in commercial wind farm site assessment have been interviewed, therefore there are generally no research projects or techniques contained within the survey results. The survey focussed on techniques for annual average wind speed assessment as in the majority of cases this was the only parameter which was assessed in any thorough way or even at all until now. However, some basic questions were asked to determine if other parameters were assessed and if so what they were. Finally, the survey was carried out on the basis that individual consultants and organizations would remain anonymous. In fact, only the person asking the questions within each country knew who the individual organizations were as all paperwork distributed and analyzed centrally within the project contained no indication of the responding organizations.

2.3 Results of Assessment Technique Survey

The results are first of all summarized and interpreted on a country by country basis. The overall results are presented and summarized in tabular form at the end of this section.

2.3.1 Denmark

Five responses were received from the survey of consultants in Denmark, all of whom mainly used wind flow models for site mean wind speed assessment. This reflects the fact that most of these consultants primarily operate in their home market where the models are well tested and the terrain is relatively simple. However, at least two Danish consultants operate in countries with more complex terrain and in these situations either wind flow models or measurement based techniques are used.

All of the consultants use the RISØ WAsP wind flow model for wind speed assessment and spatial extrapolation. Three consultants also use another Danish model called Wind Atlas System originating from Energi- og Miljødata Ålborg. The purpose of applying the models is generally concerned with resource (energy yield) assessment rather than structural integrity assessment. The experience of the

Danish consultants indicates that in Denmark, predictions are within 10 per cent of actual energy yields in most situations and indeed one consultant has evidence from more than 100 sites over periods of 3 to 6 years which indicate an average prediction error of 1 per cent and a standard deviation of 5 per cent. Using similar techniques in other countries, the same consultant assesses the prediction error to be 5 per cent. In general, the consultants assume an uncertainty of about 10 per cent on energy yield for Danish sites rising to 18-25 per cent for complex terrain sites.

Considering all of the consultants, the digitized representation of the terrain used with the models ranges from a radius of 4km to 10km depending on the memory limits of the model and hence on the complexity of the terrain height contours. Contour intervals of 2m to 5m are used in all cases and as terrain data are available in digital format in Denmark their representation should be consistent irrespective of the consultant.

The representation of obstacle and surface roughness in the models is more subjective. Each consultant has a different approach to the inclusion of obstacles and what size and position of obstacle is considered significant. However, in general roughness changes are considered to a radius of 20km (which seems inconsistent with the terrain contour domain dimensions).

Although site specific wind measurements are not a legal or contract requirement in Denmark, significant measured data exists on the performance statistics of existing wind farms. Therefore, it is relatively straightforward and common practice to confirm or validate energy yield or wind speed assessments from a proposed wind farm site on the basis of the performance of neighbouring wind farms or wind turbines.

2.3.2 Germany

Reflecting the level of growth of wind energy and legal requirements in Germany, the greatest number of consultants and other organizations involved in site assessments are located there. Forty responses were received on time although there were about sixty enquires made in total.

Terrain ranging from flat coastal regions, through moderately complex inland regions to complex mountainous terrain exists in Germany and hence a broad range of assessment techniques are used. However, the majority of consultants use a combination of modelling and measurement.

2.3.3 Greece

The responses of six developers and consultants were obtained from Greece. Additionally, a small group of old private developers, who installed wind turbines based on visual inspection of the site and using information from locals, were also identified. However, in these cases it was concluded that they adopted no reasonable site assessment technique within the concept of the present survey and so they were excluded.

The site assessment techniques used in Greece reflect the complexity of the Greek terrain (categorized as ultra complex terrain) and the wind flow uncertainties inherent therein. Therefore, most consultants use measurement based techniques. Half of the consultants use computational wind flow models in addition to or instead of measurement based techniques.

Current government regulations and subsidy schemes require an energy yield assessment to be carried out before an operation license and subsidy are granted. Hence the motivation for site assessment is primarily financial in terms of energy revenue rather than structural integrity. Despite this, most of the consultants do measure more parameters than just the bare minimum required to carry out an energy yield assessment (e.g. turbulence intensity and shear are also typically determined by measurement in addition to mean wind speed and direction).

In most cases (67 per cent), the measurements are used in conjunction with long term reference wind speed data to carry out a long-term prediction using an empirical correlation technique commonly known as Measure-Correlate-Predict (MCP). In such cases the on-site measurements are of duration's ranging from 6 months to 3 years, depending on the consultant, with most consultants typically using a minimum of 1 year of measurements.

Unusually (at least in comparison with other countries), no two consultants use the same wind flow model, with only one consultant using the commercially popular WAsP model and the other two each using different in-house numerical wind flow models.

2.3.4 Netherlands

The results contain the responses of nine out of sixteen commercial consultants identified, the remainder either not responding within the time scale or not willing to participate. In general the assessment techniques used in the Netherlands reflect the fact that the terrain is very flat and that considerable local experience of the wind characteristics and using the wind has been established over many decades. Therefore, the total picture is biased towards modelling where the term "modelling" is used in a broad sense to include local calculation codes and procedures.

A large variety of modelling based techniques are used in the Netherlands, ranging from assessments on the basis of the production of nearby wind turbines to the application of methods which take into account reference climatological data. The method which is used most is "Handbook Method III" [4], in which the energy yield of a wind turbine at a specific site is predicted on the basis of the local distribution of wind speed and the power curve of the wind turbine, the former being derived using formula and tables from the handbook. The local wind speed distribution at hub height is predicted on the basis of 30 year wind data from four reference meteorological stations which each represent a different climatological zone (maritime, coastal, lowland and inland). Large scale differences between the target and reference site wind regimes due to "macro" (i.e. roughness independent) wind speed, climatological differences and "meso" roughness effects are determined. Next, local effects are taken into account in terms of local roughness, hub height, obstacles, other single wind turbines and wind farm corrections. Finally, a stability corrected wind speed is determined. The method is restricted to hub heights less than 80m and locations excluding sites at dikes or offshore. Some of the consultants using this technique apparently assess as many as 125 sites per year.

Experience and specific studies have shown that the "Handbook Method III" generally over predicts annual energy yield by 25 ± 25 per cent reflecting a possible average annual wind speed error of up to 8 percent. Much of the variability is due to the fact that the reference wind regime period and hence prediction period is of 30 years duration which does not match well the annual average conditions used for the comparisons. However, some organizations have modified "Handbook Method III" in some unspecified ways to reduce the errors associated with certain components of the model.

The general feeling in the Netherlands is that, due to the flat terrain, measurements will not lead to a reduced uncertainty compared to existing modelling techniques unless the measurements are carried out over a long period (3 years). However, there is a trend towards more measurements particularly for large projects where there is a trade-off between the revenue from the expected yield for the wind farm and the cost of the measurement campaign. The motivation for site assessment in the Netherlands is connected with accuracy of energy yield predictions and hence potential revenue rather than turbine safety are the key issues addressed.

2.3.5 Spain

Three Spanish organizations responded to the survey. As with Greece, the terrain used for wind farms in

Spain generally ranges from complex to ultra complex, hence assessments are in all cases based on a thorough combination of measurement and modelling.

All of the consultants carry out measurements which are more comprehensive than those required to determine annual mean wind speed with the majority assessing shear, turbulence and gusts in addition to mean wind speed and direction. Two out of the three consultants also use multiple measurement masts with or without wind flow models to carry out spatial extrapolation across a proposed wind farm site.

In all three cases the long-term prediction of annual average wind speed is based on a statistical Measure-Correlate-Predict (MCP) technique. However, there is insufficient operational experience to assess how accurate the predictions based on this technique have been so far. Uncertainties of up to 15 per cent on wind speed are however assumed by two of the consultants on the basis of short term validation exercises.

Where wind flow models are used for spatial extrapolation, all three organizations use WAsP and in addition two of the organizations also use MATHEW . Although similar models are used by all three, the method of using the models seems inconsistent from consultant to consultant. For example, each consultant typically uses a terrain domain size of 10km x 10km, 15km x 15km and 40km x 40km. Surprisingly, the consultant who uses the smallest domain area also uses a coarse height contour resolution (20m to a radius of 5km and 50m thereafter), whereas at least one other consultant has access to contour data in the range 5m to 20m.

2.3.6 United Kingdom

Nine consultants and wind farm developers involved in site assessment in the UK were contacted of which eight responded within the time scales of the survey. A further consultant was also identified but upon initial contact was excluded from the survey on the basis that the methods used did not constitute a formal site or wind speed assessment, being based purely on experience. At least partly because of the perceived uncertainties arising as a result of the relatively complex terrain which characterizes typical UK wind farm sites, there is a formal requirement to carry out a minimum of 13 weeks of on-site wind measurements in the UK prior to lodging an application for a wind farm electricity supply contract. Hence measurements are used by all the UK consultants and in most cases the measurements are used in conjunction with wind models.

The statistical Measure-Correlate-Predict (MCP) technique is used by all eight UK consultants to determine the wind farm annual mean wind speed and wind speed distribution. In terms of energy yield prediction, the majority of the consultants have experience which suggests that the technique is accurate to within 5 per cent. More than half of the consultants would consider measuring for a minimum of 6-8 months and a maximum of 12 months to provide sufficient data for the correlation stage of the analysis. One organization typically executes 24 months of measurements for this purpose. No one takes the risk of using the formal minimum of 13 weeks of measurements. For the correlation stage of the analysis, somewhat surprisingly, more than half of the consultants use a least squares straight line fit forced through the origin. Other methods used are unconstrained least squares straight line fit, least squares polynomial fit and two parameter “method-of-bins” analysis. To complete the MCP process, long-term reference wind speed distribution data are required and without exception this originates from the UK Meteorological Office for sites in the UK hence all consultants are consistent in this respect.

For spatial extrapolation of the wind regime across a wind farm site, more than half of the consultants use a temporary mobile anemometer mast of typically 10m height at various locations on the proposed wind farm site. These measurements are correlated with the longer term measurement mast on the site and the results used to validate more comprehensive spatial extrapolations which are implemented using wind flow models. Of the various wind models, WAsP is the most commonly used followed by the MS family of models (MS-Micro, MS3DJH). As contour data are available in digital format, most consultants use these data with 10m contours and a 10 x 10 km domain.

2.3.7 Overall

Referring to Figure 2.1 which is based on data extracted from the survey, as the typical terrain complexity increases, the assessment technique trend moves away from using wind flow models to carrying out on-site measurements with or without supporting wind flow models.

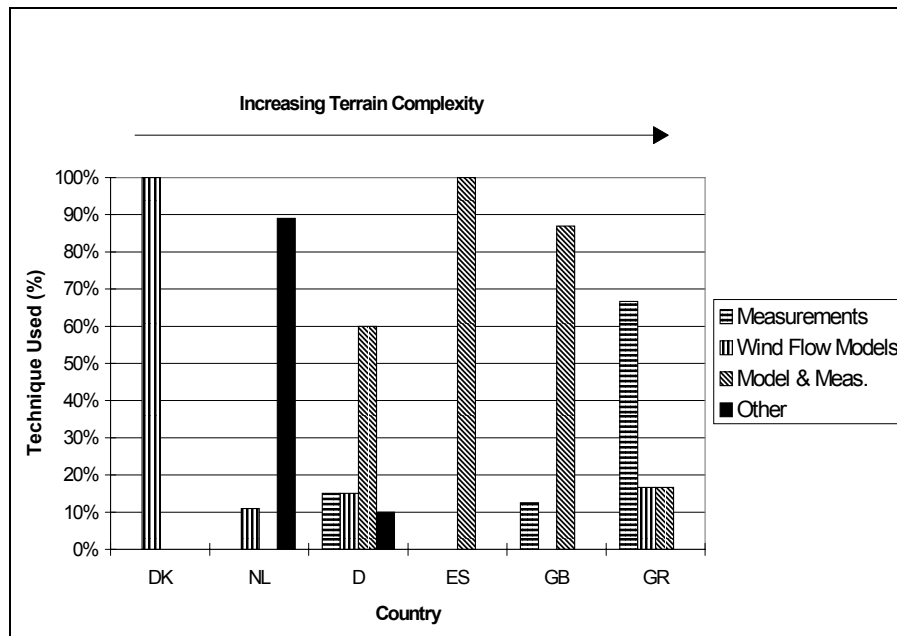


Figure 2.1 Prevalence of assessment techniques used per country

This situation reflects the perceived state-of-the-art of wind flow modelling in the commercial world and a general lack of confidence in the application of such techniques in complex terrain. From the survey results, a total of 79 consultants were identified to be using models as part of commercial site assessments (some consultants use more than one model). The breakdown by model is illustrated in Figure 2.2.

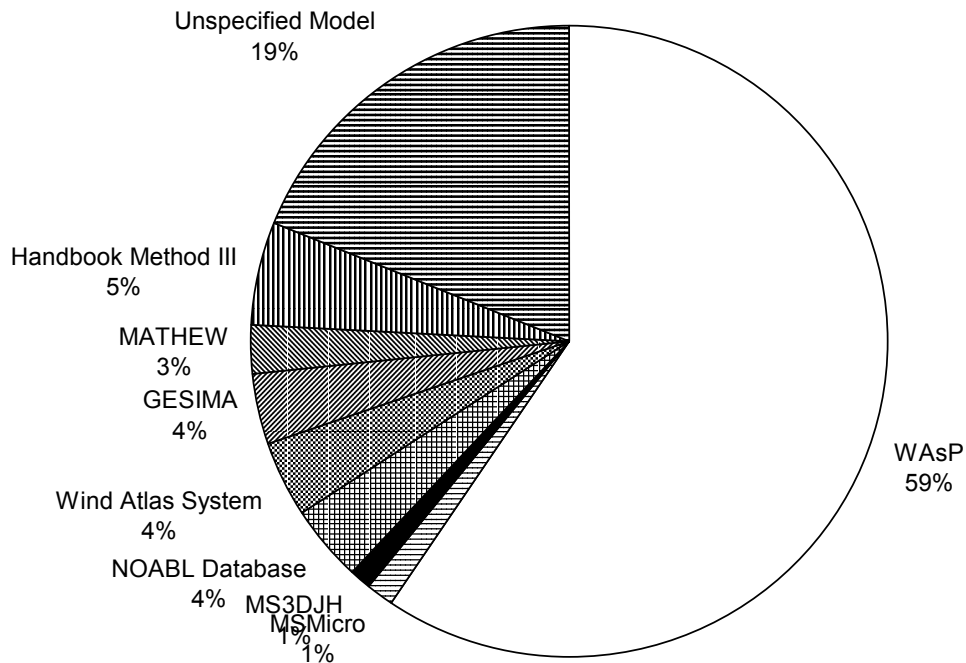


Figure 2.2 Summary of wind flow models and calculation methods in commercial use.

As WASP is clearly the most popular model, a particular emphasis was placed on assessing how consistently this was being used, how reliable the results were and suggesting guidelines for a more consistent application of the model.

2.4 Results of Input Data Survey

Various forms of input data are required by both measurement and modelling based prediction techniques. The survey was used to investigate the sources and format of reference wind speed data and terrain contour data available within each country.

2.4.1 Denmark

Terrain contours: maps are available at scales of 1:25000 and 1:100000. The 1:25000 maps are available in both printed and digital formats. The height contour resolution of the printed maps is 2.5m with additional spot heights to accurately define specific features (e.g. hill tops). However, the digital maps have a minimum height contour resolution of 5.0m.

Reference wind data: histograms of wind speed and direction are available from a number of sites (exact number unspecified) operated primarily by the Danish Meteorological Institute. Typically, the data archives cover periods of 10-20 years although there are some instances where much longer records are available (e.g. Risø has a 40-year record). According to the consultants, the quality assurance of the data is restricted to identifying instrument failures and re-calibration of the instruments.

2.4.2 Germany

Terrain contours: most of the German consultants hand digitize the height contours from printed maps although digitized data are also available. From the database of responses, the minimum contour interval available seems to be 5m.

Reference wind data: DWD, the German Meteorological Office, is the major source of long term reference data. Sometimes these data are sourced directly from DWD and in other instances the data from the European Wind Atlas are used although, for German sites, the Wind Atlas data are in fact based on DWD data. Typically a ten year data record is used. Although high quality instrumentation is used, there is some doubt over the consistency of calibrations and consideration of siting effects for such instruments. There is a lack of consistency between the techniques used by the former East and West German meteorological institutes which further complicates general assessment of the quality of the available data.

2.4.3 Greece

Terrain contours: the most commonly available printed map scale is 1:50000. However, 1:5000 scale maps are available to special order from the Hellenic Army Geographic Service provided they do not map restricted areas. The 1:50000 maps have a contour resolution of 20m and the 1:5000 scale maps have a contour resolution of 4m. The entire country is available in digitized format, however the contour resolution is only 100m. However, the Hellenic Army Geographic Service will digitize the 1:50000 maps at 20m resolution to special order.

Reference wind data: there are three sources of measured wind data in Greece; Hellenic National Meteorological Service (HNMS), Public Power Corporation (PPC) and the Centre for Renewable Energy Sources (CRES). There are 48 HNMS sites and 9 PPC sites with data records longer than 10 years, however, the data are generally only available in processed, statistical summary form. In most cases regular re-calibration of the instrumentation is carried out, ensuring some confidence of data quality.

2.4.4 Netherlands

Terrain contours: printed maps of 1:50000 scale are commonly available for the Netherlands. Due to the very flat nature of the land and the assessment technique primarily used, information on contour intervals has not been provided by any of the questionnaire recipients, although one must assume that such contours are marked on the maps.

Reference wind data: KNMI, the Royal Netherlands Meteorological Office provide long term reference data from seven stations with records extending for more than 7 years. Four of these sites constitute the reference sites for the "Handbook Method III" employed by most of the consultants.

2.4.5 Spain

Terrain contours: a variety of printed maps are available with full national coverage at 1:50000 scale, about 25 per cent coverage at 1:25000 scale and some areas where 1:10000 and even 1:5000 maps are available. The available contour resolutions depend on the scale of the map and are respectively 20m, 10m, 5m and 2m. Digitized maps are available for some areas based on the 1:50000 scale maps but with 10m contour resolution. However such data are very expensive, so most organizations hand digitize from printed maps.

Reference wind data: The Spanish Meteorological Office can provide long term wind speed data from a number of sites of which there are about 15 sites with 10-15 years of data and a further 5 sites with greater than 15 years of data available. For those sites located at airports, calibration checks are regularly carried out, however, there is no indication of what is done at other locations. Time series (half-hour interval) data

are available along with statistical summaries of wind speed and direction.

2.4.6 United Kingdom

Terrain contours: a range of printed maps are available within the UK at scales of 1:50000, 1:25000 and 1:10000. The 1:50000 and 1:25000 scale maps have contour resolutions of 10m whereas the 1:10000 maps have contours at 5m intervals in and around towns and cities and at 10m intervals in remote areas. Digitized terrain data based on the 1:50000 scale maps are available for the entire country with 10m contour resolution and a height accuracy of $\pm 3\text{m}$. Terrain data based on the 1:10000 scale maps are available to special order with contour resolutions of 5m or 10m according to the same criteria as the printed maps. In this case the height accuracy is stated to be $\pm 1.5\text{m}$.

Reference wind data: wind speed data are available in various formats from the UK Meteorological Office (MO). There are presently 180 sites operated by the MO throughout the UK from which measured wind data are available. Most of these sites are concentrated around the coast, near heavily populated areas and at military and civil airfields. Data are available to purchase in the form of hourly time series (per calendar month) and histograms of wind speed and direction by year or month. Many of the sites have records extending back for more than 15 years. The MO carry out checks at regular intervals to ensure data integrity (no details available).

2.4.7 Overall

Terrain contours: all of the countries considered are abundantly described by printed maps as would be expected. The resolution of contours available is largely dictated by the severity of the terrain in each country; the more simple the terrain, then the higher the contour resolution that is required to represent the undulations in the terrain and so the higher the contour resolution presented on maps. The economics of map production mean that it is generally not viable to produce maps with high contour resolution ($< 5\text{m}$) in complex terrain countries. In general, maps with at least 10m contour resolution seem to be readily available across Europe. Digital terrain data are available in most countries although generally at a lower contour resolution than for the best printed maps and at a perceived greater cost. However, the apparent purchase cost disadvantage must be weighed against the personnel cost, time, accuracy and consistency constraints associated with carrying out manual digitization from printed maps.

Reference wind data: as expected, the national meteorological offices in each of the countries considered are the main source of long-term wind speed records. In the main, the measurement masts are located at coastal or airport sites. The measurements are generally carried out using cup anemometers at a height of 10-20m above ground level. At this height there is a real possibility of anemometer blockage from vegetation or buildings, both of which are features which may have changed significantly over even a relatively short period of time. In the longer term, instrumentation systems may have been replaced and instrument characteristics may change as the instruments age, although this is accounted for in most cases by regular re-calibration. All of these factors combine to make the reference wind data a potentially major source of uncertainty in a site evaluation. It is recommended that this uncertainty is minimized by careful examination of the history of a reference site and its instrumentation and by inspecting the reference site via a site visit.

3. MEAN WIND SPEED ASSESSMENT

3.1 Wind Flow Modelling

3.1.1 Technology Status Review

In order to perform site assessment for wind energy applications especially in complex terrain, an accurate description of the wind flow over the terrain is needed showing the spatial variability of wind velocity and turbulence. Proper siting is necessary in terms of expected power output (maximum energy yielded compared to costs) and wind velocities and turbulence are also important for the selection of the most suitable wind turbine design in terms of fatigue resistance and strength (maximum lifetime and reliability compared to costs).

This need for reliable prediction of the wind field over complex terrain has led during the last decade to the development of various models and corresponding computer codes which differ both in complexity and accuracy. These can be divided into a number of basic categories as described in the following paragraphs.

The kinematic or mass consistent models solve the continuity equation only, assuming that the flow is inviscid. As a result, they are of low computational cost and easy to handle. This concept was initiated by Sherman's model [5], where a non divergent wind field is produced via a perturbation potential field. Traci et al [6] have developed a mass consistent model and this was the beginning of a significant modelling effort towards this direction (NOABL*, AIOLOS, WINDS, etc.). NOABL* is a mass-consistent model that solves the Poisson equation for the determination of the perturbation wind speed potential through a finite-difference scheme. The initial flow field is adjusted through the perturbation potential to satisfy mass conservation throughout the computational domain, taking into account different atmospheric stability conditions. However these models do not predict purely viscous effects such as recirculation and they do not give information on turbulence. Improvement can be accomplished by estimating the vertical velocity as solution of the turbulent momentum equation in the vertical direction (AIOLOS-T, [7]). This method accounts for stratification and uses a zero-order model or a k- ϵ model for turbulence closure.

Dynamic models solve the continuity, the momentum and the temperature equations. They vary in complexity according to the treatment of the topography, the simplifications in the equations, the turbulence model etc. In order to achieve low computational cost, dynamic models based on the boundary layer equations have been developed. The concept of the linear perturbation theory of Jackson and Hunt in two dimensions [8] and Mason and Sykes in three dimensions [9] introduced a two-layer approximation using different perturbation schemes in the inner and outer region of the boundary layer. This concept gave rise to the development of several analytical models (i.e. WASP, MS3DJH), which have given satisfactory results in geometries where no flow reversal exists (J. L. Walmsley [10]). Mason & King [11] review different J&H oriented models and compared their results against their finite difference model which is effectively identical to the model of Taylor [12]. At present analytical models based either on the potential flow theory or on boundary layer parameterisations are used for predicting the wind flow over complex terrain. The WASP program, which is capable of generalizing a long-term meteorological data series at a (reference) site which may then be used to estimate conditions at other (predicted) sites, is nowadays the most extensively used practical tool applied for this purpose. The MS3DJH family of models conserve mass but also attempt to solve momentum equations in an approximate manner by using a constant-density atmosphere. It is assumed that the physics of the flow can be simplified by using a mixing length closure for the turbulent stresses, which is only valid for statically stable conditions, and that the momentum equations subjected to the thin shear layer approximation can be linearised and then

solved using perturbation techniques. In general the models belonging to this category have inherent limitations concerning the terrain slopes and so their validity in complex terrain is not guaranteed.

To overcome the inherent limitations of the linearised flow models several researchers have recently attempted the solution of the fully 3D turbulent Navier Stokes equations [13], [14]. In the literature several models have been proposed for closure of the equations such as zero order models, one equation models, two equation models, Reynolds stress models etc. To suppress the computational cost, most Navier Stokes runs are performed on relatively coarse grids applying law of the wall type boundary conditions. Simulations with more elaborate turbulence models, like the low Reynolds $k-\epsilon$ or the algebraic Reynolds stress models, which could better estimate the wind profiles and the Reynolds stress tensor, require large memory and computer time and this renders them cost ineffective. Validation studies have confirmed that the $k-\epsilon$ is a good compromise between the simple models and the more complicated ones [15], [16].

All the previous models are unable to account for the influence that local wind systems have on the annual wind conditions especially at a complex terrain site. One important aspect of siting wind converters is a description of the local wind climate with high spatial resolution which is often not available from observations in the atmosphere. The density of operational observation networks is too poor for that purpose so that additional information is required. Therefore methods have to be applied to derive this information from the large scale state of the atmosphere and topographic parameters by applying meso-scale models. The meso-scale simulation models are able to simulate local wind systems produced by the orography and/or solar radiation, because they incorporate the appropriate physics but also because of their working domain (characteristic dimensions of time and length of the meso-scale) which is restricted in the models mentioned previously. Only at this scale, where the typical dimension of time lies between a few minutes and a 24 hour day and the typical length lies between 2.5km-mountain and valley winds to 2500km-tropical cyclone, do local wind system phenomena occur. All meso-scale models calculate the wind field by numerically solving the Navier Stokes conservation equation for mass, energy, momentum etc. The specific formulation of all equations and the approximations used depend on the specific meso-scale model that is selected. Summarizing, meso-scale models are able to describe the wind field with a high spatial resolution during short episodes in complex terrain. To gain a wind climatology from simulations with these models, available statistical information about the large scale state of the atmosphere has to be scaled down to the required resolution by applying meso-scale models, which describe principally the modification of the large scale state by meso-scale processes induced by the topography.

A number of meso-scale models that are used for site assessment applications are found in the literature, i.e. the HIRLAM model by Danish Meteorological Institute, the KAMM model by University of Karlsruhe, the GESIMA model by GKSS, the MEMO model by IEH-REG, the UK Meteorological Office model and the meso-scale model run by the University of Uppsala [17], [18], [19], [20], [7]. The tremendous computer resource needed for applying these models should be taken into account. Moreover, that the grid step used in the analysis cannot always be as small as required and the fact that the models require several basic assumptions (i.e. definition and number of episodes, assumed frequency distribution of wind velocity etc.), lead us to believe that at the moment their results are considered to allow for a qualitative description of wind statistics in regions where observations are not available but the accuracy of the absolute values resulting from these procedures is not always ensured.

Recently, research has been addressed towards the combination or nesting of models with different spatial resolutions (i.e. WAsP/local scale with KAMM or HIRLAM / meso-scale [17], [18] or WAsP with Navier Stokes solvers) and hybrid micro-siting models [21] combining the mass consistent methodology with principles of the Navier Stokes approach. During the JOULE I project, contract no JOUR0067 entitled "Wind measurements and modelling in complex terrain" it was attempted to estimate the possible zones of separating flows based on the topography input and to verify by means of the measurements obtained in the same project. In the European Wind Atlas Vol. II (to be published shortly), the KAMM model, which

is able to calculate the resource over distances of hundreds of kilometers, was used as a supplement to the WAsP model which in contrast can handle very detailed information on the topography in a radius of approximately five to ten kilometers from the sites. Preliminary results for assessing the wind potential of Ireland are quite promising [22].

In the author's opinion the most interesting idea was to include in the WAsP package a module which uses the Navier Stokes equations in a model based on the rapid distortion theory (RDT) for predicting the turbulence component spectra over moderately complex terrain.

Summarizing, the current state of the art on siting appears as follows:

Evidently, depending on its background theory each model has certain possibilities and limitations. Simple models are still in almost exclusive use. Due to their approximate character, calibration procedures (wind tunnel studies, in situ) are often needed. In some cases, additional calculations with more advanced (Navier-Stokes), generalized (meso-scale) or even statistical tools (i.e. MOS -Model Output Statistics [18]) seem necessary for improving the prediction accuracies.

Navier-Stokes models require considerable computational effort which has been a serious drawback for their widespread use.

Meso-scale models are able to simulate local wind systems produced by the orography and/or solar radiation but they are also very complicated and therefore require tremendous computational effort.

It is worth noting that most of the models discussed have been used for resource assessment purposes only. Their reliability in predicting the flow characteristics which are known to affect the operation of a wind turbine in complex terrain is by no means established. For instance, although a great number of models exist which allow, within certain limits, prediction of mean wind speed modifications due to complex terrain, only a few are capable of providing an estimate of the modification to the turbulence level and structure arising from complex terrain. The real dimensions of the problem can be appreciated by considering that the greatest bottleneck associated with complex terrain is actually the identification of the terrain parameters related to the characteristics of the wind field driving the wind turbines.

3.1.2 WAsP

3.1.2.1 Limitations

To validate the accuracy of existing flow modelling codes several factors should be considered i.e. the sensitivity to accurate model input (i.e. factors intended to be user defined) and limitations due to the physical assumptions in the coding.

The literature review was extended to papers and reports presenting results of case studies and sensitivity analyses using the WAsP package in an attempt to quantify the errors and uncertainties associated with the input data and the limitations in the physical assumptions. This revealed, in some cases, rather contradictory results regarding the importance of the resolution of the input topography.

Sensitivity studies carried out by RAL in the framework of the JOULE project contract no JOU2-CT93-0370 [7] for investigating the dependence of the prediction accuracy of these codes on the user defined input and for studying their overall usefulness when extrapolating wind speeds especially in complex terrain, revealed that the resolution of the input topography and roughness was very important to the correctness of the wind speed estimates. More specifically it was found that when the topography and the roughness were well defined and that when suitable wind speed initialization data sets were used, accurate predictions could be made. The accuracy broke down over very steep slopes and in cases where local circulations were forming. The dependence of the flow model results on some of the underlying physical assumptions of the coding was also examined. For this purpose a model of the heat fluxes in the

atmosphere was developed to divide wind speed data sets up according to the stability of the atmosphere at the time when the measurements were made. It was shown that the classified data sets had very different characteristics in terms of wind speed and direction distribution, wind shear and in terms of the magnitude and form of the correlation between data sets measured at different sites. For the case studied the errors brought in by the stability assumptions of the flow modelling were of a similar magnitude to, and could not easily be distinguished from, those brought about by the breakdown of the model's representation of the wind flow over steep slopes.

A thorough sensitivity analysis using the WAsP model for site assessment was carried out by ETSU [23] and it was revealed that estimates of the long term mean wind speed made using the WAsP model had an error of up to 30% while the corresponding wind power estimates, as expected, had an error of 70%. When trying to identify the sources of error related to the physics adopted by the model, the study referred to the fact that the WAsP model uses the Atlas file where the generalized wind data is created by forcing the measured data to fit a standard Weibull type frequency distribution. However it was found that very few of the observed wind climatologies can be stated to have come from a Weibull distribution, therefore it is evident that this procedure introduces an error the magnitude of which depends on the degree of transformation applied to the data.

Regarding the input data and additional to the points made above, it was concluded that there was no obvious pattern found relating the magnitude of the sign of the error to terrain type. The analysis also revealed that the impact of including obstacles was generally small and can not be guaranteed to improve the accuracy of the prediction. Finally, it was found that the WAsP model is relatively insensitive to the area, resolution or quality of the topographic input data, which is a rather surprising result based on the author's experience with the application of WAsP in complex terrain and taking into account that the model adopts a telescoping principle. This means that the orographic model of WAsP uses an expanding polar grid enabling a detailed description of the terrain elevations closest to the actual prediction locations which exert the strongest influence. This is also illustrated in [26], where it is evident that the prediction accuracy of WAsP depends heavily on the choice of the terrain resolution used.

The performance of WAsP in predicting wind speed variation across three sites in the UK with varying complexity, is discussed in [27] where quite accurate predictions are obtained but with the standard deviations of the differences between the observed and predicted data varying considerably, a fact which could be related to the varying severity of the terrain from site to site. In [29] a statistical treatment of the discrepancies between actual and WAsP predicted energy productions is performed using data from ten wind farms. It was found that the deviations varied from a 10% under estimate to an 8% over estimate. The difference between the forecast and actual production figures of a wind farm for a single year was up to 14% with an 8% mean value. In [30] the WAsP model was used to estimate the energy capture at potential wind turbine sites in Norway. Significant discrepancies are found between the data extrapolated from short term measurements and the predicted values which could not be explained by the statistical uncertainties generated from the use of short term measurements and by calibration errors only. Sectorwise comparison indicated that roughness effects were exaggerated and that roughness lengths outside the recommended intervals would have to be used to tune the model. This finding is in accordance with the author's experience with WAsP.

A method for estimating the uncertainty in wind energy resource among others is elaborated in [31] and it estimates the uncertainty of the estimated wind speed due to (a) the limited data quality to be 5% on the annual mean wind speed, due to (b) the application of the geostrophic drag law to be 5%, due to (c) the roughness change and choice of roughness classes to be 5% and due to (d) the incompleteness of the model for determining the flow in complex terrain to be up to 10% for certain specified cases. According to this the uncertainty related to complex terrain modeling is estimated to be of the order of 13-14% assuming the error components to be independent.

WAsP prediction errors may be significant in cases where the local climate or terrain lie outside their normal operational envelope. According to Bowen et al [24] a high level of cross correlation between wind speeds at the reference and predicted sites is an essential but not exclusive pre-requisite for an accurate prediction. The correlation coefficient itself does not indicate the sign or magnitude of the prediction error. Bowen et al concluded that the sign and approximate magnitude of the prediction error due to orography is proportional to the difference in ruggedness between the predicted and reference sites. An approximate estimate of this error may therefore be made with a performance indicator based on site ruggedness. One suitable indicator that they have developed is the difference in the fractional extent of the terrain with slopes greater than a critical value between the predicted and reference sites. This indicator (which they have called RIX for Ruggedness IndeX) is believed to provide a means of defining in quantitative terms, the orographic limits for accurate WAsP predictions and a suitable correction if those limits are exceeded. The use and effectiveness of this parameter is discussed further in section 3.3.

In [26] it was observed that in many sites where measurements were available at more than one height, the values predicted from data at different heights showed poor agreement with each other, which suggests that the wind shear profile is not being accurately modeled.

Finally, the effect of different stability (non-neutral) conditions on the predictions of WAsP are discussed in [23], [24], [25], [26] and [28]. In [26] the discrepancies between the DTI database values (consisting of NOABL estimated wind speeds across the UK) and predicted values from WAsP are considerably reduced at higher wind speeds where neutral atmospheric conditions generally occur. In [28] (addendum to [23]) it is stated that there is a separate step within WAsP which makes a correction for stability by modifying the parameters of the Weibull distribution using functions of the mean and RMS heat fluxes over land and sea defined in the parameter file. However, this stability correction is rather a climatological one and therefore misses the dynamic effect that stability has on the flow. Perhaps this is the reason why in [25] it is concluded that although the data is subdivided into stability classes and the default parameters of the model are changed, only slight improvements in the predictions are observed.

Regarding WAsP, a number of conditions that should be fulfilled for acquiring accurate predictions have been reported and it seems that users of the code all over the world agree upon this subject. The physical limitations of the model are sufficiently documented but still, there are questions arising regarding the input data.

For instance, it has been proved that the accuracy of WAsP depends on the choice of the terrain resolution used but the problem remains, considering the memory restriction on the number of data points describing the topography, how to choose a sufficient resolution without limiting the overall working domain and without performing time consuming sensitivity analysis for each site. In addition to that there seems to be no way of quantifying the effect on the user's estimate of using coarse resolution data when this is the only data available. (The 32-bit version of WAsP which is soon to be released will alleviate the terrain description resolution problem).

Another point generating uncertainty in the obtained predictions is the effect of different roughness values assigned by different observers to the same site.

The length of the reference data record used should be sufficiently long to compensate for monthly, seasonal and even yearly variations.

Finally, the length of the data averaging time is also a parameter which should be selected with care so as to allow a particular wind event to envelope physically the reference site and the site to be predicted.

Example Applications

A number of analyses were carried out within this project using WAsP to help confirm some of the findings. Sites representing terrain of varying complexity for which digitized terrain data already existed

were identified and for which measured wind speeds or performance data were available for the purpose of evaluating the prediction accuracy of WASP. Only the case of simple, flat terrain was ignored as being trivial in this instance. Sites in Germany, the UK and Greece were modelled with terrain ranging from moderately complex in Germany to ultra-complex in Greece. The results of each study are summarized below.

Germany

WASP and the European wind atlas model are widely used for prediction of annual energy yields in Germany in both inland and coastal areas. It is known from a number of publications, that the application of WASP to complex terrain situations can be associated with large errors, while the use in medium complex terrain generally gives reliable results. But this is only a generalization. The results of WASP rely very much on an exact description of surface roughness, obstacles and orography but also on reliable meteorological input data. The quality of the meteorological data depends very much on continuous data recording, calibrated and maintained anemometers, but it also depends strongly on the height of the met-mast (typically only 10m in Germany) and the influence by roughness and obstacle elements, which may vary during the measurement time (i.e. 10 years). The quality of the data and their suitability usually can not be examined by the WASP user.

To verify the results of the European wind atlas method in moderate complex terrain, WASP was applied to estimate the energy yield of an existing wind farm in southern Brandenburg. The wind farm was chosen because it consists of modern wind turbines (WT's) with a certified, measured power curve, which is an essential input to reliable energy yield estimations.

The energy yield of the wind farm in 1995 and 1996 was compared with the energy yield of a nearby single WT, operated over four years, to find out a value of the annual energy yield which is representative for a several years period. The single WT was not chosen for direct comparison because of the lack of a certified power curve. The energy yield in 1995 was chosen to be representative.

The example calculation was performed with data from different meteorological sites. The results with data from three nearby stations (distance < 45km) were extremely bad, ranging from 42 to 48 % deviation from the real energy yield. The farther met-station Leipzig (90km) gave better results (14% to 21% deviation), even though the surrounding topography is not so closely related to the wind farm area as that of the three nearby met-stations. The atlas data for Leipzig were taken from DWD and for comparison from DEWI's own generated data. The DEWI atlas data were generated conservatively giving a slightly better result. But it should be noted, that this result could be random and that the Leipzig station should not be taken generally in this area.

To help objectively assess the severity of the terrain, the RIX parameter (see section 3.3.3.2) was determined for each combination of reference and prediction sites. The RIX was calculated to a radius of 3.5km from each site using 12, 30° direction sectors. For all sites considered, the RIX was found to be zero; in other words, all terrain slopes were less than 30%. In fact, most of the slopes were less than 5 per cent. It is therefore considered unlikely that the poor prediction performance was due to poor modelling of the terrain induced flow variations. So the poor performance may have been due to poor representation of obstacles or roughness or poor quality reference wind data. Despite the only moderately complex terrain, as many of the reference sites analyzed are in very close proximity to forests and as the reference anemometers are mounted at quite low heights (12m - 18m) it is possible that a combination of all of these factors may have contributed to the poor prediction performance.

UK

Data from a complex terrain site in the North of England at which a number of meteorological masts had been installed for site assessment purposes were analyzed. Existing WASP input terrain data files were modified to determine the sensitivity of the prediction performance to the precise specification of the input terrain data. The RIX (see section 3.3.3.2) was used to characterize the terrain and an attempt was made to

derive relationships between prediction error and RIX.

Time series (hourly average) from four sites were used for the analysis, one of which was a sea level Meteorological Office reference site. The other three sites were prediction sites, one of which was at sea level and the other two at about 200m a.s.l. Digital map data obtained directly from the UK Ordnance Survey were used, after conversion to WASP format, for the analysis. The maximum available contour resolution of 10m was used in the vicinity of the prediction sites.

The terrain in this instance was characterized by RIX values of 1-2 per cent for certain directions indicating that slopes of greater than 30 per cent did exist. The relationship between prediction error and RIX was found to be less consistent than that obtained by the originators of the technique [68] possibly indicating that other factors, besides terrain ruggedness were not well represented in this model (e.g. roughness) or that the reference site (Meteorological Office station) was subject to unusual, localized meteorological effects. Consultation with the Met. Office personnel from this station did reveal experience of unusual effects from certain wind directions due to the interaction of the wind with local cliffs and sand dunes.

This analysis highlights the need to thoroughly evaluate the reference site before deciding to use it for modelling purposes.

Greece

For this case, a site on the island of Andros was identified for which a WASP terrain model existed. Measured energy and wind speed data were available from a wind farm and meteorological masts on the island from time periods both before and after the construction of the wind farm. The primary objective was to use reference wind speed data from masts located in terrain of varying complexity to predict the performance of individual wind farms. The first reference mast was located within the boundaries of the wind farm before the wind farm was built. The second mast was positioned outside the wind farm and at a distance of 1.5km from it on a well exposed site. The third reference mast was located on the edge of the wind farm in an area with relatively steep slopes (20%) in comparison to the other reference mast sites. These reference data sets were then used to predict the corresponding wind speeds at two heights on two other masts at the edge of the wind farm (before the wind farm was built). In all cases, the analysts had very good knowledge of the reference data quality, either having carried out the measurements themselves or having good access to the organization who carried out the measurements.

The results from this first study were inconsistent. It was found possible to predict the wind speeds at one mast with prediction errors of 10% to 36%, depending on the reference site. However, for the other mast, the prediction error range was 2% to 11%.

A second analysis study was carried out using the same reference sites, but targeting four masts on the boundaries of the wind farm. In this instance, the prediction error deviation was found to be 5% to 35%, although the lowest error values generally correspond to cases where the reference mast data have been used to do a self-prediction, such that the prediction and reference sites are the same site. It should be noted that due to the complexity of the terrain and the memory limitations of the model, a less detailed description of the terrain contours was used on the periphery of the wind farm. The four prediction masts in this part of the study were located in the area with less contour detail.

Finally, predictions were carried out for the energy yields of each of the seven turbines within the wind farm using the WASP WECS module to apply the turbine power curves. Measured annual energy production data for each turbine for a concurrent period were available for comparison. As it was not possible to accurately correct the WASP predictions to account for periods of turbine unavailability, both the measured and predicted energy productions for each turbine were normalized with respect to one turbine in the wind farm. So although it was found that WASP tended to overestimate the absolute energy production by between 7% and 22%, the relative prediction performance between individual turbines was

found to be quite impressive. In fact, referring to table 3.1, in all but one case, the relative prediction error is 2-3%.

Table 3.1 Relative energy production (measured and WAsP prediction)

Turbine	Measured	WAsP
1	1.00	1.00
2	0.95	0.93
3	0.89	0.87
4	0.92	0.90
5	0.85	0.83
6	0.82	0.85
7	0.79	0.91

This particular example illustrates that even in very complex terrain, when you have good quality input data, WAsP can be made to work very well, at least in relative terms.

3.1.2.2 Guidelines for Use

The general conclusion is that WAsP is a practical and, as indicated from the survey summarized in Figure 2.1, the most widespread tool for site assessment, particularly in simple terrain and for preliminary site assessment in complex terrain. The literature review shows that accurate site assessment is obtained provided that :

- both the reference and predicted sites are subject to the same weather regime
- neutral atmospheric conditions prevail
- the surrounding terrain is sufficiently gentle and smooth to ensure mostly attached flows
- the reference data are reliable
- the description of the background roughness length must be as accurate as possible

The application of WAsP to moderate complex inland areas is more difficult and should ideally only be done, if a verification with energy yield data from existing WT's or on site wind speed measurements is possible. This is particularly true if absolute predictions are required. However, in cases where relative predictions across a small area (the area of a typical wind farm say) are required, the model performance can be quite good, even in complex terrain sites. Such relative predictions would usually be carried out in conjunction with a measurement based technique. The findings of this project suggest that uncertainties in absolute resource assessment of at least 13-15 per cent can be expected for moderate to complex terrain assuming that all of the above criteria are fully addressed. There are instances when the model can perform better than this, but in most cases there will be no way of checking at the time of the assessment.

3.2 Measurement based techniques

3.2.1 Status Review

Site assessments based on measurements do not generally have the benefit of long term wind speed measurements (10 years or more) at the actual site of the proposed wind farm. To be practical, measurements can only be carried out at specific sites for periods of 1 - 2 years at most, hence fitting in with the planning (commercial, technical and legislative) time scales and financial constraints. Throughout Europe, the average wind conditions over any particular year or two will deviate substantially from the long term conditions. The longer the averaging period (say ten years), then generally the smaller the deviation from period to period. As wind farm developments have a planned life of 15 to 20 years, then

the average wind conditions must also be assessed for this longer period. The only way that this can be achieved using measurements is to relate short term wind measurements at the planned wind farm site to long term wind measurements at some reference site (e.g. national meteorological office station). There are many ways of doing this, but the general procedure is called “Measure-Correlate-Predict” (MCP) [32].

As the name suggests, the MCP procedure comprises a measurement stage, a correlation stage and a prediction stage. Each stage is described briefly in the following sections.

3.2.1.1 Measurement

Simultaneous wind speed measurements are required at two sites, one of which is at the site under assessment, the other being a reference site for which a long-term wind speed data record exists. The reference site is typically a national meteorological office station, although there may be other sources of long-term reference wind data (refer to section 2.4 for country specific guidance). As measurement of the reference data is generally beyond the control of the organization carrying out the site assessment, the format of the reference wind speed time series usually dictates the minimum format of the measured data for the prediction site. For example, the reference time series available in the UK have a minimum time step of 1-hour. Therefore, the data measured at the reference site must also be recorded or reduced to this format before it can be used in subsequent stages of the analysis. Although there are many reports documenting MCP validation studies, the measurement stage is not extensively described. However, it is generally accepted that, primarily to obtain a statistically significant directional and wind speed coverage, the “short-term” measurement campaign should be of at least 8 months duration. Furthermore, many researchers have investigated and highlighted the importance of careful reference site selection.

3.2.1.2 Correlation

In the correlation stage, relationships are derived between the short term measured wind speed time series at the reference and prediction sites. Typically, the relationships are derived separately for each 30 degree direction sector (based on the reference site wind direction). As wind vane measurements can be somewhat erratic in light winds due to vane meandering, some analysts prefer to discard data for wind speeds less than 3-4 m/s. However, there is evidence that this has, at best an inconsistent effect on subsequent prediction quality [23]. The literature confirms that the application of simple linear regression techniques with floating intercept across the complete measured wind speed range gives reasonable correlation quality in most situations [32, 23, 7]. However, in specific cases, it may be possible to decrease the statistical uncertainty carried through into the final stage of the analysis by using alternative regression functions such as polynomial, or logarithmic functions. Generally, visual inspection of the best-fit function and the raw data on a scatter plot will confirm whether or not investigation of alternative regression functions is justified. The literature suggests that more accurate predictions can be obtained, particularly at high wind speed sites, by carrying out an analysis of the relationships between discrete wind speed bins at the reference and prediction sites [33]. To the author’s knowledge and based on the evidence of the survey, this technique is not widely adopted.

In cases where the reference and prediction sites are separated by tens of kilometers, it may be possible to marginally improve correlation quality by filtering out higher frequency components from the time series before correlation [32] such that the remaining turbulent components are of scale more compatible with the site separation distance. In some situations, correlation quality for all directions may be extremely poor. This is usually indicative of an inappropriate reference site (different reference site climatology from the prediction site or inconsistent data quality) and in such cases there is no option but to identify an alternative reference site. However, it should be noted that, particularly for large separations between the reference and prediction sites the flow between the sites will not be rectilinear and will be dictated by the shape of the cyclone or anti-cyclone driving the wind and the local terrain [32]. Therefore, for a specific reference site wind direction, there are a variety of possible concurrent wind directions at the prediction

site. Particularly in complex terrain, each slight variation in local wind direction will lead to a different terrain induced wind speed effect and so, even if the reference and prediction sites are subjected to the same weather systems, scatter in the wind speed correlations is inevitable. From experience with linear regressions of wind speed data, correlation coefficients in the range 0.7 to 0.9 are typical for a well matched pair of prediction and reference sites using 30 degree direction sectors and site separations of 20 - 100km.

3.2.1.3 Prediction

The term “prediction” (implying “future”) is somewhat of a misnomer as this stage is actually a transposition of the measured (and hence “historic”) long-term reference wind regime from the reference site to the “prediction” site. This aspect is discussed further in section 3.3.4. The long-term reference wind regime is usually available in the form of a joint distribution table of wind speed and direction covering a period of 10 - 20 years. The short term wind speed relationships are applied to the uniform wind speed bin limits defining the distribution table on a direction sector-by-sector basis. Hence, the reference site wind speed distribution table with uniform wind speed bins for each direction sector is transposed to a prediction site wind speed distribution table with non-uniform wind speed bins per direction sector. By simple arithmetic manipulation the prediction site distribution table bin contents can be re-distributed to uniform bins. The long-term mean wind speed for the prediction site is determined from the sum of the products of the bin frequencies and corresponding bin mean wind speeds [32].

The technique can also be adapted to “predict” directional shifts from one direction sector at the reference site to one or more different direction sectors at the prediction site. Techniques using polynomials [32] and discrete shifts [7] are documented in the literature.

3.2.2 MCP

3.2.2.1 Recommended Applications

MCP is an extremely versatile technique which can be used in a wide variety of situations provided that:

- validated, long-term and short-term concurrent measured reference wind speed data are available at a reference site within the same climatological zone as the prediction site.
- validated prediction site wind speed measurements are available for a period of at least 8 months and more typically 12 months or more.

Subject to these few restrictions, a successful MCP analysis is always possible. However, the question which has to be answered on a project-by-project basis is that of whether an (relatively expensive) MCP analysis is required or whether modelling will suffice. The answer to that question is dictated primarily by the complexity of the terrain and the level of prediction uncertainty that is acceptable in the circumstances.

3.2.2.2 Guidelines for Use

Considering each stage of the MCP procedure in turn, the recommendations are as follows:

Measure

The reference site should satisfy the following criteria:

- located in the same climatological zone as the prediction site
- have time series data concurrent with the short-term measurement period at the prediction site available
- have long-term (10-20 years) measured distributions of wind speed and direction available.
- be subject to an investigation to determine that instrumentation and measurement quality has been consistent and is acceptable in the long-term.
- alternative reference sites should be identified for use in situations where the first-choice reference site

proves unsatisfactory.

The prediction site measurements should be carried out according to the following criteria:

- the measurement mast should be located at a position on the intended turbine or wind farm site that is at least as well exposed to the wind as the intended wind turbines or wind farm.
- measurements should be carried out according to best anemometry practice.
- the wind speed and direction data should be measured and stored using an averaging period that is either directly compatible with the reference site measurements or that can subsequently be reduced to a format that is compatible with the reference site measurements.

Correlate

The choice of correlation function is quite simply that which best represents the measured data. However, the following recommendations represent normal practice:

- it can be useful to remove particularly low wind speed data (less than 3-4 m/s) before carrying out the correlations as erratic wind vane behaviour can distort the relationships.
- (optional) for large reference and prediction site separations, filtering out of higher frequency, short-term effects can improve correlation quality.
- the correlations should be carried out for each of twelve, 30 degree directional sectors (as measured at the reference site).
- a linear regression with a floating intercept gives satisfactory results in most instances. Alternative regression functions can be tested and compared on the basis of correlation quality if time and analytical capability are available.
- all raw data and best-fit regression functions should be visually checked on a scatter plot to ensure that the regression function is sensible over the entire, expected wind speed range.
- (optional) as a separate task, a relationship between the simultaneous wind direction time series at the reference and prediction sites can be determined. This can be accomplished using polynomial or discrete (matrix) methods.

Predict

The prediction stage is simply an arithmetic transposition of a joint distribution of wind speed and direction, carried out using the regression functions identified in the correlation stage of MCP. The only important recommendations reiterate the points raised in the selection of the reference site. That is:

- ensure that the long-term reference period is sufficiently long (10-20 years) to have averaged out significant year-to-year wind speed variability.
- ensure that those measurement conditions at the reference site which are likely to influence the recorded wind speed have remained similar during the long-term reference period and the short-term reference period. That is, check that regular anemometer calibrations have been carried out and that blockage sources such as foliage, trees and buildings have not appeared, disappeared or changed significantly during the long-term.

3.3 Assessment of Uncertainty

The assessment of site mean wind speed can be considered to be a form of “site calibration”, where this term already has an accepted definition in the field of wind turbine performance measurement. It was realized several years ago, see Frandsen, 1987 [34], and Frandsen and Christensen, 1992 [35], that site calibration both for machine (performance) testing and for resource assessment constitutes a most severe uncertainty, each frequently exceeding 10% and in combination often 15-20%. The potential uncertainty when considering loads would be expected to be less, though still unacceptable. The awareness of some of the pitfalls in site calibration has in itself reduced the uncertainty. However, it appears that a necessary step in improving the applicability of site calibration is an extension of the concept itself in order to include other presumed important flow characteristics than wind speed and air density. This is done below, followed by a general discussion of the uncertainties.

3.3.1 Definition of extended (long-distance) site calibration

The objective of the site calibration is to predict flow characteristics at one geographical *prediction position* (where there is or will be a wind turbine) using information/data from another position, which we denominate *reference position*. Where the purpose of the site calibration is prediction of extreme wind speeds or kinetic energy at the prediction site there will be more solid data available from the reference position, and the site calibration effectively serves to transpose that climate information to the prediction position (this is a measure-correlate-predict process). When the site calibration is applied for machine testing (power curves, loads etc.) the purpose of the site calibration is to (by means of measurements at the reference position) estimate the simultaneous flow characteristics at the prediction position.

Site calibration is defined as the action (experimental or numerical flow modelling) that links a set of flow parameters at one geographical position to the same flow parameters at another position.

In the present context the parameters are of different importance. Thus, the mean wind speed is obviously the most important parameter. To generalize the problem and to allow for non-linearity of that particular parameter, we assume that the site calibration is carried out binwise (wind speed and direction at base position: for MCP type analyses, a single wind speed bin encompassing the entire wind speed range is usually although not exclusively used in conjunction with 30 degree direction bins. For short range site calibrations, smaller wind speed and direction bins are typically used.). Assuming that in the bin the relation between the parameters (excluding wind speed) measured at the base position and the wt position is linear, the following equation to transpose the flow parameters of the base position to the wt position is applied:

$$\mathbf{x} = \mathbf{A} {}_b\mathbf{x}^{-T} + {}_0\mathbf{x} \quad , \text{ where} \quad (1)$$

$$\mathbf{x} = \{u_r, x_2, \dots, x_n\} \quad \text{and} \quad {}_b\mathbf{x} = \{{}_b u_r, {}_b x_2, \dots, {}_b x_n\} \quad (2)$$

are the parameter sets at the wt position and the base position, respectively, and

$$\mathbf{A} = \begin{bmatrix} a_{11} & a_{12} \dots & a_{1n} \\ a_{21} & a_{22} \dots & a_{2n} \\ \dots & & \\ a_{n1} & a_{n2} \dots & a_{nn} \end{bmatrix} \quad (3)$$

is the partial regression coefficient tensor, where $a_{ij}=a_{ij}(u,d)$ are functions of wind speed and direction. The determination of \mathbf{A} and the offset vector ${}_0\mathbf{x}$ is called site calibration. The coefficients of the tensor are determined row-by-row by multi-regression analysis or estimation with a flow model.

If each parameter at the wt position is a function of only that same parameter at the base position the tensor becomes diagonal, $a_{ij} = 0$ for $i \neq j$.

3.3.2 Test parameters

It is presently not clear which (x_i) and how many parameters (n) should be included in the test to significantly improve the quality/accuracy of the test. Apart from wind speed (ideally the hub height 10-minute mean U-component), it is expected that turbulence (u but possibly also v and w), flow inclination, air density, vertical and horizontal shear and humidity are of importance. However, for MCP type analyses, the reference data (typically from a national meteorological office) are generally restricted to 1-hour averages of wind speed and direction at a single height and so the practical model is severely restricted.

3.3.3 Uncertainty components

Site calibration may be performed experimentally or by application of a flow model or by a combination of the two methods. In the practical handling of uncertainty there is good guidance in the ISO guidelines, 1993 [36], and IEC 1400-12, 1997 [37].

3.3.3.1 Experimental site calibration

Though being a matter of definition, 4 groups of uncertainties can be identified in the experimental site calibration:

- instruments' uncertainties - described in IEC 1400-12, 1997 [37].
- uncertainties on determination of regression coefficients - uncertainties related to the regression analysis are outlined in annex A.
- the uncertainty on prediction when applying regression coefficients - discussed in ISO 1993, p. 76 [36].
- intrinsic uncertainties accounting for method deficiencies: the limited number of parameters, non-linearity's, "unexplained" variation etc.

Table 3.2 Uncertainty components

Group	Site calibration uncertainties	Uncertainty	Parameter
1	Instruments' uncertainty	s_1	x and $b_x x$
2	Regression coefficients	s_2	A and x_0
3	Predicted value	s_3	$b_x x$
4	Intrinsic uncertainties	Δ	-
	Total uncertainty on param. i	s_i	x

The "propagation" of uncertainties through to the final result shall not be discussed here, however IEC 1400-12, 1997 [37], gives a good description of propagation in the case that site calibration is carried out for power performance assessment.

No detailed account of the uncertainties are offered here, merely selected, basic considerations. Should the resulting group-uncertainties be uncorrelated¹, the total uncertainty on estimate of parameter x_i at the wt site becomes

$$s_i = \sqrt{s_1^2 + s_2^2 + s_3^2 + \Delta^2} \quad (4)$$

Where the experimental site calibration action is carried out to "perfection" and with, in principle, an infinite number (m) of data sets, the lower limit of uncertainty becomes

$$s_i \xrightarrow{m \rightarrow \infty} \sqrt{s_1^2 + \Delta^2}, \quad (5)$$

because the uncertainties in group 2 and 3 are by nature statistical and therefore decrease with increasing amount of data. Thus, the uncertainty has a lower limit, determined by uncertainties of instruments and deficiencies of the site calibration model applied. Taking one step further by assuming the instruments' uncertainties to be negligible, the resulting uncertainty has a lower limit determined by the quality of the method itself and the number of physical quantities measured.

Discussion.

¹ The validity of the statement is not obvious and should be addressed in new research.

As stated, site calibration is made for two purposes, prediction of climate or for wind turbine testing. Typically, the difference in test circumstances for the two is distance between base- and wt position. When aiming at climate prediction at a prospected wind turbine (farm) site, the distance varies from a few km to tens of km, and for wind turbine performance test purposes the distance spans from about 100m to 1-2 km. The difference in separation between positions results in different needs of the extent of the data base for determination of regression coefficients and constants (group 2), and input data (group 3). However, group 2 and 3 uncertainties, as defined here, will decrease with increasing amount of data, and the uncertainties may be calculated on-line from the accumulating data base to determine when group 2 and 3 uncertainties are negligible compared to group 1 and 4 uncertainties.

Instruments' uncertainties (group 1) set limits on the integrated site calibration uncertainty. Assuming diagonality of the site calibration tensor, it could be argued that the integrated uncertainty stemming from instruments is the root-sum-square of instrumental uncertainties at the two positions. However, if e.g. anemometer calibration has an uncertainty, which is biased identically for the instruments applied at both positions, these bias errors could to some extent cancel each other. However, for an MCP type measurement/analysis, the reference wind speed measurements will usually be carried out by a third party (e.g. meteorological office) and so it may not be straightforward to gain access to and interpret calibration and uncertainty information. In this situation, it is unlikely that the bias errors at the reference and prediction sites would cancel.

An instrument uncertainty, which deserves special attention especially in complex terrain is related to the quality of the cosine response of the cup anemometers which are typically applied, Pedersen and Paulsen, 1997 [38]. The cup anemometer measures, in principle, horizontal flow speed if the mean velocity vector is horizontal, and if the vector is not horizontal, the horizontal component of the vector is ideally measured. As it is, many cup anemometers have a less than ideal cosine response. Therefore, if there is a difference in flow inclination at the two positions the site calibration results may be erroneous or directly misleading.

Summing up, the following comments to experimental site calibration can be made:

- Instrument uncertainties are fairly well covered (IEC 1400-12, 1997 [37]), though see above comment on cosine response. Uncertainties of the important wind speed measurement ranges from 1 to 5%, and may be up to 15% under special conditions². Other instruments are less uncertain, 1% or less.
- The uncertainties of regression coefficients and application of these are by nature statistical and may in principle be eliminated by sufficient data. Quantification of uncertainties still has to be evaluated.

It is known that the site calibration procedure presently used is inadequate in cases where e.g. shear and turbulence are different at base and wt position. Adopting the more general definition in this section, the great challenge in experimental site calibration is the identification of the intrinsic uncertainty (group 4), or expressed another way: the lower uncertainty limit?

3.3.3.2 Numerical site calibration

In many real life cases the experimental site calibration is ruled out as too costly and time consuming. The alternative is numerical flow modelling, which *a priori* is expected to be less accurate, but far less costly.

As outlined in Derrick et al. [39], and described in section 2.3.7, a number of different models are available and used for site evaluation. The most widely used flow model is the so-called WA^{SP} model developed at Risø National Laboratory. Nominally, the use of the model is limited to neutrally-stable wind flows over low, smooth hills with attached flows. Being easy to apply, the model is nevertheless used where terrain is excessively rugged and/or the atmosphere unstable. Mortensen and Petersen, 1997 [40], evaluate success of the model by comparison with measurements made in Portugal. A total of 3½ years of

² Note that the uncertainty of the wind speed measurement affects also uncertainty of shear, turbulence etc.

data from 8 met stations with separations of from 2 to 16 km were available for comparison. Only mean wind speed was considered and compared from station to station. The influence of ruggedness of terrain and the influence of quality/quantity of the topographical input data were analyzed, with the results presented below.

A ruggedness index (RIX) was defined as the percentage of terrain slope between two points exceeding 0.3. The results for the Portuguese sites show that a low RIX at the base (reference) position and a high RIX at the wt (predicted) site leads to over-estimation of wind speed at the wt site, and vice versa. The prediction error is with fair approximation linear in the difference in RIX of base- and wt positions, respectively. A difference in RIX of 20% corresponds to a prediction error of approx. 40%. The standard error³ is of the order 5-10%.

The importance of the size of the area covered by the flow model was investigated, the result being that the area should be 8x8 km or larger so as not to introduce significant errors this way. Also, the influence of height-contour line interval was analyzed, indicating that intervals of 20m or less should be used to avoid gross errors from this source. Finally, the accuracy of the contour representation was assessed. Referring to Figure 3.1, the accuracy was varied by removing points P2 from a contour line P1P2P3, where the distance x from that point P2 to the resulting approximate contour line, P1P3, was less than a certain distance. It was found that errors were minimized if the distance, x , was 50m or less.

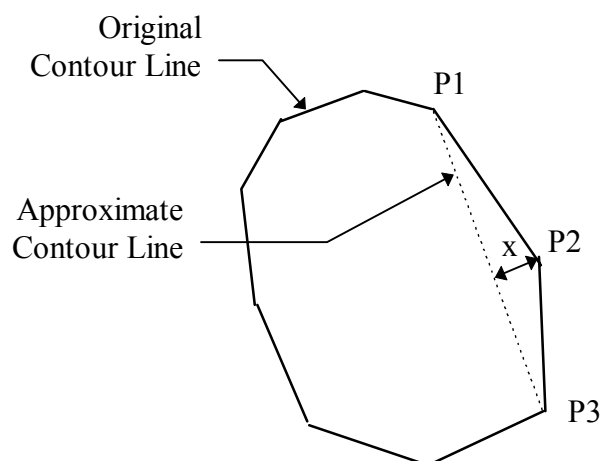


Figure 3.1 Graphical definition of contour accuracy.

The uncertainty of numerical site calibration for shorter separations (100m to 1-2 km) is poorly investigated so far. However, ongoing work in another EU financed project is expected to shed light on the issue.

Discussion

- The study referred to focuses on errors of numerical estimation of climatic information from the base- to the wt position over distances of 2 to 16 km. An important finding of Mortensen and Petersen [40] is that the prediction error seemingly is not a function of distance between base- and wt position.
- Further, the study points to the ruggedness of the terrain as the most important error source. For large ruggedness - where the WASP code is really outside its operation limits - the site calibration error may be excessive.
- The good correlation between the defined ruggedness index seems to open ground for a “ruggedness correction”. Assuming such a correction is made the remaining standard uncertainty is of the order 5-

³ Standard error: defined as the vertical root mean square deviation from a linear fit to the individual estimates, see annex A.

10%, being smallest for low ruggedness.

3.3.4 Additional Uncertainties due to Long-Term Climate Variability

The annual mean wind speed is the standard, minimum output from an MCP or Wasp analysis. As previously described, the “prediction” is derived by mapping the measured wind regime from a long-term reference site onto the prediction site using either

- relationships derived from concurrent short-term measurements at both sites (MCP) or
- a numerical wind flow model (WAsP).

Therefore, the “prediction” is in fact a historical reconstruction of what the wind regime would have been at the prediction site over the same period in time (usually of 10 to 20 years duration) that the long-term measurements were carried out at the reference site. Wind farm financiers are interested in the future wind regime which will influence the wind farm economics but all that can be delivered to them is a reconstruction based on a period in the past as we cannot predict the future. This conflict of requirements can be dealt with in numerical terms by considering extra components of uncertainty.

Consider as an example the case where an MCP analysis has been carried out on a site in the UK based on a long term reference data set of 10 years duration. Very long-term (i.e. 100 year) statistics show that the average annual wind speed at sites throughout the UK does vary from decade to decade. Therefore there is a probability that the average wind speed experienced over the next decade will differ from that experienced over the past decade and similarly, the mean wind speed experienced over a 10-year reference period, 1980-1989 say, may well be different to that experienced over the next ten years. This variability can be represented in terms of the basic statistics of these long-term measured wind speeds [41]. Therefore, it is possible to give an estimate in probabilistic terms of the most likely future wind speed based on knowledge of the historic variability.

Besides the measurement uncertainties, the uncertainties associated with the correlation and prediction stages of the MCP or WAsP include the following:

- a) the statistical uncertainty in the short term wind speed correlations (MCP) or the numerical model uncertainties, s_a .
- b) the statistical uncertainty in the reference period (e.g. ten year) sample mean due to long-term climate variability at the long-term reference site, s_b .
- c) the statistical uncertainty in the annual mean wind speed prediction due to year to year variability of the reference annual mean from the reference period (e.g. ten year) mean, s_c .

The following sections detail the assessment of these individual components of uncertainty.

a) **Uncertainties inherent in the prediction technique (MCP or WAsP)**

As applied at present, the MCP analysis technique involves determination of the relationships between the wind speeds at the reference and prediction sites over a short-term period. In most cases a simple “least-squares” analysis is used to determine the best fit line relating the wind speeds at the prediction site to those at the reference site. Other regression techniques may be used for which the principles described here still apply. Using any statistical regression technique, it is generally possible not only to derive the “best-fit” relationship but also an uncertainty due to the “goodness” of fit [37]. For example, if we have in simple, one-independent-variable regression

$$V = \alpha + \beta U \tag{6}$$

then the uncertainties on the regression parameters⁴ are

⁴ Wannacott and Wannacott, *Regression: a second course in statistics*, John Wiley & Sons, 1881.

$$s_{\alpha} = \frac{1}{\sqrt{n}} \frac{\sigma}{\sigma_u} \quad \text{and} \quad s_{\beta} = \frac{\sigma}{\sqrt{n}} \quad (7)$$

where n is the number of data sets, σ the standard error (scatter around line) and σ_u is the RMS of U_i (data normalized so that $\langle U \rangle = 0$, ensuring independence of α and β).

When the regression results are used for prediction: The standard uncertainty of the *mean of V* (V_0) when predicted with a (fixed) value of U (U_0) is then

$$s_{mean}(V_0) = \frac{\sigma}{\sqrt{n}} \sqrt{1 + \frac{U_0^2}{\sigma_u^2}} \quad (8)$$

If 1) σ_u is small (bad coverage of wind speed range), 2) U_0 large (far from mean of values used for regression analysis - the case when talking extremes), or 3) σ is large (much scatter around line, bad correlation), then we get a poorly determined prediction of V_0 . Prediction of the individual V_0 is much larger⁵. This uncertainty can be carried through to the prediction stage of the analysis and appears as an uncertainty in the predicted annual average wind speed. Experience of applying the MCP technique to many sites in the UK reveals that the value of the standard uncertainty, s_{α} , associated with correlation quality is typically 0.5 - 2.0% of the predicted annual average wind speed. If this uncertainty component is found to be much greater than this, then it suggests that the reference site is not ideal and perhaps another reference site offering a better wind speed relationship with the prediction site should be identified.

In the case of WAsP or a more sophisticated measurement based MCP (site calibration) than is presently possible, the evaluation of this component of uncertainty is as described in Sections 3.3.1 to 3.3.3.

b) Statistical Uncertainty Due to Long-Term Climate Variability

Determination of this component of the uncertainty requires detailed knowledge of the very long-term wind regime (i.e. 100 years). Such data are only available for a very limited number of sites, which are generally unlikely to be suitable for use directly as the reference site in an MCP or WAsP analysis. However, such long term trends are, within the geographical locality of a region or country such as the UK, not likely to be strongly influenced by the specific site location. Rather, such trends are driven by relatively large-scale climate variations. Therefore, in the case of the UK wind climate which is dominated by Atlantic weather systems, it is assumed that the 100 year wind speed trends observed at the few UK sites with such records can also be applied to any specific location within the UK .

Annual mean wind speed data for 31 UK Meteorological Office sites have been reconstructed for periods of 100 years and are described in a report commissioned by the UK Department of Energy [41, 42]. These data can be used to estimate the decade-to-decade wind speed variability. To do this, the statistics for the ten-year running annual average wind speed for each of the 31 sites have been extracted from [42]. For each of the 31 sites, the statistics of interest comprise the mean ten-year average wind speed and the standard deviation. These data are plotted in Figure 3.2.

$$^5 s_{one}(V_0) = \frac{\sigma}{\sqrt{n}} \sqrt{1 + \frac{U_0^2}{\sigma_u^2} + n}$$

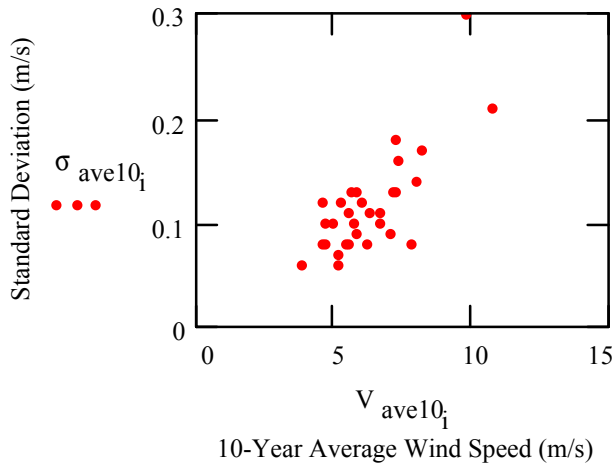


Figure 3.2 Statistics of ten-year-average wind speeds for 31 sites over a 100-year period.

The data suggest that the standard deviation of ten-year-average wind speeds at all 31 sites over 100 years is approximately proportional to the ten-year-average wind speed. Hence, for the predicted ten-year-average wind speed at the prediction site, the appropriate standard deviation can be estimated by determining and applying that relationship.

From the slope of the best-fit line to the data in Figure 3.2, the standard uncertainty, s_b , of the ten-year average due to long-term climate variability is estimated to be 2.4% of the ten-year-average wind speed for sites in the UK. The situation in other countries may however be different (e.g. a study [35] in Denmark indicated an RMS of 8 per cent on the long-term average wind speed. Due to the nature of the input data for all such analyses, the uncertainty involved is unavoidably high.

c) Statistical Uncertainty Due to Inter-Annual Variability

Continuing with the ten-year average example, the measured ten-year average wind speed, μ_{10} , over the actual historical reference period of ten years also has an uncertainty associated with the sample variance. Considering the ten annual average wind speeds from which the ten-year average is composed, which have a standard deviation σ_1 , then the standard uncertainty in the ten year mean is

$$s_c = \frac{\sigma_1}{\sqrt{10}} \quad (9)$$

Although this component of uncertainty has been derived from measurements at the reference site, it is assumed to apply also to the prediction site for that same ten year period.

Combined Uncertainty

Finally, it is assumed that all three components of uncertainty are uncorrelated and hence can be combined quadratically to give the standard uncertainty, s_{10} (excluding measurement effects) of the predicted ten year average wind speed.

$$s_{10} = \sqrt{s_a^2 + s_b^2 + s_c^2} \quad (10)$$

Exceedance Wind Speed

It is commonly required to present the predicted mean wind speed as that value which has a 90 per cent chance of exceedance. The 90 per cent exceedance wind speed is that wind speed defined by the lower boundary of the 80 per cent confidence band on the distribution of ten-year-average wind speeds. By

assuming that the ten-year-average wind speeds follow a normal distribution, the coverage factor, x , corresponding to the 80 per cent confidence band is

$$x = 1.28$$

Hence, the ten-year-average wind speed with a 90 per cent chance of exceedance, V_{e90} , is defined in terms of the central estimate, V_{10} , and the standard uncertainty s_{10} , by:

$$V_{e90} = V_{10} - xs_{10} \quad (11)$$

In illustrating this example, a ten-year averaging period has been used, however, the principles can be applied to other averaging periods. Furthermore, the long-term climate data presented here is only assumed applicable to the UK. Similar data would have to be sourced and processed for countries subject to different climates.

3.3.5 Conclusions on Uncertainty

Though some work has been done there is a fundamental lack of firm information on uncertainties related to experimental site calibration. Basic problems are the lack of a precise definition of quantities to measure, foremost “wind speed”. The presently used cup anemometer has several inherent problems such as non-ideal cosine response.

An alternative definition of site calibration has been introduced as a means to reduce the inherent uncertainties related to conventional site calibration.

A frequently used flow model has been investigated for large separations (2-16 km), showing that the quality of the model’s prediction is strongly dependent on the ruggedness of the terrain in question, but not the magnitude of separation. Assuming that corrections are made for ruggedness, the standard uncertainty was of the order 5-10%, smallest for small ruggedness.

4. OTHER PARAMETERS

This section deals with the site assessment parameters other than annual average wind speed (which is treated in other parts of the document), as these appear in the relevant standard IEC 1400-1 [2]. These parameters include the “other” parameters describing normal wind conditions and the “additional” parameters which are used in the various sub-models specified in the standard. For each parameter method(s) of measurement, analysis and uncertainty calculation are given. Since in some cases the standard leaves room for interpretation, a list of suggested changes to definitions in the standard is presented in section 4.7.

According to the standard, normal wind conditions are specified by the three so-called basic parameters;

- Reference wind speed
- Annual average wind speed at hub height, and
- Turbulence intensity at 15 m/s;

in combination with models for

- Wind speed distribution,
- Normal wind profile, and
- Normal turbulence.

These wind conditions must be assessed at the site. Since the annual average wind speed at hub height is related to the wind speed distribution model, and the turbulence intensity at 15 m/s is related to the normal turbulence model, four parameters remain to be assessed. In this chapter methods to measure these four parameters are presented: reference wind speed (section 4.1), turbulence intensity at 15 m/s (section 4.2), annual average wind speed distribution (section 4.2.1) and normal wind profile (section 4.3.1).

The theoretical background to each parameter is presented in Appendix A.

4.1 Reference Wind Speed

4.1.1 Description of Parameter

According to the standard (IEC1400-1ed2 [2]), *the reference wind speed, V_{ref} , is the extreme 10 min average wind speed at turbine hub height with a recurrence period of 50 years*. The objective thus is to specify methods to determine this reference wind speed from observed wind speeds, which must be 10 min average wind speeds.

Note that extreme wind speed is a stochastic parameter which must be expressed in terms of probabilities. This means that values of the reference wind speed are probabilistic rather than exact. That is, V_{ref} does not occur exactly once in a period of 50 years; there is a probability of $1-(0.98)^{50} = 64\%$ that V_{ref} is exceeded once or more in a period of 50 years. A more detailed investigation of the analysis of extreme wind speeds is presented in the work of sub-project 1 (Load Spectra and Extreme Winds), earlier in this report.

4.1.2 Methods of Assessment

Given the definition of the reference wind speed, determining V_{ref} requires determining the cumulative distribution function $F_e(u_e)$ of extreme wind speed u_e . More specifically, it involves determining the inverse dispersion factor α and the modal value β of the Gumbel distribution from observed extreme wind speeds. There are two methods to achieve this:

By directly estimating α and β from the extremes in a time series of wind speed, and

By indirectly estimating α and β from the Weibull parameters A and k , and the number of independent extremes M ; where A , k and M are estimated from a time series of wind speed.

In this report the “direct” method is considered to be the standard Gumbel analysis. To date, various forms and refinements of this standard analysis have been presented amongst which:

The original Gumbel method [43], which has also been presented in various forms,

The method of independent storms [44],

The Gumbel-Lieblein method [45], and

The Gumbel-Harris method [46].

In this report the “indirect” method is considered to be the generalized Gumbel analysis. It will be referred to as the Gumbel-Bergström method [47]

Only various forms of the original Gumbel method together with the Gumbel-Bergström method will be presented in this report.

4.1.2.1 Original Gumbel Method

The original Gumbel method was made operational by Shellard [43]. In this method it is assumed that a series of M independent observations of extreme wind speed is available. Furthermore it is assumed that M is large enough for the asymptotic distribution to be valid. Since how to establish a minimal value for M is not part of the method, M usually follows from the procedure to select independent extremes. For example, this is realized by finding the annual largest wind speeds from many-years of hourly average wind speeds. Since the practical value of M is usually small, generally the Gumbel distribution is not valid.

However, in the original Gumbel method the probability $F_e(u_e)$ an extreme wind speed u_e is not exceeded in one year is identified with a value

$$F_{e,j} = \frac{j}{M+1} \tag{12}$$

where j is the rank of the extreme when sorted in ascending order. Usually F_j is referred to as the plotting position. Since it is assumed the distribution

$$F_{e,j} \equiv F(u_{e,j}) = \exp(- \exp(- \alpha(u_{e,j} - \beta))) \tag{13}$$

is valid, it follows that

$$\ln(- \ln F_{e,j}) = -\alpha(u_{e,j} - \beta) \tag{14}$$

As a consequence, the Gumbel parameters α and β can be obtained from the slope and an intercept of a plot of $\ln(- \ln F_{e,j})$ versus $u_{e,j}$. When performed graphically, this method is referred to as the “Gumbel paper” method (which usually employs probability or recurrence period as the horizontal axis and extreme wind speed as the vertical axis).

To deal with the effect of too low a number of independent extremes (most probably) [48], an empirically improved plotting position was suggested [49, 50]:

$$F_{e,j} = \frac{j - 0.3}{M + 0.4} \tag{15}$$

This equation should give a more realistic probability of the smaller as well as the larger extremes.

The procedure to obtain the Gumbel parameters α and β on the basis of the original Gumbel method then is:

- Collect ten-minute average wind speeds during many years;
- Select the M annual-largest ten-minute average wind speeds $u_{e,i}$, where M is the number of years;
- Rank the extreme wind speeds $u_{e,i}$ in ascending order, so that a new series $u_{e,j}$ of extreme wind speeds is obtained (smallest extreme $j = 1$ and largest extreme $j = M$);
- Determine the M quantities $x_j = u_{e,j}$;
- Either determine the M quantities
 - (a) $y_j = \ln\left(-\ln\left(\frac{j}{M+1}\right)\right)$ or
 - (b) $y_j = \ln\left(-\ln\left(\frac{j-0.3}{M+0.4}\right)\right)$;
- On the basis of the x_j and y_j find a value for the parameters α and β by
 - (a) numerically determining the best linear fit to the relation $y = -\alpha x + B$, giving α and B , and
 - (b) solving β from $B = \alpha\beta$

The reference wind speed V_{ref} subsequently follows from

$$V_{ref} = \beta - \frac{1}{\alpha} \ln\left(-\ln\left(F_{e,V_{ref}}\right)\right) \quad \text{with} \quad F_{e,V_{ref}} = 0.98 \quad (16)$$

On that basis the uncertainty ΔV_{ref} in the reference wind speed is given by:

$$\left(\Delta V_{ref}\right)^2 = \left(\frac{\partial V_{ref}}{\partial \beta}\right)^2 (\Delta \alpha)^2 + \left(\frac{\partial V_{ref}}{\partial \alpha}\right)^2 (\Delta \beta)^2 = \frac{1}{\alpha^4} \left(\ln\left(-\ln\left(F_{e,V_{ref}}\right)\right)\right)^2 (\Delta \alpha)^2 + (\Delta \beta)^2 \quad (17)$$

Here $\Delta \alpha$ and $\Delta \beta$ are the uncertainties in the inverse dispersion factor and the modal value, as these follow from the best linear fit.

4.1.2.2 Gumbel-Bergström Method

In the Gumbel-Bergström method it is recognized that the Weibull distribution is the parent distribution of the distribution of extreme wind speed [47]. This implies the relations can be employed which express the Gumbel parameters α and β in terms of the Weibull parameters A and k , and the number of independent observations M . In other words: If the distribution of average wind speed at a site is known in terms of the two Weibull parameters, the distribution of extreme wind speed at that site is known as well when the number of independent wind speeds is known. Hence, a method is provided to determine M from a time series of average wind speed. Note this time series need not be a long-time record.

As a first step, M must be determined. Suppose now wind speed has been measured with an averaging time T_{ave} during a total time T . Then a time series with $N=T/T_{ave}$ average wind speeds is available. In general, these N observations are dependent. In order to obtain independent observations, the time series must be broken down into M independent sub-series. This number is related to the total time T via $M = T/T_M$, where T_M is the time between independent observations in the time series. Equivalently, M follows from

$$M = v_M T, \quad (18)$$

where $\nu_M = 1/T_M$ is the frequency of independent observations.

An average time between independent observations in a time series may be obtained from the average time between two observations which are correlated for 50% [47]. If $S(f)$ is the spectral density function of the time series, it can be shown that the average frequency of independent observations can be estimated from

$$\nu_M^2 = \frac{\int_{f_1}^{f_2} f^2 S(f) df}{\int_{f_1}^{f_2} S(f) df} \quad (19)$$

with $f_1 = 1/2T_c$ the lower and $f_2 = 1/2T_{ave}$ the upper integration limit; where T_c is a cut-off time scale.

It has however been found that ν_M does not depend strongly on the actual spectral density function, so that values from a typical spectrum may be used. These values are presented in Table 4.1. The data in this table allow convenient rules of thumb to be established. For example, if a time series is obtained with an averaging time of 10 min, every third observation is independent from the first one.

As a second step in the Gumbel-Bergström method, the Weibull parameters A and k must be determined from the time series with average wind speeds. To this end standard methods can be employed, which methods will not be presented here.

Having available the parameters M , A and k , the Gumbel parameters follow from

$$\frac{1}{\alpha} = \frac{A}{k} (\ln M)^{\frac{1}{k}-1} \quad \text{and} \quad \beta = A (\ln M)^{\frac{1}{k}} \quad (20)$$

It however has been reported that α 's and β 's from this equation yield a biased extreme value analysis. To solve this problem an empirical correction was suggested: *increase the value of the Weibull parameter A as obtained from the time series by 10%* [51].

Table 4.1 The frequency ν_M of independent wind speeds as a function of the averaging time T_{ave} .

T_{ave} [s]	ν_M [Hz]
3600	$2.8 \cdot 10^{-5}$
600	$7.3 \cdot 10^{-4}$
60	$1.0 \cdot 10^{-3}$
10	$4.6 \cdot 10^{-3}$
5	$7.9 \cdot 10^{-3}$
3	$1.0 \cdot 10^{-2}$
1	$2.4 \cdot 10^{-2}$

The procedure to obtain the Gumbel parameters α and β on the basis of the Gumbel-Bergström method is then:

- Collect ten-minute average wind speeds during a period T ,
 - (a) Either determine the frequency ν_M of independent wind speeds from the spectrum of the observed wind speeds, or
 - (b) use the value $\nu_M = 7.3 \cdot 10^{-4}$ Hz from a typical spectrum;
- Determine the number M of independent wind speeds from $M = \nu_M T$;
- Determine the Weibull parameters A and k from the time series with ten-minute average wind speeds using a standard method;
- (Optional) Increase the Weibull scale parameter A by 10%;

Determine the Gumbel parameters α and β from $\frac{1}{\alpha} = \frac{A}{k}(\ln M)^{\frac{1}{k}-1}$ and $\beta = A(\ln M)^{\frac{1}{k}}$

The reference wind speed V_{ref} subsequently follows from

$$V_{ref} = \beta - \frac{1}{\alpha} \ln\left(-\ln\left(F_{e,V_{ref}}\right)\right) \quad \text{with} \quad F_{e,V_{ref}} = 0.98 \quad (21)$$

The uncertainty in the reference wind speed is conveniently expressed in terms of the uncertainty in the Gumbel parameters:

$$\left(\Delta V_{ref}\right)^2 = \left(\frac{\partial V_{ref}}{\partial \alpha}\right)^2 (\Delta \alpha)^2 + \left(\frac{\partial V_{ref}}{\partial \beta}\right)^2 (\Delta \beta)^2 \quad (22)$$

Since the Gumbel parameters now depend on the Weibull parameters A and k as well as the number M of independent wind speeds, their uncertainties follow from

$$\left(\Delta \alpha\right)^2 = \frac{1}{A^2} (\ln M)^{2-\frac{2}{k}} \left[\left(\frac{k}{A}\right)^2 (\Delta A)^2 + \left(1 + \frac{1}{k} \ln \ln M\right)^2 (\Delta k)^2 + \left(\frac{k}{M}\right)^2 \left(1 - \frac{1}{k}\right)^2 (\ln M)^{-2} (\Delta M)^2 \right] \text{and}$$

$$\left(\Delta \beta\right)^2 = (\ln M)^{\frac{2}{k}} \left[(\Delta A)^2 + \frac{A^2}{k^4} (\ln \ln M)^2 (\Delta k)^2 + \left(\frac{A}{kM}\right)^2 (\ln M)^{-2} (\Delta M)^2 \right] \quad (23), (24)$$

respectively. The uncertainties ΔA and Δk in the Weibull parameters follow from the Weibull method.

The uncertainty in the number of independent wind speeds is

$$\Delta M = T \Delta v_M + v_M \Delta T \quad (25)$$

where Δv_m is the uncertainty in the frequency of independent observations and ΔT is the uncertainty in the total time. (Note these uncertainties are not statistical in nature.)

4.1.3 Instrument requirements

Since determining the reference wind speed basically comes down to measuring wind speeds and averaging over an appropriate time period, instrument requirements are as described in IEC 1400-12 [37] in relation to anemometry. However, it should be noted that the anemometer and data acquisition system measurement range should be configured to allow measurement of wind speeds over a much greater range than would be required for a power performance measurement. Whereas a power performance measurement may only require measurement of wind speeds at up to just above turbine cut-out (e.g. 30 m/s), in a site assessment all wind speeds are of interest and so the upper limit of the measurement range (depending on the site) may be 60 m/s or more. These requirements are described in section 4.3.3.

4.1.4 Further Reading

The original standard Gumbel method for extreme wind speed analysis was first presented by Shellard [43]. Overviews of this method can be found in the books by Freris [52] and Wieringa and Rijkoort [50] and the paper by Mayne [53]. Other standard Gumbel methods were described by Lieblein [45], Cook [44], and Harris [46]; the latter also providing an overview of the standard Gumbel methods. The general Gumbel method, introducing how to determine the number of independent observations from the data,

was first presented by Bergström [47]. A different approach was taken by Rijkoort [54], also described in Wieringa and Rijkoort [50], who developed a so-called compound Weibull model allowing for analysis of extreme winds. Since it deviates from the general “Gumbel” trend and requires a laborious data analysis, the Rijkoort method was not presented here.

4.2 Reference Turbulence Intensity

4.2.1 Description of Parameter

According to the standard (section 7.2 [2]), *turbulence intensity at 15 m/s I_{15} is the characteristic value (mean plus standard deviation) of hub height turbulence intensity at a 10 min average wind speed of 15 m/s. The value I_{15} shall be determined using appropriate statistical techniques applied to measured data obtained at wind speeds greater than 10 m/s. (Note, for example, turbulence intensity can be overestimated when low-frequency trends exist in the wind speed data.) Where topographical or other local effects may influence the turbulence intensity then these effects shall be represented in the data. The characteristics of the anemometer, sampling rate and averaging time used to obtain measured data can influence the assessment of turbulence intensity. These effects shall be considered when predicting the turbulence intensity from measured data.* The objective thus is to specify methods to determine this characteristic turbulence intensity from wind speeds observed over periods of 10 min.

4.2.2 Methods of Assessment

If wind speed is measured contiguously with a sampling time ΔT over a time period T , the mean μ_i and the standard deviation σ_i of the wind speed in the i th time interval follow from:

$$\mu = \frac{1}{T} \int_{t_i}^{t_i+T} u(t) dt \quad \text{and} \quad \sigma_i^2 = \frac{1}{T} \int_{t_i}^{t_i+T} (u(t) - \mu_i)^2 dt \quad (26)$$

The turbulence intensity I_i for the i th time interval subsequently is defined as the ratio of the standard deviation and the mean of the wind speed for the i th time interval:

$$I_i \equiv \frac{\sigma_i}{\mu_i} \quad (27)$$

In addition, the turbulence intensity I_u at the wind speed u is defined as

$$I_u \equiv \frac{\sigma_u}{u} \quad (28)$$

that is the ratio of the standard deviation of the wind speed at the wind speed u , and that wind speed. (Note the difference in the definition of I_u with respect to the standard; see below.)

The turbulence intensity I_u is obtained by conditionally sampling the turbulence intensities I_i . To this end those I_i are selected for which $|\mu_i - u| < \Delta u$; where Δu is the bin width. If the corresponding number of time intervals is M , the average turbulence intensity at u is

$$\mu_{i,u} = \frac{1}{M} \sum_{j=1}^M I_j \quad (29)$$

The corresponding standard deviation $\sigma_{i,u}$ of the turbulence intensity at u follows from:

$$\sigma_{I,u}^2 = \frac{1}{M} \sum_{j=1}^M (I_j - \mu_{I,u})^2 \quad (30)$$

The characteristic turbulence intensity \tilde{I}_u subsequently is defined as the sum of the mean and the standard deviation of the turbulence intensity at the wind speed u :

$$\tilde{I}_u \equiv \mu_{I,u} + \sigma_{I,u} \quad (31)$$

(Note the difference in notation with respect to the standard; see below.) It is straightforward to show that the characteristic turbulence intensity \tilde{I}_{15} at a wind speed of 15 m/s is \tilde{I}_u with $u = 15$ m/s. The bin width Δu may be selected as 0.5 m/s in line with IEC 88/1400-12.

The preceding method is based on the definition in the standard, which states that “ I_{15} ” is a characteristic turbulence intensity (rather than the turbulence intensity). To prevent “ I_{15} ” from being erroneously interpreted as *the* turbulence intensity at a wind speed of 15 m/s, as could be read from the description of symbols and units in the standard (section 1.4 [2]), in this method the symbol I_u is exclusively used for the turbulence intensity at the wind speed u . Hence the symbol \tilde{I}_u has been introduced for the characteristic turbulence intensity. See section 4.7 for suggestions for improving the terminology used in the standard with respect to turbulence.

The conditional sampling procedure, retaining only the I_i 's for which $|\mu_i - u| < \Delta u$ with $u = 15$ m/s and $\Delta u = 0.5$ m/s, automatically ensures that the value \tilde{I}_u is determined from wind speeds which are greater than 10 m/s.

In general, turbulence intensity is affected by topographical effects like orography, surface roughness and obstacles, where obstacles can be other wind turbines. Usually this implies that turbulence intensity depends on the wind direction. As a consequence, a sectorwise analysis must be performed resulting in sectorwise values of \tilde{I}_u . If a conservative approach is required, the largest sector value may subsequently be chosen as the one representing the site, otherwise, the overall average value for all directions may be adequate

The procedure to obtain the characteristic turbulence intensity \tilde{I}_{15} at a wind speed of 15 m/s is then:

- Collect ten-minute average μ_i and standard deviation σ_i data of the wind speed, and ten-minute average wind direction during a representative time period (the reference standard recommends a minimum period of 6 months);
- Determine the ten-minute turbulence intensities $I_i = \sigma_i/\mu_i$;
- For each wind direction sector (propose 30 degree sectors), select the M observations of I_i for which $14.75 \text{ m/s} < \mu_i < 15.25 \text{ m/s}$;
- For each sector determine the average turbulence intensity at 15 m/s from: $\mu_{I,15} = \frac{1}{M} \sum_{j=1}^M I_j$
- For each sector determine the standard deviation in the turbulence intensity at 15 m/s from: $\sigma_{I,15}^2 = \frac{1}{M} \sum_{j=1}^M (I_j - \mu_{I,15})^2$;
- For each sector determine the characteristic turbulence intensity at 15 m/s: $\tilde{I}_{15} \equiv \mu_{I,15} + \sigma_{I,15}$
- For a conservative assessment, select the largest sectorwise \tilde{I}_{15} as the one representing the site,

otherwise determine the overall average value of \tilde{I}_{15} to represent the site condition.

4.2.3 Measurement Requirements

4.2.3.1 Anemometer

Determining turbulence characteristics requires an anemometer which has a sufficiently fast response to measure the small-scale variations. Although the cup anemometer is not the ideal instrument for this work, compliance with the standard for power measurement as described in IEC 88/1400-12 ([section 3.2 [37]]) warrants its use.

In a turbulent wind a cup anemometer over estimates the mean wind speed. As a consequence, the resulting turbulence intensity is underestimated. This so-called overspeeding originates from a cup anemometer responding faster to an increase in wind speed than to a decrease of the same magnitude due to inertial effects. On experimental as well as theoretical grounds it has been found that the over-speeding is proportional to the turbulence intensity of the wind. If u is the mean wind speed and u_m is the mean wind speed measured by the cup anemometer, in the case of negligible vertical turbulence the relative over-speeding may be expressed as [55]:

$$\frac{u_m - u}{u} \propto J_u I_u^2 \quad (32)$$

where the factor J_u depends on the characteristics of the anemometer (in the form of the distance constant) and the wind (in the form of the inverse length scale of the energy containing eddies). It follows that the mean wind speed can be obtained from the mean wind speed measured by the cup anemometer:

$$u \approx \frac{1}{1 + J_u I_u^2} u_m \quad (33)$$

A typical expression for the factor J_u is [55]:

$$J_u = \frac{L \kappa_E}{1 + L \kappa_E} \quad (34)$$

where L is the distance constant of the cup anemometer and κ_E is the inverse length scale of the energy containing eddies. These expressions can be used to derive a requirement for L on the basis of the wind characteristics and the accepted relative over-speeding:

$$\frac{1}{L} = \kappa_E \left(\frac{u}{u_m - u} I_u^2 - 1 \right) \quad (35)$$

For example, if the expected turbulence intensity at a site is 25% and the scale of the energy containing eddies is 10m, a cup anemometer must be used with a distance constant of less than 1.9 m if the relative over-speeding is to be less than 1%. Ideally, a cup anemometer is employed which has a small intrinsic over-speeding. On the basis of an earlier recommendation (section 7.4)[56], it is recommended here to only use cup anemometers with a distance constant of less than 2 m when turbulence characteristics are to be measured.

On the other hand, these expressions can be used in order to determine the relative over-speeding of a given cup anemometer, which by the way must have a distance constant of less than 5 m to comply with the standard for power measurement (section 3.2 [37]). Since this over-speeding affects the turbulence intensity through the average wind speed, a compensated value μ'_i for the average wind speed must be

employed:

$$\mu'_i = \frac{1}{1 + J_u I_i^2} \mu_i \quad (36)$$

The compensated turbulence intensity I'_i in that interval subsequently is:

$$I'_i = \frac{\sigma_i}{\mu'_i} \quad (37)$$

Note the standard deviation σ_i of the wind speed in the interval is not compensated for the non-linear response of the cup anemometer.

The requirements for the anemometer thus are as follows:

- A cup anemometer with a distance constant of less than 2 m is recommended;
- If a different cup anemometer is used, it must have a distance constant smaller than 5 m.

Regarding application of the data from the cup anemometer:

- For each time interval the relative over-speeding must be estimated from $J_u I_i^2$, where I_i is the turbulence intensity measured in that interval;
- The over-speeding effect on mean wind speed should then be considered in the determination of the uncertainty in the turbulence intensity I_i . It is unlikely to be sensible to apply an over-speeding correction in the determination of the turbulence intensity however.

These requirements ensure that the effect of cup anemometer over-speeding on the characteristic turbulence intensity is quantified.

4.2.3.2 Data Acquisition and Pre-processing

The anemometer signals must be sampled at a rate such that all relevant wind speed variations are recorded. Since the Kolmogorov frequency f_K is the highest frequency in a turbulent wind, the sampling rate should theoretically be $2f_K$. Obviously, no cup anemometer can meet this requirement because a cup anemometer has a limited frequency response. If f_m is the cup anemometer cut-off frequency, the sampling rate must be of the order of f_m . (Note that the cup anemometer is a poor instrument for turbulence measurement because generally $f_m < f_K$.) To comply with the standard for power measurement, the minimal sampling rate must however be 0.5 Hz (section 3.7 [37]).

Turbulence, i.e. the variation of the wind speed, has a characteristic time scale τ . In the framework of the standard, in a given time interval T , the characteristic parameter is the turbulence intensity, which by definition is the ratio of the standard deviation and the average of the wind speed. By convention this standard deviation is determined with respect to the average, which implies determining turbulence intensity requires the average wind speed to be constant. Now in practice the average wind speed may change over the time interval T . If so, apart from contributions with a time scale τ , the standard deviation also contains contributions with a time scale T . In other words, in this case low-frequency events are represented in the standard deviation and, consequently, the turbulence intensity. Since, as a consequence, the standard deviation is too large, the resulting turbulence intensity is too large as well.

Having available the average μ_i and the standard deviation σ_i of the wind speed after an averaging time T , there is no method to determine after the event whether the average wind speed has changed or not during that time interval. This means one must make sure a priori that variations with a time scale of the order T (or larger) are not recorded. This is achieved by high-pass filtering the signal from the anemometer, where the lower cut-off frequency is of the order $1/T$.

Alternatively, the data acquisition system may be designed such, that based on wind speed samples recorded at intervals ΔT during the interval T , moving averages are determined on the basis of an interval proportional to τ . If these differ considerably, a trend is present. This trend must subsequently be removed, e.g. by determining the difference between the recorded samples and the moving averages. Next, mean and variance are determined from the resulting de-trended samples.

On the other hand, one must make sure that noise, i.e. variations with a small but not relevant time scale, are not recorded either. This is achieved by low-pass filtering the signal from the anemometer. Although for an ideal anemometer the higher cut-off frequency is of the order 5 times the Kolmogorov frequency, for a cup anemometer this relaxes to $5f_m$. Taken together, the requirement for data pre-processing is as follows:

The signal from the anemometer must be sampled with a sampling time of 2 s or less, but ideally with $1/f_m$, where f_m is the cup anemometer cut-off frequency;

The signal from the anemometer must be band-pass filtered for frequencies between $1/T$ and $5f_m$, where T is the averaging time.

This ensures the relevant turbulent scales are recorded, and neither low-frequency events nor noise are part of the data.

4.2.4 Further Reading

Determining a characteristic turbulence intensity mainly involves applying standard experimental and processing techniques to wind speed measurements. Although these techniques are commonly applied in wind energy, for this reason it was not possible to trace the first record of the method. Here it must however be noted that in wind energy turbulence intensity is determined in a different way than in meteorology, where it is obtained from the variation in time series of average wind speed and not from considering the standard deviation with respect to this average. This means there is no direct link with the rich literature on atmospheric turbulence.

4.3 Wind Speed Distribution

4.3.1 Description of Parameter

According to the standard (section 3.3.1a [2]), *the wind speed distribution at the site is significant for the wind turbine design because it determines the frequency of occurrence of the individual load conditions. For WTGS in the standard classes, the mean value of the wind speed over a time period of 10 min shall be assumed to be Rayleigh distributed for the purposes of design load calculations. In this case, the probability distribution of wind speed at hub height is given by:*

$$P(V < V_{hub}) = 1 - \exp\left[-\pi\left(\frac{V_{hub}}{2V_{ave}}\right)^2\right] \quad (38)$$

with $P(V < V_{hub})$ the probability of the wind speed to be smaller than V_{hub} , V_{hub} the ten minute average wind speed at hub height, and V_{ave} the annual average wind speed at hub height. The objective thus is to specify methods to determine the Rayleigh parameter “average wind speed V_{ave} ” by fitting a Rayleigh distribution to an observed (or, more likely derived/predicted) annual wind speed distribution. It should be remembered that in most cases, the Rayleigh or Weibull distributions are not good fits to real wind data in many parts of Europe and that this fitting process is mainly required to categorize the site in terms of the reference standard IEC 1400-1[2]. It should be checked that forcing a Weibull or Rayleigh distribution to fit the data does not produce a distribution which is more benign to the turbine than the actual, non-

Rayleigh distribution of winds.

For ease of notation, the equivalent cumulative distribution function $F_R(u)$ is introduced:

$$F_R(u) = 1 - \exp\left[-\frac{\pi}{4}\left(\frac{u}{\bar{u}}\right)^2\right] \quad (39)$$

which gives the probability a wind speed is smaller than u if the mean wind speed is \bar{u} . Hence

$$f_R(u) \equiv \frac{dF_R(u)}{du} = \frac{\pi}{2} \frac{u}{\bar{u}^2} \exp\left[-\frac{\pi}{4}\left(\frac{u}{\bar{u}}\right)^2\right] \quad (40)$$

is the corresponding probability density function, i.e. the probability the wind speed is u given the mean wind speed \bar{u} .

4.3.2 Methods of Assessment

The Rayleigh distribution is basically a Weibull distribution with shape parameter $k=2$. This means methods to determine the Rayleigh parameter \bar{u} can be derived from the (many) methods to determine the two Weibull parameters A and k . These methods have been grouped into five categories:

- Moment fitting method,
- Logarithmic method,
- Maximum likelihood method,
- Percentile method, and
- Least-squares method.

In the following, for each of these methods first a rough description for the Weibull case and next a more detailed description for the Rayleigh case are given. In practice, the Weibull distribution gives an accurate wind description for moderate wind speeds only [50, 57]. This is because

- Low wind speeds, less than 4 m/s, say, mainly occur under stable conditions;
- High wind speeds, more than 16 m/s, say, are not very frequent and thus can not be fit accurately.

4.3.2.1 Moment Fitting Method

In Weibull parameter estimation this method employs moments of the wind speed. The first step is to determine a value for k by deriving quantities from ratios of moments of the wind speed, such ratios, according to the Weibull distribution, depending only on k . Subsequently, k is solved on the basis of the observed values of wind speed. Examples of these ratios are the non-dimensional standard deviation (standard deviation method) and the energy pattern factor (energy pattern method). As an alternative, the energy in the wind speed distribution and the frequency of wind speeds are combined into a relation which depends on k only (European Wind Atlas method). Then a value for A is determined, again on the basis of a moment of the wind speed (usually the first) as obtained from the Weibull distribution and the observations. In Rayleigh parameter estimation only the second step can be performed, so that \bar{u} is determined from the average observed wind speed:

$$\bar{u} = \frac{1}{N} \sum_{i=1}^N u_i \quad (41)$$

where N is the number of (relevant) ten-minute records and u_i is the i th (relevant) ten-minute averaged wind speed. The uncertainty $\Delta\bar{u}$ in the moment estimate of the mean wind speed is obtained from its

variance:

$$(\Delta \bar{u})^2 = \frac{1}{N(N-1)} \sum_{i=1}^N (u_i - \bar{u})^2 \quad (42)$$

(Recall $(1/(N-1)) \sum_{i=1}^N (u_i - \bar{u})^2$ is the sample variance, which is an unbiased estimate of the variance of a random variable.) Note this uncertainty expresses variation about the mean wind speed rather than the difference between the measured and the “real” value.

The procedure to obtain the mean wind speed \bar{u} on the basis of the moment method is then:

- Collect/derive ten-minute average wind speeds u_i over a representative time period;
- Select the N observations for which $4 \text{ m/s} < u_i < 16 \text{ m/s}$;
- Determine the moment estimate of \bar{u} from $\bar{u} = \frac{1}{N} \sum_{i=1}^N u_i$;
- Determine the uncertainty $\Delta \bar{u}$ in the moment estimate of the mean wind speed from

$$(\Delta \bar{u})^2 = \frac{1}{N(N-1)} \sum_{i=1}^N (u_i - \bar{u})^2 .$$

4.3.2.2 Logarithmic method

In Weibull parameter estimation this method consists of reducing the cumulative distribution function such that a linear relation between functions of A and k is obtained. To this end the natural logarithm is taken twice of a rewritten cumulative distribution function. The coefficients of the resulting best linear fit are obtained either graphically by using so-called Weibull paper or numerically by using a standard least-squares method. Values for the two Weibull parameters are subsequently found from the slope and an intercept of the best linear fit. This method is usually referred to as the “Weibull paper” method.

In Rayleigh parameter estimation the first step to obtain the logarithmic method is to rewrite the cumulative distribution function, with as a result:

$$\frac{1}{1 - F_R(u)} = \exp \left[\frac{\pi}{4} \left(\frac{u}{\bar{u}} \right)^2 \right] \quad (43)$$

Taking the natural logarithm twice of the left and right-hand side of this equation yields:

$$\ln \ln \frac{1}{1 - F_R(u)} = \ln \frac{\pi}{4} - 2 \ln \bar{u} + 2 \ln u \quad (44)$$

Since this equation is a linear relation between $\ln(\ln(1 / (1 - F_R(u))))$ and $\ln(u)$, with slope 2 and intercept $\ln(\pi/4) - 2 \ln \bar{u}$, the mean wind speed can be obtained by solving for the intercept. As a consequence, the uncertainty $\Delta \bar{u}$ in the logarithmic estimate of the mean wind speed is determined by the uncertainty in the intercept only.

The procedure to obtain the mean wind speed \bar{u} using the logarithmic method is then:

- Collect/derive ten-minute average wind speeds u_i during a representative time period;
- Select the N observations for which $4 \text{ m/s} < u_i < 16 \text{ m/s}$;
- Create the cumulative distribution $F(u_i)$ of the selected data u_i ;

- Determine the N quantities $y_i = \ln(\ln(1 / (1 - F(u_i))))$ and $x_i = \ln(u_i)$;
- From x_i and y_i , find a value for the parameter B by numerically determining the best linear fit to the relation $y = 2x + B$;
- Determine the logarithmic estimate of \bar{u} from $2 \ln \bar{u} = \ln(\pi/4) - B$
- Determine the uncertainty $\Delta \bar{u}$ in the logarithmic estimate of the mean wind speed from, $2 \ln \Delta \bar{u} = \ln(\pi/16) - B + 2 \ln(B\Delta B)$ where ΔB is the uncertainty in B .

4.3.2.3 Maximum Likelihood Method

In Weibull parameter estimation A and k are determined such that the resulting probability density makes the observed wind speeds most likely. To this end the likelihood function (i.e. the joint probability density function) is introduced. By maximising this likelihood function (or rather its logarithm), two equations in A and k are obtained. Subsequently, by solving these equations the maximum likelihood estimates of the two Weibull parameters are obtained.

In Rayleigh parameter estimation the likelihood function L is the joint probability density function

$$L = \prod_{i=1}^N f_R(u_i) = \prod_{i=1}^N \frac{\pi}{2} \frac{u_i}{\bar{u}^2} \exp\left[-\frac{\pi}{4} \left(\frac{u_i}{\bar{u}}\right)^2\right] \quad (45)$$

where u_i is the i th observed wind speed. By taking the logarithm, this equation gives

$$\ln L = N \ln \frac{\pi}{2} + \sum_{i=1}^N \ln u_i - 2N \ln \bar{u} - \frac{\pi}{4} \frac{1}{\bar{u}^2} \sum_{i=1}^N u_i^2 \quad (46)$$

Maximising $\ln(L)$,

$$\frac{\partial \ln L}{\partial \bar{u}} = 0 \quad (47)$$

subsequently yields

$$-\frac{2N}{\bar{u}} + \frac{\pi}{2\bar{u}^3} \sum_{i=1}^N u_i^2 = 0 \quad (48)$$

The maximum likelihood estimate of \bar{u} hence follows from

$$\bar{u}^{-2} = \frac{\pi}{4N} \sum_{i=1}^N u_i^2 \quad (49)$$

Formally, the uncertainty $\Delta \bar{u}$ in the mean wind speed is given by

$$(\Delta \bar{u})^2 = V(\bar{u}) \quad (50)$$

where $V(\bar{u})$ is the variance of \bar{u} (Recall that the mean wind speed is a stochastic quantity with a distribution too.) Using $V(f(x)) = (\partial f / \partial x)^2 V(x)$ the variance of \bar{u} is expressed in terms of the variance of \bar{u}^2

$$V(\bar{u}) = \frac{1}{4} \frac{V(\bar{u}^2)}{\bar{u}^2} \quad (51)$$

Subsequently, by introducing the sample average μ_{u^2} of u_i^2 and the sample variance $\sigma_{u^2}^2$ of u_i^2 according to

$$\mu_{u^2} \equiv \frac{1}{N} \sum_{i=1}^N u_i^2 \quad \text{and} \quad \sigma_{u^2}^2 \equiv \frac{1}{N-1} \sum_{i=1}^N (u_i^2 - \mu_{u^2})^2 \quad (52)$$

it follows that

$$V(\bar{u}^2) = V\left(\frac{\pi}{4N} \sum_{i=1}^N u_i^2\right) = \frac{\pi^2}{16N} \sigma_{u^2}^2 \quad (53)$$

By inserting this equation into equation (51) it is found that the variance in the mean wind speed is:

$$V(\bar{u}) = \frac{\pi^2}{64N} \frac{\sigma_{u^2}^2}{\bar{u}^2} \quad (54)$$

so that, as a consequence, from equation (50) it follows that the uncertainty in the maximum likelihood estimate of the mean wind speed is

$$\Delta \bar{u} = \frac{\pi}{8\sqrt{N}} \frac{\sigma_{u^2}}{\bar{u}} \quad (55)$$

Here the sample standard deviation σ_{u^2} and the mean wind speed \bar{u} are given by the equations (52) and (49), respectively.

- The procedure to obtain the maximum likelihood estimate of the mean wind speed \bar{u} is then:
- Collect/derive ten-minute average wind speeds u_i over a representative time period;
- Select the N observations for which $4 \text{ m/s} < u_i < 16 \text{ m/s}$;
- Determine the maximum likelihood estimate of the mean wind speed \bar{u} from $\bar{u}^2 = \frac{\pi}{4N} \sum_{i=1}^N u_i^2$;
- Determine the uncertainty $\Delta \bar{u}$ in the maximum likelihood estimate of the mean wind speed from $\Delta \bar{u} = \frac{\pi}{8\sqrt{N}} \frac{\sigma_{u^2}}{\bar{u}}$, where σ_{u^2} is the sample standard deviation of u_i^2 .

4.3.2.4 Percentile method

In Weibull parameter estimation this method involves determining A and k by estimating two percentiles of the observed wind speeds. (The $100p$ th percentile is the wind speed for which the cumulated distribution is p .) By taking the logarithm twice of the cumulative distribution function, and employing these percentiles and the corresponding probabilities, two equations in A and k are obtained. The estimates of the two Weibull parameters are subsequently obtained by solving these equations.

In Rayleigh parameter estimation the probability p_i of the wind speed being smaller than u_i follows from the cumulative distribution function:

$$p_i = 1 - \exp\left[-\frac{\pi}{4}\left(\frac{u_i}{\bar{u}}\right)^2\right] \quad (56)$$

which is equivalent to

$$\ln \ln\left[\frac{1}{1-p_i}\right] = \ln \frac{\pi}{4} - 2 \ln \bar{u} + 2 \ln u_i \quad (57)$$

Hence, if u_x is the 100^xth percentile, this equation implies that

$$\ln \ln\left[\frac{1}{1-p_x}\right] = \ln \frac{\pi}{4} - 2 \ln \bar{u} + 2 \ln u_x \quad (58)$$

Although any percentile may be used, the 50th percentile may be preferred because it is the median of the observed wind speeds. In this case the percentile estimate of the mean wind speed is obtained from

$$2 \ln \bar{u} = -\ln \ln 2 + \ln \frac{\pi}{4} + 2 \ln u_{med} \quad (59)$$

where u_{med} is the median of the observed wind speeds. Consequently, the uncertainty in the percentile estimate of the mean wind speed is

$$\Delta \bar{u} = \frac{\bar{u}}{u_{med}} \Delta u_{med} \quad (60)$$

where

$$(\Delta u_{med})^2 = \frac{1}{N(N-1)} \sum_{i=1}^N (u_i - u_{med})^2 \quad (61)$$

gives the uncertainty Δu_{med} in the median wind speed as obtained from the variation about the median wind speed.

The procedure to obtain the mean wind speed \bar{u} using the percentile method is then:

- Collect/derive ten-minute average wind speeds u_i over a representative time period;
- Select the N observations for which $4 \text{ m/s} < u_i < 16 \text{ m/s}$;
- Determine the median wind speed u_{med} from the selected wind speeds;
- Determine the percentile estimate of the mean wind speed \bar{u} from
- $2 \ln \bar{u} = -\ln \ln 2 + \ln \frac{\pi}{4} + 2 \ln u_{med}$.
- Determine the uncertainty $\Delta \bar{u}$ in the percentile estimate of the mean wind speed from

$$\Delta \bar{u} = \frac{\bar{u}}{u_{med}} \Delta u_{med}, \text{ with } (\Delta u_{med})^2 = \frac{1}{N(N-1)} \sum_{i=1}^N (u_i - u_{med})^2$$

4.3.2.5 Least-Squares Method

In Weibull parameter estimation this method involves determining A and k by minimising the sum of squares defined by the difference between the cumulative distribution function and the observed

cumulative distribution. If the logarithms of these distributions are employed, this gives two equations in A and k from which the two Weibull parameters are obtained.

If F_R is the cumulative distribution function and F is the observed cumulative distribution, in Rayleigh parameter estimation the sum of squares is

$$\sum_{i=1}^N (F_R(u_i) - F(u_i))^2 \quad (62)$$

with u_i the i th observed wind speed. Alternatively, by using the auxiliary function

$$G(u) = \ln(1 - F(u)) \quad (63)$$

it follows that an equivalent sum of squares S is

$$S = \sum_{i=1}^N (G_R(u_i) - G(u_i))^2 \quad (64)$$

Minimising S ,

$$\frac{\partial S}{\partial u} = 0 \quad (65)$$

subsequently gives

$$\frac{\pi}{4u^{-2}} \sum_{i=1}^N u_i^4 + \sum_{i=1}^N u_i^2 \ln(1 - F(u_i)) = 0 \quad (66)$$

The least-squares estimate of \bar{u} hence follows from

$$\bar{u}^{-2} = -\frac{\pi}{4} \frac{\sum_{i=1}^N u_i^4}{\sum_{i=1}^N u_i^2 \ln(1 - F(u_i))} \quad (67)$$

(Note $\ln(1 - F(u_i)) < 0$ because $0 < F < 1$.)

Given the variance in \bar{u} from the equations (50) and (51) it follows that the uncertainty $\Delta \bar{u}$ in the mean wind speed is formally given by

$$(\Delta \bar{u})^2 = \frac{1}{4} \frac{V(\bar{u}^{-2})}{\bar{u}^{-2}} \quad (68)$$

In order to derive the variance $V(\bar{u}^{-2})$ equation (67) is rewritten in the form

$$\bar{u}^{-2} = -\frac{\pi}{4} \frac{n}{d} \quad (69)$$

where n and d are the auxiliary quantities

$$n \equiv \sum_{i=1}^N n_i \equiv \sum_{i=1}^N u_i^4 \quad \text{and} \quad d \equiv \sum_{i=1}^N d_i \equiv \sum_{i=1}^N u_i^2 \ln(1 - F(u_i)) \quad (70)$$

Equation (69) allows one to express $V(\bar{u}^{-2})$ in terms of these auxiliary quantities and their variances $V(n)$ and $V(d)$:

$$V(\bar{u}^{-2}) = \frac{\pi^2}{16} \frac{1}{d^2} \left(V(n) + \frac{n^2}{d^2} V(d) \right) \quad (71)$$

Here the variances of n and d are

$$V(n) = N\sigma_n^2 \quad \text{and} \quad V(d) = N\sigma_d^2 \quad (72)$$

respectively, where

$$\sigma_n^2 = \frac{1}{N-1} \sum_{i=1}^N (n_i - \mu_n)^2 \quad \text{with} \quad \mu_n = \frac{1}{N} \sum_{i=1}^N n_i \quad (73)$$

(sample variance σ_n^2 and sample average μ_n of n_i), and

$$\sigma_d^2 = \frac{1}{N-1} \sum_{i=1}^N (d_i - \mu_d)^2 \quad \text{with} \quad \mu_d = \frac{1}{N} \sum_{i=1}^N d_i \quad (74)$$

(sample variance σ_d^2 and sample average μ_d of d_i); recall $n_i = u_i^4$ and

$$d_i = u_i^2 \ln(1 - F(u_i)). \quad (75)$$

By inserting the equation (71) into the equation (68), and using the equations (72) and (69), it is found that the uncertainty $\Delta\bar{u}$ in the least-squares estimate of the mean wind speed is given by

$$(\Delta\bar{u})^2 = -\frac{\pi}{16} \frac{N}{nd} \left(\sigma_n^2 + \frac{n^2}{d^2} \sigma_d^2 \right) \quad (76)$$

The auxiliary quantities n and d together with their sample variances σ_n^2 and σ_d^2 , which appear in this equation, are defined in the equations (70), (73) and (74).

The procedure to obtain the mean wind speed \bar{u} using the least-squares method is then:

- Collect/derive ten-minute average wind speeds u_i during a representative time period;
- Select the N observations for which $4 \text{ m/s} < u_i < 16 \text{ m/s}$;
- Create the cumulative distribution $F(u_i)$ of the selected data u_i ;
- Determine the least-squares mean wind speed \bar{u} from $\bar{u}^{-2} = -\frac{\pi}{4} \frac{n}{d}$
- Determine the uncertainty in the least-squares mean wind speed \bar{u} from equation (75) and the associated auxiliary quantities.

4.3.3 Measurement Requirements

Determining V_{ave} basically comes down to measuring ten-minute average wind speeds which can be used to determine a wind speed distribution over a representative time period. If long term measurements are not available at the site under assessment, then this will involve using one of the extrapolation or

modelling techniques described in section 3 of this report (e.g. MCP techniques or WAsP model). According to the reference standard, the measurement time period is 6 months or longer and must include seasonal effects if these significantly contribute to the wind conditions.

The specifications for the wind speed measurement system may be taken from the Power Performance standard IEC 88/1400-12 [37], from which the following relevant requirements are identified:

- The meteorological mast shall be of a tube or cone or lattice type;
- The mast should be located in a position that represents the free wind flow that drives the planned wind turbine systems,
- Wind speed measurements shall be made with a cup anemometer;
- The cup anemometer shall have a distance constant of less than 5 m, and maintains its calibration over the duration of the measurement period.
- It is recommended that a cup anemometer shall be mounted within 2.5% of the hub height of the planned wind turbine generator system. If this is not practical due to the size of the turbine, a series of anemometers (at least 3) at various heights from about 10m height to the top of the mast should be used so that an extrapolation of wind speed to the planned hub height may be carried out from simultaneous measurements at these lower heights (see section 4.4).
- The highest anemometer should preferably be mounted on the top of a vertical circular tube standing clear of the top of the meteorological mast or alternatively on a boom clamped to the side of the mast pointing in the predominant wind direction. If booms are used, the vertical separation from the anemometer to any mounting boom should be at least 7 times the boom diameter and its horizontal separation from the mast at anemometer height should be at least 7 times the maximum mast diameter;
- Data shall be collected continuously at a sampling rate of 0.5 Hz or faster;
- The data acquisition system shall store either sampled data or pre-processed data sets, or both;
- The pre-processed data sets shall comprise the following information on the sampled data: mean value, standard deviation, maximum value, and minimum value;
- The total duration of each pre-processed data set shall be between 30 s and 10 min, and shall be 10 min divided by an integer number. If the data sets have a duration of less than 10 min, the adjacent data sets shall not be separated by a time delay.

4.3.4 Further Reading

To determine the Weibull or Rayleigh parameters essentially involves application of standard estimation techniques. For this reason it was difficult to trace the various methods to a genuine founder, apart from the percentile method which was first reported by Dubey [58]. Operational reviews of Weibull parameter estimation methods are available in the books by Wieringa and Rijkoort [50] and Lysen [59], and the report by Stevens [60]. The European Wind Atlas method, basically a moment fitting method, was, as its name suggests, first published in the European Wind Atlas [57].

4.4 Normal Wind Profile

4.4.1 Description of Parameter

As described in the standard ([2] section 3.3.1) *the wind profile $V(z)$ denotes the average wind speed as a function of height z above the ground. For WTGS designs in the standard classes, the normal wind speed profile shall be assumed to be given by the power law:*

$$V(z) = V_{hub} \left(\frac{z}{z_{hub}} \right)^\alpha \quad (77)$$

where V_{hub} is the ten minute average wind speed at hub height, z_{hub} is the hub height, and where the power law exponent α shall be assumed to be 0.2. The assumed wind profile is used to define the average wind shear across the rotor swept area. Application of this model might lead to underestimating the wind shear (and subsequently the loading), in particular when the power law exponent at the site is larger than 0.2 or when the power law is not a good model anyway. This implies that in practice, the normal wind profile should be compared to the observed profile, and, if needed, a more realistic profile must be fitted to the observations. The objective thus is to specify methods to

Determine the power law exponent from wind speed measured at various heights, and
Decide when use of the power law results in too low a loading.

Note that wind speed profiles during stable atmospheric conditions could lead to too low an estimate of the wind shear, so that one should consider taking into account diurnal variation as well.

4.4.2 Methods of Assessment

4.4.2.1 General Power Law

In a turbulent boundary layer over a smooth surface and under stable conditions, the wind speed u at height z above the surface may be described by the general power law

$$u(z) = u_{\infty} \left(\frac{z}{\delta} \right)^n \quad (78)$$

where u_{∞} is the free-stream velocity, δ is the boundary layer thickness, and n is the power law exponent {Hinze}. If the wind shear is to be determined from observed wind speeds at height z_{ref} , the general power law gives

$$u(z) = u_{z_{ref}} \left(\frac{z}{z_{ref}} \right)^n \quad (79)$$

As a consequence, for wind shear evaluation, only the power law exponent needs to be determined. By taking the logarithm of the general power law, it reduces to

$$\ln(u) = \ln(u_{\infty}) + n \ln(z) - n \ln(\delta) \quad (80)$$

This implies the power law exponent n can be obtained from the slope of the curve with $\ln(u)$ versus $\ln(z)$. As a consequence, the uncertainty in the power law exponent follows from the uncertainty in this slope.

The procedure to obtain the exponent n of the general power law is then:

Collect ten-minute average wind speeds u_i at M heights z_j over a representative time period;

Select the N observations for which $4 \text{ m/s} < u_i < 16 \text{ m/s}$;

Determine the quantities $x_j = \ln(z_j)$ and $y_{ij} = \ln(u_i(z_j))$;

Based on x_j and y_{ij} , find a value for the parameters A and B by numerically determining the best linear fit to the relation $y = Ax + B$;

Determine n from $n = A$;

Determine the uncertainty Δn from $\Delta n = \Delta A$, where ΔA is the uncertainty in A .

4.4.2.2 Logarithmic Law

In a turbulent boundary layer over a rough surface and under stable conditions, the wind speed u at height z above the surface may be described by the logarithmic law

$$u(z) = \frac{u_*}{\kappa} \ln \frac{z}{z_0} \quad (81)$$

where u_* is the friction velocity, κ is the Von Karman constant, and z_0 is the roughness length [61]. If the wind shear is to be determined from observed wind speeds at height z_{ref} , the logarithmic law gives

$$u(z) = u(z_{ref}) \frac{\ln z - \ln z_0}{\ln z_{ref} - \ln z_0} \quad (82)$$

which implies that, for wind shear evaluation, only the roughness length needs to be determined. Rewriting the power law gives

$$u(z) = \frac{u_*}{\kappa} \ln z - \frac{u_*}{\kappa} \ln z_0 \quad (83)$$

This equation reveals that the roughness length z_0 can be obtained from the root of the curve of u versus $\ln(z)$. (In addition, given the value $\kappa = 0.4$, the friction velocity u_* can be obtained from the slope of this curve.) Consequently, the uncertainty in the roughness length is obtained from the uncertainty in this root.

The procedure to obtain the roughness length z_0 of the logarithmic law is then:

Collect ten-minute average wind speeds u_i at M heights z_j during a representative time period;

Select the N observations for which $4 \text{ m/s} < u_i < 16 \text{ m/s}$;

Determine the quantities $x_j = \ln(z_j)$ and $y_{ij} = u_i(z_j)$;

Based on x_j and y_{ij} , find a value for the parameters A and B by numerically determining the best linear fit to the relation $y = Ax + B$;

Determine z_0 from $\ln(z_0) = -B/A$;

Using the uncertainties ΔA in A and ΔB in B , determine the uncertainty Δz_0 from

$$2 \ln(\Delta z_0) = -2 \ln(A) - 2B/A + \ln((B\Delta A/A)^2 + (\Delta B)^2).$$

4.4.3 Measurement Requirements

Determining the parameters in wind profiles basically comes down to measuring wind speeds at different heights. Although the minimum requirement is two anemometers, the requirement of one anemometer to be within 5% of hub height (see IEC 88/1400-12 (ed.1)[37]) warrants three anemometers to be employed. Other relevant requirements as described in IEC 88/1400-12 (ed.1) [37], are already described in section 4.3.3.

4.4.4 Method to Determine which Profile Gives the Higher Loading

4.4.4.1 Relation between Loading and Wind Profile

In the following it is assumed that the loading increases with the wind shear. This means that a high loading originates from a large vertical wind speed difference over the rotor plane. If the hub height is H and the rotor radius is R , this wind speed difference is

$$\delta u(H,R) \equiv u(H+R) - u(H-R). \quad (84)$$

In the following $\delta u(H,R)$ will be determined for wind profiles according to the general power law and the logarithmic law.

4.4.4.2 Wind Speed Difference - General Power Law

In the case of the general power law (equation (78)), if the wind speed at hub height is $u(H)$, the wind speed at the height $H + R$ is

$$\begin{aligned}
 u(H + R) &= u(H) \left(\frac{H + R}{H} \right)^n \\
 &= u(H) \left(1 + \frac{R}{H} \right)^n \\
 &= u(H) \left[1 + n \frac{R}{H} + \frac{1}{2} n(n-1) \left(\frac{R}{H} \right)^2 + \frac{1}{6} n(n-1)(n-2) \left(\frac{R}{H} \right)^3 + h.o.t \right]
 \end{aligned} \tag{85}$$

Similarly, the wind speed at the height $H - R$ is

$$u(H - R) = u(H) \left[1 - n \frac{R}{H} + \frac{1}{2} n(n-1) \left(\frac{R}{H} \right)^2 - \frac{1}{6} n(n-1)(n-2) \left(\frac{R}{H} \right)^3 + h.o.t \right] \tag{86}$$

As a consequence, the vertical wind speed difference over the rotor plane is

$$\delta u \approx 2n \frac{R}{H} u(H) \left[1 + \frac{1}{6} (n-1)(n-2) \left(\frac{R}{H} \right)^2 \right] \tag{87}$$

This means that if a general power law is used in order to describe the wind profile, the wind speed difference δu can be estimated by using equation (87).

4.4.4.3 Wind Speed Difference - Logarithmic Law

In the case of the logarithmic law (equation (81)), if the wind speed at hub height is $u(H)$, the wind speed at the height $H + R$ is

$$\begin{aligned}
 u(H + R) &= u(H) \frac{\ln(H + R) - \ln z_0}{\ln H - \ln z_0} \\
 &= u(H) \left[1 + \frac{\ln \left(1 + \frac{R}{H} \right)}{\ln H - \ln z_0} \right] \\
 &= u(H) \left[1 + \frac{\frac{R}{H} + \frac{1}{2} \left(\frac{R}{H} \right)^2 + \frac{1}{3} \left(\frac{R}{H} \right)^3 - h.o.t}{\ln H - \ln z_0} \right]
 \end{aligned} \tag{87}$$

Similarly, the wind speed at the height $H - R$ is

$$u(H-R) \approx u(H) \left[1 - \frac{\frac{R}{H} + \frac{1}{2} \left(\frac{R}{H} \right)^2 + \frac{1}{3} \left(\frac{R}{H} \right)^3 - h.o.t.}{\ln H - \ln z_0} \right] \quad (88)$$

As a consequence, the vertical wind speed difference over the rotor plane is

$$\delta u \approx \frac{2}{\ln H - \ln z_0} \frac{R}{H} u(H) \left[1 + \frac{1}{3} \left(\frac{R}{H} \right)^2 \right] \quad (89)$$

This implies that if a logarithmic law describes the wind profile, using equation (89) the wind speed difference δu can be estimated.

4.4.4.4 Profile with the Higher Loading

In order to establish which profile gives the higher loading, the general power law and the logarithmic law are fitted to wind speeds which are measured at different heights. This yields values for the power law exponent n (see section 4.4.2.1) and the roughness length z_0 (see section 4.4.2.2). This subsequently allows one to determine the corresponding wind speed differences δu_{pow} from the equation (87) and δu_{log} from the equation (89). From a comparison of the values of δu_{pow} and δu_{log} it is straightforward to decide which value is the higher, and, consequently, which profile gives the higher loading.

4.4.5 Further Reading

Determining the parameters of either a power law or a logarithmic law basically requires application of standard estimation techniques. For this reason no effort was put into finding a founder of these methods.

4.5 Wind Direction Distribution

The wind direction distribution prediction must be based on modelling (e.g. WASP) or extrapolation techniques (e.g. MCP) as described in section 3. It is therefore not considered further here.

4.6 “Other” Parameters

4.6.1 Overview

In the course of the EWTS II project, sub-project 1, “Load spectra and extreme wind conditions” additional site assessment parameters were identified. These parameters, which are used in the various models which are specified in the standard (section 3.3.1[2]), include:

- Wind direction distribution
- Wind speed distribution
- Roughness length
- Wind shear
- Turbulence length scales
- Coherence
- Standard deviation ratios
- Negative gust

Wind direction distribution and wind speed distribution have been treated in the first part of sub-project 5. Wind speed distribution is also covered in section 4.3 of this report. Furthermore, in section 4.4 roughness length and wind shear are presented.

This chapter deals with the other “additional” parameters. Since, apart from negative gust, these parameters originate from the theory of series, a review of the basics of series analysis is presented in Appendix A Assessment Of Other Parameters - Mathematical Details. On the basis of this theory turbulence length scales (section 4.6.2), coherence (section 4.6.3), and standard deviation ratios (section 4.6.4) are introduced subsequent to this chapter. In addition, negative gust is described (section 4.6.5). Finally, the requirements for measurement of these parameters are presented (section 4.6.6 and 4.6.7).

4.6.2 Turbulence Length Scale

By definition (p. 417 [62]), *integral length scale is the integral of the correlation coefficient over all separation distances*. This means a spatial description of the wind speed field is required, or, in other words, many measuring stations along a line are needed. Since this is difficult to achieve, even in a laboratory situation, the practical approach has been to consider two stations only but to vary the separation distance (section 6.4 [63], section 1.7 [61]). Accordingly, the wind speed components u_i in the positions x and $x + r$ are

$$u_i[x] \quad \text{and} \quad u_j[x + r] \tag{90}$$

where r is the distance between the two positions. From equation (A16) the corresponding covariance function is

$$R_{ij}[r] = \sum (u_j[x] - \bar{u}_j)(u_i[x + r] - \bar{u}_i) \tag{91}$$

By using equation (A18) to determine the corresponding correlation function $r_{ij}^{\text{®}}$, from the definition it follows that the integral length scale is

$$L_{ij} = \sum_{r=1-N}^{1+N} r_{ij}[r] \tag{92}$$

Note that there are nine integral length scales because there are three wind speed components. As it is unpractical to consider two measuring stations and to vary the separation distance in a field situation, an alternative approach is used (section 6.4 [63], section 1.7 [61]): an integral “length” scale L_i is obtained by using the integral time scale T_{ii} and the average wind speed \bar{u}_i via

$$L_i = \bar{u}_i T_{ii} \tag{93}$$

Here the integral time scale T_{ij} is the integral of the correlation coefficient over all time lapses:

$$T_{ij} = \sum_{\tau=1-N}^{1+N} r_{ij}[\tau] \tag{94}$$

Hence one measuring station and a temporal description of the wind speed are used. This process is described in more detail by way of an example in Appendix B, Use of sonic anemometer.. Since there are three average wind speed components, in this context there are three integral length scales: longitudinal L_1 , transversal L_2 and vertical L_3 . Although integral/turbulence length scale is not defined in the standard [2], it is assumed here that integral length scale is equivalent to turbulence length scale.

4.6.3 Coherence

By definition (p. 418 [62]), *coherence is the absolute value of the normalized cross-spectrum for two wind speeds measured at points separated in space*. This warrants a two-point spatial description of the wind speed field. If the two wind speed time series which are measured at a distance R apart are

$$u_i[x] \text{ and } u_j[x + R], \quad (95)$$

their covariance is

$$R_{ij}[R] = \sum_n (u_j[x] - \bar{u}_j[x])(u_i[x + r] - \bar{u}_i[x + R]) \quad (96)$$

where the summation and the averages are over all elements n in the time series. On basis of equation (A19) the corresponding spectral density is

$$h_{ij}[w] = \frac{1}{2\pi} \sum_k R_{ij}[R] \exp(-jwk) \quad (97)$$

Accordingly, the coherence is:

$$|c_{ij}[w]| = \left| \frac{h_{ij}[w]}{\sqrt{h_{ii}[w]h_{jj}[w]}} \right| \quad (98)$$

This means there are six cross-coherences: $|c_{12}[w]|$ and $|c_{21}[w]|$, $|c_{13}[w]|$ and $|c_{31}[w]|$, and $|c_{23}[w]|$ and $|c_{32}[w]|$; where the pairs are equal if the wind speed field is homogeneous, i.e. does not depend on the actual position. Note the three auto-coherences $|c_{11}| = |c_{22}| = |c_{33}| \equiv 1$. In the framework of the standard [appendix B]{iec1400-1ed2}, *coherency function (is) defined by the complex magnitude of the cross-spectral density of the longitudinal wind velocity components at two spatially separated points divided by the auto-spectrum function*. This suggests, according to the standard, the coherence is $|c_{11}|$; which can not be the case because $|c_{11}| \equiv 1$. A solution might be to use an alternative definition of the coherency function in the sense that the factor in the denominator of equation (A20) is $h_{ii}[0]$, $h_{jj}[0]$ rather than $h_{ii}[f]$, $h_{jj}[f]$, so that the coherence is:

$$|c_{ij}[w]| = \left| \frac{h_{ij}[w]}{\sqrt{h_{ii}[0]h_{jj}[0]}} \right| \quad (99)$$

Since in this case $|c_{11}[w]| = h_{11}[w]/h_{11}[0] \neq 1$, coherence is worthwhile. However, from neither the standard nor the literature is it clear which definition of the coherency function is employed. Equation (A20), however, is the common one in series analyses.

4.6.4 Standard Deviation Ratios

By definition, wind speed standard deviation σ is the square-root of the averaged squared difference between the wind speed realizations and the average wind speed. This means a temporal wind speed description $u_i[n]$ in a measuring position is required.

From the description of the covariance function in equation (A16) it follows that the standard deviation σ_i of the i th wind speed component is given by

$$\sigma_i^2 = \frac{1}{N_t} \sum_{n=1}^{N_t} (u_i[n_t] - \bar{u}_i)^2 = \frac{1}{N_t} R_{ii}[\tau = 0] \quad (100)$$

so that

$$\sigma_i = \sqrt{\frac{R_{ii}[0]}{N_t}} \quad (101)$$

Hence the ratio of the standard deviation of a lateral or vertical and the longitudinal wind speed component is:

$$\frac{\sigma_2}{\sigma_1} = \sqrt{\frac{R_{22}[0]}{R_{11}[0]}} \quad \text{and} \quad \frac{\sigma_3}{\sigma_1} = \sqrt{\frac{R_{33}[0]}{R_{11}[0]}} \quad (102), (103)$$

These equations show that these ratios are conveniently obtained from the auto-covariance functions of the time series with wind speed components. Although the standard does not contain a definition of wind speed standard deviation (appendix B [2]), equations (102) and (103) are in agreement with the standard's definition of turbulence intensity.

4.6.5 Negative Gust

According to the standard (section 1.3 [2]), *a gust is a temporary change in the wind speed which may be characterized by its rise-time, its magnitude and its duration*, where the change may either be an increase or a decrease. Since in general “gust” is associated with an increasing wind speed, the term “negative gust” was introduced to indicate a decreasing wind speed. It has been observed that usually a negative gust occurs before a gust [64], where the amplitude of the negative gust may be as large as 25% of the one of the gust. Therefore, the combined effect on turbine loads of a gust preceded by a negative gust could be much more severe than that of the gust alone.

Consider the time series $u_i[n]$ with the i th wind speed component. Gusts and negative gusts are detected by identifying extremes in the wind speed, e.g. by marking zeros in the derivative of the series. The wind speed extremes so determined constitute a series $u_{e,i}[m]$ with alternating minima and maxima. There is an associated series $t_{e,i}[m]$ with the time instants when the extremes in the i th component occur. The magnitude δU_i of wind speed change in the i th component is the difference between the wind speed in two subsequent extremes:

$$\delta U_i = u_{e,i}[m] - u_{e,i}[m-1] . \quad (104)$$

Likewise, the “rise time” δT_i is

$$\delta T_i = t_{e,i}[m] - t_{e,i}[m-1] . \quad (105)$$

The change is a decrease if a minimum is preceded by a maximum; otherwise it is an increase. If an increase is sufficiently strong, the wind speed change is a gust characterized by the gust magnitude $U_{g,i}$:

$$U_{g,i} = u_{e,i}[m] - u_{e,i}[m-1] > H_{g,i} \quad (106)$$

where $H_{g,i}$ is the selection level. On the other hand, the wind speed change is a negative gust if a decrease is sufficiently strong:

$$U_{ng,i} = u_{e,i}[m-1] - u_{e,i}[m] > H_{ng,i} \quad (107)$$

where $U_{ng,i}$ is the negative-gust magnitude and $H_{ng,i}$ is the selection level. In both cases the “rise time” of

the (negative) gust is:

$$T_{(n)g,i} = t_{e,i}[m] - t_{e,i}[m-1]. \quad (108)$$

Note gusts and negative gusts may be observed in the three velocity components independently, defining longitudinal, lateral and vertical (negative) gusts. If a longitudinal gust is preceded by a longitudinal negative gust, an operating gust in the sense of the standard occurs. The duration of this operating gust is the sum of the “rise time” of the gust and the one of the negative gust.

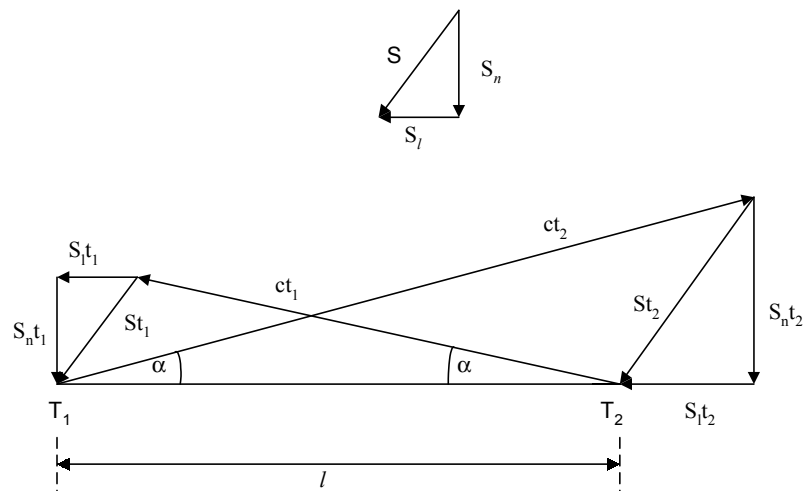
4.6.6 Instrumentation Requirements

The three dimensional characteristics of most of the “other” parameters require three-dimensional wind velocity measuring equipment. The cup-anemometer does not meet this specification. In addition, the mechanical characteristics of the cup anemometer limit the response of the instrument and so higher frequency spectral information is lost. Section 4.6.7 discusses in more detail the special instrumentation requirements of these parameters.

4.6.7 Special Instrumentation: The Ultrasonic Anemometer

4.6.7.1 Principle of operation of the sonic anemometer

Sonic anemometers make use of the propagation of sound to measure the wind velocity. An acoustic pulse is fired alternatively from two given sensors (functioning both as transmitters and receivers) and travels along a given path between the sensors. It can be proved that the time it takes for the pulse to reach the sensor depends on the wind speed component along that path. This is schematically shown in Figure 4.1 [65].



Ultrasonic sound pulses are transmitted back and forth sequentially along the same path between the transducers T1 and T2 and the elapsed times t1 and t2 are measured along the same path.

$a = \arcsin(S_n/c)$
 $S_n =$ wind speed component perpendicular to the sound path
 $S_l =$ wind speed component parallel to the sound path
 $c =$ speed of sound
 $S =$ wind speed

$$\frac{l}{t_1} = c \cdot \cos \alpha + S_l \qquad \frac{l}{t_2} = c \cdot \cos \alpha - S_l$$

$$\frac{1}{t_1} = \frac{c \cdot \cos \alpha + S_l}{l} \qquad \frac{1}{t_2} = \frac{c \cdot \cos \alpha - S_l}{l}$$

$$\frac{1}{t_1} - \frac{1}{t_2} = 2 \cdot \frac{S_l}{l} \qquad S_l = \frac{l}{2} \cdot \left(\frac{1}{t_1} - \frac{1}{t_2} \right)$$

Figure 4.1 Principle of operation of the sonic anemometer (Courtesy Ref. [65])

In reality a sonic anemometer consists, as a rule, of three pairs of sensors arranged in a three dimensional array. The form of the array depends on the manufacturer and can either have the form of an orthogonal co-ordinate system with individual paths for each sensor pair or, as in some other types of instruments, Figure 4.2, the sensor pairs are oriented at 120° azimuth intervals while being inclined at 45° to the horizontal such that the sensor paths intersect. In this way sonic anemometers can measure the three velocity components and their turbulence characteristics.

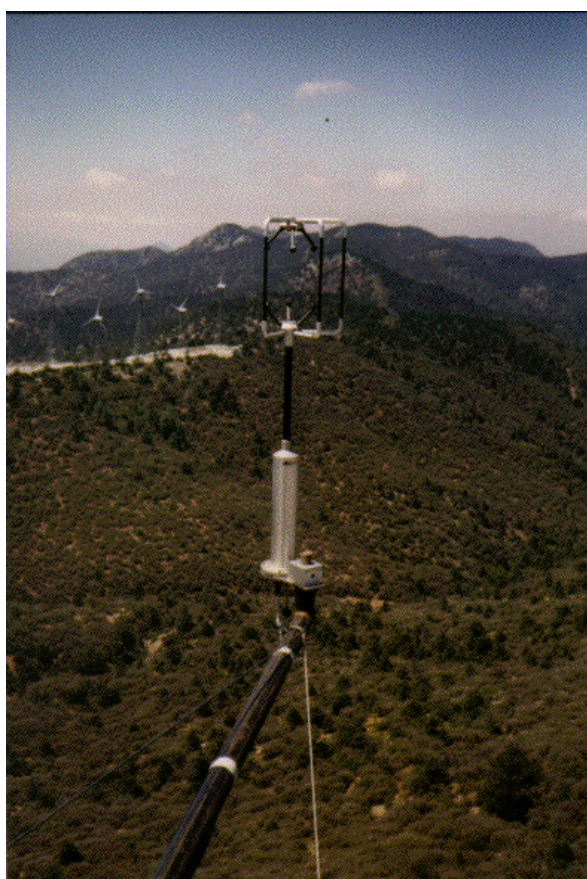


Figure 4.2 The Gill sonic anemometer

4.6.7.2 Cup- and sonic anemometers, merits and drawbacks

The most widely used instrument for the measurement of the wind speed is the cup anemometer. It is cheaper than the sonic anemometer, more robust, and its behaviour is better known and understood. Furthermore well established procedures exist for its calibration and mounting, such that measurements carried out with cup anemometers can be accepted between measuring institutes -provided these procedures are observed. Together with the mean value of the wind speed, the cup anemometer measures also the turbulence characteristics of the wind speed but its response capabilities are limited. The response of the cup anemometer (see section 4.2.3.1) is known to be a function of the mean wind speed, the degree of turbulence and the inclination of the instrument relative to the velocity vector. Performance deterioration with time is a known problem for cup anemometers and therefore they should periodically be calibrated in order to ensure that their response satisfies certain pre-defined limits.

Compared to the cup anemometer, the sonic anemometer can produce all three components of the velocity vector and their associated fluctuations as well as higher order moments. Additionally some sonic anemometers also determine the ambient temperature. The sonic anemometer has a faster response than the cup anemometer as it has no moving mechanical parts. Its response depends on the instrument's built-in electronics while a physical limitation on its response is imposed by the length of the acoustic paths, [66]. Among its drawbacks has been (and still is) the relatively high purchase price which however has become more reasonable in recent years.

There are a number of potential error sources associated with the use of the sonic anemometer. A detailed presentation of these can be found in [65, 67, 68]. The most important of them are:

- inaccuracies of the probe geometry during manufacturing, as a result of which, the actual geometric characteristics of the sensor array (i.e. positions and angles) are not as intended. To compensate for this, some of manufacturers individually calibrate their instruments and equip them with individual correction look-up tables.
- temperature sensitivity of the instrument's electronics which results in thermal drift and contamination of the measured values.
- flow distortion due to the design of the sensor array and the supporting struts of the instrument's head. To account for the above errors many manufacturers supply the sonic anemometers with instrument specific calibration tables for the on line correction of the results. The correctness or adequacy of these tables has not been documented by relevant investigations. It should be mentioned that no investigations exist showing to what extent the shape of the sonic anemometer body influences the measured wind characteristics.
- distortion of the sonic head geometry from wind loads during high wind speeds due to lack of stiffness of the construction of the sensor array.
- lack of commonly agreed procedures for the mounting of the sonic anemometers, either for boom- or for top mounting. Furthermore no agreed procedures exist as to the orientation of the sensor array so the users generally follow the manufacturers' instructions. For top mounting it is anticipated that rules corresponding to the placement of cup anemometers should be sufficient.

As a result of the aforementioned potential sources of error, and since no generally accepted procedures exist for its mounting or calibration, it is suggested that the sonic anemometer should mainly be used for the determination of the turbulent characteristics of the atmospheric flows and the relative sizes of the mean wind vector components. For the measurement of the absolute mean wind speed values the cup anemometer should be preferred.

4.7 Clarification of Standard

The preceding text has presented methods to measure and calculate the site assessment parameters which appear in the standard IEC 1400-1 [2]. Since in some cases the standard leaves room for interpretation, or even gives rise to confusion, a list of recommendations is presented.

- The definition of *reference wind speed* does not specify the meaning of recurrence period. Since several exist, it is recommended to include the appropriate description of recurrence period in the definition of reference wind speed: *the reference wind speed V_{ref} is the extreme 10 min average wind speed at turbine hub height with a recurrence period of 50 years, where this recurrence period is the inverse annual probability that V_{ref} is exceeded.*
- It is recommended to include in the list of symbols and units that recurrence period T_r is the inverse annual probability an extreme wind speed is exceeded.
- From the description in the list of symbols and units, it can be erroneously concluded that *turbulence intensity I_{15}* is the turbulence intensity at a wind speed of 15 m/s. Since this is not correct (I_{15} is a characteristic turbulence intensity at 15 m/s) it is recommended to remove I_{15} and its description from the list of symbols and units, and to introduce a specific notation for the characteristic turbulence intensity at a wind speed of 15 m/s, for example \tilde{I}_{15} , throughout the standard. Furthermore, it is recommended to include in the list of symbols and units that \tilde{I}_{15} *is the characteristic value, i.e. the sum of the average and the standard deviation, of the turbulence intensity at a wind speed of 15 m/s.*
- It is recommended to include in the standard a definition of *turbulence length scale*. Assuming that in the context of the standard turbulence length scale is equivalent to integral length scale, it is recommended that *a turbulence length scale is the integral time scale of a wind speed component multiplied by the corresponding average of the wind speed component, where this integral time scale is the integral over all time lapses of the auto-correlation function of a time series of the wind speed*

component.

- Since in the standard *coherence* is not unambiguously defined, it is recommended to include a definition which complies with the “engineering rules” for coherence that are specified in the standard.
- A definition of standard deviation ratio must be included: Standard deviation ratio is the standard deviation in the lateral or vertical wind speed component divided by the standard deviation in the longitudinal component.
- Since it has been observed that usually an increase in the wind speed is preceded by a decrease, it is recommended to change the definition of a gust accordingly: *A gust is a significant temporary increase in the wind speed. It is usually preceded by a negative gust, that being a temporary decrease in the wind speed. A gust and the preceding negative gust constitute an operating gust. A (negative) gust is characterized by its rise-time and magnitude. The duration of an operating gust is the sum of the rise times of the gust and the negative gust.*

5. REFERENCES

- [1] IEC 1400-1, Wind Turbine Generator Systems - Part 1: Safety Requirements; First Edition 1994-12
- [2] IEC 1400-1, Wind Turbine Generator Systems - Part 1: Safety Requirements; 88/69/CD (Committee Draft), Edition 2, May 1996.
- [3] Butterfield S, Holley, W, et al, Report on 88/69/CD - Wind Turbine Generator Systems Part 1: Safety Requirements, 2. edition.
- [4] Verheij F.J, Snoek L.v.d, (ed.), Handboek energie-opbrengsten van windturbines, TNO Rapport 88-145, 1989 (in Dutch).
- [5] Sherman C: A mass-consistent model for wind fields in complex terrain, J. Appl. Meteorol., 17, 312., 1978.
- [6] Traci R.M: Development of a wind energy site selection methodology, US Dept. of Energy Rept. RLO/2440-11, 205pp., 1977.
- [7] Croba D. et al: Improving techniques for statistical and physical modelling of wind resources in complex terrain, Proc. ECWEC'96, Goteborg, Sweden, pp.514, 1996.
- [8] Jackson P.S., Hunt J.C.R: Turbulent wind flow over a low hill, Q.J.R. Meteorol. Soc., 101, 929-955., 1975.
- [9] Mason P.J., Sykes R.I: Q. J.R Meteorol. Soc., 105, 383-395, 1979.
- [10] Walmsley J.L., et al: Bound. Layer Meteorol., 36, 157-186, 1986.
- [11] Mason P.J, King J.C: Measurements and prediction of flow and turbulence over an isolated hill of moderate slope, Q. J. R. Meteorol. Soc., 111, pp.617-640, 1985.
- [12] Taylor P.A: Numerical studies of neutrally stratified planetary boundary layer flow above gentle topography. I: Two dimensional cases, Bound. Layer Meteorol., 12, pp.37-60, 1977.
- [13] Tryfonopoulos D.A. , et al: Wind Engineering, 13, 324-337, 1989.
- [14] Alm L.K., Nygaard T.A: *Flow over complex terrain estimated by a general purpose Navier-Stokes solver*, Proc. EWEC'93, Travemunde, Germany, pp.591, 1993.
- [15] Tombrou M., et al: Tests of prediction effectiveness of wind energy computer models in complex terrain, Proc. ECWEC'93, Travemunde , Germany, pp599, 1993.
- [16] Bergeles G. C: *Numerical calculation of turbulent flow around two-dimensional hills*, J. Wind Eng. and Ind. Aerod., Vol.21, pp.307-321., 1985.
- [17] Petersen E. L., et al: *Measurements and modelling in complex terrain*, Proc. 1996, Goteborg, Sweden, pp.580, 1996.
- [18] Landberg L: *Implementing prediction of power from wind farms at Utilities*, Proc. 1996, Goteborg, Sweden, pp.592, 1996.
- [19] Mengelkamp H.T., et al: *Regional and local wind climatologies over heterogeneous terrain*, Proc. ECWEC'96, Goteborg, Sweden, pp.506, 1996
- [20] Hojstrup J. et al: *Wind resources in the Baltic Sea*, Proc. ECWEC'96, Goteborg, Sweden, pp.510, 1996.
- [21] Lalas D. P., et al: A hybrid micro-siting model for wind flow simulation over complex topographies, Proc. ECWEC'94, Thessaloniki, Greece, pp, 1994.
- [22] Frank H.P., Landberg L.: *Modelling the wind climate over Ireland*, Proc. ECWEC'96, Goteborg, Sweden, pp.631, 1996.
- [23] Hollis D. et al: Techniques for estimating the local wind climatology, ETSU W/11/00400/REP, 1995.
- [24] Bowen A.J., Mortensen N.G: *Exploring the limits of WAsP, the Wind Atlas Analysis and Application Program*, Proc.ECWEC'96, Goteborg, Sweden, pp.584., 1996.
- [25] Barthelmie L.J., et al: Application of the WAsP model to determine the wind resource in non-neutral conditions in coastal areas, Proc. ECWEC'96, Goteborg, Sweden, pp.627, 1996.
- [26] Brocklehurst F.K., et al, ETSU document

- [27] Hannah P., et al: Comparison of wind speed modelling techniques at existing and potential wind farm sites across the UK, Proc. Wind Energy Conversion 1995, Warwick, UK, July, 1995.
- [28] Addendum to [23]
- [29] Pedersen A.M.J, et al: Reliability of wind farm production forecasts
- [30] Nygaard T.A: Estimating expected energy capture at potential wind turbine sites in Norway, Proc. EWEC'91, Amsterdam, Netherlands, pp.787., 1991.
- [31] Frandsen S., Christensen C.J: *Accuracy of estimation of energy production from wind power plants*, Wind Engineering, Vol.16, No. 5, pp.257, 1992.
- [32] Derrick A., *Development of the Measure-Correlate-Predict strategy for site assessment*, Proc. EC Wind Energy Conf. 1993, Lubeck-Travemunde, Germany, pp681-685, 1993.
- [33] Mortimer, A., *A new correlation/prediction method for potential wind farm sites*, Proc. BWEA Conf. 1994, Stirling, Scotland, pp349, 1994.
- [34] Frandsen, S., *On Uncertainties in Power Performance measurements*. Sixth ASME Wind Energy Symposium, Dallas, Texas, USA, February 15-19, 1987.
- [35] Frandsen, S. and J.C. Christensen, *Accuracy of estimation of energy production from wind power plants*, Jour. Wind Engineering vol. 16 No. 5, 1992.
- [36] *Guide to expression of uncertainty in measurement*, International Organisation for Standardisation (ISO), 1993.
- [37] *Wind turbine generator systems, Part 12: Wind turbine power performance testing*; Final draft international standard, International Electrotechnical Commission (IEC), 1400-12 Ed. 1, FDIS 88, 1997.
- [38] Pedersen, T.F. and U.S. Paulsen, *A procedure for classification of cup anemometers*, EWEC'97, Dublin, Ireland, October, 1997.
- [39] Derrick, A. et al., *A unified approach to the evaluation of the site specific wind characteristics for use in both energy and load modelling of potential wind turbine development site*, EWEC'97, Dublin, Ireland, October, 1997.
- [40] Mortensen, N.G. and E.L. Petersen, *Influence of topographical input data on the accuracy of wind flow modelling in complex terrain*, EWEC'97, Dublin, Ireland, October, 1997.
- [41] Palutikof, J.P, et al, *The impact of climate variability on the UK wind resource*, ETSU WN 6029-P1, 1993.
- [42] Palutikof, J.P, et al, *The impact of climate variability on the UK wind resource*, ETSU WN 6029-P2, 1993
- [43] H.C. Shellard, 1965, *The estimation of design wind speed*, In: Proc. First Int. Conf. on Wind Effects on Buildings and Structures, London, 1965.
- [44] N.J. Cook, *Towards better estimation of extreme winds*, J. Wind Eng. Ind. Aerodyn. 9, p. 295. , 1982.
- [45] J. Lieblein, *Efficient methods of extreme-value methodology*, Report NBSIR 74-602, National Bureau of Standards, 1974.
- [46] R.I. Harris, *Gumbel re-visited - A new look at extreme value statistics applied to wind speeds*, J. Wind Eng. Ind. Aerodyn. 59, p. 1, 1996.
- [47] H. Bergström, *Distribution of extreme wind speed*, Wind Energy Report WE92:2, Department of Meteorology, Uppsala University, 1992.
- [48] C. Cunnane, *Unbiased plotting positions - A review*, J. Hydrol. 37, p. 205, 1978.
- [49] A. Benard and E.C. Bos-Levenbach, *The plotting of observations on probability paper*, Statistica 7, p. 163, 1953.
- [50] J. Wieringa and P.J. Rijkoort, *Windklimaat van Nederland*, Staatsdrukkerij, 1983.
- [51] A.G. Davenport, *The dependence of wind loads on meteorological parameters*, Proc. Second Int. Conf. on Wind Effects on Buildings and Structures, 1967, Ottawa, 1967.
- [52] L.L. Freris, *Wind energy conversion systems*, Prentice Hall, 1990.
- [53] J.R. Mayne, *The estimation of extreme winds*, J. Ind. Aerodyn. {bf 5}, p. 109, 1979.
- [54] P.J. Rijkoort, *A compound Weibull model for the description of surface wind velocity distributions*, Koninklijk Nederlands Meteorologisch Instituut, Report W.R. 83-13, 1983.

- [55] N.E. Busch, O. Christensen, L. Kristensen, L. Lading and S.E. Larsen, *Meteorological field instrumentation - Wind speed and direction by means of cups, vanes, propellers and lasers*, Report Risø-R-400, Risø National Laboratory, 1979.
- [56] C.J. Christensen and J.B. Dragt (ed.), *Accuracy of power curve measurements*, Report Risø-M-2632, Risø National Laboratory, 1986.
- [57] I. Troen and E.L. Petersen, *European Wind Atlas*, Commission of the European Communities, 1989.
- [58] S.D. Dubey, *Some percentile estimators for Weibull parameters*, *Technometrics* 9, p. 119, 1967.
- [59] E.H. Lysen, *Introduction to wind energy* (2nd edition), Publication CWD 82-1, Consultancy services Wind energy Developing countries, 1983.
- [60] M. Stevens, *De bruikbaarheid van Weibullfuncties bij de bepaling van de opbrengst van windenergiesystemen*, Report R-370-A, Dept. Applied Physics, Eindhoven University of Technology, 1979.
- [61] J.O. Hinze, *Turbulence* (2nd ed.), McGraw-Hill, 1975.
- [62] D.A. Spera (ed.), 1994, *Wind turbine technology*, ASME Press.
- [63] H. Tennekes and J.L. Lumley, *A first course in turbulence*, MIT Press, 1972.
- [64] C.P. Butterfield, C. Stork, W.E. Holley, P.H. Madsen and P.H. Jensen, *External condition models from the International Electrotechnical Commission 'Safety of Wind Turbine Standards (1400-1)'*, Proc. 16th ASME Wind Energy Symposium, 1997, Reno, 1997.
- [65] Mortensenn N.G. (1994), "Flow response characteristics of the Kaijo Denki omni-directional sonic anemometer (TR-61B)", Risø-R-704(EN).
- [66] Kaimal, J.C., Finnigan, J.J. (1994) "Atmospheric boundary layer flows-their structure and measurement", Oxford Univ. Press.
- [67] Mortensen, N.G. (1994), "Wind measurements for wind energy applications - a review", 16th BWEA Conference Stirling 15-17 June 1994, Scotland, pp 353-360.
- [68] Mortensen, N.G. and Højstrup Jørgen, (1995), "The Solent sonic-response and associated errors", Ninth Symposium on Meteorological Observations and Instrumentation, Charlotte, NC.

Appendix A Assessment Of Other Parameters - Mathematical Details

A.1 Extreme Wind Speeds: Distribution

In practice, wind speeds observed in a time interval are dependent rather than independent quantities. This hampers a proper statistical analysis of wind speed, with as a consequence a poor description of events which are not very frequent like high wind speeds. The situation improves when statistically independent observations of extreme wind speed are used in order to obtain a distribution of extreme wind speed.

If a quantity x has a cumulative distribution function $F(x)$, the *exact* cumulative distribution function $F_i(x)$ of M independent observations of that quantity is $F^M(x)$. If M is sufficiently large, $F_i(x)$ converges towards an asymptotic cumulative distribution function $F_d(x)$. On the other hand, for $M = 1$ the distribution of independent observation is equal to the parent distribution $F(x)$.

Now suppose a record with observations is broken down into M sub-records, and that the extreme is selected from each sub-record. If the sub-records are large enough, the extremes x_e obtained from the sub-records are independent. In this case the cumulative distribution function of the independent observations is equivalent to the cumulative distribution function of the independent extremes:

$$F_e(x_e) \equiv F_i(x_e) = F^M(x). \quad (\text{A1})$$

In the case of wind speed, the general parent cumulative distribution function is the Weibull distribution [A1]

$$F_w(u) = 1 - \exp\left[-\left(\frac{u}{A}\right)^k\right] \quad (\text{A2})$$

where F_w is the probability a wind speed is smaller than u given the scale parameter A and the shape parameter k . As a consequence, the distribution of M independent extreme wind speeds u_e is:

$$F_{e,w}(u_e) = F_w^M(u) = \left(1 - \exp\left[-\left(\frac{u}{A}\right)^k\right]\right)^M \quad (\text{A3})$$

This implies the probability an independent extreme wind speed u_e is larger than a given value u is

$$G_{e,w}(u_e) \equiv 1 - F_{e,w}(u_e) = 1 - \left(1 - \exp\left[-\left(\frac{u}{A}\right)^k\right]\right)^M \quad (\text{A4})$$

If M is large, this probability converges towards the asymptotic distribution

$$G_{e,w}(u_e) \approx 1 - \exp(-\exp(-\alpha(u - \beta))) \quad (\text{A5})$$

with

$$\frac{1}{\alpha} = \frac{A}{k} (\ln M)^{\frac{1}{k}-1} \text{ and } \beta = A (\ln M)^{\frac{1}{k}} \quad (\text{A6})$$

the dispersion factor and the modal value, respectively [A2]. These equations show that the distribution of independent extreme wind speeds can be obtained from the Weibull parameters A and k , and the number M of independent extreme wind speeds. The cumulative distribution function

$$F(x) = \exp(-\exp(-\alpha(x - \beta))) \quad (A7)$$

is the Gumbel distribution [A3], also known as the Fisher-Tippett Type 1 distribution [A4]. To facilitate calculations (see section 4.1.2.1),

$$G_{e,w}(u_e) \approx 1 - \exp(-\exp(-\alpha \cdot u + B)) \quad \text{with } B \equiv \alpha \cdot \beta \quad (A8)$$

is introduced here as an equivalent extreme winds distribution

A.2 Extreme Winds: Recurrence Period

If $F_e(u_e)$ is the probability the extreme wind speed u_e during a standard observation period, T_{obs} of one year, is *not* exceeded, the corresponding probability of exceedance is $1 - F_e(u_e)$.

If the random variable T denotes the time between consecutive occurrences of independent exceeding events then the mean value of T : $\bar{T}(u_e)$, is by definition the return period.

The return period can be related to the probability of exceedance. If an independent exceedance occurs every 50 years on the average, then the probability that such an event occurs in any given year is: $1/50 = 0.02$ or 2 percent. Thus the return period $\bar{T}(u_e)$ and the probability of exceedance $1 - F_e(u_e)$ are related as:

$$\frac{\bar{T}(u_e)}{T_{obs}} = \frac{1}{1 - F(u_e)} \quad (A9)$$

The IEC 1401-1 standard uses the term recurrence period. In the literature, as far as we know, there is however no distinction made between return period and recurrence period. In any case the IEC 1400-1 standard does not describe the meaning of recurrence period, although the reference wind speed is defined as the 10-minute average wind speed with a recurrence period of 50 years. It is therefore recommended that the definition of recurrence period is included in list of symbols and units of the IEC standard.

The use of the term 'return period' can lead to dangerous misunderstanding if one is not aware of the fact that $\bar{T}(u_e)$ is only the average value of the length of the time interval between consecutive exceedances.

After the occurrence of an exceedance there is a big chance that before $\bar{T}(u_e)$ has past, there is at least one more exceedance. Rather than choosing a return period it is better to state which risk, r , one considers to be acceptable, that u_e is exceeded within T_p standard observation periods (T_{obs}) of one year. The corresponding return period $\bar{T}(u_e)$ then follows from the relation:

$$1 - r = \left(1 - \frac{T_{obs}}{\bar{T}(u_e)}\right)^{T_p/T_{obs}} \quad (A10)$$

A.3 Series Analysis

When measuring wind speed, it is usually sampled and stored in the form of a series. The samples are obtained either in a given position during a time period or in various positions at a given time instant. Hence, a series with the i th component of the wind speed is

$$u_i[n] \quad (i = 1,2,3; n = 1,2,\dots,N) \quad (\text{A15})$$

where N is the number of observations. In the case wind speed is measured at a given position during a time period, n corresponds to time t [s]: $n \rightarrow n_t = t$. This is referred to as the temporal description of the wind speed field. On the other hand, if wind speed is measured in various positions at a give time instant, n corresponds to position x [m]: $n \rightarrow n_x = x$. This is referred to as the spatial description.

By definition, the *covariance function* of the series $u_i[n]$ and $u_j[n]$ is:

$$R_{ij}[k] = \sum_{n=1}^N (u_j[n] - \bar{u}_j)(u_i[n+k] - \bar{u}_i) \quad (k = 1 - N, \dots, 1 + N) \quad (\text{A16})$$

with

$$\bar{u}_i = \frac{1}{N} \sum_{i=1}^N u_i[n] \quad (\text{A17})$$

the average of the i th component. If n corresponds to time, k corresponds to time shift τ [s]: $k \rightarrow k_t = \tau$. Likewise, if n corresponds to position, k corresponds to separation distance r [m]: $k \rightarrow k_x = r$. The *correlation function*

$$r_{ij}[k] = \frac{R_{ij}[k]}{\sqrt{R_{ii}[0]R_{jj}[0]}} \quad (\text{A18})$$

is the non-dimensional covariance function. The *spectral density function* is obtained by Fourier transforming the covariance function:

$$h_{ij}[f] = \frac{1}{2\pi} \sum_{k=1-N}^{1+N} R_{ij}[k] \exp(-jfk) \quad (\text{A19})$$

If k corresponds to time shift, f corresponds to frequency ω [1/s]: $f \rightarrow f_t = \omega$. Alternatively, if k corresponds to separation distance, f corresponds to wave number w [1/m]: $f \rightarrow f_x = w$. The *coherency function*

$$c_{ij}[f] = \frac{h_{ij}[f]}{\sqrt{h_{ii}[f]h_{jj}[f]}} \quad (\text{A20})$$

is the non-dimensional spectral density function.

A4 References

- [A1] W. Weibull, 1951, A statistical distribution function with a wide applicability, J. Appl. Mech., p. 293.
- [A2] H. Bergström, 1992, *Distribution of extreme wind speed*, Wind Energy Report WE92:2, Department of Meteorology, Uppsala University.
- [A3] E.J. Gumbel, 1958, *Statistics of extremes*, Columbia University Press.
- [A4] R.A. Fisher and L.H.C. Tippett, 1928, Limiting forms of the frequency distribution of the largest or smallest member of a sample, Proc. Cambridge Philos. Soc., p. 180.
- [A5] H.A. Panofsky and J.A. Dutton, 1984, *Atmospheric turbulence*, John Wiley & Sons.

[A6] J. Wieringa and P.J. Rijkooft, 1983, *Windklimaat van Nederland*, Staatsdrukkerij.

[A7] L.L. Freris, 1990, *Wind energy conversion systems*, Prentice Hall.

[A8] E. Castillo, 1988, *Extreme value theory in engineering*, Academic Press.

Appendix B Use Of Sonic Anemometer

B.1 Spectral characteristics of turbulence

Before proceeding with the analysis of data from a sonic anemometer, a brief presentation is given of the power spectral density function and its relation to the turbulent kinetic energy of the wind speed components. As a result, in the following we shall limit our discussion to the variations of the three velocity components (u,v,w).

When considering the energy spectrum of the boundary layer turbulence, three distinct regions can be identified [B1,B2]:

- The *energy containing range* where energy is produced by buoyancy and shear.
- The *inertial sub-range* where energy is neither produced or dissipated, but simply transported from bigger to smaller size eddies. In the inertial sub-range the spectrum expression has the form $E_x(k) = a_1 \epsilon^{2/3} k^{-5/3}$ where x is one of the u, v or w , a_1 is the Kolmogorov constant, ϵ the dissipation rate of the turbulent kinetic energy and k the wavenumber. Kolmogorov was the first to conceive the idea of the inertial sub-range and to prove that the spectrum should have a slope of $-5/3$. According to IEC 1400-1 document “Safety of Wind Turbine Generator systems”, the inertial sub-range at 10m/s extends roughly from 0.02Hz to 2 kHz.
- The *dissipation range* where kinetic energy is converted to internal energy.

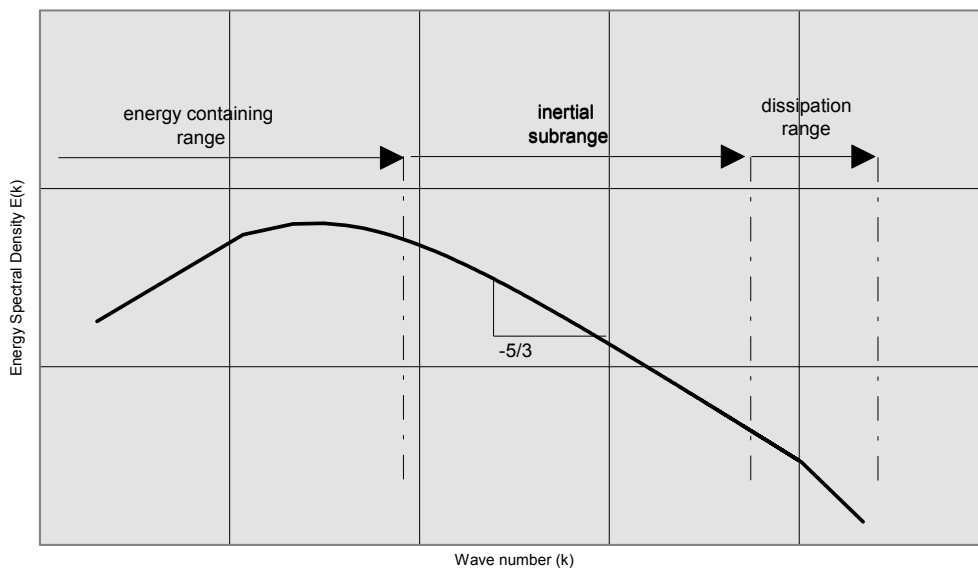


Figure B1 Spectral characteristics of the boundary layer turbulence

For the determination of the turbulence characteristics of an atmospheric flow, simultaneous measurements at a number of spatial locations are required. As this is rather difficult and has a high cost, use of the Taylor’s frozen turbulence hypothesis is made. According to Taylor, temporal and spatial measurements are equivalent since turbulence eddies do not change substantially while being convected by the mean wind speed. The equivalence between the temporal and spatial characteristics of the turbulence parameters allows their study by using one instrument (e.g. sonic anemometer) at one location.

Assuming a stationary random process we can define an autocorrelation function:

$$R(\tau) = \overline{x'(t)x'(t + \tau)} \tag{B1}$$

where τ is the time delay and x' the variation of the corresponding velocity component (u,v,w).

The Fourier transform of this function is:

$$R(\tau) = \frac{1}{2} \int_{-\infty}^{\infty} \Phi(\omega) e^{i\omega\tau} d\omega \quad (\text{B2})$$

where $\Phi(\omega)$ is the energy spectrum density (even function) and ω is the frequency expressed in radians/second.

Now for $\tau = 0$, $\Rightarrow R(0)$ is equal to twice the turbulent kinetic energy and equation (B2) becomes:

$$\sigma_x^2 = R(0) = \int_0^{\infty} \Phi(\omega) d\omega = \int_0^{\infty} S(f) df = \int_0^{\infty} fS(f) d \ln f \quad (\text{B3})$$

where $S(f) = 2\pi \cdot \Phi(\omega)$ a new spectral density function, $\omega = 2\pi f$ is the frequency in radians per second and f is the frequency in Hertz.

All expressions of equation (B3) are equivalent and their integral is seen to be the variance of the corresponding turbulent velocity component. The function $fS(f)$ is as a rule adopted for the description of the atmospheric spectra. Since the variance is finite, the function becomes practically zero at very high or very low frequencies.

B.2 Analysis stages for the calculation of the turbulent parameters

In the following the procedure for the calculation of the standard deviation, the power spectral densities and the integral length scales is presented. This is done for the Kaimal spectral model. A corresponding method can be used when the von Karman formulation is used. The power spectral density function can be approximated by an analytical expression. In the IEC 1400-1 document "Safety of Wind Turbine Generator systems", the power spectral densities are, in non-dimensional form, given by the equation:

$$\frac{fS_x(f)}{\sigma_x^2} = \frac{4fL_x / V_{hub}}{(1 + 6fL_x / V_{hub})^{5/3}}, \text{ where:} \quad (\text{B4})$$

- f the frequency in Hz
- x the corresponding velocity component
- S_x the velocity component spectrum
- σ_x the standard deviation of the x velocity component
- L_x the integral length scale of the x velocity component

The following steps are taken to calculate the power spectral density and the corresponding length scales:

Mounting of the instrument

The sonic anemometer is mounted so that the sensor array is oriented towards the wind direction that will be analysed (in this way minimum influence is experienced from the presence of the struts).

The vertical positioning of the instrument is checked with the help of a level at two orthogonal wind directions.

Data acquisition

The length of the time series used for the calculation of the turbulent parameters depends entirely on the application or on agreed procedures.

However, it is normal practice to use ten minutes time series for the calculation of the standard deviation.

For the calculation of the spectral density function and the length scales a "common practice" [B3], is to divide a ten-minutes time series into eight non-overlapping segments, calculate the spectra for each

segment and average over the eight segments. Finally, to smooth out any large variations in the values of the final spectrum, a moving average can be used. However, whether or not the above practice is followed is down to individual judgement..

The choice of the *record length* T influences automatically the value of the lowest resolvable frequency ($1/T$) and the width of the frequency band in the spectrum:

$$\Delta f = \frac{1}{T} = \frac{1}{N\Delta t} \quad (\text{B5})$$

with N : the number of data points and Δt : the time between two consecutive samples

After the FFT calculation, the number of points included in the spectrum is $N/2$ and the bandwidth of the spectrum is $(1/2\Delta t)$ Hz.

The choice of the *sampling rate* depends as a rule on the bandwidth wished to be covered. As a rule of thumb the sampling frequency should be at least twice the highest frequency that needs to be investigated (Nyquist criterion).

Finally attention is needed regarding the filtering of the data so that the results do not get contaminated from the “aliasing” process. During this process frequencies higher than $(1/2\Delta t)$ Hz are folded back on the spectrum over the lower frequencies and contaminate the results. Anti-aliasing filter should therefore be employed in the measurement system.

Data reduction

The time series chosen for the analysis should not contain large variations or trends in the magnitude of the wind velocity or wind direction. The existence of trends in the data violates the stationarity assumption and, as will be seen later, introduces uncertainties in the calculation of the length scales.

The output of the sonic anemometer is given as three velocities in an orthogonal co-ordinate system, fixed to the anemometer. Assuming this is a right-hand system (which is not always the case), a two-step transformation is applied (Figure B2), where the “fixed to the anemometer” co-ordinate system (x_1, y_1, z_1) is translated to the (x_3, y_3, z_3) system. Thus the resultant wind speed u_3 is aligned to the x_3 axis and the mean values of the two other components are equal to zero ($v_3=w_3=0$).

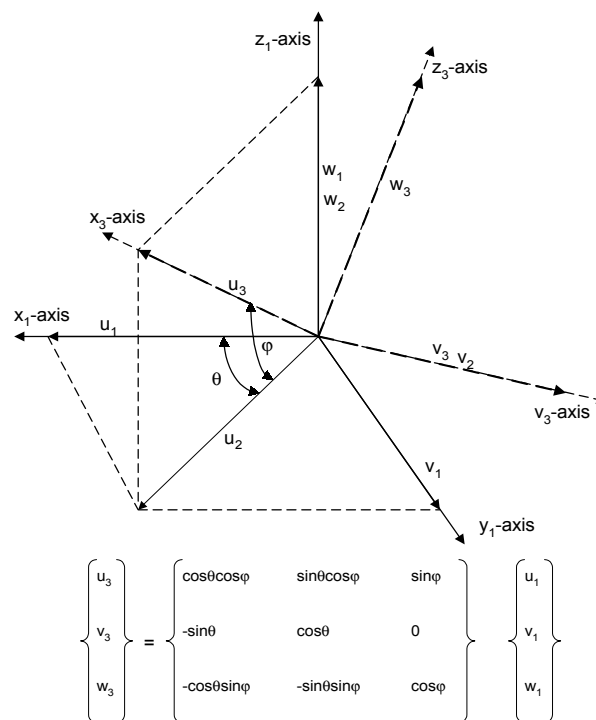


Figure B2 Transformation of the fixed-to-the-anemometer co-ordinate system

Calculate and subtract the mean value (either of the whole time series or of each segment) of the u_3 velocity and find the corresponding standard deviations for all three velocity components. The difference between subtracting the mean value and de-trending (by using a linear or higher order approximation) is that it affects the standard deviation and variance of the resulting series. This is illustrated in Figure B3 where, for the time series (top), the standard deviation is 1.79m/s for the time series in the middle (mean value removed) and 1.39m/s for the bottom one (linear de-trend) while both have zero mean values.

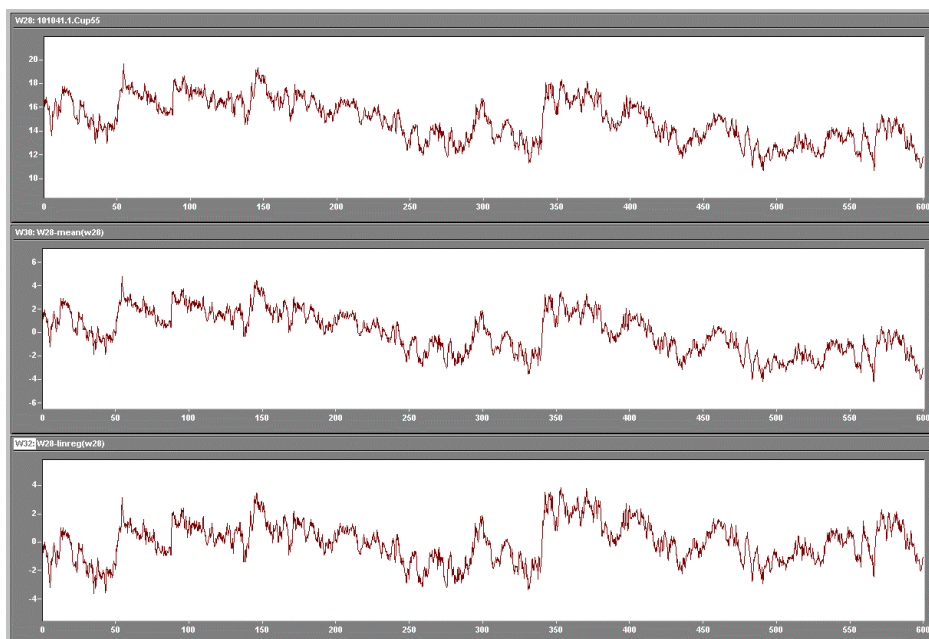


Figure B3 From top to bottom: a) original time series, b) mean value subtracted (std. dev=1.79m/s), c) linear de-trending (std. dev.=1.39m/s)

The difference in the value of the standard deviation influences both the lower spectral frequencies and the values of the length scales. This is also predicted from equation (B4), where a higher standard deviation is connected to higher length scale values.

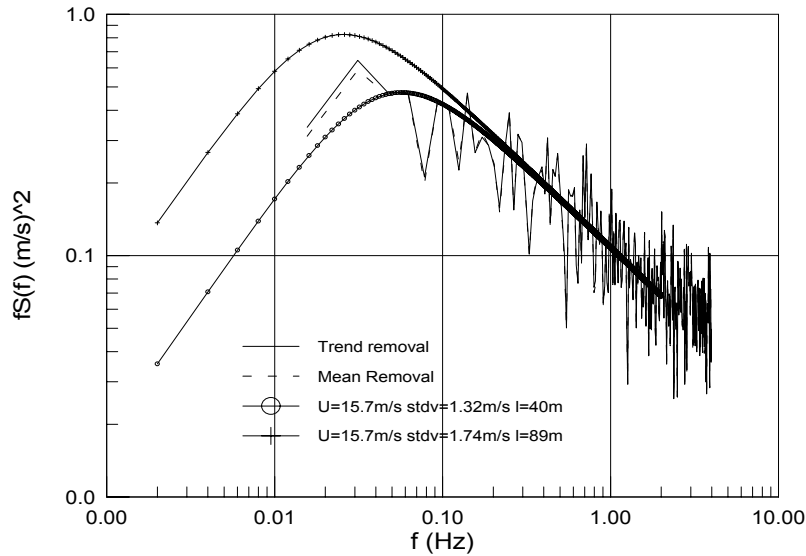


Figure B4 Different ways of removing the mean velocity value affect both the lower spectral frequencies and the magnitude of the length scale

Further evidence is presented in the example of Figure B4 where the spectra of the time series of a wind velocity with a mean value of 15.7m/s are shown both after removing the mean value and by linear de-trend. As a result of the different standard deviations, the length scales differ also. In Figure B4 the power spectral density curves as derived from equation (B4), and corresponding to the two different standard deviation values and length scales, are plotted.

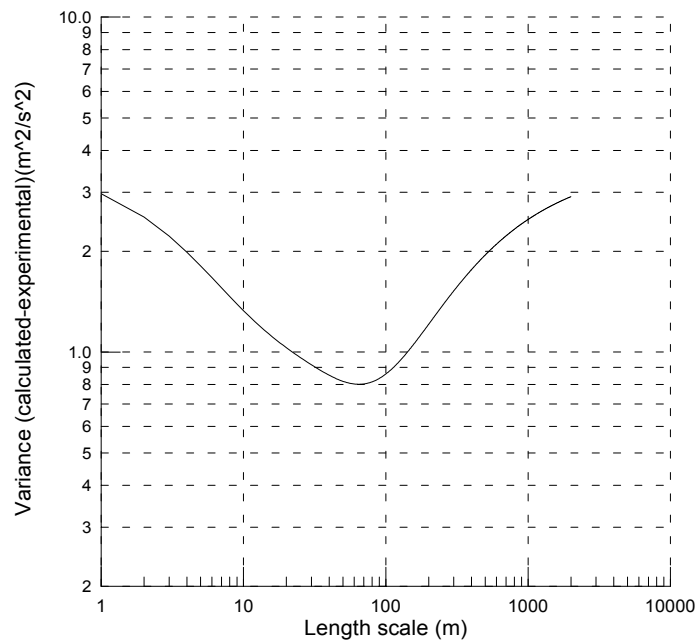


Figure B5 Calculating the length scale from the least square fit

Use an FFT transformation to derive the power spectral density of the time series and a Rectangular window for data filtering.. With the help of equation (B4) fit the linear part of the analytical spectrum to the experimental data (linear part) using a least squares method. This “best-fit” procedure then gives the magnitude of the length scale. The results of this procedure are seen in Figure B5 where the correct length scale is given by the minimum of the curve.

The frequency interval where fitting takes place depends on the response characteristics of the sonic anemometer but as a minimum, a band from 0.25Hz and covering one frequency decade is recommended. It must however be emphasized that there are really no clear rules on this topic and care is needed since the choice of the fitting interval interacts with the fitting procedure and this results in length scales of different size. Thus it really depends on the person carrying out the data analysis to look at the data and take a sound decision.

Experience has shown that the number of observations plotted against the logarithm of the length scale (for a large number of observations) is normally distributed. This means that the individual length scale calculated using the above described procedure is not necessarily representative and that a large number of measurements are required before the “true” length scale is determined.

B3 References

- [B1] Kaimal, J.C., Finnigan, J.J. (1994) “Atmospheric Boundary Layer Flows-Their Structure and Measurement”, Oxford Univ. Press.
- [B2] Sorbjan, Z., (1989), “Structure of the Atmospheric Boundary Layer”, Prentice Hall.
- [B3] “MOUNTURB-Data Analysis Benchmark Test”, C.R.E.S. (1996).

